The Development of Aminopeptidase N Inhibitors as Potential Anti-Cancer Agents

Jisook Lee

Bachelor of Pharmaceutical Sciences (Honours) Medicinal Chemistry

A thesis submitted for the degree of *Doctor of Philosophy*

Medicinal Chemistry Theme
Monash Institute of Pharmaceutical Sciences
Faculty of Pharmacy and Pharmaceutical Sciences
Monash University

August 2019

Table of Contents

Copyright notice

Notice 1

Under the Copyright Act 1968, this thesis must be used only under the normal conditions of scholarly fair dealing. In particular, no results or conclusions should be extracted from it, nor should it be copied or closely paraphrased in whole or in part without the written consent of the author. Proper written acknowledgement should be made for any assistance obtained from this thesis.

Notice 2

I certify that I have made all reasonable efforts to secure copyright permissions for third-party content included in this thesis and have not knowingly added copyright content to my work without the owner's permission.

Abstract

Aminopeptidase N (APN) is a ubiquitous transmembrane ectoenzyme that is widely present in different types of cells. APN is a member of the zinc dependent M1 aminopeptidase superfamily of enzymes. APN is one of the most extensively studied metalloaminopeptidases as an anti-cancer target due to its significant role in the regulation of metastasis and angiogenesis. Compelling evidence has demonstrated a strong relationship between dysregulation of APN activity and the development of human malignancies through extracellular matrix (ECM) degradation, tumour cell migration, and invasion. Despite continuous efforts over the past decades, few inhibitors have demonstrated desirable efficacy. Thus, there is an on-going interest to develop potent APN inhibitors as potential anti-cancer drug candidates.

Previous research identified a hydroxamic acid containing analogue, *N*-(2-(hydroxyamino)-2-oxo-1-(3',4',5'-trifluoro-[1,1'-biphenyl]-4-yl)ethyl)pivalamide (**1**) as a potent inhibitor of the APN homologue from the malaria parasite, *Plasmodium falciparum,* (*Pf*A-M1). This thesis describes the rationale behind the repurposing of **1** as a novel APN inhibitor for the treatment of cancer. A series of hydroxamic acid analogues were designed using a structure-based design approach. The *N*-pivaloyl group of **1** was replaced with various alkyl and aromatic linkers, and the synthesised compounds were evaluated for their inhibitory activity against APN. Among the series of compounds, the methylsulfonamide analogue **6ad** was identified as an extremely potent inhibitor of APN, which was 26-fold more potent than compound **1**. Computational modelling studies demonstrated that **6ad** engaged in several hydrophobic and hydrogen bonding interactions at the S1 and S1′ subsites of APN. The inhibitor was also selective against other zinc dependent enzymes such as matrix metalloproteases (MMPs), possessed limited cytotoxicity against Ad293 cells and had favourable metabolic and plasma stability properties.

Physicochemical property studies found that **6ad** had sub-optimal kinetic solubility. Therefore, a number of modifications to the lipophilic 3,4,5-trifluorophenyl ring were made to optimise the binding interactions at the S1 subsite of APN, which has not been explored in the previous studies, as well as to improve the solubility. A variety of synthetic strategies were extensively explored for optimisation of multiple synthetic pathways. Suzuki-Miyaura coupling reaction condition between aryl bromide, arylboronic acids and cycloalkylboronic acids were successfully optimised to synthesise analogues containing biphenyl and cycloalkyl-aryl scaffolds. A diverse set of synthetic approaches were employed to generate piperidyl and piperazinyl compounds through Buchwald-Hartwig aminations. *In vitro* enzymatic assays revealed that the 3-fluorophenyl analogue **6f** was the most potent inhibitor of this project, exhibiting a remarkable inhibitory activity of $K_i^{(app)}$ = 0.66 nM. This was 178-fold more potent than compound **1** with reduced cLogP value of 1.81. Molecular docking studies of selected compounds were performed to investigate the differences in the binding interactions between each inhibitor. Cell-based assays were conducted to measure the potential anti-proliferative activity of selected compounds in a cellular environment. Despite being a potent enzyme inhibitor, compound **6f** showed weak anti-proliferative activity against certain types of cancer cell lines.

Finally, the central phenyl group of the scaffold was proposed to replace with heteroaromatics such as pyridine and pyrimidine or acetylene group. A number of synthetic pathways were developed to synthesise a small series of compounds. However, the optimisation of the synthesis was challenging and requires further investigation in the future.

General Declaration

I hereby declare that this thesis contains no material which has been accepted for the award of any other degree or diploma at any university or equivalent institution and that, to the best of my knowledge and belief, this thesis contains no material previously published or written by another person, except where due reference is made in the text of the thesis.

This thesis includes 2 original papers published in peer reviewed journals. The core theme of the thesis is the development of novel Aminopeptidase N inhibitors through structure-based approaches. The ideas, development and writing up of all the papers in the thesis were the principal responsibility of myself, the student, working within the Department of Medicinal Chemistry and the Department of Microbiology under the supervision of Prof Peter. J. Scammells, Dr Sheena McGowan, and Dr Natalie Vinh.

The inclusion of co-authors reflects the fact that the work came from active collaboration between researchers and acknowledges input into team-based research.

In the case of *Chapter 1* and *Chapter 2*, my contribution to the work involved the following:

Thesis Chapter	Publication Title	Status	Nature and extent of student contribution	Co-author name(s) Nature and extent of Co-author's contribution	Co-author(s), Monash student
Section 1.3 and 1.4 of Chapter 1	M1 aminopeptidases as drug targets: broad applications or therapeutic niche?	Published	Writing part of the review article, 10%	**Drinkwater, N., McGowan, S.** Article preparation, literature search (35%) **Yang, W.** Writing part of article (10%) **Malcolm, T. R.** Writing part of article (10%)	Malcolm, T. R.
Section 1.8 of Chapter 1 & Chapter 2	Novel Human Aminopeptidase N Inhibitors: Discovery and Optimization of Subsite Binding Interactions	Published	Data acquisition, analysis, manuscript preparation, 80%	**Vinh, N., Drinkwater, N., Yang, W.** Skill training, data acquisition, manuscript preparation (1%) **Sivaraman, K. K.** Skill training, data acquisition (1%) **Schembri, L., Gazdik, M., Grin, P., Butler, G., Overall, C., Charman, S.** Data acquisition and analysis (1%) **McGowan, S.** Manuscript preparation, idea generation, supervision (5%) **Scammells, P. J.** Manuscript preparation, idea generation, supervision (5%)	

I have not renumbered sections of submitted or published papers in order to generate a consistent presentation within the thesis.

Student name: Jisook Lee

Student signature: **Date:** 31 July 2019

I hereby certify that the above declaration correctly reflects the nature and extent of the student's and co-authors' contributions to this work. In instances where I am not the responsible author, I have consulted with the responsible author to agree on the respective contributions of the authors.

Main Supervisor name: Peter J Scammells

Main Supervisor signature: **Date:** 31 July 2019

Publications during enrolment

Drinkwater, N.; Lee, J.; Yang, W.; Malcolm, T. R.; McGowan, S. M1 aminopeptidases as drug targets: broad applications or therapeutic niche? *FEBS J.* **2017**, *284*, 1473-1488.

Lee, J.; Vinh, N. B.; Drinkwater, N.; Yang, W.; Kannan Sivaraman, K.; Schembri, L. S.; Gazdik, M.; Grin, P. M.; Butler, G. S.; Overall, C. M.; Charman, S. A.; McGowan, S.; Scammells, P. J. Novel Human Aminopeptidase N Inhibitors: Discovery and Optimization of Subsite Binding Interactions. *J. Med. Chem.* **2019**, *published asap online* (DOI: 10.1021/acs.jmedchem.9b00757).

Acknowledgements

Firstly, I would like to express my deepest gratitude to my amazing supervisors Prof Peter Scammells, Dr Sheena McGowan and Dr Natalie Vinh for their continuous support and guidance throughout my PhD journey. Without their valuable advice and direction, I would not have been able to overcome challenges that I have faced during the candidature and complete this thesis. Peter, thank you so much for all the opportunities you have provided me with. I was very fortunate and privileged to attend several unforgettable conferences and to work on this exciting project with kind and warm-hearted people. I was able to not lose momentum and motivation thanks to your encouragement. Sheena, thank you so much for helping me to expand my knowledge and skills in biology and computational studies. Having no biology and computational background, this aspect of the project was always the toughest for me, but I was able to pass the huge learning curve thanks to your patience and understanding. Nat, thank you so much for training me since the day one I joined Scammells group. I really appreciate the effort you put into improving my chemistry, writing, and presentation skills. I also thank you not only for giving me advice in the lab, but also providing me with emotional and mental support. Once again, thank you very much for your caring and sincere support. The past 3.5 years would not have been so memorable if I did not have all three of you as my supervisors.

I would also like to thank Dr Nyssa Drinkwater and Komagal Kannan Sivaraman from McGowan group for teaching me how to conduct enzyme assays. I am also grateful to Dr Wei Yang who taught me computational works from the basics with patience.

I would also like to thank my panel members Prof Philip Thompson and Dr Ben Capuano who always provided me with valuable advice and encouragement.

I wish to acknowledge our collaborators Prof Christopher Overall, Dr Georgina Butler, and Peter Mathew Grin from the University of British Columbia for conducting enzymatic assays. This project would have not been possible without their support.

I also appreciate the support from CDCO and Prof Susan Charman for the metabolic stability, plasma stability studies, and analysis of physicochemical properties of testing compounds.

I thank Dr Jason Dang for NMR and mass spectrometry services. Also, Dr David Chalmers was always willing to provide me with advice regarding computational chemistry and appropriate resources for the research.

To all past and present members of the Scammells lab: Dr Shane Devine, Dr Leigh Ford, Dr Manuela Jorg, Dr Michelle Gazdik, Dr Luke Schembri, Anthony Lai, Tim Fyfe, Cassandra Yong, Kyle Awalt, Ricki Wilcox, Benjamin Jeges, Mahta Mansouri Jajaei, Peter Calic, and Jomo Kigotho. I am so glad that I was able to spend my PhD years with wonderful people. Working in Scammells lab was truly an amazing experience and I will never forget the kindness I have received from all the members.

I would like to thank my fellow PhD students: Cassandra Yong, Hanson Law, Matthew Bentley, Mitchell Silk, Shayna Jia and Emma Xu. Thank you so much for making my PhD years more enjoyable and memorable. I would have not been able to survive this tough journey without such brilliant friends.

I appreciate the financial support from Monash University, Sir James McNeil Foundation, and Cancer Therapeutics CRC for this project with Monash International Postgraduate Research Scholarship, Sir James McNeil Scholarship, and CTx Top-up Scholarship.

한국에서 나를 응원하는 가족들 그리고 호주에서 만난 소중한 사람들, 항상 저를 응원해 주셔서 감사합니다. 그리고 항상 내가 우주 최고라고 해주는 사람, 지난 5 년간 내 옆에 있으면서 날 지켜줘서 고마워요.

마지막으로 세상에서 가장 사랑하는 엄마. 엄마의 희생과 기도 덕분에 여기까지 올 수 있었어요. 절 키워주셔서 감사하고 항상 나의 편이 되어주셔서 감사합니다.

Abbreviations

^{1}H NMR	Proton nuclear magnetic resonance
^{13}C NMR	Carbon-13 nuclear magnetic resonance
^{19}F NMR	Fluorine-19 nuclear magnetic resonance
Ac	Acetyl
ADMET	Absorption, distribution, metabolism, excretion, toxicity
AHNPA	(2*S*,3*R*)-2-amino-3-hydroxy-3-(4-nitrophenyl)propanoic acid
AKT	Protein kinase B
APA	Aminopeptidase A
APN	Aminopeptidase N
app.	Apparent
Bcl-2	B-cell lymphoma 2
bFGF	Basic fibroblast growth factor
Bis_2pin_2	Bis(pinacolato)diboron
Bn	Benzyl
Boc	*tert*-Butyl carbamate
Bu	Butyl
Cbz	Carboxybenzyl
CCoV	Canine coronavirus
CDCO	Monash Centre for Drug Candidate Optimisation
CDK	Cyclin-dependent kinase
CEL	Chan-Evans-Lam
cLogP	Calculated logarithm of a compound's partition coefficient between *n*-octanol and water *in silico*
CNS	Central nervous system
CoV	Coronavirus
d	Day

δ	Chemical shift
DMSO-d_6	*hexa*-Deuterated dimethylsulfoxide
DANP	(1*S*,2*S*)-2,3-Diamino-1-(4-nitrophenyl)propan-1-ol
DCE	1,2-Dichloroethane
DCM	Dichloromethane
DIPEA	*N*,*N*-Diisopropylethylamine
DMAP	*N*,*N*-Dimethyl-4-aminopyridine
DME	Dimethoxyethane
DMF	*N*,*N*-Dimethylformamide
DMSO	Dimethyl sulfoxide
DPPF	1,1'-Bis(diphenylphosphino)ferrocene
DPP-IV	Dipeptidyl peptidase 4
ECM	Extracellular matrix
EDCI	1-Ethyl-3-(3-dimethylaminopropyl)carbodiimide
EMA	European Medicines Agency
eq.	Equivalence
ERK	Extracellular signal-regulated kinase
Et	Ethyl
FAK	Focal adhesion kinase
FCoV	Feline coronavirus
FDA	Food and Drug Administration
g	Gram
GRB2	Growth factor receptor-bound protein 2
h	Hour
HCoV229E	Human coronavirus 229E
HCTU	*O*-(1*H*-6-Chlorobenzotriazole-1-yl)-1,1,3,3-tetramethyluronium hexafluorophosphate
HDACs	Histone deacetylases
HOBt	1-Hydroxybenzotriazole
HPLC	High Performance Liquid Chromatography
HRMS	High-resolution mass spectrometry
*h*TNF	Human tumour necrosis factor
HUVEC	Human Umbilical Vein Endothelial Cells

IC_{50}	Concentration of compound required to produce 50% inhibition
IGF-1	Insulin-like growth factor 1
IKK	IκB kinase
J	J coupling
JNK	c-Jun N-terminal kinase
$K_i^{(app)}$	Apparent inhibition constant
K_i	Inhibition constant
LAP	Leucine aminopeptidase
LC-MS	Liquid chromatography–mass spectrometry
LogD	Logarithm of a compound's ionisable species partition coefficient between n-octanol and water at specific pH
M	Molar
m/z	Mass to charge ratio
mAb	Monoclonal antibody
MARK	Mitogen-activated protein kinase
MD	Molecular dynamic
Me	Methyl
MeCN	Acetonitrile
mg	Milligram
MKK3	Mitogen-activated protein kinase kinase 3
mL	Millilitre
mmol	Millimole
MMP	Matrix metalloproteinase
mRNA	Messenger ribonucleic acid
MsCl	Methanesulfonyl chloride
mTOR	Mammalian target of rapamycin
NAD^+	Nicotinamide adenine dinucleotide
NBS	N-Bromosuccinimide
NCI	National Cancer Institute
NF-κB	Nuclear factor kappa light chain enhancer of activated B cells
nM	Nanomolar
NMR	Nuclear magnetic resonance
O/N	Overnight

OTf	Triflate
*p*APN	Porcine Aminopeptidase N
$Pd_2(dba)_3$	Tris(dibenzylideneacetone)dipalladium(0)
PDB	Protein Data Bank
PDCoV	porcine deltacoronavirus
PE	Petroleum ether
*Pf*A-M17	*Plasmodium falciparum* M17 aminopeptidase
*Pf*A -M1	*Plasmodium falciparum* M1 aminopeptidase
PI3K	Phosphoinositide 3-kinases
PMF	Peptide Mass Fingerprinting
ppm	Parts per million
PRCV	Porcine respiratory coronavirus
RhoA	Ras homolog gene family, member A
RMSD	Root mean square deviation
rt	Room temperature
SAR	Structure activity relationships
SEM	Standard error of the mean
SFXC	Surflex-Dock GeomX
shRNA	Short hairpin ribonucleic acid
SI	Supporting information
SRB	Sulforhodamine B
TBS	*tert*-butyldimethylsilyl
TCA	Trichloroacetic acid
TFA	Trifluoroacetic acid
TGEV	Porcine transmissible gastroenteritis virus
THF	Tetrahydrofuran
TIPS	Triisopropylsilyl
TIPSCl	Triisopropylsilyl chloride
TNFα	Tumor necrosis factor alpha
TOF	Time of flight
µL	Microlitre
µM	Micromolar
VEGF	Vascular endothelial growth factor

VEGF-A	Vascular endothelial growth factor-A
VEGFR	Vascular endothelial growth factor receptor
VEGFR-2	Vascular endothelial growth factor-2
Xphos	2-Dicyclohexylphosphino-2′,4′,6′-triisopropylbiphenyl
ZBG	Zinc binding group

Nb. Amino acids are referred to as their standard one or three letter codes. All chemical reagents are given by standard chemical formulas.

Chapter 1: Introduction

1.1 Cancer

Cancer is one of the most concerning health problems in Australia. There are over one million people who are either living with or have lived with cancer, and the number of new cancer cases in Australia was estimated to reach 145,000 in 2019.[1] Although there has been a promising increase in cancer survival rates and reduced rates of cancer mortality, cancer is still the second most common cause of death in Australia and accounts for approximately three in every 10 medical deaths.[1] Chemotherapeutic agents to treat cancer can range from small molecules to antibodies and include effective block-buster drugs such as methotrexate,[2, 3] actinomycin-D,[4, 5] 5-fluorouracil,[6] and trastuzumab[7] (Figure 1.1).

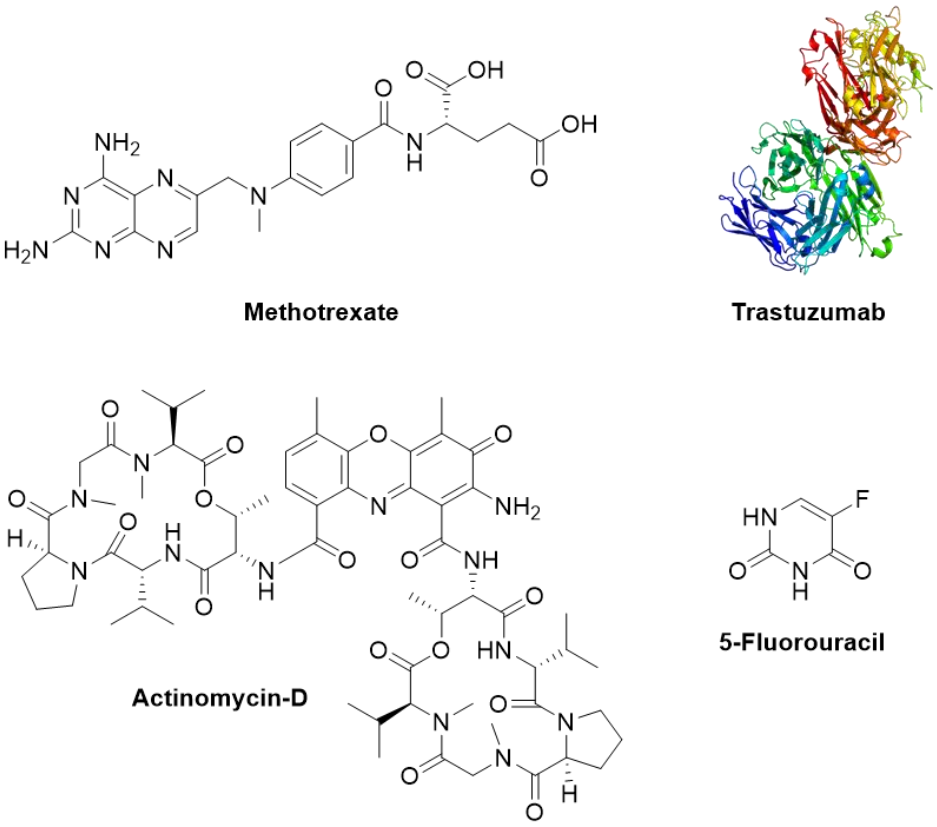

Figure 1.1. Structures of block-buster anti-cancer drugs (PDB ID 5XHG for trastuzumab).

However, many cancer drugs are associated with undesirable side effects, primarily due to their non-selective activity toward non-cancerous cells. Complications from these adverse side effects can lead to detrimental cardiac, hepatic, renal, pulmonary and haematological toxicities.[8-12] In addition, the chronic use of anti-cancer drugs inevitably accompanies drug resistance and reduces its efficacy.[13, 14] Therefore, the development of novel anti-cancer drugs with less toxicity, improved efficacy, and higher selectivity continues to be critically important.

1.2 Cancer Targets and Drugs

With the ever-growing interests in the discovery of less toxic and more selective anti-cancer agents, extensive research has been conducted to identify and characterise therapeutic targets for cancer.[15, 16] In the last few decades, identification of new anti-cancer targets at the molecular level has focused on the biological processes that are important for cancer progression, such as angiogenesis and metastasis.[15, 17-19] Better understanding of the cell cycle and apoptosis pathways have also allowed researchers to develop diverse anti-cancer agents.[15, 20, 21] Insights into cancer biology revealed a variety of molecules regulating the cellular signal transduction machinery, and the most extensively researched area was on protein kinases.[15, 22] The following section provides brief explanations on various cancer targets involved in angiogenesis, cell cycle, and apoptosis, as well as inhibitors that disrupt these three pathways.

1.2.1 Protein Targets Involved in Angiogenesis and Current Drugs

Angiogenesis is the formation of new blood vessels from pre-existing microvasculature.[23] In normal physiological conditions, angiogenesis occurs during embryogenesis, menstruation, and wound healing, and the level of angiogenesis is tightly controlled.[24, 25] However in abnormal conditions such as cancer, uncontrolled level of angiogenesis persists and stimulates the cancer growth by providing nutrients and oxygen to cancer cells.[25, 26] Therefore, angiogenesis is a requirement not only for continuous cancer growth, but also for metastasis.[27, 28]

According to compelling experimental and clinical data, it has been shown that most human cancers can survive for months to years without blood supply until a set of cancer cells acquires an angiogenic phenotype by a phenomenon called ‘angiogenic switch’.[28-30] The activation of the angiogenic switch is characterised by the increased release of angiogenic factors, mobilised angiogenic proteins from the extracellular matrix (ECM), and activation of host cells such as macrophages which produce their own angiogenic molecules.[15, 26, 28, 30] The angiogenic

molecules released send signals to the surrounding normal host tissue and activate genes to produce proteins that stimulate the growth of new blood vessels.[15]

After decades of research on the biology of cancer angiogenesis, a number of molecular targets for angiogenesis inhibition have been uncovered.[15, 19, 31, 32] Currently, most of the targets of angiogenesis are classified into three groups – endothelial cells, endothelial cell growth factor receptors, and extracellular matrix proteinases.[15, 33] The early studies of angiogenesis inhibitors focussed on the discovery of molecules that disrupt the formation of tube networks by endothelial cells, which are the major components constituting blood vessels.[15] Angiostatin and endostatin are the two peptidyl compounds discovered that effectively antagonised the angiogenic actions of endogenous angiogenic protein, angiogenin.[15] Previous studies indicated that these 20 – 38 kDa proteins inhibited endothelial cells proliferation, angiogenesis and tumour growth.[34-37]

Considerable efforts in anti-angiogenic cancer drug discovery have also been focussed on the growth factors and growth factor receptors that involve in endothelial cell proliferation.[15] The most studied targets among this class of anti-cancer agents are the vascular endothelial growth factor (VEGF) and its receptor VEGFR-2.[38, 39] VEGF is an angiogenesis inducer responsible for stimulating growth and proliferation of endothelial cells, as well as regulating the vascular permeability.[40-42] VEGF is also a survival factor for endothelial cells by preventing the apoptosis.[43] VEGFR-2 is a transmembrane tyrosine kinase that is exclusively expressed in endothelial cells, therefore it is a promising target for angiogenesis inhibitors.[38] Bevacizumab is a recombinant humanised monoclonal antibody to VEGF and blocks tumour cell-derived VEGF-A to impair the development of new vessels, leading to cancer growth inhibition.[44] Combination therapy of bevacizumab with other cancer drugs was assessed against various types of cancer in clinical trial settings, and bevacizumab was approved by the Food and Drug Administration (FDA) for the treatment of colorectal, non-small-cell lung, and glioblastoma multiforme.[15, 45-48] Sunitinib and Sorafenib are orally available VEGFR inhibitors, and they were approved by the FDA for renal cell carcinoma (Figure 1.2).[15, 49, 50]

Another class of targets for angiogenesis inhibition that have been much studied is extracellular matrix proteinases, particularly the matrix metalloproteinases family (MMPs).[51, 52] MMPs belong to the metzincin superfamily of metalloproteinases, and there are 28 subtypes of MMPs identified (MMP1 – MMP28).[53] MMPs induce angiogenesis by degrading ECM proteins which

allow the endothelial cells to invade the surrounding matrix.[15] Studies also suggest that MMP2 is up-regulated in all human cancers.[54] Many small molecule MMP inhibitors with extremely potent activity at nanomolar to picomolar range have been developed.[53, 54] Some of the first-generation MMP inhibitors contained hydroxamic acid as the zinc binding group (ZBG).[55] Hydroxamic acid based inhibitor, batimastat, and its more water-soluble analogue, marimastat (Figure 1.2), underwent clinical trials, however, their clinical performance was disappointing.[53, 56-58] More than 50 MMP inhibitors have been studied in clinical trials, and all of these trials failed due to varied reasons including poor trial design, unstable metabolism, poor oral bioavailability, dose-limiting toxicities, and poor knowledge of the complexity of biological roles of MMPs .[53, 54, 59, 60]

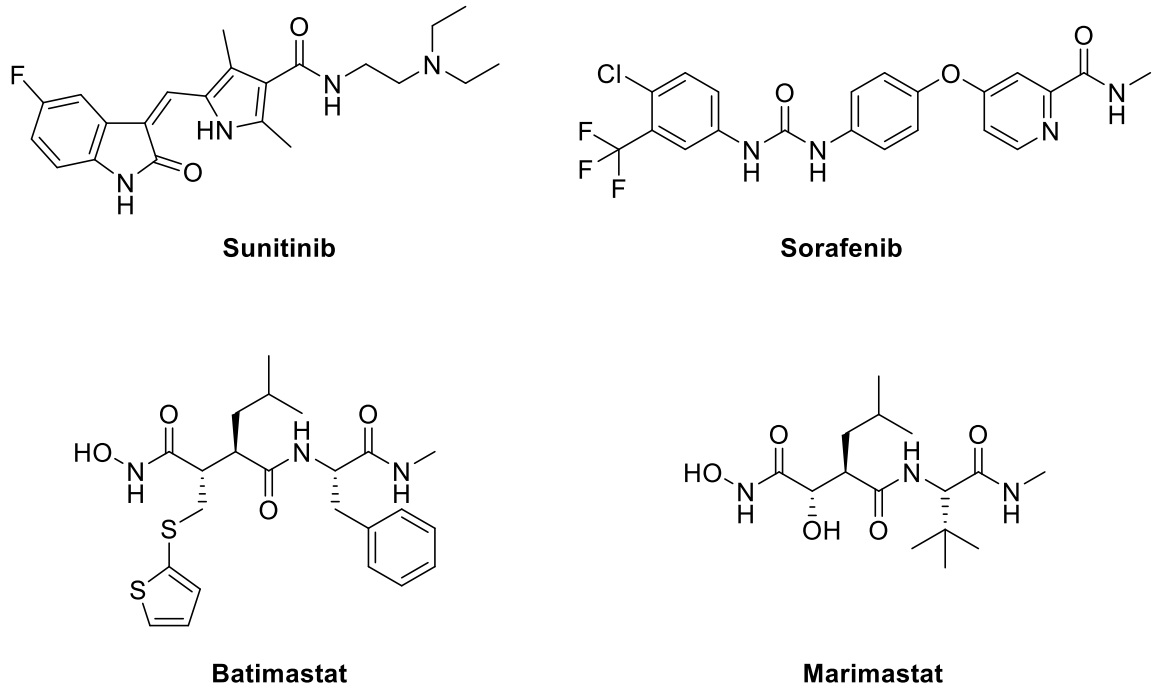

Figure 1.2. Structures of selected anti-angiogenic agents targeting VEGFR (Sunitinib and Sorafenib) and MMPs (batimastat and marimastat).

1.2.2 Cell Cycle Regulators and Current Drugs

The cell cycle is a complex process consisting of mitosis (M), which is the cell division, and interphase, which comprises the G_1 (pre-DNA synthesis), S (DNA synthesis), and G_2 (pre-division) phases.[20, 61] After interphase, the cell cycle returns to the G_0 phase (quiescence).[20, 61] The cell cycle is tightly regulated by different checkpoints under normal physiological conditions, however, many human cancers are characterised by dysregulated cell cycle, resulting in uncontrolled growth of cancer cells.[15, 62, 63] Each stage in the cell cycle is meticulously regulated by cyclin-dependent kinases (CDKs), a family of serine/threonine protein kinases, and their regulatory partners, the cyclins.[20, 64-66] CDK-cyclin complexes are the key regulatory molecules of the cell cycle, therefore intensive studies have been conducted to design various CDK inhibitors in order to disturb aberrant cell growth.[20, 64] Among the first-generation CDK inhibitors, Flavopiridol is one of the most tested in clinical trials (Figure 1.3). Flavopiridol is a semi-synthetic flavonoid derived from an alkaloid isolated from *Dysoxylum binectariferum* and it was primarily used for the treatment of rheumatoid arthritis.[67] Flavopiridol induces cell cycle arrest at the G_1 or G_2/M phase by association with CDKs 1, 2, 4, 6, 7, and 9.[68] Despite comprehensive clinical trials, Flavopiridol failed to receive an approval as an effective anti-cancer agent due to dose-limiting toxicities from poor selectivity.[20] Therefore, a new generation of compounds that are capable of inhibiting selective CDKs were discovered.[20] For example, Palbociclib is an oral, reversible, and selective CDK4/6 inhibitor that inactivates early G_1 kinases (Figure 1.3).[20, 69] Palbociclib was approved by the FDA for certain advanced or metastatic breast cancer in combination with other anti-cancer drugs.[70]

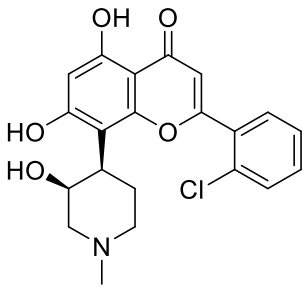

Flavopiridol

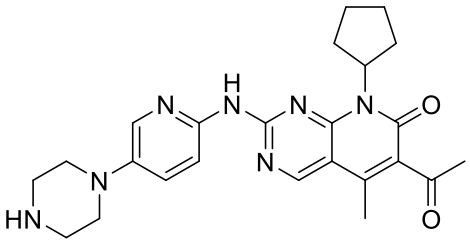

Palbociclib

Figure 1.3. Structures of CDK inhibitors Flavopiridol and Palbociclib.

1.2.3 Apoptosis Modulators and Current Drugs

Alongside angiogenesis and cell cycle modulators, apoptotic cell death is an attractive pathway for anti-cancer drug discovery.[15] Apoptosis is caused by chronological activation of protease enzymes caspases via two distinct but congregating signalling pathways – the intrinsic and extrinsic pathways.[71, 72] The intrinsic pathway, also known as mitochondrial pathway, is mainly controlled by Bcl-2 protein family.[72] A study has established that Bcl-2 protein family determines the survival of cells and increased level of anti-apoptotic proteins are responsible for the progression of various cancers.[73] Oblimersen sodium is an 18-base antisense phosphorothioate oligonucleotide that binds to Bcl-2 mRNA to downregulate the expression of Bcl-2.[21, 74, 75] According to several clinical trials, Oblimersen sodium is the most promising inhibitor of anti-apoptotic Bcl-2 protein for lymphoma.[76] In addition, its effectiveness as combination therapy has been evaluated in numerous clinical settings for other types of cancers such as multiple myeloma and small-cell lung cancer.[77, 78]

Histone deacetylases (HDACs) are an important class of enzymes involved in tumorigenesis. HDACs enzymatic activity involves the removal of an acetyl group from histones, and over-expression of HDACs has been observed during critical events of tumorigenesis.[79-81] A genetic knock-down of HDAC-1, -2, -3, and -6 resulted in an induced apoptosis and cell cycle arrest in different cancer types, suggesting that HDAC activity is a critical marker for survival and tumorigenic capacity.[82] A range of HDAC inhibitors have been discovered to be anti-cancer agents targeting cell apoptosis.[21] Among them, Vorinostat, Romidepsin, and Belinostat have been approved by the FDA for the treatment of refractory cutaneous T-cell lymphoma or peripheral T-cell lymphoma (Figure 1.4).[83-85]

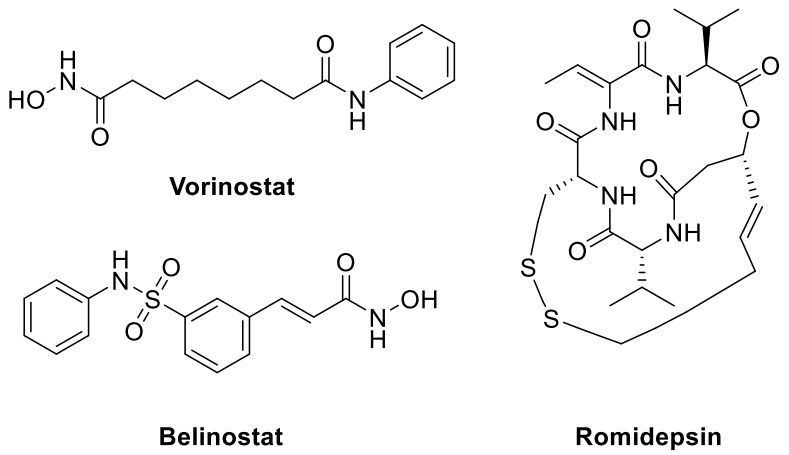

Figure 1.4. Structures of selected HDAC inhibitors.

1.3 Aminopeptidase N

Aminopeptidase N (APN/CD13; EC 3.4.11.2) is a member of M1 aminopeptidase superfamily of enzymes (protease clan MA) that catalyse the cleavage of amino acids from the N-terminus of polypeptide substrates.[86] APN is a ubiquitous transmembrane ectoenzyme that can be found in various cell types including renal, intestinal, fibroblast, endothelial and tumour cells.[87, 88] APN displays an identical gene sequence to the human lymphocyte surface cluster of differentiation CD13 antigen, therefore APN is also called as CD13.[89-91] The enzyme is involved in various biological responses with different roles.[92] Many peptides including Angiotensin III and IV, neuropeptides and chemokines are processed by APN.[93-95] In addition, APN acts as a signalling molecule for cell adhesion and endocytosis and is also a receptor for coronavirus.[92, 96, 97]

APN is one of the most studied metalloaminopeptidases associated with cancer.[86] A strong correlation between the level of APN expression of a cell and its invasive characteristics has been established through multiple studies.[98] Dysregulation of APN has been found to evolve in almost all types of human malignancies.[90] Over-expression of APN has been observed in small cell lung carcinoma,[99] thyroid carcinoma,[100] acute myeloid leukaemia,[101] colon carcinoma[102] and prostate carcinoma.[103] Selective expression of APN was also found on the surface of angiogenic blood vessels that are mostly absent in normal blood vessels.[104, 105] In addition, APN activity affects metastasis, which contributes to more than 90% of cancer related deaths, by promoting cell adhesion, cell motility, angiogenesis and ECM degradation.[106, 107, 108]

1.4 Multi-functionality of APN

1.4.1 Enzymatic Activity of APN

APN is described as a "moonlighting" enzyme due to its multi-functional roles: an enzyme to cleave peptide substrates, a receptor, and a signalling molecule (Figure 1.5).[92] The proteolytic activity of APN involves the removal of N-terminal amino acids from unsubstituted oligopeptides, amide, or arylamide.[109] APN has a broad substrate specificity from hydrophobic to basic amino acid residues, and the order of favoured substrates is: Ala>Phe>Tyr>Leu>Arg>Thr>Trp>Lys>Ser>Asp>His>Val.[109, 110] The most well-known enzymatic function of APN is hydrolysis of the N-terminal Arg residue of Angiotensin III to produce Angiotensin IV as a part of renin-angiotensin system to control blood pressure.[92, 111]

APN is also responsible for the inactivation of the neuropeptide hormones, endorphins and enkephalins.[112, 113] Other peptides or proteins such as tuftsin, kinins, hemorphins, chemokines, and ECM proteins are also substrates of APN.[108, 112, 114-116]

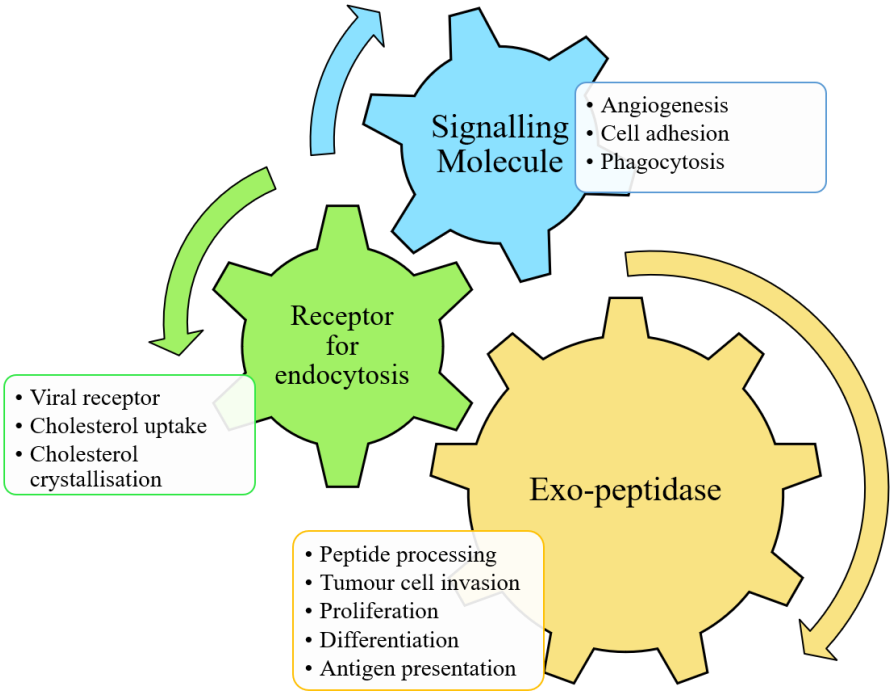

Figure 1.5. Various biological roles of APN as enzyme, receptor, and signalling molecule.

1.4.2 APN is a Cell Surface Receptor

One of the intensively investigated functions of APN is its role as a viral receptor in various species.[92] Mammalian APN has been reported to behave as the cell entry receptor for canine enteric coronavirus (CCoV), feline enteric coronavirus (FCoV), porcine transmissible gastroenteritis virus (TGEV), porcine deltacoronavirus (PDCoV), and human respiratory coronavirus 229E (HCoV229E).[97, 117-121] CoV recognition of APN was known to be species specific which was associated with N-linked glycosylations in APN.[122] Reguera *et al*. disclosed crystal structures of the receptor-binding domains of TGEV and porcine respiratory CoV (PRCV) bound to porcine APN (*p*APN) or neutralising antibodies.[123] The results indicated that these CoVs attached to the cell surface of APN for entry into host cells, and the potent TGEV neutralising antibodies 6AC3 mAb was able to prevent infection.[123] In addition, more recent research by Santiago *et al*. demonstrated the significance of APN dynamics in its activities as a receptor and an enzyme.[124] The crystal structures of human and porcine APN were obtained

as closed, intermediate and open conformations which represented characteristic functional states.[124] The studies also revealed that CoVs specifically recognised the open conformation and the allosteric binding of virus proteins prevented conformational change to the closed state, which consequently disrupted enzymatic activity of APN.[124]

Furthermore, APN has been known to involve in cholesterol absoprtion.[125] The mechanism of how Ezetimibe, an inhibitor of cholesterol intestinal absorption, was not understood until Kramer *et al*. found out that Ezetimibe analogues specifically bound to APN.[125, 126] The results also proposed that the cellular trafficking of APN between plasma membrane and intracellular compartments were disturbed by Ezetimibe.[125]

1.4.3 APN is a Signalling Molecule

Another role of APN unrelated to its enzymatic activity could be explained as a signalling molecule involved in signalling transduction cascades. [107] A series of research using APN mAbs by Santos *et al*. demonstrated that APN increased the calcium ion release to activate monocytes either by phosphorylating tyrosine kinases such as mitogen-activated protein kinase (MAPK), or by activating inositol triphosphate receptor coupled calcium ion channels.[127] It was hypothesised that the signalling transduction of APN was likely to involve other auxiliary proteins due to its short cytoplasmic domain that does not possess any signalling sequences.[92, 127, 128] Later studies identified a number of proteins that were associated with APN in signalling transduction and they included galectin-3, galectin-4, and reversion-inducing cysteine-rich protein with kazal motifs and tumour-associated antigen L6.[107, 129-131] Biological processes involving the signalling function of APN include angiogenesis, cell adhesion, and phagocytosis.[92, 107, 132, 133]

1.5 APN as a Therapeutic Target for Cancer

APN has been intensively studied as a therapeutic target for a variety of diseases including auto-immune diseases of the central nervous system (CNS), inflammatory bowel diseases, collagen vascular diseases, systemic sclerosis, rheumatoid arthritis, and infective viral diseases.[98, 134-137] However, the most heavily researched area is focussed on developing APN inhibitors for the treatment of various cancers.[98] Numerous *in vitro* and *in vivo* experiments have proven that APN contributes to angiogenesis, tumour growth, and metastasis, suggesting that it is an attractive therapeutic target for various cancers.[90]

1.5.1 Role of APN in Angiogenesis

Angiogenesis is the formation of new blood vessels from pre-existing vasculature.[105, 138] In normal cells, the process stays transient, but in tumour cells angiogenesis is persistent.[105, 139] *In vivo* studies by Pasqualini *et al*. demonstrated that APN is responsible for increasing the level of angiogenesis.[104] An asparagine-glycine-arginine (NGR) motif was discovered during *in vitro* screenings using phage-display libraries to identify non-arginine-glycine-aspartic acid (RGD) integrin binding motifs.[140-142] The NGR peptides was shown to bind strictly to the endothelium of angiogenic blood vessels.[143] Further studies discovered that an APN isoform that is expressed in angiogenic blood vessels acts as a vascular receptor, rather than an enzyme for the NGR motif.[104] Due to specific binding to APN, the NGR motif is considered as a homing device for targeted drug delivery, and it has been conjugated with anti-cancer agents in clinical studies.[140] In a Phase I study, human tumour necrosis factor integrated NGR (NGR-*h*TNF) in combination with cisplatin displayed anti-tumour activity with a favourable toxicity profile.[144] NGR-*h*TNF is currently in Phase II clinical trials for further evaluation in combination with standard chemotherapy for metastatic colorectal cancer.[145]

A study by Bhagwat *et al*. showed that APN aminopeptidase activity is an important regulator of endothelial morphogenesis during angiogenesis.[146] Up-regulation of APN levels in primary endothelial cells and cell lines were observed in response to hypoxia, angiogenic growth factors (bFGF, VEGF, TNFα and IGF-1) and signals regulating capillary tube formation.[146] In addition, treating HUVECs on Matrigel with APN inhibitors bestatin or amastatin, or with mAb MY7 that interferes APN activity resulted in disrupted capillary tube formation.[146] However, the proliferation of primary vascular endothelial cells was not affected by APN inhibitors, indicating that APN is important in controlling endothelial cell morphogenesis.[146]

1.5.2 Role of APN in Tumour Growth

The level of APN expression in both tumour and host cells was found to affect tumour growth.[147] Rangel and colleagues generated APN-null mice, which displayed impaired neovascularisation in response to hypoxia or growth factor.[148] Subsequent studies by Guzman-Rojas *et al.* investigated the role of APN in tumour growth by injecting B16F10 melanoma cells expressing control-shRNA and APN-shRNA into wild-type and APN-null mice.[147] Post injection analysis indicated that the wild-type mice that received APN-positive cancer cells developed an enlarged tumour.[147] In contrast, a reduction in tumour weight and volume were observed in APN-null mice.[148] Tumours generated from APN-shRNA cells showed a notable reduction in the tumour growth in wild-type mice.[148] The most remarkable inhibition of tumorigenesis was found when APN-shRNA cells were injected into APN-null mice, which showed almost negligible growth after two weeks of administration.[148] These results indicated the importance of the level of APN expression in both tumour cells and host cells.

1.5.3 Role of APN in Metastasis

Metastasis is a complex multistep process of cell migration, cell invasion, and angiogenesis, and it is the major cause of cancer related deaths worldwide.[106, 149-151] Multiple studies have shown that APN enzymatic activity is involved in ECM degradation, an essential step for metastasis.[108, 152, 153] Yoneda and co-workers demonstrated that bestatin inhibits tumour cell invasion and aminopeptidase activity of both murine and human metastatic cells.[152] *In vitro* studies conducted by Saiki *et al*. showed that APN is responsible for an increased level of tumour metastasis by facilitating ECM degradation.[108] Later, Liang *et al.* determined the correlation between enzymatic and signalling functions of APN in osteosarcoma invasion.[153] Their studies indicated that APN plays an imperative role in modulating the signalling pathway by the activation of MAPK, phosphoinositide 3-kinases (PI3K) and transcription factor NF-κB.[153] The activation of MAPK/PI3K signalling cascade triggers MMP-2 and MMP-9 to promote migration and invasion (Figure 1.6).[153]

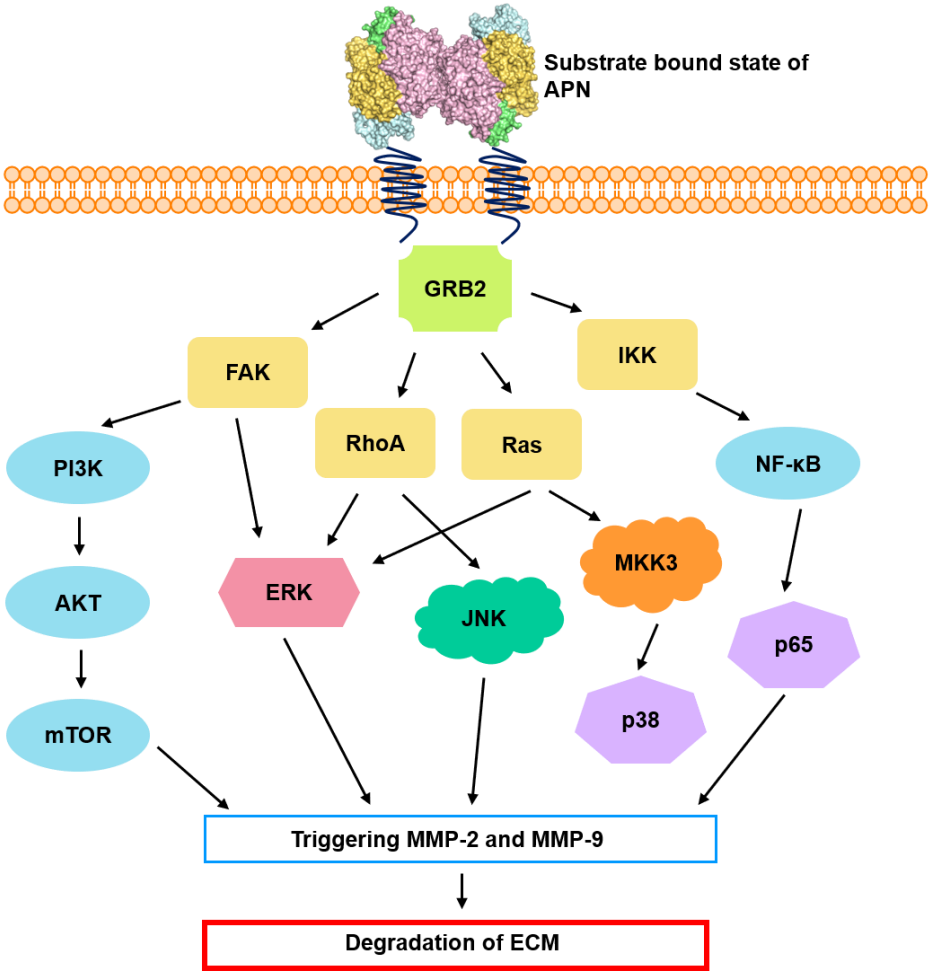

Figure 1.6. Proposed signalling pathways of substrate-bound APN to achieve degradation of ECM. Adapted from Liang *et al*.[153]

1.6 Structure of APN

1.6.1 M1 Aminopeptidase Superfamily

The M1 aminopeptidases superfamily are zinc-dependent enzymes that can be found in all kingdoms of life except viruses.[110] The M1 metallo-exopeptidases can exist as monomers and/or dimers, and can be membrane-bound, surface-exposed, or cytosolic.[92, 154, 155] Generally, M1 aminopeptidases consist of a short tail from the transmembrane anchor and a large ectodomain which contains relatively conserved three of four domains.[156] Sequence comparison and site-directed mutagenesis have demonstrated that most M1 aminopeptidases family members possess identical zinc coordination and mechanism of action to

thermolysin.[157-159] In addition, domain II of M1 metalloaminopeptidases is known as a catalytic domain where the two important consensus zinc binding motif $HEXXHX_{18}E$ and substrate-recognising motif GXMEN are found.[110, 156, 160, 161]

1.6.2 Crystal Structure of APN

APN is a zinc dependent aminopeptidase consisting of 967 amino acids with a relative molecular mass of ~110 kDa.[110] As a member of the M1 aminopeptidase superfamily, APN shares many structural similarities with other M1 metalloaminopeptidases. Figure 1.7 shows the structure of APN consisting of seven domains characteristic of M1 family proteins.[110]

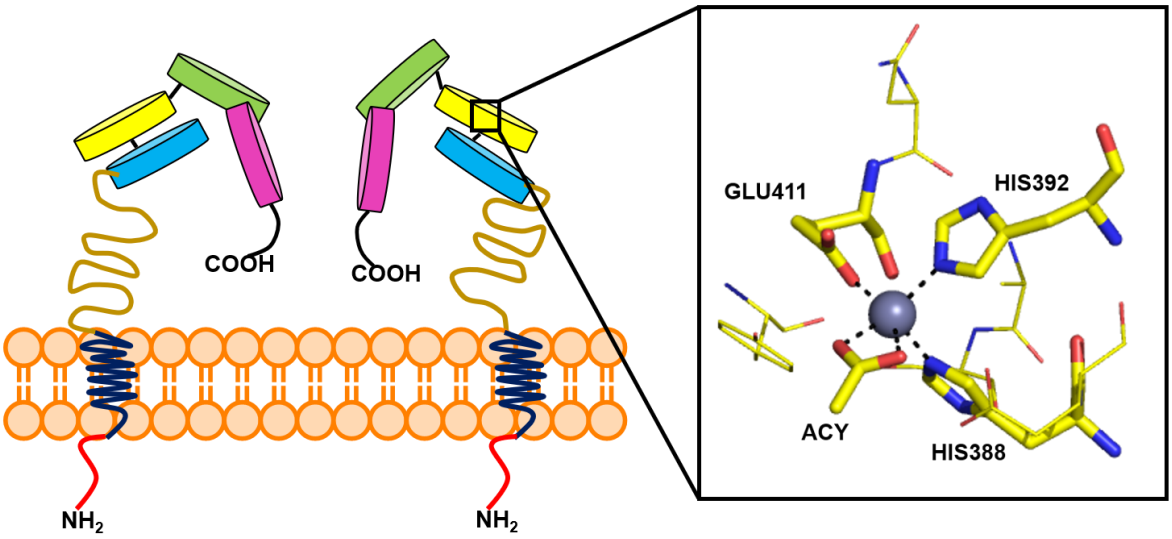

Figure 1.7. Schematic illustration of APN dimer structure and the zinc coordination in the native state of APN. Proposed structure of the seven domains of APN are illustrated in a dimer formation on the left. The key zinc binding residues and acetate from crystallisation buffer are shown as yellow sticks on the right. The catalytic zinc is the grey sphere. Interactions between the zinc and residues are shown as black dashed lines (PDB ID 4FYQ).[110]

APN is comprised of cytoplasmic domain (residues 1-9, red), transmembrane segment (residues 10-32, navy), and the serine/threonine-rich stalk (residues 33-65, brown).[110] The ecto-domain(s) of APN structure continues with domain I (residues 66-287, blue) and domain II (residues 288-549, yellow).[110] Domain II also referred to as the catalytic domain and is where the enzymatic activity occurs, and the catalytic zinc metal, consensus $^{388}HEXXHX_{18}E^{411}$ and $^{352}GXMEN^{356}$ motifs are found.[110] Wong *et al*. also disclosed that the catalytic zinc of unbound APN state forms a pentahedral complex with His^{388}, His^{392}, Glu^{411}, and acetate oxygen atoms

from crystallisation buffer (Figure 1.7).[110] Domain III (residues 549-636, green), adopts a β-sandwich fold and lastly, domain IV (residues 637-967, magenta) assumes a six α-helical superhelix appearance, and it is responsible for creating the dimeric interface through hydrophobic interactions and salt-bridge network.[110] Structures of APN complexed with peptidomimetic inhibitors such as bestatin and amastatin, and as well as its endogenous substrate angiotensin IV have also been reported.[110]

A dimer arrangement of M1 aminopeptidases is rare in lower order species that to date have only been identified as functional monomers.[156, 161-166] Interestingly, APN is typically reported as a dimeric ectoenzyme with a short N-terminal cytoplasmic domain and large cellular ectodomain containing the active site, although a soluble form of monomeric APN has also been identified in the blood.[110, 138, 156, 167, 168] The crystal structure of APN revealed the dimeric arrangement of the enzyme (Figure 1.8) where two monomers of APN are connected by non-covalent interactions, including hydrogen bonding and salt-bridge interactions at domain IV.[110]

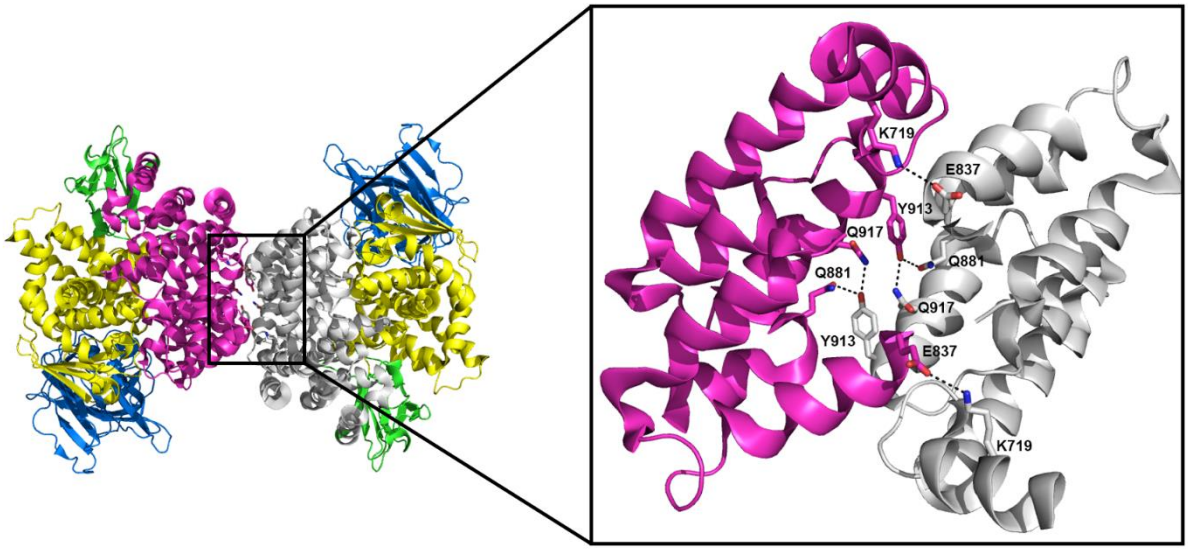

Figure 1.8. Structure of *h*APN dimer. Highlighted are the four domains; domain I (blue), II (yellow), III (green), IV (magenta, grey). Domain IV of each monomer and key residues involved in the dimeric interaction are shown in magenta and grey. Interactions between the key residues are illustrated as black dashed lines (PDB ID 4FYQ).[110]

Functional reasons for the dimer formation of APN have been proposed by Chen *et al*.[156] Firstly, cell-surface ectoenzymes encounter harsher environments than intracellular enzymes, therefore, dimerisation may be essential for stability.[156] Secondly, the M1 aminopeptidase family enzymes undergo a large conformational change, from a closed or open conformation as part of their proteolytic activity, and the dimer formation may provide flexibility to facilitate conformational changes of APN.[156]

1.6.3 APN's Catalytic Mechanism

APN has a relatively broad specificity towards N-terminal amino acids of peptide substrates.[110, 156] The catalytic mechanism by which APN can cleave an N-terminal amino acid is thought to be similar to that of thermolysin where an activated water molecule attacks the scissile bond of peptide substrates.[169, 170] By performing site-directed mutagenesis, Luciani *et al*. proposed the mechanism of substrate hydrolysis and revealed the significance of Glu^{355} in stabilising the transition state of the enzyme (Figure 1.9).[170] The zinc ion is coordinated to three amino acid residues (His^{338}, His^{392}, Glu^{411}) and a water molecule. Upon binding of a peptide substrate, the water molecule is displaced to Glu^{389}. The carbonyl oxygen of the scissile bond and the free amino group of the peptide substrate are near the zinc ion, forming a hexa-coordinated zinc complex (Figure 1.9A). The water molecule is polarised by Glu^{389} which enhances its nucleophilicity. In addition, the carbonyl carbon of the scissile bond becomes more electrophilic due to the coordination of the carbonyl oxygen to the zinc ion. The water molecule attacks the carbonyl carbon, while the zinc metal loses a bond with the free α-amino group, which creates additional hydrogen bonds with Glu^{355} (Figure 1.9B). In this transition state, the zinc ion forms a penta-coordinated complex and the peptide bond carbon has a tetrahedral geometry. A proton is transferred from Glu^{389} to the nitrogen atom (Figure 1.9C), then the terminal amino acid is cleaved, followed by a second proton transfer (Figure 1.9D).

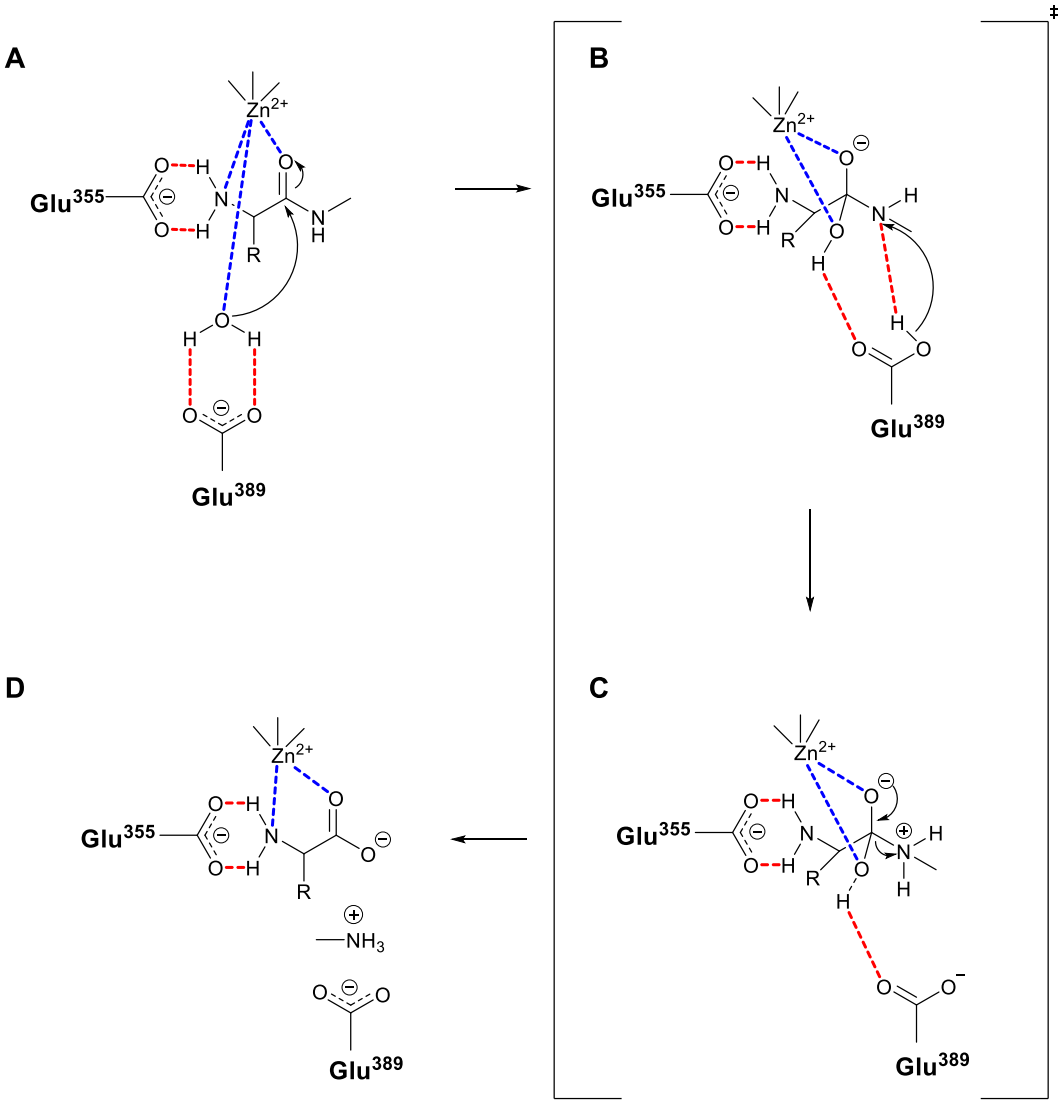

Figure 1.9. APN mechanism of action. Coordination of the zinc ion is shown in blue dashed lines. Hydrogen bonds between the water molecule, substrate and residues are shown in red dashed lines. Curly arrows indicate the mechanism of chemical reactions occurring. Adapted from Luciani *et al.*[170]

1.7 Current Inhibitors of APN

Since abundant scientific evidence has proposed APN as a potential therapeutic target for cancer, a wide range of APN inhibitors have been discovered and evaluated for their anti-cancer activity. Current inhibitors of APN have been extensively reviewed in a number of literatures.[90, 98, 171-173] Despite the tremendous effort to develop drug candidates for the treatment of cancer, neither the European Medicines Agency (EMA) nor the FDA has approved any APN inhibitor in an anti-cancer treatment setting.[86] The main reasons for developed APN inhibitors to fail in earlier stages of research include low efficacy, poor selectivity and unfavourable physicochemical properties. There are ongoing clinical trials to assess the efficacy of two APN inhibitors: the natural inhibitor, bestatin and a synthetic inhibitor Tosedostat.

1.7.1 Natural Inhibitors

1.7.1.1 Bestatin

One of the most studied and widely used APN inhibitors is bestatin (also known as Ubenimex, Figure 1.10).[150, 174] Bestatin is a natural dipeptide originally isolated from *Streptomyces olivoreticuli*.[175] This dipeptide analogue was initially used as an immuno-modulating agent by inhibiting aminopeptidase B (inhibition constant (K_i) = 6 μM) and leucine aminopeptidase (LAP, K_i = 9 nM).[176-178] Bestatin was later found to inhibit APN with a K_i value of 3.03 μM and exhibited anti-tumour activity.[171, 178] Bestatin showed therapeutic activity against acute myeloid leukaemia and lung cancer in clinical trials, and it is available in Japan as an adjuvant therapy for acute non-lymphatic leukaemia.[177, 179-181] A randomised study of bestatin in patients with non-small cell lung cancer demonstrated that bestatin significantly improved survival rates.[182] Another randomised, double-blind placebo controlled clinical study on patients with completely resected stage I squamous cell lung carcinoma demonstrated improved five-year cancer-free survival.[179] However, combination therapy with bestatin for inoperable primary lung cancer patients did not show a statistically significant difference compared to the control group.[183] Adjuvant treatment with other anti-cancer drugs for resectable gastric cancer patients showed positive results for a restricted subgroup of stage III + IV patients.[184]

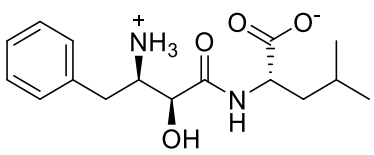

Figure 1.10. Structure of bestatin at physiological pH.

Bestatin inhibits APN by binding in the catalytic site and competing with natural substrates.[178] Scornik *et al.* and Rich *et al*. found that bestatin binds slowly at a low concentration resulting in a delayed inhibition of APN.[178, 185] The crystal structure of bestatin bound to APN showed that bestatin has novel binding pose compared to all of the other available M1 aminopeptidase - bestatin complexes.[110, 154] The most significant difference was observed from the zinc chelation. In APN, the terminal carboxylic acid of bestatin coordinated to the zinc, whereas in other M1 aminopeptidases, the backbone hydroxy ketone of bestatin formed a complex with the zinc (Figure 1.11).[110, 154] APN is unable to hydrolyse bestatin because of the unique α-hydroxy-β-amino acid group.[110] Figure 1.11A illustrates the interactions that APN makes with bestatin where its carboxylate group coordinates to the catalytic zinc.[110] A number of direct and water-mediated interactions between Ser^{895} and Asp^{189}, Leu^{190}, Asp^{216}, and Gln^{213} residues are formed. On the other hand, when bestatin is bound to porcine APN, the zinc forms a complex with the backbone hydroxy ketone and the key zinc binding residues (Figure 1.11B).[156]

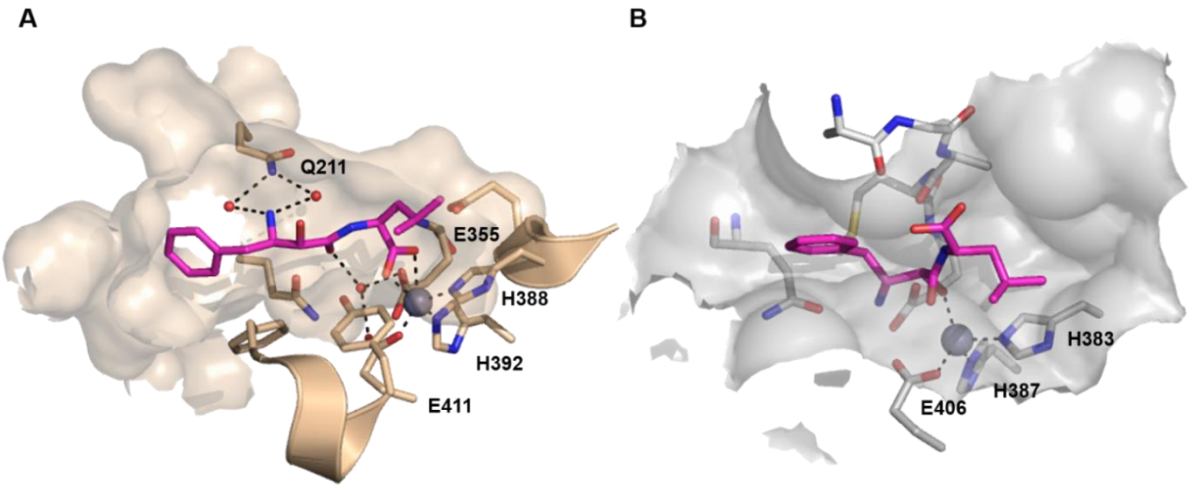

Figure 1.11. Crystal structures of bestatin bound to APN (A) and *p*APN (B). Interactions between bestatin and enzymes are shown in black dashed lines. Bestatin is illustrated as a magenta stick. Key residues of APN and porcine APN are shown in wheat and grey, respectively. (PDB ID 4FYR and 4FYS).[110]

1.7.1.2 Other Natural APN Inhibitors

Besides bestatin, several other natural APN inhibitors have been identified. Figure 1.8 shows some examples of natural APN inhibitors including amastatin, curcumin, probestin, psammaplin A, actinonin and betulinic acid (Figure 1.12).

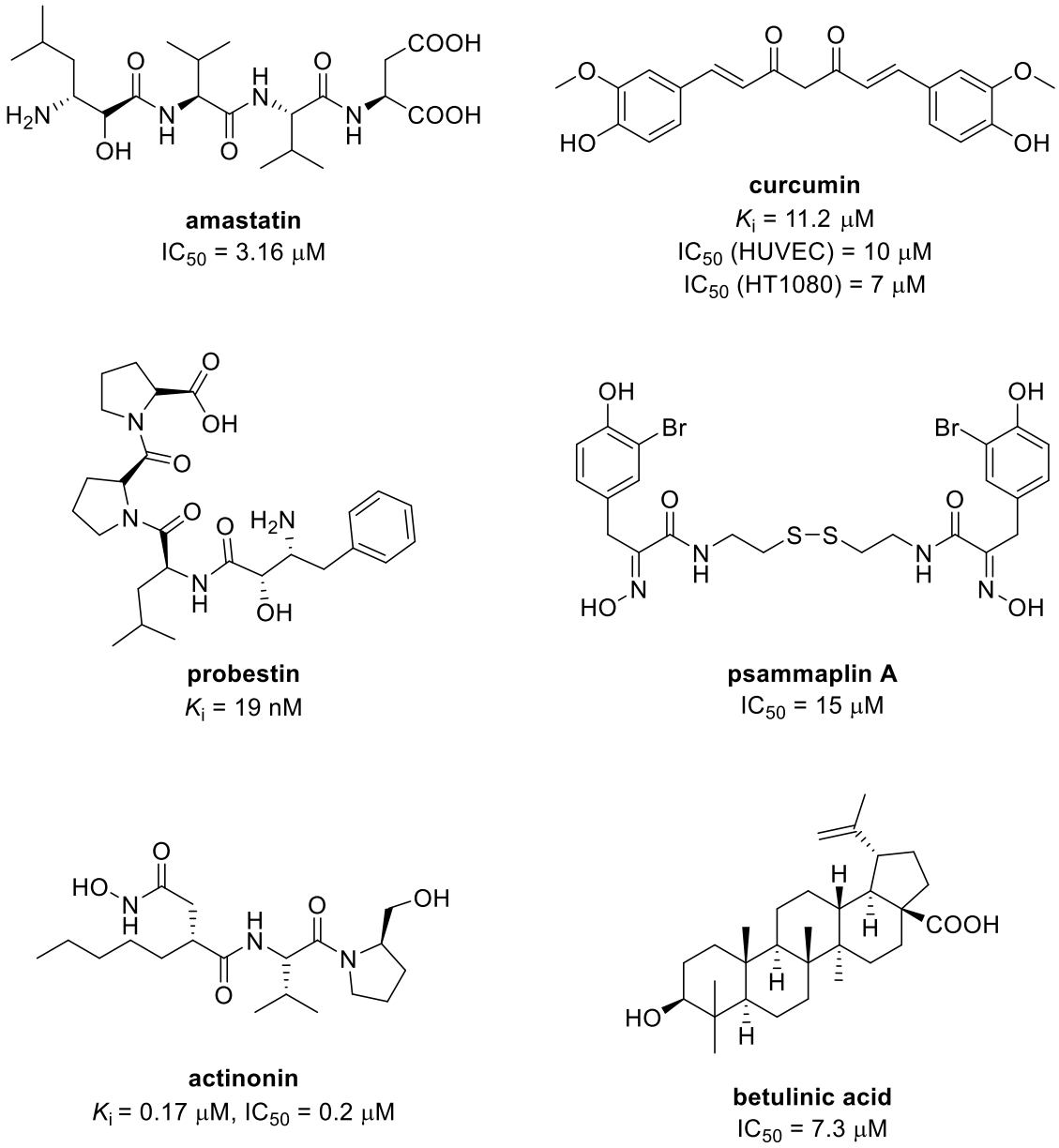

Figure 1.12. Structures of selected natural APN inhibitors.

Amastatin was first isolated in 1978 from *Streptomyces sp*. ME98-83 as an aminopeptidase A inhibitor.[186] Similar to bestatin, amastatin is a slow-binding competitive inhibitor of APN.[185] *In vitro* fluorometric assays in the presence of L-Ala-4-methyl-1-coumarylamide as the competitive substrate confirmed that amastatin possessed weak inhibition activity against

porcine APN with an IC_{50} value of 3.16 μM.[187] The X-ray structure of human APN bound to amastatin was revealed by Wong *et al.* which showed that amastatin has similar non-canonical binding conformation to bestatin where the α-hydroxy-β-amino group coordinating with the zinc ion to inhibit APN activity.[110, 185]

Probestin is a tetrapeptide compound discovered from a program designed to find microorganism-produced inhibitors of APN from *Streptomyces azureus* MH663-2F6.[188] Aoyagi *et al*. performed an absorbance enzyme assay with L-Leu β-naphthylamide as substrate, and pobestin inhibited APN with a K_i value of 19 nM.[188]

Actinonin is a natural hydroxamic acid compound which was first isolated from a Malayan strain of *Actynomycetes* as an antibiotic.[189, 190] Screening the inhibitory activities of actinonin against various aminopeptidases including leucine aminopeptidase, aminopeptidase A and aminopeptidase B revealed that it was a selective APN inhibitor (K_i = 0.17 μM, IC_{50} = 0.2 μM).[187, 191] Subsequent studies by Xu *et al*. indicated that actinonin showed anti-tumour activity against both APN-positive (HL60) and APN-negative (RAJI) leukaemic cell lines.[192] Moreover, actinonin induced G_1 arrest and apoptosis in human leukaemic and lymphoma cells.[192]

Curcumin is a natural product isolated from rhizomes of Asian perennial herbs and the most well-known representative is *Curcuma longa L.*[171] Fluorometric *in vitro* high throughput screenings showed that curcumin was an irreversible APN inhibitor with K_i value of 11.2 μM.[193] It was also revealed that curcumin possessed APN inhibition activity *in vivo* against human umbilical vein endothelial cells (HUVECs) and fibrosarcoma HT1080 cells IC_{50} values of 10 μM and 7 μM, respectively.[193] Curcumin has been recognised as a potential therapeutic anti-cancer agents due to its capacity to suppress tumour progression, and to induce S and G_2/M phase arrest and apoptosis.[194, 195] Moreover, curcumin has been extensively studied in innumerable clinical settings to determine its efficacy against a wide range of diseases including cancers, inflammatory diseases and diabetes.[196] However, curcumin exhibited limited efficacy in clinical trials due to poor absorption, rapid metabolism and systemic elimination, which consequently led to limited bioavailability.[196, 197]

Psammaplin A was first isolated from three different research groups in 1987 from unidentified species of marine sponge, *Psammaplysilla sp.*, and *Thorectopsamma xana*.[198-200] This phenolic natural product was found to inhibit APN in a non-competitive manner with a K_i value of 15

μM and also suppressed angiogenesis *in vitro*.[201] In addition, psammaplin A was cytotoxic against various cancer cell lines.[202, 203]

Betulinic acid is a pentacyclic that can be found from various vegetal species, and one of the major source of betulinic acid is bark of several species of plants.[171] *In vitro* studies conducted by Melzig *et al.* measured the inhibitory activity of betulinic acid against APN spectrophotometrically, which was IC_{50} value of 7.3 μM.[204] Moreover, compelling evidence supported that betulinic acid inhibited angiogenesis, metastasis, cell growth, and tumour invasion, however the mechanism of action proposed was largely related to signalling transductions instead of APN activity.[205-207]

1.7.2 Synthetic Inhibitors

Despite the discovery of a number of natural products, most of them could not be pursued further due to various reasons such as low efficacy, poor bioavailability, proteolytic lability, rapid excretion, and short duration of action. Therefore, many research groups focussed on developing a broad range of small molecule APN inhibitors with diverse chemotypes to overcome these problems. Several synthetic APN inhibitors, including Tosedostat, cyclic imides, 3-amino-2-tetralones, 3-amino-2-hydroxypriopionaldehydes, 3-amino-1-hydroxypropan-2-ones, flavone-8-acetic acids, chloramphenicol amines, boronic acid derivatives, and phosphonic and phosphinic acids are introduced in the following sections.

1.7.2.1 Tosedostat

The APN inhibitor Tosedostat (CHR2797) is an orally bioavailable hydrophobic prodrug that is converted to the pharmacologically active drug (CHR79888) inside cells.[208] CHR79888 is a potent inhibitor of multiple intracellular aminopeptidases and also displays anti-proliferative activity against a range of cancer cell lines *in vitro* and *in vivo*.[208] In addition, Tosedostat displayed 300-fold improved anti-proliferative activity against leukaemic cell lines compared to that of bestatin and favourable cytotoxic profile with myeloma cells.[209, 210] Extensive phase I and II clinical trials of Tosedostat were conducted for the treatment of actue myeliod leukaemia, pancreatic cancer, and non-squamous non small cell lung cancer.[98, 208, 211] In addition, Tosedostat demonstrated significant anti-leukemic activity in elderly or relapsing patients with acute myeloid leukaemia.[212]

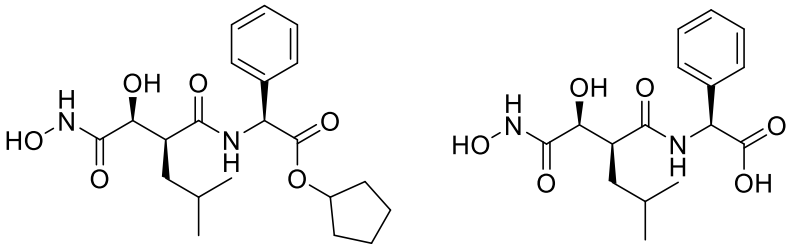

CHR2797 CHR79888

Figure 1.13. Structure of CHR2797 and CHR79888.

1.7.2.2 Cyclic imides

Cyclic imides scaffolds were first introduced as novel non-peptide APN inhibitors by Miyachi *et al.*[213] Inhibition activity of the novel cyclic imides against APN and dipeptidyl peptidase IV (DPP-IV) were measured by intact-cell assays using human acute lymphoblastic leukaemia cells.[213] The selective inhibition of two *N*-phenylhomophthalimide analogues towards APN was confirmed (Figure 1.14A).[213]

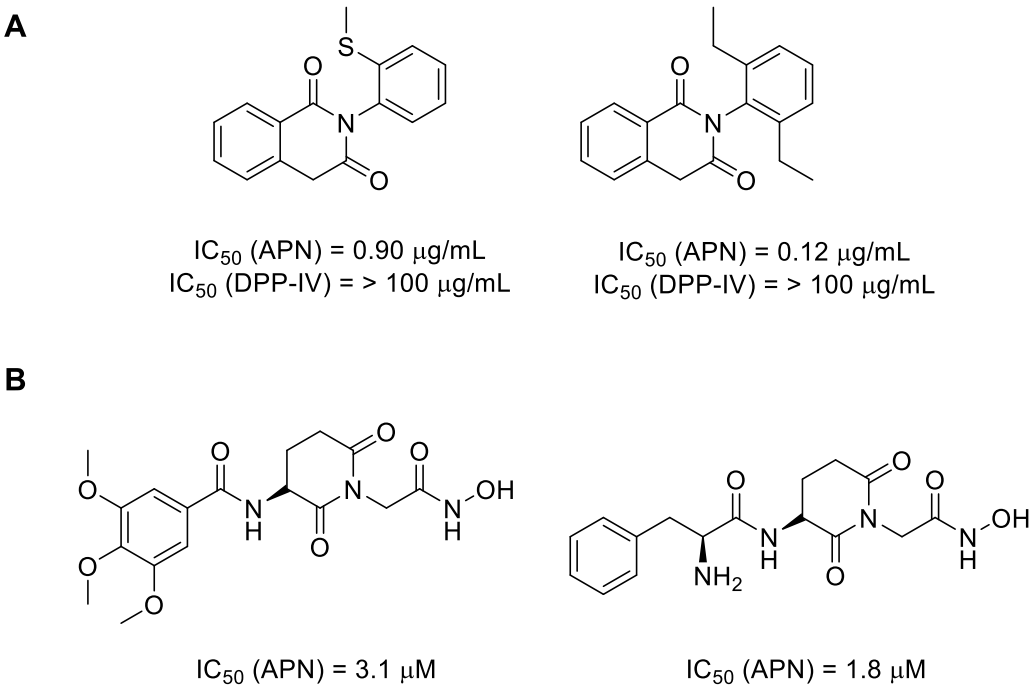

Figure 1.14. Structures of cyclic imide APN inhibitors containing (A) *N*-phenylhomophthalimide and (B) hydroxamic acid.

Later, Li *et al*. employed cyclic imide scaffold to improve selectivity between APN and MMPs of L-iso-glutamate derivatives by adding conformational constraints into molecules.[214] In their studies a hydroxamic acid bearing compound displayed potent activity with a IC_{50} value of 3.1 µM, and the potency was further improved to IC_{50} = 1.8 µM by replacing the trimethoxyphenyl with benzyl group (Figure 1.14B).[214] This compound also showed significant inhibition in the growth and migration of ovarian cancer cell line ES-2 and hepatocellular cancer cell line HuH-7.[215, 216]

1.7.2.3 3-Amino-2-tetralones

3-Amino-2-tetralone derivatives were first reported as competitive zinc dependent aminopeptidases inhibitors by Schalk *et al*.[217] *In vitro* studies of the compounds synthesised revealed two compounds that were very selective toward APN compared to aminopeptidase A and aminopeptidase B.[217] It was proposed that the aminotetralone moiety would act as a bidentate ligand to interact with the catalytic zinc ion in the active site.[218] In addition, Albrecht and co-workers synthesised aminobenzosuberone analogues to improve the stability profile of aminotetralones.[219] Aminobenzosuberone showed the best potency of K_i = 1000 nM against porcine APN and this compound was further pursued by Maiereanu *et al*. to synthesise extremely potent and selective APN inhibitor biphenyl aminobenzosuberone which showed a K_i value of 0.06 nM.[219, 220] Despite its excellent potency and selectivity, biphenyl aminobenzosuberone could not be pursued further to *in vivo* studies due to undesirable physicochemical and *in vitro* pharmacokinetic properties.[221]

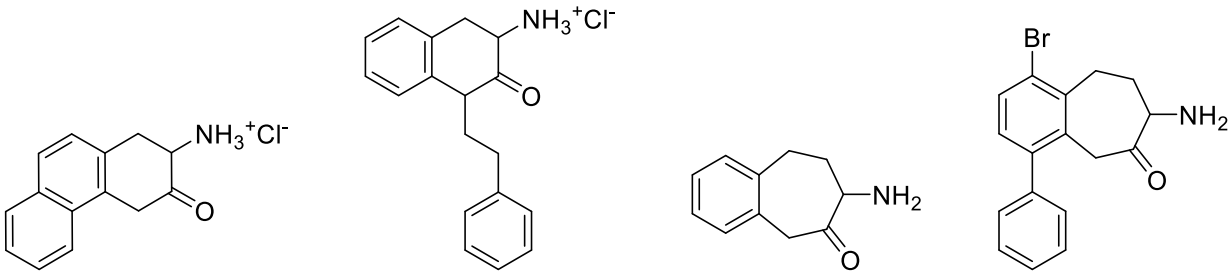

K_i(pAPN) = 0.02 µM K_i(pAPN) = 0.08 µM K_i(pAPN) = 1000 nM K_i(pAPN) = 0.06 nM

Figure 1.15. Structures of 3-amino-2-tetralone APN inhibitors

1.7.2.4 Flavone-8-acetic acid

Flavone-8-acetic acid derivatives have been first synthesised in 1985 and studied as a treatment for various solid tumours.[173, 222] Bauvois *et al.* reported that among a series of novel flavone acetic acid synthesised, 2′,3-dinitroflavone-9-acetic acid (Figure 1.16) was the most potent reversible APN inhibitor with a IC_{50} value of 25 μM.[223] The flavone compound was not cytotoxic to cultured human cells U937 and did not induce apoptosis.[223] Moreover, the compound was inactive on other various proteases such as MMPs, angiotensin converting enzyme, and DPP-IV.[223]

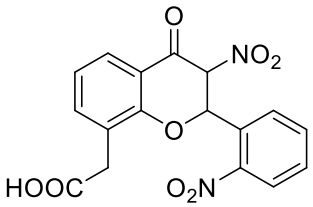

IC_{50} = 25 μM

Figure 1.16. Structure of a flavone-8-acetic acid APN inhibitor.

1.7.2.5 Chloramphenicol amines

Yang and co-workers generated a series of chloramphenicol amine derivatives (Figure 1.17), and the (2S,3R)-2-amino-3-hydroxy-3-(4-nitrophenyl)propanoic acid (AHNPA) dipeptide derivative was the most potent APN inhibitor with a IC_{50} value of 7.1 μM.[224] Inspired by the previous work, Jia *et al*. investigated the effect of modifying chloramphenicol amine to (1S,2S)-2,3-diamino-1-(4-nitrophenyl)propan-1-ol (DANP) scaffold on APN inhibition activity.[225] Most of these compounds exhibited moderate selectivity over MMP-2. Aniline chloroamphenicol compound (Figure 1.17, right) was the most potent inhibitor against APN (IC_{50} = 6.1 μM) and leukaemic cell line HL-60 (IC_{50} = 1.64 μM).

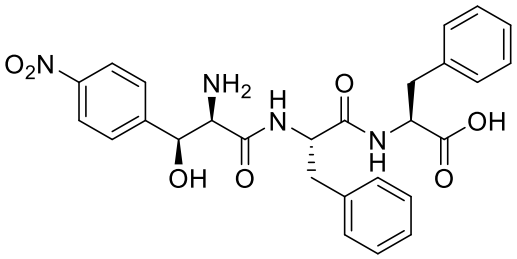

IC_{50} = 7.1 μM

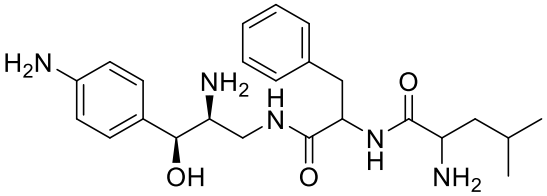

IC_{50} = 6.1 μM

Figure 1.17. Structures of chloramphenicol amine APN inhibitors

1.7.2.6 Boronic acid derivatives

Aliphatic boronic acid derivatives have been proposed to act as transition-state analogues by forming tetrahedral boronate ion to inhibit APN activity.[226] Shenvi *et al*. synthesised *α*-aminoboronic acid derivatives, which showed inhibitory activity against APN in the nanomolar range.[227] In addition, these boronic acids also showed time-dependent inhibition against cytosolic and microsomal leucine aminopeptidases.[227]

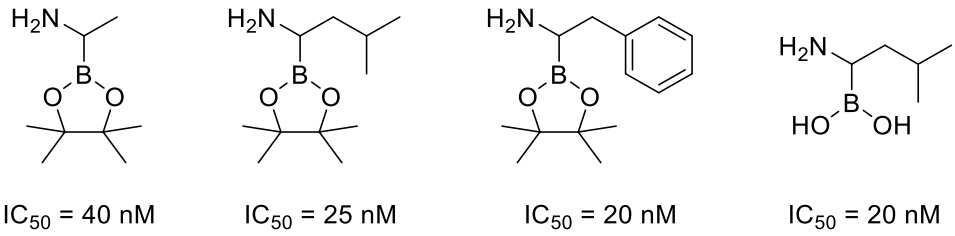

Figure 1.18. **Structures of boronic acid derivative APN inhibitors.**

1.7.2.7 Phosphonic and phosphinic acid derivatives

Due to the tetrahedral shape of the phosphonate or phosphinate groups, phosphonic acids served as ZBGs.[98] Lejczak and colleagues, who were inspired by the earlier studies on phosphorous amino acids and dipeptide analogues affecting aminopeptidase activity, synthesised aminophosphonate derivatives which showed inhibitory activity against cytosolic and microsomal aminopeptidases.[228] Cyclohexyl aminophosphonate compound (Figure 1.19, left) was the most potent inhibitor of the series of analogues with a K_i value of 870 nM.[228] Chen *et al*. designed new phosphino peptides as transition state analogues that had potential to interact with the S1, S1′, and S2′ subsite of APN, and two compounds showed significant inhibitory activities and selectivity towards APN over other aminopeptidases (Figure 1.19).[229]

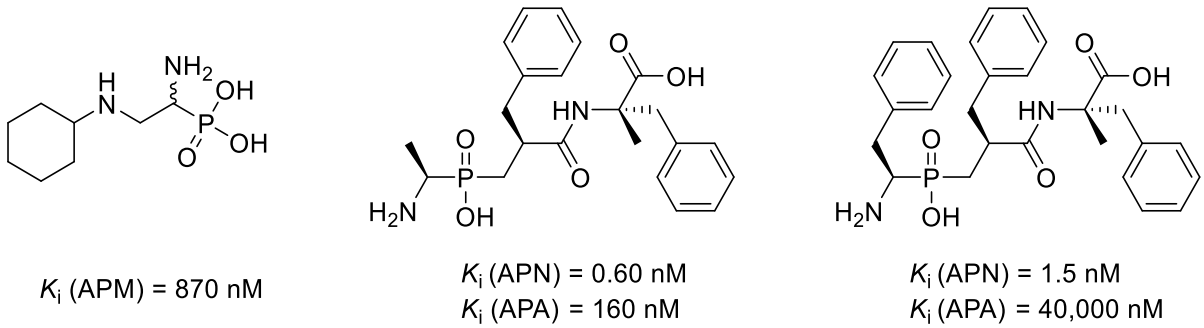

Figure 1.19. Structures of phosphonic acid derivatives as APN inhibitors.

1.8 Previous Work: Repurposing an anti-malarial agent as a novel APN inhibitor

Previous work by our group generated a series of dual inhibitors of the *Plasmodium falciparum* aminopeptidases *Pf*A-M1 and *Pf*A-M17 that show anti-parasitic activity.[230-232] *Pf*A-M1 is an M1 metalloaminopeptidase from *P falciparum*, and it is the parasitic homologue of APN, while *Pf*A-M17 is also a metalloaminopeptidase from the unrelated M17 superfamily (protease clan MF).[161, 233] One of our compounds, *N*-(2-(hydroxyamino)-2-oxo-1-(3',4',5'-trifluoro-[1,1'-biphenyl]-4-yl)ethyl)pivalamide (**1**) (Figure 1.20), was a potent inhibitor of both *Pf*A-M1 and *Pf*A-M17 in the nanomolar range.

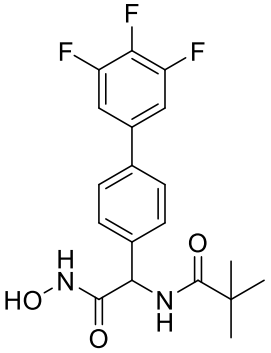

Figure. 1.20 Structure of *Pf*A-M1 and *Pf*A-M17 dual inhibitor 1.

Interestingly, **1** displayed a stronger inhibitory activity to the *Pf*A-M1 than bestatin ($K_i^{(app)}$ = 331 nM, Table 1.1). Preliminary *in vitro* studies showed that **1** ($K_i^{(app)}$ = 118 nM) exhibited more potent inhibition of APN activity compared to other APN inhibitors bestatin ($K_i^{(app)}$ = 2370 nM) and Tosedostat ($K_i^{(app)}$ = 1180 nM). Therefore, we decided to repurpose **1** as a novel APN inhibitor.

Table 1.1. Inhibition activities of bestatin, Tosedostat, and compound **1** against APN and *Pf*A-M1.

Compound	$K_i^{(app)}$(APN) ± SEM (nM)	$K_i^{(app)}$(*Pf*A-M1) ± SEM (nM)
Bestatin	2370 ± 350	1530 ± 58
Tosedostat	1180 ± 8	6150 ± 275
1	118 ± 3	331 ± 12

Please note that compound **1** and all other synthesised inhibitors that are discussed in the following chapters were evaluated for the inhibitory activities against APN as racemic mixtures. Resolutions of racemates by diastereomeric salt formation and chiral HPLC were attempted, but this proved to be challenging and only afforded small amounts of compounds, which was insufficient to progress. For the efficient progress of this project, all inhibitors were initially evaluated as racemates, and the resolution can be addressed in the future using chiral reagents in parallel with optimisation of the cellular activity and *in vivo* PK profile.

The ability of **1** to inhibit both enzymes can be explained by their common mechanism of action and the conserved features of the active site of the enzymes. Both APN and *Pf*A-M1 contain the consensus HEXXHXE zinc binding motif and GXMEN substrate recognising motif in the catalytic domain.[110, 161] The co-crystal structure of **1** bound to *Pf*A-M1 (PDB ID 4ZX4) and molecular modelling of **1** into the crystal structure of APN (PDB ID 4FYQ) are shown in Figure 1.21.

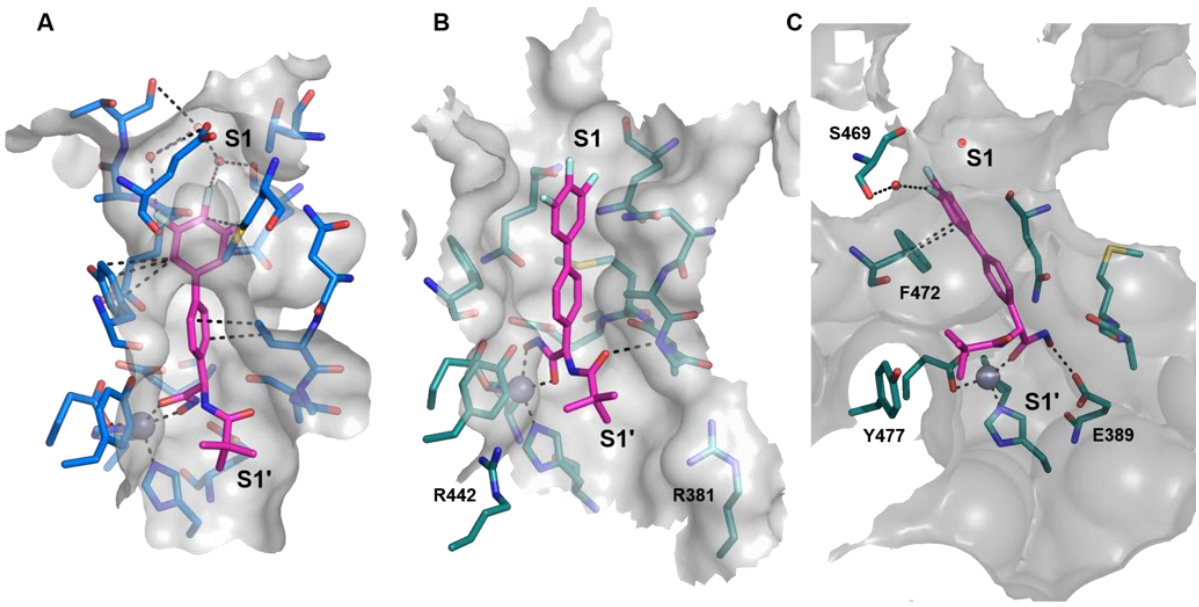

Figure 1.21. (A) X-ray crystal structure of **1** bound to *Pf*A-M1 (PDB ID 4ZX4). (B) A predicted binding pose of **1** bound to APN obtained from docking (PDB ID 4FYQ). (C) MD simulation of **1** docked to APN. The ligand is shown in magenta and residues of *Pf*A-M1 and APN are coloured in blue and dark green, respectively. Interactions between the ligand and proteins are depicted as black dashed lines. The zinc is represented by the grey sphere.

Chelation of the hydroxamic acid to the catalytic zinc ion was observed in both *Pf*A-M1 and APN. In *Pf*A-M1, compound **1** formed water-mediated hydrogen bonding interactions with nearby backbone residues where fluorines act as acceptors.[230] Val[459] and Tyr[575] residues provided key edge π-π hydrophobic interactions to the biaryl system of **1** (Figure 1.21A).[230] According to the predicted binding pose of **1** in APN, the 3,4,5-trifluorophenyl ring was positioned deep into the S1 pocket, and the *N*-pivaloyl group occupied the S1′ subsite of APN (Figure 1.21B). Charged residues Arg[381] and Arg[442] located in the extended region of S1′ pocket of APN was also observed. Further molecular dynamic (MD) simulations of the docked pose of **1** into APN indicated that the 3,4,5-trifluorophenyl ring engaged in interactions with a single water molecule and largely maintained face-face stacking interactions with relatively rigid Phe[472] at the S1 pocket of APN (Figure 1.21C). In addition, the pivaloyl group was facing the aromatic side chain of Tyr[477] residue. Based on the computational modelling studies, it was therefore hypothesised that compounds that are capable of improved interactions in the S1′ subsite, as well as extend further to engage residues beyond the S1' pocket of APN might contribute to improved inhibitory activity toward APN (Figure 1.21C).

As a part of my Honours project, a total of 11 hydroxamic acid analogues with various S1′ anchors were synthesised (Figure 1.22). The *N*-pivaloyl group of **1** was replaced with a longer alkyl chain with carboxylate and its derivatives (compound **3**-**6**) to reach Arg[381] or Arg[442] residues. Aromatic linkers containing hydrogen bond donors and acceptors (compound **7**-**12**) were also introduced to attract additional hydrophobic interactions with Tyr[477] residue at the S1′ pocket. Studies on the structure-activity relationships (SAR) concluded that the substituted aromatic compounds were more favoured than alkyl compounds. Among the series of compounds, the 3-fluoro-4-hydroxy compound **11** showed the strongest potency with a $K_i^{(app)}$ value of 29.1 nM, which was 82-fold and 4-fold improved activity compared to bestatin and compound **1**, respectively.

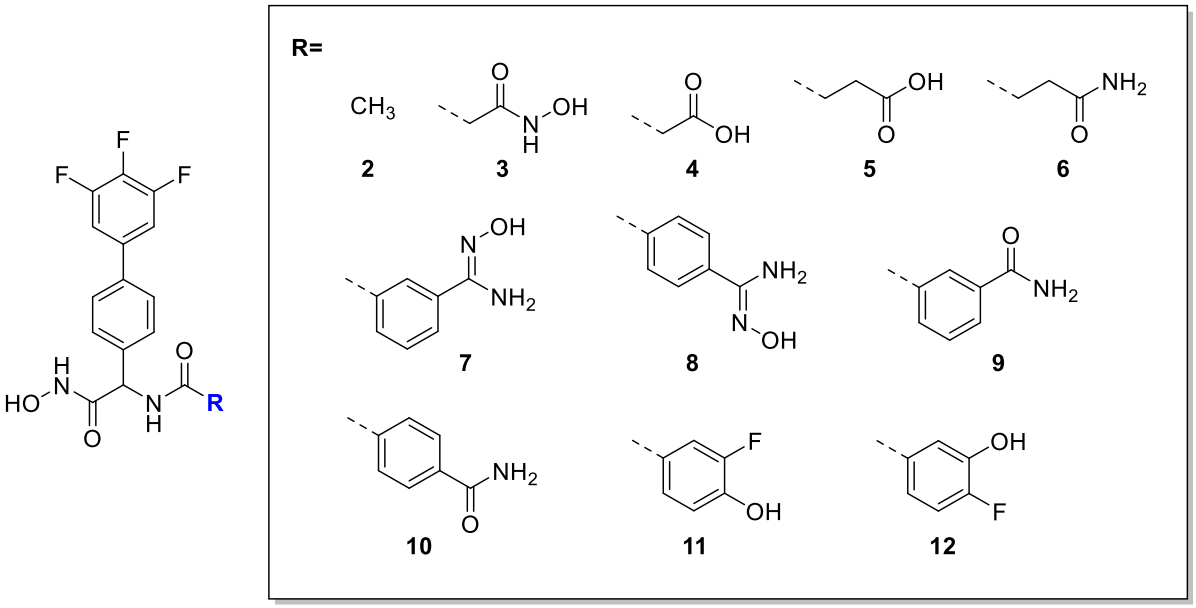

Figure 1.22. Hydroxamic acid APN inhibitors synthesised previously.

1.9 Project Aims

Continuing from previous work, this project aims to synthesise diverse sets of hydroxamic acid analogues to improve inhibitory activity toward APN, and hence develop novel lead candidate(s) for the treatment of cancer. The project proposes to achieve this aim in three different perspectives (Figure 1.23). Firstly, aromatic compounds containing more variety of hydrogen bonding groups will be synthesised to probe and optimise the binding interactions at the S1′ pocket of APN further, and build comprehensive structure-activity relationships. Appropriate molecular modelling, using the structures of compounds bound to the related *Pf*A-M1, may be able to guide the design of novel APN inhibitors for optimal binding to APN.

The second part of the project involves replacement of the 3,4,5-trifluorophenyl ring of the lead compound **1**, which was optimised for the S1 pocket of *Pf*A-M1. We aim to investigate the effect of modifications in the 3,4,5-trifluorophenyl group on the inhibitory activity at the S1 pocket of APN. In addition, earlier studies on compound **1** indicated that the compound possesses moderate aqueous solubility.[230] In order to improve solubility, the 3,4,5-trifluorophenyl ring can be modified to more hydrophilic aromatic or alkyl groups through various synthetic chemistry approaches. The hydrophobicity of synthesised compounds will be compared to that of compound **1**, and structure-activity relationships will be discussed in-depth.

Lastly, the project proposes to expand the chemical space being investigated around the central aromatic group of compound **1**. The central aromatic ring was identified to be engaging in significant hydrophobic interactions in *Pf*A-M1.[230] Modifications to the central aromatic ring may result in substantial structural changes to the core biphenyl system. Installation of heteroaromatic or acetylene groups will allow us to gain insights on how the structural changes in the core biphenyl moiety affect APN activity.

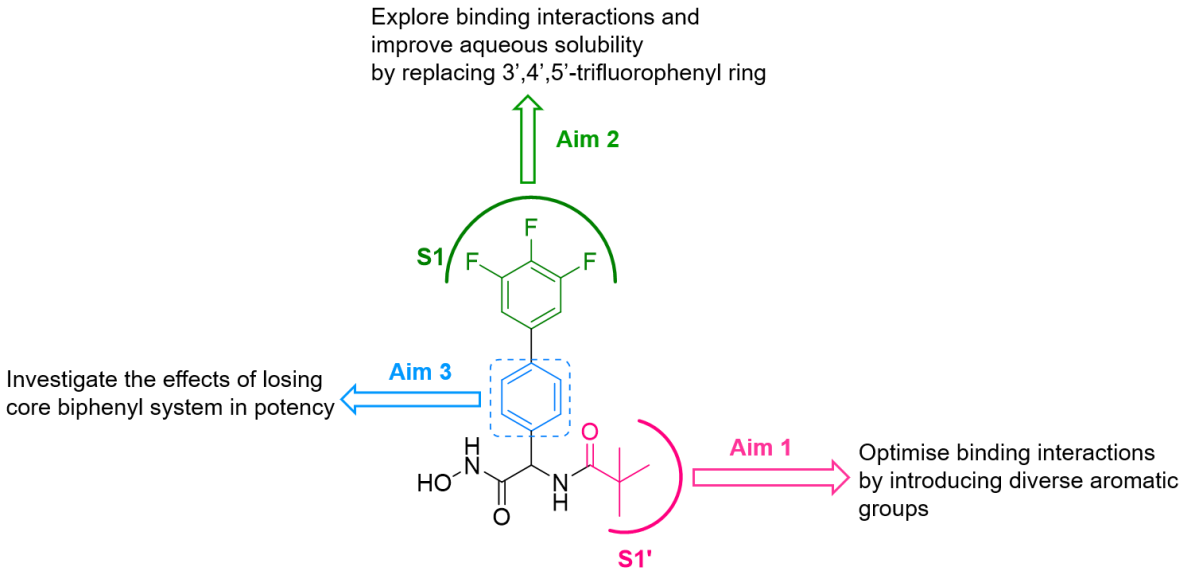

Figure 1.23. Schematic representation of proposed aims.

The biological activity of the synthesised compounds will be evaluated using a variety of assays. Target based activity will be assessed via *in vitro* fluorescence enzymatic assay to determine the inhibitory activity of compounds against the aminopeptidase activity of APN. Molecular modelling studies will be performed to investigate the interactions between selected compounds and APN. In collaboration with the National Cancer Institute (NCI), anti-proliferative activities of potent APN inhibitors will also be measured using high-content imaging in cell viability assays across 60 different cancer cell lines. The hydroxamic acid moiety in the molecules has a strong chelating property that may allow the inhibitors to interact with other metalloaminopeptidases.[234] Thus, selectivity studies against metal-dependent enzymes such as MMPs will be completed to investigate potential off-target effects of selective inhibitors. Lastly, the preliminary absorption, disposition, metabolism, excretion and toxicity (ADMET) will be assessed in collaboration with the Monash Centre for Drug Candidate Optimisation (CDCO).

Chapter 2: Design and Synthesis of Novel APN Inhibitors to Optimise Binding Interactions at the Subsites of APN

2.1 Introduction

Previous research to repurpose the anti-parasitic agent **1**, a potent *Pf*A-M1 inhibitor, as a novel APN inhibitor generated a series of 11 hydroxamic analogues. The *N*-pivaloyl group of compound **1** was replaced with various carboxylic acid derivative alkyl linkers and substituted aromatic linkers to achieve optimal binding interactions, and hence improve the inhibitory activity against APN. From this study, the potency of synthesised APN inhibitors was improved significantly compared to the lead compound **1**. With the promising results obtained, this project firstly aimed to further probe the binding interactions within the active site of APN.

The design, synthesis, pharmacology, and computational modelling works involved in developing series of novel APN inhibitors are described in this chapter which is presented as a journal article: Lee *et al*. Novel Human Aminopeptidase N Inhibitors: Discovery and Optimization of Subsite Binding Interactions. *J. Med. Chem.*, **2019**, *published asap online*, (DOI: 10.1021/acs.jmedchem.9b00757).

2.2 Journal Article

Journal of Medicinal Chemistry

Article

Cite This: J. Med. Chem. XXXX, XXX, XXX−XXX

pubs.acs.org/jmc

Novel Human Aminopeptidase N Inhibitors: Discovery and Optimization of Subsite Binding Interactions

Jisook Lee,[†] Natalie B. Vinh,[†] Nyssa Drinkwater,[§] Wei Yang,[§] Komagal Kannan Sivaraman,[§] Luke S. Schembri,[†] Michelle Gazdik,[†] Peter M. Grin,[∥,#] Georgina S. Butler,[∥,⊥,#] Christopher M. Overall,[∥,⊥,#] Susan A. Charman,[‡] Sheena McGowan,*[,§] and Peter J. Scammells*[,†]

[†]Medicinal Chemistry, Monash Institute of Pharmaceutical Sciences and [‡]Centre for Drug Candidate Optimisation, Monash Institute of Pharmaceutical Sciences, Monash University, Parkville Campus, Parkville, VIC 3052, Australia

[§]Infection and Immunity Program, Biomedicine Discovery Institute and Department of Microbiology, Monash University, Clayton Campus, Clayton, VIC 3800, Australia

[∥]Department of Biochemistry & Molecular Biology, [⊥]Department of Oral Biological & Medical Sciences, and [#]Centre for Blood Research, Life Sciences Institute, University of British Columbia, Vancouver, British Columbia V6T 1Z3, Canada

Supporting Information

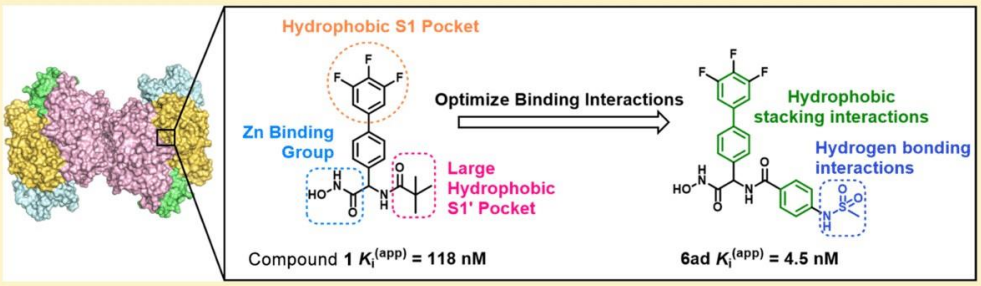

ABSTRACT: Aminopeptidase N (APN/CD13) is a zinc-dependent M1 aminopeptidase that contributes to cancer progression by promoting angiogenesis, metastasis, and tumor invasion. We have previously identified hydroxamic acid-containing analogues that are potent inhibitors of the APN homologue from the malarial parasite *Plasmodium falciparum* M1 aminopeptidase (*Pf*A-M1). Herein, we describe the rationale that underpins the repurposing of *Pf*A-M1 inhibitors as novel APN inhibitors. A series of novel hydroxamic acid analogues were developed using a structure-based design approach and evaluated their inhibition activities against APN. *N*-(2-(Hydroxyamino)-2-oxo-1-(3′,4′,5′-trifluoro-[1,1′-biphenyl]-4-yl)ethyl)-4-(methylsulfonamido)benzamide (**6ad**) proved to be an extremely potent inhibitor of APN activity in vitro, selective against other zinc-dependent enzymes such as matrix metalloproteases, and possessed limited cytotoxicity against Ad293 cells and favorable physicochemical and metabolic stability properties. The combined results indicate that compound **6ad** may be a useful lead for the development of anticancer agents.

■ INTRODUCTION

Aminopeptidase N (APN/CD13; EC 3.4.11.2) is a ubiquitous transmembrane ectoenzyme that is widely present in different types of cells, including renal, intestinal, fibroblast, endothelial, and tumor cells.[1,2] APN is described as a "moonlighting" enzyme due to its multifunctional roles: an enzyme to cleave peptide substrates, a receptor, and a signaling molecule.[3] The enzyme cleaves hydrophobic and basic amino acid residues from the N-terminus of polypeptides with broad substrate specificity.[4] For example, APN catalyzes the metabolism of angiotensin III to generate angiotensin IV to regulate the renin−angiotensin system[5] and levels of neuropeptides such as enkephalins.[6,7] APN also acts as a viral receptor for mammalian coronavirus, and is a signaling molecule in phagocytosis, angiogenesis, and cell adhesion.[8−13]

APN is a member of the zinc-dependent M1 aminopeptidase superfamily of enzymes (protease clan MA) that can be found in all kingdoms of life except viruses.[4] M1 aminopeptidases are characterized by a thermolysin fold and two consensus sequence motifs: an $HEXXHX_{18}E$ zinc-binding motif and a GXMEN substrate-guiding motif.[4,14−16] Wong et al. reported the X-ray crystal structure of human APN, as well as the structures of APN bound to generic inhibitors bestatin and amastatin, and an endogeneous peptide substrate, Angiotensin IV.[4] Human APN consists of a short intracellular tail, a transmembrane anchor, a small serine-/threonine-rich extracellular stalk, and a large ectodomain, composed of four domains (I−IV) characteristic of M1 aminopeptidase super-

Received: May 8, 2019
Published: June 28, 2019

DOI: 10.1021/acs.jmedchem.9b00757
J. Med. Chem. XXXX, XXX, XXX−XXX

family.[4,14] The catalytic domain II contains the consensus motifs ^{352}GXMEN^{356} and ^{388}HEXXHX$_{18}$E^{411}, the latter of which includes the catalytic triad His^{388}, His^{392}, and Glu^{411} that coordinates the essential zinc ion.[4]

APN has been extensively studied due to its significant role in the regulation of metastasis and angiogenesis.[17] A significant body of evidence supports the rationale that APN is an effective therapeutic target for malignancies.[17−20] Dysregulated activity of APN has been found to develop into a wide spectrum of human malignancies.[21−27] Metastasis is a complex multistep process of cell migration, cell invasion, and angiogenesis, and it is the major cause of cancer-related deaths worldwide.[28−31] Multiple studies have shown that APN activity is involved in extracellular matrix (ECM) degradation, an essential step for metastasis, which was later determined to increase tumor cell migration and invasion by stimulating mitogen-activated protein kinases/phosphoinositide 3-kinase signaling cascade.[24,32,33] Thus, there is an ongoing interest to develop potent APN inhibitors as effective anticancer drug candidates.

A variety of APN inhibitors have been developed as potential anticancer candidates.[18,19,34,35] Among them, a natural peptidomimetic, bestatin, is the most widely studied competitive APN inhibitor. Originally isolated from *Streptomyces olivoreticuli* as an immunomodulating agent, bestatin was found to have antitumor activity[36,37] as well as clinical efficacy against acute myeloid leukemia and lung cancer in clinical trials.[38−41] Another APN inhibitor Tosedostat (CHR2797) is an orally bioavailable prodrug that is converted to a pharmacologically active drug (CHR79888) inside cells.[42] Tosedostat demonstrated significant antileukemic activity in phase II clinical trials in elderly or relapsing patients with acute myeloid leukemia.[43]

Previous work by our group generated a series of hydroxamic acid-containing compounds that were inhibitors of the *Plasmodium falciparum* M1 aminopeptidase, *Pf*A-M1.[44−46] We described *N*-(2-(hydroxyamino)-2-oxo-1-[3′,4′,5′-trifluoro(1,1′-biphenyl)-4-yl]ethyl)pivalamide (**1**) (Figure 1) as a potent inhibitor of *Pf*A-M1, exhibiting an

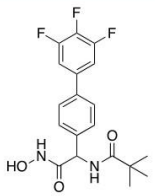

Figure 1. Structure of *N*-(2-(hydroxyamino)-2-oxo-1-[3′,4′,5′-trifluoro(1,1′-biphenyl)-4-yl]ethyl)pivalamide (**1**).

inhibitory constant ($K_i^{(app)}$) in the nanomolar range.[44] Here, we show that **1** is also active toward APN and is more potent than both bestatin and Tosedostat. We have repurposed compound **1** as a novel APN inhibitor and developed a new series of analogues with improved potency against APN through structure-based approaches.

RESULTS AND DISCUSSION

Compound 1 Can Inhibit Recombinant Human APN.

*Pf*A-M1 is a homologue of APN found in *P. falciparum*, which is one of the parasites that causes malaria. Being part of the same M1 aminopeptidase family, *Pf*A-M1 shares a number of structural similarities with APN, particularly within the catalytic domain II. Overall, *Pf*A-M1 and APN share 19% sequence identity (35% similarity); however, in the highly conserved catalytic domain II, this sequence identity increases to 24% (43% similarity). This conserved catalytic domain II adopts a thermolysin-like fold and in *Pf*A-M1, contains an H^{496}EYFHX$_{17}$KE^{519} zinc-binding motif as well as a G^{490}AMEN substrate-guiding motif.[16] The catalytic zinc in the active site is coordinated by a catalytic triad His^{496}, His^{500}, and Glu^{519} in the unbound state.[16] Therefore, we were interested to see how the potent *Pf*A-M1 inhibitor **1** would interact with human APN.

Our standard fluorescence-based aminopeptidase inhibition assay was used to measure the inhibitory activities of bestatin, Tosedostat, and **1** against human APN. This assay used recombinant human APN and a commercially available fluorophore 7-amino-4-methylcoumarin as the competitive substrate to determine an inhibitory constant ($K_i^{(app)}$). We compared the inhibitory activities of bestatin, Tosedostat, and **1** against human APN as well as *Pf*A-M1 (Table 1). Bestatin

Table 1. $K_i^{(app)}$ Comparison of Bestatin, Tosedostat, and Compound 1 against Human APN and *Pf*A-M1

compound	$K_i^{(app)}$(APN) ± SEM (nM)	$K_i^{(app)}$(*Pf*A-M1) ± SEM (nM)
bestatin	2370 ± 350	1530 ± 58
Tosedostat	1180 ± 8	6150 ± 275
1	118 ± 3	331 ± 12

showed a moderate loss in potency toward APN compared to *Pf*A-M1, whereas Tosedostat exhibited a 6-fold improved potency toward APN compared to *Pf*A-M1. Interestingly, compound **1** was significantly more potent than Tosedostat and bestatin, displaying a 10- to 20-fold increase in APN inhibition activity.

To understand the mechanism by which **1** was able to inhibit both APN and *Pf*A-M1, we investigated the interactions the compound made with the active site of the enzymes. To do this, we used the X-ray crystal structure of *Pf*A-M1 bound to compound **1** [Protein Data Bank (PDB) ID 4ZX4][44] as a scaffold to dock **1** into the active site of APN (PDB 4FYQ).[4] The catalytic domains of the two proteins share 24% sequence identity and have a root-mean-square deviation (RMSD) of only 1.244 Å (over 257 Cα atoms in domain II). The co-crystal structure of **1** bound to *Pf*A-M1 revealed extensive water-mediated interactions of the 3,4,5-trifluorophenyl ring with backbone residues located at the S1 substrate binding pocket, as well as key hydrophobic interactions with the biaryl system of **1** (Figure 2A).[44] Our docking analysis of **1** bound to APN showed a similar pose to that observed when bound to *Pf*A-M1 (Figure 2B). Each of the poses obtained from docking **1** were similar and showed the 3,4,5-trifluorophenyl ring in the same position, located deep within the S1 pocket of APN, and minor rotations of the position of the *N*-pivaloyl group were observed. In general, there were significantly less interactions observed between **1** and the active site residues of APN than that of *Pf*A-M1 (Figure 2B).

To evaluate any potential dynamics of **1** bound within the active site of APN as well as any effect from water-mediated interactions, we performed molecular dynamics (MD) simulations of **1** docked into APN. Molecular modeling for metallo-proteins presents significant challenges, and traditional force fields are often not appropriate for simulation.[47] In the case of APN, the presence of zinc in the active site means that

DOI: 10.1021/acs.jmedchem.9b00757
J. Med. Chem. XXXX, XXX, XXX−XXX

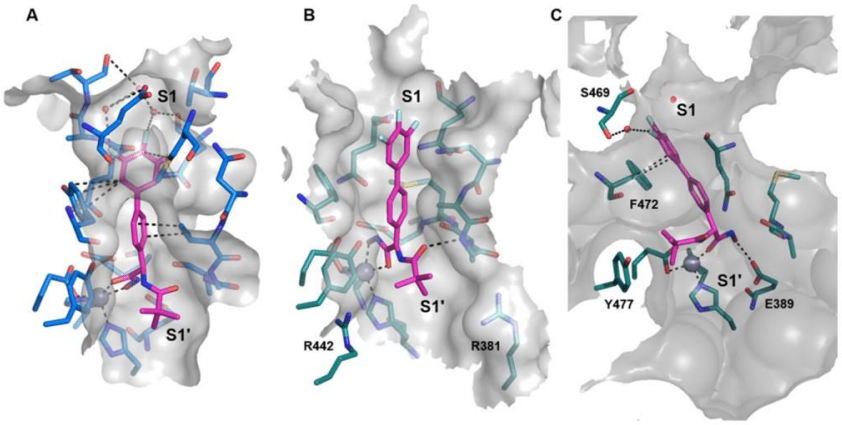

Figure 2. (A) X-ray crystal structure of **1** bound to *Pf*A-M1 (PDB ID 4ZX4). (B) Predicted binding pose of **1** bound to APN obtained from docking (PDB ID 4FYQ). (C) Molecular dynamics (MD) simulation of **1** docked to APN showed that the trifluorophenyl group formed stable interactions in the S1 pocket. The ligand is shown in magenta, and residues of *Pf*A-M1 and APN are colored in blue and dark green, respectively. Interactions between the ligand and proteins are depicted as black dashed lines. The zinc is represented by the gray sphere.

this problem cannot be computationally ignored. Recently, our team has produced the necessary parameters to use the zinc Amber force field (ZAFF) to simulate the active site of *Pf*A-M1.[48,49] We used this system to simulate our docking of APN bound to **1**. MD simulations (n = 3) were performed for the duration of 50 ns, which should be sufficient to observe the movements of small molecules. The results were surprising and showed that in two of the three MD runs, **1** experienced significant movement within the active site (Figure S2). Investigation into the motion of **1** indicated that the 3,4,5-trifluorophenyl ring engaged in interactions with a single water molecule and largely maintained face−face stacking interactions with relatively rigid Phe^{472} at the S1 pocket of APN (Figure 2C). In addition, the pivaloyl group was facing the aromatic side chain of Tyr^{477} residue. We hypothesized therefore that compounds that are capable of improved interactions in the S1′ subsite as well as extending further to engage residues beyond the S1′ pocket of APN may contribute to improved inhibitory activity toward APN. To this end, we turned our attention to residues Tyr^{477}, Arg^{381}, and Arg^{442} that are located within the S1′ and beyond the S1′ pocket of APN which may allow the formation of hydrophobic interactions as well as polar interactions with inhibitor compound(s).

Substitution of the *N*-Pivaloyl Group To Optimize Binding at the S1′ Subsite of APN. The molecular modeling revealed the potential to achieve enhanced binding interactions at, and beyond, the S1′ pocket of APN by replacing the *N*-pivaloyl group of **1** with aromatic groups that target the Tyr^{477} residue. We designed and produced a series of hydroxamic acid analogues that contained elongated alkyl and aryl linkers to reach deeper into the pocket (Figure 3). Various hydrogen-bonding groups were also incorporated to capture additional interactions with Arg^{381} or Arg^{442} residues and improve inhibition activities of the designed compounds. In addition, we were interested to investigate the effect of various heteroaromatic groups, such as indole and indoline. Analogues with benzyl linkers that contain an additional methylene group were also designed to increase flexibility and allow the phenyl group to penetrate more deeply beyond the S1′ pocket.

Chemistry. The synthesis of the key intermediate, the phenyl glycine derivative **4** (Scheme 1), was adapted from

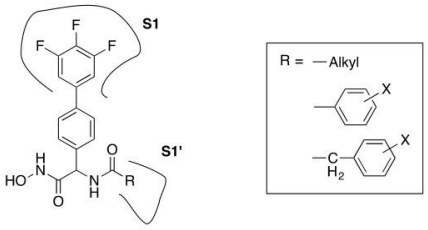

Figure 3. Structures of targeted hydroxamic acid analogues.

Mistry et al.[46] Installation of the 3,4,5-trifluorophenyl ring was successfully achieved using a Suzuki coupling reaction between 4′-bromoacetophenone and (3,4,5-trifluorophenyl)boronic acid under reported conditions producing acetophenone **2** in excellent yield (99%).[44] Oxidation of **2** with selenium dioxide in anhydrous pyridine[50] afforded the corresponding α-keto acid **3** in quantitative yield. The product produced from the reductive amination of **3** underwent an acid-catalyzed esterification and subsequent debenzylation to successfully afford key precursor **4** in 47% yield over three steps.

The key intermediate (**4**) was then used to incorporate a range of functionalities in place of the *N*-pivaloyl group present in **1**, which was predominately achieved with traditional peptide coupling reagents such as HCTU or EDCI. The first synthetic attempt to obtain benzamide analogues **5r** and **5s** involved the synthesis of their respective acid chlorides in situ and subsequent acylation with intermediate **4**. However, benzonitriles **5n** and **5o** were produced instead by dehydration of the carboxamide group. Ring-opening reactions of cyclic acid anhydrides were also performed to synthesize alkyl carboxylate analogues. Cyclic anhydrides such as succinic anhydride and Meldrum's acid have been commonly used in the literature to form amide bonds through ring-opening reactions.[51−59] The butyric acid analogue (**5e**) was synthesized from intermediate **4** via nucleophilic attack on the carbonyl π system present in succinic anhydride. Subsequent (benzotriazol-1-yloxy)tripyrrolidinophosphonium hexafluorophosphate (PyBOP) amide coupling of **5e** converted the acid moiety to the corresponding carboxamide **5f**. However,

DOI: 10.1021/acs.jmedchem.9b00757
J. Med. Chem. XXXX, XXX, XXX−XXX

Scheme 1. Synthesis of Hydroxamic Acid Inhibitors[a]

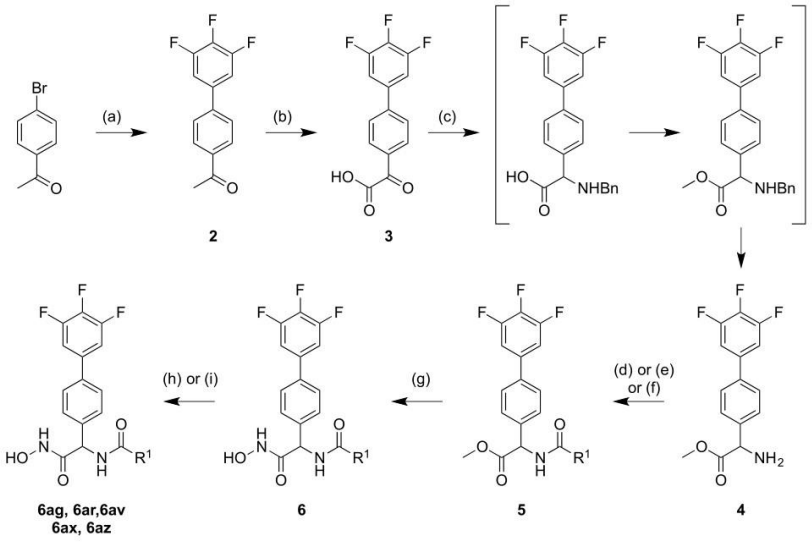

a	$-CH_3$	**r**	$-C_6H_4C(O)NH_2$ (*m*)	**aj**	-indol-5-yl
b	$-CH_2C(O)O^tBu$	**s**	$-C_6H_4C(O)NH_2$ (*p*)	**ak**	-indazol-5-yl
c	$-CH_2C(O)OH$ (**6c** from **5b**)	**t**	$-C_6H_4C(O)NHMe$ (*p*)	**al**	-benzotriazol-5-yl
d	$-CH_2C(O)NHOH$ (**6d** from **5b**)	**u**	$-C_6H_4C(O)NMe_2$ (*p*)	**am**	-benzimidazol-5-yl
e	$-CH_2CH_2C(O)OH$	**v**	$-C_6H_4C(O)NHEt$ (*p*)	**an**	-(2-oxoindolin-5-yl)
f	$-CH_2CH_2C(O)NH_2$	**w**	$-C_6H_4C(O)NH^iPr$ (*p*)		
		x	$-C_6H_4C(O)NHCH_2CH_2OH$ (*p*)	**ao**	$-CH_2C_6H_5$
g	$-C_6H_5$	**y**	$-C_6H_4SO_2NH_2$ (*p*)	**ap**	$-CH_2C_6H_4F$ (*m*)
h	$-C_6H_4F$ (*m*)	**z**	$-C_6H_4NHBoc$ (*m*)	**aq**	$-CH_2C_6H_4F$ (*p*)
i	$-C_6H_4F$ (*p*)	**aa**	$-C_6H_4NHBoc$ (*p*)	**ar**	$-CH_2C_6H_4OMe$ (*p*)
j	$-C_6H_4OMe$ (*m*)	**ab**	$-C_6H_4NH_2$ (*m*) (**6ab** from **5z**)	**as**	$-CH_2C_6H_4OH$ (*p*) (**6as** from **6ar**)
k	$-C_6H_4OMe$ (*p*)	**ac**	$-C_6H_4NH_2$ (*p*) (**6ac** from **5aa**)	**at**	$-CH_2C_6H_4C(O)NH_2$ (*p*)
l	$-C_6H_4OH$ (*m*) (**6l** from **6j**)	**ad**	$-C_6H_4NHSO_2Me$ (*p*)	**au**	$-CH_2C_6H_3$ (3,4-OMe)
m	$-C_6H_4OH$ (*p*) (**6m** from **6k**)	**ae**	$-C_6H_4NHSO_2NH_2$ (*p*)	**av**	$-CH_2C_6H_3$ (3,4-OH) (**6av** from **6au**)
n	$-C_6H_4CN$ (*m*)	**af**	$-C_6H_3$(3,4-OMe)	**aw**	$-CH_2C_6H_3$ (3-F,4-OMe)
o	$-C_6H_4CN$ (*p*)	**ag**	$-C_6H_3$ (3,4-OH) (**6ag** from **6af**)	**ax**	$-CH_2C_6H_3$ (3-F,4-OH) (**6ax** from **6aw**)
p	$-C_6H_4C(NHOH)NH_2$ (*m*) (**6p** from **5n**)	**ah**	$-C_6H_3$(3-F, 4-OH)	**ay**	$-CH_2C_6H_3$ (4-F,3-OMe)
q	$-C_6H_4C(NHOH)NH_2$ (*p*) (**6q** from **5o**)	**ai**	$-C_6H_3$(4-F, 3-OH)	**az**	$-CH_2C_6H_3$ (4-F,3-OH) (**6az** from **6ay**)

[a]Reagents and conditions: (a) 3,4,5-trifluorophenylboronic acid, $Pd(PPh_3)_2Cl_2$, 1 M Na_2CO_3, tetrahydrofuran (THF), reflux, 2 h; (b) SeO_2, anhyd. pyridine, reflux, 24 h; (c) (i) benzylamine, $Na(OAc)_3BH$, dichloroethane (DCE), room temperature (rt), 24 h; (ii) concd H_2SO_4, MeOH, reflux, 24 h; (iii) H_2, 10% Pd/C, cat. HCl MeOH, rt, 24 h; (d) (i) carbamoylbenzoic acid, $(COCl)_2$, dimethylformamide (DMF), dichloromethane (DCM), rt, 1 h; (ii) **4**, *N*,*N*-diisopropylethylamine (DIPEA), DCM, rt, 30 min; (e) carboxylic acid, *O*-(1*H*-6-chlorobenzotriazol-l-yl)-1,1,3,3-tetramethyluronium hexafluorophosphate (HCTU), DIPEA, DMF, DCM, rt, 24 h; (f) carboxylic acid, 1-ethyl-3-(3-dimethylaminopropyl)-carbodiimide (EDCI), 4-dimethylamonipyridine (DMAP), DCM, rt, 24 h; (g) $NH_2OH{\cdot}HCl$, 5 M KOH in anhyd. MeOH, rt; (h) 20% trifluoroacetyl (TFA) in DCM, rt; (i) 1 M BBr_3 in DCM, −78 °C to rt, 2−24 h.

reaction with Meldrum's acid under identical reaction conditions resulted in decarboxylation, generating the acetamide analogue (**5a**) instead of the expected propionic analogue.

The methyl ester in **5** was converted to the corresponding hydroxamic acids (**6**) using hydroxylamine hydrochloride and methanolic potassium hydroxide. In some cases, minor conversion to the carboxylic acid through base-mediated hydrolysis was detected. Occasionally, complete conversion to the desired product was not successful due to unexpected side reactions. For instance, liquid chromatography−mass spectrometry (LC−MS) analysis of the *tert*-butyl propanoate analogue (**5b**) indicated only partial conversion. Interestingly, when more of the reagents were added to the reaction mixture, condensation of both methyl and *tert*-butyl esters occurred, generating the desired mono-hydroxamic acid **6b** and dihydroxamic acid analogue **6d**. For the benzonitrile compounds **5n** and **5o**, nucleophilic attack of hydroxylamine on the electrophilic nitrile carbon resulted in the formation of amidoxime compounds **6p** and **6q**, respectively.[60,61] The APN inhibitory activity of these unintended analogues was still evaluated due to their potential ability to form hydrogen bonds or ionic interactions at the S1′ pocket. Compounds with acidic functionality (**5c**, and phenolic analogues) showed poor solubility in methanol when deprotonated by potassium hydroxide, which consequently resulted in a longer reaction times and poor reaction yields.

Further deprotection reactions were required to produce carboxylic acid **6c**, anilines **6ab** and **6ac**, and phenols **6ag**, **6as**, **6av**, **6ax**, and **6az**. The *tert*-butyl propanoate analogue (**5b**) and Boc-protected aniline analogues (**5z**, **5aa**) were hydrolyzed under mild acidic conditions to give propionic acid **6c** and

DOI: 10.1021/acs.jmedchem.9b00757
J. Med. Chem. XXXX, XXX, XXX−XXX

Scheme 2. Synthesis of Benzylamine Analogue 9[a]

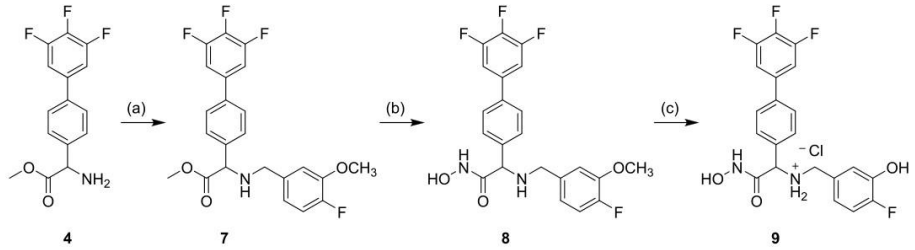

[a]Reagents and conditions: (a) benzaldehyde, $Na(OAc)_3BH$, anhyd. DCE, rt, 24 h; (b) $NH_2OH{\cdot}HCl$, 5 M KOH in anhyd. MeOH, rt; (c) (i) 1 M BBr_3 in DCM, −78 °C to rt, 2−24 h; (ii) 1 M HCl, MeOH, rt, 24 h.

Table 2. Summary of Inhibitory Activity of Hydroxamic Acid Analogues against APN

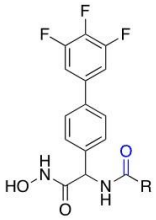

6a-6az

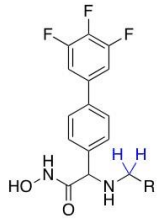

9

compound	R	$K_i^{(app)}$ ± SEM (nM)
bestatin		2370 ± 350
Tosedostat		1180 ± 77
1	$-C(CH_3)_3$	118 ± 3
6a	$-CH_3$	560 ± 50
6c	$-CH_2COOH$	188 ± 9
6d	$-CH_2C(O)NHOH$	348 ± 33
6e	$-CH_2CH_2COOH$	172 ± 9
6f	$-CH_2CH_2C(O)NH_2$	497 ± 35
6g	$-C_6H_5$	522 ± 37
6h	$-C_6H_4F$ (*m*)	919 ± 160
6i	$-C_6H_4F$ (*p*)	704 ± 68
6j	$-C_6H_4OMe$ (*m*)	462 ± 6
6k	$-C_6H_4OMe$ (*p*)	745 ± 53
6l	$-C_6H_4OH$ (*m*)	366 ± 31
6m	$-C_6H_4OH$ (*p*)	102 ± 5
6p	$-C_6H_4C(NHOH)NH_2$ (*m*)[a]	37.3 ± 2.9
6q	$-C_6H_4C(NHOH)NH_2$ (*p*)[a]	49.1 ± 3.7
6r	$-C_6H_4C(O)NH_2$ (*m*)	71.2 ± 6.5
6s	$-C_6H_4C(O)NH_2$ (*p*)[a]	82.1 ± 9.8
6t	$-C_6H_4C(O)NHMe$ (*p*)	185 ± 22
6u	$-C_6H_4C(O)NMe_2$ (*p*)	182 ± 5
6v	$-C_6H_4C(O)NEt$ (*p*)	277 ± 22
6w	$-C_6H_4C(O)NH^iPr$ (*p*)	631 ± 70
6x	$-C_6H_4C(O)NHCH_2CH_2OH$ (*p*)	163 ± 26
6y	$-C_6H_4SO_2NH_2$ (*p*)	240 ± 7
6ab	$-C_6H_4NH_2$ (*m*)	131 ± 10
6ac	$-C_6H_4NH_2$ (*p*)	205 ± 17
6ad	$-C_6H_4NHSO_2Me$ (*p*)[a]	4.50 ± 0.80
6ae	$-C_6H_4CNHSO_2NH_2$ (*p*)[a]	8.20 ± 0.90
6af	$-C_6H_3$ (3,4-OMe)	175 ± 16
6ag	C_6H_3 (3,4-OH)	430 ± 42
6ah	$-C_6H_3$ (3-F,4-OH)[a]	29.1 ± 3.6
6ai	$-C_6H_3$ (4-F,3-OH)[a]	40.0 ± 2.2
6aj	-indol-5-yl	111 ± 3
6ak	-indazol-5yl[a]	19.2 ± 2.5
6al	-benzotriazol-5-yl[a]	23.4 ± 2.3
6am	-benzimidazol-5-yl[a]	170 ± 17
6an	-(2-oxoindolin-5-yl)	156 ± 9
6ao	$-CH_2C_6H_5$	4420 ± 720
6ap	$-CH_2C_6H_4F$ (*m*)	442 ± 36
6aq	$-CH_2C_6H_4F$ (*p*)	158 ± 5
6ar	$-CH_2C_6H_4OMe$ (*p*)	978 ± 120
6as	$-CH_2C_6H_4OH$ (*p*)	235 ± 24
6at	$-CH_2C_6H_4C(O)NH_2$ (*p*)	604 ± 66
6au	$-CH_2C_6H_3$ (3,4-OMe)	119 ± 12
6av	$-CH_2C_6H_3$ (3,4-OH)	137 ± 6
6ax	$-CH_2C_6H_3$ (3-F,4-OH)	43.1 ± 5.0
6az	$-CH_2C_6H_3$ (4-F,3-OH)	138 ± 5
9	$-CH_2C_6H_3$ (4-F,3-OH)[b]	>1 mM

[a]Biological triplicates were performed for inhibitors with $K_i^{(app)}$ < 100 nM from initial triage screenings. [b]The compound is secondary amine derivative.

anilines **6ab** and **6ac**, respectively. O-Demethylation was carried out in the presence of boron tribromide to form the corresponding phenols/catechols **6ag**, **6as**, **6av**, **6ax**, and **6az**.

In addition to the analogues with an amide linker, a benzylamine analogue (**9**) was also synthesized (Scheme 2). Further physicochemical studies on the parent compound (**1**) indicate that it has an aqueous solubility ranging between 12 and 25 μM and a Log *D* of 3.0.[44] This study demonstrated that there was room to improve its physicochemical properties for optimal pharmacokinetic profiles. Incorporating bulkier groups inevitably increases the hydrophobicity of molecules, consequently decreasing aqueous solubility. However, the introduction of a secondary amine would allow the molecule to be formulated as a salt to overcome solubility issues. As described previously, reductive amination of intermediate **4** with 4-fluoro-3-methoxybenzylaldehyde yielded **7**, which was converted to the corresponding hydroxamic acid (**8**). The methoxy group in **8** was readily deprotected using boron tribromide, then reacted with hydrochloric acid to obtain the 4-fluoro-3-hydroxybenzylamine analogue (**9**) as a hydrochloride salt.

Substituted Aromatic Group Is Important for Potency toward Human APN. The inhibitory activities ($K_i^{(app)}$) of the synthesized hydroxamic acids were measured against recombinant human APN (Table 2). Initial experimental triplicates were performed for all compounds to

DOI: 10.1021/acs.jmedchem.9b00757
J. Med. Chem. XXXX, XXX, XXX−XXX

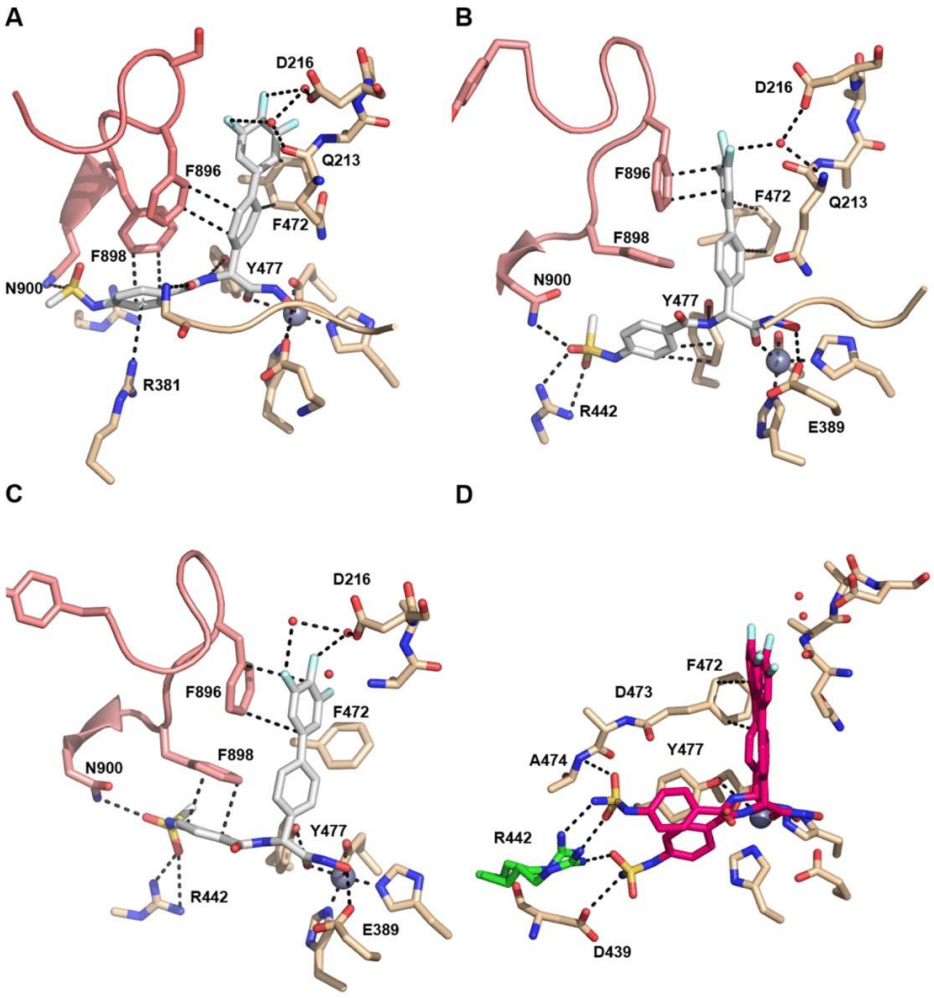

Figure 4. Three conformations of compound **6ad** (A–C) observed during MD simulation. The carbon atoms of the flexible loop are colored in light pink, and other residues in the binding site are wheat-colored. Interactions between compound **6ad** (carbon atoms in white) and APN are shown in black dashed lines. (D) Overlay of two predicted binding poses of compound **6ae**. Residues around compound **6ae** (carbon atoms in magenta) are wheat-colored (PDB ID 4FYQ). Overlaid Arg^{442} residues are shown in green. Interactions between the compound and APN are depicted in black dashed lines.

determine compounds of higher priority with $K_i^{(app)} \leq 100$ nM, which were assessed further in biological triplicate. In general, the aliphatic carboxamides (**6a–f**) were less potent than the lead compound (**1**) but more potent than bestatin and Tosedostat (Table 2). This suggests that the appended carboxylic acid and carboxamide moieties (in the case of **6a**, **6e**, and **6f**) were unable to make the intended polar interactions with the S1′ subsite of APN, potentially due to the short linker length. The unsubstituted benzamide **6g** showed over 4-fold loss in inhibitory activity compared to **1**. However, introduction of hydrogen-bond-donating groups to the phenyl ring led to a recovery in potency. For example, hydroxyl, amidoxime, and carboxamide monosubstituted benzamides **6m–s** were all more potent than compound **1**. On the other hand, hydrogen-bond acceptors such as fluorine (**6h** and **6i**) and methoxy (**6j** and **6k**) were not well tolerated. We also examined eight functionalized carboxamides (**6t–x**), sulfonamides (**6y** and **6ad**), and sulfamide (*para*-(sulfamoylamino)benzoic acid) (**6ae**) analogues, which have the capacity to increase ligand binding interactions in the S1′ pocket via hydrogen-bonding interactions. The benzamide derivatives **6t–x** exhibited a decrease in activity ranging from 2- to 8-fold compared to carboxamide **6s**. A trend of decreasing activity was observed from the benzamide derivatives as the size of the hydrophobic group increases from methyl, dimethyl, ethyl, and isopropyl, indicating that a loss in polar contacts may result in reduced binding to APN. Additionally, the inhibitory activities of the methyl (**6t**) and dimethyl (**6u**) analogues were essentially identical, suggesting that the hydrogen-bond-donating capability of benzamide does not play a significant role in potency. 4-Methylsulfonamide **6ad** ($K_i^{(app)}$ = 4.5 nM) and sulfamide **6ae** ($K_i^{(app)}$ = 8.2 nM) were the most potent inhibitors of the series and showed a greater than 10-fold improvement in potency compared to **1**, potentially due to its multiple hydrogen-bond-forming capacity for strong binding interactions with APN.

DOI: 10.1021/acs.jmedchem.9b00757
J. Med. Chem. XXXX, XXX, XXX–XXX

Among the disubstituted benzamides (**6af**–**ai**), the fluorohydroxyl analogues (**6ah** and **6ai**) showed improved activity relative to **1**. Compared to the corresponding monosubstituted benzamide derivatives, disubstituted analogues showed stronger inhibition activity. For example, 3-fluorobenzamide **6h** and 4-hydroxybenzamide **6m** displayed activities of 919 and 366 nM, respectively, whereas the potency of the 3-fluoro-4-hydroxyl analogue (**6ah**) significantly increased to 29 nM, suggesting that both fluoro and hydroxyl are making important interactions with APN. A similar result was observed for the 4-fluoro-3-hydroxy analogue (**6ai**), which exhibited significantly greater potency ($K_i^{(app)}$ = 40 nM) than the corresponding monosubstituted analogues 4-fluorobenzamide **6i** ($K_i^{(app)}$ = 704 nM) and 3-hydroxybenzamide **6l** ($K_i^{(app)}$ = 102 nM). Similarly, the 3,4-dimethoxy analogue (**6af**) exhibited an increased potency compared to 3- and 4-methoxy analogues, **6j** and **6k**, respectively.

The activities of compounds where benzamide was replaced with various heterocyclic amides (**6aj**–**an**) were also investigated. The indole analogue (**6aj**) was equipotent with the parent compound (**1**). A significant increase in the potency was observed from indazole **6ak** ($K_i^{(app)}$ = 19.2 nM) and benzotriazole **6al** ($K_i^{(app)}$ = 23.4 nM).

In general, replacement of benzamide with acetamide to introduce sp^2 characteristics for increased flexibility resulted in a significant loss in potency (**6ao**–**ay**). The 3-fluoro-4-hydroxyl analogue **6ax** was the only compound in this series that proved to be more potent than **1** with an inhibition activity of 43.1 nM. Inconsistent relationships were observed between the benzamide and matching acetamide analogues. For instance, the potency observed for the benzyl analogue (**6ao**) reduced drastically compared to the phenyl analogue (**6g**). This trend was also observed for the 4-methoxy (**6k** and **6ar**), 4-hydroxy (**6m** and **6as**), 4-fluoro-3-hydroxy (**6ai** and **6az**), and 4-benzamide (**6s** and **6at**) pairs. In contrast, an increase in potency was observed for the fluoro analogues (**6h**, **6i**, **6ap**, **6aq**) and the 3,4-dimethoxy analogues (**6af** and **6au**), while 3-fluoro-4-hydroxyl compounds **6ah** and **6ax** were the most potent compounds in each series. The 4-fluoro-3-hydroxybenzylamine analogue (**9**) was the weakest inhibitor of this series; full inhibition was not achieved at a concentration of 1 mM, suggesting that carbonyl oxygen of the amide linker is crucial for potent activity, potentially by providing appropriate rigidity and also hydrogen-bonding interaction with nearby residues.

Structure–activity relationship (SAR) investigations around the S1′ pocket of APN through modifications of the *N*-pivaloyl group of compound **1** indicated that substituted aryls were essential for inhibitory activity, where hydrogen-bond donors were more favored than hydrogen-bond acceptors. A substantial decrease in activity observed from acetamide and secondary amine analogues revealed that rigidity and the carbonyl oxygen of the benzamide were vital. In addition, studies on functionalized carboxamides and sulfonamides showed that there was a decreasing trend in activity as the size of the hydrophobic group increases, while incorporating polar groups led to a significant rise in activity. This suggested that hydrogen-bonding interactions played a major role to enhance activity against APN.

Core Biaryl System Engages in Hydrophobic Interactions with Flexible Loop at the S1 Pocket of APN. To understand why **6ad** and **6ae** displayed such an improvement in potency, we undertook molecular docking followed by MD simulations to generate a model of APN bound to both inhibitors. A rigid-docking into the APN crystal structure (PDB ID 4FYQ) of compounds **6ad** and **6ae** was performed based on the docked pose of compound **1** into APN using Surflex Docking software available from SYBYL2.1. The common fragments of the biphenyl core structure and the hydroxamic group were set as constraints. Similar to the molecular docking of compound **1**, the most preferred structures of **6ad** and **6ae** bound to APN were selected based on the total docking score (Table S6). MD simulations showed that the ligands occupy different conformations in a time-dependent manner (Movies S1 and S2). Compound **6ad** participated in water-mediated hydrogen-bonding interactions with the fluorine atoms and the nearby residues at the S1 subsite of APN, both of which were also observed in the co-crystal structure of compound **1** bound to *Pf*A-M1.[44] One compelling result from the MD simulation was a flexible loop located at domain IV acting as an effective "cap" to close the active site of APN (Figure 4). The flexible loop and the Phe^{896} residue are believed to play important roles in conformational changes of APN.[4] The flexible loop consists of eight amino acid residues (^{891}YGGGSFSF^{898}) and has been shown to undergo a dramatic change in conformation upon complex formation with a peptide substrate.[4] The binding mode of bestatin, which binds APN differently to other M1 aminopeptidases (noncanonical binding pose), is also thought to be related to the flexible loop, in particular Phe^{896}. As opposed to other M1–bestatin complexes in which the loop is shorter and different in sequence and therefore does not impede bestatin from binding with canonical geometry, the Phe^{896} of APN was positioned away from the binding pocket to accommodate the bulky phenyl group of bestatin at the S1 pocket.[4] In our simulations, we saw that the biphenyl ring system of **6ad** maintained face-to-face stacking interactions with Phe^{896} to keep the inhibitor locked in the active site of APN; however, it was clear that this interaction varied within the biphenyl system between different poses. Generally, the side chain of Phe^{896} interacted with the top trifluorophenyl (Figure 4B,C), but interactions with the central aromatic ring of compound **6ad** were also observed (Figure 4A).

Interestingly, stable hydrophobic stacking interactions between the flexible loop and compound **6ae** were not observed (Figure 4). Without the flexible loop stabilizing the biaryl core moiety and restricting the movement of the molecule, the flat biphenyl system of **6ae** gained freedom to move within the S1 pocket. Although prominent stacking interactions that were observed with **6ad** were missing from **6ae**, the phenylalanine-rich region provided a favorable environment for the hydrophobic biaryl group to maintain its overall position within the pocket.

Sulfonamide Moiety Provides Multiple Hydrogen-Bonding Interactions at the S1′ Pocket of APN. Based on our MD simulations, the large arylsulfonamide derivatives of both **6ad** and **6ae** were able to reach the S1′ pocket of APN. The bottom aromatic group of **6ad** was flexible enough to interact with the side chain of Phe^{898} or Tyr^{477} (Figure 4A–C). Due to the high flexibility of the sulfonamide moiety, these interactions were occasionally lost and replaced with a cation–π interaction between the Arg^{381} side chain and the electron-rich aromatic ring of arylsulfonamide. The results also revealed that the sulfonyl oxygen atoms can engage in dual hydrogen bonds with Asn^{900} and Arg^{442} (Table S3), where the

DOI: 10.1021/acs.jmedchem.9b00757
J. Med. Chem. XXXX, XXX, XXX–XXX

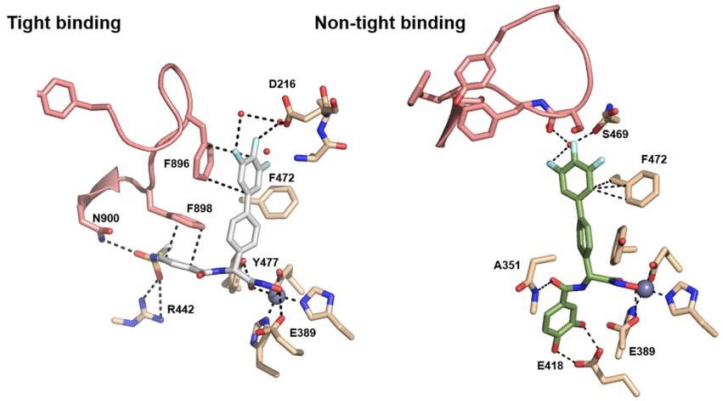

Figure 5. Comparison of the binding interactions occurred with tight-binding inhibitor **6ad** (left) and the weaker inhibitor **6ag** (right) (4FYQ). The carbon atoms of the flexible loop are colored in light pink, and other residues in the binding site are wheat-colored. Compounds **6ad** and **6ag** are colored in white and green, respectively. Interactions between the ligands and APN are shown in black dashed lines.

arginine residue stayed in a relatively rigid manner throughout simulations.

Compound **6ae** behaved similarly to **6ad**, exhibiting multiple binding positions. The aromatic ring located in the S1′ pocket of APN displayed extensive interactions with the side chain of Arg^{442} and Asn^{900}. As described above, the flexible loop was not accessible to the molecule, but the bottom aromatic was located closer to Tyr^{477}, forming hydrophobic edge-face stacking interactions (Figure 4D). The backbone amide of Ala^{474} could also participate in a hydrogen-bond interaction with a sulfonyl oxygen atom of **6ae** (Table S4). In the case, where the sulfamide was pointing deeper into the S1′ subsite of APN, the amino group is located in close proximity to Asp^{439}.

To rationalize our SAR analysis, we also investigated the interactions between one of the weaker inhibitors, **6ag** ($K_i^{(app)}$ = 430 nM), which contains 3,4-hydroxyl group (Figure 5). In contrast to compounds **6ad** and **6ae**, which showed extensive hydrophobic interactions with the flexible loop, the biphenyl system of compound **6ag** made no interactions with the key phenylalanine residues of the flexible loop. Throughout most of the simulation, the trifluorophenyl moiety participated in a water-mediated hydrogen-bonding network with Ser^{469} and hydrophobic interactions between Phe^{472}. However, the flexible loop was located too far away from the biphenyl system to capture essential nonpolar interactions, which may explain the significant decrease in the potency. Hydrogen-bonding interactions between the catechol group and the side chain of Glu^{418} residue were also observed. However, these interactions appear not able to compensate the missing stacking interactions between the S1′ aromatic group and Tyr^{477} or the Phe^{898} residues, which may contribute to the reduced inhibition activity of **6ag** against APN.

Role of Glu^{389} Residue as the Zinc−Hydroxamic Acid Complex Stabilizer. Another intriguing phenomenon was observed from the formation of the zinc−hydroxamic acid complex. In the M1 aminopeptidases, inhibitors often bind with a pentahedral coordination to the zinc, which mimic the transition state of the activated enzyme.[4,62] In the simulations we performed, the hydroxyl group of hydroxamic acid readily lost contact with the zinc, with bond distance ranging from 2.2 to 3.4 Å while the carbonyl oxygen possessed a very stable coordination with a bond distance range of 1.9−2.0 Å, resulting in tetrahedral coordination. Given the challenges associated with metallo-protein simulations, this observation is possibly biased by the ZAFF parameters used. To accurately simulate the change in ligand interaction with the zinc ion, a quantum mechanics/molecular mechanics simulation would be needed. However, we did observe that the loss of pentahedral coordination of **6ad** and **6ae** to the zinc ion resulted in the formation of a hydrogen bond with Glu^{389} (Figure 6). This

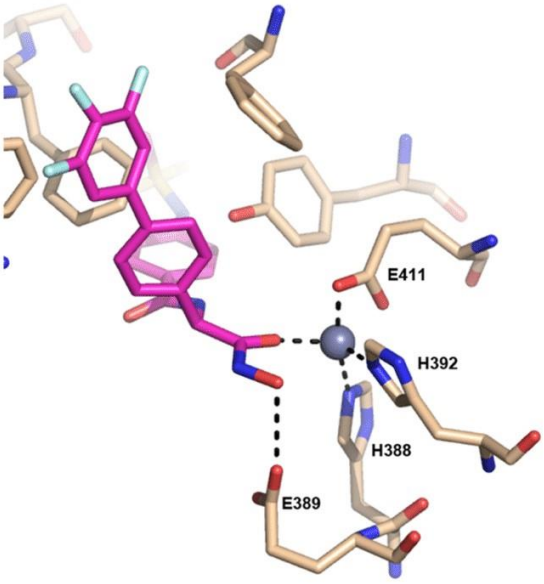

Figure 6. Hydroxamic acid−zinc complex in the active site of APN. APN residues are wheat-colored, and the ligand is shown in magenta. Interactions between the ligand and the catalytic triad and Glu^{389} are illustrated in black dashed lines (PDB ID 4FYQ).

interaction was extremely stable and maintained a bond distance of 2.4−2.9 Å throughout our simulations (Tables S3 and S4). Further computational and experimental investigation is required to determine whether this interaction plays a role in the catalytic mechanism by stabilizing the zinc−ligand complex.

DOI: 10.1021/acs.jmedchem.9b00757
J. Med. Chem. XXXX, XXX, XXX−XXX

Table 3. Physicochemical and Metabolic Properties of 6ad and 6ae

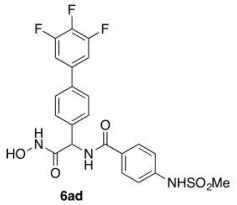

6ad

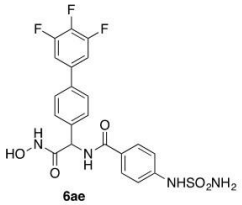

6ae

	kinetic solubility		liver microsome stability		plasma stability	
compound	$Sol_{pH\ 2.0}$	$Sol_{pH\ 6.5}$	mouse $t_{1/2}$ (min)	human $t_{1/2}$ (min)	mouse $t_{1/2}$ (min)	human $t_{1/2}$ (min)
6ad	12.5−25	12.5−25	>250	>250	>1020	>1020
6ae	6.3−12.5	12.5−25	>250	>250	>1020	>1020

Compounds 6ad and 6ae Show Selectivity for APN over Matrix Metalloproteinases (MMPs). As the hydroxamic acid moiety is a strong zinc chelator, there is a possibility that our potent APN inhibitors may interact with other zinc-dependent enzymes. To assess the selectivity and potential off-target effects of **6ad** and **6ae**, we performed quenched fluorescence assays with MMP2, 7, 8, 9, and 13 (Figure S1). The activity of the parent compound (**1**), Tosedostat, and the broad spectrum MMP inhibitor, Marimastat, were also evaluated as comparison and controls (Table 1). MMP2 and 9 were effectively inhibited by Marimastat (IC_{50} 0.43 and 3.1 nM, respectively) and weakly by Tosedostat (IC_{50}: 0.19 and 1.5 μM, respectively), whereas **6ad** and **6ae** weakly inhibited MMP2 (1.3 and 2.1 μM, respectively) and only inhibited MMP9 at relatively high concentrations (IC_{50} > 100 μM). Similar observations were made for collagenases MMP8 and MMP13 as well as matrilysin MMP7, which were all inhibited with low nM IC_{50} by Marimastat, high nM IC_{50} by Tosedostat, and μM to mM IC_{50} by the novel inhibitors, with **1** demonstrating the lowest extent of inhibition (Figure S1). Collectively, these findings show that the novel APN inhibitors demonstrate low off-target inhibitory effects on MMPs.

Cellular Toxicity, and Physicochemical and Pharmacokinetic Properties of 6ad and 6ae. Evaluation of cellular toxicity, and physicochemical and stability properties provide important early-stage data to determine whether or not a compound has the necessary features to be pursued further as a drug candidate. In our cellular toxicity study, we used Ad293 cell line, which was used to measure cell toxicity in other literature reports, is derived from the human embryonic kidney 293 (HEK293) cell line, but transfected with a special gene for improved cell adherence to make cell handling easier during cell cultures and assays.[63] The compounds show limited cytotoxicity against Ad293 cells with CC_{50} values of 41 ± 2 μM for **6ad** and 149 ± 13 μM for **6ae**. In vitro physicochemical properties and metabolic/plasma stabilities of two potent APN inhibitors **6ad** and **6ae** were measured (Table 3). The kinetic solubility of each compound was determined by nephelometry. Both compounds showed moderate solubility under pH conditions representative of the stomach (pH 2) and upper fasted state small intestine (pH 6.5) suggesting that solubility could be a factor that limits oral absorption. The partition coefficients at pH 7.4 ($Log\ D_{pH\ 7.4}$) were estimated using a chromatographic method and found to be 2.8 and 2.6, respectively. The metabolic stabilities were assessed by incubating compounds in mouse and human hepatic microsomes at 37 °C and a protein concentration of 0.4 mg/mL. The compounds showed minimal degradation and very long half-lives of longer than 4 h in both mouse and human microsomes, resulting in low in vitro intrinsic clearance values [CL_{int} < 7 μL/(min mg protein)]. In vitro plasma stability studies were performed by incubating compounds in human and mouse plasma at 37 °C for up to 4 h. Both compounds displayed minimal loss, indicating that they are not readily susceptible to the action of hydrolytic enzymes present in the plasma.

■ CONCLUSIONS

Rapid metastasis of cancer cells through complex mechanisms of ECM degradation, angiogenesis, cell invasion, and cell adhesion is a major burden in effective cancer therapy. Therefore, continuous development of novel anticancer agents targeting metastasis is urgently required. Being involved in mechanisms of angiogenesis and metastasis, APN has been broadly studied as a therapeutic target for cancer. Here, we have reported the design, synthesis, and biological evaluations of novel APN inhibitors that were derived from a potent inhibitor of parasitic homologue *Pf*A-M1. Through comprehensive structure-based design, we were able to generate a small library of novel hydroxamic acid analogues targeting APN and discover a potent compound **6ad** that showed 527-fold improved inhibition activity than a known APN inhibitor bestatin. Molecular docking and MD simulations highlighted the significance of the flexible loop in domain VI in providing hydrophobic interactions at the S1 pocket. The results also revealed the combination of stacking and dual hydrogen-bonding interactions was crucial to optimize the binding at the S1′ subunit of APN. In addition, cross-activity studies showed that **6ad** and **6ae** possessed low off-target activity on MMPs. The evaluation of the cellular activities of **6ad** and **6ae** against Ad293 cell line also indicated that they displayed limited cytotoxicity. Moreover, **6ad** and **6ae** had favorable metabolic and plasma stability in both human and mouse models. However, the solubility of these compounds is suboptimal and should be addressed by further medicinal chemistry approaches.

■ EXPERIMENTAL SECTION

Chemistry. Chemicals and solvents were purchased from standard suppliers and used without further purification unless otherwise indicated. ^{1}H NMR, ^{19}F NMR, and ^{13}C NMR spectra were recorded on a Bruker Avance Nanobay III 400 MHz Ultrashield Plus spectrometer at 400.13, 376.46, and 100.61 MHz, respectively. NMR experiments were obtained at the temperature of 298 K. Data acquisition and processing was managed using Topspin software package version 3. Chemical shifts (δ) are recorded in parts per

DOI: 10.1021/acs.jmedchem.9b00757
J. Med. Chem. XXXX, XXX, XXX−XXX

million with reference to the chemical shift of the deuterated solvent. Coupling constants (J) and carbon−fluorine coupling constants (J_{CF}) are recorded in hertz, and multiplicities are described as singlet (s), doublet (d), triplet (t), multiplet (m), doublet of doublets (dd), doublet of triplets (dt), doublet of doublets of doublets (ddd), and broad (br). Overlapped nonequivalent ^{13}C peaks were identified by heteronuclear single quantum coherence and heteronuclear multiple-bond correlation NMR.

Analytical thin-layer chromatography (TLC) was performed on Merck silica gel $60F_{254}$ aluminum-backed plates, which were visualized by fluorescence quenching under a UV lamp at 254 nm or by $Fe(III)Cl_3$ staining for hydroxamic acid compounds. Flash chromatography was performed with silica gel 60 (particle size, 0.040−0.063 μm).

Analytical high-performance liquid chromatography (HPLC) was performed using an Agilent 1260 Infinity Analytical HPLC with a Zorbax Eclipse Plus C18 Rapid Resolution 4.6 × 100 mm^2, 3.5 μm column. Buffer A: 0.1% TFA in H_2O and buffer B: 0.1% TFA in MeCN were used. Samples were run at a gradient of 5% buffer B/buffer A (0−9 min) to 100% buffer B (9−10 min) at a flow rate of 1 mL/min. Unless otherwise indicated, all compounds were >95% pure by HPLC (254 and 214 nm) prior to biological evaluation.

Preparative HPLC was performed using an Agilent 1260 Infinity instrument coupled with a binary preparative pump and an Agilent 1260 FC-PS fraction collector using Agilent OpenLAB CDS software (revision C.01.04) and an Altima C8 22 × 250 mm^2, 5 μM column, and a 1260 Infinity diode array detector VL. The following buffers were used: buffer A: 0.1% TFA in H_2O and buffer B: 0.1% TFA in MeCN. The sample was run at a gradient of 30−100% buffer B over 10 min at a flow rate of 20 mL/min.

LC−MS was performed using system A or B. System A: Agilent 6100 series single quadrupole instrument coupled to an Agilent 1200 series HPLC instrument fitted with a Luna 120 C8(2) 5 μm 50 × 4.6 mm^2 column. Samples were run at a flow rate of 0.5 mL/min for 12 min: 5% buffer B/buffer A (0−4 min), 100% buffer B (4−7 min), and 5% buffer B/buffer A (7−12 min). Mass spectra were obtained in positive- and negative-ion modes with a scan range of 100−1000 m/z. UV detection was carried out at 254 nm. System B: Agilent 6120 series single quadrupole instrument coupled to an Agilent 1260 series HPLC instrument fitted with a Poroshell 120 EC-C18 50 × 3.0 mm^2, 2.7 μm column. The following buffers were used: buffer A: 0.1% formic acid in H_2O and buffer B: 0.1% formic acid in MeCN. Samples were run at a flow rate of 0.5 mL/min for 5 min: 5% buffer B/buffer A (0−1 min), 100% buffer B (1−2.5 min), and held at this composition until 3.8 min, 5% buffer B/buffer A (3.8−4 min), and held until 5 min at this composition. Mass spectra were obtained in positive- and negative-ion modes with a scan range of 100−1000 m/z. UV detection was carried out at 214 and 254 nm.

High-resolution mass spectrometry (HRMS) was carried out using an Agilent 6224 TOF LC−MS mass spectrometer coupled to an Agilent 1290 Infinity device. All data were acquired and referenced via dual-spray electrospray ionization source. Acquisition was performed using Agilent Mass Hunter Data Acquisition software version B.05.00 Build 5.0.5042.2, and analysis was conducted using Mass Hunter Qualitative Analysis version B.05.00 Build 5.0.519.13.

Instant JChem was used for data management: Instant JChem 16.9.12.0, ChemAxon (http://www.chemaxon.com).

General Procedure A: Amide Coupling Using HCTU and DIPEA. Carboxylic acid (1.1 equiv) and HCTU (1.2 equiv) were dissolved in anhydrous DMF (2 mL/mmol) and stirred for 30 min in a N_2-flushed microwave vial. DIPEA (2.1 equiv) was added dropwise followed by compound **4** (1.0 equiv) in anhydrous DCM (2 mL/mmol). The reaction mixture was stirred at rt for 1 day. If the reaction did not reach completion after 1 day, then a further 1.2 equiv HCTU and 2.1 equiv DIPEA were added. After completion, the reaction mixture was diluted with sat. $NaHCO_3$ (10 mL) and extracted with DCM (3 × 15 mL). The combined organic layers were washed with water (2 × 10 mL) and brine (15 mL). The organic layer was dried over anhydrous Na_2SO_4, filtered, and concentrated in vacuo. The crude was purified by column chromatography using either DCM/MeOH or petroleum ether (PE)/EtOAc as the eluent.

General Procedure B: Amide Coupling Using EDCI and DMAP. Compound **4** (1.0 equiv), carboxylic acid (1.2 equiv), EDCI (1.2 equiv), and DMAP (1.3 equiv) were dissolved in DCM (8 mL/mmol) or DMF (8 mL/mmol) and stirred at rt overnight. If the reaction did not reach completion, then a further 1.2 equiv EDCI and 1.3 equiv DMAP were added. The reaction mixture was diluted with sat. $NaHCO_3$ (10 mL) and extracted with DCM (3 × 10 mL). The combined organic layers were washed with a 1 M HCl solution (15 mL), dried over anhydrous Na_2SO_4, filtered, and concentrated in vacuo. The crude residue was purified by column chromatography using PE/EtOAc as the eluent.

General Procedure C: Direct Aminolysis of Methyl Ester to the Hydroxamic Acid. To a solution of methyl ester (1.0 equiv) in anhydrous MeOH (3 mL/mmol) was added $NH_2OH{\cdot}HCl$ (4−10 equiv) followed by KOH (5 M in MeOH, 5−10 equiv). The reaction mixture was stirred at rt and monitored by LC−MS and TLC using an $Fe(III)Cl_3$ stain. Once the reaction was complete, the suspension was dry-loaded onto silica and purified by column chromatography.

General Procedure D: O-Demethylation Using BBr_3. To a solution of the methyl ether substrate (1.0 equiv) in DCM (2 mL/mmol) was added BBr_3 (1 M in DCM, 5.0 equiv for mono O-demethylation, 10.0 equiv for double O-demethylation) at −78 °C. The reaction mixture was stirred at rt for 2 h to 1 day. The reaction was quenched by the addition of a 1 M HCl and stirred vigorously for 10 min. The resulting precipitate was filtered and purified by preparative HPLC.

*1-(3′,4′,5′-Trifluoro-[1,1′-biphenyl]-4-yl)ethan-1-one (**2**).* To a nitrogen-flushed 500 mL round-bottom flask were added 4′-bromoacetophenone (5.00 g, 25.1 mmol), 3,4,5-trifluorophenylboronic acid (5.74 g, 32.7 mmol), anhydrous THF (180 mL), and a 1 M Na_2CO_3 solution (60 mL). $PdCl_2(PPh_3)_2$ (529 mg, 0.754 mmol) was added, and the mixture was heated at reflux for 2 h. The reaction mixture was concentrated under reduced pressure and extracted with Et_2O (3 × 50 mL). The combined organic layers were dried over anhydrous Na_2SO_4, filtered, and concentrated in vacuo. The crude product was purified by column chromatography (PE/EtOAc 100:0−50:50) to afford compound **2** as a yellow-brown solid (6.29 g, 100%); ^1H NMR [d_6-dimethyl sulfoxide (DMSO)] δ 8.03 (d, J = 8.6 Hz, 2H), 7.89 (d, J = 8.5 Hz, 2H), 7.80 (dd, J = 9.6, 6.8 Hz, 2H), 2.62 (s, 3H); ^{19}F NMR (d_6-DMSO) δ −134.6 (d, J = 21.7 Hz), −162.1 (dd, J = 21.7/21.7 Hz); ^{13}C NMR (d_6-DMSO) δ 197.5, 150.6 (ddd, J_{CF} = 247.0/9.8/4.2 Hz), 141.1−141.0 (m), 138.79 (dt, J_{CF} = 250.5/15.6 Hz), 136.5, 135.6 (dt, J_{CF} = 12.8/6.4 Hz), 128.8, 127.1, 112.2−111.3 (m), 26.8; m/z MS $C_{14}H_{10}F_3O$ $[MH]^+$ calcd 251.1, found 251.0.

*2-Oxo-2-(3′,4′,5′-trifluoro-[1,1′-biphenyl]-4-yl)acetic Acid (**3**).* Compound **2** (6.29 g, 25.1 mmol) and SeO_2 (4.18 g, 37.7 mmol) were dissolved in anhydrous pyridine (200 mL). The reaction mixture was sonicated and then heated at 110 °C overnight under nitrogen. Once the reaction was complete, the mixture was filtered through Celite and the filtrate was concentrated in vacuo. A 1 M HCl solution (20 mL) was added, and the compound was extracted with EtOAc (3 × 50 mL). The combined organic layers were dried over anhydrous Na_2SO_4, filtered and concentrated under reduced pressure to afford compound **3** as a brown solid (7.04 g, 100%); ^1H NMR (d_6-DMSO) δ 8.05−7.93 (m, 4H), 7.84 (dd, J = 9.5/6.7 Hz, 2H); ^{19}F NMR (d_6-DMSO) δ −134.4 (d, J = 21.7 Hz), −161.3 (dd, J = 21.7/21.7 Hz); ^{13}C NMR (d_6-DMSO) δ 188.0, 165.8, 150.7 (ddd, J_{CF} = 247.2/9.8/4.1 Hz), 142.9−142.8 (m), 139.1 (dt, J_{CF} = 248.4/14.2 Hz), 135.8−134.5 (m), 131.6, 130.2, 127.7, 116.5−105.3 (m); m/z MS $C_{14}H_6F_3O_3$ $[M - H]^-$ calcd 279.0, found 279.0.

*Methyl 2-Amino-2-(3′,4′,5′-trifluoro-[1,1′-biphenyl]-4-yl)acetate (**4**).* Compound **3** (7.04 g, 25.1 mmol) and benzylamine (4.12 mL, 37.7 mmol) were dissolved in anhydrous DCE (200 mL) and stirred for 30 min. $Na(OAc)_3BH$ (7.99 g, 56.6 mmol) was added, and the mixture was stirred at rt overnight. Once the reaction was complete, water (30 mL) was added and the mixture was stirred vigorously for 5 min. DCE was removed in vacuo and the solid was filtered and washed with ethanol to give 9.33 g of 2-(benzylamino)-2-(3′,4′,5′-

DOI: 10.1021/acs.jmedchem.9b00757
J. Med. Chem. XXXX, XXX, XXX−XXX

trifluoro-[1,1′-biphenyl]-4-yl)acetic acid as a yellow solid. The crude solid was dissolved in MeOH (250 mL) and conc. H_2SO_4 (5.36 mL, 101 mmol) was added dropwise. The reaction mixture was refluxed for 16 h and then concentrated under reduced pressure. Sat. $NaHCO_3$ was added and the mixture was extracted with DCM (3 × 150 mL). The combined organic layers were dried over anhydrous Na_2SO_4, filtered, and concentrated under reduced pressure to afford 7.86 g of methyl 2-(benzylamino)-2-(3′,4′,5′-trifluoro-[1,1′-biphenyl]-4-yl)-acetate. The crude ester was subsequently dissolved in MeOH (200 mL), and 32% HCl (5 mL) was added. The flask was evacuated and flushed with nitrogen three times before the addition of 10% Pd/C (1.60 g). The reaction mixture was stirred vigorously under a hydrogen atmosphere at rt overnight. Upon completion, the reaction mixture was filtered through Celite and washed with MeOH (50 mL). The filtrate was concentrated in vacuo followed by dilution with sat. $NaHCO_3$ and extraction with EtOAc (3 × 100 mL). The organic layer was dried over anhydrous Na_2SO_4, filtered, and concentrated under reduced pressure. The crude product was purified by column chromatography (PE/EtOAc 50:50−0:100) to afford compound **4** as a sticky yellow solid (3.51 g, 47% over three steps). ^{1}H NMR ($CDCl_3$) δ 7.47 (m, 4H), 7.20−7.10 (m, 2H), 4.67 (s, 1H), 3.72 (s, 3H), 2.30 (s, 2H); ^{19}F NMR ($CDCl_3$) δ −134.0 (d, J = 20.5 Hz), −162.4 (dd, J = 20.6/20.6 Hz); ^{13}C NMR ($CDCl_3$) δ 174.3, 151.5 (ddd, J_{CF} = 249.6/10.0/4.3 Hz), 140.5, 140.9−137.9 (m), 138.1−137.9 (m), 136.8 (td, J_{CF} = 7.8/4.7 Hz), 127.7, 127.3, 111.3−110.9 (m), 58.4, 52.6; m/z MS $C_{15}H_{13}F_3NO_2$ $[MH]^+$ calcd 296.1, found 296.1.

*Methyl 2-Acetamido-2-(3′,4′,5′-trifluoro-[1,1′-biphenyl]-4-yl)-acetate (**5a**).* To a mixture of compound **4** (300 mg, 1.01 mmol) in anhydrous toluene (4 mL) was added Meldrum's acid (161 mg, 1.12 mmol). The reaction mixture was refluxed for 3 h. After cooling to rt, the resulting precipitate was filtered and washed with Et_2O to afford compound **5a** as a white solid (172 mg, 50%). ^{1}H NMR (d_6-DMSO) δ 8.80 (d, J = 7.3 Hz, 1H), 7.89−7.64 (m, 4H), 7.48 (d, J = 8.3 Hz, 2H), 5.48 (d, J = 7.3 Hz, 1H), 3.63 (s, 3H), 1.91 (s, 3H); ^{19}F NMR (d_6-DMSO) δ −134.8 (d, J = 21.8 Hz), −163.3 (dd, J = 21.7/21.7 Hz); ^{13}C NMR (d_6-DMSO) δ 171.0, 169.3, 150.6 (ddd, J_{CF} = 246.6/9.7/4.2 Hz), 138.4 (dt, J_{CF} = 249.5/15.7 Hz), 136.9−136.8 (m), 136.7, 136.3 (td, J_{CF} = 8.1/4.5 Hz), 128.4, 127.2, 117.8−108.1 (m), 55.8, 52.3, 22.2; m/z MS $C_{17}H_{15}F_3NO_3$ $[MH]^+$ calcd 338.1, found 338.1.

*tert-Butyl 3-((2-Methoxy-2-oxo-1-(3′,4′,5′-trifluoro-[1,1′-biphenyl]-4-yl)ethyl)amino)-3-oxopropanoate (**5b**).* 3-(*tert*-Butoxy)-3-oxopropanoic acid (198 mg, 1.24 mmol) was coupled to compound **4** (330 mg, 1.12 mmol) according to General Procedure A. The crude product was purified by column chromatography (PE/EtOAc 0:100−50:50) to afford compound **5b** (185 mg, 38%) as an orange oil. ^{1}H NMR (d_6-DMSO) δ 9.00 (d, J = 7.3 Hz, 1H), 7.80−7.67 (m, 4H), 7.50 (d, J = 8.3 Hz, 2H), 5.52 (d, J = 7.3 Hz, 1H), 3.65 (s, 3H), 3.31−3.21 (m, 2H), 1.39 (s, 9H); ^{19}F NMR (d_6-DMSO) δ −134.9 (d, J = 21.7 Hz), −163.3 (dd, J = 21.7/21.7 Hz); ^{13}C NMR (d_6-DMSO) δ 170.6, 166.9, 165.5, 150.6 (ddd, J_{CF} = 246.6/9.8/4.2 Hz), 138.4 (dt, J_{CF} = 249.7/15.6 Hz), 136.9−136.8 (m), 136.6, 136.3 (m), 128.3, 127.2, 111.7−111.0 (m), 80.6, 55.8, 52.4, 43.2, 27.7; m/z MS $C_{22}H_{21}F_3NO_5$ $[M - H]^-$ calcd 436.1, found 436.1.

*4-((2-Methoxy-2-oxo-1-(3′,4′,5′-trifluoro-[1,1′-biphenyl]-4-yl)-ethyl)amino)-4-oxobutanoic Acid (**5e**).* To a mixture of compound **4** (428 mg, 1.45 mmol) in anhydrous toluene (10 mL) was added succinic anhydride (160 mg, 1.60 mmol). The reaction mixture was refluxed for 3 h. After cooling to rt, the resulting precipitate was filtered and washed with Et_2O to afford compound **5e** as a white solid (267 mg, 49%). ^{1}H NMR (d_6-DMSO) δ 12.11 (s, 1H), 8.83 (d, J = 7.3 Hz, 1H), 7.80−7.65 (m, 4H), 7.49 (d, J = 8.3 Hz, 2H), 5.49 (d, J = 7.3 Hz, 1H), 3.63 (s, 3H), 2.46−2.39 (m, 4H); ^{19}F NMR (d_6-DMSO) δ −134.82 (d, J = 21.8 Hz), −163.24 (dd, J = 21.8/21.8 Hz); ^{13}C NMR (d_6-DMSO) δ 173.7, 171.2, 171.0, 150.6 (ddd, J_{CF} = 246.4/9.6/4.0 Hz), 138.4 (m), 137.0 (m), 136.8, 136.3 (m), 128.4, 127.1, 111.5−111.2 (m), 55.8, 52.3, 29.6, 28.9; m/z MS $C_{19}H_{17}F_3NO_5$ $[MH]^+$ calcd 396.1, found 396.1.

*Methyl 2-(4-Amino-4-oxobutanamido)-2-(3′,4′,5′-trifluoro-[1,1′-biphenyl]-4-yl)acetate (**5f**).* Compound **5e** (272 mg, 0.688 mmol) and PyBOP (531 mg, 1.02 mmol) in DMF (10 mL) were stirred for 10 min. DIPEA (0.2 mL, 1.02 mmol) and ammonium carbonate (332 mg, 3.45 mmol) were added to the reaction mixture which was stirred at rt overnight. After completion, the mixture was diluted with water (10 mL) and extracted with DCM (3 × 15 mL). The combined organic layers were washed with sat. $NaHCO_3$ (2 × 30 mL) and brine (30 mL). The organic layer was dried over anhydrous Na_2SO_4, filtered, and concentrated in vacuo. The crude product was purified by column chromatography (PE/EtOAc 50:50−0:100) to afford compound **5f** as a white solid (84 mg, 31%). ^{1}H NMR (d_6-DMSO) δ 8.81 (d, J = 7.3 Hz, 1H), 7.87−7.60 (m, 4H), 7.49 (d, J = 8.3 Hz, 2H), 7.29 (br s, 1H), 6.75 (br s, 1H), 5.49 (d, J = 7.3 Hz, 1H), 3.63 (s, 3H), 2.47−2.25 (m, 4H); ^{19}F NMR (d_6-DMSO) δ −134.8 (d, J = 21.8 Hz), −163.3 (dd, J = 21.8/21.8 Hz); ^{13}C NMR (d_6-DMSO) δ 173.4, 171.7, 171.0, 150.6 (ddd, J_{CF} = 246.5/9.7/4.2 Hz), 138.4 (dt, J_{CF} = 249.6/15.7 Hz), 136.8 (2C), 136.34 (td, J_{CF} = 8.2/4.2 Hz), 128.4, 127.2, 111.6−110.9 (m), 55.8, 52.3, 30.2, 30.1; m/z MS $C_{19}H_{18}F_3N_2O_4$ $[MH]^+$ calcd 395.1, found 395.1.

*Methyl 2-Benzamido-2-(3′,4′,5′-trifluoro-[1,1′-biphenyl]-4-yl)-acetate (**5g**).* Benzoic acid (99.3 mg, 0.813 mmol) was coupled to compound **4** (200 mg, 0.678 mmol) according to General Procedure B. The crude product was purified by column chromatography (PE/EtOAc 100:0−50:50) to afford compound **5g** as a bright yellow foam (244 mg, 90%). ^{1}H NMR (d_6-DMSO) δ 9.26 (d, J = 7.3 Hz, 1H), 8.00−7.91 (m, 2H), 7.79−7.66 (m, 4H), 7.61 (d, J = 8.3 Hz, 2H), 7.58−7.53 (m, 1H), 7.51−7.45 (m, 2H), 5.79 (d, J = 7.3 Hz, 1H), 3.69 (s, 3H); ^{19}F NMR (d_6-DMSO) δ −134.8 (d, J = 21.7 Hz), −163.4 (dd, J = 21.6/21.6 Hz); ^{13}C NMR (d_6-DMSO) δ 170.9, 166.5, 150.6 (ddd, J_{CF} = 246.7/9.7/4.2 Hz), 138.4 (dt, J_{CF} = 249.5/15.6 Hz), 136.8, 136.8−136.7 (m), 136.5−136.3 (td, J_{CF} = 8.1/4.4 Hz), 133.5, 131.6, 128.9, 128.2, 127.7, 127.0, 111.6−111.0 (m), 56.4, 52.3; m/z MS $C_{22}H_{17}F_3NO_3$ $[MH]^+$ calcd 400.1, found 400.1.

*Methyl 2-(3-Fluorobenzamido)-2-(3′,4′,5′-trifluoro-[1,1′-biphenyl]-4-yl)acetate (**5h**).* 3-Fluorobenzoic acid (114 mg, 0.812 mmol) was coupled to compound **4** (200 mg, 0.677 mmol) according to General Procedure B. The crude product was purified by column chromatography (PE/EtOAc 100:0−50:50) to afford compound **5h** as a bright yellow foam (243 mg, 86%). ^{1}H NMR (d_6-DMSO) δ 9.35 (d, J = 7.1 Hz, 1H), 7.82−7.66 (m, 6H), 7.60 (d, J = 8.3 Hz, 2H), 7.54 (ddd, J = 8.0/7.9/5.9 Hz, 1H), 7.44−7.38 (m, 1H), 5.77 (d, J = 7.1 Hz, 1H), 3.69 (s, 3H); ^{19}F NMR (d_6-DMSO) δ −112.9, −134.8 (d, J = 21.7 Hz), −163.3 (dd, J = 21.7/21.7 Hz); ^{13}C NMR (d_6-DMSO) δ 170.7, 165.2 (d, J_{CF} = 2.5 Hz), 161.9 (d, J_{CF} = 244.3 Hz), 150.6 (ddd, J_{CF} = 246.7/9.7/4.1 Hz), 138.4 (dt, J_{CF} = 249.5/15.7 Hz), 136.9−136.6 (m), 136.5, 136.4−136.2 (m), 135.7 (d, J_{CF} = 6.9 Hz), 130.4 (d, J_{CF} = 8.0 Hz), 129.0, 127.0, 123.9 (d, J_{CF} = 2.8 Hz), 118.5 (d, J_{CF} = 21.2 Hz), 114.5 (d, J_{CF} = 22.9 Hz), 112.1−110.6 (m), 56.5, 52.4; m/z MS $C_{22}H_{16}F_4NO_3$ $[MH]^+$ calcd 418.1, found 418.1.

*Methyl 2-(4-Fluorobenzamido)-2-(3′,4′,5′-trifluoro-[1,1′-biphenyl]-4-yl)acetate (**5i**).* 4-Fluorobenzoic acid (114 mg, 0.812 mmol) was coupled to compound **4** (200 mg, 0.677 mmol) according to General Procedure B. The crude product was purified by column chromatography (PE/EtOAc 100:0−50:50) to afford compound **5i** as a bright yellow foam (150 mg, 53%). ^{1}H NMR (d_6-DMSO) δ 9.28 (d, J = 7.2 Hz, 1H), 8.08−7.97 (m, 2H), 7.75 (d, J = 8.3 Hz, 2H), 7.72−7.64 (m, 2H), 7.60 (d, J = 8.3 Hz, 2H), 7.34−7.25 (m, 2H), 5.77 (d, J = 7.2 Hz, 1H), 3.69 (s, 3H); ^{19}F NMR (d_6-DMSO) δ −108.8, −134.8 (d, J = 21.6 Hz), −163.4 (dd, J = 21.6/21.6 Hz); ^{13}C NMR (d_6-DMSO) δ 170.8, 165.4, 164.1 (d, J_{CF} = 249.1 Hz), 150.6 (ddd, J_{CF} = 246.8/9.7/4.1 Hz), 138.4 (dt, J_{CF} = 249.6/15.6 Hz), 136.8−136.7 (m), 136.6, 136.4 (td, J_{CF} = 8.1/4.4 Hz), 130.4 (d, J_{CF} = 9.1 Hz), 123.0 (d, J_{CF} = 2.9 Hz), 128.9, 127.0, 115.1 (d, J_{CF} = 21.8 Hz), 111.2 (m), 56.5, 52.3; m/z MS $C_{22}H_{16}F_4NO_3$ $[MH]^+$ calcd 418.1, found 417.8.

*Methyl 2-(3-Methoxybenzamido)-2-(3′,4′,5′-trifluoro-[1,1′-biphenyl]-4-yl)acetate (**5j**).* 3-Methoxybenzoic acid (247 mg, 1.63 mmol) was coupled to compound **4** (400 mg, 1.36 mmol) according to General Procedure B. The crude product was purified by column

DOI: 10.1021/acs.jmedchem.9b00757
J. Med. Chem. XXXX, XXX, XXX−XXX

chromatography (PE/EtOAc 100:0−50:50) to afford compound **5j** as a bright yellow foam (578 mg, 99%). ^{1}H NMR (d_6-DMSO) δ 9.25 (d, J = 7.2 Hz, 1H), 7.75 (d, J = 8.4 Hz, 2H), 7.69 (m, 2H), 7.61 (d, J = 8.3 Hz, 2H), 7.56−7.51 (m, 1H), 7.51−7.48 (m, 1H), 7.39 (t, J = 7.9 Hz, 1H), 7.15−7.09 (m, 1H), 5.78 (d, J = 7.2 Hz, 1H), 3.81 (s, 3H), 3.69 (s, 3H); ^{19}F NMR (d_6-DMSO) δ −134.8 (d, J = 21.7 Hz), −163.3 (dd, J = 21.6/21.6 Hz); ^{13}C NMR (d_6-DMSO) δ 170.9, 166.2, 159.1, 150.6 (ddd, J_{CF} = 246.8/9.8/4.2 Hz), 138.4 (dt, J_{CF} = 249.5/15.6 Hz), 136.9−136.7 (m, 2C), 136.4 (td, J_{CF} = 8.1/4.4 Hz), 134.9, 129.4, 128.9, 127.0, 120.0, 117.5, 112.8, 112.0−110.4 (m), 56.5, 55.3, 52.3; m/z MS $C_{23}H_{19}F_3NO_4$ $[MH]^+$ calcd 430.1, found 429.9.

*Methyl 2-(4-Methoxybenzamido)-2-(3′,4′,5′-trifluoro-[1,1′-biphenyl]-4-yl)acetate (**5k**).* 4-Methoxybenzoic acid (199 mg, 1.31 mmol) was coupled to compound **4** (322 mg, 1.09 mmol) according to General Procedure B. The crude product was purified by column chromatography (PE/EtOAc 100:0−50:50) to afford compound **5k** as a white solid (154 mg, 33%). ^{1}H NMR ($CDCl_3$) δ 7.80 (d, J = 8.9 Hz, 2H), 7.54−7.49 (m, 2H), 7.48−7.42 (m, 2H), 7.29 (d, J = 6.7 Hz, 1H), 7.13 (m, 2H), 6.90 (d, J = 8.9 Hz, 2H), 5.81 (d, J = 6.8 Hz, 1H), 3.82 (s, 3H), 3.78 (s, 3H); ^{19}F NMR ($CDCl_3$) δ −134.0 (d, J = 20.5 Hz), −162.3 (dd, J = 20.5 Hz); ^{13}C NMR ($CDCl_3$) δ 171.5, 166.3, 162.7, 151.5 (ddd, J_{CF} = 249.7/9.9/4.2 Hz), 139.5 (dt, J_{CF} = 252.2/15.5 Hz), 138.6−138.4 (m), 137.2, 136.7 (td, J_{CF} = 7.7/4.6 Hz), 129.2, 128.2, 127.5, 125.7, 113.9, 111.1 (m), 56.6, 55.5, 53.1; m/z MS $C_{23}H_{19}F_3NO_4$ $[MH]^+$ calcd 430.1, found 429.9.

*Methyl 2-(3-Cyanobenzamido)-2-(3′,4′,5′-trifluoro-[1,1′-biphenyl]-4-yl)acetate (**5n**).* Oxalyl chloride (130 μL, 1.51 mmol) was added dropwise to a mixture of 3-carbamoylbenzoic acid (167 mg, 1.01 mmol) in DCM (10 mL) containing a catalytic amount of DMF (20 μL). After stirring the mixture at rt for 1 h, the DCM was concentrated in vacuo. A mixture of DIPEA (126 μL, 1.31 mmol) and compound **4** (300 mg, 1.01 mmol) in DCM (10 mL) was added to the acid chloride. The reaction mixture was stirred at rt for 30 min and then diluted with water (15 mL) and extracted with DCM (3 × 10 mL). The combined organic layers were dried over Na_2SO_4, filtered, and concentrated in vacuo. LC−MS of the crude product indicated dehydration of the carboxamide group occurred to form a cyano analogue. The crude product was purified by column chromatography (PE/EtOAc 100:0−0:100) to afford compound **5n** as a clear oil (383 mg, 89%). ^{1}H NMR ($CDCl_3$) δ 8.12 (s, 1H), 8.06 (d, J = 7.9 Hz, 1H), 7.80 (d, J = 7.8 Hz, 1H), 7.58 (t, J = 7.7 Hz, 1H), 7.54−7.48 (m, 4H), 7.44 (d, J = 6.7 Hz, 1H), 7.19−7.10 (m, 2H), 5.79 (d, J = 6.7 Hz, 1H), 3.81 (s, 3H); ^{19}F NMR ($CDCl_3$) δ −133.7 (d, J = 20.6 Hz), −161.9 (dd, J = 20.6/20.6 Hz); ^{13}C NMR ($CDCl_3$) δ 171.1, 164.7, 151.6 (ddd, J_{CF} = 250.0/10.1/4.2 Hz), 139.6 (dt, J_{CF} = 252.4/15.4 Hz), 138.9−138.7 (m), 136.6−136.5 (m), 136.4, 135.3, 134.7, 131.5, 131.2, 129.8, 128.2, 127.7, 117.9, 113.2, 112.0−110.2 (m), 56.8, 53.4; m/z MS $C_{23}H_{14}F_3N_2O_3$ $[M - H]^-$ calcd 423.1, found 423.1.

*Methyl 2-(4-Cyanobenzamido)-2-(3′,4′,5′-trifluoro-[1,1′-biphenyl]-4-yl)acetate (**5o**).* Oxalyl chloride (130 μL, 1.51 mmol) was added dropwise to a mixture of 4-carbamoylbenzoic acid (167 mg, 1.01 mmol) in DCM (10 mL) containing a catalytic amount of DMF (20 μL). After stirring the mixture at rt for 1 h, the DCM was removed in vacuo. A mixture of DIPEA (126 μL, 1.31 mmol) and compound **4** (300 mg, 1.01 mmol) in DCM (10 mL) was added to the acid chloride. The reaction mixture was stirred at rt for 30 min, then diluted with water (15 mL), and extracted with DCM (3 × 10 mL). The combined organic layers were dried over anhydrous Na_2SO_4, filtered, and concentrated in vacuo. LC−MS of the crude product indicated dehydration of the carboxamide group occurred to form a cyano analogue. The crude product was purified by column chromatography (PE/EtOAc 100:0−0:100) to afford compound **5o** as a yellow oil (185 mg, 43%). ^{1}H NMR ($CDCl_3$) δ 7.98−7.73 (m, 4H), 7.54−7.45 (m, 4H), 7.34 (app. t, J = 6.6 Hz, 1H), 7.19−7.11 (m, 2H), 5.79 (d, J = 6.6 Hz, 1H), 3.81 (s, 3H); ^{19}F NMR ($CDCl_3$) δ −133.7 (d, J = 20.5 Hz), −161.9 (dd, J = 20.5/20.5 Hz); ^{13}C NMR ($CDCl_3$) δ 171.1, 164.9, 151.6 (ddd, J_{CF} = 250.0/10.1/4.3 Hz), 139.6 (dt, J_{CF} = 252.5/15.3 Hz), 139.0−138.8 (m), 137.4, 136.8−136.3 (m, 2C), 132.7, 128.2, 128.0, 127.7, 118.0, 115.8, 111.9−110.6 (m), 56.7, 53.5; m/z MS $C_{23}H_{16}F_3N_2O_3$ $[MH]^+$ calcd 425.1, found 425.1.

*Methyl 2-(3-Carbamoylbenzamido)-2-(3′,4′,5′-trifluoro-[1,1′-biphenyl]-4-yl)acetate (**5r**).* 3-Carbamoylbenzoic acid (205 mg, 1.24 mmol) was coupled to compound **4** (332 mg, 1.13 mmol) according to General Procedure A. The crude product was purified by column chromatography (PE/EtOAc 50:50−0:100) to afford compound **5r** as a light yellow solid (328 mg, 66%). ^{1}H NMR (d_6-DMSO) δ 9.37 (d, J = 7.1 Hz, 1H), 8.42 (t, J = 1.6 Hz, 1H), 8.07 (br s, 1H), 8.06−7.99 (m, 2H), 7.78−7.69 (m, 4H), 7.64−7.54 (m, 3H), 7.50 (br s, 1H), 5.78 (d, J = 7.1 Hz, 1H), 3.69 (s, 3H); ^{19}F NMR (d_6-DMSO) δ −134.8 (d, J = 21.7 Hz), −163.3 (dd, J = 21.7/21.7 Hz); ^{13}C NMR (d_6-DMSO) δ 170.9, 167.5, 166.2, 150.7 (ddd, J_{CF} = 246.6/9.7/4.1 Hz), 138.4 (dt, J_{CF} = 249.5/15.6 Hz), 136.9−136.8 (m), 136.7, 136.4 (td, J_{CF} = 8.1/4.4 Hz), 134.5, 133.6, 130.5, 130.4, 129.0, 128.4, 127.1, 126.9, 112.9−109.9 (m), 56.6, 52.5; m/z MS $C_{23}H_{18}F_3N_2O_4$ $[MH]^+$ calcd 443.1, found 443.1.

*Methyl 2-(4-Carbamoylbenzamido)-2-(3′,4′,5′-trifluoro-[1,1′-biphenyl]-4-yl)acetate (**5s**).* 4-Carbamoylbenzoic acid (246 mg, 1.49 mmol) was coupled to compound **4** (400 mg, 1.35 mmol) according to General Procedure A. The crude product was purified by column chromatography (PE/EtOAc 50:50−0:100) to afford compound **5s** as a light yellow solid (383 mg, 64%). ^{1}H NMR (d_6-DMSO) δ 9.38 (d, J = 7.2 Hz, 1H), 8.10 (br s, 1H), 8.02−7.91 (m, 4H), 7.84−7.68 (m, 4H), 7.60 (d, J = 8.3 Hz, 2H), 7.52 (br s, 1H), 5.77 (d, J = 7.1 Hz, 1H), 3.68 (s, 3H); ^{19}F NMR (d_6-DMSO) δ −134.8 (d, J = 21.8 Hz), −163.2 (dd, J = 21.7/21.7 Hz); ^{13}C NMR (d_6-DMSO) δ 170.8, 167.2, 165.9, 150.6 (ddd, J_{CF} = 246.4/9.5/4.1 Hz), 138.4 (dt, J_{CF} = 249.8/15.7 Hz), 136.9, 136.4 (td, J_{CF} = 8.2/5.5 Hz), 135.8−135.7 (m), 133.4, 132.2, 129.0, 127.7, 127.4, 127.1, 111.6−111.1 (m), 56.5, 52.5; m/z MS $C_{23}H_{18}F_3N_2O_4$ $[MH]^+$ calcd 443.1, found 443.1.

*Methyl 2-(4-(Methylcarbamoyl)benzamido)-2-(3′,4′,5′-trifluoro-[1,1′-biphenyl]-4-yl)acetate (**5t**).* 4-(Methylcarbamoyl)benzoic acid (97.3 mg, 0.504 mmol) was coupled to compound **4** (107 mg, 0.364 mmol) according to General Procedure B. Upon completion, the mixture was added to a 0.1 M HCl solution (50 mL) and extracted with EtOAc (3 × 50 mL). The combined organic layers were washed with brine (50 mL), dried over anhydrous Na_2SO_4, filtered, and concentrated under reduced pressure. The residue was then taken up in minimal DMF and added to an ice−water mixture. The precipitate was filtered and washed with minimal MeOH to afford compound **5t** as a yellow solid (98.4 mg, 59%). ^{1}H NMR (d_6-DMSO) δ 9.38 (d, J = 7.1 Hz, 1H), 8.57 (d, J = 4.5 Hz, 1H), 8.04−7.96 (m, 2H), 7.92 (d, J = 8.4 Hz, 2H), 7.79−7.67 (m, 4H), 7.60 (d, J = 8.3 Hz, 2H), 5.78 (d, J = 7.1 Hz, 1H), 3.69 (s, 3H), 2.80 (d, J = 4.5 Hz, 3H); ^{19}F NMR (d_6-DMSO) δ −134.8 (d, J = 21.7 Hz), −163.3 (dd, J = 21.7/21.7 Hz); ^{13}C NMR (d_6-DMSO) δ 170.8, 166.0 (2C), 150.7 (ddd, J_{CF} = 246.4/9.7/4.2 Hz), 139.9−137.1 (m), 137.2, 136.9 (br s), 136.6, 136.5−136.4 (m), 129.0, 127.8, 127.1, 127.0, 112.7−108.5 (m), 56.6, 52.5, 26.3; m/z MS $C_{24}H_{20}F_3N_2O_4$ $[MH]^+$ calcd 457.1, found 456.8.

*Methyl 2-(4-(Dimethylcarbamoyl)benzamido)-2-(3′,4′,5′-trifluoro-[1,1′-biphenyl]-4-yl)acetate (**5u**).* 4-(Dimethylcarbamoyl)-benzoic acid (102 mg, 0.491 mmol) was coupled to compound **4** (114 mg, 0.385 mmol) according to General Procedure B. Upon completion, the mixture was added to a 0.1 M HCl solution (50 mL) and extracted with EtOAc (3 × 50 mL). The combined organic layers were washed with brine (50 mL), dried over anhydrous Na_2SO_4, filtered, and concentrated under reduced pressure. The residue was then taken up in minimal DMF and added to an ice−water mixture. The precipitate was filtered and washed with minimal MeOH to afford compound **5u** as a white solid (92.0 mg, 51%) ^{1}H NMR (d_6-DMSO) δ 9.36 (d, J = 7.2 Hz, 1H), 8.07−7.86 (m, 2H), 7.79−7.68 (m, 4H), 7.60 (d, J = 8.3 Hz, 2H), 7.53−7.46 (m, 2H), 5.77 (d, J = 7.2 Hz, 1H), 3.68 (s, 3H), 2.99 (s, 3H), 2.88 (s, 3H); ^{19}F NMR (d_6-DMSO) δ −134.8 (d, J = 21.7 Hz), −163.3 (dd, J = 21.8/21.8 Hz); ^{13}C NMR (d_6-DMSO) δ 171.0, 169.7, 166.3, 150.8 (ddd, J_{CF} = 14.1/9.4/3.6 Hz), 139.9−137.2 (m), 139.7, 137.0 (d, J_{CF} = 1.5 Hz), 136.8, 136.69−136.36 (m), 134.2, 129.2, 128.0, 127.2, 127.0, 111.4 (dd, J_{CF} = 16.2/5.3 Hz), 56.7, 52.6, 34.9; m/z MS $C_{25}H_{22}F_3N_2O_4$ $[MH]^+$ calcd 471.2, found 470.9.

DOI: 10.1021/acs.jmedchem.9b00757
J. Med. Chem. XXXX, XXX, XXX−XXX

*Methyl 2-(4-(Ethylcarbamoyl)benzamido)-2-(3′,4′,5′-trifluoro-[1,1′-biphenyl]-4-yl)acetate (**5v**).* Carboxylic acid **12** (102 mg, 0.491 mmol) was coupled to compound **4** (114 mg, 0.385 mmol) according to General Procedure B. Upon completion, the mixture was added to a 0.1 M HCl solution (50 mL) and extracted with EtOAc (3 × 50 mL). The combined organic layers were washed with brine (50 mL), dried over anhydrous Na_2SO_4, filtered, and concentrated under reduced pressure. The residue was then taken up in minimal DMF and added to an ice−water mixture. The precipitate was filtered and washed with minimal MeOH to afford compound **5v** as a yellow solid (92.0 mg, 51%). ^{1}H NMR (d_6-DMSO) δ 9.39 (d, J = 7.1 Hz, 1H), 8.61 (t, J = 5.5 Hz, 1H), 8.03−7.98 (m, 2H), 7.93 (d, J = 8.4 Hz, 2H), 7.76 (d, J = 8.3 Hz, 2H), 7.71 (dd, J = 9.4, 6.8 Hz, 2H), 7.61 (d, J = 8.3 Hz, 2H), 5.78 (d, J = 7.1 Hz, 1H), 3.69 (s, 3H), 3.34−3.26 (m, 2H), 1.14 (t, J = 7.2 Hz, 3H); ^{19}F NMR (d_6-DMSO) δ −134.8 (d, J = 21.7 Hz), −163.3 (dd, J = 21.7/21.7 Hz); ^{13}C NMR (d_6-DMSO) δ 170.8, 165.9, 165.2, 150.6 (ddd, J_{CF} = 246.8/9.6/4.4 Hz), 138.4 (dt, J_{CF} = 33.6/15.7 Hz), 137.3, 136.8, 136.6, 136.4 (td, J_{CF} = 8.1/4.6 Hz), 129.0, 127.7, 127.07, 127.05, 111.3 (dd, J_{CF} = 15.9/5.5 Hz), 56.5, 52.4, 34.2, 14.7; m/z MS $C_{25}H_{22}F_3N_2O_4$ $[MH]^+$ calcd 471.2, found 470.9.

*Methyl 2-(4-(Isopropylcarbamoyl)benzamido)-2-(3′,4′,5′-trifluoro-[1,1′-biphenyl]-4-yl)acetate (**5w**).* 4-(Isopropylcarbamoyl)-benzoic acid (119 mg, 0.573 mmol) was coupled to compound **4** (118 mg, 0.401 mmol) according to General Procedure B. Upon completion, the mixture was added to a 0.1 M HCl solution (50 mL) and extracted with EtOAc (3 × 50 mL). The combined organic layers were washed with brine (50 mL), dried over anhydrous Na_2SO_4, filtered, and concentrated under reduced pressure. The residue was then taken up in minimal DMF and added to an ice−water mixture. The precipitate was filtered and washed with minimal MeOH to afford compound **5w** as a white solid (177 mg, 91%). ^{1}H NMR (d_6-DMSO) δ 9.40 (d, J = 7.1 Hz, 1H), 8.37 (d, J = 7.7 Hz, 1H), 8.02 (d, J = 8.5 Hz, 2H), 7.95 (d, J = 8.4 Hz, 2H), 7.76 (d, J = 8.3 Hz, 2H), 7.69 (dd, J = 9.3, 6.8 Hz, 2H), 7.62 (d, J = 8.3 Hz, 2H), 5.80 (d, J = 7.1 Hz, 1H), 4.22−4.00 (m, 1H), 3.70 (s, 3H), 1.18 (d, J = 6.6 Hz, 6H); ^{19}F NMR (d_6-DMSO) δ −130.0 (d, J = 21.6 Hz), −158.5 (dd, J = 21.6/21.6 Hz); ^{13}C NMR (d_6-DMSO) δ 170.90, 166.0, 164.7, 153.0−148.6 (m), 138.4 (dt, J_{CF} = 30.9/13.8 Hz), 137.5, 136.9, 136.6, 136.5−136.3 (m), 135.5, 129.0, 127.7, 127.2, 127.1, 111.3 (dd, J_{CF} = 18.9/2.5 Hz), 56.6, 52.4, 41.2, 22.3; m/z MS $C_{26}H_{24}F_3N_2O_4$ $[MH]^+$ calcd 485.2, found 484.9.

*Methyl 2-(4-((2-Hydroxyethyl)carbamoyl)benzamido)-2-(3′,4′,5′-trifluoro-[1,1′-biphenyl]-4-yl)acetate (**5x**).* A sealed vessel containing (1-cyano-2-ethoxy-2-oxoethylidenaminooxy)-dimethylamino-morpholino-carbenium hexafluorophosphate (2.23 g, 0.584 mmol), triethylamine (1.10 mL, 7.89 mmol), carboxylic acid **14** (746 mg, 3.56 mmol), and compound **4** (761 mg, 2.58 mmol) was purged twice with nitrogen and charged with DMF (5 mL). The reaction mixture was allowed to stir at rt overnight. The mixture was then added to a half saturated $NaHCO_3$ solution (80 mL) and extracted with EtOAc (3 × 80 mL). The combined organic layers were washed with brine (50 mL), dried over anhydrous Na_2SO_4, filtered, and concentrated under reduced pressure. The residue was then taken up in minimal DMF and added to an ice−water mixture. The precipitate was filtered and washed with minimal MeOH and further purified by column chromatography (DCM/MeOH 98:2−94:6) to afford compound **5x** as a cream solid after lyophilization (182 mg, 14%). ^{1}H NMR (d_6-DMSO) δ 9.41 (d, J = 7.2 Hz, 1H), 8.61 (t, J = 5.7 Hz, 1H), 8.06−7.99 (m, 2H), 8.00−7.93 (m, 2H), 7.78−7.72 (m, 2H), 7.67 (dd, J = 9.4, 6.6 Hz, 2H), 7.65−7.58 (m, 2H), 5.80 (d, J = 7.1 Hz, 1H), 4.81 (br s, 1H), 3.70 (s, 3H), 3.56 (t, J = 6.2 Hz, 2H), 3.38 (q, J = 6.0, 2H); ^{19}F NMR (d_6-DMSO) δ −134.8 (d, J = 21.8 Hz), −163.2 (dd, J = 21.7/21.7 Hz); ^{13}C NMR (d_6-DMSO) δ 170.9, 166.1, 165.8, 150.7 (ddd, J_{CF} = 246.8/9.7/4.2 Hz), 138.5 (dt, J_{CF} = 30.6/12.4 Hz), 137.3, 137.0, 136.7, 136.5 (td, J_{CF} = 8.1/4.4 Hz), 135.7, 129.1, 127.8, 127.3, 127.1, 111.3 (dd, J_{CF} = 16.0/5.5 Hz), 59.8, 56.7, 52.5, 42.4; m/z MS $C_{25}H_{22}F_3N_2O_5$ $[MH]^+$ calcd 487.1, found 486.8.

*Methyl 2-(4-Sulfamoylbenzamido)-2-(3′,4′,5′-trifluoro-[1,1′-biphenyl]-4-yl)acetate (**5y**).* 4-Carboxybenzenesulfonamide (274 mg, 1.36 mmol) was coupled to compound **4** (290 mg, 0.981 mmol) according to General Procedure B. Upon completion, the mixture was added to a 0.1 M HCl solution (50 mL) and extracted with EtOAc (3 × 50 mL). The combined organic layers were washed with brine (50 mL), dried over anhydrous Na_2SO_4, filtered, and concentrated under reduced pressure. The residue was then taken up in minimal DMF and added to an ice−water mixture. The fine precipitate was centrifuged, the supernatant removed, and the solid resuspended in EtOAc twice to afford compound **5y** as a light yellow solid after lyophilization (101 mg, 22%). ^{1}H NMR (d_6-DMSO) δ 9.46 (d, J = 7.1 Hz, 1H), 8.07 (d, J = 8.4 Hz, 2H), 7.91 (d, J = 8.3 Hz, 2H), 7.79−7.69 (m, 4H), 7.60 (d, J = 8.2 Hz, 2H), 7.51 (s, 2H), 5.76 (d, J = 7.0 Hz, 1H), 3.68 (s, 3H); ^{19}F NMR (d_6-DMSO) δ −134.8 (d, J = 21.4 Hz), −163.2 (dd, J = 21.5/21.5 Hz); ^{13}C NMR (d_6-DMSO) δ 171.2, 166.1, 151.1 (ddd, J_{CF} = 13.9/9.3/3.7 Hz), 147.1, 140.8−137.5 (m), 137.4, 136.9, 136.8, 129.5, 128.9, 127.5, 126.1, 111.8 (dd, J_{CF} = 16.0/5.4 Hz), 57.1, 52.9; m/z MS $C_{22}H_{18}F_3N_2O_5S$ $[MH]^+$ calcd 479.1, found 478.8.

*Methyl 2-(3-((tert-Butoxycarbonyl)amino)benzamido)-2-(3′,4′,5′-trifluoro-[1,1′-biphenyl]-4-yl)acetate (**5z**).* 3-((*tert*-Butoxycarbonyl)amino)benzoic acid (289 mg, 1.22 mmol) was coupled to compound **4** (300 mg, 1.02 mmol) according to General Procedure B. The crude product was purified by column chromatography (PE/EtOAc 100:0−50:50) to afford compound **5z** as a yellow oil (353 mg, 67%). ^{1}H NMR (d_6-DMSO) δ 9.48 (s, 1H), 9.17 (d, J = 7.3 Hz, 1H), 7.99 (m, 1H), 7.78−7.66 (m, 4H), 7.63−7.56 (m, 3H), 7.54−7.48 (m, 1H), 7.34 (t, J = 7.9 Hz, 1H), 5.74 (d, J = 7.1 Hz, 1H), 3.68 (s, 3H), 1.48 (s, 9H); ^{19}F NMR (d_6-DMSO) δ −134.8 (d, J = 21.7 Hz), −163.4 (dd, J = 21.7/21.7 Hz); ^{13}C NMR (d_6-DMSO) δ 170.8, 166.7, 152.8, 150.6 (ddd, J_{CF} = 246.7/9.7/4.3 Hz), 139.9−136.9 (m) (2C), 136.8, 136.7−136.6 (m), 136.4 (td, J_{CF} = 8.1/4.4 Hz), 134.3, 128.9, 128.4, 127.0, 121.2, 121.2, 117.8, 113.1−110.3 (m), 79.2, 56.4, 52.3, 28.1; m/z MS $C_{27}H_{26}F_3N_2O_5$ $[MH]^+$ calcd 515.2, found 515.1.

*Methyl 2-(4-((tert-Butoxycarbonyl)amino)benzamido)-2-(3′,4′,5′-trifluoro-[1,1′-biphenyl]-4-yl)acetate (**5aa**).* 4-((*tert*-Butoxycarbonyl)amino)benzoic acid (289 mg, 1.22 mmol) was coupled to compound **4** (300 mg, 1.02 mmol) according to General Procedure B. The crude product was purified by column chromatography (PE/EtOAc 100:0−50:50) to afford compound **5aa** as a bright yellow foam (370 mg, 70%). ^{1}H NMR (d_6-DMSO) δ 9.62 (s, 1H), 9.04 (d, J = 7.2 Hz, 1H), 7.86 (d, J = 8.8 Hz, 2H), 7.78−7.67 (m, 4H), 7.58 (d, J = 8.3 Hz, 2H), 7.53 (d, J = 8.8 Hz, 2H), 5.74 (d, J = 8.5 Hz, 1H), 3.67 (s, 3H), 1.48 (s, 9H); ^{19}F NMR (d_6-DMSO) δ −134.8 (d, J = 21.7 Hz), −163.3 (dd, J = 21.7/21.7 Hz); ^{13}C NMR (d_6-DMSO) δ 171.0, 166.0, 152.6, 150.6 (ddd, J_{CF} = 246.5/9.7/4.1 Hz), 142.7, 138.4 (dt, J_{CF} = 249.9/15.7 Hz), 136.9, 136.8−136.6 (m), 136.4 (td, J_{CF} = 8.1/4.3 Hz), 128.9, 128.6, 127.0, 126.7, 117.0, 111.5−111.0 (m), 79.5, 56.4, 52.3, 28.0; m/z MS $C_{27}H_{24}F_3N_2O_5$ $[M - H]^-$ calcd 513.2, found 512.9.

*Methyl 2-(4-(Methylsulfonamido)benzamido)-2-(3′,4′,5′-trifluoro-[1,1′-biphenyl]-4-yl)acetate (**5ad**).* 4-((Methyl)-sulfonylamino)benzoic acid (106 mg, 0.494 mmol) was coupled to compound **4** (118 mg, 0.401 mmol) according to General Procedure B. Upon completion, the mixture was added to a 0.1 M HCl solution (50 mL) and extracted with EtOAc (3 × 50 mL). The combined organic layers were washed with brine (50 mL), dried over anhydrous Na_2SO_4, filtered, and concentrated under reduced pressure. The residue was then taken up in minimal DMF and added to an ice−water mixture. The precipitate was filtered and washed with minimal MeOH to afford compound **5ad** as a light yellow solid (142 mg, 72%). ^{1}H NMR (d_6-DMSO) δ 10.14 (s, 1H), 9.14 (d, J = 7.2 Hz, 1H), 7.95−7.88 (m, 2H), 7.78−7.68 (m, 4H), 7.58 (d, J = 8.3 Hz, 2H), 7.30−7.18 (m, 2H), 5.74 (d, J = 7.2 Hz, 1H), 3.67 (s, 3H), 3.07 (s, 3H); ^{19}F NMR (d_6-DMSO) δ −134.8 (d, J = 21.8 Hz), −163.3 (dd, J = 21.7/21.7 Hz); ^{13}C NMR (d_6-DMSO) δ 171.0, 165.9, 150.7 (ddd, J_{CF} = 246.7/9.7/4.2 Hz), 141.6, 136.8−136.7(m), 136.8, 136.4 (td, J_{CF} = 7.8/4.2 Hz), 129.2, 129.0, 128.2, 127.0, 117.9, 111.3 (dd,

DOI: 10.1021/acs.jmedchem.9b00757
J. Med. Chem. XXXX, XXX, XXX−XXX

J_{CF} = 16.0/5.5 Hz), 56.5, 52.4, 40.6; *m/z* MS $C_{23}H_{20}F_3N_2O_5S$ $[MH]^+$ calcd 493.1, found 492.8.

*Methyl 2-(4-(Sulfamoylamino)benzamido)-2-(3′,4′,5′-trifluoro-[1,1′-biphenyl]-4-yl)acetate (**5ae**).* Carboxylic acid **15** (160 mg, 0.742 mmol) was coupled to compound **4** (191 mg, 0.645 mmol) according to General Procedure B. Upon completion, the mixture was added to a 0.1 M HCl solution (50 mL) and extracted with EtOAc (3 × 50 mL). The combined organic layers were washed with brine (50 mL), dried over anhydrous Na_2SO_4, filtered, and concentrated under reduced pressure. The residue was then taken up in minimal DMF and added to an ice−water mixture. The precipitate was sonicated in Et_2O for 10 min and then centrifuged. The supernatant was removed and the solid resuspended in Et_2O twice to afford compound **5ae** as a cream solid (170 mg, 53%). ^{1}H NMR (d_6-DMSO) δ 9.94 (s, 1H), 9.05 (d, J = 7.2 Hz, 1H), 7.86 (d, J = 8.8 Hz, 2H), 7.80−7.63 (m, 4H), 7.58 (d, J = 8.3 Hz, 2H), 7.29 (s, 2H), 7.18 (d, J = 8.8 Hz, 2H), 5.73 (d, J = 7.2 Hz, 1H), 3.67 (s, 3H); ^{19}F NMR (d_6-DMSO) δ −134.8 (d, J = 21.7 Hz), −163.3 (dd, J = 21.7/21.7 Hz); ^{13}C NMR (d_6-DMSO) δ 171.1, 166.1, 150.7 (ddd, J_{CF} = 246.3/9.6/4.0 Hz), 142.8, 138.5 (dt, J_{CF} = 30.9/15.2 Hz), 137.0, 136.8, 136.5 (td, J_{CF} = 8.1/4.4 Hz), 129.0, 128.9, 127.0, 126.3, 116.3, 111.3 (dd, J_{CF} = 16.0/5.4 Hz), 56.5, 52.4; *m/z* MS $C_{22}H_{19}F_3N_3O_5S$ $[MH]^+$ calcd 494.1, found 493.8.

*Methyl 2-(3,4-Dimethoxybenzamido)-2-(3′,4′,5′-trifluoro-[1,1′-biphenyl]-4-yl)acetate (**5af**).* 3,4-Dimethoxybenzoic acid (148 mg, 0.813 mmol) was coupled to compound **4** (200 mg, 0.677 mmol) according to General Procedure B. The crude product was purified by column chromatography (PE/EtOAc 100:0−50:50) to afford compound **5af** as a bright yellow foam (233 mg, 75%). ^{1}H NMR (d_6-DMSO) δ 9.10 (d, J = 7.1 Hz, 1H), 7.80−7.65 (m, 4H), 7.64−7.56 (m, 3H), 7.53 (d, J = 2.0 Hz, 1H), 7.03 (d, 7.1 Hz, 1H), 5.76 (d, J = 7.2 Hz, 1H), 3.82 (s, 3H), 3.81 (s, 3H), 3.69 (s, 3H); ^{19}F NMR (d_6-DMSO) δ −134.8 (d, J = 21.7 Hz), −163.3 (dd, J = 21.7/21.7 Hz); ^{13}C NMR (d_6-DMSO) δ 171.1, 165.9, 151.7, 150.6 (ddd, J_{CF} = 246.7/9.7/4.2 Hz), 148.2, 138.4 (dt, J_{CF} = 249.7/15.7 Hz), 136.9, 136.8−136.7 (m), 136.4 (td, J_{CF} = 8.1/4.5 Hz), 129.0, 127.0, 125.6, 121.3, 111.4−111.1 (m), 111.0, 110.8, 56.5, 55.60, 55.58, 52.3; *m/z* MS $C_{24}H_{21}F_3NO_5$ $[MH]^+$ calcd 460.1, found 460.1.

*Methyl 2-(1H-Indole-5-carboxamido)-2-(3′,4′,5′-trifluoro-[1,1′-biphenyl]-4-yl)acetate (**5aj**).* 1*H*-Indole-5-carboxylic acid (98 mg, 0.610 mmol) was coupled to compound **4** (150 mg, 0.508 mmol) according to General Procedure B. Upon completion, the DCM was concentrated in vacuo. The solution was quenched with a 1 M HCl solution and extracted with EtOAc (1 × 30 mL). The organic phase was then washed with a saturated $NaHCO_3$ solution (20 mL) and finally brine (20 mL). The organic phase was dried over anhydrous Na_2SO_4, filtered, and concentrated in vacuo. The crude product was purified by flash column chromatography (PE/EtOAc 100:0−60:40) to afford compound **5aj** as a maroon solid (220 mg, 99%). ^{1}H NMR (MeOD) δ 8.19 (dd, J = 1.7/0.5 Hz, 1H), 7.69−7.58 (m, 5H), 7.46−7.39 (m, 3H), 7.32 (d, J = 3.2 Hz, 1H), 6.56 (dd, J = 3.2/0.8 Hz, 1H), 5.81 (s, 1H), 3.77 (s, 3H); ^{19}F NMR (MeOD) δ −136.9 (d, J = 19.8 Hz), −166.0 (dd, J = 19.8/19.8 Hz); ^{13}C NMR (MeOD) δ 172.8, 171.4, 152.6 (ddd, J_{CF} = 247.8/9.8/4.1 Hz), 141.9−139.2 (m), 139.7, 139.2, 138.5−138.3 (m), 138.3, 129.8 (2C), 129.0, 128.3 (2C), 127.3, 125.6, 121.9, 121.9, 112.3−112.0 (m, 3C), 103.7, 58.4, 53.2; *m/z* MS (system A) $C_{24}H_{16}F_3N_2O_3$ $[M - H]^-$ calcd 437.1, found 437.1.

*Methyl 2-(1H-Indazole-5-carboxamido)-2-(3′,4′,5′-trifluoro-[1,1′-biphenyl]-4-yl)acetate (**5ak**).* 1*H*-Indazole-5-carboxylic acid (59 mg, 0.366 mmol) was coupled to compound **4** (90 mg, 0.305 mmol) according to General Procedure B. Upon completion, the DCM was concentrated in vacuo. The solution was quenched with a 1 M HCl solution and extracted with EtOAc (1 × 30 mL). The organic phase was then washed with a saturated $NaHCO_3$ solution (20 mL) and finally brine (20 mL). The organic phase was dried over anhydrous Na_2SO_4, filtered, and concentrated in vacuo. The crude product was purified by flash chromatography (PE/EtOAc 100:0−40:60) to afford compound **5ak** as a white solid (76 mg, 57%). ^{1}H NMR (d_6-DMSO) δ 9.24 (d, J = 7.2 Hz, 1H), 8.46 (s, 1H), 8.22 (s, 1H), 7.91 (dd, J = 8.8/1.5 Hz, 1H), 7.80−7.68 (m, 5H), 7.65−7.56 (m, 3H), 5.79 (d, J = 7.2 Hz, 1H), 3.69 (s, 3H); ^{19}F NMR (d_6-DMSO) δ −134.8 (d, J = 21.7 Hz), −163.3 (dd, J = 21.7/21.7 Hz); ^{13}C NMR (d_6-DMSO) δ 171.0, 166.8, 150.6 (ddd, J_{CF} = 246.7/9.7/4.1 Hz), 141.0, 139.8−136.9 (m), 136.9, 136.7, 136.6−136.3 (m), 134.9, 128.9 (2C), 127.0 (2C), 126.0, 125.7, 122.3, 121.4, 111.3 (dd, J_{CF} = 16.1/5.4 Hz), 109.7, 56.5, 52.3; *m/z* MS $C_{23}H_{17}F_3N_3O_3$ $[MH]^+$ calcd 440.1, found 439.8.

*Methyl 2-(1H-Benzo[d][1,2,3]triazole-5-carboxamido)-2-(3′,4′,5′-trifluoro-[1,1′-biphenyl]-4-yl)acetate (**5al**).* 1*H*-Benzo[*d*]-[1,2,3]triazole-5-carboxylic acid (60 mg, 0.366 mmol) was coupled to compound **4** (90 mg, 0.305 mmol) according to General Procedure B. Upon completion, the DCM was concentrated in vacuo. The solution was quenched with a 1 M HCl solution and extracted with EtOAc (1 × 30 mL). The organic phase was then washed with a saturated $NaHCO_3$ solution (20 mL) and finally brine (20 mL). The organic phase was dried over anhydrous Na_2SO_4, filtered, and concentrated in vacuo. The crude product was purified by flash chromatography (PE/EtOAc 100:0−40:60) to afford compound **5al** as a white solid (100 mg, 75%). ^{1}H NMR (MeOD) δ 8.47 (s, 1H), 7.98 (dd, J = 8.7/1.5 Hz, 1H), 7.88 (d, J = 8.7 Hz, 1H), 7.66−7.56 (m, 4H), 7.43−7.35 (m, 2H), 5.82 (s, 1H), 3.78 (s, 3H); ^{19}F NMR (MeOD) δ −136.8 (d, J = 19.9 Hz), −165.8 (dd, J = 19.8/19.8 Hz); ^{13}C NMR (MeOD) δ 172.5, 169.5, 152.7 (ddd, J_{CF} = 248.0/9.9/4.2 Hz), 141.9−139.0 (m), 139.5, 139.2, 138.5−138.2 (m), 137.8,[a] 132.5, 129.9 (2C), 129.8, 128.4, 128.4 (2C), 126.8, 112.4−112.1 (m, 2C), 58.6, 53.2; *m/z* MS $C_{22}H_{16}F_3N_4O_3$ $[MH]^+$ calcd 441.1, found 440.8.

*Methyl 2-(1H-Benzo[d]imidazole-5-carboxamido)-2-(3′,4′,5′-trifluoro-[1,1′-biphenyl]-4-yl)acetate (**5am**).* 1*H*-Benzo[*d*]imidazole-5-carboxylic acid (99 mg, 0.610 mmol) was coupled to compound **4** (150 mg, 0.508 mmol) according to General Procedure B. Upon completion, the DCM was concentrated in vacuo. The solution was quenched with a 1 M HCl solution and extracted with EtOAc (1 × 30 mL). The organic phase was then washed with a saturated $NaHCO_3$ solution (20 mL) and finally brine. The organic phase was dried over anhydrous Na_2SO_4, filtered, and concentrated in vacuo. The crude product was purified by flash column chromatography (DCM/MeOH 100:0−90:10) to afford compound **5am** as a dull yellow/brown solid (174 mg, 78%). ^{1}H NMR (MeOD) δ 8.30 (s, 1H), 8.21 (d, J = 1.1 Hz, 1H), 7.83 (dd, J = 8.5/1.6 Hz, 1H), 7.69−7.58 (m, 5H), 7.45−7.37 (m, 2H), 5.81 (s, 1H), 3.78 (s, 3H); ^{19}F NMR (MeOD) δ −136.8 (d, J = 19.8 Hz), −165.9 (dd, J = 19.8/19.8 Hz); ^{13}C NMR (MeOD) δ 172.6, 170.3, 152.6 (ddd, J_{CF} = 248.1/10.0/4.1 Hz), 144.8, 141.0−140.8 (m), 141.8−138.8 (m), 139.3, 139.1, 138.6−138.1 (m), 137.9, 129.8 (2C), 129.5, 128.3 (2C), 123.5, 116.9, 115.8, 112.1 (m, 2C), 58.5, 53.3; *m/z* MS (system A) $C_{23}H_{17}F_3N_3O_3$ $[MH]^+$ calcd 440.1, found 439.8.

*Methyl 2-(2-Oxoindoline-5-carboxamido)-2-(3′,4′,5′-trifluoro-[1,1′-biphenyl]-4-yl)acetate (**5an**).* 2-Oxoindoline-5-carboxylic acid (72 mg, 0.406 mmol) was coupled to compound **4** (100 mg, 0.339 mmol) in DMF according to General Procedure B. Upon completion, the reaction mixture was poured onto ice-cold water. The precipitate was filtered and washed thoroughly with water and Et_2O to afford compound **5an** as a brown solid (152 mg, 99%). ^{1}H NMR (MeOD) δ 7.83−7.76 (m, 2H), 7.67−7.62 (m, 2H), 7.59−7.55 (m, 2H), 7.42 (dd, J = 9.3/6.6 Hz, 2H), 6.94 (dd, J = 8.1/0.5 Hz, 1H), 5.76 (s, 1H), 3.76 (s, 3H); ^{19}F NMR (MeOD) δ −136.8 (d, J = 19.8/19.8 Hz), −165.9 (dd, J = 19.8/19.8 Hz); ^{13}C NMR (MeOD) δ 179.9, 172.6, 169.7, 152.7 (ddd, J_{CF} = 248.0/10.0/4.1 Hz), 148.3, 141.9−138.9 (m), 139.4−139.1 (m), 138.4−138.2 (m), 138.0, 129.8 (2C), 129.5, 128.6, 128.3 (2C), 127.2, 125.2, 112.2 (m, 2C), 110.3, 58.4, 53.2, 39.6; *m/z* MS (system A) $C_{24}H_{18}F_3N_2O_4$ $[MH]^+$ calcd 455.1, found 455.7.

*Methyl 2-(2-Phenylacetamido)-2-(3′,4′,5′-trifluoro-[1,1′-biphenyl]-4-yl)acetate (**5ao**).* Phenylacetic acid (99.6 mg, 0.732 mmol) was coupled to compound **4** (180 mg, 0.610 mmol) according to General Procedure B. The crude product was purified by column chromatography (PE/EtOAc 100:0−50:50) to afford compound **5ao** as a yellow solid (100 mg, 40%). ^{1}H NMR ($CDCl_3$) δ 7.43−7.37 (m, 2H), 7.37−7.19 (m, 7H), 7.16−7.04 (m, 2H), 6.60 (d, J = 6.9 Hz, 1H), 5.57 (d, J = 7.0 Hz, 1H), 3.68 (s, 3H), 3.59 (s, 2H); ^{19}F NMR

DOI: 10.1021/acs.jmedchem.9b00757
J. Med. Chem. XXXX, XXX, XXX−XXX

($CDCl_3$) δ −133.9 (d, J = 20.5 Hz), −162.2 (dd, J = 20.5/20.5 Hz); ^{13}C NMR ($CDCl_3$) δ 171.1, 170.5, 151.5 (ddd, J_{CF} = 249.8/10.0/4.3 Hz), 139.5 (dt, J_{CF} = 252.4/15.4 Hz), 138.5−138.4 (m), 136.9, 136.6 (td, J_{CF} = 7.7/4.5 Hz), 129.5, 129.2, 127.9, 127.6, 127.5, 111.5−110.9 (m), 56.2, 53.1, 43.6; m/z MS $C_{23}H_{19}F_3NO_3$ $[MH]^+$ calcd 414.1, found 413.9.

*Methyl 2-(2-(3-Fluorophenyl)acetamido)-2-(3′,4′,5′-trifluoro-[1,1′-biphenyl]-4-yl)acetate (**5ap**).* 2-(3-Fluorophenyl)acetic acid (125 mg, 0.813 mmol) was coupled to compound **4** (200 mg, 0.667 mmol) according to General Procedure B. The crude product was purified by column chromatography (PE/EtOAc 100:0−50:50) to afford compound **5ap** as a white solid (248 mg, 85%). ^{1}H NMR (d_6-DMSO) δ 9.08 (d, J = 7.1 Hz, 1H), 7.75 (d, J = 8.4 Hz, 2H), 7.72−7.63 (m, 2H), 7.51 (d, J = 8.3 Hz, 2H), 7.38−7.28 (m, 1H), 7.12 (m, 2H), 7.08−6.98 (m, 1H), 5.51 (d, J = 7.1 Hz, 1H), 3.64 (s, 3H), 3.61 (app. d, J = 4.3 Hz, 2H); ^{19}F NMR (d_6-DMSO) δ −113.9, −134.8 (d, J = 21.6 Hz), −163.3 (dd, J = 21.7/21.7 Hz); ^{13}C NMR (d_6-DMSO) δ 170.8, 169.7, 162.0 (d, J_{CF} = 242.9 Hz), 150.6 (ddd, J_{CF} = 246.7/9.7/4.1 Hz), 138.8 (d, J_{CF} = 7.9 Hz), 138.4 (dt, J_{CF} = 249.7/15.7 Hz), 136.9 (d, J = 1.2 Hz), 136.5, 136.3 (td, J_{CF} = 8.1/4.4 Hz), 123.0 (d, J_{CF} = 8.4 Hz), 128.4, 127.2, 125.2 (d, J_{CF} = 2.7 Hz), 115.8 (d, J_{CF} = 21.4 Hz), 113.2 (d, J_{CF} = 20.8 Hz), 111.8−110.3 (m), 56.0, 52.3, 41.1; m/z MS $C_{23}H_{18}F_4NO_3$ $[MH]^+$ calcd 432.1, found 431.8.

*Methyl 2-(2-(4-Fluorophenyl)acetamido)-2-(3′,4′,5′-trifluoro-[1,1′-biphenyl]-4-yl)acetate (**5aq**).* 2-(4-Fluorophenyl)acetic acid (94.0 mg, 0.610 mmol) was coupled to compound **4** (150 mg, 0.508 mmol) according to General Procedure B. The crude product was purified by column chromatography (PE/EtOAc 100:0−50:50) to afford compound **5aq** as a white solid (155 mg, 71%). ^{1}H NMR ($CDCl_3$) δ 7.35 (d, J = 8.4 Hz, 2H), 7.27 (d, J = 8.3 Hz, 2H), 7.19−7.12 (m, 2H), 7.08−7.01 (m, 2H), 6.98−6.91 (m, 2H), 6.61 (d, J = 6.9 Hz, 1H), 5.51 (d, J = 7.0 Hz, 1H), 3.63 (s, 3H), 3.50 (s, 2H); ^{19}F NMR ($CDCl_3$) δ −115.1, −133.9 (d, J = 20.5 Hz), −162.1 (dd, J = 20.5/20.5 Hz); ^{13}C NMR ($CDCl_3$) δ 171.1, 170.2, 162.3 (d, J_{CF} = 246.1 Hz), 151.5 (ddd, J_{CF} = 249.8/10.0/4.3 Hz), 140.9−137.8 (dt, J_{CF} = 252.2/15.2 Hz), 138.7−138.5 (m), 136.8, 136.6 (td, J_{CF} = 7.8/4.7 Hz), 131.0 (d, J_{CF} = 8.1 Hz), 130.3 (d, J_{CF} = 3.3 Hz), 128.0, 127.5, 115.9 (d, J_{CF} = 21.5 Hz), 111.1 (m), 56.2, 53.1, 42.5; m/z MS $C_{23}H_{18}F_4NO_3$ $[MH]^+$ calcd 432.1, found 431.8.

*Methyl 2-(2-(4-Methoxyphenyl)acetamido)-2-(3′,4′,5′-trifluoro-[1,1′-biphenyl]-4-yl)acetate (**5ar**).* 2-(4-Methoxyphenyl)acetic acid (270 mg, 1.63 mmol) was coupled to compound **4** (400 mg, 1.35 mmol) according to General Procedure B. The crude product was purified by column chromatography (PE/EtOAc 100:0−50:50) to afford compound **5ar** as a white solid (195 mg, 32%). ^{1}H NMR ($CDCl_3$) δ 7.42 (d, J = 8.3 Hz, 2H), 7.35 (d, J = 8.3 Hz, 2H), 7.19 (d, J = 8.6 Hz, 2H), 7.12 (m, 2H), 6.89 (d, J = 8.6 Hz, 2H), 6.70 (d, J = 7.0 Hz, 1H), 5.61 (d, J = 7.1 Hz, 1H), 3.80 (s, 3H), 3.71 (s, 3H), 3.55 (s, 2H); ^{19}F NMR ($CDCl_3$) δ −133.9 (d, J = 20.5 Hz), −162.2 (dd, J = 20.5/20.5 Hz); ^{13}C NMR ($CDCl_3$) δ 171.1, 170.9, 159.0, 151.5 (ddd, J_{CF} = 249.8/10.0/4.2 Hz), 139.5 (dt, J_{CF} = 32.4/15.4 Hz), 138.4−138.4 (m), 136.9, 136.6 (td, J_{CF} = 7.8/4.6 Hz), 130.5, 127.9, 127.4, 126.4, 114.5, 111.1 (m), 56.1, 55.3, 53.0, 42.6; m/z MS $C_{24}H_{21}F_3NO_4$ $[MH]^+$ calcd 444.1, found 443.9.

*Methyl 2-(2-(4-Carbamoylphenyl)acetamido)-2-(3′,4′,5′-trifluoro-[1,1′-biphenyl]-4-yl)acetate (**5at**).* 2-(4-Carbamoylphenyl)-acetic acid (146 mg, 0.813 mmol) was coupled to compound **4** (200 mg, 0.677 mmol) according to General Procedure B. Upon completion, the reaction mixture was diluted with sat. $NaHCO_3$ (15 mL) and extracted with DCM (3 × 15 mL). The combined organic layers were dried over anhydrous Na_2SO_4, filtered, and concentrated in vacuo to afford compound **5at** as a white solid (261 mg, 85%). ^{1}H NMR (d_6-DMSO) δ 9.09 (d, J = 7.2 Hz, 1H), 7.91 (br s, 1H), 7.87−7.65 (m, 6H), 7.51 (d, J = 8.3 Hz, 2H), 7.34 (d, J = 8.3 Hz, 2H), 7.30 (br s, 1H), 5.50 (d, J = 7.1 Hz, 1H), 3.64 (s, 3H), 3.62 (d, J = 2.3 Hz, 2H); ^{19}F NMR (d_6-DMSO) δ −134.8 (d, J = 21.7 Hz), −163.2 (dd, J = 21.7/21.7 Hz); ^{13}C NMR (d_6-DMSO) δ 170.9, 169.8, 167.8, 150.6 (ddd, J_{CF} = 246.7/9.7/4.2 Hz), 139.4, 138.4 (dt, J_{CF} = 249.5/15.5 Hz), 137.0−136.8 (m), 136.6, 136.2 (td, J_{CF} = 8.1/4.3 Hz), 132.5, 128.9, 128.5, 127.4, 127.2, 111.6−111.0 (m), 56.0, 52.4, 41.4; m/z MS $C_{24}H_{20}F_3N_2O_4$ $[MH]^+$ calcd 457.1, found 456.9.

*Methyl 2-(2-(3,4-Dimethoxyphenyl)acetamido)-2-(3′,4′,5′-trifluoro-[1,1′-biphenyl]-4-yl)acetate (**5au**).* 2-(3,4-Dimethoxyphenyl)-acetic acid (319 mg, 1.63 mmol) was coupled to compound **4** (400 mg, 1.35 mmol) according to General Procedure B. The crude product was purified by column chromatography (PE/EtOAc 100:0−50:50) to afford compound **5au** as a white solid (446 mg, 70%). ^{1}H NMR (d_6-DMSO) δ 9.03 (d, J = 7.3 Hz, 1H), 7.87−7.62 (m, 4H), 7.51 (d, J = 8.3 Hz, 2H), 6.94−6.75 (m, 3H), 5.51 (d, J = 7.2 Hz, 1H), 3.72 (s, 3H), 3.71 (s, 3H), 3.64 (s, 3H), 3.48 (s, 2H); ^{19}F NMR (d_6-DMSO) δ −134.8 (d, J = 21.7 Hz), −163.3 (dd, J = 21.7/21.7 Hz); ^{13}C NMR (d_6-DMSO) δ 170.9, 170.4, 150.6 (ddd, J_{CF} = 246.8/9.8/4.3 Hz), 148.5, 147.5, 138.4 (dt, J_{CF} = 30.6/15.6 Hz), 136.9−136.8 (m), 136.7, 136.3 (td, J_{CF} = 8.1/4.4 Hz), 128.5, 128.4, 127.1, 121.0, 112.9, 111.7, 111.3 (dd, J_{CF} = 16.0/5.6 Hz), 55.9, 55.5, 55.3, 52.3, 41.2; m/z MS $C_{25}H_{23}F_3NO_5$ $[MH]^+$ calcd 474.1, found 473.9.

*Methyl 2-(2-(3-Fluoro-4-methoxyphenyl)acetamido)-2-(3′,4′,5′-trifluoro-[1,1′-biphenyl]-4-yl)acetate (**5aw**).* 2-(3-Fluoro-4-methoxyphenyl)acetic acid (187 mg, 1.02 mmol) was coupled to compound **4** (250 mg, 0.847 mmol) according to General Procedure B. The crude product was purified by column chromatography (PE/EtOAc 100:0−50:50) to afford compound **5aw** as a yellow solid (134 mg, 34%). ^{1}H NMR ($CDCl_3$) δ 7.45 (d, J = 8.4 Hz, 2H), 7.36 (d, J = 8.2 Hz, 2H), 7.14 (m, 2H), 7.05−6.90 (m, 3H), 6.60 (d, J = 6.9 Hz, 1H), 5.59 (d, J = 7.0 Hz, 1H), 3.89 (s, 3H), 3.73 (s, 3H), 3.54 (s, 2H); ^{19}F NMR ($CDCl_3$) δ −133.9 (d, J = 20.5 Hz), −134.2, −162.1 (dd, J = 20.5/20.5 Hz); ^{13}C NMR ($CDCl_3$) δ 171.1, 170.2, 152.5 (d, J_{CF} = 246.9 Hz), 151.6 (ddd, J_{CF} = 249.8/10.0/4.2 Hz), 147.2 (d, J_{CF} = 10.6 Hz), 139.6 (dt, J_{CF} = 252.3/15.3 Hz), 138.7−138.5 (m), 136.82, 136.6 (td, J_{CF} = 7.8/4.7 Hz), 128.0, 127.6, 127.2 (d, J_{CF} = 6.4 Hz), 125.3 (d, J_{CF} = 3.6 Hz), 117.2 (d, J_{CF} = 18.6 Hz), 113.9 (d, J_{CF} = 2.2 Hz), 111.2 (m), 56.4, 56.3, 53.2, 42.5 (d, J_{CF} = 1.0 Hz); m/z MS $C_{23}H_{20}F_4NO_4$ $[MH]^+$ calcd 462.1, found 461.9.

*Methyl 2-(2-(4-Fluoro-3-methoxyphenyl)acetamido)-2-(3′,4′,5′-trifluoro-[1,1′-biphenyl]-4-yl)acetate (**5ay**).* 2-(4-Fluoro-3-methoxyphenyl)acetic acid (225 mg, 1.22 mmol) was coupled to compound **4** (300 mg, 1.02 mmol) according to General Procedure B. The crude product was purified by column chromatography (PE/EtOAc 100:0−50:50) to afford compound **5ay** as a white solid (410 mg, 87%). ^{1}H NMR ($CDCl_3$) δ 7.47−7.32 (m, 4H), 7.18−7.10 (m, 2H), 7.08−7.00 (m, 1H), 6.89 (dd, J = 8.1/2.1 Hz, 1H), 6.78 (ddd, J = 8.2/4.2/2.1 Hz, 1H), 6.66 (d, J = 7.0 Hz, 1H), 5.60 (d, J = 7.0 Hz, 1H), 3.85 (s, 3H), 3.72 (s, 3H), 3.57 (s, 2H); ^{19}F NMR ($CDCl_3$) δ −133.8 (d, J = 20.5 Hz), −137.0, −162.1 (dd, J = 20.5/20.5 Hz); ^{13}C NMR ($CDCl_3$) δ 171.1, 170.1, 151.9 (d, J_{CF} = 245.8 Hz), 151.53 (ddd, J_{CF} = 249.9/10.0/4.2 Hz), 147.97 (d, J_{CF} = 10.8 Hz), 139.5 (dt, J_{CF} = 252.4/15.4 Hz), 138.6 (d, J_{CF} = 1.6 Hz), 136.8, 136.5 (td, J_{CF} = 7.8/4.7 Hz), 130.76 (d, J = 4.0 Hz), 128.0, 127.5, 121.6 (d, J_{CF} = 6.9 Hz), 116.4 (d, J_{CF} = 18.4 Hz), 114.5 (d, J_{CF} = 2.0 Hz), 111.1 (dd, J_{CF} = 15.9/6.0 Hz), 56.3, 56.2, 53.1, 43.0; m/z MS $C_{24}H_{20}F_4NO_4$ $[MH]^+$ calcd 462.1, found 461.8.

*2-Acetamido-N-hydroxy-2-(3′,4′,5′-trifluoro-[1,1′-biphenyl]-4-yl)acetamide (**6a**).* Compound **5a** (101 mg, 0.300 mmol) was converted to the corresponding hydroxamic acid according to General Procedure C. The crude product was purified by column chromatography (DCM/MeOH/AcOH 99:0:1−90:9:1) to afford compound **6a** as a pink solid (64 mg, 65%). ^{1}H NMR (d_6-DMSO) δ 11.02 (s, 1H), 9.01 (s, 1H), 8.71 (d, J = 8.4 Hz, 1H), 7.86−7.64 (m, 4H), 7.49 (d, J = 8.3 Hz, 2H), 5.41 (d, J = 8.4 Hz, 1H), 1.91 (s, 3H); ^{19}F NMR (d_6-DMSO) δ −134.9 (d, J = 21.8 Hz), −163.5 (dd, J = 21.8/21.8 Hz); ^{13}C NMR (d_6-DMSO) δ 169.1, 166.5, 150.7 (ddd, J_{CF} = 13.6/9.8/4.3 Hz), 139.4, 134.0−136.8 (m), 136.7−136.4 (m), 136.3−135.9 (m), 127.7, 126.8, 111.3 (dd, J_{CF} = 16.0/5.4 Hz), 53.5, 22.4; m/z HRMS (TOF ES$^+$) $C_{16}H_{14}F_3N_2O_3$ $[MH]^+$ calcd 339.0951, found 339.0953.

*3-((2-(Hydroxyamino)-2-oxo-1-(3′,4′,5′-trifluoro-[1,1′-biphenyl]-4-yl)ethyl)amino)-3-oxopropanoic Acid (**6c**).* Compound **5b** (185 mg, 0.485 mmol) was converted to the corresponding hydroxamic acid according to General Procedure C. After 1 day, only partial

DOI: 10.1021/acs.jmedchem.9b00757
J. Med. Chem. XXXX, XXX, XXX−XXX

conversion had occurred and therefore $NH_2OH{\cdot}HCl$ (135 mg, 1.94 mmol) and KOH (5 M in MeOH, 0.486 mL) were added. The reaction mixture was stirred for a further 24 h. LC−MS indicated that **5b** was converted to the desired product and the dihydroxamic acid N^1-hydroxy-N^3-(2-(hydroxyamino)-2-oxo-1-(3′,4′,5′-trifluoro-[1,1′-biphenyl]-4-yl)ethyl)malonamide (**6d**). These two compounds were isolated by column chromatography (DCM/MeOH/AcOH 99:0:1−90:9:1). The desired hydroxamic acid was treated with 20% TFA/DCM (5 mL) and stirred at rt overnight. The reaction mixture was concentrated in vacuo and extracted with EtOAc (3 × 5 mL). The combined organic layers were dried over Na_2SO_4, filtered, and concentrated in vacuo. The crude product was purified by column chromatography (DCM/MeOH/AcOH 99:0:1−90:9:1) to afford compound **6c** as a light brown oil (10 mg, 6% over two steps). ^{1}H NMR (d_6-DMSO) δ 11.28 (s, 1H), 9.29 (d, J = 8.2 Hz, 1H), 7.86−7.58 (m, 4H), 7.49 (d, J = 8.3 Hz, 2H), 5.41 (d, J = 8.2 Hz, 1H), 3.26−3.06 (m, 2H); ^{19}F NMR (d_6-DMSO) δ −134.9 (d, J = 21.7 Hz), −163.5 (dd, J = 21.8/21.8 Hz); ^{13}C NMR (d_6-DMSO) δ 170.2, 166.9, 166.3, 150.6 (ddd, J_{CF} = 246.5/9.7/4.1 Hz), 139.3, 138.3 (dt, J_{CF} = 251.1/16.7 Hz), 136.6 (td, J_{CF} = 8.1/4.5 Hz), 136.2−136.1 (m), 127.6, 126.8, 113.1−108.6 (m), 53.7, 43.3; m/z HRMS (TOF ES$^+$) $C_{17}H_{14}F_3N_2O_5$ $[MH]^+$ calcd 383.0849, found 383.0857.

*N^1-Hydroxy-N^3-(2-(hydroxyamino)-2-oxo-1-(3′,4′,5′-trifluoro-[1,1′-biphenyl]-4-yl)ethyl)malonamide (**6d**).* The title compound was synthesized by aminolysis of both methyl and *tert*-butyl esters of compound **5b** as explained above. ^{1}H NMR (d_6-DMSO) δ 10.64 (s, 2H), 9.08 (s, 1H), 8.94 (s, 1H), 8.84 (d, J = 8.2 Hz, 1H), 7.81−7.58 (m, 4H), 7.49 (d, J = 8.3 Hz, 2H), 5.39 (d, J = 8.2 Hz, 1H), 3.07 (s, 2H); ^{19}F NMR (d_6-DMSO) δ −134.9 (d, J = 21.7 Hz), −163.5 (dd, J = 21.7/21.7 Hz); ^{13}C NMR (d_6-DMSO) δ 166.1, 165.9, 163.8, 150.6 (ddd, J = 246.5/9.7/4.4 Hz), 139.4, 138.3 (dt, J = 249.8/19.6 Hz), 136.6 (td, J = 8.2/4.5 Hz), 136.2−136.0 (m), 127.5, 126.8, 111.8−109.8 (m), 53.8, 40.3; m/z MS (TOF ES$^-$) $C_{17}H_{13}F_3N_3O_5$ $[M-H]^-$ calcd 396.1, found 396.0; m/z HRMS (TOF ES$^+$) $C_{17}H_{15}F_3N_3O_5$ $[MH]^+$ calcd 398.0958, found 398.0954.

*4-((2-(Hydroxyamino)-2-oxo-1-(3′,4′,5′-trifluoro-[1,1′-biphenyl]-4-yl)ethyl)amino)-4-oxobutanoic Acid (**6e**).* Compound **5c** (267 mg, 0.675 mmol) was converted to the corresponding hydroxamic acid according to General Procedure C. After 1 day, only partial conversion had occurred; therefore, $NH_2OH{\cdot}HCl$ (188 mg, 2.71 mmol) was added and the reaction mixture was heated at 40 °C for 2 h. The reaction progressed slowly and therefore the temperature was increased to 50 °C overnight. LC−MS showed degradation of **5e** to **4**. The reaction was stopped, and compounds **4**, **5e**, and **6e** were isolated by column chromatography (DCM/MeOH/AcOH 99:0:1−95:4:1). Compound **6e** was obtained as a white solid (15 mg, 6%). ^{1}H NMR (d_6-DMSO) δ 11.95 (s, 1H), 11.01 (s, 1H), 9.04 (s, 1H), 8.72 (d, J = 8.3 Hz, 1H), 8.08−7.61 (m, 4H), 7.49 (d, J = 8.3 Hz, 2H), 5.41 (d, J = 8.3 Hz, 1H), 2.49−2.02 (m, 4H); ^{19}F NMR (d_6-DMSO) δ −134.9 (d, J = 21.8 Hz), −163.5 (dd, J = 21.8/21.8 Hz); ^{13}C NMR (d_6-DMSO) δ 174.1, 171.1, 166.5, 150.7 (ddd, J_{CF} = 246.4/9.7/4.1 Hz), 139.4, 138.4 (dt, J_{CF} = 248.9/15.1 Hz), 136.6 (td, J_{CF} = 8.0/4.3 Hz), 136.3−136.0 (m), 127.7, 126.8, 111.5−111.0 (m), 53.6, 29.9, 29.2; m/z HRMS (TOF ES$^+$) $C_{18}H_{16}F_3N_2O_5$ $[MH]^+$ calcd 397.1006, found 397.1018.

*N^1-(2-(Hydroxyamino)-2-oxo-1-(3′,4′,5′-trifluoro-[1,1′-biphenyl]-4-yl)ethyl)succinamide (**6f**).* Compound **5f** (84 mg, 0.213 mmol) was converted to the corresponding hydroxamic acid according to General Procedure C. The crude product was purified by column chromatography (DCM/MeOH/AcOH 95:4:1−90:9:1) to afford compound **6f** as a white solid (43 mg, 52%). ^{1}H NMR (d_6-DMSO) δ 11.00 (s, 1H), 9.01 (s, 1H), 8.66 (d, J = 8.3 Hz, 1H), 7.79−7.62 (m, 4H), 7.49 (d, J = 8.4 Hz, 2H), 7.27 (br s, 1H), 6.74 (br s, 1H), 5.41 (d, J = 8.3 Hz, 1H), 2.43 (t, J = 7.9 Hz, 2H), 2.28 (t, J = 7.2 Hz, 2H); ^{19}F NMR (d_6-DMSO) δ −134.9 (d, J = 21.7 Hz), −163.5 (dd, J = 21.8/21.8 Hz);^{13}C NMR (d_6-DMSO) δ 173.5, 171.4, 166.4, 150.6 (ddd, J_{CF} = 246.4/9.8/4.3 Hz), 139.4, 138.3 (dt, J_{CF} = 258.4/15.8 Hz), 136.6 (td, J_{CF} = 8.1/4.2 Hz), 136.2−135.9 (m), 127.7, 126.8, 111.2 (dd, J_{CF} = 16.0/5.4 Hz), 53.6, 30.4, 30.3; m/z HRMS (TOF ES$^+$) $C_{18}H_{17}F_3N_3O_4$ $[MH]^+$ calcd 396.1166, found 396.1173.

*N-(2-(Hydroxyamino)-2-oxo-1-(3′,4′,5′-trifluoro-[1,1′-biphenyl]-4-yl)ethyl)benzamide (**6g**).* Compound **5g** (50 mg) was converted to the corresponding hydroxamic acid according to General Procedure C. The crude product was purified by column chromatography (DCM/MeOH 100:0−90:10) followed by preparative HPLC to afford compound **6g** as a white solid (10.7 mg, 21%). ^{1}H NMR (d_6-DMSO) δ 11.08 (s, 1H), 9.06 (s, 1H), 8.94 (d, J = 8.1 Hz, 1H), 7.93 (d, J = 7.3 Hz, 2H), 7.78−7.60 (m, 6H), 7.58−7.39 (m, 3H), 5.68 (d, J = 8.1 Hz, 1H); ^{19}F NMR (d_6-DMSO) δ −134.9 (d, J = 21.6 Hz), −163.5 (dd, J = 21.7/21.7 Hz); ^{13}C NMR (d_6-DMSO) δ 166.5, 166.3, 150.6 (ddd, J_{CF} = 246.6/9.7/4.2 Hz), 138.9, 138.3 (dt, J_{CF} = 249.1/15.4 Hz), 136.6 (td, J_{CF} = 8.0/4.3 Hz), 136.3−136.1 (m), 133.8, 131.5, 128.2, 128.1, 127.8, 126.8, 113.5−109.6 (m), 54.4; m/z HRMS (TOF ES$^+$) $C_{21}H_{16}F_3N_2O_3$ $[MH]^+$ calcd 401.1108, found 401.1104.

*3-Fluoro-N-(2-(hydroxyamino)-2-oxo-1-(3′,4′,5′-trifluoro-[1,1′-biphenyl]-4-yl)ethyl)benzamide (**6h**).* Compound **5h** (50 mg, 0.120 mmol) was converted to the corresponding hydroxamic acid according to General Procedure C. The crude product was purified by column chromatography (DCM/MeOH 100:0−90:10) followed by preparative HPLC to afford compound **6h** as a white solid (28.6 mg, 57%). ^{1}H NMR (d_6-DMSO) δ 11.08 (s, 1H), 9.11 (d, J = 8.0 Hz, 1H), 9.06 (s, 1H), 7.84−7.59 (m, 8H), 7.52 (dd, J = 13.9/7.9 Hz, 1H), 7.43−7.36 (m, 1H), 5.66 (d, J = 8.0 Hz, 1H); ^{19}F NMR (d_6-DMSO) δ −113.1, −134.9 (d, J = 21.7 Hz), −163.5 (dd, J = 21.6/21.6 Hz); ^{13}C NMR (d_6-DMSO) δ 166.3, 165.0 (d, J_{CF} = 2.4 Hz), 161.8 (d, J_{CF} = 244.0 Hz), 150.6 (ddd, J_{CF} = 246.5/9.7/4.2 Hz), 138.6, 138.3 (dt, J_{CF} = 248.8/15.4 Hz), 136.5 (td, J_{CF} = 8.2/4.7 Hz), 136.4−136.2 (m), 136.1 (d, J_{CF} = 6.9 Hz), 130.3 (d, J_{CF} = 7.9 Hz), 128.2, 126.8, 124.0 (d, J_{CF} = 2.7 Hz), 118.3 (d, J_{CF} = 21.1 Hz), 114.6 (d, J_{CF} = 22.9 Hz), 111.9−110.5 (m), 54.5; m/z HRMS (TOF ES$^+$) $C_{21}H_{15}F_4N_2O_3$ $[MH]^+$ calcd 419.1013, found 419.1020.

*4-Fluoro-N-(2-(hydroxyamino)-2-oxo-1-(3′,4′,5′-trifluoro-[1,1′-biphenyl]-4-yl)ethyl)benzamide (**6i**).* Compound **5i** (100 mg, 0.240 mmol) was converted to the corresponding hydroxamic acid according to General Procedure C. The crude product was purified by column chromatography (DCM/MeOH 100:0−90:10) to afford compound **6i** as a white solid (48 mg, 48%). ^{1}H NMR (d_6-DMSO) δ 11.06 (s, 1H), 9.13−8.97 (m, 2H), 8.08−7.96 (m, 2H), 7.78−7.60 (m, 6H), 7.36−7.22 (m, 2H), 5.67 (d, J = 8.0 Hz, 1H); ^{19}F NMR (d_6-DMSO) δ −109.1, −135.0 (d, J = 21.7 Hz), −163.5 (dd, J = 21.6/21.6 Hz); ^{13}C NMR (d_6-DMSO) δ 166.5, 165.3, 164.0 (d, J_{CF} = 241.0 Hz), 150.6 (ddd, J_{CF} = 246.6/9.7/4.2 Hz), 138.8, 138.3 (dt, J_{CF} = 249.4/15.6 Hz), 136.6 (td, J_{CF} = 8.0/4.3 Hz), 136.3−136.2 (m), 130.5 (d, J_{CF} = 9.0 Hz), 130.3 (d, J_{CF} = 2.9 Hz), 128.1, 126.8, 115.1 (d, J_{CF} = 21.7 Hz), 111.2 (m), 54.5; m/z HRMS (TOF ES$^+$) $C_{21}H_{15}F_4N_2O_3$ $[MH]^+$ calcd 419.1013, found 419.1019.

*N-(2-(Hydroxyamino)-2-oxo-1-(3′,4′,5′-trifluoro-[1,1′-biphenyl]-4-yl)ethyl)-3-methoxybenzamide (**6j**).* Compound **5j** (528 mg, 1.23 mmol) was converted to the corresponding hydroxamic acid according to General Procedure C. The crude product was purified by column chromatography (DCM/MeOH 100:0−90:10) to afford compound **6j** as a white solid (350 mg, 66%). ^{1}H NMR (d_6-DMSO) δ 8.99 (d, J = 8.1 Hz, 1H), 7.76−7.61 (m, 6H), 7.53 (m, 2H), 7.37 (dd, J = 7.9/7.9 Hz, 1H), 7.10 (dd, J = 8.1/2.3 Hz, 1H), 5.72 (d, J = 8.0 Hz, 1H), 3.81 (s, 3H); ^{19}F NMR (d_6-DMSO) δ −134.9 (d, J = 21.6 Hz), −163.5 (dd, J = 21.6/21.6 Hz); ^{13}C NMR (d_6-DMSO) δ 166.6, 166.2, 159.2, 150.7 (ddd, J_{CF} = 246.7/9.7/4.1 Hz), 139.0, 138.4 (dt, J_{CF} = 249.5/15.6 Hz), 136.7 (td, J_{CF} = 8.0/4.4 Hz), 136.5−136.0 (m), 135.3, 129.4, 128.2, 126.8, 120.1, 117.6, 112.9, 111.2 (m), 55.3, 54.5; m/z HRMS (TOF ES$^+$) $C_{22}H_{18}F_3N_2O_4$ $[MH]^+$ calcd 431.1213, found 431.1207.

*N-(2-(Hydroxyamino)-2-oxo-1-(3′,4′,5′-trifluoro-[1,1′-biphenyl]-4-yl)ethyl)-4-methoxybenzamide (**6k**).* Compound **5k** (154 mg, 0.359 mmol) was converted to the corresponding hydroxamic acid according to General Procedure C. The crude product was purified by column chromatography (DCM/MeOH 100:0−90:10) to afford compound **6k** as a white solid (95.3 mg, 62%). ^{1}H NMR (d_6-DMSO) δ 11.06 (s, 1H), 9.05 (s, 1H), 8.76 (d, J = 8.2 Hz, 1H), 7.93 (d, J = 8.9 Hz, 2H), 7.81−7.65 (m, 4H), 7.61 (d, J = 8.4 Hz, 2H), 6.99 (d, J = 8.9 Hz, 2H), 5.66 (d, J = 8.1 Hz, 1H), 3.81 (s, 3H); ^{19}F NMR (d_6-

DOI: 10.1021/acs.jmedchem.9b00757
J. Med. Chem. XXXX, XXX, XXX−XXX

DMSO) δ −134.9 (d, J = 21.7 Hz), −163.5 (dd, J = 21.7/21.7 Hz); ^{13}C NMR (d_6-DMSO) δ 166.6, 165.7, 161.8, 150.6 (ddd, J_{CF} = 246.6/9.7/4.2 Hz), 139.1, 138.3 (dt, J_{CF} = 249.3/15.5 Hz), 136.6 (td, J_{CF} = 8.1/4.5 Hz), 136.2−136.0 (m), 129.7, 128.1, 126.7, 126.0, 113.4, 111.2 (m), 55.4, 54.3; m/z HRMS (TOF ES$^+$) $C_{22}H_{18}F_3N_2O_4$ [MH]$^+$ calcd 431.1213, found 431.1216.

*3-Hydroxy-N-(2-(hydroxyamino)-2-oxo-1-(3′,4′,5′-trifluoro-[1,1′-biphenyl]-4-yl)ethyl)benzamide (**6l**).* Compound **6j** (230 mg, 0.534 mmol) was treated with BBr_3 (1 M in DCM, 2.67 mL, 2.67 mmol) according to General Procedure D. The crude product was purified by preparative HPLC to afford compound **6l** as a white solid (62 mg, 28%). ^{1}H NMR (d_6-DMSO) δ 11.07 (s, 1H), 9.61 (br s, 1H), 8.79 (d, J = 8.1 Hz, 1H), 7.68 (m, 6H), 7.37 (d, J = 7.8 Hz, 1H), 7.33−7.20 (m, 2H), 6.94 (dd, J = 8.0/1.7 Hz, 1H), 5.65 (d, J = 8.1 Hz, 1H); ^{19}F NMR (d_6-DMSO) δ −134.9 (d, J = 21.7 Hz), −163.5 (dd, J = 21.7/21.7 Hz); ^{13}C NMR (d_6-DMSO) δ 166.6, 166.4, 157.3, 150.7 (ddd, J_{CF} = 246.5/9.7/4.1 Hz), 139.0, 138.4 (dt, J_{CF} = 249.4/15.6 Hz), 136.6 (td, J_{CF} = 8.0/4.3 Hz), 136.4−136.1 (m), 135.3, 129.3, 128.1, 126.8, 118.5, 118.3, 114.7, 111.2 (m), 54.4; m/z HRMS (TOF ES$^+$) $C_{21}H_{16}F_3N_2O_4$ [MH]$^+$ calcd 417.1057, found 417.1064.

*4-Hydroxy-N-(2-(hydroxyamino)-2-oxo-1-(3′,4′,5′-trifluoro-[1,1′-biphenyl]-4-yl)ethyl)benzamide (**6m**).* Compound **6k** (125 mg, 0.290 mmol) was treated with BBr_3 (1 M in DCM, 2.90 mL, 2.90 mmol) according to General Procedure D. The crude product was purified by column chromatography (DCM/MeOH 100:0−90:10) followed by preparative HPLC to afford compound **6m** as a white solid (3.00 mg, 2.5%). ^{1}H NMR (d_6-DMSO) δ 11.03 (s, 1H), 10.0 (s, 1H), 9.03 (s, 1H), 8.60 (d, J = 8.2 Hz, 1H), 7.83−7.78 (m, 2H), 7.76−7.65 (m, 4H), 7.60 (d, J = 8.4 Hz, 2H), 6.83−6.77 (m, 2H), 5.63 (d, J = 8.1 Hz, 1H); ^{19}F NMR (d_6-DMSO) δ −134.9 (d, J = 21.7 Hz), −163.5 (dd, J = 21.7/21.7 Hz); ^{13}C NMR (d_6-DMSO) δ 166.6, 165.8, 160.4, 150.6 (ddd, J_{CF} = 246.5/9.8/4.3 Hz), 139.2, 138.2 (dt, J_{CF} = 247.8/15.7 Hz), 136.8−136.3 (m), 136.2−136.1 (m), 129.7, 128.0, 126.7, 124.4, 114.7, 111.7−110.8 (m), 54.2; m/z HRMS (TOF ES$^+$) $C_{21}H_{16}F_3N_2O_4$ [MH]$^+$ calcd 417.1057, found 417.1072.

*N-(2-(Hydroxyamino)-2-oxo-1-(3′,4′,5′-trifluoro-[1,1′-biphenyl]-4-yl)ethyl)-3-(N′-hydroxycarbamimidoyl)benzamide (**6p**).* Compound **5n** (372 mg, 0.883 mmol) was converted to the amidoxime **6j** according to General Procedure C. After stirring at rt for 1 day, the nitrile of **5n** was completely converted to the corresponding amidoxime, but none of the ester had converted to the hydroxamic acid. The reaction was left for a further 3 days, but only partial conversion to the desired hydroxamic acid **6p** was observed. NH_2OH·HCl (244 mg, 3.51 mmol) and KOH (5 M in MeOH, 0.876 mL) were added. After stirring the reaction mixture at rt for 1 day, the reaction was complete and the mixture was purified by column chromatography (DCM/MeOH 100:0−90:10) to afford compound **6p** as white flakes (132 mg, 33%). ^{1}H NMR (d_6-DMSO) δ 11.11 (s, 1H), 9.72 (s, 1H), 9.08 (s, 1H), 8.98 (d, J = 8.2 Hz, 1H), 8.20 (s, 1H), 7.86 (dd, J = 20.8/7.9 Hz, 2H), 7.76−7.67 (m, 4H), 7.62 (d, J = 8.4 Hz, 2H), 7.46 (t, J = 7.8 Hz, 1H), 5.93 (s, 2H), 5.68 (d, J = 8.1 Hz, 1H); ^{19}F NMR (d_6-DMSO) δ −134.9 (d, J = 21.7 Hz), −163.5 (dd, J = 21.8/21.8 Hz); ^{13}C NMR (d_6-DMSO) δ 166.4, 166.1, 150.6 (ddd, J_{CF} = 246.5/9.7/4.2 Hz), 150.3, 139.0, 138.3 (dt, J_{CF} = 247.1/14.4 Hz), 136.7−136.4 (m), 136.4−136.2 (m), 133.7, 133.3, 128.3 (2C), 128.2, 128.0, 126.8, 124.7, 112.2−109.2 (m), 54.3; m/z HRMS (TOF ES$^+$) $C_{22}H_{18}F_3N_4O_4$ [MH]$^+$ calcd 459.1275, found 459.1276.

*N-(2-(Hydroxyamino)-2-oxo-1-(3′,4′,5′-trifluoro-[1,1′-biphenyl]-4-yl)ethyl)-4-(N′-hydroxycarbamimidoyl)benzamide (**6q**).* Compound **5o** (212 mg, 0.500 mmol) was converted to the corresponding amidoxime **6q** according to General Procedure C. The crude product was purified by column chromatography (DCM/MeOH 100:0−95:5) to afford **6q** as a white solid (34 mg, 15%). ^{1}H NMR (d_6-DMSO) δ 11.05 (s, 1H), 9.81 (s, 1H), 9.07 (s, 1H), 9.00 (d, J = 8.1 Hz, 1H), 7.92 (d, J = 8.5 Hz, 2H), 7.79−7.66 (m, 6H), 7.62 (d, J = 8.4 Hz, 2H), 5.91 (s, 2H), 5.66 (d, J = 8.1 Hz, 1H); ^{19}F NMR (d_6-DMSO) δ −134.9 (d, J = 21.8 Hz), −163.5 (dd, J = 21.7/21.7 Hz); ^{13}C NMR (d_6-DMSO) δ 166.5, 165.9, 150.6 (ddd, J_{CF} = 246.2/9.5/4.1 Hz), 150.2, 138.9, 138.3 (m), 136.7−136.4 (m), 136.3−136.2 (m), 136.1, 133.9, 128.1, 127.7, 126.8, 125.0, 111.2 (m), 54.4; m/z HRMS (TOF ES$^+$) $C_{22}H_{18}F_3N_4O_4$ [M + H]$^+$ calcd 459.1275, found 459.1281; purity 85%.

*N-(2-(Hydroxyamino)-2-oxo-1-(3′,4′,5′-trifluoro-[1,1′-biphenyl]-4-yl)ethyl)isophthalamide (**6r**).* Compound **5r** (328 mg, 0.741 mmol) was converted to the corresponding hydroxamic acid according to General Procedure C. The crude product was purified by column chromatography (DCM/MeOH 95:5−90:10) to afford compound **6r** as a white solid (153 mg, 47%). ^{1}H NMR (d_6-DMSO) δ 11.11 (s, 1H), 9.09 (s, 1H), 9.07 (d, J = 8.2 Hz, 1H), 8.41 (br s, 1H), 8.07 (br s, 1H), 8.05−7.95 (m, 2H), 7.77−7.67 (m, 4H), 7.62 (d, J = 8.4 Hz, 2H), 7.55 (dd, J = 7.8/7.8 Hz, 1H), 7.50 (s, 1H), 5.68 (d, J = 8.1 Hz, 1H); ^{19}F NMR (d_6-DMSO) δ −134.9 (d, J = 21.8 Hz), −163.4 (dd, J = 21.7/21.7 Hz); ^{13}C NMR (d_6-DMSO) δ 167.5, 166.4, 165.9, 150.6 (ddd, J_{CF} = 246.5/9.7/4.1 Hz), 140.2−136.8 (m), 138.9, 136.6 (td, J_{CF} = 8.0/4.3 Hz), 136.4−136.3 (m), 134.3, 133.9, 130.6, 130.4, 128.3, 128.1, 126.8, 126.7, 112.6−109.7 (m), 54.4; m/z HRMS (TOF ES$^+$) $C_{22}H_{17}F_3N_3O_4$ [MH]$^+$ calcd 444.1166, found 444.1172.

*N-(2-(Hydroxyamino)-2-oxo-1-(3′,4′,5′-trifluoro-[1,1′-biphenyl]-4-yl)ethyl)terephthalamide (**6s**).* Compound **5s** (383 mg, 0.865 mmol) was converted to the corresponding hydroxamic acid according to General Procedure C. The crude product was purified by column chromatography (DCM/MeOH 100:0−90:10) to afford compound **6s** as a white solid (38 mg, 10%). ^{1}H NMR (d_6-DMSO) δ 11.08 (s, 1H), 9.11 (d, J = 8.1 Hz, 1H), 9.07 (br s, 1H), 8.09 (br s, 1H), 8.01−7.89 (m, 4H), 7.78−7.58 (m, 6H), 7.50 (br s, 1H), 5.67 (d, J = 8.1 Hz, 1H); ^{19}F NMR (d_6-DMSO) δ −134.9 (d, J = 21.8 Hz), −163.5 (dd, J = 21.7/21.7 Hz); ^{13}C NMR (d_6-DMSO) δ 167.2, 166.4, 165.8, 150.6 (ddd, J_{CF} = 246.5/9.9/4.3 Hz), 138.7, 138.2 (dt, J_{CF} = 262.9/14.7 Hz), 136.7, 136.5 (dt, J_{CF} = 6.4/5.2 Hz), 136.4−136.2 (m), 136.1, 128.1, 127.8, 127.3, 126.8, 112.3 (dd, J_{CF} = 16.0/5.4 Hz), 54.4; m/z HRMS (TOF ES$^+$) $C_{22}H_{17}F_3N_3O_4$ [MH]$^+$ calcd 444.1166, found 444.1172.

*N^1-(2-(Hydroxyamino)-2-oxo-1-(3′,4′,5′-trifluoro-[1,1′-biphenyl]-4-yl)ethyl)-N^4-methylterephthalamide (**6t**).* Compound **5t** (52.7 mg, 0.115 mmol) was converted to the corresponding hydroxamic acid according to General Procedure C. Upon completion, the mixture was purified by preparative HPLC to afford compound **6t** as a white fluffy solid after lyophilization (24.5 mg, 47%). ^{1}H NMR (d_6-DMSO) δ 11.09 (s, 1H), 9.11 (d, J = 8.1 Hz, 1H), 9.07 (br s, 1H), 8.57 (d, J = 4.6 Hz, 1H), 8.00 (d, J = 8.4 Hz, 2H), 7.90 (d, J = 8.4 Hz, 2H), 7.78−7.66 (m, 4H), 7.62 (d, J = 8.3 Hz, 2H), 5.67 (d, J = 8.0 Hz, 1H), 2.80 (d, J = 4.5 Hz, 3H); ^{19}F NMR (d_6-DMSO) −134.9 (d, J = 21.8 Hz), −163.5 (dd, J = 21.8/21.8 Hz); ^{13}C NMR (d_6-DMSO) δ 166.4, 165.9, 165.8, 150.6 (ddd, J_{CF} = 246.2/9.3/3.9 Hz), 138.8, 139.8−137.0 (m), 137.0, 136.6 (td, J_{CF} = 7.9/4.8 Hz), 136.3, 135.9, 128.1, 127.8, 126.9, 126.8, 111.2 (dd, J_{CF} = 16.2/5.2 Hz), 54.4, 26.3; m/z HRMS (TOF ES$^+$) $C_{23}H_{19}N_3O_4F_3$ [MH]$^+$ calcd 458.1322, found 458.1323.

*N^1-(2-(Hydroxyamino)-2-oxo-1-(3′,4′,5′-trifluoro-[1,1′-biphenyl]-4-yl)ethyl)-N^4,N^4-dimethylterephthalamide (**6u**).* Compound **5u** (51.3 mg, 0.109 mmol) was converted to the corresponding hydroxamic acid according to General Procedure C. Upon completion, the mixture was purified by column chromatography (DCM/PE/AcOH 1:1:0.1 to DCM/MeOH/AcOH 95:5:0.1) followed by preparative HPLC to afford compound **6u** as a white fluffy solid after lyophilization (8.0 mg, 16%). ^{1}H NMR (d_6-DMSO) δ 11.07 (s, 1H), 9.08 (d, J = 8.1 Hz, 2H), 7.96 (d, J = 8.4 Hz, 2H), 7.78−7.64 (m, 4H), 7.62 (d, J = 8.4 Hz, 2H), 7.47 (d, J = 8.4 Hz, 2H), 5.66 (d, J = 8.0 Hz, 1H), 2.99 (s, 3H), 2.89 (s, 3H); ^{19}F NMR (d_6-DMSO) δ −134.9 (d, J = 21.7 Hz), −163.5 (dd, J = 21.6/21.6 Hz); m/z HRMS (TOF ES$^+$) $C_{24}H_{21}N_3O_4F_3$ [MH]$^+$ calcd 472.1479, found 472.1480.

*N^1-Ethyl-N^4-(2-(hydroxyamino)-2-oxo-1-(3′,4′,5′-trifluoro-[1,1′-biphenyl]-4-yl)ethyl)terephthalamide (**6v**).* Compound **5v** (50.7 mg, 0.108 mmol) was converted to the corresponding hydroxamic acid according to General Procedure C. Upon completion, the resulting mixture was purified by column chromatography (DCM/PE/AcOH 1:1:0.1 to DCM/MeOH/AcOH 95:5:0.1) followed by preparative HPLC to afford compound **6v** as a white fluffy solid after lyophilization (10.0 mg, 13%). ^{1}H NMR (d_6-DMSO) δ 11.08 (s, 1H), 9.10 (d, J = 8.1 Hz, 1H), 9.06 (br s, 1H), 8.59 (t, J = 5.2 Hz,

DOI: 10.1021/acs.jmedchem.9b00757
J. Med. Chem. XXXX, XXX, XXX−XXX

1H), 7.99 (d, J = 8.4 Hz, 2H), 7.90 (d, J = 8.3 Hz, 2H), 7.75−7.68 (m, 4H), 7.62 (d, J = 8.3 Hz, 2H), 5.66 (d, J = 8.0 Hz, 1H), 3.30 (q, J = 7.1 Hz, 2H), 1.13 (t, J = 7.2 Hz, 3H); ^{19}F NMR (d_6-DMSO) δ −134.9 (d, J = 21.8 Hz), −163.5 (dd, J = 21.6/21.6 Hz); m/z HRMS (TOF ES$^+$) $C_{24}H_{21}N_3O_4F_3$ [MH]$^+$ calcd 472.1479, found 472.1480.

*N^1-(2-(Hydroxyamino)-2-oxo-1-(3′,4′,5′-trifluoro-[1,1′-biphenyl]-4-yl)ethyl)-N^4-isopropylterephthalamide (**6w**).* Compound **5w** (56.8 mg, 0.117 mmol) was converted to the corresponding hydroxamic acid according to General Procedure C. Upon completion, the mixture was purified by column chromatography (DCM/PE/AcOH 1:1:0.1 to DCM/MeOH/AcOH 95:5:0.1) followed by preparative HPLC to afford compound **6w** as a white fluffy solid after lyophilization (11.6 mg, 20%). ^{1}H NMR (d_6-DMSO) δ 11.09 (s, 1H), 9.10 (d, J = 8.1 Hz, 1H), 9.07 (d, J = 0.8 Hz, 1H), 8.35 (d, J = 7.7 Hz, 1H), 7.99 (d, J = 8.5 Hz, 2H), 7.91 (d, J = 8.5 Hz, 2H), 7.77−7.66 (m, 4H), 7.62 (d, J = 8.4 Hz, 2H), 5.67 (d, J = 8.1 Hz, 1H), 4.19−3.97 (m, 1H), 1.18 (d, J = 6.6 Hz, 6H); ^{19}F NMR (d_6-DMSO) δ −134.9 (d, J = 21.8 Hz), −163.5 (dd, J = 21.8/21.8 Hz); m/z HRMS (TOF ES$^+$) $C_{25}H_{23}N_3O_4F_3$ [MH]$^+$ calcd 486.1635, found 486.1638.

*N^1-(2-(Hydroxyamino)-2-oxo-1-(3′,4′,5′-trifluoro-[1,1′-biphenyl]-4-yl)ethyl)-N^4-(2-hydroxyethyl)terephthalamide (**6x**).* Compound **5x** (54.1 mg, 0.111 mmol) was converted to the corresponding hydroxamic acid according to General Procedure C. Upon completion, the mixture was purified by preparative HPLC to afford compound **6x** as a white fluffy solid after lyophilization (18.4 mg, 34%). ^{1}H NMR (d_6-DMSO) δ 11.08 (s, 1H), 9.11 (d, J = 8.1 Hz, 1H), 9.07 (s, 1H), 8.57 (t, J = 5.6 Hz, 1H), 8.00 (d, J = 8.4 Hz, 2H), 7.92 (d, J = 8.4 Hz, 2H), 7.78−7.66 (m, 4H), 7.62 (d, J = 8.3 Hz, 2H), 5.67 (d, J = 8.0 Hz, 1H), 4.74 (s, 1H), 3.52 (q, J = 9.7 Hz, 2H), 3.40−3.30 (m, 2H); ^{19}F NMR (d_6-DMSO) δ −134.9 (d, J = 21.7 Hz), −163.4 (dd, J = 21.7/21.7 Hz); ^{13}C NMR (d_6-DMSO) δ 166.4, 165.8, 165.7, 150.6 (ddd, J_{CF} = 246.8/9.5/4.3 Hz), 138.7, 138.3 (dt, J_{CF} = 31.2/16.1 Hz), 137.0, 136.6 (td, J_{CF} = 8.2/4.7 Hz), 136.3, 135.9, 128.2, 127.8, 127.1, 126.8, 112.4−109.4 (m), 59.7, 54.4, 42.3; m/z HRMS (TOF ES$^+$) $C_{24}H_{21}N_3O_5F_3$ [MH]$^+$ calcd 488.1428, found 488.1425.

*N-(2-(Hydroxyamino)-2-oxo-1-(3′,4′,5′-trifluoro-[1,1′-biphenyl]-4-yl)ethyl)-4-sulfamoylbenzamide (**6y**).* Compound **5y** (55.2 mg, 0.115 mmol) was converted to the corresponding hydroxamic acid according to General Procedure C. Upon completion, the mixture was then purified by column chromatography (DCM/PE/AcOH 1:1:0.1 to DCM/MeOH/AcOH 95:5:0.1) followed by preparative HPLC to afford compound **6y** as a white fluffy solid after lyophilization (10.0 mg, 18%). ^{1}H NMR (d_6-DMSO) δ 11.09 (d, J = 0.9 Hz, 1H), 9.22 (d, J = 8.0 Hz, 1H), 9.07 (d, J = 1.1 Hz, 1H), 8.15−7.99 (m, 2H), 7.97−7.84 (m, 2H), 7.71 (dt, J = 10.6/6.2 Hz, 4H), 7.62 (d, J = 8.4 Hz, 2H), 7.50 (s, 2H), 5.66 (d, J = 8.0 Hz, 1H); ^{19}F NMR (d_6-DMSO) δ −134.9 (d, J = 21.7 Hz), −163.4 (dd, J = 21.6/21.6 Hz); m/z HRMS (TOF ES$^+$) $C_{21}H_{17}F_3N_3O_5S$ [MH]$^+$ calcd 480.0836, found 480.0835.

*3-Amino-N-(2-(hydroxyamino)-2-oxo-1-(3′,4′,5′-trifluoro-[1,1′-biphenyl]-4-yl)ethyl)benzamide TFA Salt (**6ab**).* Compound **5z** (228 mg, 0.443 mmol) was converted to the corresponding hydroxamic acid according to General Procedure C. Upon completion, the mixture was purified by column chromatography (DCM/MeOH 100:0−95:5) to afford *tert*-butyl (3-((2-(hydroxyamino)-2-oxo-1-(3′,4′,5′-trifluoro-[1,1′-biphenyl]-4-yl)ethyl)carbamoyl)phenyl)-carbamate (108 mg). This was dissolved in 20% TFA/DCM and stirred at rt for 4 h to remove the boc group. The reaction mixture was concentrated in vacuo and purified by preparative HPLC to afford compound **6ab** as a pale brown solid (28.5 mg, 12% over two steps). ^{1}H NMR (d_6-DMSO) δ 11.09 (s, 1H), 8.82 (d, J = 8.0 Hz, 1H), 7.77−7.65 (m, 4H), 7.61 (d, J = 8.3 Hz, 2H), 7.51−7.42 (m, 2H), 7.33 (t, J = 7.8 Hz, 1H), 7.09 (dd, J = 7.9/1.3 Hz, 1H), 6.72 (br s, 3H), 5.64 (d, J = 8.0 Hz, 1H); ^{19}F NMR (d_6-DMSO) δ −74.5, −134.9 (d, J = 21.7 Hz), −163.5 (dd, J = 21.7/21.7 Hz); ^{13}C NMR (d_6-DMSO, TFA signals are not included) δ 166.4, 166.1, 150.7 (ddd, J_{CF} = 246.6/9.7/4.0 Hz), 141.2−141.0 (m), 138.9, 138.3 (dt, J_{CF} = 31.0/13.9 Hz), 136.6 (td, J_{CF} = 8.3/4.6 Hz), 136.3, 135.0, 129.2, 128.0, 126.8, 121.1, 120.6, 117.5, 111.7−110.6 (m), 54.3; m/z HRMS (TOF ES$^+$) $C_{21}H_{17}F_3N_3O_3$ [MH]$^+$ calcd. 416.1217, found 416.1229.

*4-Amino-N-(2-(hydroxyamino)-2-oxo-1-(3′,4′,5′-trifluoro-[1,1′-biphenyl]-4-yl)ethyl)benzamide TFA Salt (**6ac**).* Compound **5aa** (235 mg, 0.457 mmol) was converted to the corresponding hydroxamic acid according to General Procedure C. Upon completion, the mixture was purified by column chromatography (DCM/MeOH 100:0−95:5) to afford *tert*-butyl (4-((2-(hydroxyamino)-2-oxo-1-(3′,4′,5′-trifluoro-[1,1′-biphenyl]-4-yl)ethyl)carbamoyl)-phenyl)carbamate (128 mg). This was dissolved in 20% TFA/DCM and stirred at rt for 4 h to remove the boc group. The reaction mixture was concentrated in vacuo and purified by preparative HPLC to afford compound **6ac** as a pale brown solid (69 mg, 28% over two steps). ^{1}H NMR (d_6-DMSO) δ 11.08 (br s, 1H), 8.53 (d, J = 8.1 Hz, 1H), 7.78 (d, J = 8.6 Hz, 2H), 7.74−7.56 (m, 6H), 7.17 (br s, 3H), 6.80 (d, J = 8.5 Hz, 2H), 5.66 (d, J = 8.0 Hz, 1H); ^{19}F NMR (d_6-DMSO) δ −74.5, −134.9 (d, J = 21.6 Hz), −163.6 (dd, J = 21.6/21.6 Hz); ^{13}C NMR (d_6-DMSO, TFA signals are not included) δ 166.8, 166.0, 150.7 (ddd, J_{CF} = 246.6/9.7/4.2 Hz), 147.5, 139.4, 138.4 (dt, J_{CF} = 249.4/15.6 Hz), 136.7 (td, J_{CF} = 8.1/4.6 Hz), 136.3 (m), 129.4, 128.1, 127.0, 123.9, 115.4, 111.7−110.6 (m), 54.3; m/z HRMS (TOF ES$^+$) $C_{21}H_{17}F_3N_3O_3$ [MH]$^+$ calcd 416.1217, found 416.1234.

*N-(2-(Hydroxyamino)-2-oxo-1-(3′,4′,5′-trifluoro-[1,1′-biphenyl]-4-yl)ethyl)-4-(methylsulfonamido)benzamide (**6ad**).* Compound **5ad** (65.2 mg, 0.132 mmol) was converted to the corresponding hydroxamic acid according to General Procedure C. Upon completion, the mixture was purified by column chromatography (DCM/PE/AcOH 1:1:0.1 to DCM/MeOH/AcOH 95:5:0.1) followed by preparative HPLC to afford compound **6ad** as a white fluffy solid after lyophilization (30.0 mg, 46%). ^{1}H NMR (d_6-DMSO) δ 11.07 (s, 1H), 10.13 (s, 1H), 9.06 (s, 1H), 8.83 (d, J = 8.1 Hz, 1H), 7.92 (d, J = 8.8 Hz, 2H), 7.79−7.65 (m, 4H), 7.60 (d, J = 8.4 Hz, 2H), 7.25 (d, J = 8.8 Hz, 2H), 5.65 (d, J = 8.1 Hz, 1H), 3.07 (s, 3H); ^{19}F NMR (d_6-DMSO) δ −134.9 (d, J = 21.8 Hz), −163.5 (dd, J = 21.8/21.8 Hz); ^{13}C NMR (d_6-DMSO) δ 166.5, 165.6, 150.6 (ddd, J_{CF} = 246.5/9.6/4.3 Hz), 141.4, 139.0, 138.3 (dt, J_{CF} = 31.4/16.1 Hz), 136.6 (td, J_{CF} = 8.2/4.2 Hz), 136.3−136.1 (m), 129.2, 128.5, 128.0, 126.8, 117.8, 111.2 (dd, J_{CF} = 15.8/5.5 Hz), 54.3, 40.6; m/z HRMS (TOF ES$^+$) $C_{22}H_{19}F_3N_3O_5S$ [MH]$^+$ calcd 494.0992, found 494.0993.

*N-(2-(Hydroxyamino)-2-oxo-1-(3′,4′,5′-trifluoro-[1,1′-biphenyl]-4-yl)ethyl)-4-(sulfamoylamino)benzamide (**6ae**).* Compound **5ae** (54.2 mg, 0.110 mmol) was converted to the corresponding hydroxamic acid according to General Procedure C. Upon completion, the mixture was purified by preparative HPLC to afford compound **6ae** as a beige fluffy solid after lyophilization (39.3 mg, 72%). ^{1}H NMR (d_6-DMSO) δ 11.07 (s, 1H), 9.93 (s, 1H), 8.75 (d, J = 8.2 Hz, 1H), 7.88 (d, J = 8.7 Hz, 2H), 7.81−7.65 (m, 4H), 7.61 (d, J = 8.4 Hz, 2H), 7.29 (s, 2H), 7.19 (d, J = 8.8 Hz, 2H), 5.66 (d, J = 8.1 Hz, 1H); ^{19}F NMR (d_6-DMSO) δ −134.9 (d, J = 21.7 Hz), −163.5 (dd, J = 21.7/21.7 Hz); ^{13}C NMR (d_6-DMSO) δ 166.6, 165.8, 150.7 (ddd, J_{CF} = 246.7/9.8/4.3 Hz), 142.5, 139.1, 138.3 (dt, J_{CF} = 31.1/15.9 Hz), 136.6 (td, J_{CF} = 8.1/4.6 Hz), 136.2 (d, J = 1.5 Hz), 128.8, 128.1, 126.8, 126.6, 116.2, 111.2 (dd, J_{CF} = 16.0/5.4 Hz), 54.2; m/z HRMS (TOF ES$^+$) $C_{21}H_{18}F_3N_4O_5S$ [MH]$^+$ calcd 495.0945, found 495.0947.

*N-(2-(Hydroxyamino)-2-oxo-1-(3′,4′,5′-trifluoro-[1,1′-biphenyl]-4-yl)ethyl)-3,4-dimethoxybenzamide (**6af**).* Compound **5af** (183 mg, 0.398 mmol) was converted to the corresponding hydroxamic acid according to General Procedure C. The crude product was purified by column chromatography (DCM/MeOH 100:0−90:10) to afford compound **6af** as a white solid (93.4 mg, 51%). ^{1}H NMR (d_6-DMSO) δ 11.08 (s, 1H), 9.07 (s, 1H), 8.86 (d, J = 8.2 Hz, 1H), 7.79−7.47 (m, 8H), 7.01 (d, J = 8.6 Hz, 1H), 5.68 (d, J = 8.1 Hz, 1H), 3.82 (s, 3H), 3.81 (s, 3H); ^{19}F NMR (d_6-DMSO) δ −134.9 (d, J = 21.7 Hz), −163.5 (dd, J = 21.7/21.7 Hz); ^{13}C NMR (d_6-DMSO) δ 166.6, 165.8, 151.5, 150.6 (ddd, J_{CF} = 246.6/9.7/4.2 Hz), 148.1, 139.1, 138.3 (dt, J_{CF} = 248.0/15.7 Hz), 136.6 (td, J_{CF} = 8.2/4.5 Hz), 136.3−135.7 (m), 128.1, 126.8, 126.0, 121.3, 111.4−111.1 (m), 111.1, 110.8, 55.6 (2C), 54.3; m/z HRMS (TOF ES$^+$) $C_{23}H_{20}F_3N_2O_5$ [MH]$^+$ calcd 461.1319, found 461.1322.

DOI: 10.1021/acs.jmedchem.9b00757
J. Med. Chem. XXXX, XXX, XXX−XXX

*3,4-Dihydroxy-N-(2-(hydroxyamino)-2-oxo-1-(3′,4′,5′-trifluoro-[1,1′-biphenyl]-4-yl)ethyl)benzamide (**6ag**).* Compound **6af** (200 mg, 0.434 mmol) was treated with BBr_3 (1 M in DCM, 4.34 mL, 4.34 mmol) according to General Procedure D to form the corresponding catechol. The crude product was purified by preparative HPLC to afford compound **6ag** as a white solid (69.3 mg, 37%). ^{1}H NMR (d_6-DMSO) δ 11.05 (s, 1H), 9.49 (s, 1H), 9.15 (s, 1H), 9.06 (s, 1H), 8.49 (d, J = 8.1 Hz, 1H), 7.80−7.64 (m, 4H), 7.61 (d, J = 8.3 Hz, 2H), 7.39−7.21 (m, 2H), 6.78 (d, J = 8.2 Hz, 1H), 5.63 (d, J = 8.1 Hz, 1H); ^{19}F NMR (d_6-DMSO) δ −134.9 (d, J = 21.6 Hz), −163.5 (dd, J = 21.7/21.7 Hz); ^{13}C NMR (d_6-DMSO) δ 166.8, 166.0, 150.7 (ddd, J_{CF} = 246.6/9.7/4.2 Hz), 148.8, 144.9, 139.3, 138.4 (dt, J_{CF} = 249.5/15.8 Hz), 136.7 (td, J_{CF} = 8.1/4.4 Hz), 136.3−136.2 (m), 128.1, 126.8, 125.0, 119.7, 115.5, 114.9, 112.7−109.9 (m), 54.3; m/z HRMS (TOF ES$^+$) $C_{21}H_{16}F_3N_2O_5$ $[MH]^+$ calcd 433.1006, found 433.1003.

*3-Fluoro-4-hydroxy-N-(2-(hydroxyamino)-2-oxo-1-(3′,4′,5′-trifluoro-[1,1′-biphenyl]-4-yl)ethyl)benzamide (**6ah**).* 3-Fluoro-4-hydroxybenzoic acid (194 mg, 1.24 mmol) was coupled to compound **4** (330 mg, 1.12 mmol) according to General Procedure A. Upon completion, the reaction mixture was diluted with a 1 M HCl solution (10 mL) and extracted with DCM (3 × 15 mL). The combined organic layers were washed with water (2 × 20 mL) and brine (20 mL). The organic layer was dried over anhydrous Na_2SO_4, filtered, and concentrated under reduced pressure. The crude product was purified by column chromatography (DCM/MeOH 100:0−95:5) to afford 430 mg of the desired product (64% of purity). The crude product was converted to the corresponding hydroxamic acid according to General Procedure C. The mixture was purified by column chromatography (DCM/MeOH 100:0−90:10) to afford compound **6ah** as a white solid (30 mg, 7%). ^{1}H NMR (d_6-DMSO) δ 11.05 (s, 1H), 10.53 (s, 1H), 9.05 (s, 1H), 8.82 (d, J = 8.1 Hz, 1H), 7.85−7.47 (m, 8H), 6.99 (t, J = 8.7 Hz, 1H), 5.63 (d, J = 8.1 Hz, 1H); ^{19}F NMR (d_6-DMSO) δ −134.9 (d, J = 21.8 Hz), −136.6, −163.5 (dd, J = 21.8/21.8 Hz); ^{13}C NMR (d_6-DMSO) δ 166.5, 164.9 (d, J_{CF} = 2.0 Hz), 150.6 (ddd, J_{CF} = 246.5/9.8/4.2 Hz), 150.3 (d, J_{CF} = 241.0 Hz), 148.1 (d, J_{CF} = 12.1 Hz), 138.9, 138.3 (dt, J_{CF} = 249.1/15.9 Hz), 136.8−136.4 (m), 136.3−136.1 (m), 128.1, 126.7, 125.0 (d, J_{CF} = 2.8 Hz), 124.9 (d, J_{CF} = 5.3 Hz), 117.0 (d, J_{CF} = 2.9 Hz), 115.9 (d, J_{CF} = 19.6 Hz), 111.6−110.6 (m), 54.4; m/z HRMS (TOF ES$^+$) $C_{21}H_{15}F_4N_2O_4$ $[MH]^+$ calcd 435.0962, found 435.0968.

*4-Fluoro-3-hydroxy-N-(2-(hydroxyamino)-2-oxo-1-(3′,4′,5′-trifluoro-[1,1′-biphenyl]-4-yl)ethyl)benzamide (**6ai**).* 4-Fluoro-3-hydroxybenzoic acid (233 mg, 1.49 mmol) was coupled to compound **4** (400 mg, 1.35 mmol) according to General Procedure A. Upon completion, the reaction mixture was diluted with a 1 M HCl solution (10 mL) and extracted with DCM (3 × 15 mL). The combined organic layers were washed with water (2 × 20 mL) and brine (20 mL). The organic layer was dried over anhydrous Na_2SO_4, filtered, and concentrated under reduced pressure. The crude was purified by column chromatography (DCM/MeOH 98:2−90:10) to afford 577 mg of a white solid (53% purity). The product was converted to the corresponding hydroxamic acid according to General Procedure C. After stirring at rt for 1 day, 40% of the starting material had converted to compound **6ai**. The reaction was left for a further 6 days reaching 70% conversion according to LC−MS. The reaction was stopped, and the starting material and compound **6ai** were isolated by column chromatography (DCM/MeOH 100:0−90:10), in which 68 mg (13%) of compound **6ai** was obtained as a pale yellow solid and 10 mg of the starting material was recovered. ^{1}H NMR (d_6-DMSO) δ 11.04 (s, 1H), 10.11 (s, 1H), 9.04 (s, 1H), 8.87 (d, J = 8.1 Hz, 1H), 7.74−7.66 (m, 4H), 7.60 (d, J = 8.4 Hz, 2H), 7.49 (dd, J = 8.6/2.2 Hz, 1H), 7.41 (ddd, J = 8.4/4.3/2.2 Hz, 1H), 7.21 (dd, J = 11.0/8.5 Hz, 1H), 5.60 (d, J = 8.1 Hz, 1H); ^{19}F NMR (d_6-DMSO) δ −132.2, −134.9 (d, J = 21.7 Hz), −163.5 (dd, J = 21.7/21.7 Hz); ^{13}C NMR (d_6-DMSO) δ 166.5, 165.5, 153.1 (d, J_{CF} = 246.2 Hz), 150.6 (ddd, J_{CF} = 246.4/10.2/4.0 Hz), 144.6 (d, J_{CF} = 12.4 Hz), 138.9, 138.3 (dt, J_{CF} = 243.0/12.5 Hz), 136.6 (td, J_{CF} = 7.9/4.6 Hz), 136.3−136.1 (m), 130.6 (d, J_{CF} = 3.1 Hz), 128.1, 126.8, 119.3 (d, J_{CF} = 7.4 Hz), 117.7 (d, J_{CF} = 3.9 Hz), 115.8 (d, J_{CF} = 18.9 Hz), 111.9−110.6 (m), 54.4; m/z MS (TOF ES$^-$) $C_{21}H_{13}F_4N_2O_4$ $[M - H]^-$ calcd 433.1, found 433.1; m/z HRMS (TOF ES$^+$) $C_{21}H_{15}F_4N_2O_4$ $[MH]^+$ calcd 435.0962, found 435.0973.

*N-(2-(Hydroxyamino)-2-oxo-1-(3′,4′,5′-trifluoro-[1,1′-biphenyl]-4-yl)ethyl)-1H-indole-5-carboxamide (**6aj**).* Compound **5aj** (200 mg, 0.456 mmol) was converted to the corresponding hydroxamic acid according to General Procedure C. Upon completion, the solvent was concentrated in vacuo. An aqueous 10% citric acid solution was added dropwise to the crude residue. The precipitate was filtered and purified by flash column chromatography (PE/EtOAc 100:0−15:85) to afford compound **6aj** as a white solid (129 mg, 64%). ^{1}H NMR (MeOD) δ 8.19 (d, J = 1.3 Hz, 1H), 7.69−7.59 (m, 5H), 7.47−7.36 (m, 3H), 7.32 (d, J = 3.2 Hz, 1H), 6.56 (dd, J = 3.2, 0.8 Hz, 1H), 5.73 (s, 1H); ^{19}F NMR (MeOD) δ −136.9 (d, J = 19.8 Hz), −166.0 (dd, J = 19.9/19.9 Hz); ^{13}C NMR (MeOD) δ 171.0, 169.5, 152.6 (ddd, J_{CF} = 247.9/9.9/4.2 Hz), 141.8−139.2 (m), 139.7, 139.5, 139.0, 138.5 (td, J_{CF} = 7.8/4.5 Hz), 129.2 (2C), 129.0, 128.2 (2C), 127.4, 125.6, 121.8, 121.7, 112.3−111.9 (m, 3C), 103.7, 56.2; m/z HRMS (TOF ES$^+$) $C_{23}H_{17}F_3N_3O_3$ $[MH]^+$ calcd 440.1217, found 440.1210.

*N-(2-(Hydroxyamino)-2-oxo-1-(3′,4′,5′-trifluoro-[1,1′-biphenyl]-4-yl)ethyl)-1H-indazole-5-carboxamide (**6ak**).* Compound **5ak** (45 mg, 0.102 mmol) was converted to the corresponding hydroxamic acid according to General Procedure C. Upon completion, the solvent was concentrated in vacuo. An aqueous 10% citric acid solution was added dropwise to the crude residue. The precipitate was filtered and washed thoroughly with water, then triturated with Et_2O to afford compound **6ak** as an off-white solid (40 mg, 89%). ^{1}H NMR (d_6-DMSO) δ 13.32 (s, 1H), 11.11 (s, 1H), 9.09 (s, 1H), 8.93 (d, J = 8.1 Hz, 1H), 8.48 (s, 1H), 8.21 (s, 1H), 7.91 (dd, J = 8.8/1.2 Hz, 1H), 7.80−7.52 (m, 7H), 5.70 (d, J = 8.0 Hz, 1H); ^{19}F NMR (d_6-DMSO) δ −134.9 (d, J = 21.7 Hz), −163.5 (dd, J = 21.7/21.7 Hz); ^{13}C NMR (d_6-DMSO) δ 167.0, 166.9, 150.9 (ddd, J_{CF} = 246.9/9.7/4.2 Hz), 141.4, 139.2, 138.6 (dt, J_{CF} = 31.4/15.9 Hz), 136.8 (td, J_{CF} = 7.9/4.4 Hz), 136.6, 135.3, 128.4 (2C), 127.1 (2C), 126.4, 126.0, 122.6, 121.7, 111.4 (m, 2C), 110.1, 54.8; m/z HRMS (TOF ES$^+$) $C_{22}H_{16}F_3N_4O_3$ $[MH]^+$ calcd 441.1169, found 441.1176.

*N-(2-(Hydroxyamino)-2-oxo-1-(3′,4′,5′-trifluoro-[1,1′-biphenyl]-4-yl)ethyl)-1H-benzo[d][1,2,3]triazole-5-carboxamide (**6al**).* Compound **5al** (90 mg, 0.204 mmol) was converted to the corresponding hydroxamic acid according to General Procedure C. Upon completion, the solvent was concentrated in vacuo. An aqueous 10% citric acid solution was added dropwise to the crude residue. The precipitate was filtered and washed thoroughly with water, then triturated in Et_2O to afford compound **6al** as a yellow solid (75 mg, 83%). ^{1}H NMR (d_6-DMSO) δ 11.09 (s, 1H), 9.22 (d, J = 8.0 Hz, 1H), 9.07 (s, 1H), 8.60 (s, 1H), 8.02−7.91 (m, 2H), 7.79−7.61 (m, 7H), 5.75−5.63 (m, 1H); ^{19}F NMR (d_6-DMSO) δ −134.9 (d, J = 21.7 Hz), −163.5 (dd, J = 21.7/21.7 Hz); ^{13}C NMR (d_6-DMSO, rotamers) δ 171.9, 171.5, 166.6, 166.3, 150.8 (ddd, J_{CF} = 246.8/9.8/4.3 Hz), 138.9 (2C), 138.5 (dt, J_{CF} = 248.9/15.7 Hz), 136.8−136.6 (m),[a] 136.5, 129.0, 128.4 (3C), 127.0, 126.9 (3C), 111.6−111.2 (m), 54.8; m/z HRMS (TOF ES$^+$) $C_{21}H_{15}F_3N_5O_3$ $[MH]^+$ calcd 442.1122, found 442.1127.

*N-(2-(Hydroxyamino)-2-oxo-1-(3′,4′,5′-trifluoro-[1,1′-biphenyl]-4-yl)ethyl)-1H-benzo[d]imidazole-5-carboxamide (**6am**).* Compound **5am** (80 mg, 0.182 mmol) was converted to the corresponding hydroxamic acid according to General Procedure C. Upon completion, the solvent was concentrated in vacuo. An aqueous 10% citric acid solution was added dropwise to the crude residue. The resultant solid was filtered and washed thoroughly with water, then triturated in Et_2O to afford compound **6am** as an off-white solid (75 mg, 94%). ^{1}H NMR (MeOD) δ 8.33 (s, 1H), 8.22 (d, J = 1.0 Hz, 1H), 7.85 (dd, J = 8.5/1.6 Hz, 1H), 7.71−7.61 (m, 5H), 7.46−7.37 (m, 2H), 5.73 (s, 1H); ^{19}F NMR (MeOD) δ −136.8 (d, J = 19.8 Hz), −165.9 (dd, J = 19.8/19.8 Hz); ^{13}C NMR (MeOD) δ 170.0, 169.4, 152.6 (ddd, J_{CF} = 247.9/9.9/4.1 Hz), 144.8, 141.9−138.3 (m), 140.7, 139.2, 139.1, 138.6, 138.5−138.3 (m), 129.8, 129.3 (2C), 128.2 (2C), 123.6, 116.8, 115.8, 112.1 (m, 2C), 56.5; m/z HRMS (TOF ES$^+$) $C_{22}H_{16}F_3N_4O_3$ $[MH]^+$ calcd 441.1169, found 441.1176.

DOI: 10.1021/acs.jmedchem.9b00757
J. Med. Chem. XXXX, XXX, XXX−XXX

*N-(2-(Hydroxyamino)-2-oxo-1-(3′,4′,5′-trifluoro-[1,1′-biphenyl]-4-yl)ethyl)-2-oxoindoline-5-carboxamide (**6an**).* Compound **5an** (70 mg, 0.154 mmol) was converted to the corresponding hydroxamic acid according to General Procedure C. Upon completion, the solvent was concentrated in vacuo. An aqueous 10% citric acid solution was added dropwise to the crude residue. The resultant solid was filtered and washed thoroughly with water. The solid was purified by flash column chromatography (DCM/MeOH 100:0−90:10) to afford compound **6an** as a dull yellow solid (30 mg, 43%). ^{1}H NMR (d_6-DMSO) δ 11.05 (s, 1H), 10.63 (s, 1H), 9.05 (s, 1H), 8.72 (d, J = 8.1 Hz, 1H), 7.82 (d, J = 7.7 Hz, 2H), 7.76−7.65 (m, 4H), 7.60 (d, J = 8.4 Hz, 2H), 6.86 (d, J = 8.5 Hz, 1H), 5.64 (d, J = 8.1 Hz, 1H), 3.53 (s, 2H); ^{19}F NMR (d_6-DMSO) δ −134.9 (d, J = 21.8 Hz), −163.5 (dd, J = 21.7/21.7 Hz); ^{13}C NMR (d_6-DMSO) δ 177.9, 167.3, 166.9, 151.2 (ddd, J_{CF} = 247.0/9.8/4.2 Hz), 147.18, 139.12, 138.9 (dt, J_{CF} = 32.1/15.4 Hz), 137.1−136.8 (m, 2C), 128.6 (3C), 127.4 (2C), 127.2, 126.3, 124.5, 111.7 (m, 2C), 109.3, 54.9, 36.1; m/z HRMS (TOF ES$^+$) $C_{23}H_{17}F_3N_3O_4$ [MH]$^+$ calcd 456.1166, found 456.1172.

*N-Hydroxy-2-(2-phenylacetamido)-2-(3′,4′,5′-trifluoro-[1,1′-biphenyl]-4-yl)acetamide (**6ao**).* Compound **5ao** (54.0 mg, 0.131 mmol) was converted to the corresponding hydroxamic acid according to General Procedure C. The crude product was purified by column chromatography (DCM/MeOH 100:0−90:0) to afford compound **6ao** as a white solid (26.7 mg, 49%). ^{1}H NMR (d_6-DMSO) δ 11.0 (s, 1H), 9.04 (s, 1H), 8.92 (d, J = 8.3 Hz, 1H), 7.76−7.64 (m, 4H), 7.50 (d, J = 8.3 Hz, 2H), 7.32−7.17 (m, 5H), 5.42 (d, J = 8.3 Hz, 1H), 3.58 (s, 2H); ^{19}F NMR (d_6-DMSO) δ −134.9 (d, J = 21.7 Hz), −163.5 (dd, J = 21.7/21.7 Hz); ^{13}C NMR (d_6-DMSO) δ 169.9, 166.3, 150.6 (ddd, J_{CF} = 246.4/9.8/4.3 Hz), 139.3, 138.3 (dt, J_{CF} = 31.3/16.9 Hz), 136.5 (td, J_{CF} = 7.8/4.1 Hz), 136.4, 136.2−136.1 (m), 129.1, 128.2, 127.5, 126.8, 126.3, 111.8−110.3 (m), 53.5, 41.7; m/z HRMS (TOF ES$^+$) $C_{22}H_{18}F_3N_2O_3$ [MH]$^+$ calcd 415.1264, found 415.1264.

*2-(2-(3-Fluorophenyl)acetamido)-N-hydroxy-2-(3′,4′,5′-trifluoro-[1,1′-biphenyl]-4-yl)acetamide (**6ap**).* Compound **5ap** (198 mg, 0.459 mmol) was converted to the corresponding hydroxamic acid according to General Procedure C. The crude product was purified by column chromatography (DCM/MeOH 100:0−90:10) followed by preparative HPLC to afford compound **6ap** as a white solid (101 mg, 51%). ^{1}H NMR (d_6-DMSO) δ 11.07 (s, 1H), 9.07 (s, 1H), 8.99 (d, J = 8.2 Hz, 1H), 7.84−7.61 (m, 4H), 7.51 (d, J = 8.2 Hz, 2H), 7.32 (dd, J = 14.5/7.5 Hz, 1H), 7.18−6.90 (m, 3H), 5.43 (d, J = 8.2 Hz, 1H), 3.63 (s, 2H); ^{19}F NMR (d_6-DMSO) δ −113.8, −134.9 (d, J = 21.7 Hz), −163.5 (dd, J = 21.6/21.6 Hz); ^{13}C NMR (d_6-DMSO) δ 169.4, 166.4, 162.0 (d, J_{CF} = 243.0 Hz), 150.6 (ddd, J_{CF} = 246.7/9.7/4.1 Hz), 139.2 (d, J = 4.3 Hz), 139.1, 138.3 (dt, J_{CF} = 249.5/15.7 Hz), 136.5 (td, J_{CF} = 8.1/4.4 Hz), 136.3 (m), 130.0 (d, J_{CF} = 8.4 Hz), 127.6, 126.8, 125.2 (d, J_{CF} = 2.5 Hz), 115.8 (d, J_{CF} = 21.3 Hz), 113.2 (d, J_{CF} = 20.8 Hz), 111.2 (m), 53.6, 41.3; m/z HRMS (TOF ES$^+$) $C_{22}H_{17}F_4N_2O_3$ [MH]$^+$ calcd 433.1170, found 433.1188.

*2-(2-(4-Fluorophenyl)acetamido)-N-hydroxy-2-(3′,4′,5′-trifluoro-[1,1′-biphenyl]-4-yl)acetamide (**6aq**).* Compound **5aq** (47 mg, 0.109 mmol) was converted to the corresponding hydroxamic acid according to General Procedure C. The crude product was purified by column chromatography (DCM/MeOH 100:0−90:10) followed by preparative HPLC to afford compound **6aq** as a white solid (40.6 mg, 38%). ^{1}H NMR (d_6-DMSO) δ 11.05 (s, 1H), 9.06 (s, 1H), 8.94 (d, J = 8.3 Hz, 1H), 7.82−7.61 (m, 4H), 7.50 (d, J = 8.2 Hz, 2H), 7.31 (m, 2H), 7.10 (t, J = 8.8 Hz, 2H), 5.42 (d, J = 8.3 Hz, 1H), 3.58 (s, 2H); ^{19}F NMR (d_6-DMSO) δ −116.78 (s), −134.9 (d, J = 21.7 Hz), −163.5 (dd, J = 21.7/21.7 Hz); ^{13}C NMR (d_6-DMSO) δ 169.8, 166.4, 161.0 (d, J_{CF} = 241.9 Hz), 150.6 (ddd, J_{CF} = 246.7/9.8/4.2 Hz), 139.2, 138.3 (dt, J_{CF} = 249.5/15.6 Hz), 136.5 (td, J_{CF} = 8.0/4.4 Hz), 136.3−136.1 (m), 132.5 (d, J_{CF} = 3.0 Hz), 130.9 (d, J_{CF} = 8.0 Hz), 127.5, 126.8, 114.9 (d, J = 21.1 Hz), 111.5−110.7 (m), 53.5, 40.8; m/z HRMS (TOF ES$^+$) $C_{22}H_{17}F_4N_2O_3$ [MH]$^+$ calcd 433.1170, found 433.1173.

*N-Hydroxy-2-(2-(4-methoxyphenyl)acetamido)-2-(3′,4′,5′-trifluoro-[1,1′-biphenyl]-4-yl)acetamide (**6ar**).* Compound **5ar** (195 mg, 0.440 mmol) was converted to the corresponding hydroxamic acid according to General Procedure C. The crude product was purified by column chromatography (DCM/MeOH 100:0−90:10) to afford compound **6ar** as a white solid (124 mg, 64%). ^{1}H NMR (d_6-DMSO) δ 11.03 (s, 1H), 9.04 (s, 1H), 8.83 (d, J = 8.4 Hz, 1H), 7.95−7.61 (m, 4H), 7.49 (d, J = 8.3 Hz, 2H), 7.19 (d, J = 8.7 Hz, 2H), 6.84 (d, J = 8.7 Hz, 2H), 5.41 (d, J = 8.3 Hz, 1H), 3.71 (s, 3H), 3.50 (s, 2H); ^{19}F NMR (d_6-DMSO) δ −134.9 (d, J = 21.7 Hz), −163.5 (dd, J = 21.7/21.7 Hz); ^{13}C NMR (d_6-DMSO) δ 170.2, 166.4, 157.9, 150.6 (ddd, J_{CF} = 246.6/9.7/4.1 Hz), 139.3, 138.3 (dt, J_{CF} = 249.2/15.6 Hz), 136.5 (td, J_{CF} = 8.1/4.4 Hz), 136.2−136.0 (m), 130.0, 128.3, 127.5, 126.8, 113.6, 111.2 (m), 55.0, 53.4, 40.9; m/z HRMS (TOF ES$^+$) $C_{23}H_{20}F_3N_2O_4$ [MH]$^+$ calcd 445.1370, found 445.1362.

*N-Hydroxy-2-(2-(4-hydroxyphenyl)acetamido)-2-(3′,4′,5′-trifluoro-[1,1′-biphenyl]-4-yl)acetamide (**6as**).* Compound **6ar** (184 mg, 0.414 mmol) was treated with BBr_3 (1 M in DCM, 2.07 mL, 2.07 mmol) according to General Procedure D. The crude product was purified by preparative HPLC to afford compound **6as** as a white solid (58 mg, 32%). ^{1}H NMR (d_6-DMSO) δ 11.05 (s, 1H), 9.21 (s, 1H), 9.05 (s, 1H), 8.78 (d, J = 8.4 Hz, 1H), 7.75−7.63 (m, 4H), 7.50 (d, J = 8.3 Hz, 2H), 7.07 (d, J = 8.5 Hz, 2H), 6.68 (d, J = 8.5 Hz, 2H), 5.42 (d, J = 8.3 Hz, 1H), 3.45 (s, 2H); ^{19}F NMR (d_6-DMSO) δ −134.9 (d, J = 21.7 Hz), −163.5 (dd, J = 21.7/21.7 Hz); ^{13}C NMR (d_6-DMSO) δ 170.5, 166.4, 155.9, 150.6 (ddd, J_{CF} = 246.6/9.7/4.2 Hz), 139.4, 138.3 (dt, J_{CF} = 249.3/15.7 Hz), 136.6 (td, J_{CF} = 8.1/4.4 Hz), 136.3−136.0 (m), 130.0, 127.5, 126.8, 126.5, 115.0, 111.6−110.9 (m), 53.5, 41.0; m/z HRMS (TOF ES$^+$) $C_{22}H_{18}F_3N_2O_4$ [MH]$^+$ calcd 431.1213, found 431.1214.

*4-(2-((2-(Hydroxyamino)-2-oxo-1-(3′,4′,5′-trifluoro-[1,1′-biphenyl]-4-yl)ethyl)amino)-2-oxoethyl)benzamide (**6at**).* Compound **5at** (198 mg, 0.434 mmol) was converted to the corresponding hydroxamic acid according to General Procedure C. The crude product was purified by column chromatography followed by preparative HPLC to afford compound **6at** as a white solid (33.5 mg, 17%). ^{1}H NMR (d_6-DMSO) δ 11.05 (s, 1H), 9.05 (s, 1H), 8.99 (d, J = 8.3 Hz, 1H), 7.90 (br s, 1H), 7.78 (d, J = 8.2 Hz, 2H), 7.74−7.64 (m, 4H), 7.50 (d, J = 8.3 Hz, 2H), 7.33 (d, J = 8.2 Hz, 2H), 7.29 (br s, 1H), 5.41 (d, J = 8.3 Hz, 1H), 3.64 (s, 2H); ^{19}F NMR (d_6-DMSO) δ −134.9 (d, J = 21.7 Hz), −163.5 (dd, J = 21.7/21.7 Hz); ^{13}C NMR (d_6-DMSO) δ 169.5, 167.8, 166.3, 150.6 (ddd, J_{CF} = 246.3/9.4/4.6 Hz), 139.7, 139.9−139.0 (m), 139.2, 136.5 (td, J_{CF} = 5.3/2.2 Hz), 136.3−136.1 (m), 132.5, 128.9, 127.5, 127.4, 126.8, 111.4−111.0 (m), 53.5, 41.5; m/z HRMS (TOF ES$^+$) $C_{23}H_{19}F_3N_3O_4$ [MH]$^+$ calcd 458.1322, found 458.1320.

*2-(2-(3,4-Dimethoxyphenyl)acetamido)-N-hydroxy-2-(3′,4′,5′-trifluoro-[1,1′-biphenyl]-4-yl)acetamide (**6au**).* Compound **5au** (413 mg, 0.872 mmol) was converted to the corresponding hydroxamic acid according to General Procedure C. The crude product was purified by column chromatography (DCM/MeOH 100:0−90:0) to afford compound **6au** as a white solid (100 mg, 24%). ^{1}H NMR (d_6-DMSO) δ 11.04 (s, 1H), 9.04 (s, 1H), 8.84 (d, J = 8.4 Hz, 1H), 7.75−7.63 (m, 4H), 7.50 (d, J = 8.3 Hz, 2H), 6.92 (d, J = 1.9 Hz, 1H), 6.85 (d, J = 8.2 Hz, 1H), 6.78 (dd, J = 8.2/1.9 Hz, 1H), 5.42 (d, J = 8.4 Hz, 1H), 3.72 (s, 3H), 3.71 (s, 3H), 3.49 (s, 2H); ^{19}F NMR (d_6-DMSO) δ −134.9 (d, J = 21.7 Hz), −163.5 (dd, J = 21.7/21.7 Hz); ^{13}C NMR (d_6-DMSO) δ 170.1, 166.4, 150.6 (ddd, J_{CF} = 246.5,/9.7/4.2 Hz), 148.5, 147.5, 139.3, 138.3 (dt, J_{CF} = 31.0/15.7 Hz), 136.5 (td, J_{CF} = 8.0/4.3 Hz), 136.2−136.1 (m), 128.8, 127.5, 126.8, 121.0, 112.9, 111.8, 111.5−110.5 (m), 55.5, 55.4, 53.4, 41.4; m/z HRMS (TOF ES$^+$) $C_{24}H_{22}F_3N_2O_5$ [MH]$^+$ calcd 475.1475, found 475.1477.

*2-(2-(3,4-Dihydroxyphenyl)acetamido)-N-hydroxy-2-(3′,4′,5′-trifluoro-[1,1′-biphenyl]-4-yl)acetamide (**6av**).* Compound **6au** (213 mg, 0.449 mmol) was treated with BBr_3 (1 M in DCM, 4.49 mL, 4.49 mmol) according to General Procedure D to form the corresponding catechol. The crude product was purified by preparative HPLC to afford compound **6av** as a white solid (97.9 mg, 49%). ^{1}H NMR (d_6-DMSO) δ 11.05 (s, 1H), 9.05 (br s, 1H), 8.85−8.53 (m, 3H), 7.76−7.62 (m, 4H), 7.49 (d, J = 8.3 Hz, 2H), 6.69 (d, J = 2.0 Hz, 1H), 6.64 (d, J = 8.0 Hz, 1H), 6.53 (dd, J = 8.0/2.0 Hz, 1H), 5.41 (d, J = 8.3 Hz,

DOI: 10.1021/acs.jmedchem.9b00757
J. Med. Chem. XXXX, XXX, XXX−XXX

1H), 3.39 (s, 2H); ^{19}F NMR (d_6-DMSO) δ −134.9 (d, J = 21.7 Hz), −163.5 (dd, J = 21.7/21.7 Hz); ^{13}C NMR (d_6-DMSO) δ 170.5, 166.4, 150.7 (ddd, J_{CF} = 246.5/9.6/4.1 Hz), 145.0, 143.9, 139.4, 138.3 (dt, J_{CF} = 236.0/15.9 Hz), 136.6 (td, J_{CF} = 8.2/4.4 Hz), 136.3−136.2 (m), 127.5, 127.1, 126.8, 119.9, 116.6, 115.4, 112.6−109.0 (m), 53.4, 41.3; m/z HRMS (TOF ES$^+$) $C_{22}H_{18}F_3N_2O_5$ $[MH]^+$ calcd 447.1162, found 444.1162.

*2-(2-(3-Fluoro-4-hydroxyphenyl)acetamido)-N-hydroxy-2-(3′,4′,5′-trifluoro-[1,1′-biphenyl]-4-yl)acetamide (**6ax**).* Compound **5aw** (104 mg, 0.225 mmol) was converted to the corresponding hydroxamic acid according to General Procedure C, affording 67.2 mg of 2-(2-(3-fluoro-4-methoxyphenyl)acetamido)-*N*-hydroxy-2-(3′,4′,5′-trifluoro-[1,1′-biphenyl]-4-yl)acetamide (**6aw**). This was treated with BBr_3 (1 M in DCM, 0.724 μL, 0.724 μmol) according to General Procedure D. The resulting precipitate was filtered to afford compound **6ax** as an off-white solid (46.5 mg, 72%). ^{1}H NMR (d_6-DMSO) 11.07 (s, 1H), 9.71 (br s, 1H), 8.84 (d, J = 8.2 Hz, 1H), 7.79−7.60 (m, 4H), 7.49 (d, J = 8.3 Hz, 2H), 7.11−6.98 (m, 1H), 6.93−6.74 (m, 2H), 5.40 (d, J = 8.2 Hz, 1H), 3.47 (s, 2H); ^{19}F NMR (d_6-DMSO) δ −134.8 (d, J = 21.7 Hz), −136.8, −163.5 (dd, J = 21.6/21.6 Hz); ^{13}C NMR (d_6-DMSO) δ 170.2, 166.5, 150.8 (d, J = 240.0 Hz), 150.7 (ddd, J = 12.7/9.6/4.2 Hz), 143.4 (d, J = 12.1 Hz), 139.3, 138.4 (dt, J = 249.1/15.4 Hz), 136.6 (td, J = 8.2/4.5 Hz), 136.4−136.3 (m), 127.7, 127.6, 126.9, 125.2 (d, J = 3.0 Hz), 117.5 (d, J = 3.0 Hz), 116.7 (d, J = 18.4 Hz), 111.3 (m), 53.6, 40.7; m/z HRMS (TOF ES$^+$) $C_{22}H_{17}F_4N_2O_4$ $[MH]^+$ calcd 449.1117, found 449.1125.

*2-(2-(4-Fluoro-3-methoxyphenyl)acetamido)-N-hydroxy-2-(3′,4′,5′-trifluoro-[1,1′-biphenyl]-4-yl)acetamide (**6ay**).* Compound **5ay** (367 mg, 0.795 mmol) was converted to the corresponding hydroxamic acid according to General Procedure C. The crude product was purified by column chromatography (DCM/MeOH 100:0−90:0) to afford the desired hydroxamic acid analogue as a white solid (**6ay**) (226 mg, 61%). ^{1}H NMR (d_6-DMSO) δ 11.05 (s, 1H), 9.05 (s, 1H), 8.95 (d, J = 8.3 Hz, 1H), 7.81−7.63 (m, 4H), 7.50 (d, J = 8.3 Hz, 2H), 7.19−7.01 (m, 2H), 6.81 (ddd, J = 8.2/4.3/2.0 Hz, 1H), 5.41 (d, J = 8.3 Hz, 1H), 3.80 (s, 3H), 3.55 (s, 2H); ^{19}F NMR (d_6-DMSO) δ −134.9 (d, J = 21.7 Hz), −138.9 (s), −163.5 (dd, J = 21.7/21.7 Hz); ^{13}C NMR (d_6-DMSO) δ 169.7, 166.3, 150.6 (ddd, J_{CF} = 246.7/9.8/4.3 Hz), 150.4 (d, J_{CF} = 242.0 Hz), 146.7 (d, J_{CF} = 10.6 Hz), 139.3, 138.3 (dt, J_{CF} = 31.4/15.9 Hz), 136.5 (td, J_{CF} = 8.1/4.4 Hz), 136.3−136.1 (m), 133.1 (d, J_{CF} = 3.7 Hz), 127.5, 126.8, 121.2 (d, J_{CF} = 6.7 Hz), 115.4 (d, J_{CF} = 17.9 Hz), 114.6 (d, J_{CF} = 1.5 Hz), 111.7−110.4 (m), 55.8, 53.5, 41.3; m/z MS $C_{23}H_{19}F_4N_2O_4$ $[MH]^+$ calcd 463.1, found 462.8.

*2-(2-(4-Fluoro-3-hydroxyphenyl)acetamido)-N-hydroxy-2-(3′,4′,5′-trifluoro-[1,1′-biphenyl]-4-yl)acetamide (**6az**).* Compound **6ay** (205 mg, 0.443 mmol) was treated with BBr_3 (1 M in DCM, 2.22 mL, 2.22 mmol) according to General Procedure D to form the corresponding phenol. The crude product was purified by preparative HPLC to afford compound **6az** as a white solid (156 mg, 78%). ^{1}H NMR (d_6-DMSO) δ 11.05 (s, 1H), 9.73 (s, 1H), 9.06 (s, 1H), 8.89 (d, J = 8.3 Hz, 1H), 7.76−7.63 (m, 4H), 7.49 (d, J = 8.3 Hz, 2H), 7.07−6.96 (m, 1H), 6.88 (dd, J = 8.7/2.1 Hz, 1H), 6.67 (ddd, J = 8.2/4.3/2.1 Hz, 1H), 5.40 (d, J = 8.3 Hz, 1H), 3.48 (s, 2H); ^{19}F NMR (d_6-DMSO) δ −134.9 (d, J = 21.7 Hz), −139.8, −163.5 (dd, J = 21.7/21.7 Hz); ^{13}C NMR (d_6-DMSO) δ 169.9, 166.4, 150.6 (ddd, J_{CF} = 246.5/9.7/4.1 Hz), 150.0 (d, J_{CF} = 239.0 Hz), 144.4 (d, J_{CF} = 12.2 Hz), 139.3, 138.3 (dt, J_{CF} = 249.1/15.5 Hz), 136.6 (td, J_{CF} = 8.0/4.1 Hz), 136.3−136.0 (m), 132.7 (d, J_{CF} = 3.4 Hz), 127.5, 126.8, 119.9 (d, J_{CF} = 6.4 Hz), 118.5 (d, J_{CF} = 2.7 Hz), 115.6 (d, J_{CF} = 18.0 Hz), 111.8−110.8 (m), 53.5, 41.0; m/z HRMS (TOF ES$^+$) $C_{22}H_{17}F_4N_2O_4$ $[MH]^+$ calcd 449.1117, found 449.1113.

*Methyl 2-((4-Fluoro-3-methoxybenzyl)amino)-2-(3′,4′,5′-trifluoro-[1,1′-biphenyl]-4-yl)acetate (**7**).* 4-Fluoro-3-methoxybenzaldehyde (172 mg, 1.12 mmol) was added to a solution of compound **4** (300 mg, 1.02 mmol) in DCE (10 mL) and stirred for 30 min before adding $Na(OAc)_3BH$ (540 mg, 2.55 mmol). The reaction mixture was stirred at rt overnight. Upon completion, the reaction mixture was diluted with sat. $NaHCO_3$ (20 mL) and extracted with DCM (3 × 20 mL). The combined organic layers were dried over anhydrous Na_2SO_4, filtered, and concentrated in vacuo. The crude product was purified by column chromatography (PE/EtOAc 100:0−50:50) to afford compound **7** as a clear oil (405 mg, 92%). ^{1}H NMR ($CDCl_3$) δ 7.53−7.41 (m, 4H), 7.22−7.13 (m, 2H), 7.01−6.93 (m, 2H), 6.83−6.76 (m, 1H), 4.41 (s, 1H), 3.87 (s, 3H), 3.72 (s, 3H), 3.71 (s, 2H), 2.42 (br s, 1H); ^{19}F NMR ($CDCl_3$) δ −134.0 (d, J = 20.6 Hz), −137.4, −162.3 (dd, J = 20.5/20.5 Hz); ^{13}C NMR ($CDCl_3$) δ 173.2, 151.7 (d, J_{CF} = 244.9 Hz), 151.5 (ddd, J_{CF} = 249.7/10.1/4.3 Hz), 147.6 (d, J_{CF} = 10.8 Hz), 140.9−137.9 (m), 138.3, 138.1−138.0 (m), 136.7 (td, J_{CF} = 7.8/4.7 Hz), 135.6 (d, J_{CF} = 3.7 Hz), 128.3, 127.3, 120.5 (d, J_{CF} = 6.8 Hz), 115.8 (d, J_{CF} = 18.3 Hz), 113.4 (d, J_{CF} = 1.9 Hz), 111.4−110.6 (m), 63.9, 56.2, 52.5, 51.1; m/z MS $C_{23}H_{20}F_4NO_3$ $[MH]^+$ calcd 434.1, found 433.9.

*2-((4-Fluoro-3-methoxybenzyl)amino)-N-hydroxy-2-(3′,4′,5′-trifluoro-[1,1′-biphenyl]-4-yl)acetamide (**8**).* Compound **7** (365 mg, 0.842 mmol) was converted to the corresponding hydroxamic acid according to General Procedure C. The crude product was purified by column chromatography (DCM/MeOH 100:0−90:0) to afford compound **8** as a white solid (242 mg, 66%). ^{1}H NMR (d_6-DMSO) δ 10.80 (s, 1H), 8.95 (s, 1H), 7.77−7.61 (m, 4H), 7.51 (d, J = 8.3 Hz, 2H), 7.18−7.06 (m, 2H), 6.85 (ddd, J = 8.1/4.4/1.8 Hz, 1H), 4.09 (s, 1H), 3.82 (s, 3H), 3.61 (s, 2H), 3.10 (br s, 1H); ^{19}F NMR (d_6-DMSO) δ −135.0 (d, J = 21.7 Hz), −138.4, −163.7 (dd, J = 21.7/21.7 Hz); ^{13}C NMR (d_6-DMSO) δ 168.3, 150.6 (ddd, J_{CF} = 246.5/9.7/4.2 Hz), 150.5 (d, J_{CF} = 242.0 Hz), 146.9 (d, J_{CF} = 10.6 Hz), 140.3, 139.8−136.9 (m), 137.0 (d, J_{CF} = 3.5 Hz), 136.7 (td, J_{CF} = 8.1/4.3 Hz), 136.1−135.9 (m), 128.0, 126.6, 119.9 (d, J_{CF} = 6.7 Hz), 115.3 (d, J_{CF} = 17.8 Hz), 113.3 (d, J_{CF} = 1.4 Hz), 111.9−110.6 (m), 61.8, 55.8, 49.9; m/z MS $C_{22}H_{19}F_4N_2O_3$ $[MH]^+$ calcd 435.1, found 434.9

*2-((4-Fluoro-3-hydroxybenzyl)amino)-N-hydroxy-2-(3′,4′,5′-trifluoro-[1,1′-biphenyl]-4-yl)acetamide HCl Salt (**9**).* Compound **8** (200 mg, 0.460 mmol) was treated with BBr_3 (1 M in DCM, 2.30 mL, 2.30 mmol) according to General Procedure D. Upon completion, the reaction was quenched with a 1 M HCl solution (3 mL) and stirred vigorously for 10 min. The mixture was neutralized to pH 7 with sat. $NaHCO_3$ and extracted with EtOAc (3 × 10 mL). The combined organic layers were dried over anhydrous Na_2SO_3, filtered, and concentrated in vacuo. To convert the neutralized product to the corresponding HCl salt, the crude product (126 mg, 0.300 mmol) was dissolved in MeOH (8 mL) before addition of 1 M HCl (600 μL, 0.600 mmol) and stirred overnight at rt. The reaction mixture was concentrated in vacuo and lyophilized to remove excess HCl to afford compound **9** as a white solid (125 mg, 27%). ^{1}H NMR (d_6-DMSO) δ 11.55 (s, 1H), 10.21 (s, 1H), 10.13 (br s, 2H), 9.40 (br s, 1H), 7.84 (d, J = 8.4 Hz, 2H), 7.81−7.73 (m, 2H), 7.70 (d, J = 8.4 Hz, 2H), 7.23−7.09 (m, 2H), 6.90 (ddd, J = 8.1/4.0/2.1 Hz, 1H), 4.84 (s, 1H), 3.93 (q, J = 12.6 Hz, 2H); ^{19}F NMR (d_6-DMSO) δ −134.7 (d, J = 21.7 Hz), −135.7, −162.8 (dd, J = 21.7/21.7 Hz); ^{13}C NMR (d_6-DMSO) δ 162.8, 151.5 (d, J_{CF} = 242.8 Hz), 150.7 (ddd, J_{CF} = 246.7/9.7/4.2 Hz), 144.9 (d, J = 12.3 Hz), 138.6 (dt, J_{CF} = 249.0/15.5 Hz), 137.89−137.7 (m), 135.9 (dt, J_{CF} = 8.4/4.0 Hz), 132.4, 129.1, 127.2, 121.7 (d, J_{CF} = 6.6 Hz), 120.2 (d, J_{CF} = 2.9 Hz), 116.1 (d, J_{CF} = 18.5 Hz), 111.8−110.9 (m), 59.3, 48.5; m/z HRMS (TOF ES$^+$) $C_{21}H_{17}F_4N_2O_3$ $[MH]^+$ calcd 421.1170, found 421.1175.

Biology. *Protein Expression and Purification.* A soluble form of human APN ectodomain was expressed and purified as reported previously.[4] In brief, human APN was expressed in a stably transfected HEK293S GnT1$^-$ cell line, which was a kind gift from Prof. James Rini from the University of Toronto, Canada. The cell growth and passaging of the cells, as well as collection of the culture supernatant, were conducted by Monash Protein Production Unit. Cells were grown in Dulbecco's modified Eagle's medium (DMEM)/F-12 supplemented with 3% fetal bovine serum (FBS) Invitrogen, 1× penicillin−streptomycin (Invitrogen), 1 mg/L doxycycline (Sigma), and 1 mg/L aprotinin (Bioshop Canada). The APN−protein A fusion protein was purified by IgG-Sepharose (GE Healthcare) affinity chromatography. The protein A tag was removed by on-column tobacco etch virus protease digestion and the liberated APN was further purified by size exclusion chromatography on a Superdex S200

DOI: 10.1021/acs.jmedchem.9b00757
J. Med. Chem. XXXX, XXX, XXX−XXX

10/300 column in 50 mM *N*-(2-hydroxyethyl)piperazine-*N*′-ethanesulfonic acid pH 8.0, 300 mM NaCl, and 5% glycerol buffer. Biochemical parameters K_m (31 ± 5 μM) and k_{cat} (456 ± 14 FU/s) were determined in the presence of L-leucine-7-amido-4-methylcoumarin hydrochloride (H-Leu-NHMec) (Sigma L2145).

APN Enzymatic Analysis. Aminopeptidase assays were based on the modified report of Drinkwater et al.[44] The activity of APN was determined by measuring the release of the fluorogenic leaving group, NH_2Mec, from the fluorogenic peptide H-Leu-NHMec (Sigma L2145). The reactions were carried out in 384-well microtiter plates, 50 μL total volume at 37 °C using a spectrofluorimeter (BMG FLUOstar) with excitation at 355 nm and emission at 460 nm. APN was preincubated in 100 mM Tris pH 8.0 at 37 °C with the inhibitors for 10 min prior to the addition of substrate (25 μM). Inhibitor concentrations were assayed with highest working concentrations of 2−320 μM, diluted 1:4 to assess an overall 1000-fold concentration series. Initially, assays were performed in experimental triplicate, and if a $K_i^{(app)}$ value of ≤100 nM was calculated, the inhibitor was considered of high priority, and assessed further in biological triplicate. The fluorescence signal was monitored for 1 h at 37 °C. Only a linear range of velocity was considered in data analysis. $K_i^{(app)}$ values were then calculated by using the Morrison equation for competitive and tight-binding inhibitors.[64,65] Analysis and graphical output were performed in GraphPad Prism 7.

Ad293 Cellular Viability Assay. Compounds were prepared as a 0.1 M stock solution in DMSO. A total of 5000 cells/well were plated out in a 96-well sterile clear TC plates in 100 μL of DMEM + 10% FBS + 1% Penstrep (Invitrogen). The plates were incubated at 37 °C and 5% CO_2 overnight. Media was aspirated off followed by washing with 100 μL of PBS pH 7.4 (Invitrogen). In a separate plate, 240 μL of each compound was prepared at the working concentration by diluting the stock solutions with the media. This was serially diluted in 1:2 ratios across well plate. From the dilution plate, 100 μL of each compound dose was dispensed into the cell-seeded plate. Final concentration ranges of 0−800 μM (bestatin) and 0−400 μM (compound **6ad** and **6ae**) were achieved. After addition of the compound, the plate was incubated for an additional 72 h. At the 72 h mark, 10 μL of CellTiter-Blue (Promega) was added to the cells followed by an additional 4 h of incubation. Fluorescence readings were obtained on EnVision (PerkinElmer) at 565/595 nm. The results were expressed as % proliferation relative to a negative DMSO control. CC_{50} values were calculated from dose−response curves (log[compound concentration] vs % proliferation) using GraphPad Prism 7.

Estimation of Kinetic Solubility Using Nephelometry. Compounds in DMSO was spiked into either pH 6.5 phosphate buffer or 0.01 M HCl (pH ∼ 2.0) with the final DMSO concentration being 1%. After 30 min had elapsed, the samples were then analyzed via Nephelometry to determine a solubility range.[66]

Estimation of Distribution Coefficient Using Chromatography. Partition coefficient values (Log *D*) of the test compounds were estimated at pH 7.4 by correlation of their chromatographic retention properties against the characteristics of a series of standard compounds with known partition coefficient values. The method employed is a gradient HPLC-based derivation of the method developed by Lombardo et al.[67]

In Vitro Metabolic Stability. The metabolic stability assay was performed by incubating each compound in human or mouse liver microsomes at 37 °C and a protein concentration of 0.4 mg/mL. The metabolic reaction was initiated by the addition of a reduced nicotinamide adenine dinucleotide phosphate (NADPH)-regenerating system and quenched at various time points over a 60 min incubation period by the addition of acetonitrile containing diazepam as internal standard. Control samples (containing no NADPH) were included (and quenched at 2, 30, and 60 min) to monitor for potential degradation in the absence of cofactor. The human liver microsomes used in this experiment were supplied by XenoTech, lot # 1410230. The mouse liver microsomes used in this experiment were supplied by XenoTech, lot # 1510256. Microsomal incubations were performed at a substrate concentration of 1 μM.

In Vitro Plasma Stability. Human plasma (pooled; n = 3 donors) was separated from whole blood procured from the Victorian Blood Donor Registry. Mouse plasma (pooled; multiple mice) from male Swiss outbred mice was collected in-house. Aliquots of plasma were spiked with DMSO/MeCN/H_2O solutions of test compound to a nominal compound concentration of 1000 ng/mL. The maximum final DMSO and acetonitrile concentrations were 0.2% (v/v) and 0.4% (v/v), respectively. Immediately after compound spiking, plasma was vortex-mixed and aliquots of spiked plasma (50 μL) were transferred into fresh microcentrifuge tubes and maintained at 37 °C under 10% CO_2 conditions. At various time points over the 240 min incubation period, triplicate plasma samples were taken and immediately snap-frozen in dry ice. All samples were stored frozen at −80 °C until analysis by LC−MS. Plasma samples were quantified relative to calibration standards prepared using blank plasma of the same species. Calibration standards were spiked with test compound over the range of 0.5−10 000 ng/mL. Internal standard (diazepam) was added to calibration standards and incubation samples and then immediately quenched using two volumes of MeCN to precipitate plasma proteins. Samples were vortex-mixed and centrifuged (10 000 rpm for 3 min) in a microcentrifuge and the supernatant analyzed by LC−MS (Water Micromass Quattro Premier coupled to a Waters Acquity UPLC). The bioanalytical method was validated with respect to calibration range, linearity, accuracy, and precision. The mean and standard deviation of measured plasma concentrations were calculated for each time point and expressed as a percentage remaining relative to the initial time point (5 min).

Computational Chemistry. *Molecular Modeling.* Molecular docking of compounds **1**, **6ad**, **6ae**, and **6ag** were carried out using Surflex docking interfaced with SYBYL2.1.1 in SFXC mode. The domain II of reference *Pf*A-M1 structure (PDB ID 4ZX4, residues 392−649) and APN structure (PDB ID 4FYQ, residues 287−546) were chosen for alignment due to the fact this domain incorporates the active site of interest and also shares the highest structural and sequence similarity across M1 aminopeptidase superfamily. A superimposed structural alignment was then performed using Pymol 1.8.23[68] with domain II of both *Pf*A-M1 and APN. The coordinates of compound **1** in the superimposed APN was subsequently extracted for later use of fragment constraints. The bond constants and charge distribution for **1** were derived using the GAFF[69] and AM1-BCC models,[70,71] respectively. To prepare the crystal structures, water molecules were removed and any missing regions were modeled using the program Modeller v9.10.[72] The flexible loop ^{891}YGGGSFSF^{898} was not resolved in the unbound structure of APN (PDB ID 4FYQ); however, it was resolved in electron density when APN was bound to either small-molecule inhibitors such as bestatin (PDB ID 4FYR) and amastatin (PDB ID 4FYT) or a peptide substrate angiotensin IV (PDB ID 4FYS).[4] We rebuilt the missing loop in 4FYQ using Modeller, and the structure was overlaid with the bound APN structures to examine if the flexible loop was modeled into a sensible position. Side-chain amides were protonated and fixed alongside charge addition using the Gasteiger−Marsili method.[73] The charge for zinc metal was 2.0. The two-dimensional ligand structures were prepared with default settings from SYBYL2.1.1. In grid generation, the core biphenyl system and hydroxamic acid were set as fragment constraints with a constraint penalty of 10. A total of 20 poses were produced for each ligand that were similar in their conformations and interactions. The differences in the total docking score between the most preferred pose and the second best pose of **1**, **6ad**, **6ae**, and **6ag** were 0.02, 0.003, 0.127, and 0.046, respectively. The best pose according to the total docking scores was selected to perform MD simulations.

MD Simulations. The APN−ligand complex models were solvated in a rectangular simulation box leaving at least 12 Å of water shell thickness at all sides of the protein with a periodic box of 117 Å × 125 Å × 120 Å. System charges were neutralized with sodium counterions.[74] Proteins and ions were modeled using the AMBER force field FF14SB and waters represented using the three-particle TIP3P model.[74,75] M1 aminopeptidase zinc and zinc-binding residues (His^{388}, His^{392}, and Glu^{411}) were prepared as described previously.[48]

DOI: 10.1021/acs.jmedchem.9b00757
J. Med. Chem. XXXX, XXX, XXX−XXX

MD simulations were performed using NAMD 2.9 on an IBM Blue Gene/Q.[76] Equilibration was performed in three stages. First, potential steric clashes in the initial configuration were relieved with 2000 steps of energy minimization. Initial velocities for each system were then assigned randomly according to a Maxwell–Boltzmann distribution at 100 K. Each system was then heated to 300 K over 0.1 ns, under the isothermal–isometric ensemble (NVT) conditions, with the protein atoms (excluding hydrogens) harmonically restrained [with a force constant of 10 kcal/(mol A^2)]. Following this, each system was simulated for another 0.1 ns under the isothermal–isobaric ensemble (NPT) with applied harmonic restraints. For each system, we repeated the above process three times to initiate the production simulations with different initial velocities in NPT. Simulation time step was set to 2 fs and the SHAKE algorithm was used to constrain all bonds involving hydrogen atoms.[77] All simulations were run at constant temperature (300 K) and pressure (1 atm), using a Langevin damping coefficient of 0.5 fs^{-1} and a Berendsen thermostat relaxation time of τ_p = 1.0 ps.[78,79] For each simulated system, periodic boundary conditions were used together with the particle-mesh Ewald method for long-range electrostatic interactions, and a real space cutoff of 10 Å was used.[80] To increase the efficiency of sampling, production MD simulations for APN were run in triplicate for 50 ns. The conformation was sampled every 5000 steps (one snapshot per 10 ps). We then used one snapshot per 100 ps to analyze the MD trajectories.

■ ASSOCIATED CONTENT

Supporting Information

The Supporting Information is available free of charge on the ACS Publications website at DOI: 10.1021/acs.jmedchem.9b00757.

Synthetic procedures (compounds **10**–**16**); MMP enzymatic analysis; RMSD of the Cα and ligands of **1**, **6ad**, **6ae**, and **6ag** along the molecular modeling trajectory; hydrogen-bond occupancy analysis of **1**, **6ad**, **6ae**, and **6ag** with APN; binding scores for the docked poses of **1**, **6ad**, **6ae**, and **6ag** into APN; and HPLC traces of biologically evaluated compounds (**6a**–**6az** and **9**) (PDF)

Molecular formula strings (CSV)

PDB file for compound **1** docking (PDB)

MD simulations of APN **6ad** (MP4)

MD simulations of APN **6ae** (MP4)

Accession Codes

The atomic coordinates for the X-ray crystal structures used as templates for molecular docking are available from the Protein Data Bank (PDB). *Pf*A-M1-**1** PDB ID 4ZX4 and human APN PDB ID 4FYQ.

■ AUTHOR INFORMATION

Corresponding Authors

*E-mail: Sheena.McGowan@monash.edu. Phone: +61 (0)3 9902 9309 (S.M.).

*E-mail: Peter.Scammells@monash.edu. Phone: +61 (0)3 9903 9542 (P.J.S.).

ORCID

Luke S. Schembri: 0000-0001-5588-1077

Christopher M. Overall: 0000-0001-5844-2731

Sheena McGowan: 0000-0001-6863-1106

Peter J. Scammells: 0000-0003-2930-895X

Author Contributions

The manuscript was written through contributions of all authors. All authors have given approval to the final version of the manuscript.

Notes

The authors declare no competing financial interest.

■ ACKNOWLEDGMENTS

This work was supported by the National Health and Medical Research Council (Project Grant 1063786 to S.M. and P.J.S.). The authors thank Prof. James Rini at the University of Toronto, Canada, for the generous donation of the cell line that expresses the recombinant human APN ectodomain. They also thank Miss Cassandra Yong for the kind donation of the Ad293 cell line and for training to perform the cell toxicity assay. They acknowledge the Monash Platforms (Protein Production and Crystallization) for technical assistance. J.L. was supported by Monash University, Sir James McNeil Foundation, and the Cancer Therapeutics CRC, CTx. W.Y. was supported by a postgraduate scholarship from Monash University.

■ ABBREVIATIONS

DIPEA, *N*,*N*-diisopropylethylamine; HCTU, *O*-(1*H*-6-chlorobenzotriazol-l-yl)-1,1,3,3-tetramethyluronium hexafluorophosphate; DMAP, 4-dimethylamonipyridine; EDCI, 1-ethyl-3-(3-dimethylaminopropyl)carbodiimide; PyBOP, (benzotriazol-1-yloxy)tripyrrolidinophosphonium hexafluorophosphate

■ ADDITIONAL NOTE

[a]May account for two carbons, as there are many overlapping quaternary carbons in this region.

■ REFERENCES

(1) Maroux, S.; Louvard, D.; Baratti, J. The aminopeptidase from hog intestinal brush border. *Biochim. Biophys. Acta, Enzymol.* **1973**, *321*, 282–295.

(2) Dixon, J.; Kaklamanis, L.; Turley, H.; Hickson, I. D.; Leek, R. D.; Harris, A. L.; Gatter, K. C. Expression of aminopeptidase-n (CD 13) in normal tissues and malignant neoplasms of epithelial and lymphoid origin. *J. Clin. Pathol.* **1994**, *47*, 43–47.

(3) Mina-Osorio, P. The moonlighting enzyme CD13: old and new functions to target. *Trends Mol. Med.* **2008**, *14*, 361–371.

(4) Wong, A. H.; Zhou, D.; Rini, J. M. The X-ray crystal structure of human aminopeptidase N reveals a novel dimer and the basis for peptide processing. *J. Biol. Chem.* **2012**, *287*, 36804–36813.

(5) Zini, S.; Fournie-Zaluski, M. C.; Chauvel, E.; Roques, B. P.; Corvol, P.; Llorens-Cortes, C. Identification of metabolic pathways of brain angiotensin II and III using specific aminopeptidase inhibitors: predominant role of angiotensin III in the control of vasopressin release. *Proc. Natl. Acad. Sci. U.S.A.* **1996**, *93*, 11968–11973.

(6) Giros, B.; Gros, C.; Solhonne, B.; Schwartz, J. C. Characterization of aminopeptidases responsible for inactivating endogenous (Met5)enkephalin in brain slices using peptidase inhibitors and anti-aminopeptidase M antibodies. *Mol. Pharmacol.* **1986**, *29*, 281–287.

(7) Xu, Y.; Wellner, D.; Scheinberg, D. A. Substance P and bradykinin are natural inhibitors of CD13/aminopeptidase N. *Biochem. Biophys. Res. Commun.* **1995**, *208*, 664–674.

(8) Bosch, B. J.; Smits, S. L.; Haagmans, B. L. Membrane ectopeptidases targeted by human coronaviruses. *Curr. Opin. Virol.* **2014**, *6*, 55–60.

(9) Kolb, A. F.; Hegyi, A.; Maile, J.; Heister, A.; Hagemann, M.; Siddell, S. G. Molecular analysis of the coronavirus-receptor function of aminopeptidase N. *Adv. Exp. Med. Biol.* **1998**, *440*, 61–67.

(10) Yeager, C. L.; Ashmun, R. A.; Williams, R. K.; Cardellichio, C. B.; Shapiro, L. H.; Look, A. T.; Holmes, K. V. Human aminopeptidase N is a receptor for human coronavirus 229E. *Nature* **1992**, *357*, 420–422.

DOI: 10.1021/acs.jmedchem.9b00757
J. Med. Chem. XXXX, XXX, XXX–XXX

(11) Mina-Osorio, P.; Ortega, E. Aminopeptidase N (CD13) functionally interacts with FcgammaRs in human monocytes. *J. Leukocyte Biol.* **2005**, *77*, 1008−1017.
(12) Pasqualini, R.; Koivunen, E.; Kain, R.; Lahdenranta, J.; Sakamoto, M.; Stryhn, A.; Ashmun, R. A.; Shapiro, L. H.; Arap, W.; Ruoslahti, E. Aminopeptidase N is a receptor for tumor-homing peptides and a target for inhibiting angiogenesis. *Cancer. Res.* **2000**, *60*, 722−727.
(13) Mina-Osorio, P.; Shapiro, L. H.; Ortega, E. CD13 in cell adhesion: aminopeptidase N (CD13) mediates homotypic aggregation of monocytic cells. *J. Leukocyte Biol.* **2006**, *79*, 719−730.
(14) Chen, L.; Lin, Y. L.; Peng, G.; Li, F. Structural basis for multifunctional roles of mammalian aminopeptidase N. *Proc. Natl. Acad. Sci. U.S.A.* **2012**, *109*, 17966−17971.
(15) Drag, M.; Bogyo, M.; Ellman, J. A.; Salvesen, G. S. Aminopeptidase fingerprints, an integrated approach for identification of good substrates and optimal inhibitors. *J. Biol. Chem.* **2010**, *285*, 3310−3318.
(16) McGowan, S.; Porter, C. J.; Lowther, J.; Stack, C. M.; Golding, S. J.; Skinner-Adams, T. S.; Trenholme, K. R.; Teuscher, F.; Donnelly, S. M.; Grembecka, J.; Mucha, A.; Kafarski, P.; Degori, R.; Buckle, A. M.; Gardiner, D. L.; Whisstock, J. C.; Dalton, J. P. Structural basis for the inhibition of the essential *Plasmodium falciparum* M1 neutral aminopeptidase. *Proc. Natl. Acad. Sci. U.S.A.* **2009**, *106*, 2537−2542.
(17) Hitzerd, S. M.; Verbrugge, S. E.; Ossenkoppele, G.; Jansen, G.; Peters, G. J. Positioning of aminopeptidase inhibitors in next generation cancer therapy. *Amino Acids* **2014**, *46*, 793−808.
(18) Bauvois, B.; Dauzonne, D. Aminopeptidase-N/CD13 (EC 3.4.11.2) inhibitors: chemistry, biological evaluations, and therapeutic prospects. *Med. Res. Rev.* **2006**, *26*, 88−130.
(19) Wickström, M.; Larsson, R.; Nygren, P.; Gullbo, J. Aminopeptidase N (CD13) as a target for cancer chemotherapy. *Cancer Sci.* **2011**, *102*, 501−508.
(20) Amin, S. A.; Adhikari, N.; Jha, T. Design of aminopeptidase N inhibitors as anti-cancer agents. *J. Med. Chem.* **2018**, *61*, 6468−6490.
(21) Ashmun, R. A.; Look, A. T. Metalloprotease activity of CD13/aminopeptidase N on the surface of human myeloid cells. *Blood* **1990**, *75*, 462−469.
(22) Hashida, H.; Takabayashi, A.; Kanai, M.; Adachi, M.; Kondo, K.; Kohno, N.; Yamaoka, Y.; Miyake, M. Aminopeptidase N is involved in cell motility and angiogenesis: its clinical significance in human colon cancer. *Gastroenterology* **2002**, *122*, 376−386.
(23) Kawamura, J.; Shimada, Y.; Kitaichi, H.; Komoto, I.; Hashimoto, Y.; Kaganoi, J.; Miyake, M.; Yamasaki, S.; Kondo, K.; Imamura, M. Clinicopathological significance of <tep-common:author-query>AQ7: Please provide a DOI number for ref 23 or indicate if one doesn’t exist.</tep-common:author-query>aminopeptidase N/CD13 expression in human gastric carcinoma. *Hepatogastroenterology* **2007**, *54*, 36−40.
(24) Liang, W.; Gao, B.; Xu, G.; Weng, D.; Xie, M.; Qian, Y. Possible contribution of aminopeptidase N (APN/CD13) to migration and invasion of human osteosarcoma cell lines. *Int. J. Oncol.* **2014**, *45*, 2475−2485.
(25) Nohara, S.; Kato, K.; Fujiwara, D.; Sakuragi, N.; Yanagihara, K.; Iwanuma, Y.; Kajiyama, Y. Aminopeptidase N (APN/CD13) as a target molecule for scirrhous gastric cancer. *Clin. Res. Hepatol. Gastroenterol.* **2016**, *40*, 494−503.
(26) Schmidt, L. H.; Brand, C.; Stucke-Ring, J.; Schliemann, C.; Kessler, T.; Harrach, S.; Mohr, M.; Gorlich, D.; Marra, A.; Hillejan, L.; Muller-Tidow, C.; Lenz, G.; Wardelmann, E.; Wiewrodt, R.; Berdel, W. E.; Schwoppe, C.; Hartmann, W. Potential therapeutic impact of CD13 expression in non-small cell lung cancer. *PLoS One* **2017**, *12*, No. e0177146.
(27) Tokuhara, T.; Hattori, N.; Ishida, H.; Hirai, T.; Higashiyama, M.; Kodama, K.; Miyake, M. Clinical significance of aminopeptidase N in non-small cell lung cancer. *Clin. Cancer Res.* **2006**, *12*, 3971−3978.
(28) Valastyan, S.; Weinberg, R. A. Tumor metastasis: molecular insights and evolving paradigms. *Cell* **2011**, *147*, 275−292.
(29) Su, L.; Cao, J.; Jia, Y.; Zhang, X.; Fang, H.; Xu, W. Development of synthetic aminopeptidase N/CD13 inhibitors to overcome cancer metastasis and angiogenesis. *ACS. Med. Chem. Lett.* **2012**, *3*, 959−964.
(30) Wirtz, D.; Konstantopoulos, K.; Searson, P. C. The physics of cancer: the role of physical interactions and mechanical forces in metastasis. *Nat. Rev. Cancer.* **2011**, *11*, 512−522.
(31) Chaffer, C. L.; Weinberg, R. A. A perspective on cancer cell metastasis. *Science* **2011**, *331*, 1559−1564.
(32) Saiki, I.; Fujii, H.; Yoneda, J.; Abe, F.; Nakajima, M.; Tsuruo, T.; Azuma, I. Role of aminopeptidase N (CD13) in tumor-cell invasion and extracellular matrix degradation. *Int. J. Cancer* **1993**, *54*, 137−143.
(33) Yoneda, J.; Saiki, I.; Fujii, H.; Abe, F.; Kojima, Y.; Azuma, I. Inhibition of tumor invasion and extracellular matrix degradation by ubenimex (bestatin). *Clin. Exp. Metastasis* **1992**, *10*, 49−59.
(34) Mucha, A.; Drag, M.; Dalton, J. P.; Kafarski, P. Metalloaminopeptidase inhibitors. *Biochimie* **2010**, *92*, 1509−1529.
(35) Zhang, X.; Fang, H.; Zhang, J.; Yuan, Y.; Xu, W. Recent advance in aminopeptidase N (APN/CD13) inhibitor research. *Curr. Med. Chem.* **2011**, *18*, 5011−5021.
(36) Scornik, O. A.; Botbol, V. Bestatin as an experimental tool in mammals. *Curr. Drug Metab.* **2001**, *2*, 67−85.
(37) Umezawa, H.; Aoyagi, T.; Suda, H.; Hamada, M.; Takeuchi, T. Bestatin, an inhibitor of aminopeptidase B, produced by actinomycetes. *J. Antibiot.* **1976**, *29*, 97−99.
(38) Ichinose, Y.; Genka, K.; Koike, T.; Kato, H.; Watanabe, Y.; Mori, T.; Iioka, S.; Sakuma, A.; Ohta, M. Randomized double-blind placebo-controlled trial of bestatin in patients with resected stage I squamous-cell lung carcinoma. *JNCI, J. Natl. Cancer Inst.* **2003**, *95*, 605−610.
(39) Ota, K. Review of ubenimex (Bestatin): clinical research. *Biomed. Pharmacother.* **1991**, *45*, 55−60.
(40) Ota, K.; Kurita, S.; Yamada, K.; Masaoka, T.; Uzuka, Y.; Ogawa, N. Immunotherapy with bestatin for acute nonlymphocytic leukemia in adults. *Cancer Immunol. Immunother.* **1986**, *23*, 5−10.
(41) Urabe, A.; Mutoh, Y.; Mizoguchi, H.; Takaku, F.; Ogawa, N. Ubenimex in the treatment of acute nonlymphocytic leukemia in adults. *Ann. Hematol.* **1993**, *67*, 63−66.
(42) Krige, D.; Needham, L. A.; Bawden, L. J.; Flores, N.; Farmer, H.; Miles, L. E.; Stone, E.; Callaghan, J.; Chandler, S.; Clark, V. L.; Kirwin-Jones, P.; Legris, V.; Owen, J.; Patel, T.; Wood, S.; Box, G.; Laber, D.; Odedra, R.; Wright, A.; Wood, L. M.; Eccles, S. A.; Bone, E. A.; Ayscough, A.; Drummond, A. H. CHR-2797: an antiproliferative aminopeptidase inhibitor that leads to amino acid deprivation in human leukemic cells. *Cancer Res.* **2008**, *68*, 6669−6679.
(43) Lowenberg, B.; Morgan, G.; Ossenkoppele, G. J.; Burnett, A. K.; Zachee, P.; Duhrsen, U.; Dierickx, D.; Muller-Tidow, C.; Sonneveld, P.; Krug, U.; Bone, E.; Flores, N.; Richardson, A. F.; Hooftman, L.; Jenkins, C.; Zweegman, S.; Davies, F. Phase I/II clinical study of Tosedostat, an inhibitor of aminopeptidases, in patients with acute myeloid leukemia and myelodysplasia. *J. Clin. Oncol.* **2010**, *28*, 4333−4338.
(44) Drinkwater, N.; Vinh, N. B.; Mistry, S. N.; Bamert, R. S.; Ruggeri, C.; Holleran, J. P.; Loganathan, S.; Paiardini, A.; Charman, S. A.; Powell, A. K.; Avery, V. M.; McGowan, S.; Scammells, P. J. Potent dual inhibitors of *Plasmodium falciparum* M1 and M17 aminopeptidases through optimization of S1 pocket interactions. *Eur. J. Med. Chem.* **2016**, *110*, 43−64.
(45) Kannan Sivaraman, K.; Paiardini, A.; Sienczyk, M.; Ruggeri, C.; Oellig, C. A.; Dalton, J. P.; Scammells, P. J.; Drag, M.; McGowan, S. Synthesis and structure-activity relationships of phosphonic arginine mimetics as inhibitors of the M1 and M17 aminopeptidases from *Plasmodium falciparum*. *J. Med. Chem.* **2013**, *56*, 5213−5217.
(46) Mistry, S. N.; Drinkwater, N.; Ruggeri, C.; Sivaraman, K. K.; Loganathan, S.; Fletcher, S.; Drag, M.; Paiardini, A.; Avery, V. M.; Scammells, P. J.; McGowan, S. Two-pronged attack: dual inhibition of *Plasmodium falciparum* M1 and M17 metalloaminopeptidases by a

DOI: 10.1021/acs.jmedchem.9b00757
J. Med. Chem. XXXX, XXX, XXX−XXX

novel series of hydroxamic acid-based inhibitors. *J. Med. Chem.* **2014**, *57*, 9168−9183.
(47) Li, P.; Merz, K. M., Jr. Metal ion modeling using classical mechanics. *Chem. Rev.* **2017**, *117*, 1564−1686.
(48) Yang, W.; Riley, B. T.; Lei, X.; Porebski, B. T.; Kass, I.; Buckle, A. M.; McGowan, S. Generation of AMBER force field parameters for zinc centres of M1 and M17 family aminopeptidases. *J. Biomol. Struct. Dyn.* **2018**, 2595−2604.
(49) Yang, W.; Riley, B.; Lei, X.; Porebski, B. T.; Kass, I.; Buckle, A. M.; McGowan, S. Mapping the pathway and dynamics of bestatin inhibition of the *Plasmodium falciparum* M1 aminopeptidase, PfA-M1. *ChemMedChem* **2018**, *13*, 2504−2513.
(50) Beebe, X.; Nilius, A. M.; Merta, P. J.; Soni, N. B.; Bui, M. H.; Wagner, R.; Beutel, B. A. Synthesis and SAR evaluation of oxadiazolopyrazines as selective Haemophilus influenzae antibacterial agents. *Bioorg. Med. Chem. Lett.* **2003**, *13*, 3133−3136.
(51) Adediran, S. A.; Cabaret, D.; Lohier, J. F.; Wakselman, M.; Pratt, R. F. Substituted aryl malonamates as new serine beta-lactamase substrates: structure-activity studies. *Bioorg. Med. Chem.* **2010**, *18*, 282−291.
(52) Im, I.; Lee, E. S.; Choi, S. J.; Lee, J. Y.; Kim, Y. C. Structure-activity relationships of heteroaromatic esters as human rhinovirus 3C protease inhibitors. *Bioorg. Med. Chem. Lett.* **2009**, *19*, 3632−3636.
(53) Kam, Y. L.; Rhee, H. K.; Kim, H. J.; Back, S. K.; Na, H. S.; Choo, H. Y. Synthesis and bradykinin inhibitory activity of novel non-peptide compounds, and evaluation of in vivo analgesic activity. *Bioorg. Med. Chem.* **2010**, *18*, 2327−2336.
(54) Williams, S. J.; Zammit, S. C.; Cox, A. J.; Shackleford, D. M.; Morizzi, J.; Zhang, Y.; Powell, A. K.; Gilbert, R. E.; Krum, H.; Kelly, D. J. 3′,4′-Bis-difluoromethoxycinnamoylanthranilate (FT061): an orally-active antifibrotic agent that reduces albuminuria in a rat model of progressive diabetic nephropathy. *Bioorg. Med. Chem. Lett.* **2013**, *23*, 6868−6873.
(55) Butters, M.; Davies, C. D.; Elliott, M. C.; Hill-Cousins, J.; Kariuki, B. M.; Ooi, L. L.; Wood, J. L.; Wordingham, S. V. Synthesis and stereochemical determination of batzelladine C methyl ester. *Org. Biomol. Chem.* **2009**, *7*, 5001−5009.
(56) Sun, W. S.; Park, Y. S.; Yoo, J.; Park, K. D.; Kim, S. H.; Kim, J. H.; Park, H. J. Rational design of an indolebutanoic acid derivative as a novel aldose reductase inhibitor based on docking and 3D QSAR studies of phenethylamine derivatives. *J. Med. Chem.* **2003**, *46*, 5619−5627.
(57) Sadovoy, A.; K, A.; Golubeva, G.; Sviridova, L. Regioselective synthesis of 1-alkyl-5-(indol-3-yl- and -2-yl)pyrrolidin-2-ones from available reagents. *Chem. Heterocycl. Compd.* **2011**, *46*, 1215−1223.
(58) Romeo, G.; Salerno, L.; Pittala, V.; Modica, M. N.; Siracusa, M. A.; Materia, L.; Buccioni, M.; Marucci, G.; Minneman, K. P. High affinity ligands and potent antagonists for the alpha1D-adrenergic receptor. Novel 3,8-disubstituted [1]benzothieno[3,2-d]pyrimidine derivatives. *Eur. J. Med. Chem.* **2014**, *83*, 419−432.
(59) Valla, A.; Cartier, D.; Zentz, F.; Labia, R. Atypical oxidation reaction by thionyl chloride: easy two-step synthesis of N-Alkyl-1,4-dithiines. *Synth. Commun.* **2006**, *36*, 3591−3597.
(60) Arulsamy, N.; Bohle, D. S. Nucleophilic addition of hydroxylamine, methoxylamine, and hydrazine to malononitrileoxime. *J. Org. Chem.* **2000**, *65*, 1139−1143.
(61) Vörös, A.; Mucsi, Z.; Baán, Z.; Timári, G.; Hermecz, I.; Mizsey, P.; Finta, Z. An experimental and theoretical study of reaction mechanisms between nitriles and hydroxylamine. *Org. Biomol. Chem.* **2014**, *12*, 8036−8047.
(62) Luciani, N.; Marie-Claire, C.; Ruffet, E.; Beaumont, A.; Roques, B. P.; Fournie-Zaluski, M. C. Characterization of Glu350 as a critical residue involved in the N-terminal amine binding site of amino-peptidase N (EC 3.4.11.2): insights into its mechanism of action. *Biochemistry* **1998**, *37*, 686−692.
(63) Graham, F. L.; Smiley, J.; Russell, W. C.; Nairn, R. Characteristics of a human cell line transformed by DNA from human adenovirus type 5. *J. Gen. Virol.* **1977**, *36*, 59−74.
(64) Morrison, J. F. Kinetics of the reversible inhibition of enzyme-catalysed reactions by tight-binding inhibitors. *Biochim. Biophys. Acta, Enzymol.* **1969**, *185*, 269−286.
(65) Williams, J. W.; Morrison, J. F. The kinetics of reversible tight-binding inhibition. *Methods Enzymol.* **1979**, *63*, 437−467.
(66) Bevan, C. D.; Lloyd, R. S. A high-throughput screening method for the determination of aqueous drug solubility using laser nephelometry in microtiter plates. *Anal. Chem.* **2000**, *72*, 1781−1787.
(67) Lombardo, F.; Shalaeva, M. Y.; Tupper, K. A.; Gao, F. ElogD(oct): a tool for lipophilicity determination in drug discovery. 2. Basic and neutral compounds. *J. Med. Chem.* **2001**, *44*, 2490−2497.
(68) Schrödinger. *The PyMOL Molecular Graphics System*, version 1.8; Schrödinger, LLC, 2017.
(69) Wang, J.; Wolf, R. M.; Caldwell, J. W.; Kollman, P. A.; Case, D. A. Development and testing of a general amber force field. *J. Comput. Chem.* **2004**, *25*, 1157−1174.
(70) Jakalian, A.; Bush, B. L.; Jack, D. B.; Bayly, C. I. Fast, efficient generation of high-quality atomic charges. AM1-BCC model: I. Method. *J. Comput. Chem.* **2000**, *21*, 132−146.
(71) Jakalian, A.; Jack, D. B.; Bayly, C. I. Fast, efficient generation of high-quality atomic charges. AM1-BCC model: II. Parameterization and validation. *J. Comput. Chem.* **2002**, *23*, 1623−1641.
(72) Fiser, A.; Šali, A. Modeller: generation and refinement of homology-based protein structure models. *Methods Enzymol.* **2003**, *374*, 461−491.
(73) Gasteiger, J.; Marsili, M. Iterative partial equalization of orbital electronegativity—a rapid access to atomic charges. *Tetrahedron* **1980**, *36*, 3219−3228.
(74) Jorgensen, W. L.; Chandrasekhar, J.; Madura, J. D.; Impey, R. W.; Klein, M. L. Comparison of simple potential functions for simulating liquid water. *J. Chem. Phys.* **1983**, *79*, 926−935.
(75) Case, D. A.; Cheatham, T. E., 3rd; Darden, T.; Gohlke, H.; Luo, R.; Merz, K. M., Jr.; Onufriev, A.; Simmerling, C.; Wang, B.; Woods, R. J. The Amber biomolecular simulation programs. *J. Comput. Chem.* **2005**, *26*, 1668−1688.
(76) Phillips, J. C.; Braun, R.; Wang, W.; Gumbart, J.; Tajkhorshid, E.; Villa, E.; Chipot, C.; Skeel, R. D.; Kale, L.; Schulten, K. Scalable molecular dynamics with NAMD. *J. Comput. Chem.* **2005**, *26*, 1781−1802.
(77) Ryckaert, J.-P.; Ciccotti, G.; Berendsen, H. J. C. Numerical integration of the cartesian equations of motion of a system with constraints: molecular dynamics of n-alkanes. *J. Comput. Phys.* **1977**, *23*, 327−341.
(78) Kawasaki, K. Simple derivations of generalized linear and nonlinear Langevin equations. *J. Phys. A: Math., Nucl. Gen.* **1973**, *6*, 1289.
(79) Berendsen, H. J. C.; Postma, J. P. M.; van Gunsteren, W. F.; DiNola, A.; Haak, J. R. Molecular dynamics with coupling to an external bath. *J. Chem. Phys.* **1984**, *81*, 3684−3690.
(80) Essmann, U.; Perera, L.; Berkowitz, M. L.; Darden, T.; Lee, H.; Pedersen, L. G. A smooth particle mesh Ewald method. *J. Chem. Phys.* **1995**, *103*, 8577−8593.

DOI: 10.1021/acs.jmedchem.9b00757
J. Med. Chem. XXXX, XXX, XXX−XXX

2.3 Supplementary information

The following section discloses data that was not included in the publication Lee *et al*., *J. Med. Chem*, **2019** to show that the research completed in this doctoral research.

2.3.1 Cell-based assays of APN inhibitors betatin, Tosedostat, 6ad, and 6ae

Cell-based assays are one of the most commonly used methods to measure the level of living cells or to determine the cytotoxic effects of testing compounds. These assays are developed based on biological processes that take place in healthy cells. There are various types of cell proliferation assays, such as tetrazolium reduction, resazurin reduction, protease markers, and ATP detection.[235] In this project, the resazurin reduction assay was performed to determine the effects of **6ad** and **6ae** on cell proliferation.

In order to detect the level of viable cells, a small volume of resazurin dye is added to cell culture after treating the cells with testing compounds for an adequate period of time. Resazurin is a non-fluorescent blue dye that is irreversibly reduced to pink fluorogenic resorufin by active metabolism in viable cells (Figure SI.1). Therefore, the level of fluorescence generated from resorufin indicates the number of functioning cells. The more pink fluorescence that is generated, the higher the number of viable cells present and hence, less active the testing compounds are in the cell environment. Resorufin can be further reduced to a colourless and non-fluorescent compound hydroresorufin when cells are overgrown.

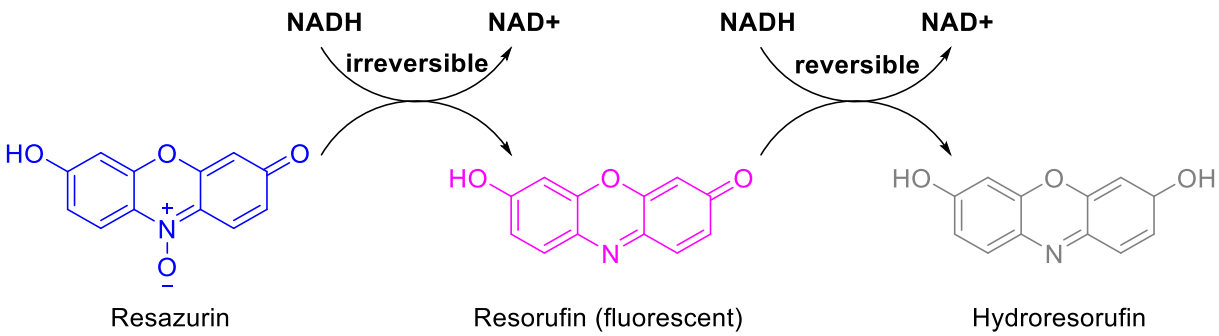

Figure SI.1. Reduction of resazurin to resorufin and hydroresorufin in viable cells.

In this project, the resazurin assay was conducted to estimate the effects of **6ad** and **6ae** on cancer cell proliferation in the presence of bestatin as a positive control. Two types of cancer

cell lines were used - ES-2 ovarian cancer cell line is (high APN-expressing) and REH acute lymphatic leukemic cell line (low-APN expressing). The use of these cancer cell lines may allow us to investigate how **6ad** and **6ae** behave in cellular environments with different levels of APN. The fluorescence signals detected were calculated as percentage proliferation relative to DSMO control and the concentration where 50% loss in cell proliferation was represented as IC_{50} (Table SI.1). In both APN-positive ES-2 and APN-negative REH cell lines, bestatin reached approximately 80% cell proliferation at the working concentration of 400 µM. Although both **6ad** and **6ae** were more potent than bestatin, they only displayed weak anti-proliferative activities in a micromolar range. Compound **6ad** was more potent than **6ae** by approximately 3-fold in both ES-2 and REH cells. Anti-proliferative activities of both compounds were significantly stronger in APN-negative REH cell line, indicating the cell proliferation might not be related to APN activity. There is also the possibility of off-target effects where the inhibitors interact with other proteases in the cells other than APN to reduce the efficacy. Further investigations are required to determine the factors that cause significant loss in cellular efficacy in the future.

Table SI.1. Anti-proliferative activities of bestatin, 6ad, and 6ae on cell proliferation in ES-2, and REH cell lines.

Compound	ES-2 (IC_{50} / µM)	REH (IC_{50} / µM)
Bestatin	> 400	> 400
6ad	63.7 ± 2.1	9.78 ± 0.29
6ae	185 ± 6	39.9 ± 1.9

Consistent results were obtained when the inhibitors were tested against 60 different cancer cell lines at a single dose of 10 µM in collaboration with NCI (Figure SI.2). Compounds **6ad** and **6ae** exhibited very weak activity against certain leukaemic, renal, and prostate cancer cell lines. This was comparable to that of Tosedostat which showed growth inhibition in several cancer cell lines, but the most notable results were renal cancer cell RXF 393 and breast cancer cell MDA-MB-231, which showed very low growth rate of 7.55% and 9.77%, respectively (Figure SI.2).

Developmental Therapeutics Program

One Dose Mean Graph

NSC: D-806014 / 1	Conc: 1.00E-5 Molar	Test Date: Jul 30, 2018
Experiment ID: 1807OS85		Report Date: Oct 03, 2018

Panel/Cell Line	Growth Percent
Leukemia	
CCRF-CEM	81.26
HL-60(TB)	77.99
K-562	88.93
MOLT-4	87.05
RPMI-8226	84.14
SR	84.90
Non-Small Cell Lung Cancer	
A549/ATCC	90.23
EKVX	98.80
HOP-62	97.73
HOP-92	102.98
NCI-H226	108.61
NCI-H23	99.67
NCI-H322M	99.03
NCI-H460	105.15
NCI-H522	92.85
Colon Cancer	
COLO 205	113.54
HCC-2998	111.84
HCT-116	95.16
HCT-15	95.35
HT29	106.50
KM12	98.30
SW-620	96.06
CNS Cancer	
SF-268	91.85
SF-295	98.83
SF-539	103.70
SNB-19	83.22
SNB-75	100.56
U251	80.24
Melanoma	
LOX IMVI	89.24
MALME-3M	102.04
M14	100.99
MDA-MB-435	99.02
SK-MEL-2	93.65
SK-MEL-28	101.87
SK-MEL-5	99.82
UACC-257	100.88
UACC-62	89.83
Ovarian Cancer	
IGROV1	90.58
OVCAR-3	96.12
OVCAR-4	92.45
OVCAR-5	101.77
OVCAR-8	90.32
NCI/ADR-RES	100.38
Renal Cancer	
786-0	98.76
A498	98.37
ACHN	101.76
CAKI-1	99.92
RXF 393	95.11
SN12C	93.29
TK-10	94.26
UO-31	80.76
Prostate Cancer	
PC-3	76.29
DU-145	111.54
Breast Cancer	
MCF7	89.25
MDA-MB-231/ATCC	86.78
HS 578T	102.78
BT-549	117.81
T-47D	79.05
MDA-MB-468	86.34
Mean	95.52
Delta	19.23
Range	41.52

Mean Growth Percent - Growth Percent

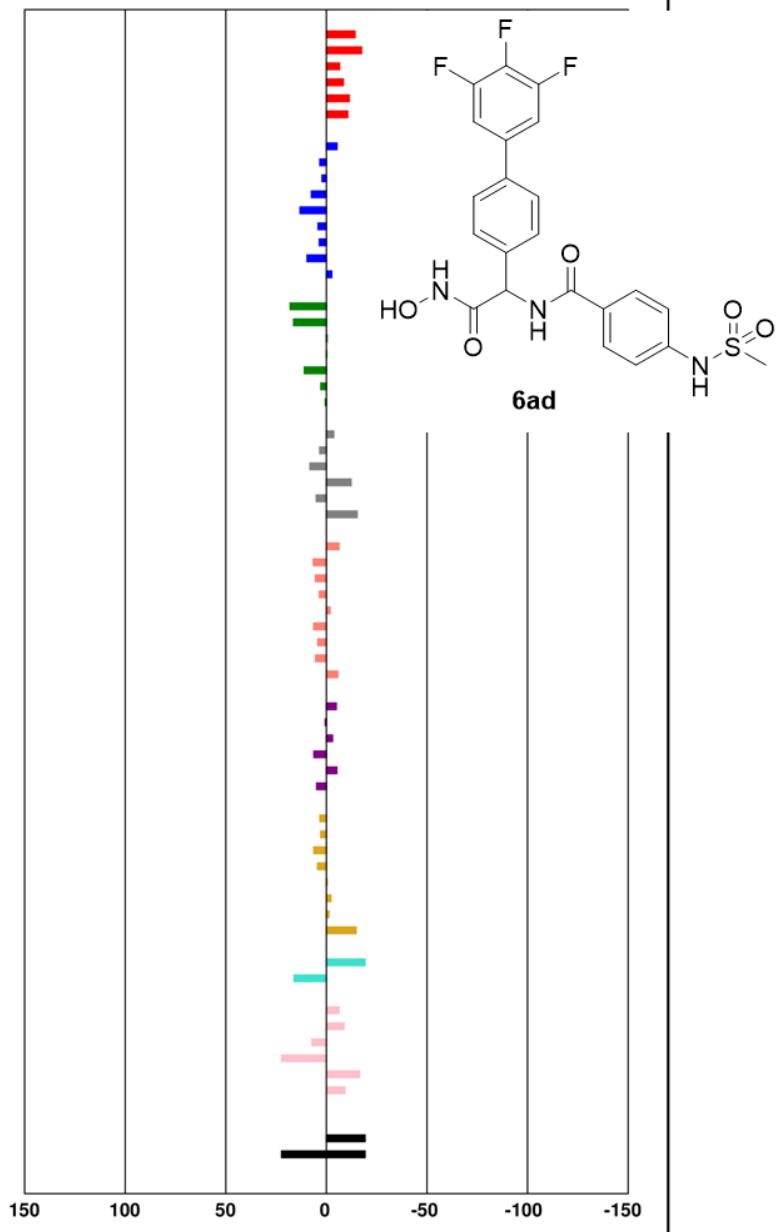

6ad

Developmental Therapeutics Program

One Dose Mean Graph

NSC: D-806015 / 1	Conc: 1.00E-5 Molar	Test Date: Jul 30, 2018
Experiment ID: 1807OS85		Report Date: Oct 03, 2018

Panel/Cell Line	Growth Percent
Leukemia	
CCRF-CEM	91.25
HL-60(TB)	80.15
K-562	84.78
MOLT-4	86.03
RPMI-8226	92.00
SR	93.49
Non-Small Cell Lung Cancer	
A549/ATCC	96.94
EKVX	101.28
HOP-62	95.67
HOP-92	113.67
NCI-H226	100.17
NCI-H23	103.17
NCI-H322M	96.44
NCI-H460	107.52
NCI-H522	77.76
Colon Cancer	
COLO 205	115.47
HCC-2998	112.58
HCT-116	91.48
HCT-15	101.32
HT29	98.69
KM12	100.89
SW-620	97.42
CNS Cancer	
SF-268	99.79
SF-295	103.46
SF-539	99.19
SNB-19	91.65
SNB-75	111.05
U251	91.87
Melanoma	
LOX IMVI	96.57
MALME-3M	100.91
M14	100.65
MDA-MB-435	93.93
SK-MEL-2	110.14
SK-MEL-28	106.31
SK-MEL-5	105.20
UACC-257	99.07
UACC-62	98.23
Ovarian Cancer	
IGROV1	95.40
OVCAR-3	99.17
OVCAR-4	95.68
OVCAR-5	104.80
OVCAR-8	94.64
NCI/ADR-RES	100.48
Renal Cancer	
786-0	96.16
A498	89.73
ACHN	96.33
CAKI-1	98.04
RXF 393	108.58
SN12C	100.47
TK-10	102.55
UO-31	74.75
Prostate Cancer	
PC-3	79.65
DU-145	106.62
Breast Cancer	
MCF7	93.21
MDA-MB-231/ATCC	99.87
HS 578T	106.65
BT-549	104.29
T-47D	89.82
MDA-MB-468	100.00
Mean	98.02
Delta	23.27
Range	40.72

Mean Growth Percent - Growth Percent

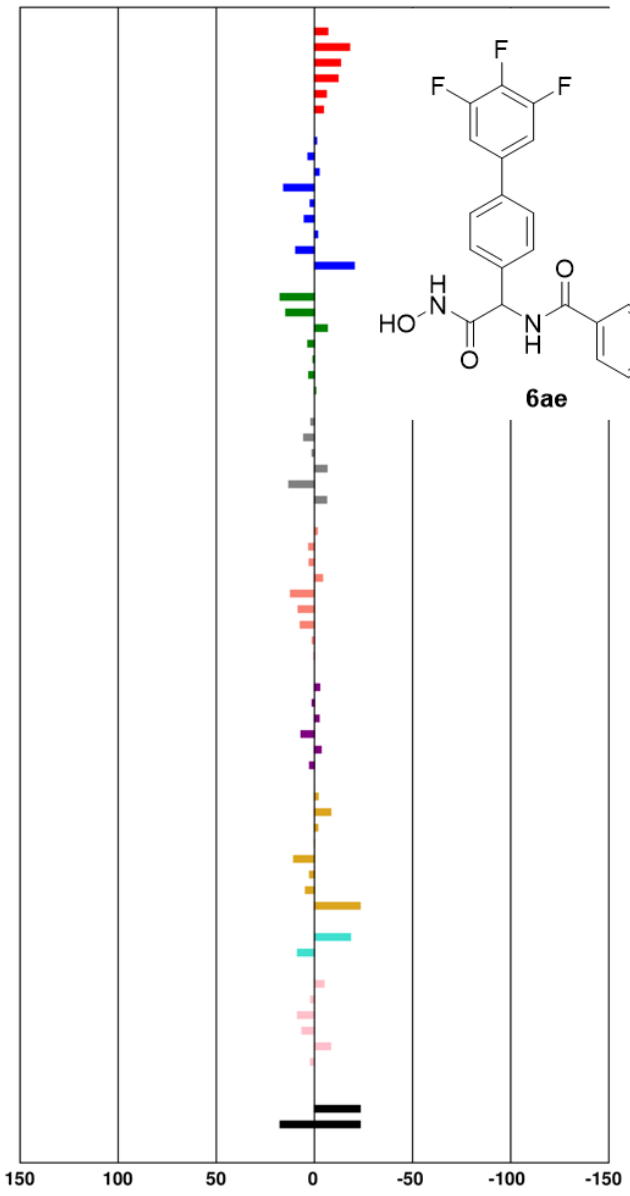

6ae

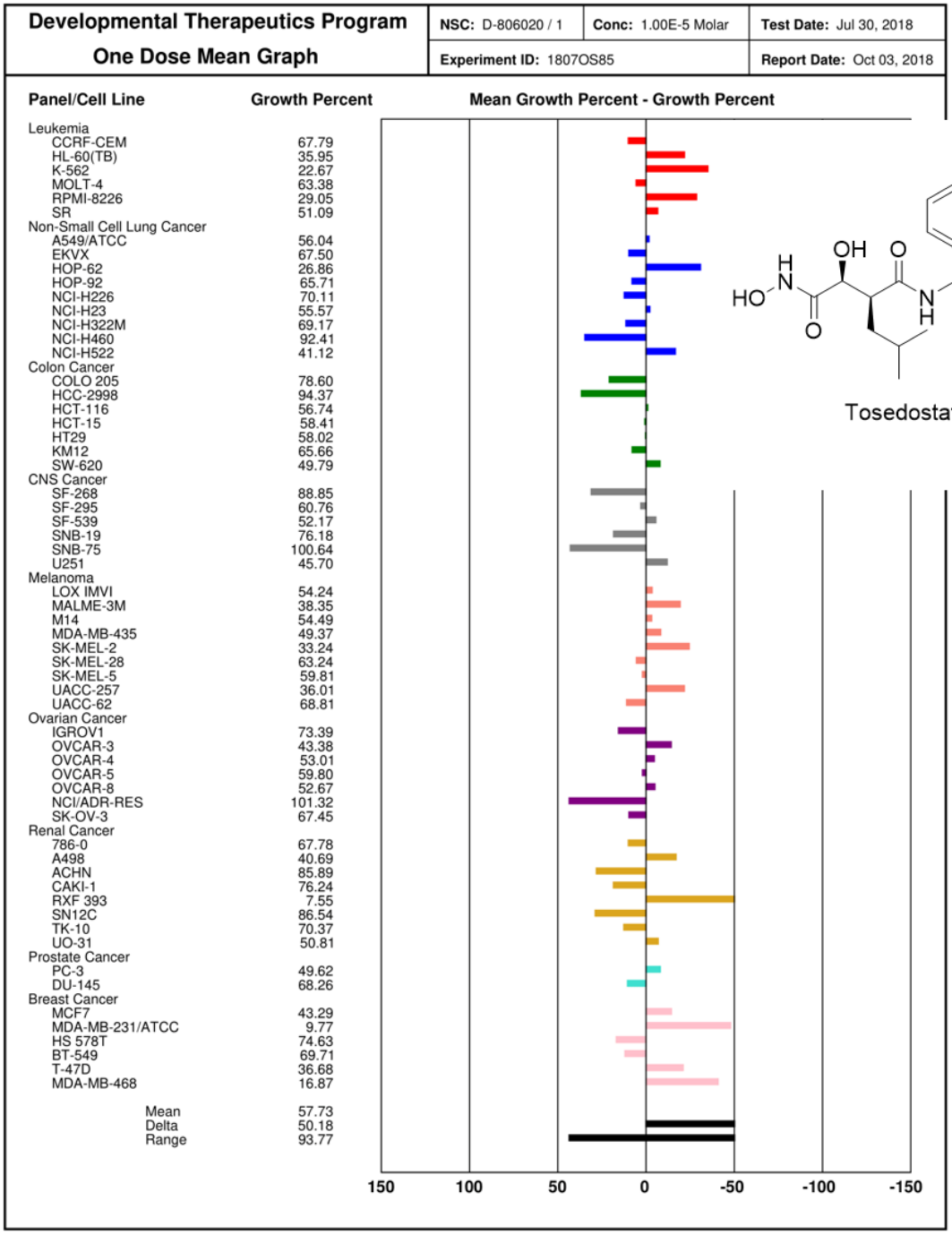

Figure SI.2. One-dose mean growth graph of compound 6ad, 6ae, and Tosedostat. Testing compounds were evaluated for growth inhibition activity at a single dose of 10 μM. Data acquisition and analysis were completed by NCI.

2.3.2 Experimental

Resazurin assays of bestatin, **6ad**, and **6ae** were performed as described in the journal article.

NCI-60 Screening

The sulforhodamine B (SRB) assays were performed by the NCI-60 screening service (https://dtp.cancer.gov/discovery_development/nci-60/methodology.htm). The protocol used is reported as follows. The human cancer cell lines are grown in RPMI 1640 medium containing 5% fetal bovine serum and 2 mM L-glutamine. Cells are seeded into 96 well microtiter plates in 100 µL at cell densities ranging from 5,000 to 40,000 cells/well. The seeded plates are incubated at 37 °C, 5% CO_2, 95% air and 100% relative humidity for 24 h.

After 24 h, two plates of each cell line are fixed with trichloroacetic acid (TCA) *in situ*. Tosedostat, **6ad**, and **6ae** are solubilised in DMSO at 400-fold the desired final test concentration (10 µM) and stored frozen. When testing compounds are added, an aliquot of frozen concentrate is thawed and diluted to 20 µM with complete medium containing 50 µg/ml gentamicin. Aliquots of 100 µL from each testing compound are added to the appropriate microtiter wells already containing 100 µl of the medium.

After drug addition, the plates are incubated for an additional 48 h at 37 °C, 5% CO_2, 95% air, and 100% relative humidity. For adherent cells, the assay is terminated by adding cold TCA. Cells are fixed *in situ* by the addition of 50 µl of cold 50% (w/v) TCA and incubated for 1 h at 4 °C. The supernatant is discarded, and the plates are washed five times with tap water and air-dried. SRB solution (100 µl) at 0.4% (w/v) in 1% acetic acid is added to each well, and plates are incubated for 10 min at room temperature. After staining, unbound dye is removed by washing with 1% acetic acid and the plates are air-dried. Bound stain is subsequently solubilised with 10 mM trizma base, and the absorbance is read using an automated plate reader at a wavelength of 515 nm. For suspension cells, the assay is terminated by fixing settled cells at the bottom of the wells by adding 50 µL of 80% TCA (final concentration, 16 % TCA). Using the three absorbance measurements [time zero, (Tz), no-drug control, (C), and test growth in the presence of drug at 10 µM (Ti)], the percentage growth is calculated of the drug at the testing concentration level. The growth inhibition calculated is reported as a mean graph of the percentage growth of treated cells.

2.4 Appendices

Supplementary information of Lee *et al*., *J. Med. Chem.*, **2019** is provided as appendices in the following section.

The molecular formula strings of all synthesised compounds, PDB file of the docked pose of compound **1**, and MD simulations of compound **6ad** and **6ae** are available at https://pubs.acs.org/doi/10.1021/acs.jmedchem.9b00757.

SUPPORTING INFORMATION

Novel Human Aminopeptidase N Inhibitors: Discovery and Optimization of Subsite Binding Interactions

Jisook Lee[†], Natalie B. Vinh[†], Nyssa Drinkwater[‡], Wei Yang[‡], Komagal Kannan Sivaraman[‡], Luke S. Schembri[†], Michelle Gazdik[†], Peter M. Grin[▽⊥], Georgina S. Butler[▽⊥O], Christopher M. Overall[▽⊥O], Susan A. Charman[§], Sheena McGowan[‡], Peter J. Scammells*[†]*

[†] Medicinal Chemistry, Monash Institute of Pharmaceutical Sciences, Monash University, Parkville Campus, VIC 3052, Australia.

[‡] Infection and Immunity Program, Biomedicine Discovery Institute and Department of Microbiology, Monash University, Clayton Campus, VIC 3800, Australia.

[§] Centre for Drug Candidate Optimisation, Monash Institute of Pharmaceutical Sciences, Monash University, Parkville Campus, VIC 3052, Australia

[▽] Department of Biochemistry & Molecular Biology and [O] Department of Oral Biological & Medical Sciences, University of British Columbia, Vancouver, BC V6T 1Z3, Canada

[⊥] Centre for Blood Research, Life Sciences Institute, University of British Columbia, Vancouver, BC V6T 1Z3, Canada

Table of Contents **Page #**

General Procedure E: Amide coupling of mono-methyl terephthalate using HCTU and TEA. A sealed vessel containing HCTU (1.6 eq.), mono-methyl terephthalate (1.0 eq.) and amine (2.0 eq.) in anhydrous DMF (0.5 mL) was purged twice with dry N_2(g) and charged with TEA (5.0 eq.). The mixture was allowed to stir at rt for 17 h. The mixture was then added to a solution of half-saturated $NaHCO_3$ (60 mL) and extracted with EtOAc (3 × 50 mL). The combined organic extracts were washed with additional half-saturated $NaHCO_3$ (2 × 60 mL), dried with brine (30 mL) and Na_2SO_4, filtered and the solvent evaporated under reduced pressure. The residue was then taken up in a solution of MeOH, THF and 1 M LiOH (1:1:1, 6 mL) and stirred at rt for 17 h. Sodium hydroxide solution (0.1 M, 100 mL) was added and the aqueous layer washed with EtOAc (3 × 50 mL). The aqueous layer was acidified with concentrated HCl (6 M, 5 mL) and extracted with a mixture of isopropanol and $CHCl_3$ (1:3, 3 × 50 mL). The combined organic extracts were dried with Na_2SO_4, filtered and the solvent evaporated under reduced pressure. The residue was purified by column chromatography (DCM:MeOH:AcOH 98.9:1:0.1 to 95.9:4:0.1)

4-(Methylcarbamoyl)benzoic acid (10). The compound was generated according to General Procedure E, which was a different synthetic route reported previously.[1] Mono-methyl terephthalate (248 mg, 1.38 mmol) was coupled to $MeNH_2$.HCl (195 mg, 2.89 mmol) in the presence of HCTU (925 mg, 2.24 mmol) and TEA (1 ml, 7.17 mmol). The crude product was purified by column chromatography (DCM:MeOH:AcOH 98.9:1:0.1 to 95.9:4:0.1) followed by lyophilization to obtain compound **10** as a white, fluffy solid (182 mg, 73%). ^{1}H NMR (d_6-DMSO) δ 8.64–8.55 (m, 1H), 8.02–7.97 (m, 2H), 7.94–7.88 (m, 2H), 2.79 (d, J = 4.6 Hz, 3H); ^{13}C NMR (d_6-DMSO) δ 166.8, 166.0, 138.3, 132.9, 129.3, 127.3, 26.3; *m/z* MS $C_9H_8NO_3$ $[M-H]^-$ calcd 178.1, found 178.0.

4-(Dimethylcarbamoyl)benzoic acid (11). The compound was generated according to General Procedure E, which was a different synthetic route reported previously.[2] Mono-methyl terephthalate (259 mg, 1.44 mmol) was coupled to Me_2NH.HCl (266 mg, 3.26 mmol) in the presence of HCTU (1.22 g, 2.24 mmol) and TEA (1 ml, 7.17 mmol). The crude product was purified by column chromatography (DCM:MeOH:AcOH 98.9:1:0.1 to 95.9:4:0.1) followed by lyophilization to obtain compound **11** as a white, fluffy solid after lyophilization (260 mg, 94%).

^{1}H NMR (d_6-DMSO) δ 7.98 (d, J = 8.4 Hz, 2H), 7.49 (d, J = 8.4 Hz, 2H), 2.98 (s, 3H), 2.86 (s, 3H); ^{13}C NMR (d_6-DMSO) δ 169.4, 166.9, 140.7, 131.4, 129.4, 127.1, 34.7; *m/z* MS $C_{10}H_{10}NO_3$ $[M-H]^-$ calcd 192.1, found 192.0.

4-(Ethylcarbamoyl)benzoic acid (12). A sealed vessel containing HCTU (1.28 g, 3.10 mmol), mono-methyl terephthalate (246 mg, 1.37 mmol) and $EtNH_2$.HCl (239 mg, 2.92 mmol) in anhydrous DMF (1 ml) was purged twice with nitrogen and charged with TEA (1 mL, 7.17 mmol). The mixture was allowed to stir at rt overnight. The mixture was then added to a solution of half-saturated $NaHCO_3$ (60 ml) and extracted with EtOAc (3 × 50 mL). The combined organic layers were washed with additional half-saturated $NaHCO_3$ (2 × 60 mL), brine (30 mL) and dried over anhydrous Na_2SO_4, filtered and the solvent evaporated under reduced pressure. The residue was then taken up in a solution of MeOH, THF and 1M LiOH (1:1:1, 6 mL) and stirred at rt overnight. A 0.1 M NaOH solution (100 mL) was added and the aqueous layer washed with EtOAc (3 × 50 mL). The aqueous layer was acidified with concentrated HCl (6 M, 5 mL) and extracted with a mixture of isopropanol and $CHCl_3$ (1:3, 3 × 50 mL). The combined organic layers were dried with anhydrous Na_2SO_4, filtered and the solvent evaporated under reduced pressure. The residue was purified by column chromatography with a gradient mixture of MeOH (1 - 4%) and AcOH (0.1%) in DCM to afford compound **12** as a white fluffy solid after lyophilization (252 mg, 94%). ^{1}H NMR (d_4-MeOD) δ 8.63 (t, J = 5.4 Hz, 1H), 8.00 (d, J = 8.5 Hz, 2H), 7.92 (d, J = 8.6 Hz, 2H), 3.31–3.24 (m, 2H), 1.13 (t, J = 7.2 Hz, 3H); ^{13}C NMR (d_4-MeOH) δ 166.9, 165.4, 138.5, 132.9, 129.3, 127.4, 34.3, 14.7; *m/z* MS $C_{10}H_{10}NO_3$ $[M-H]^-$ calcd 192.1, found 192.0.

4-(Isopropylcarbamoyl)benzoic acid (13). The compound was generated according to General Procedure E, which was a different synthetic route reported previously.[3] Mono-methyl terephthalate (403 mg, 2.23 mmol) was coupled to isopropylamine (500 µL, 5.87 mmol) in the presence of HCTU (1.52 g, 3.67 mmol). The crude product was purified by column chromatography (DCM:MeOH:AcOH 98.9:1:0.1 to 95.9:4:0.1) followed by lyophilization to obtain compound **13** as a white, fluffy solid (233 mg, 50%). ^{1}H NMR (d_6-DMSO) δ 8.38 (d, J = 7.7 Hz, 1H), 8.00 (d, J = 8.4 Hz, 2H), 7.93 (d, J = 8.4 Hz, 2H), 4.22–3.99 (m, 1H), 1.17 (s, J = 3.7 Hz, 3H),

1.15 (s, 3H); ^{13}C NMR (d_6-DMSO) δ 167.0, 164.8, 138.7, 132.9, 129.2, 127.6, 41.3, 22.3; *m/z* MS $C_{11}H_{12}NO_3$ $[M-H]^-$ calcd 206.1, found 206.0.

4-((2-Hydroxyethyl)carbamoyl)benzoic acid (14). A sealed vessel containing PyBOP (1.95 g, 3.75 mmol), mono-methyl terephthalate (332 mg, 1.84 mmol) and ethanolamine (550 µL, 9.09 mmol) in anhydrous DMF (3.0 ml) was purged twice with nitrogen. The mixture was allowed to stir at rt for 1 h. The mixture was then added to a 0.1 M KOH solution (100 mL) and extracted with 1:3 isopropanol:EtOAc (5 × 50 mL). The combined organic layers were dried over anhydrous Na_2SO_4, filtered and concentrated under reduced pressure. The residue was then taken up in a solution of MeOH, THF and 1 M LiOH (1:1:1, 6 mL) and stirred at 40 °C overnight. A NaOH solution (0.1 M, 100 mL) was added and the aqueous layer was washed with 1:3 isopropanol:$CHCl_3$ (3 × 100 mL). The aqueous layer was acidified with concentrated HCl (6 M, 5 mL) and extracted with 1:3 isopropanol:EtOAc (5 × 100 mL). The combined organic layers were dried over anhydrous Na_2SO_4, filtered and concentrated under reduced pressure. The crude product was purified by column chromatography (10% MeOH and 0.1% AcOH in DCM) to afford compound **14** as a white fluffy solid after lyophilization (195 mg, 51%). ^{1}H NMR (1:5 d_6-DMSO:D_2O) δ 8.04 (d, J = 8.0 Hz, 2H), 7.83 (d, J = 8.0 Hz, 2H), 3.73 (t, J = 5.3 Hz, 2H), 3.51 (t, J = 5.3 Hz, 2H); ^{13}C NMR (1:5 d_6-DMSO:D_2O) δ 170.6, 170.3, 139.5, 134.1, 131.4, 128.9, 61.3, 43.6; *m/z* MS $C_{10}H_{10}NO_4$ $[M-H]^-$ calcd 208.1, found 208.0.

4-(Sulfamoylamino)benzoic acid (15). To a stirring solution of CSI (550 µL, 7.37 mmol) in DCM (50 mL) at 0 °C was added *t*-BuOH (705 µL, 7.37 mmol) dropwise. The solution was stirred for 30 min at 0 °C. This solution was then added portion-wise to a solution of ethyl 4-aminobenzoate (1.01 g, 6.14 mmol) and TEA (1.70 mL, 12.2 mmol) in DCM at 0°C. The solution was allowed to warm to rt and stirred overnight. DCM (100 mL) was added and the solution washed with a 0.2 M HCl (2 × 100 mL) followed by brine (50 mL) and dried with Na_2SO_4. The mixture was filtered and the solvent evaporated. The residue was taken up in TFA (20 mL) and DCM (80 mL) and stirred at rt for 17 h. The solvent was evaporated and the residue taken up in a solution of MeOH, THF and 2 M LiOH (3:1:1, 25 mL) and stirred at rt for 6 h. H_2O (80 mL) was

added and the solution extracted with 1:3 isopropanol:$CHCl_3$ (3 × 100 mL). The aqueous layer was acidified with HCl (6M, 5 mL) and extracted with 1:3 isopropanol:EtOAc (3 × 100 mL). The latter organic layers were dried with Na_2SO_4, filtered and the solvent evaporated. The solid was taken up in Et_2O and triturated twice followed by purification by column chromatography (10% MeOH and 0.1% AcOH in DCM) to give the title compound as a pale brown solid (484 mg, 36%). ^{1}H NMR (*d*$_6$-DMSO) δ 10.06 (s, 1H), 7.94–7.78 (m, 2H), 7.32 (s, 2H) 7.29–7.14 (m, 2H); ^{13}C NMR (*d*$_6$-DMSO) δ 167.1, 143.7, 130.5, 123.5, 116.4; *m/z* MS $C_7H_7N_2O_4S$ $[M-H]^-$ calcd 215.0, found 214.9.

2-Oxoindoline-5-carboxylic acid (16). The title compound was synthesized according to a previously described procedure.[4] Briefly, indolin-2-one (2.00 g, 15 mmol) was added to a stirred suspension $AlCl_3$ (6.91 g, 51.8 mmol) in DCE (9 mL) in an ice bath. Chloroacetyl chloride (2.39 mL, 30.0 mmol) was slowly added and HCl gas evolved. After 10 minutes of stirring, the reaction was warmed to 40 - 50 °C for 1.5 h. The mixture was cooled to room temperature and poured into ice water. The precipitate was collected by vacuum filtration, washed with water, and dried under vacuum to afford 5-(2-chloroacetyl)indolin-2-one (2.63 g, 84%). The solid was stirred in pyridine (25 mL, 314 mmol) at 80 – 90 °C for 3 h and then cooled to room temperature. The precipitate was collected by vacuum filtration and washed with EtOH (10 mL). The solid was dissolved in a 2.5 N sodium hydroxide solution (25 mL, 63 mmol) and stirred at 70 – 80 °C for 3 hours. The mixture was cooled to room temperature and acidified with a 0.5 N HCl solution until no more precipitate formed. The precipitate was collected by vacuum filtration and washed thoroughly with water to afford compound **16** as a dark brown solid. After standing overnight, the filtrate provided more of **16** as a yellow solid. The combined yield was 85% (1.88 g). ^{1}H NMR (*d*$_6$-DMSO) δ 12.55 (s, 1H), 10.70 (s, 1H), 7.82 (dd, *J* = 8.2, 1.0 Hz, 1H), 7.75 (s, 1H), 6.88 (d, *J* = 8.1 Hz, 1H), 3.54 (s, 2H). ^{13}C NMR (*d*$_6$-DMSO) δ 176.76, 167.34, 147.99, 130.02, 125.96, 125.45, 123.58, 108.77, 35.55. *m/z* MS $C_9H_8NO_3$ $[MH]^+$ calcd 178.0, found 177.9.

MMP Enzymatic Analysis. Purified matrix metalloproteinases (MMPs) were activated using 1 mM 4-aminophenylmercuric acetate in buffer containing 50 mM HEPES, 150 mM NaCl, 5 mM $CaCl_2$, pH 7.0 for 1 h at rt, at working MMP concentrations of 1 μM (MMP2, 9 or 13) or 10 μM (MMP7 or 8). Each activated MMP was incubated at 2 – 20 nM concentrations with increasing inhibitor concentrations (0.1 pM–100 μM) of **1**, **6ad**, **6ae**, marimastat, or tosedostat in fluorimetry assay buffer (100 mM Tris-HCl, 100 mM NaCl, 10 mM $CaCl_2$, 0.15% Brij-35, pH 7.5) for 1 h at rt. Quenched fluorescent (QF)-24 substrate (ChinaPeptides Co. Ltd., Shanghai, China) was dissolved in DMSO and diluted to 10 μM working concentrations in fluorimetry assay buffer. QF assays were performed by incubating each MMP-inhibitor solution with 1 μM QF24 substrate at 37 °C and measuring fluorescence at excitation and emission wavelengths of 320 and 405 nm, respectively, at 1-minute intervals over 1 h using a Fluorescence Plate Reader (POLARStar, OPTIMA, BMG Labtech, Ortenberg, Germany). IC_{50} values for each inhibitor were calculated by plotting log(inhibitor concentration) vs. activity rate (pmol of QF24 substrate cleaved/h) and applying the 4-parameter Hill equation (GraphPad Prism 5.0, La Jolla, CA). Each MMP was assayed with all inhibitors in 3 independent experiments.

Table S1 Inhibition activity of APN inhibitors (**6ad** and **6ae**) and controls (Marimastat, Tosedostat, and **1**) against MMP2 and MMP9.

Compound	**MMP2** IC_{50} (μM)	**MMP9** IC_{50} (μM)
Marimastat	0.43 nM	3.1 nM
Tosedostat	0.19	1.5
1	26	> 10 mM
6ad	1.3	> 10 mM
6ae	2.1	> 10 mM

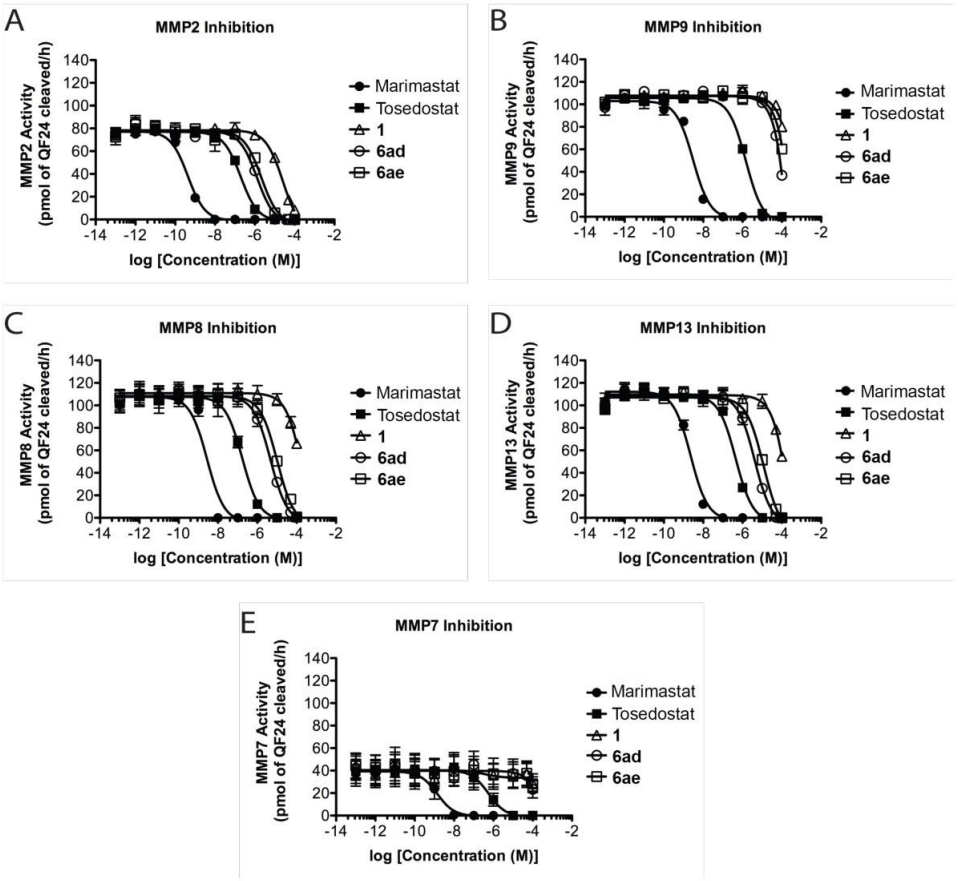

Figure S1. MMP2 (A), MMP9 (B), MMP8 (C), MMP13 (D), and MMP7 (E) activity in response to increasing concentrations of potent APN inhibitors (**6ad** and **6ae**) and controls (Marimastat, Tosedostat, and **1**).

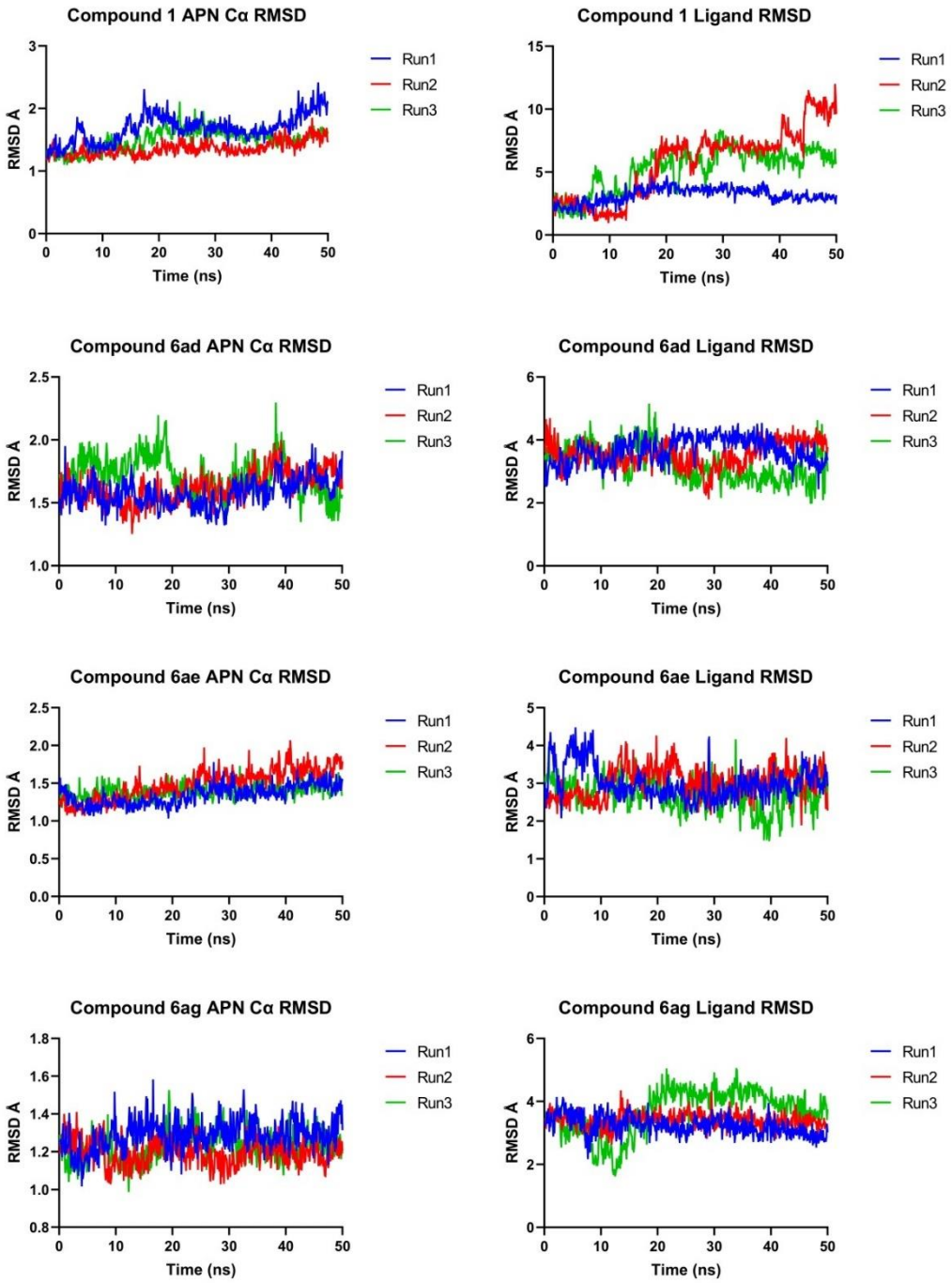

Figure S2. RMSD of the Cα and ligands for **1**, **6ad**, **6ae**, and **6ag** along the molecular modeling trajectory.

Table S2 Hydrogen bond occupancy analysis of **1** with APN. Bonds with occupancy fraction ≥ 0.005 are shown.

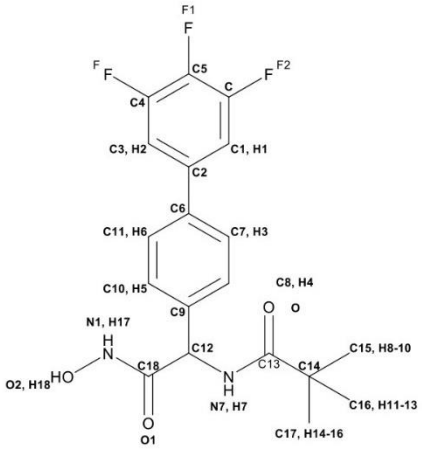

Acceptor	DonorH	Donor	Occupancy	Average Distance (Å)	Average Angle (°)
Protein acceptor / ligand donor					
GLU389@OE1	LIG@H18	LIG@O2	0.2520	2.5802	166.3056
GLU389@OE2	LIG@H18	LIG@O2	0.2107	2.5728	166.5114
GLU411@OE2	LIG@H7	LIG@N	0.0707	2.9110	153.8766
ALA353@O	LIG@H17	LIG@N1	0.0593	2.8692	154.3729
GLN213@OE1	LIG@H17	LIG@N1	0.0567	2.8736	149.9532
GLN857@OE1	LIG@H18	LIG@O2	0.0173	2.6792	162.9816
PHE472@O	LIG@H18	LIG@O2	0.0080	2.7487	163.1202
Ligand acceptor / protein donor					
LIG@O	GLY352@H	GLY352@N	0.1300	2.8611	152.7941
LIG@O2	GLN213@HE21	GLN213@NE2	0.1113	2.9039	160.2485
LIG@N1	GLN213@HE21	GLN213@NE2	0.0467	2.9389	145.4461
LIG@O	ASN900@HD21	ASN900@ND2	0.0380	2.8658	160.1753
LIG@O1	GLY352@H	GLY352@N	0.0320	2.8792	151.2775
LIG@O1	TYR477@HH	TYR477@OH	0.0153	2.8069	161.3428
LIG@O2	GLU355@H	GLU355@N	0.0147	2.9276	146.5107
LIG@F2	ALA214@H	ALA214@N	0.0120	2.8815	150.6386
LIG@O1	ASN900@HD22	ASN900@ND2	0.0080	2.8366	159.1932
LIG@F1	ALA214@H	ALA214@N	0.0080	2.8823	144.4548
LIG@H17	GLN213@HE21	GLN213@NE2	0.0080	2.8839	137.8437

Table S3 Hydrogen bond occupancy analysis of **6ad** with APN. Bonds with occupancy fraction ≥ 0.005 are shown.

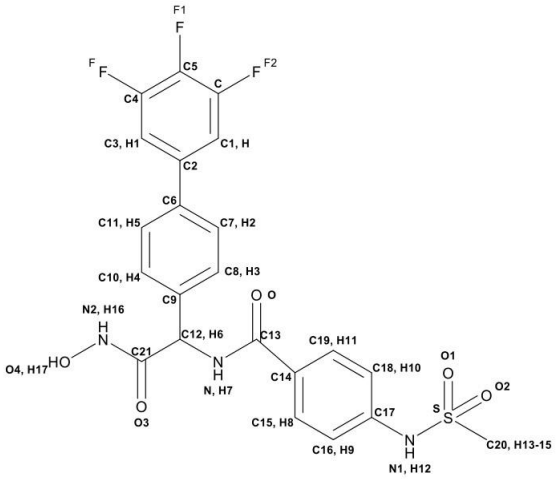

Acceptor	DonorH	Donor	Occupancy	Average Distance (Å)	Average Angle (°)
Protein acceptor / ligand donor					
GLU389@OE1	LIG@H17	LIG@O4	1.0000	2.5791	168.2348
GLN213@OE1	LIG@H16	LIG@N2	0.1380	2.8715	146.2220
ALA353@O	LIG@H16	LIG@N2	0.1240	2.8845	150.7804
TYR477@OH	LIG@H7	LIG@N	0.0960	2.9075	149.0200
TYR477@HH	LIG@H7	LIG@N	0.0300	2.8436	140.4882
MET354@HA	LIG@H16	LIG@N2	0.0187	2.8892	139.2854
TYR477@HH	LIG@H4	LIG@C10	0.0047	2.8975	144.3194
TYR477@HE1	LIG@H7	LIG@N	0.0047	2.9320	150.9237
Ligand acceptor / protein donor					
LIG@O4	GLN213@HE21	GLN213@NE2	0.1947	2.9159	163.3118
LIG@O3	TYR477@HH	TYR477@OH	0.1787	2.8295	156.5810
LIG@O1	ARG442@HH12	ARG442@NH1	0.1667	2.8322	156.6878
LIG@O2	ASN900@HD21	ASN900@ND2	0.1033	2.8622	160.1093
LIG@O	GLY352@H	GLY352@N	0.1000	2.8582	154.0260
LIG@O2	ARG442@HH12	ARG442@NH1	0.0840	2.8292	156.4282
LIG@O1	ARG442@HH22	ARG442@NH2	0.0560	2.8530	149.4766
LIG@N2	GLN213@HE21	GLN213@NE2	0.0540	2.9426	146.4858
LIG@O2	ASN900@HD22	ASN900@ND2	0.0373	2.8383	160.1685
LIG@H16	MET354@HA	MET354@CA	0.0360	2.9151	147.1097
LIG@O1	ASN900@HD21	ASN900@ND2	0.0227	2.8467	157.9495
LIG@O2	ARG442@HH22	ARG442@NH2	0.0153	2.8501	150.4100
LIG@H16	GLN213@HE21	GLN213@NE2	0.0100	2.9016	145.0138
LIG@F2	ASN350@HD21	ASN350@ND2	0.0093	2.8718	146.1015
LIG@O2	ASN900@H	ASN900@N	0.0080	2.8918	152.3064
LIG@O1	ALA474@H	ALA474@N	0.0067	2.8767	144.1850
LIG@F	ALA214@H	ALA214@N	0.0067	2.9107	144.1248
LIG@O1	ASN900@H	ASN900@N	0.0060	2.9234	143.2368
LIG@H	ASN350@HD21	ASN350@ND2	0.0047	2.8587	143.0663
LIG@H2	ASN350@HD21	ASN350@ND2	0.0047	2.9156	143.5178

Table S4 Hydrogen bond occupancy analysis of **6ae** with APN. Bonds with occupancy fraction ≥ 0.005 are shown.

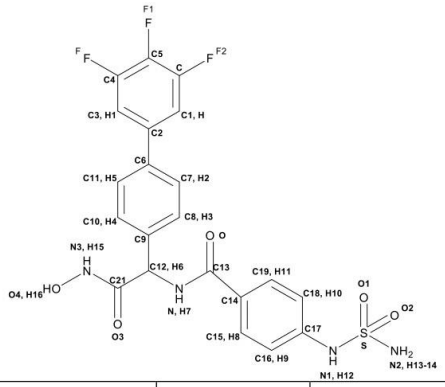

Acceptor	DonorH	Donor	Occupancy	Average Distance (Å)	Average Angle (°)
Protein acceptor / ligand donor					
GLU389@OE1	LIG@H16	LIG@O4	0.9960	2.5813	167.3761
TYR477@OH	LIG@H7	LIG@N	0.1387	2.9007	150.3463
GLN213@OE1	LIG@H15	LIG@N3	0.1293	2.8880	146.4075
ALA353@O	LIG@H15	LIG@N3	0.0867	2.8793	153.3946
TYR477@HH	LIG@H7	LIG@N	0.0307	2.8377	141.3187
MET354@HA	LIG@H15	LIG@N3	0.0133	2.8283	141.1887
TYR477@HE2	LIG@H7	LIG@N	0.0113	2.8993	147.6918
GLU389@OE2	LIG@H16	LIG@O4	0.0080	2.7863	150.2529
Ligand acceptor / protein donor					
LIG@O2	ARG442@HH12	ARG442@NH1	0.2113	2.8374	156.1366
LIG@O4	GLN213@HE21	GLN213@NE2	0.2113	2.9167	163.6767
LIG@O3	TYR477@HH	TYR477@OH	0.1420	2.8081	158.7084
LIG@O2	ARG442@HH22	ARG442@NH2	0.1333	2.8594	154.9591
LIG@N2	ARG442@HH12	ARG442@NH1	0.1307	2.8818	156.2908
LIG@N3	GLN213@HE21	GLN213@NE2	0.0880	2.9378	145.7857
LIG@N2	ARG442@HH22	ARG442@NH2	0.0553	2.8708	159.5539
LIG@O	GLY352@H	GLY352@N	0.0353	2.8268	158.1149
LIG@O1	ARG442@HH12	ARG442@NH1	0.0260	2.8424	150.8653
LIG@O1	ASN900@HD21	ASN900@ND2	0.0260	2.8861	162.2496
LIG@H15	MET354@HA	MET354@CA	0.0227	2.9171	154.1892
LIG@H14	ARG442@HH12	ARG442@NH1	0.0180	2.9059	147.0976
LIG@O1	ARG442@HH22	ARG442@NH2	0.0147	2.8693	151.4265
LIG@H15	GLN213@HE21	GLN213@NE2	0.0120	2.8362	139.8136
LIG@O2	ASN900@HD21	ASN900@ND2	0.0113	2.8790	158.3034
LIG@O1	ARG442@HH11	ARG442@NH1	0.0093	2.8357	155.6258
LIG@N2	ARG442@HH21	ARG442@NH2	0.0093	2.8508	152.0718
LIG@O2	ALA474@H	ALA474@N	0.0087	2.8470	153.6096
LIG@H14	ARG442@HH22	ARG442@NH2	0.0073	2.8993	148.6655
LIG@F	ALA214@H	ALA214@N	0.0073	2.9115	148.2595
LIG@F	ASN350@HD21	ASN350@ND2	0.0073	2.9227	146.3335
LIG@O1	ARG442@HH21	ARG442@NH2	0.0067	2.8224	150.3570
LIG@O2	ARG442@HH21	ARG442@NH2	0.0047	2.8020	159.3886
LIG@H13	ARG442@HH12	ARG442@NH1	0.0047	2.9248	145.1204

Table S5 Hydrogen bond occupancy analysis of **6ag** with APN. Bonds with occupancy fraction ≥ 0.005 are shown.

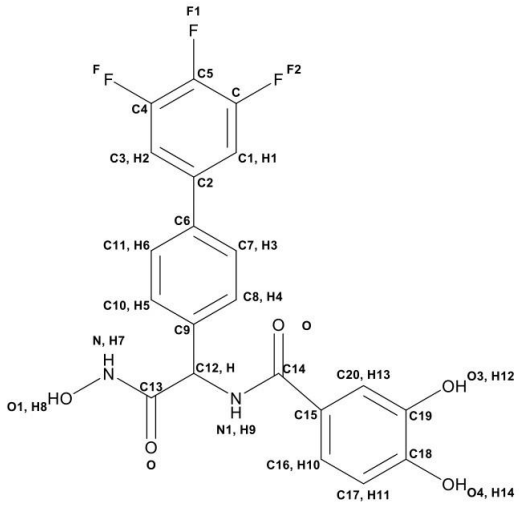

Acceptor	DonorH	Donor	Occupancy	Average Distance (Å)	Average Angle (°)
Protein acceptor / ligand donor					
GLU389@OE1	LIG@H8	LIG@O1	0.9620	2.6167	164.2574
ALA353@O	LIG@H7	LIG@N	0.4407	2.8838	160.7565
GLU418@OE2	LIG@H12	LIG@O3	0.4280	2.6369	163.8371
GLU418@OE2	LIG@H14	LIG@O4	0.4120	2.6671	164.9260
GLU418@OE1	LIG@H14	LIG@O4	0.2613	2.6822	164.3662
GLU418@OE1	LIG@H12	LIG@O3	0.2353	2.6495	161.1446
GLU418@CD	LIG@H12	LIG@O3	0.1833	2.9159	144.1679
GLU389@OE2	LIG@H8	LIG@O1	0.0767	2.8019	148.5760
MET354@HA	LIG@H7	LIG@N	0.0087	2.8315	137.7612
Ligand acceptor / protein donor					
LIG@O2	GLY352@H	GLY352@N	0.4333	2.8641	152.7699
LIG@O1	GLN213@HE21	GLN213@NE2	0.2413	2.9059	152.5440
LIG@O	TYR477@HH	TYR477@OH	0.2213	2.8370	162.4522
LIG@H7	MET354@HA	MET354@CA	0.1060	2.9029	145.4880
LIG@O4	ARG442@HH12	ARG442@NH1	0.0120	2.8819	160.7464
LIG@N	GLN213@HE21	GLN213@NE2	0.0080	2.9678	154.1978
LIG@F1	SER932@HG	SER932@OG	0.0060	2.8474	149.4747
LIG@O	GLN213@HE21	GLN213@NE2	0.0053	2.9063	146.4989
LIG@O1	GLU355@H	GLU355@N	0.0047	2.9364	142.7386

Table S6 Binding scores[5] for the 20 docked poses of compounds **1**, **6ad**, **6ae** and **6ag** into APN.

Total Score	Crash	Polar	FragRMSD	D score	PMF score	G score	ChemScore
Compound **1**							
5.5168	-2.196	5.3507	0.336	-107.649	-92.0788	-189.614	-26.2188
5.4958	-2.212	5.4135	0.338	-108.816	-96.8674	-192.487	-26.5314
5.4269	-2.3433	5.334	0.374	-112.527	-98.3004	-186.06	-27.3774
5.4012	-2.2669	5.2499	0.361	-114.814	-98.8207	-226.585	-27.223
5.3868	-2.2993	5.3371	0.366	-109.331	-96.1585	-193.538	-26.916
5.3705	-2.1395	5.3176	0.332	-110.069	-95.2558	-192.922	-26.3935
5.3633	-2.496	5.3551	0.356	-111.901	-93.7594	-193.568	-26.7976
5.3613	-2.2278	5.2936	0.339	-111.678	-96.8794	-193.496	-26.6659
5.3008	-2.4363	4.996	0.348	-117.902	-94.6245	-204.726	-27.2519
5.2984	-2.173	5.3541	0.328	-108.817	-94.8249	-192.42	-26.3421
5.2711	-1.8023	5.1592	0.393	-110.572	-101.67	-172.7	-26.6053
5.2514	-1.7674	5.0289	0.439	-110.879	-99.2608	-176.785	-26.9812
5.218	-1.7974	5.1087	0.386	-110.741	-103.267	-173.22	-26.6771
5.2031	-2.4108	5.0072	0.326	-115.454	-97.0622	-200.346	-27.0806
5.1086	-1.7438	5.1422	0.411	-112.608	-103.59	-175.295	-26.8849
4.979	-2.184	5.2913	0.342	-106.761	-92.4709	-188.953	-26.0689
4.8863	-1.4284	4.913	0.361	-107.271	-104.323	-169.793	-26.2131
4.8234	-1.6138	4.5525	0.384	-117.515	-105.801	-184.214	-27.4717
4.7917	-2.4203	5.1049	0.332	-113.284	-99.9642	-197.087	-26.7167
4.5379	-2.9104	4.3485	0.412	-129.67	-77.8838	-269.542	-24.4934
Compound **6ad**							
5.8499	-1.2187	4.4618	0.36	-129.864	-95.2487	-171.214	-27.3399
5.8468	-1.1179	4.388	0.339	-129.899	-95.6599	-171.589	-27.3589
5.8264	-0.836	4.1447	0.394	-121.268	-91.5471	-161.455	-27.1541
5.7242	-0.8378	4.1269	0.384	-126.91	-92.6742	-156.682	-27.0187
5.6828	-1.0987	3.247	0.318	-134.482	-106.566	-164.536	-28.5796
5.6673	-0.7936	3.0018	0.423	-132.813	-95.9156	-150.614	-27.5169
5.6449	-1.1563	3.146	0.3	-133.42	-104.013	-166.65	-28.2581
5.6425	-0.9737	4.1944	0.376	-130.353	-95.2522	-161.614	-26.8992
5.6403	-0.9503	3.2781	0.341	-131.533	-100.453	-156.215	-28.2825
5.5951	-0.9387	4.5847	0.327	-115.07	-91.6739	-160.234	-25.8054
5.5893	-0.7583	2.9547	0.385	-133.565	-97.1698	-149.767	-28.4505
5.57	-0.7301	4.102	0.38	-117.285	-94.0912	-154.209	-26.5293
5.5421	-0.9936	4.4991	0.308	-125.669	-95.7022	-159.998	-26.6003
5.5121	-0.924	4.4976	0.29	-114.561	-91.8541	-154.425	-26.4597
5.5079	-0.8562	4.1001	0.366	-118.155	-94.6052	-151.898	-26.3575
5.5032	-1.0251	3.2799	0.379	-132.158	-100.976	-157.126	-28.7218
5.4784	-0.9002	4.4717	0.306	-115.264	-94.0283	-158.46	-26.0446
5.4709	-0.9747	4.502	0.299	-118.238	-94.5523	-154.11	-26.1766
5.4613	-0.7275	4.114	0.366	-117.02	-95.0333	-153.068	-26.3349
5.4591	-1.0214	4.4808	0.295	-118.625	-98.004	-154.895	-26.2492
Compound **6ae**							
6.0707	-1.1883	5.6459	0.301	-125.682	-99.0949	-181.189	-27.818
5.9437	-1.2319	5.6375	0.289	-125.115	-98.0537	-176.38	-28.4462

5.8116	-1.2712	5.6558	0.295	-127.208	-102.879	-172.85	-29.0811
5.6174	-0.865	4.9957	0.301	-124.946	-104.303	-192.885	-31.3854
5.5122	-1.0416	3.933	0.299	-127.993	-105.324	-146.123	-29.0573
5.4358	-0.9888	4.3904	0.347	-124.433	-93.4953	-157.373	-26.4973
5.3932	-0.9039	4.141	0.414	-119.555	-92.347	-156.987	-26.8237
5.382	-1.4015	4.8294	0.455	-127.948	-93.2636	-179.224	-28.805
5.3717	-0.8674	4.1633	0.356	-125.602	-98.474	-162.585	-26.3388
5.3353	-1.1759	3.8065	0.366	-130.348	-100.769	-159.586	-30.5242
5.33	-1.0346	4.4353	0.307	-118.368	-97.6234	-164.415	-26.2954
5.2738	-0.9636	3.9164	0.374	-119.622	-88.0054	-167.277	-24.3176
5.2529	-0.8757	4.1268	0.365	-119.682	-95.8169	-162.93	-26.38
5.2118	-1.0272	4.4276	0.376	-117.723	-91.3257	-158.062	-26.2028
5.2071	-0.9486	4.4796	0.281	-111.437	-93.6697	-153.771	-25.5381
5.1782	-1.0788	4.3393	0.349	-118.855	-94.5424	-163.362	-26.4993
5.1679	-1.1769	4.6263	0.404	-126.94	-89.9427	-173.302	-26.5427
5.0913	-1.002	4.5224	0.293	-116.931	-91.1068	-156.104	-25.3769
5.0695	-1.024	4.516	0.317	-124.183	-93.3478	-153.998	-25.6391
5.055	-1.0947	4.494	0.333	-116.963	-96.842	-163.411	-26.1729
Compound **6ag**							
6.6773	-0.7386	4.8505	1.639	-115.418	-84.8864	-205.277	-27.3128
6.6312	-0.8802	4.961	1.551	-114.597	-85.299	-212.382	-27.2732
6.5302	-0.8628	4.7152	1.622	-109.365	-91.8747	-200.08	-25.2895
6.4185	-0.8727	4.7579	1.583	-111.191	-84.8147	-207.023	-26.8443
6.3751	-1.3271	4.9491	0.59	-117.496	-84.2348	-222.182	-27.7804
6.3363	-0.8763	4.8536	1.653	-110.104	-79.8375	-203.14	-26.6084
6.3207	-0.9768	4.7708	1.816	-108.075	-91.0772	-194.016	-25.3876
6.2477	-1.8158	4.4148	2.095	-115.51	-83.9242	-195.924	-24.6921
6.246	-0.8582	4.729	1.433	-109.313	-91.1799	-212.594	-28.6567
6.2416	-0.9981	4.6943	1.451	-114.706	-85.2842	-225.084	-26.6986
6.1699	-0.7661	4.4429	1.547	-107.257	-93.5184	-194.802	-26.5301
6.1616	-0.6594	5.7827	8.772	-101.835	-36.6042	-145.23	-20.791
6.127	-1.2146	4.4754	0.518	-117.098	-82.7772	-221.425	-25.1872
5.9032	-1.3043	4.7958	0.621	-115.549	-84.3334	-210.164	-26.9125
5.899	-0.8463	5.4005	8.754	-110.007	-31.2335	-155.423	-22.9152
5.8757	-1.2952	4.4566	0.475	-119.744	-87.698	-180.363	-24.9448
5.7147	-1.3885	4.5657	0.558	-116.718	-88.161	-227.894	-27.0993
5.6105	-1.0328	3.6727	1.718	-108.97	-81.9326	-202.927	-24.4841
5.5915	-0.8496	5.8074	7.902	-100.012	-103.046	-158.24	-22.1368
5.5905	-1.3058	3.5781	1.452	-114.892	-95.8201	-202.188	-25.0279

HPLC Traces of Biologically Evaluated Compounds (6a - 6az and 9).

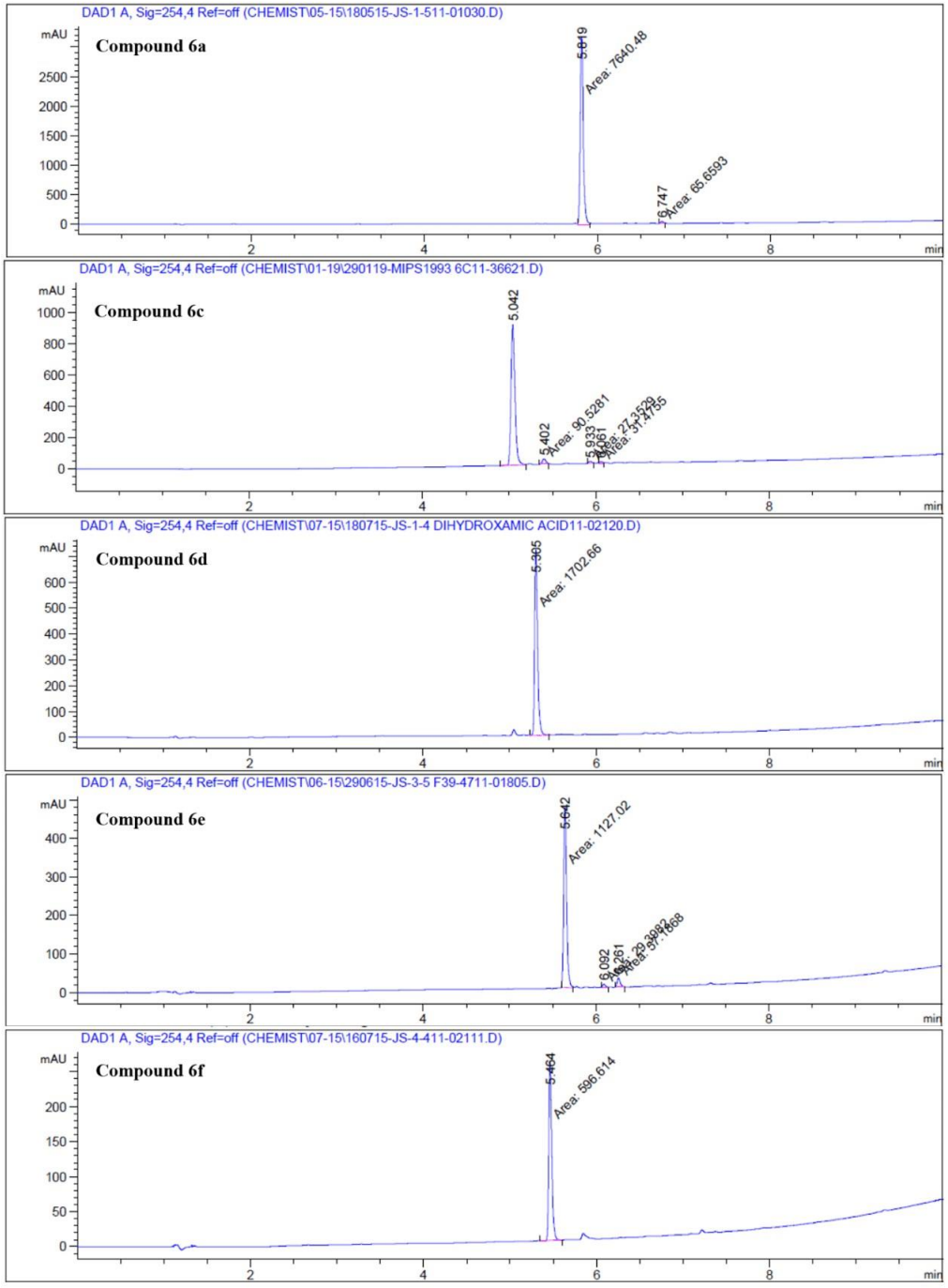

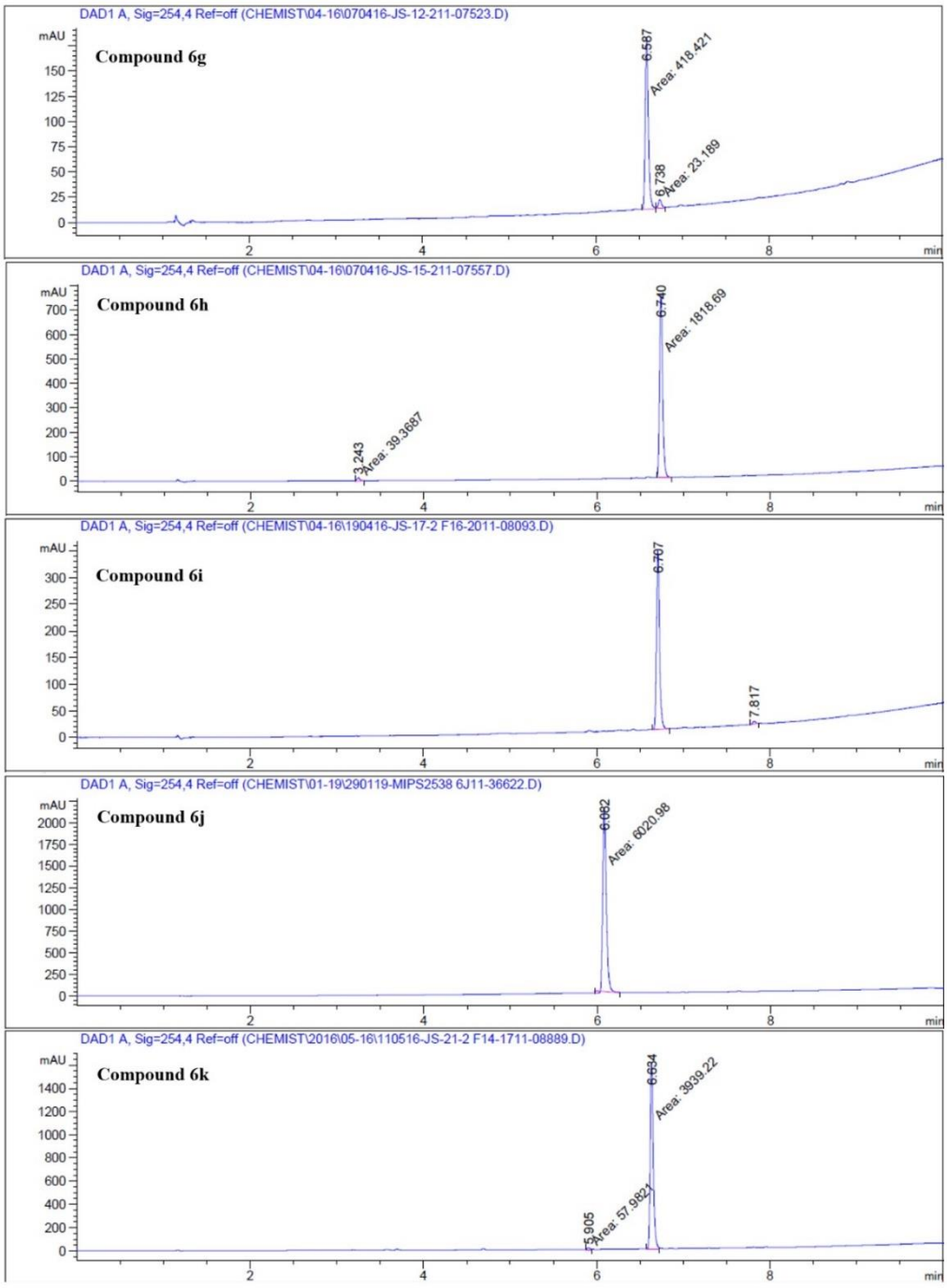
DAD1 A, Sig=254,4 Ref=off (CHEMIST\04-16\070416-JS-12-211-07523.D)
Compound 6g
6.587
Area: 418.421
6.738
Area: 23.189
DAD1 A, Sig=254,4 Ref=off (CHEMIST\04-16\070416-JS-15-211-07557.D)
Compound 6h
6.740
Area: 1818.69
3.243
Area: 39.3687
DAD1 A, Sig=254,4 Ref=off (CHEMIST\04-16\190416-JS-17-2 F16-2011-08093.D)
Compound 6i
6.767
7.817
DAD1 A, Sig=254,4 Ref=off (CHEMIST\01-19\290119-MIPS2538 6J11-36622.D)
Compound 6j
6.662
Area: 6020.98
DAD1 A, Sig=254,4 Ref=off (CHEMIST\2016\05-16\110516-JS-21-2 F14-1711-08889.D)
Compound 6k
6.634
Area: 3939.22
5.905
Area: 57.9821
mAU
min

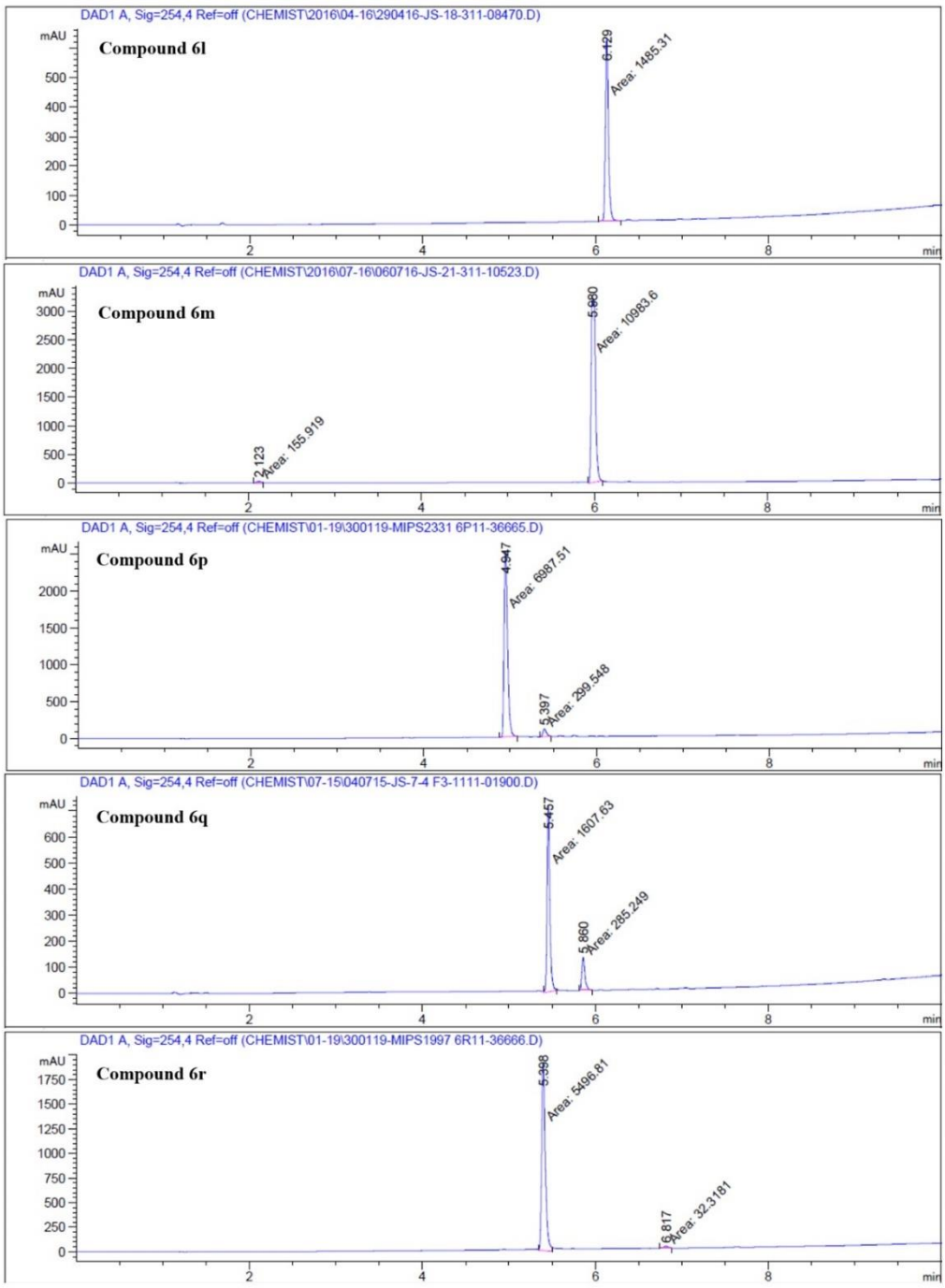
DAD1 A, Sig=254,4 Ref=off (CHEMIST\2016\04-16\290416-JS-18-311-08470.D)
Compound 6l
mAU
6.129
Area: 1485.31
min
DAD1 A, Sig=254,4 Ref=off (CHEMIST\2016\07-16\060716-JS-21-311-10523.D)
Compound 6m
mAU
5.860
Area: 10983.6
2.123
Area: 155.919
min
DAD1 A, Sig=254,4 Ref=off (CHEMIST\01-19\300119-MIPS2331 6P11-36665.D)
Compound 6p
mAU
4.947
Area: 6987.51
5.397
Area: 299.548
min
DAD1 A, Sig=254,4 Ref=off (CHEMIST\07-15\040715-JS-7-4 F3-1111-01900.D)
Compound 6q
mAU
5.457
Area: 1607.63
5.860
Area: 285.249
min
DAD1 A, Sig=254,4 Ref=off (CHEMIST\01-19\300119-MIPS1997 6R11-36666.D)
Compound 6r
mAU
5.398
Area: 5496.81
6.817
Area: 32.3181
min

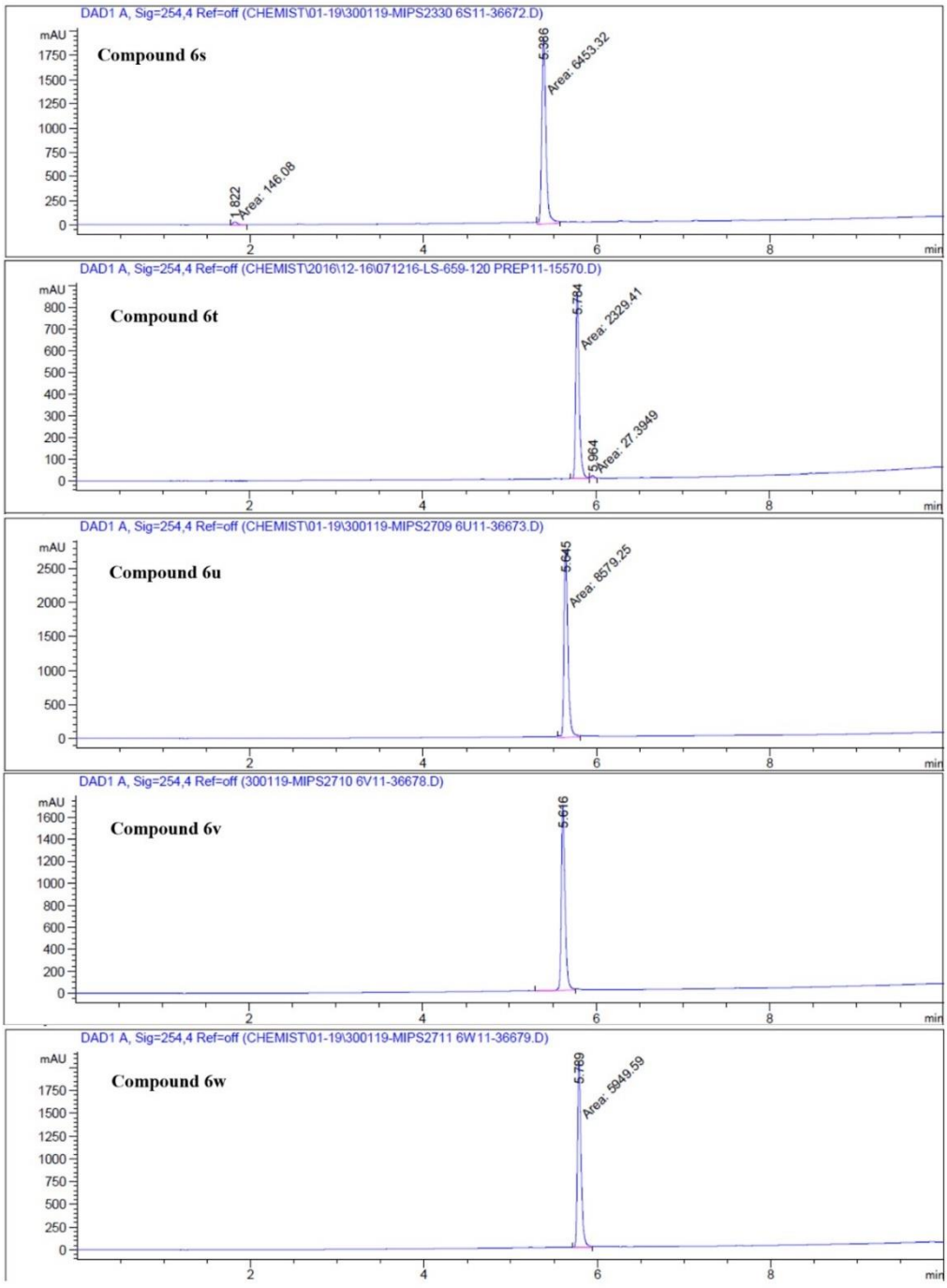
DAD1 A, Sig=254,4 Ref=off (CHEMIST\01-19\300119-MIPS2330 6S11-36672.D)
Compound 6s
5.386
Area: 6453.32
1.822
Area: 146.08
DAD1 A, Sig=254,4 Ref=off (CHEMIST\2016\12-16\071216-LS-659-120 PREP11-15570.D)
Compound 6t
5.784
Area: 2329.41
5.964
Area: 27.3949
DAD1 A, Sig=254,4 Ref=off (CHEMIST\01-19\300119-MIPS2709 6U11-36673.D)
Compound 6u
5.645
Area: 8579.25
DAD1 A, Sig=254,4 Ref=off (300119-MIPS2710 6V11-36678.D)
Compound 6v
5.616
DAD1 A, Sig=254,4 Ref=off (CHEMIST\01-19\300119-MIPS2711 6W11-36679.D)
Compound 6w
5.789
Area: 5949.59
mAU
min

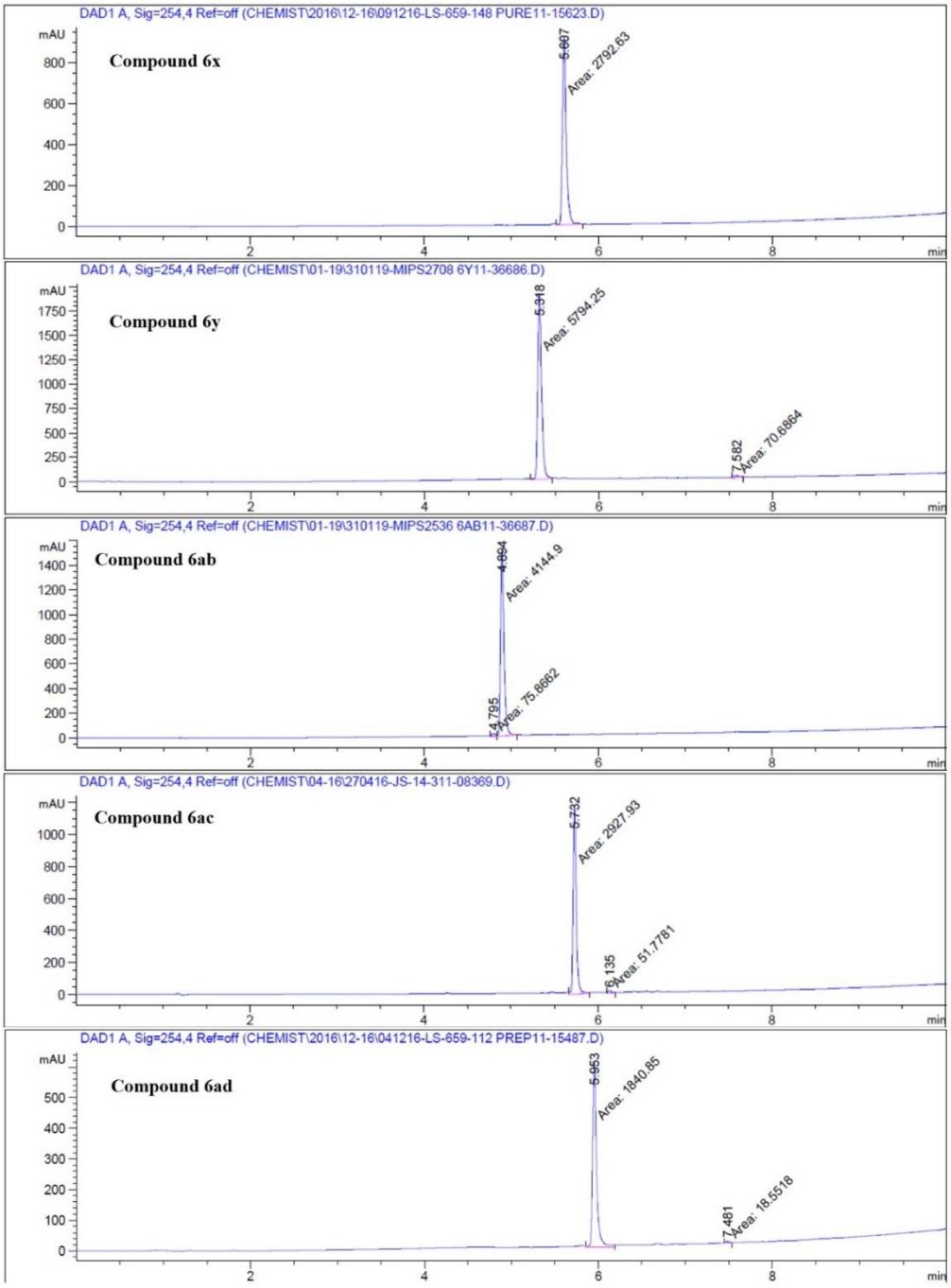
DAD1 A, Sig=254,4 Ref=off (CHEMIST\2016\12-16\091216-LS-659-148 PURE11-15623.D)
Compound 6x
mAU
5.667
Area: 2792.63
min
DAD1 A, Sig=254,4 Ref=off (CHEMIST\01-19\310119-MIPS2708 6Y11-36686.D)
Compound 6y
mAU
5.318
Area: 5794.25
7.582
Area: 70.6864
min
DAD1 A, Sig=254,4 Ref=off (CHEMIST\01-19\310119-MIPS2536 6AB11-36687.D)
Compound 6ab
mAU
4.864
Area: 4144.9
4.795
Area: 75.8662
min
DAD1 A, Sig=254,4 Ref=off (CHEMIST\04-16\270416-JS-14-311-08369.D)
Compound 6ac
mAU
5.732
Area: 2927.93
6.135
Area: 51.7781
min
DAD1 A, Sig=254,4 Ref=off (CHEMIST\2016\12-16\041216-LS-659-112 PREP11-15487.D)
Compound 6ad
mAU
5.953
Area: 1840.85
7.481
Area: 18.5518
min

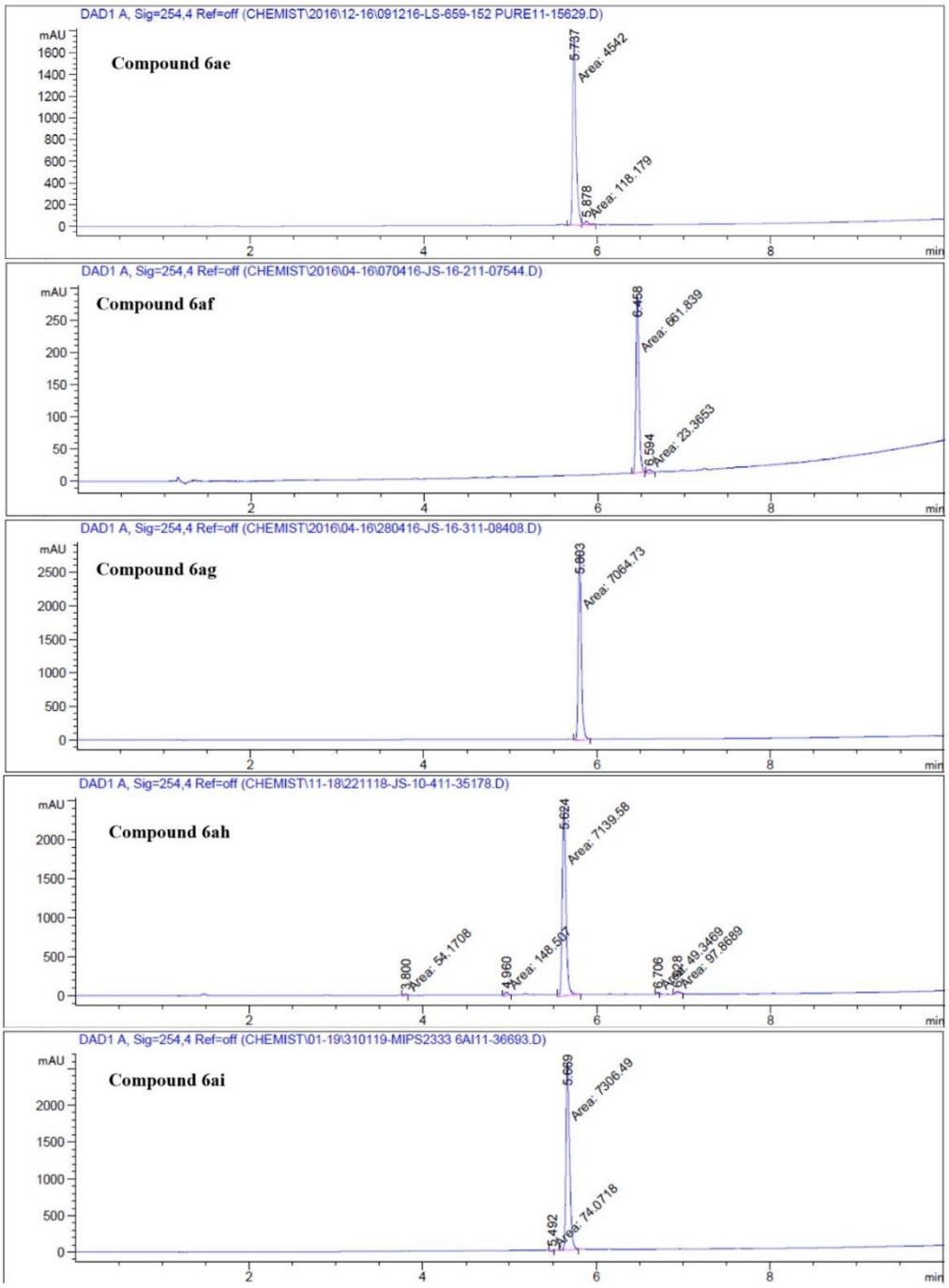
DAD1 A, Sig=254,4 Ref=off (CHEMIST\2016\12-16\091216-LS-659-152 PURE11-15629.D)
Compound 6ae
5.737
Area: 4542
5.878
Area: 118.179
DAD1 A, Sig=254,4 Ref=off (CHEMIST\2016\04-16\070416-JS-16-211-07544.D)
Compound 6af
6.458
Area: 861.839
6.594
Area: 23.3653
DAD1 A, Sig=254,4 Ref=off (CHEMIST\2016\04-16\280416-JS-16-311-08408.D)
Compound 6ag
5.803
Area: 7064.73
DAD1 A, Sig=254,4 Ref=off (CHEMIST\11-18\221118-JS-10-411-35178.D)
Compound 6ah
5.624
Area: 7139.58
3.800
Area: 54.1708
4.960
Area: 148.507
DAD1 A, Sig=254,4 Ref=off (CHEMIST\01-19\310119-MIPS2333 6AI11-36693.D)
Compound 6ai
5.669
Area: 7306.49
5.492
Area: 74.0718
mAU
min

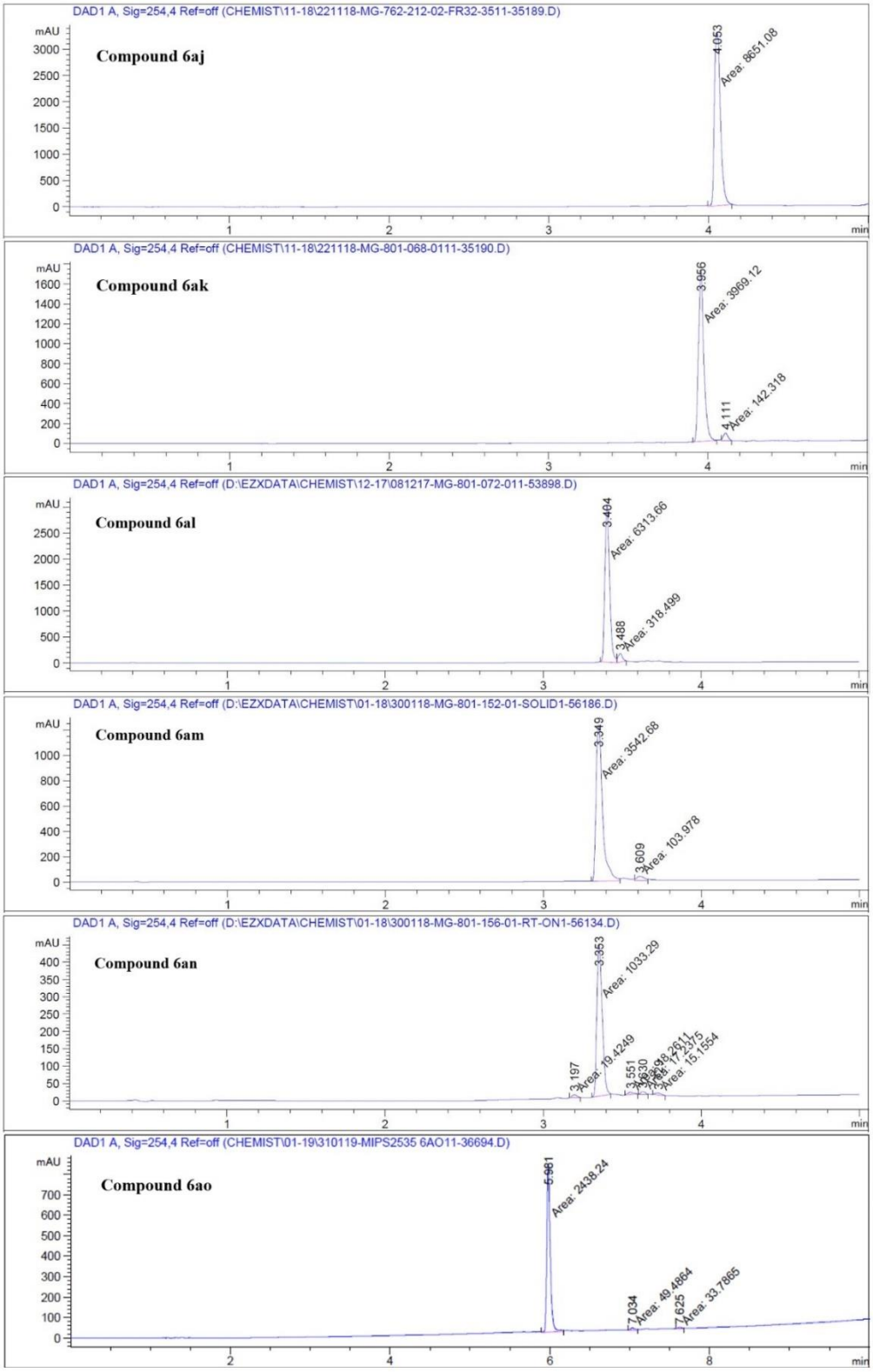
DAD1 A, Sig=254,4 Ref=off (CHEMIST\11-18\221118-MG-762-212-02-FR32-3511-35189.D)
Compound 6aj
4.053
Area: 8651.08
DAD1 A, Sig=254,4 Ref=off (CHEMIST\11-18\221118-MG-801-068-0111-35190.D)
Compound 6ak
3.956
Area: 3969.12
4.111
Area: 142.318
DAD1 A, Sig=254,4 Ref=off (D:\EZXDATA\CHEMIST\12-17\081217-MG-801-072-011-53898.D)
Compound 6al
3.464
Area: 6313.66
3.488
Area: 318.499
DAD1 A, Sig=254,4 Ref=off (D:\EZXDATA\CHEMIST\01-18\300118-MG-801-152-01-SOLID1-56186.D)
Compound 6am
3.349
Area: 3542.68
3.609
Area: 103.978
DAD1 A, Sig=254,4 Ref=off (D:\EZXDATA\CHEMIST\01-18\300118-MG-801-156-01-RT-ON1-56134.D)
Compound 6an
3.353
Area: 1033.29
3.197
Area: 19.4249
3.551
Area: 15.1554
DAD1 A, Sig=254,4 Ref=off (CHEMIST\01-19\310119-MIPS2535 6AO11-36694.D)
Compound 6ao
5.981
Area: 2438.24
7.034
Area: 49.4864
7.625
Area: 33.7865
mAU
min

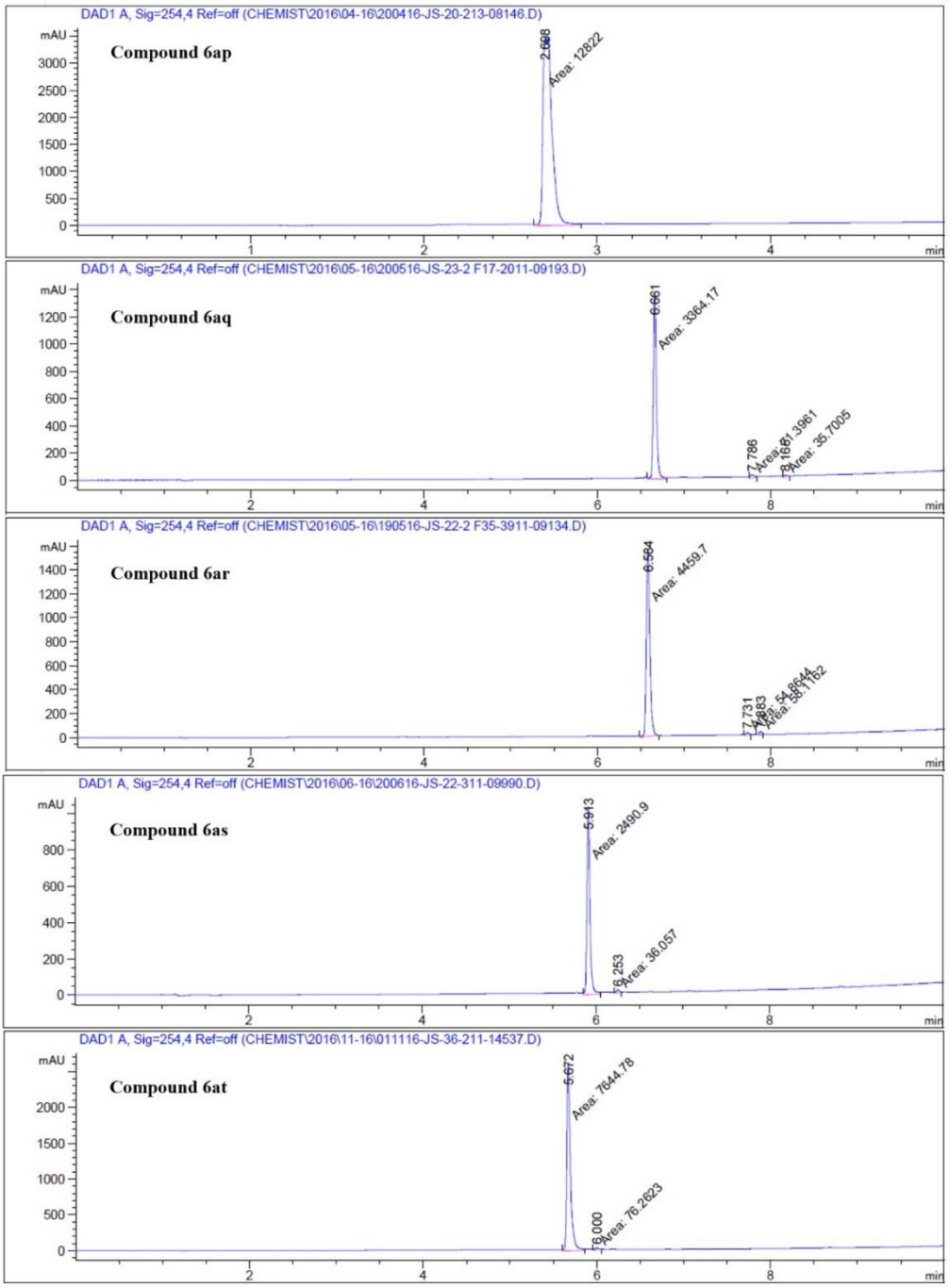
DAD1 A, Sig=254,4 Ref=off (CHEMIST\2016\04-16\200416-JS-20-213-08146.D)
Compound 6ap
Area: 12822
DAD1 A, Sig=254,4 Ref=off (CHEMIST\2016\05-16\200516-JS-23-2 F17-2011-09193.D)
Compound 6aq
6.661
Area: 3364.17
7.786
Area: 61.3961
Area: 35.7005
DAD1 A, Sig=254,4 Ref=off (CHEMIST\2016\05-16\190516-JS-22-2 F35-3911-09134.D)
Compound 6ar
6.584
Area: 4459.7
7.731
DAD1 A, Sig=254,4 Ref=off (CHEMIST\2016\06-16\200616-JS-22-311-09990.D)
Compound 6as
5.913
Area: 2490.9
6.253
Area: 36.057
DAD1 A, Sig=254,4 Ref=off (CHEMIST\2016\11-16\011116-JS-36-211-14537.D)
Compound 6at
5.672
Area: 7644.78
6.000
Area: 76.2623
mAU
min

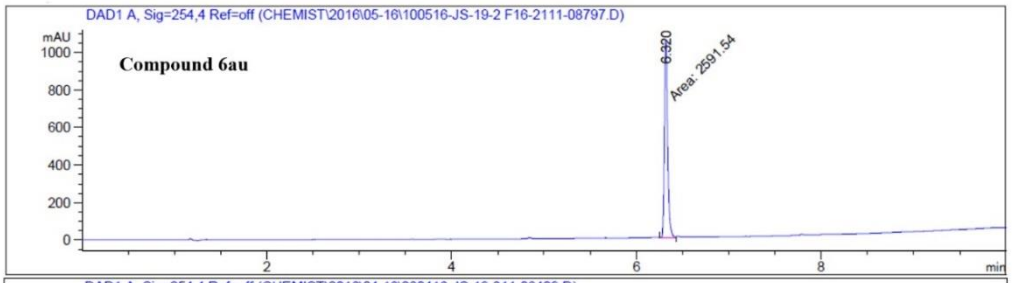
DAD1 A, Sig=254,4 Ref=off (CHEMIST\2016\05-16\100516-JS-19-2 F16-2111-08797.D)
Compound 6au
mAU
6.920
Area: 2591.54
min

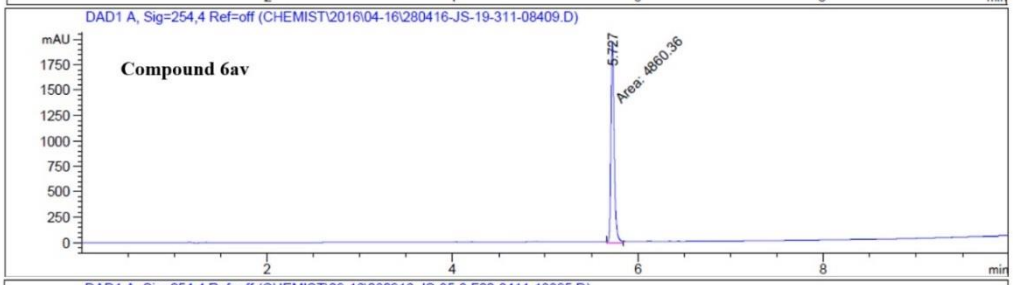
DAD1 A, Sig=254,4 Ref=off (CHEMIST\2016\04-16\280416-JS-19-311-08409.D)
Compound 6av
mAU
5.727
Area: 4860.36
min

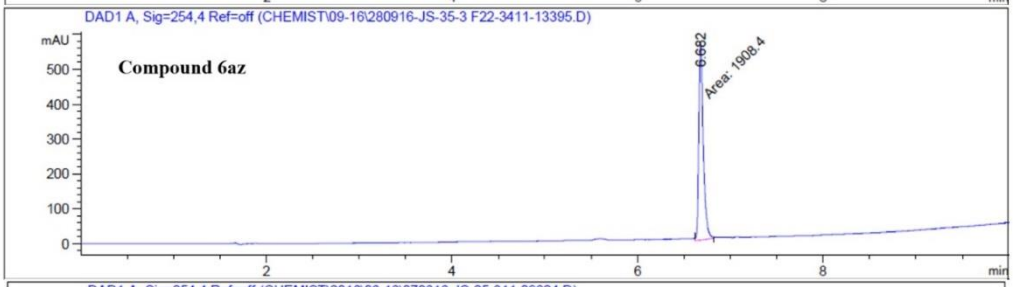
DAD1 A, Sig=254,4 Ref=off (CHEMIST\09-16\280916-JS-35-3 F22-3411-13395.D)
Compound 6az
mAU
6.682
Area: 1908.4
min

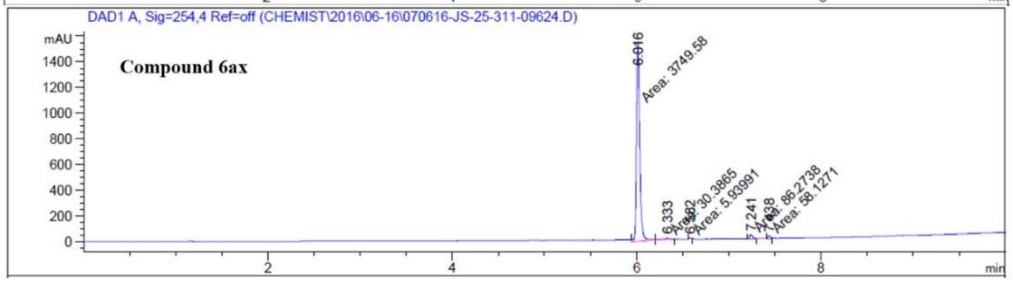
DAD1 A, Sig=254,4 Ref=off (CHEMIST\2016\06-16\070616-JS-25-311-09624.D)
Compound 6ax
mAU
6.916
Area: 3749.58
Area: 5.53991
Area: 86.2738
Area: 58.1271
min

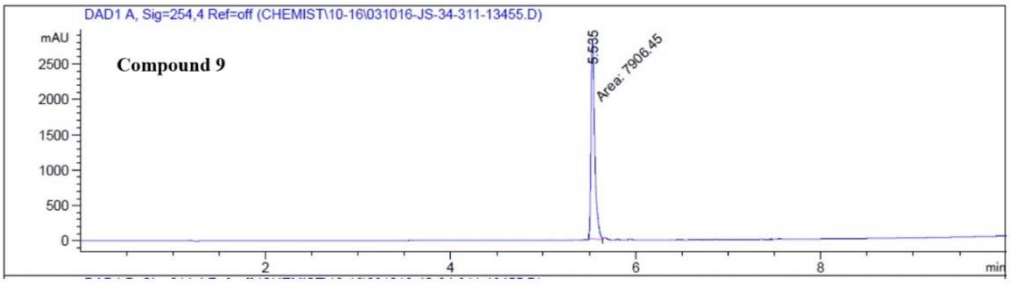
DAD1 A, Sig=254,4 Ref=off (CHEMIST\10-16\031016-JS-34-311-13455.D)
Compound 9
mAU
5.595
Area: 7906.45
min

References

(1) Ochiai, H.; Uetake, Y.; Niwa, T.; Hosoya, T. Rhodium-Catalyzed Decarbonylative Borylation of Aromatic Thioesters for Facile Diversification of Aromatic Carboxylic Acids. *Angew. Chem. Int. Ed. Engl.* **2017,** 56, 2482-2486.

(2) Tinnis, F.; Volkov, A.; Slagbrand, T.; Adolfsson, H. Chemoselective Reduction of Tertiary Amides under Thermal Control: Formation of either Aldehydes or Amines. *Angew. Chem. Int. Ed. Engl.* **2016,** 55, 4562-6.

(3) Zheng, Y.; Liu, B.; Gou, Z.; Li, Y.; Zhang, X.; Wang, Y.; Yu, S.; Li, Y.; Sun, D. Design of novel CSA analogues as potential safeners and fungicides. *Bioorg. Med. Chem. Lett.* **2015,** 25, 791-4.

(4) Sun, L.; Tran, N.; Liang, C.; Tang, F.; Rice, A.; Schreck, R.; Waltz, K.; Shawver, L. K.; McMahon, G.; Tang, C. Design, synthesis, and evaluations of substituted 3-[(3- or 4-carboxyethylpyrrol-2-yl)methylidenyl]indolin-2-ones as inhibitors of VEGF, FGF, and PDGF receptor tyrosine kinases. *J. Med. Chem.* **1999,** 42, 5120-30.

(5) Jain, A. N. Surflex: fully automatic flexible molecular docking using a molecular similarity-based search engine. *J. Med. Chem.* **2003,** 46, 499-511.

Chapter 3: Replacing the 3,4,5-Trifluorophenyl for Improved Solubility and Optimised Activity at the S1 Pocket of APN

3.1 Introduction

In *Chapter 2*, a series of hydroxamic acid analogues were synthesised to optimise the binding interactions around and beyond the S1′ subsite of the target protein, APN for the treatment of cancer. Among them, the 4-methylsulfonyl analogue **6ad** showed the most potent inhibition against APN with a $K_i^{(app)}$ value of 4.8 nM, which was a 500-fold improvement in activity compared to a known APN inhibitor bestatin ($K_i^{(app)}$ = 2.4 μM). Compound **6ad** also showed favourable metabolic and plasma stability *in vitro*. Despite its potent activity and promising pharmacokinetic properties, **6ad** could not be pursued further as an anti-cancer lead candidate due to its sub-optimal aqueous solubility (12.5 – 25 μg/mL in pH 2.0 and 6.0) which could potentially limit the absorption into the body, and poor efficacy in the cellular environment.

Therefore, the focus of this project changed to the modifications of the 3,4,5-trifluorophenyl moiety of **6ad** that is positioned at the S1 binding site of APN. The 3,4,5-trifluorophenyl group was derived from the SAR studies and structure-guided optimisations of the parasitic homologue *Pf*A-M1.[230] However there was limited exploration to the S1 subsite of APN for optimised binding interactions. According to the molecular modelling studies described in *Chapter 2*, the trifluorophenyl ring formed various hydrophobic interactions with the flexible loop ^{891}YGGGSFSF^{898} in domain IV, creating a stable binding site for the inhibitors within APN. Therefore, complete removal of the trifluorophenyl group may allow us to investigate if the biphenyl system is essential for obtaining potency against APN and if the result is consistent with our molecular modelling studies. In addition, replacing the hydrophobic 3,4,5-trifluorophenyl to various heteroaromatic groups may improve the solubility as well as binding interactions by introducing additional polar atoms into the molecule, which may also increase the hydrogen bonding capacity. Moreover, previous studies heavily focussed on the biaryl or

4-haloaryl units, therefore, incorporating sp^3 – rich groups as replacements of trifluorophenyl moiety may create new chemical scaffolds to probe the activities around the S1 pocket of APN.

Chapter 3 aims to investigate the S1 pocket of APN by modifying the 3,4,5-trifluorophenyl moiety to less hydrophobic substituted aromatic, heteroaromatic or cycloalkyl groups. A number of hydroxamic acid analogues were designed to achieve improved aqueous solubility and optimised binding interactions at the S1 subsite of APN based on the molecular modelling studies conducted in *Chapter 2*. Diverse synthetic strategies such as Suzuki-Miyaura couplings and Buchwald-Hartwig aminations are employed to produce the designed molecules efficiently. Compounds synthesised were evaluated for inhibitory activity against APN *in vitro* and SAR was developed from biological data to identify the essential properties required for the desired activity. In addition, the hydrophobicity of molecules was compared using the cLogP parameter as an indication of aqueous solubility. Finally, molecular docking studies were performed for selected compounds to investigate binding interactions made between the ligands and APN.

3.2 Design and syntheses of new hydroxamic acid analogues with diverse S1 head groups

3.2.1 Design of the target compounds

A new series of compounds was designed to explore the S1 pocket of APN by replacing the trifluorophenyl moiety with other substituents. Instead of the methanesulfonyl group of **6ad**, which was the most potent inhibitor discovered in the previous chapter, the sulfamide group of **6ae** ($K_i^{(app)}$ = 8.2 nM) was retained as the S1′ tail group to increase the polarity of molecules (Figure 3.1). In addition, the compounds were carefully developed to ensure that they have lower cLogP values compared to compound **6ae**. Various phenylglycine analogues where the 3,4,5-fluorophenyl ring is completely removed may determine if the biphenyl system is crucial for activity. In addition, halogen groups of substituted phenylglycines create dipole moments which can involve in dipole-dipole interactions. Mono- or di-fluorophenyls are also included to reduce the hydrophobicity of compounds and assess which position of the substituent is preferred for potency.

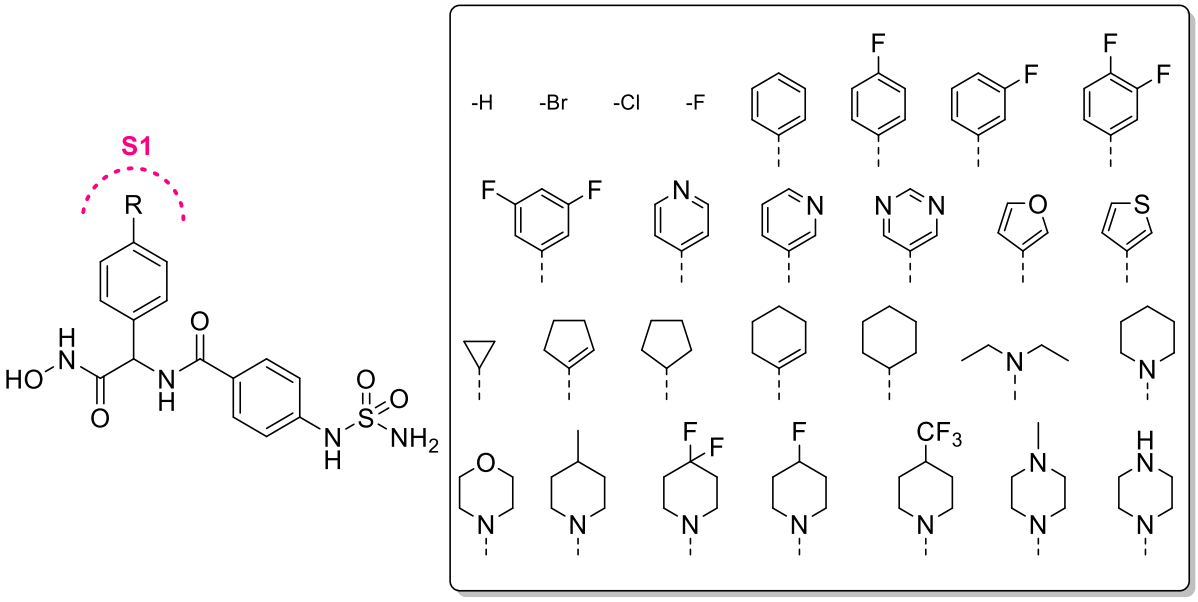

Figure 3.1. Structure of designed hydroxamic analogues to investigate the binding interactions at the S1 subsite of APN.

Nitrogen containing heteroaromatic groups such as pyridine and pyrimidine can be introduced as they are known as isosteres of a benzene ring. Meanwell *et al*. and Dalvie *et al*. extensively reviewed the use of heteroaromatics in drug development and details the advantages of replacing phenyl ring with other heteroaromatic groups.[236-238] Firstly, the additional electronegative nitrogen atom(s) of pyridine and pyrimidine create larger dipole moment, allowing molecules to be involved in intermolecular dipole-dipole interactions with the target protein.[236, 237] Additionally, the nitrogen atoms could act as hydrogen bond acceptors to form hydrogen bonding interactions with the backbone residues.[236, 237] Moreover, physicochemical or pharmacokinetic properties could be enhanced while maintaining activity.[237, 238]

The molecular sizes of pyridine and pyrimidine are comparable to that of benzene, and the designed analogues would retain the biphenyl core scaffold so that the compounds could engage in π-stacking hydrophobic interactions with the phenylalanine residues of domain IV as described in *Chapter 2*. However, incorporating nitrogen-containing heteroaromatics may changes the physicochemical properties significantly due to lowered LogP/LogD, increased hydrogen bond capacity and polar surface area.[238] These changes would improve aqueous solubility and other aspects of pharmacokinetic profiles such as ADMET.[238]

Apart from six-membered heteroaromatic, five-membered heteroaryl groups such as furan and thiophene would be interesting to investigate its effect on APN activity. Furan bears an electronegative oxygen atom which is capable of capturing additional hydrogen bonding interactions with the nearby residues. Thiophene is one of the most widely exploited sulfur-containing heteroaromatics in medicinal chemistry due to its unique structural and chemical properties. A sulfur atom is electropositive because it donates p_z electron to the aromatic π system. Therefore, sulfur is able to interact with electronegative oxygen atoms.[239] The S-O interactions have been much discussed in the context of intramolecular interactions.[237, 239] However, there is growing evidence of intermolecular interactions between sulfur of a ligand and the carbonyl oxygen of backbone residue.[239]

Moreover, the installation of sp^3-rich cycloalkyl groups such as cyclohexyl and cyclopropyl may increase the solubility of the compounds by removing the aromaticity and symmetry of the biphenyl scaffold. This strategy has few advantages over introducing a hydrophilic group to enhance solubility.[240] Firstly, reducing cLogP by adding hydrophilic atoms is the general approach; however, such methods may not be effective because polar groups can interfere with target-drug interactions.[240] Secondly, the change of crystal polymorphs for better solubility may be able to reach an ideal balance between solubility and hydrophobicity, which is essential for optimal oral bioavailability.[240] Piperidine and piperazine derivatives may have advantages in two-fold because they are not only sp^3-rich but also contain additional nitrogen atom(s) that can be ionised as salt to achieve improved solubility.

3.2.2 Optimisation of Suzuki-Miyaura coupling reactions to form a C-C bond of designed compounds

Successful syntheses of designed analogues containing biaryl or cycloalkyl-aryl scaffolds involve the formation of aryl-aryl and aryl-alky C-C bonds, respectively. There are numerous reported reactions that used to form C-C bonds, but the most widely known would be Suzuki-Miyaura coupling, which is the palladium catalysed the reaction between aryl halides and boronic acids. In the following sections, synthesis optimisations to generate biaryl and cycloalkyl-aryl analogues are discussed in detail.

3.2.2.1 Synthetic strategies employed to form an aryl-aryl C-C bond

Synthesis of sulfamide analogues was attempted as described in Scheme 3.1. Acid catalysed esterification was performed to form methyl 2-amino-2-(4-bromophenyl)acetate (**1d**) in an excellent yield of 90% yield. The amino group of **1d** was coupled to pre-synthesised 4-((*N*-(*tert*-butoxycarbonyl)sulfamoyl)amino)benzoic acid in the presence of EDCI and DMAP, generating the intermediate compound **2**. The synthesis of the benzoic acid was performed as described in Lee *et al*.[241] Following deprotection of the *tert*-butyl carbamate group (Boc) through acid hydrolysis with 20% TFA/DCM efficiently produced the free sulfamide compound **3** in 50% yield. Suzuki-Miyaura coupling reactions were attempted in various conditions to replace the bromide of intermediate **3** with 4-fluorophenylboronic acid. (Table 3.1).

Scheme 3.1. Proposed multi-step synthesis to generate sulfamide analogues.

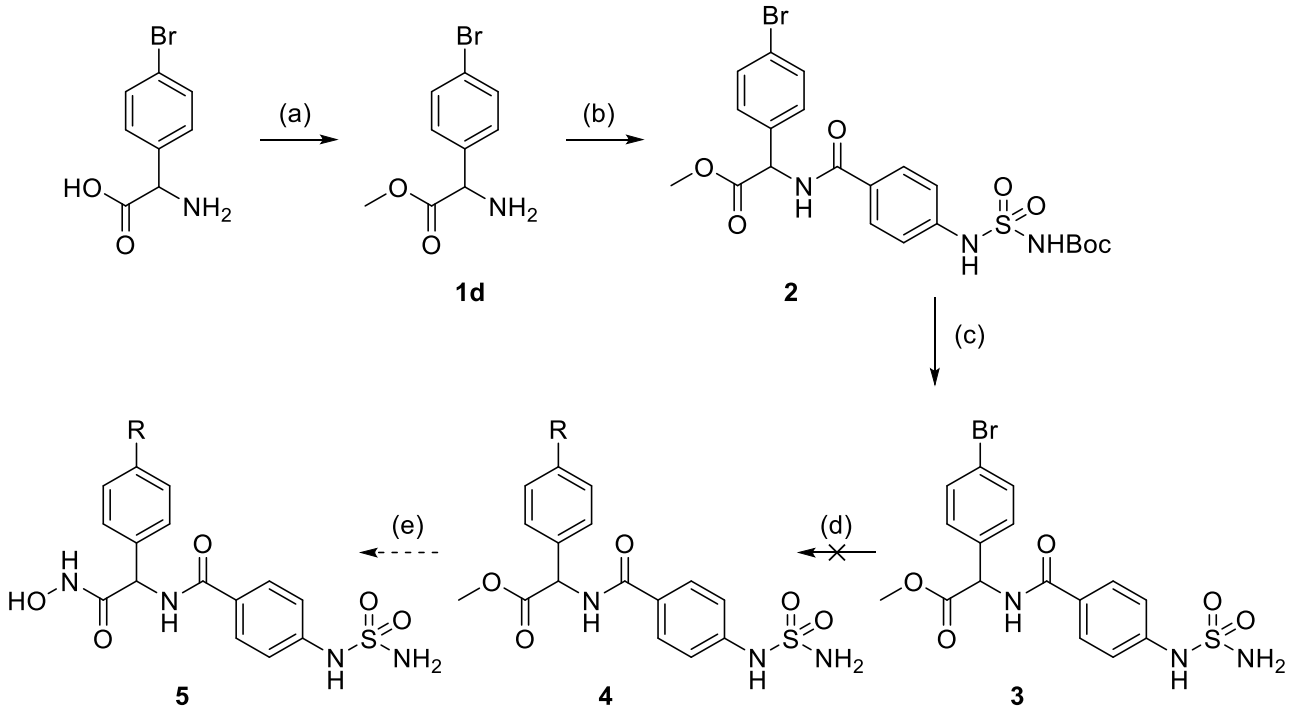

Reagents and conditions: (a) conc. H_2SO_4, MeOH, reflux, overnight, 90%; (b) 4-((*N*-(*tert*-butoxycarbonyl)sulfamoyl)amino)benzoic acid, EDCI, DMAP, DCM, rt, overnight, 78%; (c) 20% TFA/DCM, rt, 3 h, 50%; (d) Suzuki-Miyaura coupling; (e) $NH_2OH{\cdot}HCl$, 5 M KOH/MeOH, anhydrous MeOH, rt, overnight.

When a mixture of compound **3**, 4-fluoroboronic acid, 1 M Na_2CO_3, and $Pd(PPh_3)_2Cl_2$ in THF was heated at reflux for 2 hours (Table 3.1, Entry 1), 40% of **3** was hydrolysed to the corresponding carboxylic acid. When the reaction was refluxed for another 2 hours, minimal conversion to the desired product was observed. The base hydrolysis was easily prevented by changing the base to triethylamine in an anhydrous condition (Table 3.1, Entry 2). However, the reaction failed to achieve complete conversion despite the prolonged reaction time of 20 hours. After isolation, a mixture of the desired product and aniline compound was obtained, indicating that the desired product was formed, but degraded to aniline by sulfonamide cleavage. Similar results were obtained when $Pd(PPh_3)_4$, K_2CO_3, DME and a minimal amount of water were heated at 150 °C for 10 minutes in a microwave (Table 3.1, Entry 3); the cleavage of the sulfonamide group still occurred together with debromination of compound **3**.

Coupling reactions between free sulfamide intermediate **3** and 4-fluoroboronic acid were not successful, mainly due to the base-mediated methyl ester hydrolysis and sulfonamide cleavage. One causative factor of the unsuccessful reactions could be the presence of sulfonamide group, which are also known as zinc (II) chelators.[242] Being one of the sulfonamide derivatives, sulfamide may have potential to chelate metals including palladium, which can be detrimental for metal-catalysed reaction to work effectively. Therefore, the Boc-protected intermediate **2** was used as the new starting molecule to provide sufficient steric hindrance so that chelation of sulfamide to palladium could be prevented. With the conditions described in Table 3.1, Entry 4, compound **2** was converted to the desired product by 10%. Unfortunately, most of compound **2** remained unreacted, or the Boc group was cleaved to produce compound **3**. Heating the reaction mixture in a microwave reactor for a short period of time was able to minimise the Boc-deprotection, however complete conversion to the product was not achieved (Table 3.1, Entry 5). Isolation of the product from starting material **2** by column chromatography was challenging due to the poor resolution on silica gel, suggesting a complete conversion of the starting material is essential. An increase in the reaction time (Table 3.1, Entry 6) or a reduction in the temperature with increased reaction time (Table 3.11, Entry 7) led to sulfonamide cleavage and minimal formation of the product

Table 3.1. Summary of Suzuki-Miyaura coupling reactions attempted from compound 3 (Entry 1-3) and 2 (Entry 4-7).

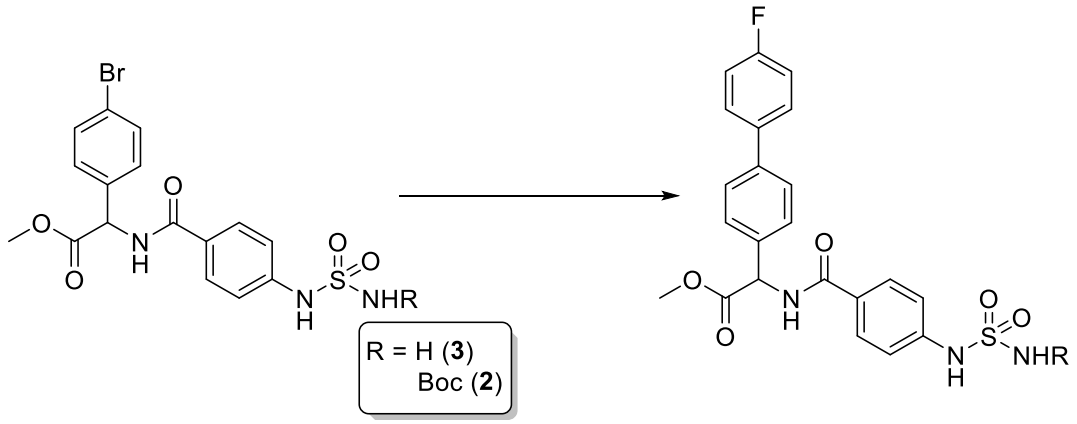

Entry	Catalyst	Base	Solvent	Conditions	Results
1	$Pd(PPh_3)_2Cl_2$	1 M Na_2CO_3	THF	Reflux, 2 – 4 h	Base hydrolysis
2	$Pd(PPh_3)_2Cl_2$	Et_3N	THF	Reflux, 2 – 20 h	Partial conversion and sulfonamide cleavage
3	$Pd(PPh_3)_4$	K_2CO_3	DME/water	Microwave 10 min, 150 °C	Sulfonamide cleavage
4	$Pd(PPh_3)_2Cl_2$	1 M Na_2CO_3	THF	Reflux, overnight	Boc deprotection and 10% conversion
5	$Pd(PPh_3)_2Cl_2$	1 M Na_2CO_3	THF	Microwave 10 min, 100 °C	A mixture of **2** and product after isolation.
6	$Pd(PPh_3)_2Cl_2$	1 M Na_2CO_3	THF	Microwave 30 min, 100 °C	Minimal conversion and sulfonamide cleavage
7	$Pd(PPh_3)_2Cl_2$	1 M Na_2CO_3	THF	Microwave 30 min, 90 °C	Minimal conversion and sulfonamide cleavage

From Suzuki-Miyaura coupling reactions with sulfamide derivatives **2** and **3**, it was concluded that the sulfamide group was unstable in both anhydrous and biphasic conditions. Therefore, our focus turned to the sulfonamide group of **6ad** (cLogP = 2.10), which showed the best activity in the S1′ region of APN but was slightly more hydrophobic than **6ae** (cLogP = 1.64).

The synthesis of intermediate **4** was accomplished by applying the synthetic approach described in Scheme 3.2.

Scheme 3.2. Optimised synthetic pathway to produce mono-aryl analogues 6a-d and biaryl analogues 6e-s.

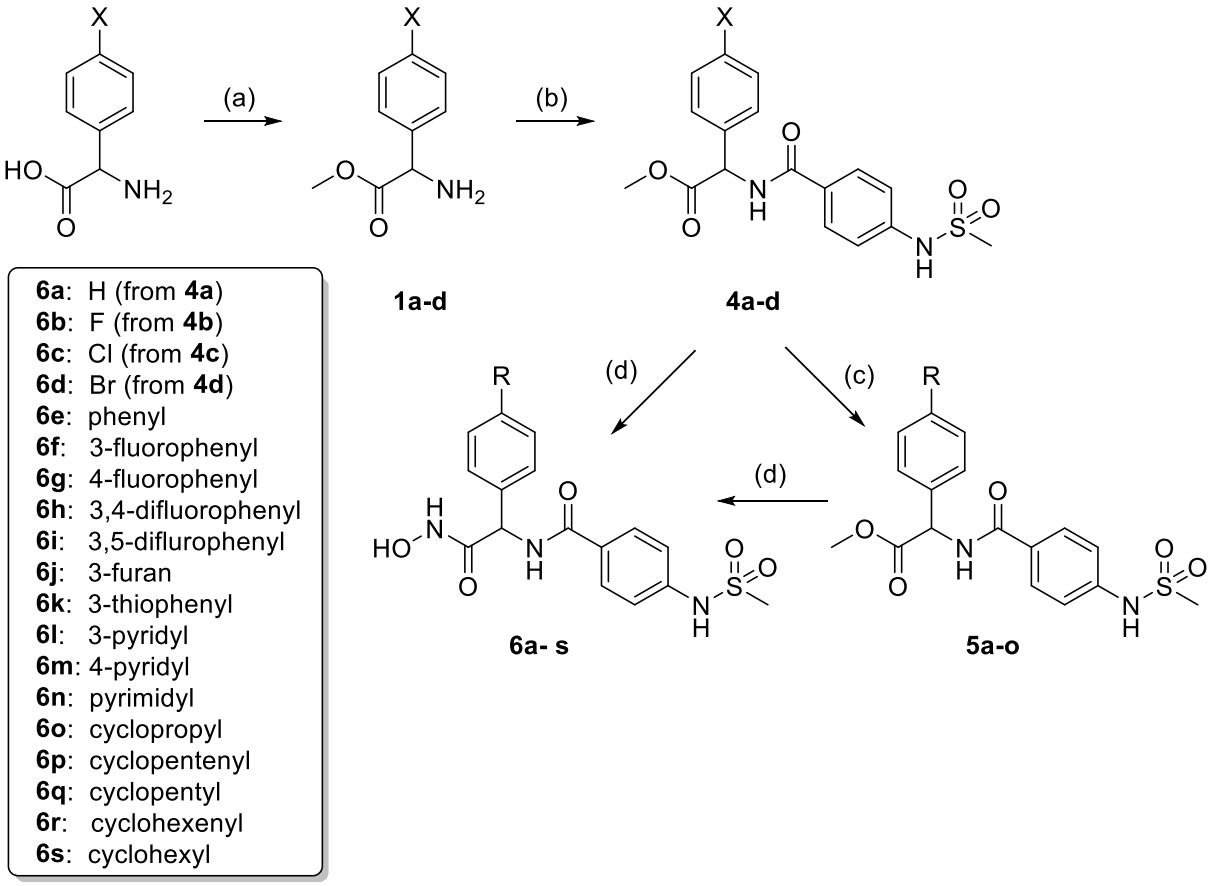

Reagents and conditions: (a) conc. H_2SO_4, MeOH, reflux, overnight, 75–90%; (b) 4-(methylsulfonamido)benzoic acid, EDCI, DMAP, DCM, rt, overnight, 61–92%; (c) Suzuki-Miyaura coupling reactions; (d) $NH_2OH{\cdot}HCl$, 5 M KOH/MeOH, anhydrous MeOH, rt, overnight, 5-78%.

Suzuki-Miyaura coupling reactions between the aryl bromide **4d** and aryl boronic acids were successfully optimised (Table 3.2). The microwave-assisted reaction was able to generate compound **5c** in 34% yield after purification (Table 3.2, Entry 1). However, this result was not reproducible when the same reaction conditions were applied to the coupling of 3-fluorophenyl boronic acid (Table 3.2, Entry 2). The purified compound **5b** was obtained in a low yield of 14%, and a mixture of **5b** and the methyl ester hydrolysed product was generated in 20% yield.

The yield of **5b** was significantly improved to 73% when the reaction was conducted under anhydrous conditions in the presence of powdered K_3PO_4 to avoid hydrolysis (Table 3.2, Entry 3). It was also noted that longer reaction time was required to reach complete conversion in the absence of water. The optimised coupling reaction condition was deployed for the synthesis of compounds **5a-o**.

Table 3.2. Summary of Suzuki-Miyaura coupling reactions attempted from compound 4 with aryl boronic acids.

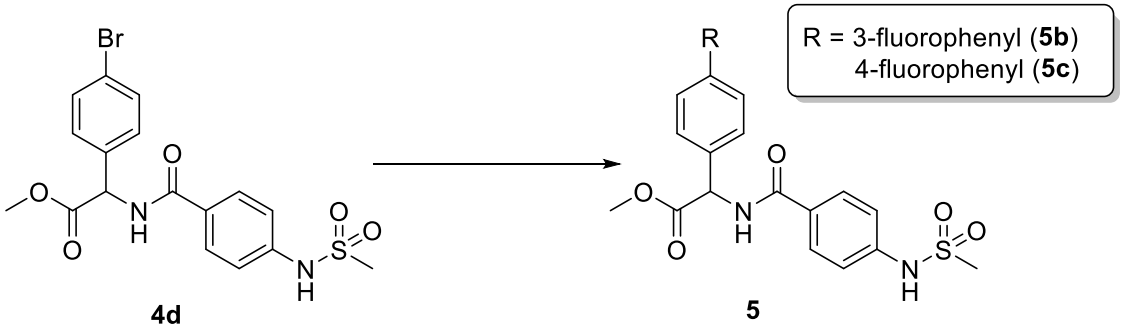

Entry	R	Catalyst	Base	Solvent	Conditions	Results
1	4-fluorophenyl	$Pd(PPh_3)_2Cl_2$	1 M Na_2CO_3	DMF	Microwave 10 min, 100 °C	34% yield
2	3-fluorophenyl	$Pd(PPh_3)_2Cl_2$	1 M Na_2CO_3	DMF	Microwave 10 min, 100 °C	Mixture of product + hydrolysed dimer (20% yield)
3	3-fluorophenyl	$Pd(PPh_3)_2Cl_2$	K_3PO_4	DMF	Microwave 2 h, 100 °C	73% yield

While the introduction of the hydroxamic acid could be achieved by direct aminolysis of methyl ester in the presence of hydroxylamine hydrochloride and potassium hydroxide (Scheme 3.2), we also investigated alternative synthetic routes which involved the formation of protected hydroxamic acid from a carboxylic acid via amide coupling (Scheme 3.3). Synthesis of protected hydroxamic acid consists of the use of weak organic bases. Therefore, hydrolysis of methyl ester, which was occasionally observed from direct aminolysis due to

excess strong base, may be eradicated. Additionally, the protected hydroxamic acid may also prevent potential chelation to metal effectively, which is essential for palladium-catalysed reactions such as Suzuki-Miyaura and Buchwald-Hartwig coupling reactions to work successfully.

Scheme 3.3. Proposed scheme to synthesise protected hydroxamic acid.

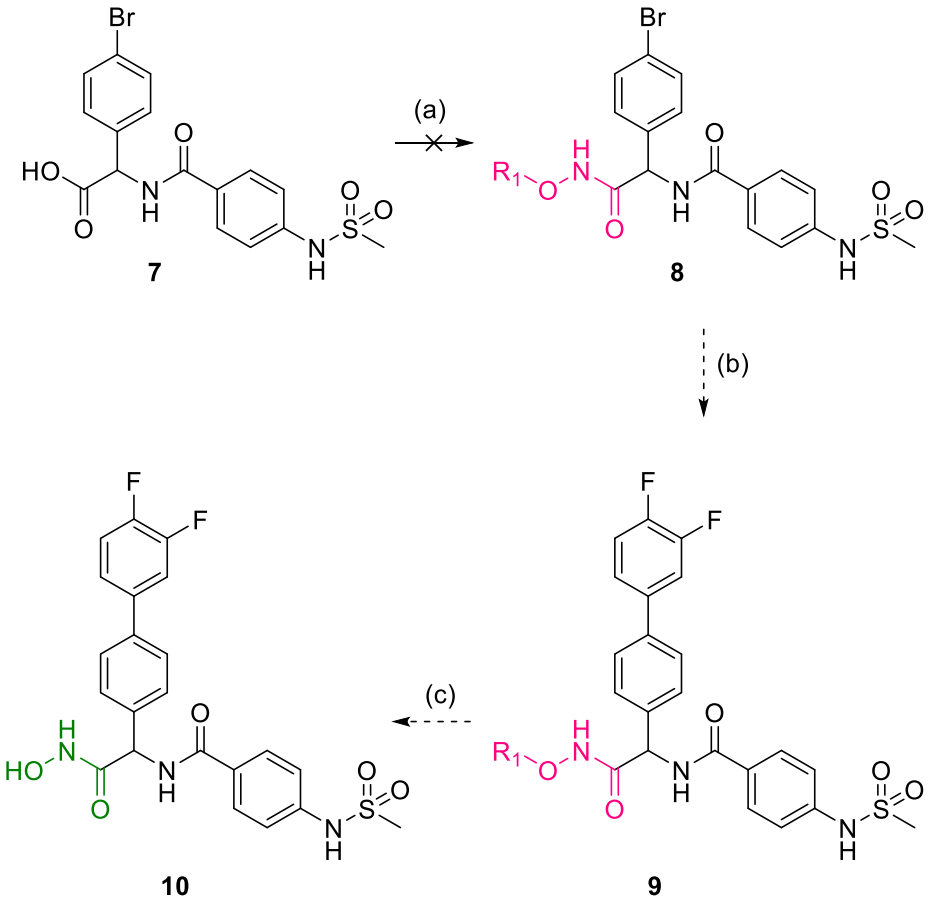

Reagents and conditions: (a) **7**, *O*-protected hydroxylamine, EDCI, bases, HOBt, anhydrous DMF, rt, overnight; (b) 3,4-difluorophenylboronic acids, $Pd(PPh_3)_2Cl_2$, K_3PO_4, anhydrous DMF, 100 °C, 15 min, microwave reactor; (c) silyl deprotection.

Protecting groups that were attempted to install included *tert*-butyldimethylsilyl (TBS), benzyl (Bn), and *tri*-isopropyldimethylsilyl (TIPS). Amide coupling reactions between the carboxylic acid **7** and commercially available *O*-TBS hydroxylamine and *O*-Bn hydroxylamine hydrochloride were conducted in the presence of EDCI as an activator, different bases (Et_3N, DMAP, and DIPEA), and additive (HOBt). However, there was no conversion to the desired

product observed. ^{1}H NMR and LC-MS of crude indicated the presence of multiple compounds, including the starting material **7**. Isolation of each compound through column chromatography was not successful because of the poor separation on silica gel.

Since the synthesis of intermediate **8** from carboxylic acid **7** was disappointing, several reactions were attempted to introduce protecting groups from hydroxamic acid **6d** to investigate how stable the protected hydroxamic acid would be in coupling reaction conditions (Scheme 3.4). A classical TBS protection with free hydroxamic acid **6d** was carried out in the presence of imidazole under anhydrous conditions. Despite increasing the amount of the reagents and the reaction temperature, the hydroxamic acid **6d** was not converted to the TBS-protected intermediate **8a**. This could be explained by the steric hindrance of the bulky *tert*-butyl groups that potentially limited the access to hydroxamic acid, which adversely affected forming the desired product. When the silylating agent changed to less bulky TIPS chloride, the reaction was able to reach a moderate conversion. Complete conversion was achieved by adding 10% mol loading of DMAP as a catalyst to obtain the TIPS-protected hydroxamic acid intermediate **8b** in 50% of yield. Unfortunately, subsequent Suzuki-Miyaura coupling reaction resulted in the removal of TIPS group from compound **9**.

Scheme 3.4. Synthesis of TBS/TIPS protected hydroxamic acid from compound 6d.

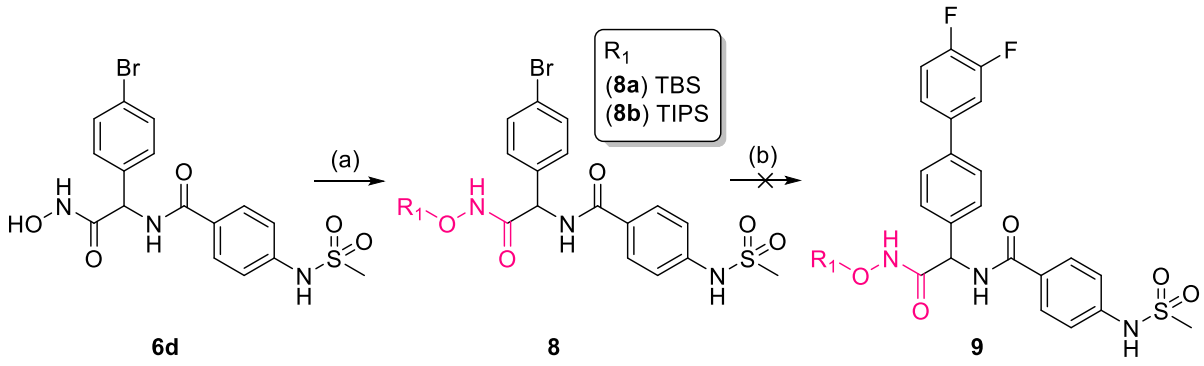

Reagents and conditions: (a) **6d**, imidazole, anhydrous DMF, TIPSCl, rt, overnight, 0–50%; (b) 3,4-difluorophenylboronic acid, $Pd(PPh_3)_2Cl_2$, K_3PO_4, anhydrous DMF, 100 °C, 15 min, microwave reactor.

3.2.2.2 Synthetic approaches attempted to form an alkyl-aryl C-C bond

The optimised synthetic pathway developed for compounds biphenyl scaffold was applied to generate compounds containing an alky-aryl core, except that the Suzuki-Miyaura coupling reaction involved the use of alkylboronic acids instead of arylboronic acids. Innumerable Suzuki-Miyaura couplings have been established to form C-C bonds between aryl halides and arylboronic acids through extensive research in the past.[243] In contrast, cross-coupling reactions of alkylboronic acids still remain challenging because of a number of serious issues such as decomposition of palladium-alkyl intermediate via β-elimination, slow transmetallation, and generation of unwanted side products.[244] Doucet *et al*. reviewed a wide range of Suzuki-Miyaura reactions focussed on alkylboronates.[243]. Selected reactions from previously reported procedures were applied to synthesise cyclopropyl analogue **5k** from aryl bromide **4d** (Table 3.3). It was surprising that the complete hydrolysis of methyl ester occurred when the optimised reaction conditions for arylboronic acids was performed (Table 3.3, Entry 1), which could arise from using a solvent that was potentially contaminated by water

Table 3.3. Reactions attempted to synthesise cyclopropyl analogue 5k from aryl bromide 4d.

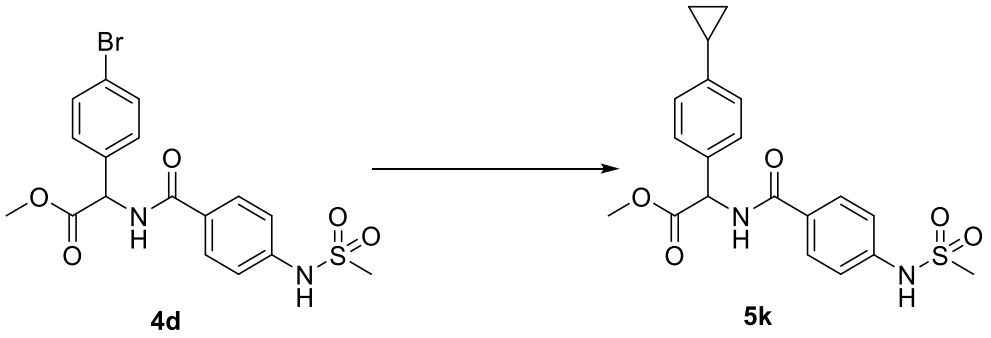

Entry	Catalyst/ligand	Base	Solvent	Conditions	Results
1	$Pd(PPh_3)_2Cl_2$	K_3PO_4	DMF	Microwave 1 h, 100 °C	Complete hydrolysis
2	$Pd(dppf)Cl_2$	K_2CO_3	THF	80 °C, O/N	94% yield

The reaction outcome was significantly improved when ferrocene-containing palladium catalyst $Pd(dppf)Cl_2$ was used. Molander *et al*. reported successful coupling reactions between alkylboronic acids and either electron-deficient or electron-excessive aryl bromides in the presence of $Pd(dppf)Cl_2$, potassium carbonate, and biphasic solvent THF/water.[245] It was also noted that $Pd(dppf)Cl_2$ was commonly used catalyst for coupling reactions with alkylboronic acids which usually required forcing conditions.[243] Therefore, using the reaction conditions

reported by Molander *et al*. but in an anhydrous environment to avoid hydrolysis of the methyl ester group, the product **5k** was obtained in an excellent yield of 94% (Table 3.3, Entry 2). Unfortunately, the reaction conditions described in Entry 2 of Table 3.3 were not able to couple the cyclobutyl and cyclopentylboronic acids to compound **4d**. There was no conversion to the desired product, and the starting material **4d** was completely recovered. Several literatures reported that cyclopropylboronic acid derivatives are widely explored as a competent nucleophile in Suzuki-Miyaura coupling reactions due to its unique hybridisation and aromaticity characteristics.[243, 245] In contrast, there is extremely limited evidence for coupling reactions of other secondary alkylboronic acids because of steric hindrance, which leads to slow transmetallation rates with palladium.[243, 246] A strategy applied to accelerate the transmetallation step involves the use of silver(II) oxide (Ag_2O) as an additive.[243, 247, 248] However, when this approach was applied to couple aryl bromide **4d** with cyclopentylboronic acid, only resulted in a complete debromination of **4d**. Therefore, an alternative method was used; cyclopentenyl and cyclohexenyl boronic acids that have more planarity were coupled to **4d**. The C=C bond was reduced in the subsequent transfer catalytic reduction reaction (Scheme 3.5).

Scheme 3.5. Synthesis of cyclopentyl and cyclohexyl analogues.

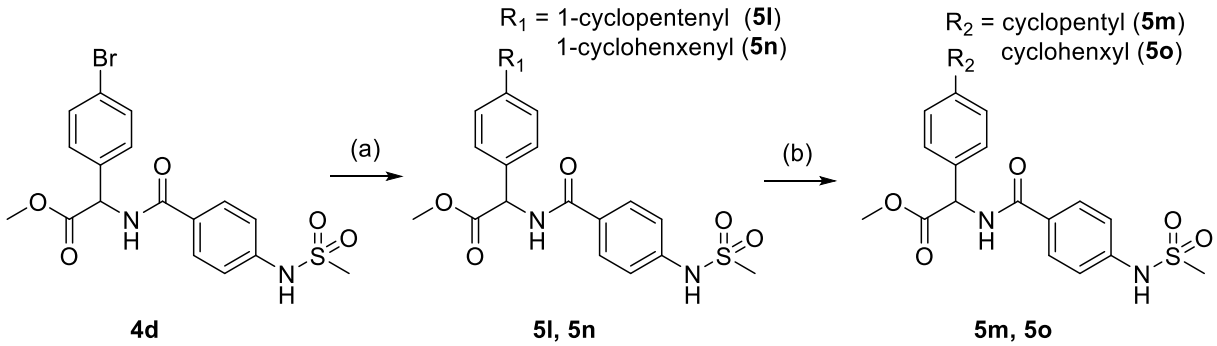

Reagents and conditions: (a) boronic acid, K_2CO_3, $Pd(dppf)Cl_2$, THF, 80 °C, overnight, 78-87%; (b) ammonium formate, 10% Pd/C EtOH or MeOH, reflux, 2 h, 80–83 %.

With the introduction of additional C=C bond, the cycloalkenyl substrates gained sp^2 characteristics which were favoured in Suzuki-Miyaura coupling reactions. Indeed, the reaction outcome was significantly improved when the reaction conditions described in Table 3.3, Entry 2 were applied. Cyclopentenyl and cyclohexenyl analogues **5l** and **5n** were synthesised

smoothly with 87% and 78% of yield, respectively. The C=C bond present in the molecules were reduced effortlessly via transfer catalytic hydrogenation and generated fully saturated cyclopentyl and cyclohexyl analogues **5m** and **5o** in good yields of 80% and 83%, respectively.

3.2.3 Synthesis of amine-containing analogues through metal catalysed reactions: chemistry optimisation to form C-N bonds

In order to synthesise analogues containing piperidine and piperazine derivatives, various metal-catalysed reactions were attempted. Such reactions included palladium catalysed Buchwald-Hartwig amination and copper catalysed Chan-Evans-Lam (CEL) coupling reactions which are widely used to form C-N bonds.

Firstly, series of studies was conducted to optimise Buchwald-Hartwig amination reaction of **4d** with 1-methylpiperazine and 4-methylpiperidine with different combinations of commonly used catalyst $Pd_2(dba)_3$, ligands (XPhos and BINAP), and bases (NaO*t*Bu, K_3PO_4, and Cs_2CO_3) (Table 3.4). Unfortunately, the outcomes were discouraging. Debromination of the aryl bromide **4d** was observed when the reaction was carried out under conditions described in Table 3.4, Entry 1. The reaction was attempted again in a microwave reactor with reduced reaction time to achieve a conversion to the desired product and to prevent debromination that could potentially occur from prolonged reaction time, simultaneously (Table 3.4, Entry 2). When the catalyst and base were changed to BINAP and K_3PO_4 there was no conversion of compound **4d**, but this could be because the reactant was completely insoluble in toluene (Table 3.4, Entry 3). To solve this problem, the solvent was replaced with DMF for improved solubilisation of compound **4d**. However, the result was not promising as a mixture of unidentifiable compounds was obtained, and a similar effect was observed when the base was changed to NaO*t*Bu (Table 3.4, Entry 4 and 5).

Table 3.4. Summary of Buchwald-Hartwig Reactions attempted between aryl bromide 4d and 1-methylpiperazine (Entry 1-2) or 4-methylpiperidine (Entry 3-7).

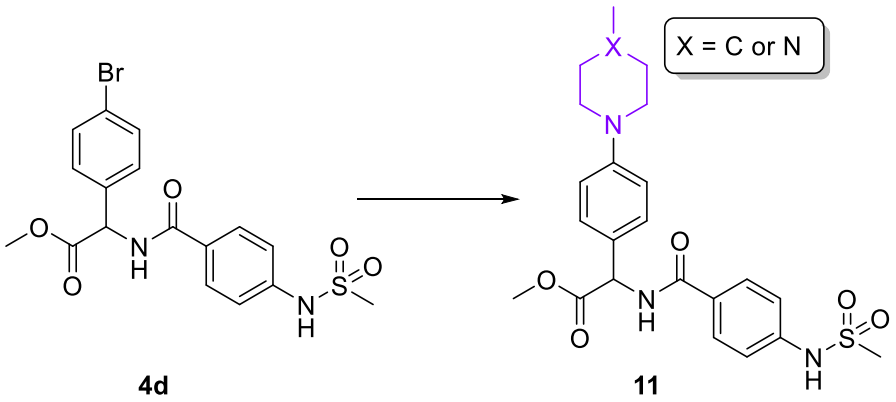

Entry	Catalyst/Ligand	Base	Solvent	Condition	Results
1	$Pd_2(dba)_3$/Xphos	NaO*t*Bu	Dioxane	reflux, O/N	Debromination, hydrolysis
2	$Pd_2(dba)_3$/Xphos	NaO*t*Bu	Dioxane	microwave reflux, 4 h	No conversion
3	$Pd_2(dba)_3$/BINAP	K_3PO_4	Toluene	reflux, O/N	No conversion due to poor solubility
4	$Pd_2(dba)_3$/BINAP	K_3PO_4	DMF	100 °C, O/N	Mixture of unidentifiable products
5	$Pd_2(dba)_3$/BINAP	NaO*t*Bu	DMF	100 °C, O/N	Mixture of unidentifiable products
6	$Pd_2(dba)_3$/Xphos	Cs_2CO_3	Toluene	reflux, O/N	No conversion
7	$Pd_2(dba)_3$/Xphos	Cs_2CO_3	DMF	100 °C, O/N	Mixture of unidentifiable products

It was hypothesised that the sulfonamide group of **4d** might be interfering the reaction progression by interacting with the palladium catalyst or being deprotonated in a basic reaction condition. Therefore, a model study was performed to investigate if the sulfonamide substituent was the main cause of the failure of amination reactions. Methyl 2-benzamido-2-(4-(4-methylpiperidin-1-yl)phenyl)acetate (**12**) was selected as the model system to attempt Buchwald-Hartwig aminations under the conditions adapted from *Piscitelli et al*. (Scheme 3.6).[249] A mixture of compound **12**, 4-methylpiperidine or 4,4-difluoropiperidine, $Pd_2(dba)_3$,

XPhos, and cesium carbonate in anhydrous toluene was heated at reflux to successfully generate 4-methylpiperidyl analogue **13a** and 4,4-difluoropiperidyl analogue **13b** in 41% and 72% of yield, respectively.

Scheme 3.6. Buchwald-Hartwig amination of 2-benzamido-2-(4-(4-methylpiperidin-1-yl)phenyl)acetate (12) with piperidine derivatives.

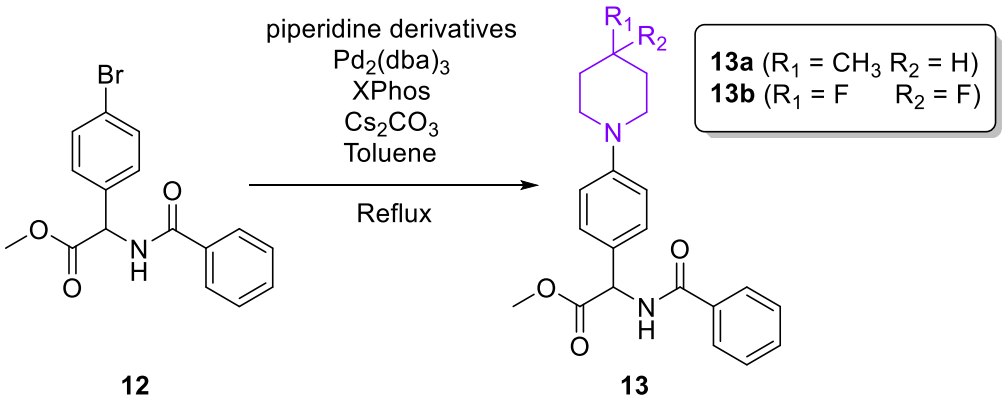

However, the result was disappointing when the identical reaction conditions were employed to couple 4-methylpiperidine to aryl bromide **4d**, suggesting that unsuccessful Buchwald-Hartwig amination was originated from the sulfonamide substituent of compound **4d**. Not surprisingly, there was no conversion of compound **4d** due to its poor solubility in toluene (Table 3.4, Entry 6). Changing of the solvent to DMF was not able to improve the outcome, and a mixture of unidentifiable compounds was produced (Table 3.4, Entry 7).

Since the results acquired from the model study indicated that the sulfonamide group of compound **4d** was detrimental for successful Buchwald-Hartwig amination, an alternative synthetic approach was proposed as illustrated in Scheme 3.7. As a replacement of sulfonamide, nitro-containing intermediate **14** was synthesised, hoping that the alternative substituent is more favoured in the following Buchwald-Hartwig amination reaction. The nitro group could be easily reduced to the aniline intermediate **15** by hydrogenation, and methansulfonyl chloride could react with the aniline to successfully incorporate sulfonamide group. The reaction conditions discussed in Scheme 3.6 were applied to install 4-methylpiperidine into compound **14**. However, the reaction struggled to achieve a complete conversion even with an excess amount of reagents and longer reaction time. Most of the aryl bromide **14** were recovered, therefore, the desired product was obtained in an extremely low yield.

Scheme 3.7. Proposed synthetic scheme to generate sulfonamide analogue 5s from nitro intermediate 14.

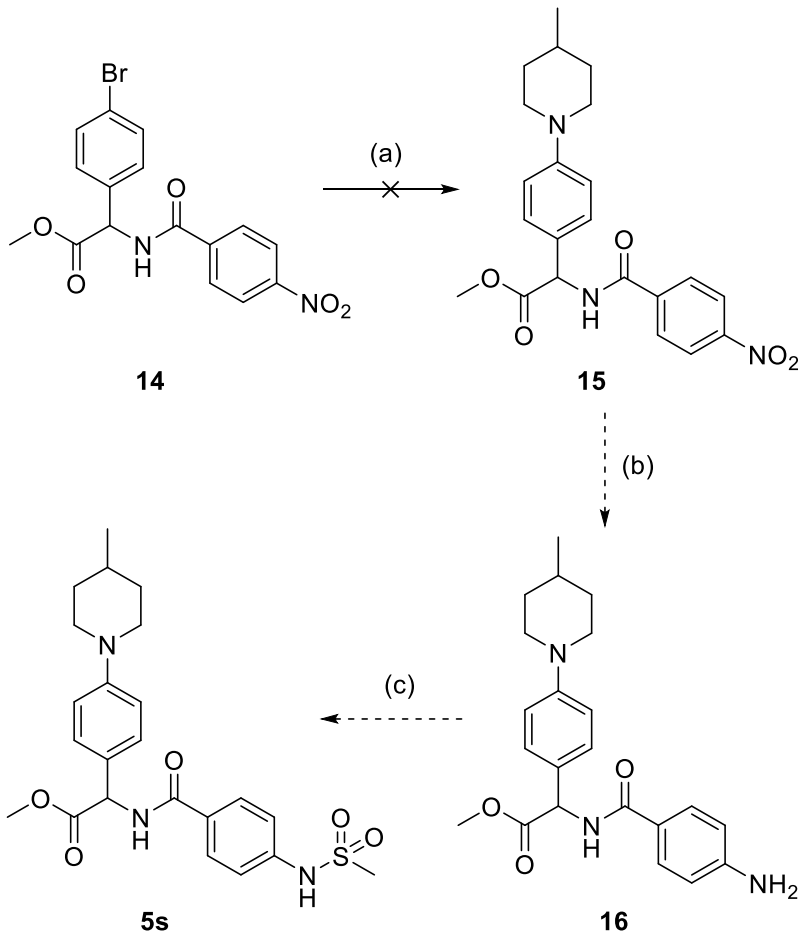

Reagents and conditions: (a) **14**, 4-methylpiperidine, $Pd_2(dba)_3$, XPhos, Cs_2CO_3, anhydrous toluene, reflux, overnight; (b) 10% Pd/C, MeOH, H_2, rt, overnight; (c) DIPEA, anhydrous DCM, 0 °C, MsCl, rt, overnight.

Despite substantial efforts to optimise the synthesis of piperidyl and piperazinyl analogues through Buchwald-Hartwig amination with different aryl bromides, we were not able to generate the desired compounds successfully. As such, an alternative synthetic pathway was established, which involved the use of relatively simple molecule methyl 2-(4-bromophenyl)-2-((*tert*-butoxycarbonyl)amino)acetate (**17**) as the key aryl bromide intermediate (Scheme 3.8).

Scheme 3.8. Optimised synthetic pathway of amino-containing hydroxamic acid analogues through Buchwald-Hartwig amination

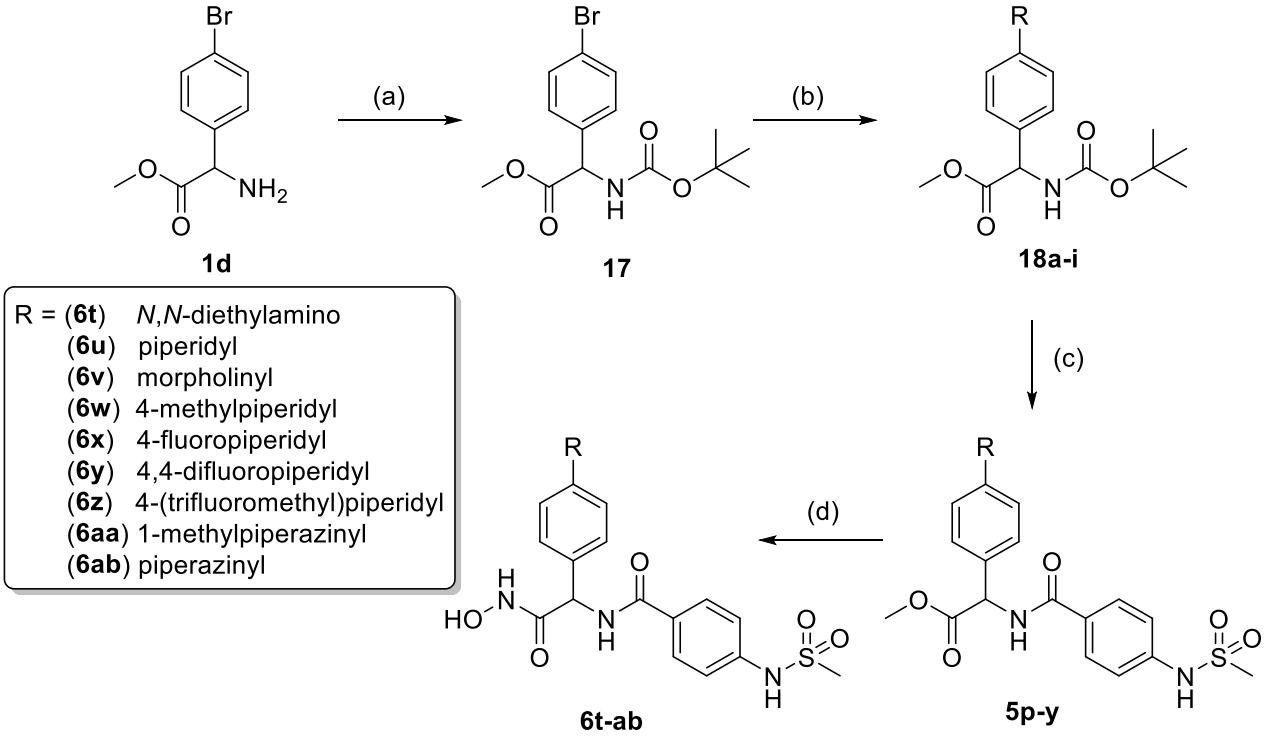

Reagents and conditions: (a) **1d**, Boc_2O, sat. $NaHCO_3$, water, THF, rt, overnight; 75%; (b) amines, Cs_2CO_3, $Pd_2(dba)_3$, XPhos, anhydrous toluene, reflux, overnight, 50–99%; (c) (i) 20% TFA/DCM, rt, 3 h, quantitative; (ii) HCTU, DIPEA, 4-(methylsulfonamido)benzoic acid, rt, overnight, 41–70%; (d) $NH_2OH{\cdot}HCl$, 5 M KOH/MeOH, rt, overnight, 35–73%.

The intermediate **17** was synthesised by Boc protection of the amino acid derivative **1d**. A total of 10 alkyl amines were coupled with **17** smoothly using the identical reaction conditions described in Scheme 3.6. Unlike other cyclic amino analogues, the installation of *N*,*N*-diethyl moiety resulted in a low yield of 42%, because *N*,*N*-diethylamine is volatile (b.p. = 56 °C) and it can be quickly evaporated at high reaction temperature of 120 °C, particularly when such a small volume of amine (350 µL) was used for reaction. This problem was easily rectified by increasing the amount of *N*,*N*-diethylamine added and by heating the reaction mixture in a closed microwave vessel, which significantly improved the yield to 84%. Synthesis of free piperazinyl analogue **5y** required additional steps because the piperazine contained two unprotected nitrogen atoms that had equal capacity to participate in the coupling reaction. In order to avoid potential complications, mono-benzyl carbamate (Cbz) protected piperazine was

used as the source of amine. The Cbz group was removed effortlessly by a transfer catalytic hydrogenation with ammonium formate and 10% Pd/C. The Boc group of intermediates **18a-i** was removed by acid hydrolysis with 20% TFA in DCM to give the corresponding free amines as TFA salts. The following amide coupling reaction was performed in the presence of excess DIPEA, HCTU, and 4-(methylsulfonamido)benzoic acid to produce methyl ester intermediates **5p-y**. Finally, the methyl ester group of **5p-y** underwent aminolysis to generate hydroxamic acid analogues **6t-ab**.

Alongside the synthesis optimisation through Buchwald-Hartwig amination, copper-catalysed coupling reaction was investigated as an alternative pathway. The new synthetic approach involved Chan-Evans-Lam (CEL) reaction, which is a coupling reaction between boronic acid derivatives and amines to form C-N bonds.

Scheme 3.9. Proposed synthetic pathway of 4-methylpiperidyl analogue 5s using CEL coupling reaction.

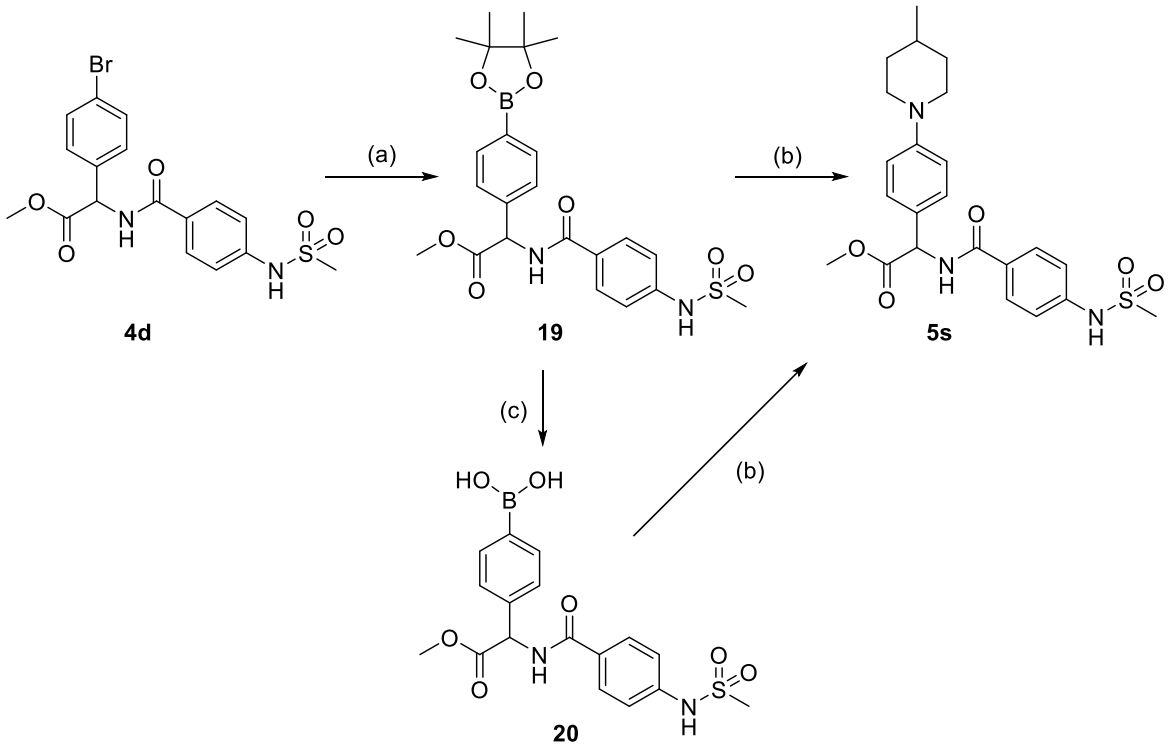

Reactions and conditions: (a) Bis_2pin_2, AcOK, $Pd(dppf)Cl_2$.DCM, DPPF, dioxane, reflux, 2 d, 86%; (b) 4-methylpiperidine, $Cu(OAc)_2$, $B(OH)_3$ or Et_3N, powdered MS 3 Å, anhydrous DCM or MeCN, rt or reflux, overnight; (c) ammonium acetate, sodium periodate, acetone/water (1:1), rt, overnight, 49 %.

The proposed synthetic route to 4-methylpiperidyl analogue **5s** is shown in Scheme 3.9. The first step involved the synthesis of pinacol ester **19** from aryl bromide **4d** by heating a mixture of Bis_2pin_2, AcOK, $Pd(dppf)Cl_2$.DCM and DPPF at reflux for 2 days. The corresponding pinacol ester was produced with an excellent yield of 86%. Intermediate **19** was as the essential precursor of the subsequent CEL coupling reactions, or it underwent an additional step of deprotection to generate free boronic acid **20**. Various conditions were applied to achieve a successful CEL coupling reaction from pinacol ester **19** or boronic acid **20** in the presence of copper acetate, boric acid, and molecular sieves using previously reported procedures (Table 3.6).[250, 251]

Table 3.6. Reaction conditions applied of CEL couplings between pinacol ester 18 or boronic acid 19 with 4-methylpiperidine.

Entry	Starting material	Catalyst	Additive	Solvent	Conditions	Results
1	19	$Cu(OAc)_2$	$B(OH)_3$	MeCN (0.03 M)	80 °C, O/N	oxidation and photodeboronation
2	19	$Cu(OAc)_2$	Et_3N	MeCN (0.03 M)	80 °C, O/N	complete conversion, inseparable by-products
3	20	$Cu(OAc)_2$	$B(OH)_3$	DCM or MeCN (0.03 M)	rt, O/N	starting material not soluble.
4	20	$Cu(OAc)_2$	$B(OH)_3$	MeCN (0.03 M)	80 °C, O/N	product + oxidation + photodeboronation
5	20	$Cu(OAc)_2$	$B(OH)_3$	MeCN (0.5 M)	80 °C, O/N	product + oxidation + photodeboronation

Under the reaction conditions described in Table 3.6, Entry 1, oxidation and photodeboronation, which are the commonly observed side reactions in CEL couplings occurred. The pinacol ester group of compound **19** was oxidised to hydroxyl or completely cleaved (Figure 3.2). Change

of the additive from boric acid to triethylamine resulted in the complete consumption of the starting material **19**. However, four other unknown compounds were also produced, which made isolation of **5s** from other impurities extremely challenging (Table 3.6, Entry 2).

Coupling reactions with free boronic acid **20** were also attempted. The reaction temperature was decreased to room temperature initially to prevent unwanted side reactions from oxidation and photodeboronation. However, compound **20** was utterly insoluble in both DCM and MeCN at room temperature, which consequently led to no consumption of compound **20** (Table 3.6, Entry 3). Increasing the reaction temperature indeed improved the conversion rate, however, oxidation and photodeboronation could not be avoided (Table 3.6, Entry 4). Vantourout *et al*. reported that the reaction concentration affects the rate of side-product formations from oxidation and photodeboronation.[250] However, the occurrence of two side-reactions was still detected, although there was an increase in the reaction concentration from 0.03 M to 0.5 M (Table 3.6, Entry 4 and 5).

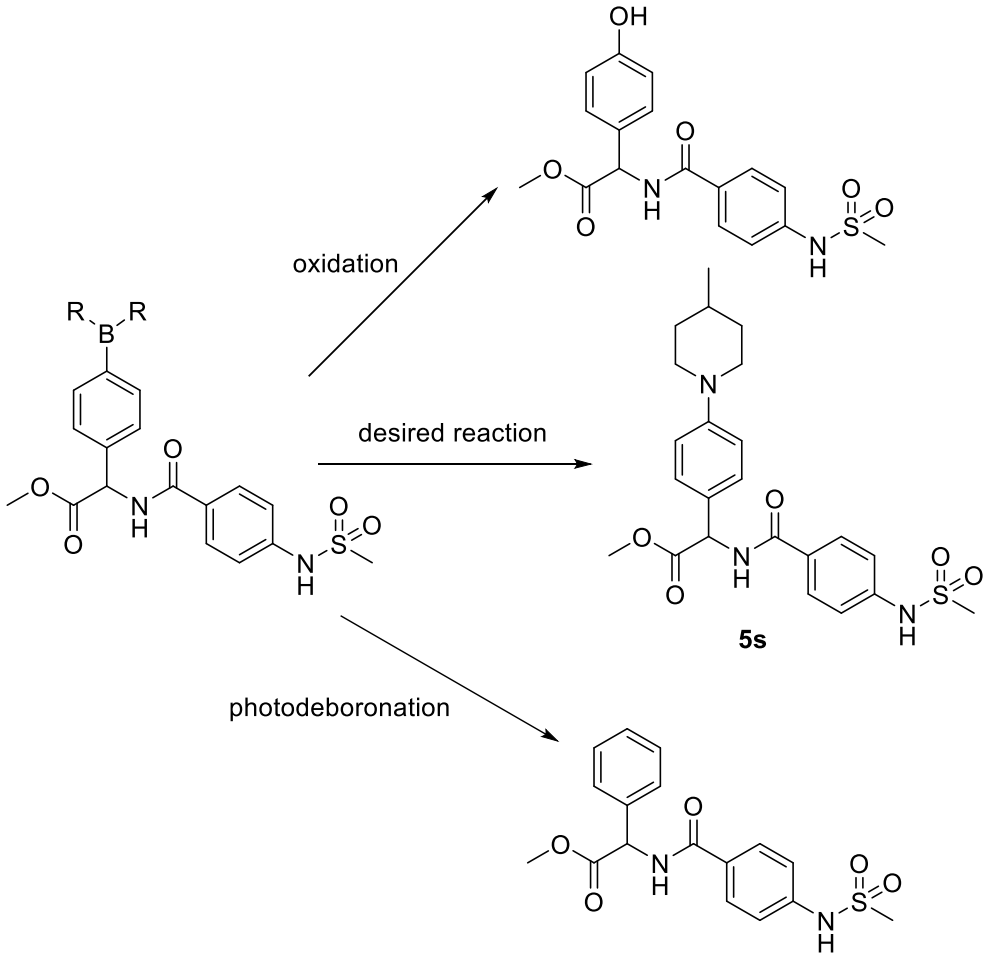

Figure 3.2. Products formed from a CEL coupling reaction.

3.3 Relationships between the structure and inhibitory activity, and the comparisons of solubility of novel hydroxamic acids

A total of 28 novel hydroxamic acid analogues were successfully synthesised (**6a**–**ab**) to probe the interactions occurring at the S1 pocket of APN as well as to improve aqueous solubility by replacing the hydrophobic 3,4,5-trifluorophenyl ring of our best APN inhibitor **6ad** (from *Chapter 2*). The inhibitory activities of these compounds were evaluated by a fluorescence-based assay using recombinant human APN in the presence of Leu-Mec as a competitive substrate (Table 3.7), as described in *Chapter 2* (pg. 51). The measured inhibition constants ($K_i^{(app)}$) were compared between different analogues comprehensively based on their structural variations to determine which group successfully replaced the 3,4,5-trifluorophenyl group without sacrificing the activity.

Considering phenylglycine analogues **6a**-**d**, it was noted that a complete removal of the 3,4,5-trifluorophenyl group resulted in a significant loss in the activity from $K_i^{(app)}$ = 4.90 nM (**6ad**) to $K_i^{(app)}$ = 116 nM (**6a**). However, activity was regained once halogen groups introduced in the descending order of Cl > Br > F, indicating dipole-induced interactions play a role in improving potency. It was also interesting to observe that phenyl analogue **6e** ($K_i^{(app)}$ = 4.1 nM) was comparable to that of the lead compound **6ad** but more potent than the bromophenylglycine analogue **6d** ($K_i^{(app)}$ = 9.47 nM) which contained bromo group as a bioisostere of phenyl. The result suggested that biphenyl is the preferred scaffold over phenylglycines.

The fluorine substituted phenyl compounds **6f-i** were well tolerated. For example, 3-fluorophenyl analogue **6f** was determined to be the most potent inhibitor of this project with a $K_i^{(app)}$ value of 0.660 nM. There was a decrease in potency when fluorine was substituted at the 4-position. For instance, 4-fluorophenyl analogue **6g** showed a reduced inhibitory activity of $K_i^{(app)}$ = 9.54 nM compared to 3-fluorophenyl **6f**. Similarly, 3,4-difluorophenyl analogue **6h** possessed potency of $K_i^{(app)}$ = 6.15 nM, which was approximately 6-fold less potent than 3,5-difluorophenyl analogue **6i** ($K_i^{(app)}$ = 1.1.9 nM). Based on these results, it was proposed that substituent at 3-position is preferred to 4-position and trifluoro group is not required for achieving the potent activity.

Table 3.7. Inhibition activities ($K_i^{(app)}$) of synthesised compounds against APN.

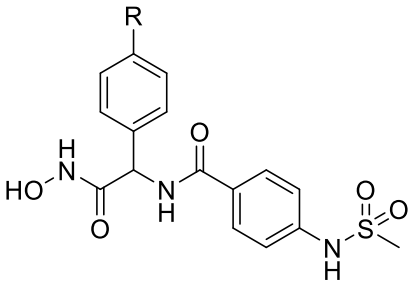

Compound	R	$K_i^{(app)}$ ± SEM / nM	cLogP
6ad	3,4,5-Trifluorophenyl	4.90 ± 0.80	2.10
6a	H	166 ± 15	0.0200
6b	F	48.6 ± 1.3	0.170
6c	Cl	7.38 ± 0.17	0.630
6d	Br	9.47 ± 0.17	0.790
6e	Phenyl	4.15 ± 0.24	1.67
6f	3-Fluorophenyl	0.660 ± 0.060	1.81
6g	4-Fluorophenyl	9.54 ± 0.97	1.81
6h	3,4-Difluorophenyl	6.15 ± 0.29	1.96
6i	3,5-Difluorophenyl	1.19 ± 0.13	1.96
6j	3-Furan	34.6 ± 1.2	0.810
6k	3-Thiophene	10.2 ± 1.0	1.45
6l	3-Pyridyl	9.77 ± 0.19	0.450
6m	4-Pyridyl	2.41 ± 0.30	0.450
6n	Pyrimidyl	49.0 ± 4.4	-0.250
6o	Cyclopropyl	9.74 ± 0.62	0.810
6p	1-Cyclopentenyl	90.6 ± 4.1	1.43
6q	Cyclopentyl	11.4 ± 1.2	1.70
6r	1-Cyclohexenyl	343 ± 5	1.87
6s	Cyclohexyl	4.87 ± 0.34	2.14
6t	*N*,*N*-Diethylamino	54.8 ± 4.1	0.850
6u	Piperidyl	151 ± 13	0.980
6v	Morpholine	224 ± 6	-0.0900
6w	4-Methylpiperidyl	212 ± 9	1.27
6x	4-Fluoropiperidyl	54.8 ± 4.6	0.340

6y	4,4-Difluoropiperidyl	63.5 ± 6.2	1.20
6z	4-(Trifluoromethyl)piperidyl	158 ± 10	1.55
6aa	1-Methylpiperazinyl	42.4 ± 1.8	-0.0200
6ab	Piperazinyl	27.0 ± 1.9	-0.400

Most heteroaromatic analogues **6j**-**n** displayed decreased level of activity against APN, except 4-pyridyl analogue **6m** which showed enhanced inhibitory activity of $K_i^{(app)}$ = 2.41 nM. The potent activity of compound **6m** compared to phenyl analogue **6e** could be possibly due to the pyridine moiety that is capable of participating in hydrogen bonding interaction as a hydrogen bond donor. Five-membered heteroaromatic furan analogue **6j** and thiophene analogue **6k** displayed potency of $K_i^{(app)}$ = 34.6 nM and 10.2 nM, respectively. In addition, pyrimidyl analogue **6n** exhibited a reduced inhibition activity ($K_i^{(app)}$ = 49.0 nM) compared to 3-pyridyl analogue **6l** and 4-pyridyl analogue **6m** by 5- and 10-fold. The preference towards pyrimidyl compound over pyridyl compounds could be explained by the differences in electronic characteristics and basicity. The basicity of pyridine is triggered by the sp^2 hybridised nitrogen atom which possesses one pair of electrons available outside the π system for protonation. On the other hand, pyrimidine bears two sp^2 hybridised nitrogen atoms with one pair of electrons outside the aromatic ring individually. Due to the electron-withdrawing and inductive effect, protonation at the second nitrogen atom is unlikely, making pyrimidine less basic than pyridine. Therefore, it can be suggested that less basic group is favoured at the S1 subsite of APN.

According to the molecular modelling studies discussed in *Chapter 2*, the biphenyl scaffold engaged in multiple hydrophobic interactions with a flexible loop located in domain IV, and it was proposed that these interactions may play an imperative role in locking inhibitors within the active site of APN effectively. Therefore, it was hypothesised that analogues containing alkyl groups as replacement of 3,4,5-trifluorophenyl (i.e. compounds **6o**-**ab**) would display significantly reduced potency. Indeed, a decreased level of potency was observed from the majority of alkyl analogues, and cyclopropyl analogue **6o** and cyclohexyl analogue **6s** displayed tight-bindings to APN. Despite the small size and less degree of planarity, the cyclopropyl analogue **6o** retained good activity ($K_i^{(app)}$ = 9.74 nM). Interestingly, a trend of decreasing activities was observed from cycloalkenyl analogues compared to its saturated cycloalkyl pairs. Cyclopentyl **6q** showed a $K_i^{(app)}$ value of 11.4 nM but its unsaturated pair cyclopentenyl **6p** showed a decreased potency ($K_i^{(app)}$ of 90.6 nM). Similarly, cyclohexyl **6s**

($K_i^{(app)}$ = 4.87 nM) which was equipotent to **6ad**, was nearly 70-fold more active than cyclohexenyl **6r** ($K_i^{(app)}$ = 343 nM). However, there was an exceptional case as well, where the phenyl analogue **6e** was equally potent to cyclohexyl **6s**.

Unfortunately, amine analogues **6t**-**ab** were not well tolerated and showed significantly diminished inhibitory activities. *N*,*N*-Diethyl analogue **6t** showed a potency of $K_i^{(app)}$ = 54.8 nM and the activity even more deteriorated when cyclised amino groups were incorporated (**6u**-**6w**). Additional fluorine(s) of 4-fluoropiperidyl **6x** and 4,4-difluoropiperidyl **6y** were able to enhance the potency ($K_i^{(app)}$ = 63.5 nM) compared to the unsubstituted piperidyl analogue **6u** ($K_i^{(app)}$ = 151 nM) or the 4-methylpiperidyl analogue **6w** ($K_i^{(app)}$ = 212 nM). Piperazinyl analogues were determined to be more potent than its corresponding piperidyl compounds. For example, piperazinyl analogue **6ab** ($K_i^{(app)}$ = 27.0 nM) was nearly 6-fold more active than piperidyl analogue **6u** ($K_i^{(app)}$ = 212 nM). A similar relationship was observed between 4-methylpiperidyl analogue **6w** and 1-methylpiperazinyl **6aa** ($K_i^{(app)}$ = 27.0 nM). There are two aspects that potentially contributed to the enhanced potency of piperazinyl compounds compared to piperidyl compounds. Firstly, piperazine derivatives possess an additional basic aliphatic nitrogen atom that can be readily ionised in physiological pH condition. However, the nitrogen atom present in piperidine derivatives would have similar properties as arylamines, which are significantly less basic than aliphatic amines. With the greater capacity of ionisation, piperazinyl analogues may form strong ionic interactions with nearby basic residues. Secondly, the aliphatic amine of piperazinyl is also able to engage in hydrogen bonding interactions acting as a hydrogen bond donor.

Alongside optimisation of inhibition activity at the S1 subsite of APN, improving the solubility of novel hydroxamic acid compounds by replacing hydrophobic 3,4,5-trifluorophenyl ring was another goal to achieve in this chapter. Therefore, hydrophobicity of compounds was compared to the lead compound **6ad**, and investigation of the relationships between potency and solubility of analogues was also attempted. As a measure of solubility, partition coefficient cLogP, which reflects the partitioning of a molecule between lipophilic and aqueous layers was used. High cLogP of a molecule indicates high lipophilicity, suggesting the molecule is likely to have low aqueous solubility whereas a low cLogP implies low hydrophobicity. Negative cLogP value of a molecule demonstrates that the molecule is more likely to partition into the aqueous layer, hence more aqueous soluble. The cLogP values of synthesised compounds were calculated *in silico* by ChemAxon Instant JChem software 16.9.12.0. The analogues

synthesised displayed smaller cLogP values than the lead compound **6ad** (cLogP = 2.10), suggesting that this series of analogues could potentially have improved solubility than **6ad**. We attempted to establish relationships between the potency and cLogP of this series of compounds, however, there was no striking trend observed. Morpholine analogue **6v** showed the second weakest potency among the series of analogues ($K_i^{(app)}$ = 224 nM) although the analogue was hydrophilic with a cLogP value of -0.09. On the other hand, the best inhibitor of this series, 3-fluorophenyl **6f**, displayed a relatively high cLogP compared to other analogues.

3.4 Predicted binding poses of selected APN inhibitors and their interactions within the S1 pocket of APN

According to the inhibitory activities of APN inhibitors synthesised, the S1 subsite of APN turned out to be capable of tolerating various chemical moieties. A number of substituted aromatic and heteroaromatic analogues were extremely potent. In addition, some cycloalkyl and amine-containing analogues also displayed good inhibition activity against APN in nanomolar rage, although most of them were not as potent as the parent compound **6ad**. In order to investigate how different chemical moieties may interact within the S1 pocket of APN APN and how the differences in these interactions affected the potency of each compound, a series of molecular modelling studies were performed.

Among the series of hydroxamic acids, seven analogues were selected based on their activities for molecular docking studies. Compounds with diverse chemical structures were chosen so that binding interactions across different structures from aromatics, alkyls, and amines could be explored. Docking studies of phenylglycine analogue **6a** would allow us to understand how the complete removal of the top aromatic ring affected the potency adversely. The two best inhibitors of this series, 3-fluorophenyl analogue **6f** and 4-pyridyl analogue **6m** were also selected. In addition, cyclopropyl analogue **6o** and cyclohexyl analogue **6s** were included to assess how these inhibitors were able to maintain potent activity despite drastic structural changes compared to **6ad**. Lastly, the binding interactions of piperazinyl analogue **6ab**, which was the most potent inhibitor among the amine analogues, were also studied.

Molecular docking was carried out using Surflex docking available in Sybyl 2.1.1, as described in *Chapter 2*.[241] The final APN-**6ad** bound structure obtained at the end of MD simulations in previous studies was used as the template structure for ligand docking. The structures of ligand **6a**, **6e**, **6f**, **6m**, **6o**, **6s**, and **6ab** were prepared with the default settings from Sybyl 2.1.1, and the hydroxamic acid group was set as fragment constraint to ensure that the crucial coordination to catalytic zinc is not lost during the modelling process. A maximum of 20 different poses were obtained for each ligand, and they were superimposed in order to visualise the differences between each pose (Figure 3.3).

Compound **6a** showed the most dynamic changes in the hydroxamic acid position (Figure 3.3A). Among 20 poses obtained, six poses had the hydroxamic acid positioned relatively far from the catalytic zinc to form a metal complex. The coordination between hydroxamic acid and zinc became more stable when ligands possessed biaryl or alkyl-aryl scaffolds (Figure 3.3B-G). Significant changes in the aryl sulfonamide position between different poses were commonly observed from all the ligands, where the most notable conformational changes were detected from cyclohexyl analogue **6s** (Figure 3.3F). The biaryl analogues **6e**, **6f**, and **6m** showed negligible changes in the conformations of the top aryl group, whereas alkyl-aryl analogues **6o**, **6s**, and **6ab** had considerable movements in the cyclic alkyl groups.

The binding energy scores of each predicted binding pose were tabulated (Appendix A) and used as a guide to determine the most plausible pose of each ligand. The binding pose that showed the highest total score was considered to possess a more favoured conformation. Moreover, the conformation of the hydroxamic acid and the core scaffolds were manually interrogated to exclude any poses that were distant from catalytic zinc ion (six poses from compound **6a** and one pose from **6o**), or the position of core scaffolds and aryl sulfonamide were flipped (2 poses from **6s**). Figure 3.4 illustrates the selected binding pose of each ligand.

The docked pose of ligands showed coordination between the hydroxamic acid and the zinc ion that was coordinated by the catalytic triad His^{388}, His^{392} and Glu^{411} residues. Another interaction that was observed in common was a hydrogen bonding interaction between Glu^{389} and the hydroxyl group of hydroxamic acid. This result was consistent with the MD simulations discussed in *Chapter 2*, where the role of Glu^{389} was hypothesised to stabilise the relatively weak coordination bond between hydroxyl of hydroxamic acid and zinc ion.[241] Phenylglycine analogue **6a** showed a similar binding pose as the trifluorophenyl analogue **6ad**, except that **6a**

did not have an additional aromatic ring to engage in π-π stacking interactions with Phe^{896} of the flexible loop in domain IV (Figure 3.4A). A decreased potency of compound **6a** could be explained by the absence of hydrophobic interactions. Enzymatic assay results also indicated that phenyl analogue **6e** was equipotent to **6ad**. With a phenyl group introduced, the analogue might have regained potency by participating in additional hydrophobic interactions with Phe^{896} residue (Figure 3.4B).

However, the information gained from docking studies was not sufficient to analyse the predicted binding interactions of from the docked poses of 3-fluorophenyl **6f**, cyclopropyl **6o**, and cyclohexyl **6s** analogues comprehensively. Polar interactions such as water-mediated hydrogen bonding interactions that the fluorine or nitrogen atom of **6f** and **6m** may engage could not be observed due to the absence of water molecules in the docked poses. Moreover, there were no distinct differences found in the binding interactions of cycloalkyl analogues to investigate how the different sizes (**6o** and **6s**) and polarity (**6s** and **6ab**) of the cyclic alkyl group lead to different binding modes. Therefore, further studies will be required in the future for a comprehensive analysis of the binding interactions by performing extensive computational studies such as MD simulations or producing X-ray crystal structures of the APN-inhibitor complexes.

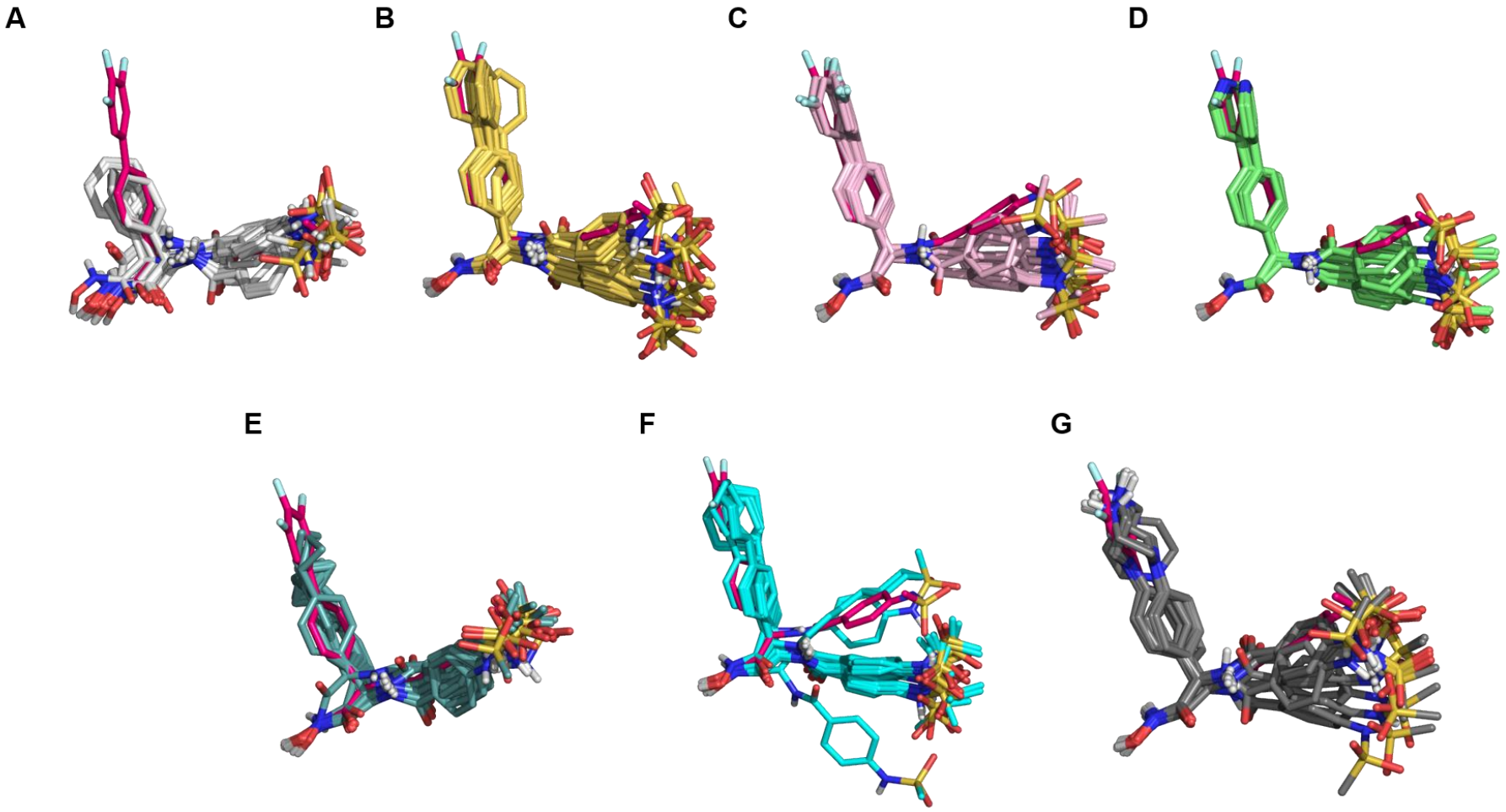

Figure 3.3. Superimposed predicted binding poses of 6a (A), 6e (B), 6f (C), 6m (D), 6o (E), 6s (F), and 6ab (G) into APN. The predicted binding pose of compound **6ad** (magenta stick) obtained from MD simulation was included for comparison. Ligands **6a**, **6e**, **6f**, **6m**, **6o**, **6s**, and **6ab** are depicted as sticks in white, yellow, pink, green, tilt green, cyan, and grey, respectively.

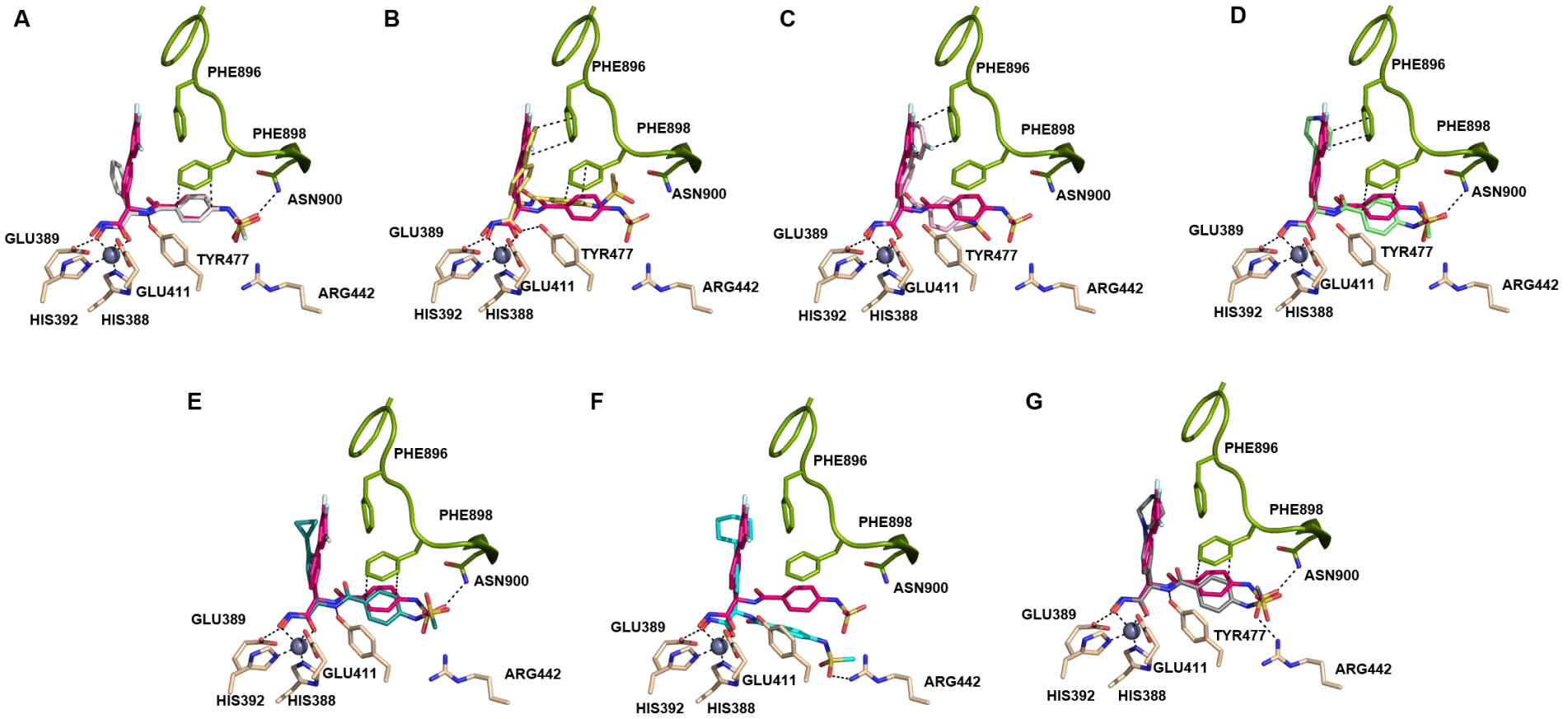

Figure 3.4. The most plausible binding pose of 6a (A), 6e (B), 6f (C), 6m (D), 6o (E), 6s (F), and 6ab (G). Compound **6ad** is shown as a magenta stick. Ligands **6a**, **6e**, **6f**, **6m**, **6o**, **6s**, and **6ab** are depicted as sticks in white, yellow, pink, green, tilt green, cyan, and grey, respectively. Key residues near the ligands are illustrated as a wheat stick, and the flexible loop is shown as a green cartoon. Interactions between ligands and APN are shown as black dashed lines.

3.5 Anti-proliferative activity of hydroxamic acids against various cancer cell lines

Selected novel hydroxamic acid analogues were also evaluated for anti-proliferative activity in cellular environment to measure how effectively potent APN inhibitors could disrupt cancer cell proliferation. The top ten compounds (**6c**, **6e**, **6f**, **6i**, **6m**, **6o**, **6q**, **6s**, **6x**, and **6ab**) were selected based on the potency. As described in *Chapter 2* (pg. 60), single-dose assays were carried out by NCI to screen the compounds chosen across 60 different cancer cell lines. Although the inhibitors exhibited excellent potency towards APN, they showed limited activity against cancer cell lines, which was consistent with the screening results of compound **6ad** and **6ae** in *Chapter 2* (Appendix B). The most potent APN inhibitor **6f** displayed weak anti-proliferative activities against certain cancer cell lines such as HOP-92, NCI-H522 (non-small cell lung cancer cell line), SNB-75 (CNS cancer cell line), and UO-31 (renal cancer cell line) with mean growth inhibition of 30% at 10 μM. The low cellular efficacy could arise by various reasons such as poor permeability and off-target effect. Therefore, extensive research will be required in order to identify the reasons for such a drastic change in the potency against purified APN and cancer cells.

3.6 Conclusion

In this chapter, a new series of hydroxamic acid analogues were designed to probe the binding interactions at the S1 pocket of APN and to enhance solubility by modulating hydrophobicity. The 3,4,5-trifluorophenyl moiety of the lead compound **6ad** was modified to substituted aromatic and heteroaromatic groups so that the biaryl system is maintained and hydrophobicity of the molecule is reduced. Microwave-assisted Suzuki-Miyaura coupling reaction was successfully optimised to form an aryl-aryl C-C bond between key precursor aryl bromide **4d** and various arylboronic acids to produce biaryl analogues **6e**-**6n**. In addition, an alternative synthetic route by the formation of *O*-Bn, TBS, and TIPS protected hydroxamic acids were also explored. Installation of cycloalkyl groups was attempted through diverse synthetic approaches. Synthesis of cyclopropyl analogue **6o** was achieved using previously reported conditions. However, direct coupling reactions with cyclopentyl and cyclohexylboronic acids were challenging. This problem was solved by changing the boronic acid to the corresponding cycloalkenylboronic acids. The C=C bond of cyclopentenyl and cyclohexenyl intermediates synthesised were further reduced to generate fully saturated cyclopentyl **6s** and cyclohexyl **6s** analogues.

A diverse range of synthetic methods was employed to couple amines with aryl bromide **4d** to generate amine-containing analogues **6t**-**6ab**. A number of model studies were performed on palladium catalysed Buchwald-Hartwig amination was attempted and found out that the sulfonamide group of **4d** is detrimental to achieve a successful conversion. Therefore, new synthetic strategies were applied and Boc-protected aryl bromide 1**7** was used as the key intermediate for Buchwald-Hartwig aminations. Alkyl amine, piperidine, and piperazine derivatives reacted with 1**7** to generate desired analogues successfully. Copper-catalysed CEL coupling reactions between amines and boronic acid derivative of **4d** were also investigated. Unfortunately, CEL coupling reactions were not pursued further due to limited conversion to product and formation of by-products via oxidation and photodeboronation.

A total of 28 novel hydroxamic acids were synthesised through optimised synthetic pathways, and their inhibitory activity against APN was measured by *in vitro* enzyme assays to establish comprehensive structure-activity relationships. Majority of the hydroxamic acid analogues showed inhibition at a low nanomolar range, and four compounds were more potent than the lead compound **6ad**. The results revealed that various chemical moieties could be tolerated at the S1 pocket of APN. The halo-phenylglycine analogues **6b-d** showed improved potency compared to phenylglycine analogue **6a**. Unsubstituted phenyl analogue **6e** was equipotent to **6ad**, and the potency was enhanced with additional fluorine atoms. The most potent inhibitor identified in the series of analogues was 3-fluorophenyl analogue **6f** which displayed a remarkable $K_i^{(app)}$ of 0.66 nM, and this was 7-fold and 3600-fold more active than **6ad** and bestatin, respectively. Intriguing results were obtained from cycloalkyl analogues; fully saturated cyclopentyl **6q** and cyclohexyl **6s** analogues were preferred to its corresponding unsaturated analogues. Moreover, a considerable decrease in the activity was observed from amine analogues.

Binding interactions between selected compounds and APN were investigated through molecular docking studies. Some predicted binding poses of phenylglycine analogue **6a** showed movements in the hydroxamic acid position, and the significant loss in potency compared **6ad** could be explained by a complete loss of hydrophobic interactions with Phe^{896}. Analogues containing biaryl scaffold **6e**, **6f**, **6m**, and **6o** possessed extremely stable hydroxamic acid – zinc coordination and the movement of the biaryl scaffold at the S1 pocket was almost negligible. Cycloalkyl moiety of alkyl-aryl analogues **6s** and **6ab** displayed some differences in conformation between each pose. Unfortunately, the fragment-based docking

provided limited information to understand the differences in potency observed between the APN inhibitors.

Anti-proliferative activities of top ten APN inhibitors were also determined by NCI single-dose screening assays. Compounds **6c**, **6e**, **6f**, **6i**, **6m**, **6o**, **6q**, **6s**, **6x**, and **6ab** were selected not only because they showed most active potency, but also they possessed distinct chemical scaffolds. The selected compounds were screened against 60 different cancer cell lines of diverse cancer types. The most potent inhibitor **6f** was the only analogue that showed a weak anti-proliferative activity against certain cancer cell lines. Other chosen analogues showed no activity in the cellular environment. The reasons for the extremely weak anti-proliferative activity of these potent APN inhibitors is not yet understood, and more extensive investigation of target selectivity and the role of APN in these cancer lines is required in the future.

3.7 Experimental

3.7.1 Biology

Protein expression and purification, enzymatic assay, and NCI-60 screenings were performed as per *Chapter 2*, pg 52-53.[241]

3.7.2 Chemistry

General experimental

The general instrument information is provided in *Chapter 2*, pg 40-41.[241]

General Procedure A: Acid catalysed the esterification of substituted 2-amino-2-phenylacetic acids. To a round bottom flask was added appropriate 2-amino-2-phenylacetic acid (1.0 eq.), MeOH (13 mL/mmol) and conc. H_2SO_4 (4.0 eq.) dropwise. The mixture was heated at reflux for overnight. Upon completion, the mixture was concentrated *in vacuo* and neutralised by sat. $NaHCO_3$ to pH 7–8 and extracted with EtOAc (3 × 20 mL). The combined organic layer was dried over anhydrous Na_2SO_4 and concentrated *in vacuo*. The crude product obtained was used for subsequent reactions without further purifications.

General Procedure B: Amide coupling using EDCI and DMAP. Methyl 2-amino-2-phenylacetate (1.0 eq.), carboxylic acid (1.2 eq.), EDCI (1.2 eq.) and DMAP (1.3 eq.) were dissolved in DCM/DMF (1:1) mixture (10 mL/mmol) and stirred at room temperature for overnight. DCM was removed *in vacuo*, and the resulting mixture was diluted with a 1 M HCl (20 mL) and extracted with EtOAc (3 × 15 mL). The combined organic layer was washed with water (2 × 20 mL) and brine (20 mL), which was then dried over Na_2SO_4 and concentrated *in vacuo*. The crude was taken up into a minimum amount of DMF and added to ice-water dropwise. The solid was filtered with minimal MeOH wash and dried under vacuum overnight.

General Procedure C: Suzuki-coupling reaction of aryl bromide containing sulfonamide. To a N_2 flushed 0.5–2 mL microwave vial was added the aryl bromide (1.0 eq.), boronic acid (1.2 eq.), K_3PO_4 (2.4 eq.) and anhydrous DMF (2 mL), which was stirred and degassed for 5 min before adding Pd $(PPh_3)_2Cl_2$ (0.05 eq.). The mixture was heated at 100 °C for 1–20 h in a microwave reactor until completion. The reaction mixture was diluted with a 1 M HCl (20 mL) and extracted with EtOAc (3 × 15 mL). The combined organic layer was further washed with water (2 × 20 mL) and brine (20 mL) which was then dried over anhydrous Na_2SO_4 followed

by concentration *in vacuo*. The crude was taken up into a minimal amount of DMF and added to ice-water dropwise. The solid was filtered with minimal MeOH wash and dried under vacuum overnight.

General Procedure D: Buchwald-Hartwig amination between aryl bromide and alkylamines. A mixture of aryl bromide (1.0 eq.), $Pd_2(dba)_3$ (0.03 eq.), XPhos (0.1 eq.), Cs_2CO_3 (2.5–5.0 eq.), and amine (2.5 eq.) in degassed anhydrous toluene (10 mL) was heated at reflux for overnight. After cooling, the mixture was diluted with water (6 mL) and extracted with EtOAc (3 × 20 mL). The combined organic layer was washed with brine, dried over anhydrous Na_2SO_4 and concentrated *in vacuo*. The crude was purified by column chromatography.

*General Procedure E: Synthesis of aryl sulfonamide compounds **5p-y** from Boc-protected intermediates **18a-i***. A round bottom flask was charged with Boc-protected intermediate (1.0 eq.) and 20% TFA in DCM (10 mL/mmol). The mixture was stirred at room temperature for 3 h. Upon completion, excess TFA was removed *in vacuo*, and the residue was dried under vacuum overnight. The residue was dissolved in DCM (5 mL/mmol), and DIPEA (3.0 eq.) was added before stirring for 30 min (mixture 1). To a separate dried round bottom flask was added 4-(methylsulfonamido)benzoic acid (1.1 eq.), HCTU (1.2 eq.), DIPEA (2.0 eq.), and DMF (5 mL/mmol) and stirred for 30 min (mixture 2). Mixture 1 and 2 were combined and stirred at room temperature for overnight. Upon completion, the mixture was concentrated *in vacuo* and diluted with a half sat. $NaHCO_3$ (10 mL) and extracted with EtOAc (3 × 15 mL). The combined organic layer was further washed with water (3 × 20 mL) and brine (20 mL) followed by drying over anhydrous Na_2SO_4 and concentration *in vacuo*. The crude was purified by column chromatography.

General Procedure F: Direct aminolysis of methyl ester to the hydroxamic acid. To a solution of methyl ester (1.0 eq.) in anhydrous MeOH (3 mL/mmol) was added $NH_2OH{\cdot}HCl$ (8.0 eq.), followed by 5 M KOH in anhydrous MeOH (10 eq.). The reaction was stirred at room temperature for overnight. Upon completion, the suspension was concentrated *in vacuo* followed by addition of a 10% citric acid (10 mL) and extraction with EtOAc (3 × 10 mL). The combined organic layer was dried over anhydrous Na_2SO_4 and concentration *in vacuo*. The crude product was purified by column chromatography or Preparative HPLC.

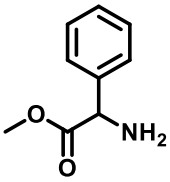

*Methyl 2-amino-2-phenylacetate (**1a**).* Compound **1a** was synthesised from 2-amino-2-phenylacetic (200 mg, 1.32 mmol) according to General Procedure A. The crude product (164 mg) was obtained as a brown oil in 75% of yield. ^{1}H NMR ($CDCl_3$) δ 7.42–7.29 (m, 5H), 4.65 (s, 1H), 3.70 (s, 3H), 2.49 (br. s, 2H); ^{13}C NMR ($CDCl_3$) δ 170.6, 129.0, 128.3, 128.2, 127.0, 58.9, 52.6.

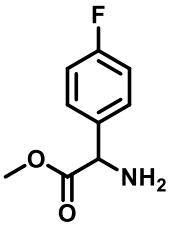

*Methyl 2-amino-2-(4-fluorophenyl)acetate (**1b**).* Compound **1b** was synthesised from 2-amino-2-(4-fluorophenyl)acetic acid (200 mg, 1.18 mmol) according to General Procedure A. The crude product (188 mg) was obtained as a brown oil in 87% of yield. ^{1}H NMR ($CDCl_3$) δ 7.41–7.29 (m, 2H), 7.11–6.96 (m, 2H), 4.63 (s, 1H), 3.70 (s, 3H), 2.27 (br. s, 2H); ^{19}F NMR ($CDCl_3$) δ -114.1; ^{13}C NMR ($CDCl_3$) δ 174.2, 162.6 (d, J_{CF} = 246.7 Hz), 135.8 (d, J_{CF} = 3.3 Hz), 128.7 (d, J_{CF} = 8.2 Hz), 115.8 (d, J_{CF} = 21.6 Hz), 58.1, 52.7.

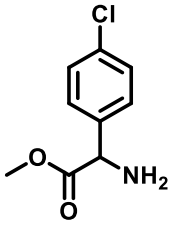

*Methyl 2-amino-2-(4-chlorophenyl)acetate (**1c**).* Compound **1c** was synthesised from 2-amino-2-(4-chlorophenyl)acetic acid (200 mg, 1.08 mmol) according to General Procedure A. The crude product (181 mg) was obtained as a brown oil in 84% of yield. ^{1}H NMR ($CDCl_3$) δ 7.33 (app. s, 4H), 4.61 (s, 1H), 3.70 (s, 3H), 2.13 (br. s, 2H); ^{13}C NMR ($CDCl_3$) δ 174.0, 138.5, 134.11, 129.1, 128.4, 58.6, 52.7.

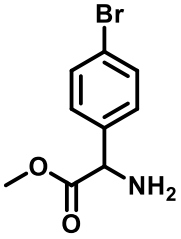

*Methyl 2-amino-2-(4-bromophenyl)acetate (**1d**).* Compound **1d** was synthesised from 2-amino-2-(4-bromophenyl)acetic acid (2.00 g, 8.69 mmol) according to General Procedure A. The crude product (1.90 g) was obtained as a brown oil in 90% of yield. ^{1}H NMR ($CDCl_3$) δ 7.48 (d, J = 7.4 Hz, 2H), 7.30 (d, J = 7.9 Hz, 2H), 4.70 (s, 1H), 3.70 (s, 3H), 3.42 (br. s, 2H).

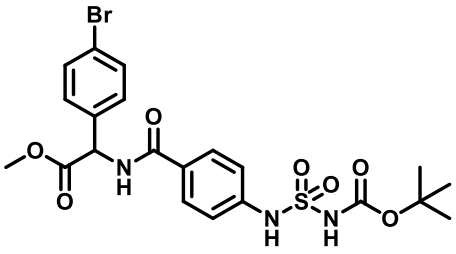

*Methyl 2-(4-bromophenyl)-2-(4-((N-(tert-butoxycarbonyl)sulfamoyl)amino)benzamido)acetate (**2**).* 4-((*N*-(*tert*-butoxycarbonyl)sulfamoyl)amino)benzoic acid (1.24 g, 3.93 mmol) was coupled to compound **1d** (800 mg, 3.28 mmol) according to General Procedure B. The crude was purified by column chromatography using PE/EtOAc (100:0 to 50:50) afford 1.38 g (76%) of the desired product as a creamy yellow solid. ^{1}H NMR (DMSO-d_6) δ 11.46 (s, 1H), 10.71 (s, 1H), 9.10 (d, J = 7.1 Hz, 1H), 7.87 (d, J = 8.6 Hz, 2H), 7.60 (d, J = 8.4 Hz, 2H),

7.44 (d, *J* = 8.4 Hz, 2H), 7.21 (d, *J* = 8.6 Hz, 2H), 5.67 (d, *J* = 7.1 Hz, 1H), 3.66 (s, 3H), 1.32 (s, 9H); ^{13}C NMR (DMSO-d_6) δ 170.7, 165.8, 149.9, 140.8, 135.8, 131.4, 130.5, 128.9, 127.9, 121.5, 117.6, 81.8, 56.2, 52.4, 27.6; *m/z* MS $C_{21}H_{25}BrN_3O_7S$ $[MH]^+$ calcd 542.1, found 541.7.

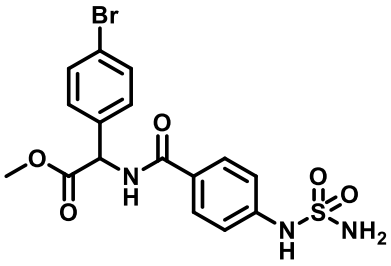

*Methyl 2-(4-bromophenyl)-2-(4-(sulfamoylamino)benzamido)acetate (**3**).* Compound **2** (100 mg, 184 μmol) was dissolved in DCM (20 mL). To this mixture was added TFA (4 mL) at 0 ºC and stirred at room temperature for 3 h. Excess TFA was removed by concentrating under reduced pressure. The residue was diluted with EtOAc (30 mL) and washed with sat. $NaHCO_3$ (3 × 30 mL). The organic layer was dried over anhydrous Na_2SO_4, filtered, and concentrated *in vacuo*. The crude (49.3 mg, 60%) showed > 95% purity based on NMR, therefore it was used without further purification. ^{1}H NMR (DMSO-d_6) δ 9.94 (s, 1H), 9.02 (d, *J* = 7.1 Hz, 1H), 7.84 (d, *J* = 8.8 Hz, 2H), 7.68–7.54 (m, 2H), 7.43 (d, *J* = 8.5 Hz, 2H), 7.29 (s, 2H), 7.17 (d, *J* = 8.8 Hz, 2H), 5.66 (d, *J* = 7.1 Hz, 1H), 3.66 (s, 3H); ^{13}C NMR (DMSO-d_6) δ 170.8, 165.9, 142.6, 135.9, 131.4, 130.5, 128.7, 126.1, 121.4, 116.2, 56.1, 52.4; *m/z* MS $C_{16}H_{17}BrN_3O_5S$ $[MH]^+$ calcd 442.0, found 441.7.

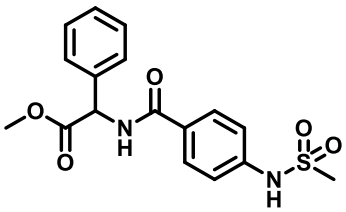

*Methyl 2-(4-(methylsulfonamido)benzamido)-2-phenylacetate (**4a**).* Compound **1a** (164 mg, 0.993 mmol) was coupled to (methylsulfonamido)benzoic acid (228 mg, 1.19 mmol) according to General Procedure B. The crude was dissolved in minimal amount of DMF and added into ice-water mixture dropwise. The precipitate was filtered and washed with minimal MeOH to produce 220 mg (61%) of a white solid. ^{1}H NMR (DMSO-d_6) δ 10.13 (s, 1H), 9.06 (d, *J* = 7.1 Hz, 1H), 8.01–7.79 (m, 2H), 7.47 (m, 2H), 7.44–7.33 (m, 3H), 7.30–7.09 (m, 2H), 5.65 (d, *J* = 7.1 Hz, 1H), 3.65 (s, 3H), 3.06 (s, 3H); ^{13}C NMR (DMSO-d_6) δ 171.1, 165.8, 141.5, 136.2, 129.2, 128.5, 128.2, 128.2, 128.1, 117.8, 56.9, 52.2, 39.5; *m/z* MS $C_{17}H_{19}N_2O_5S$ $[MH]^+$ calcd 363.1, found 362.8.

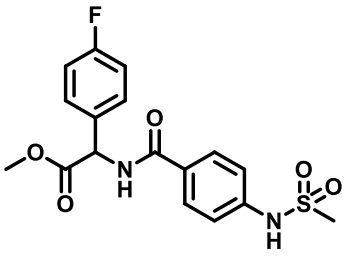

*Methyl 2-(4-fluorophenyl)-2-(4-(methylsulfonamido)benzamido)acetate (**4b**).* Compound **1b** (188 mg, 1.03 mmol) was coupled to (methylsulfonamido)benzoic acid (236 mg, 1.23 mmol) according to General Procedure B. The crude was dissolved in minimal amount of DMF and added into

ice-water mixture dropwise. The precipitate was filtered and washed with minimal MeOH to produce 300 mg (77%) of a white solid. ^{1}H NMR (DMSO-d_6) δ 10.13 (s, 1H), 9.07 (d, J = 7.1 Hz, 1H), 7.89 (d, J = 8.8 Hz, 2H), 7.59–7.45 (m, 2H), 7.27–7.21 (m, 4H), 5.67 (d, J = 7.0 Hz, 1H), 3.65 (s, 3H), 3.06 (s, 3H); ^{19}F NMR (DMSO-d_6) δ -114.1; ^{13}C NMR (DMSO-d_6) δ 171.0, 165.8, 161.9 (d, J_{CF} = 244.4 Hz), 141.5, 132.5, 130.4 (d, J_{CF} = 8.4 Hz), 129.2, 128.1, 117.8, 115.3 (d, J_{CF} = 21.5 Hz), 56.1, 52.3, 39.6; *m/z* MS $C_{17}H_{18}FN_2O_5S$ $[MH]^+$ calcd 381.1, found 380.8.

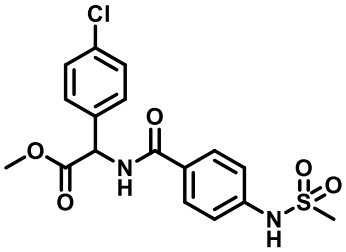

*Methyl 2-(4-chlorophenyl)-2-(4-(methylsulfonamido)benzamido)acetate (**4c**)*. Compound **1c** (181 mg, 0.907 mmol) was coupled to (methylsulfonamido)benzoic acid (209 mg, 1.09 mmol) according to General Procedure B. The reaction produced 332 mg (92%) of the crude product, and it was used for the next reaction without further purification. ^{1}H NMR (DMSO-d_6) δ 10.14 (s, 1H), 9.10 (d, J = 7.1 Hz, 1H), 7.89 (d, J = 8.8 Hz, 2H), 7.53–7.44 (m, 4H), 7.25 (d, J = 8.8 Hz, 2H), 5.69 (d, J = 7.1 Hz, 1H), 3.66 (s, 3H), 3.06 (s, 3H); ^{13}C NMR (DMSO-d_6) δ 171.3, 166.3, 142.1, 135.9, 133.4, 130.7, 129.7, 129.0, 128.5, 118.3, 56.6, 52.8, 40.2; *m/z* MS $C_{17}H_{18}ClN_2O_5S$ $[MH]^+$ calcd 397.1, found 396.8.

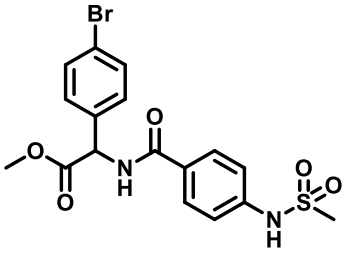

*Methyl 2-(4-bromophenyl)-2-(4-(methylsulfonamido)benzamido)acetate (**4d**)*. 4-(Methylsulfonamido)benzoic acid (2.06 g, 9.59 mmol) was coupled to compound **1d** (1.95 g, 7.99 mmol) according to General Procedure B. The crude was dissolved in minimal amount of DMF and added into ice-water mixture dropwise. The precipitate was filtered and washed with minimal MeOH to afford 2.32 g (66%) of a light yellow solid. ^{1}H NMR (DMSO-d_6) δ 10.15 (s, 1H), 9.11 (d, J = 7.1 Hz, 1H), 7.97–7.81 (m, 2H), 7.64–7.56 (m, 2H), 7.48–7.39 (m, 2H), 7.31–7.20 (m, 2H), 5.67 (d, J = 7.1 Hz, 1H), 3.66 (s, 3H), 3.07 (s, 3H); ^{13}C NMR (DMSO-d_6) δ 170.7, 165.8, 141.6, 135.8, 131.4, 130.5, 129.2, 128.0, 121.5, 117.8, 56.2, 52.4, 39.6; *m/z* MS $C_{17}H_{18}BrN_2O_5S$ $[MH]^+$ calcd 441.0, found 441.3.

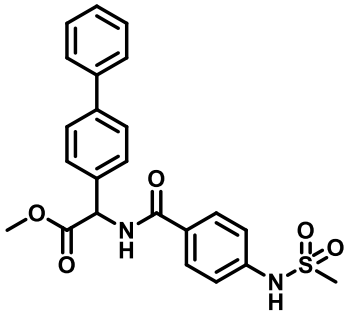

*Methyl 2-([1,1'-biphenyl]-4-yl)-2-(4-(methylsulfonamido)benzamido)acetate (**5a**).* Phenylboronic acid (49.7 mg, 0.408 mmol) was coupled to compound **4d** (150 mg, 0.340 mmol) according to General Procedure C. The reaction mixture was heated at 120 °C for 4 h to complete. The crude was dissolved in minimum amount of DMF and added into ice-water mixture dropwise. The precipitate was filtered and washed with minimal MeOH to produce 58.5 mg (39%) of the desired product as a white solid. ^{1}H NMR (DMSO-d_6) δ 10.13 (s, 1H), 9.11 (d, J = 7.0 Hz, 1H), 7.92 (d, J = 8.6 Hz, 2H), 7.73–7.62 (m, 4H), 7.56 (d, J = 8.2 Hz, 2H), 7.52–7.43 (m, 2H), 7.42–7.34 (m, 1H), 7.25 (d, J = 8.6 Hz, 2H), 5.71 (d, J = 7.0 Hz, 1H), 3.68 (s, 3H), 3.07 (s, 3H); ^{13}C NMR (DMSO-d_6) δ 171.1, 165.8, 141.5, 140.1, 139.7, 135.4, 129.2, 129.0, 128.9, 128.1, 127.6, 126.9, 126.7, 117.8, 56.6, 52.3, 39.6; *m/z* MS $C_{23}H_{23}N_2O_5S$ $[MH]^+$ calcd 439.1, found 438.8.

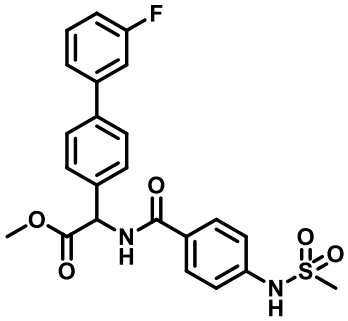

*Methyl 2-(3'-fluoro-[1,1'-biphenyl]-4-yl)-2-(4-(methylsulfonamido)benzamido)acetate (**5b**).* (3-Fluorophenyl)boronic acid (57.1 mg, 0.406 mmol) was coupled to compound **4d** (150 mg, 0.340 mmol) according to General Procedure C. The reaction mixture was heated at 100 °C for 1.5 h to complete. The crude was dissolved in minimum amount of DMF and added into ice-water mixture dropwise. The precipitate was filtered and washed with minimal MeOH to produce 114 mg (74%) of a light pink solid. ^{1}H NMR (DMSO-d_6) δ 10.14 (s, 1H), 9.13 (d, J = 7.1 Hz, 1H), 8.00–7.84 (m, 2H), 7.78–7.70 (m, 2H), 7.58 (d, J = 8.3 Hz, 2H), 7.56–7.48 (m, 3H), 7.29–7.24 (m, 2H), 7.23–7.18 (m, 1H), 5.73 (d, J = 7.1 Hz, 1H), 3.68 (s, 3H), 3.07 (s, 3H); ^{19}F NMR (DMSO-d_6) δ -112.7; ^{13}C NMR (DMSO-d_6) δ 171.0, 165.8, 162.7 (d, J_{CF} = 243.3 Hz), 142.1 (d, J_{CF} = 7.8 Hz), 141.6, 138.6 (d, J_{CF} = 2.2 Hz), 136.1, 130.9 (d, J_{CF} = 8.6 Hz), 129.2, 128.9, 128.1, 127.0, 122.8, 117.8, 114.3 (d, J_{CF} = 21.0 Hz), 113.4 (d, J_{CF} = 22.1 Hz), 56.5, 52.3, 39.6; *m/z* MS $C_{23}H_{22}FN_2O_5S$ $[MH]^+$ calcd 457.1, found 456.7.

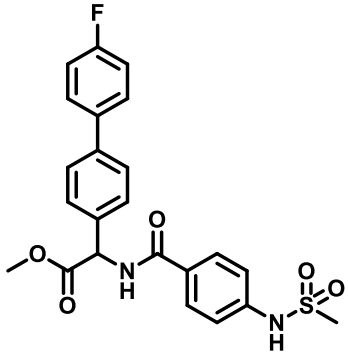

*Methyl 2-(4'-fluoro-[1,1'-biphenyl]-4-yl)-2-(4-(methylsulfonamido)benzamido)acetate (**5c**).* A nitrogen flushed 5 mL microwave vial was charged with compound **4d** (150 mg, 0.340 mmol), (4-fluorophenyl)boronic acid (57.1 mg, 0.408 mmol), 1 M Na_2CO_3 (1 mL) and degassed DMF (3 mL). The mixture was bubble through N_2 while stirring for 5 min before adding $Pd(PPh_3)_2Cl_2$ (11.9 mg, 0.017 mmol). The mixture was heated at 100 °C for 15 min. After cooling, the mixture was diluted with a 1 M HCl (10 mL) and extracted with EtOAc (3 × 10 mL). The combined organic layer was washed with water (2 × 20 mL) and brine (20 mL) and then dried over anhydrous Na_2SO_4 before concentration *in vacuo*. The crude product was purified by column chromatography using DCM/MeOH (95:5 to 90:10) to obtain 118 mg (77%) of a pale yellow solid. ^{1}H NMR (DMSO-d_6) δ 10.14 (s, 1H), 9.12 (d, J = 7.1 Hz, 1H), 8.00–7.87 (m, 2H), 7.75–7.69 (m, 2H), 7.68–7.64 (m, 2H), 7.56 (d, J = 8.3 Hz, 2H), 7.36–7.21 (m, 4H), 5.72 (d, J = 7.0 Hz, 1H), 3.68 (s, 3H), 3.07 (s, 3H); ^{19}F NMR (DMSO-d_6) δ -115.2; ^{13}C NMR (DMSO-d_6) δ 171.1, 165.9, 162.0 (d, J_{CF} = 244.5 Hz), 141.6, 139.1, 136.2 (d, J_{CF} = 3.0 Hz), 135.4, 129.2, 128.9, 128.7 (d, J_{CF} = 8.2 Hz), 128.2, 126.8, 117.8, 115.8 (d, J_{CF} = 21.4 Hz), 56.6, 52.3, 39.6; *m/z* MS $C_{23}H_{22}FN_2O_5S$ $[MH]^+$ calcd 457.1, found 456.8.

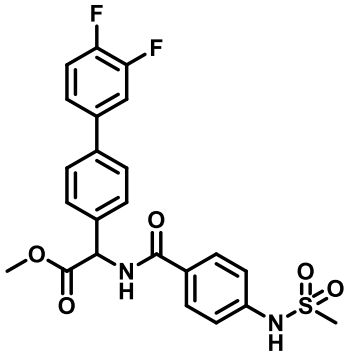

*Methyl 2-(3',4'-difluoro-[1,1'-biphenyl]-4-yl)-2-(4-(methylsulfonamido)benzamido)acetate (**5d**).* (3,4-Difluorophenyl)boronic acid (51.5 mg, 0.326 mmol) was coupled to compound **4d** (120 mg, 0.271 mmol) according to General Procedure C. The reaction mixture was heated at 100 °C for 1.5 h to complete. The crude was dissolved in minimum amount of DMF and added into ice-water mixture dropwise. The precipitate was filtered and washed with minimal MeOH to produce 95.0 mg (74%) of the desired product as a light beige solid. ^{1}H NMR (DMSO-d_6) δ 10.14 (s, 1H), 9.13 (d, J = 7.1 Hz, 1H), 7.92 (d, J = 8.8 Hz, 2H), 7.84–7.75 (m, 1H), 7.71 (d, J = 8.4 Hz, 2H), 7.61–7.50 (m, 4H), 7.26 (d, J = 8.8 Hz, 2H), 5.73 (d, J = 7.1 Hz, 1H), 3.68 (s, 3H), 3.07 (s, 3H); ^{19}F NMR (DMSO-d_6) δ -138.1 (d, J = 22.5 Hz), -140.6 (d, J = 22.5 Hz); ^{13}C NMR (DMSO-d_6) δ 171.0, 165.8, 149.8 (dd, J_{CF} = 245.3/12.6 Hz), 149.2 (dd, J_{CF} = 246.4/12.7 Hz), 141.6, 137.8, 137.3 (dd, J_{CF} = 6.1/3.9 Hz), 136.1, 129.2, 128.9, 128.1, 126.9, 123.5 (dd, J_{CF} = 6.6/3.3 Hz), 118.0 (d, J_{CF} = 17.0 Hz), 117.8,

115.8 (d, J_{CF} = 17.8 Hz), 56.5, 52.3, 39.64; *m/z* MS $C_{23}H_{21}F_2N_2O_5S$ $[MH]^+$ calcd 475.1, found 474.8.

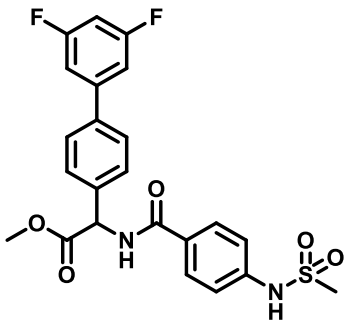

*Methyl 2-(3',5'-difluoro-[1,1'-biphenyl]-4-yl)-2-(4-(methylsulfonamido)benzamido)acetate (**5e**).* (3,5-Difluorophenyl)boronic acid (51.5 mg, 0.326 mmol) was coupled to compound **4d** (120 mg, 0.271 mmol) according to General Procedure C. The reaction mixture was heated at 100 °C for 1.5 h to complete. The crude was dissolved in minimal amount of DMF and added into ice-water mixture dropwise. The precipitate was filtered and washed with minimal MeOH to produce 69.0 mg (53%) of the desired product as a yellow solid. ^{1}H NMR (DMSO-d_6) δ 10.14 (s, 1H), 9.14 (d, *J* = 7.2 Hz, 1H), 7.92 (d, *J* = 8.8 Hz, 2H), 7.77 (d, *J* = 8.4 Hz, 2H), 7.59 (d, *J* = 8.3 Hz, 2H), 7.47 (dd, *J* = 9.0/2.2 Hz, 2H), 7.32–7.18 (m, 3H), 5.74 (d, *J* = 7.1 Hz, 1H), 3.68 (s, 3H), 3.07 (s, 3H); ^{19}F NMR (DMSO-d_6) δ -109.4; ^{13}C NMR (DMSO-d_6) δ 171.0, 165.8, 162.9 (dd, J_{CF} = 245.6/13.7 Hz), 143.3 (t, J_{CF} = 9.8 Hz), 141.6, 137.4 (t, J_{CF} = 2.4 Hz), 136.9, 129.2, 128.9, 128.1, 127.1, 117.8, 111.2–109.1 (m), 102.9 (t, J_{CF} = 26.0 Hz), 56.5, 52.4, 39.6; *m/z* MS $C_{23}H_{21}F_2N_2O_5S$ $[MH]^+$ calcd 475.1, found 474.8.

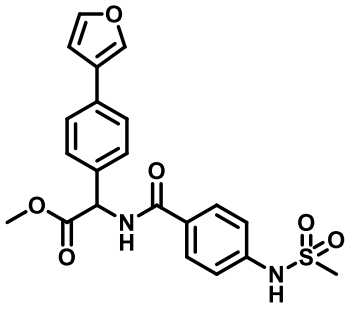

*Methyl 2-(4-(furan-3-yl)phenyl)-2-(4-(methylsulfonamido)benzamido)acetate (**5f**).* Furan-3-ylboronic acid (36.5 mg, 0.326 mmol) was coupled to compound **4d** (120 mg, 0.271 mmol) according to General Procedure C. The reaction mixture was heated at 100 °C for 1 h to complete. The crude was dissolved in minimum amount of DMF and added into ice-water mixture dropwise. The precipitate was filtered and washed with minimal MeOH to produce 96 mg (82%) of the desired product as a pale yellow solid. ^{1}H NMR (DMSO-d_6) δ 10.13 (s, 1H), 9.06 (d, *J* = 7.0 Hz, 1H), 8.26–8.08 (m, 1H), 7.91 (d, *J* = 8.8 Hz, 2H), 7.78–7.68 (m, 1H), 7.63 (d, *J* = 8.3 Hz, 2H), 7.48 (d, *J* = 8.3 Hz, 2H), 7.30–7.20 (m, 2H), 6.97 (dd, *J* = 1.9/0.8 Hz, 1H), 5.65 (d, *J* = 7.0 Hz, 1H), 3.66 (s, 3H), 3.06 (s, 3H); ^{13}C NMR (DMSO-d_6) δ 170.9, 165.5, 141.5, 134.8, 131.9, 129.2 (2C), 128.7, 128.1, 125.6, 125.4, 117.8, 108.6, 56.5, 52.3, 39.6; *m/z* MS $C_{21}H_{21}N_2O_6S$ $[MH]^+$ calcd 429.1, found 428.8.

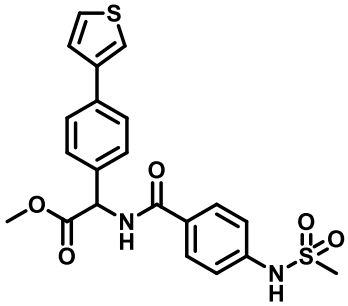

*Methyl 2-(4-(methylsulfonamido)benzamido)-2-(4-(thiophen-3-yl)phenyl)acetate (**5g**).* Thiophen-3-ylboronic acid (41.8 mg, 0.326 mmol) was coupled to compound **4d** (120 mg, 0.271 mmol) according to General Procedure C. The reaction mixture was heated at 100 °C for 1 h to complete. The crude obtained (116 mg, 95%) was for the subsequent reaction without further purification. ^{1}H NMR (DMSO-d_6) δ 10.13 (s, 1H), 9.08 (d, J = 7.1 Hz, 1H), 7.94–7.90 (m, 2H), 7.90–7.85 (m, 1H), 7.76–7.71 (m, 2H), 7.67–7.64 (m, 1H), 7.57–7.54 (m, 2H), 7.52–7.49 (m, 1H), 7.25 (d, J = 8.8 Hz, 2H), 5.67 (d, J = 7.0 Hz, 1H), 3.67 (s, 3H), 3.06 (s, 3H); ^{13}C NMR (DMSO-d_6) δ 169.5, 158.2, 141.5, 140.9, 135.1, 134.9, 129.2, 128.9, 128.8, 128.7, 126.2, 126.1, 121.3, 117.8, 56.6, 52.3, 39.6; *m/z* MS $C_{21}H_{19}N_2O_5S_2$ $[M-H]^-$ calcd 443.1, found 442.8.

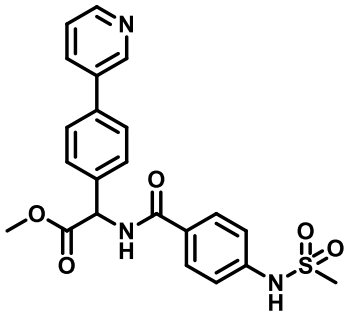

*Methyl 2-(4-(methylsulfonamido)benzamido)-2-(4-(pyridin-3-yl)phenyl)acetate (**5h**).* Pyridin-3-ylboronic acid (40.4 mg, 0.326 mmol) was coupled to compound **4d** (120 mg, 0.272 mmol) according to General Procedure C. Only 70% of conversion to the desired product was observed based on LC-MS after heating at 100 °C for 20 h. After cooling, the solvent was removed by concentrating *in vacuo*. 1 M HCl was added dropwise to the residue to adjust pH to 8–9 and extracted with EtOAc (3 × 10 mL). The combined organic layer was washed with water (2 × 20 mL) and brine (20 mL) and then dried over anhydrous Na_2SO_4 before concentration *in vacuo*. The crude was dissolved in minimum amount of DMF and added into ice-water mixture dropwise. The precipitate was filtered and washed with minimal MeOH to obtain 40.0 mg (33%) of the product as an off-white solid. ^{1}H NMR (DMSO-d_6) δ 10.14 (s, 1H), 9.13 (d, J = 7.1 Hz, 1H), 8.96–8.86 (m, 1H), 8.64–8.53 (m, 1H), 8.14–8.04 (m, 1H), 7.92 (d, J = 8.8 Hz, 2H), 7.79–7.73 (m, 2H), 7.64–7.58 (m, 3H), 7.25 (d, J = 8.8 Hz, 2H), 5.74 (d, J = 7.1 Hz, 1H), 3.68 (s, 3H), 3.07 (s, 3H); ^{13}C NMR (DMSO-d_6) δ 171.0, 165.8, 148.7, 147.7, 141.6, 137.0, 136.3, 135.1, 134.2, 129.3, 129.1, 128.1, 127.1, 124.0, 117.8, 56.5, 52.3, 39.6; *m/z* MS $C_{22}H_{22}N_3O_5S$ $[MH]^+$ calcd 440.1, found 439.8.

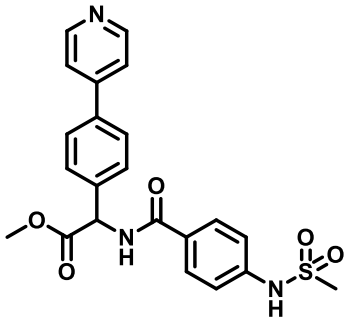

*Methyl 2-(4-(methylsulfonamido)benzamido)-2-(4-(pyridin-4-yl)phenyl)acetate (**5i**).* Pyridin-4-ylboronic acid (40.1 mg, 0.326 mmol) was coupled to compound **4d** (120 mg, 0.271 mmol) according to General Procedure C. The reaction mixture was heated at 100 °C for 1.5 h to complete. The crude was dissolved in minimum amount of DMF and added into ice-water mixture dropwise. The precipitate was filtered and washed with minimal MeOH to produce 67.4 mg (56%) of the desired product as a yellow solid. ^{1}H NMR (DMSO-d_6) δ 10.14 (s, 1H), 9.15 (d, J = 7.1 Hz, 1H), 8.65 (d, J = 6.1 Hz, 2H), 7.92 (d, J = 8.8 Hz, 2H), 7.86–7.81 (m, 2H), 7.75–7.69 (m, 2H), 7.65–7.59 (m, 2H), 7.25 (d, J = 8.8 Hz, 2H), 5.75 (d, J = 7.1 Hz, 1H), 3.68 (s, 3H), 3.07 (s, 3H); ^{13}C NMR (DMSO-d_6) δ 170.9, 165.8, 150.3, 147.2, 141.4, 137.4, 137.0, 129.2, 129.1, 128.2, 127.0, 121.2, 117.8, 56.5, 52.4, 39.6; *m/z* MS $C_{22}H_{22}N_3O_5S$ $[MH]^+$ calcd 440.1, found 439.8.

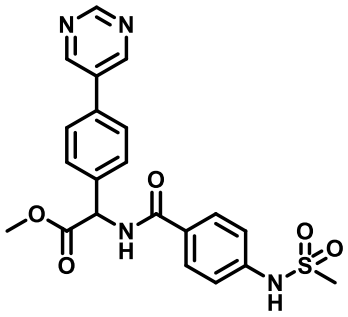

*Methyl 2-(4-(methylsulfonamido)benzamido)-2-(4-(pyrimidin-5-yl)phenyl)acetate (**5j**).* Pyrimidin-5-ylboronic acid (40.4 mg, 0.326 mmol) was coupled to compound **4d** (120 mg, 0.272 mmol) according to General Procedure C. The reaction mixture was heated at 100 °C for 6 h to complete. After cooling, the solvent was removed by concentrating *in vacuo*. 1 M HCl was added dropwise to the concentrated residue and sonicated for 2 min. The precipitate formed was filtered and washed with minimal Et_2O to afford 70 mg (58%) of the product as a white solid. ^{1}H NMR (DMSO-d_6) δ 10.14 (s, 1H), 9.20 (s, 1H), 9.18–9.14 (m, 3H), 7.91 (d, J = 8.8 Hz, 2H), 7.84 (d, J = 8.4 Hz, 2H), 7.65 (d, J = 8.3 Hz, 2H), 7.25 (d, J = 8.8 Hz, 2H), 5.76 (d, J = 7.2 Hz, 1H), 3.68 (s, 3H), 3.07 (s, 3H); ^{13}C NMR (DMSO-d_6) δ 170.9, 165.8, 154.8, 141.6, 137.2, 133.6, 132.8, 129.3, 129.2, 128.1, 127.1, 126.9, 117.8, 56.4, 52.4, 39.6; *m/z* MS $C_{21}H_{21}N_4O_5S$ $[MH]^+$ calcd 441.1, found 440.8.

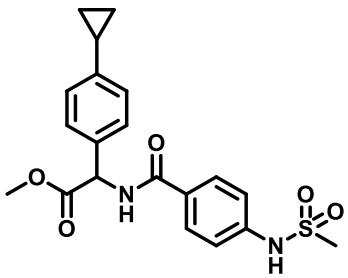

*Methyl 2-(4-cyclopropylphenyl)-2-(4-(methylsulfonamido)benzamido)acetate (**5k**).* To a N_2 flushed 5 mL microwave vial was added compound **4d** (100 mg, 0.227 mmol), cyclopropylboronic acid (21.4 mg, 0.245 mmol), K_2CO_3 (94 mg, 0.680 mmol) and anhydrous THF (4 mL). The mixture was degassed while stirring for 2 min before adding $Pd(dppf)Cl_2$

(16.6 mg, 0.023 mmol), and heated at reflux for overnight. The reaction mixture was diluted with a 1 M HCl (5 mL) and extracted with EtOAc (3 × 10 mL). The combined organic layer was dried over anhydrous Na_2SO_4 and concentrated under reduced pressure. The crude obtained (85.9 mg, 94%) was used for the subsequent reaction without further purification. ^{1}H NMR (DMSO-d_6) δ 10.13 (s, 1H), 8.98 (d, *J* = 7.0 Hz, 1H), 7.89 (d, *J* = 8.7 Hz, 2H), 7.33 (d, *J* = 8.2 Hz, 2H), 7.24 (d, *J* = 8.7 Hz, 2H), 7.09 (d, *J* = 8.2 Hz, 2H), 5.57 (d, *J* = 6.9 Hz, 1H), 3.64 (s, 3H), 3.06 (s, 3H), 1.95–1.79 (m, 1H), 1.06–0.83 (m, 2H), 0.77–0.53 (m, 2H); ^{13}C NMR (DMSO-d_6) δ 171.2, 165.8, 143.9, 141.5, 133.0, 129.2, 128.2, 125.5, 117.8, 56.6, 52.2, 39.6, 14.8, 9.5, 9.4; *m/z* MS $C_{20}H_{23}N_2O_5S$ $[MH]^+$ calcd 403.1, found 402.8.

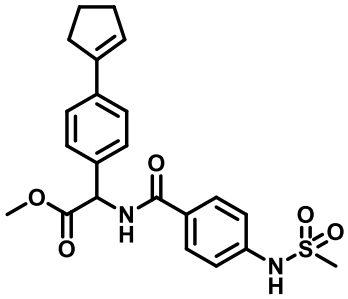

*Methyl 2-(4-(cyclopent-1-en-1-yl)phenyl)-2-(4-(methylsulfonamido)benzamido)acetate (**5l**)*. A dry round bottom flask was charged with compound **4d** (400 mg, 906 µmol), 1-cyclopentenylboronic acid (162 mg, 1.45 mmol), K_2CO_3 (564 mg, 4.08 mmol), and anhydrous THF (2 mL). The mixture was bubbled through N_2 for 10 min prior to addition of Pd(dppf)Cl_2 (99.5 mg, 136 µmol). The mixture was refluxed for overnight. Upon completion, THF was removed *in vacuo*, the residue was acidified with a 1 M HCl (10 mL) and extracted with EtOAc (3 × 10 mL). The combined organic layer was dried over anhydrous Na_2SO_4 and concentrated *in vacuo*. The crude product triturated with Et_2O and the filtered solid was washed with minimum amount of 1:2 MeOH/Et_2O to obtain 337 mg (87%) of the desired product as a dark brown solid. ^{1}H NMR (DMSO-d_6) δ 10.13 (s, 1H), 9.04 (d, *J* = 7.1 Hz, 1H), 7.93–7.85 (m, 2H), 7.47 (d, *J* = 8.4 Hz, 2H), 7.42 (d, *J* = 8.4 Hz, 2H), 7.29–7.17 (m, 2H), 6.35–6.18 (m, 1H), 5.63 (d, *J* = 7.0 Hz, 1H), 3.65 (s, 3H), 3.06 (s, 3H), 2.73–2.58 (m, 2H), 2.49–2.44 (m, 2H), 2.04–1.84 (m, 2H); ^{13}C NMR (DMSO-d_6) δ 171.1, 165.8, 141.5 (2C), 136.1, 134.7, 129.2, 128.3, 128.2, 126.6, 125.6, 117.8, 56.6, 52.2, 39.6, 32.9, 32.7, 22.7; *m/z* MS $C_{22}H_{25}N_2O_5S$ [MH]+ calcd 429.1, found 429.0.

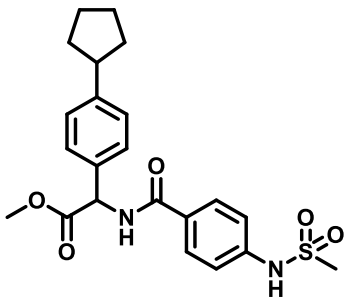

*Methyl 2-(4-cyclopentylphenyl)-2-(4-(methylsulfonamido)benzamido)acetate (**5m**)*. A 50 mL round bottom flask was charged with compound **5l** (174 mg, 406 µmol), ammonium formate (256 mg, 4.06 mmol) and EtOH (10 mL). The mixture was stirred and purged with N_2 thoroughly before adding 10% Pd/C (20 mg), which was refluxed for 2 h. Upon completion,

the reaction mixture was cooled to room temperature and filtered through Celite. The filtrate was concentrated *in vacuo* and extracted with EtOAc (3 × 10 mL) from water (10 mL). The combined organic layers were dried over anhydrous Na_2SO_4 and concentrated *in vacuo* to obtain 144 mg (83%) of the desired product as a white solid. The crude product was used for subsequent reaction without further purification. ^{1}H NMR (DMSO-d_6) δ 10.12 (s, 1H), 8.99 (d, J = 6.9 Hz, 1H), 7.94–7.87 (m, 2H), 7.37 (d, J = 8.2 Hz, 2H), 7.31–7.20 (m, 4H), 5.58 (d, J = 6.9 Hz, 1H), 3.64 (s, 3H), 3.06 (s, 3H), 3.00–2.90 (m, 1H), 2.06–1.89 (m, 2H), 1.82–1.71 (m, 2H), 1.71–1.59 (m, 2H), 1.59–1.45 (m, 2H); ^{13}C NMR (DMSO-d_6) δ 171.2, 165.8, 146.0, 141.5, 133.5, 129.2, 128.2, 128.1, 127.2, 117.8, 56.7, 52.2, 45.1, 39.6, 34.2, 25.0; *m/z* MS $C_{22}H_{27}N_2O_5S$ $[MH]^+$ calcd 431.2, found 431.0.

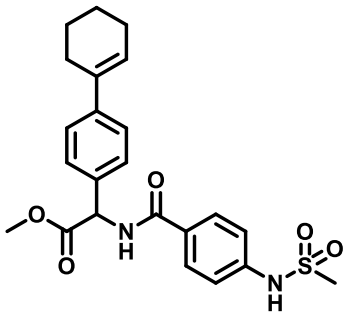

*Methyl 2-(4-(methylsulfonamido)benzamido)-2-(2',3',4',5'-tetrahydro-[1,1'-biphenyl]-4-yl)acetate (**5n**)*. A dry round bottom flask was charged with compound **4d** (404 mg, 915 µmol), 1-cyclohexenylboronic acid (185 mg, 1.46 mmol), K_2CO_3 (569 mg, 4.12 mmol), and anhydrous THF (15 mL). The mixture was bubbled through N_2 for 10 min prior to addition of Pd(dppf)Cl_2 (100 mg, 137 µmol). The mixture was refluxed for overnight. Upon completion, the reaction mixture was concentrated *in vacuo*, and the resulting residue was acidified with a 1 M HCl (10 mL) and extracted with EtOAc (3 × 10 mL). The combined organic layer was dried over anhydrous Na_2SO_4 and concentrated *in vacuo*. The crude product was purified by column chromatography using PE/EtOAc (70:30 to 0:100) to obtain 315 mg (78%) of the desired product as a brown solid. ^{1}H NMR (DMSO-d_6) δ 10.13 (s, 1H), 9.03 (d, J = 7.0 Hz, 1H), 8.03–7.79 (m, 2H), 7.40 (app. s, 4H), 7.29–7.19 (m, 2H), 6.23–6.09 (m, 1H), 5.62 (d, J = 7.0 Hz, 1H), 3.65 (s, 3H), 3.06 (s, 3H), 2.41–2.27 (m, 2H), 2.26–2.05 (m, 2H), 1.82–1.68 (m, 2H), 1.67–1.47 (m, 2H); ^{13}C NMR (DMSO-d_6) δ 171.1, 165.8, 141.8, 141.5, 135.6, 134.4, 129.2, 128.2, 128.2, 124.8, 124.7, 117.8, 56.6, 52.2, 39.6, 26.7, 25.3, 22.5, 21.6; *m/z* MS $C_{23}H_{27}N_2O_5S$ $[MH]^+$ calcd 443.2, found 443.0.

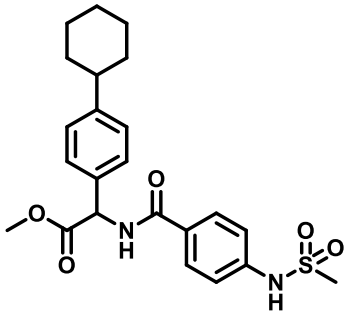

*Methyl 2-(4-cyclohexylphenyl)-2-(4-(methylsulfonamido)benzamido)acetate (**5o**)*. A 50 mL round bottom flask was charged with compound **5n** (263 mg, 594 µmol), ammonium formate (375 mg, 5.94 mmol) and MeOH (10 mL). The mixture was stirred and purged with N_2 thoroughly before adding 10% Pd/C (20 mg), which was refluxed for overnight. Upon completion, DMF was added until the reaction mixture becomes a homogeneous black solution to dissolve solid formed. Pd was filtered through Celite and the filtrate was concentrated *in vacuo* and extracted with EtOAc (3 × 20 mL) from water (30 mL). The combined organic layer was further washed with water (3 × 50 mL) and brine (50 mL). The combined organic layer was dried over anhydrous Na_2SO_4 and concentrated *in vacuo* to obtain 210 mg (80%) of the desired product as a beige solid. ^{1}H NMR (DMSO-d_6) δ 10.10 (s, 1H), 9.00 (d, J = 6.9 Hz, 1H), 7.97–7.76 (m, 2H), 7.36 (d, J = 8.2 Hz, 2H), 7.28–7.21 (m, 4H), 5.58 (d, J = 6.9 Hz, 1H), 3.64 (s, 3H), 3.06 (s, 3H), 1.87–1.49 (m, 6H), 1.49–1.09 (m, 5H); ^{13}C NMR (DMSO-d_6) δ 171.2, 165.8, 147.6, 141.5, 133.5, 129.2, 128.2, 128.1, 126.9, 117.8, 56.7, 52.2, 43.5, 39.6, 33.9, 33.8, 26.3, 25.6; *m/z* MS $C_{23}H_{29}N_2O_5S$ $[MH]^+$ calcd 445.2, found 445.0.

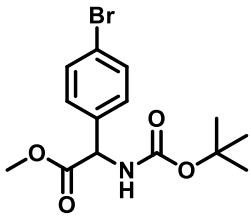

*Methyl 2-(4-bromophenyl)-2-((tert-butoxycarbonyl)amino)acetate (**17**)*. In a round bottom flask was added compound **1d** (3.10 g, 12.7 mmol), sat. $NaHCO_3$ (30 mL) and water (30 mL). The mixture was stirred at room temperature for 30 min after adding Boc_2O (2.77 g, 12.7 mmol). Additional Boc_2O (1.39 g, 6.35 mmol) and THF (90 mL) were added. The reaction mixture was stirred at room temperature for overnight. Upon completion, THF was removed under reduced pressure. 1 M HCl was added to the residue until pH 3 and the mixture was extracted with EtOAc (3 × 50 mL). The combined organic layer was dried over anhydrous Na_2SO_4 and concentrated *in vacuo*. The crude was purified by column chromatography using PE/EtOAc (100:0 to 40:60) to obtain 3.28 g (75%) of the desired product as a pale-yellow foam. ^{1}H NMR (DMSO-d_6) δ 7.84 (d, J = 8.1 Hz, 1H), 7.55 (d, J = 8.4 Hz, 2H), 7.43–7.12 (m, 2H), 5.23 (d, J = 8.1 Hz, 1H), 3.61 (s, 3H), 1.38 (s, 9H); ^{13}C NMR (DMSO-d_6) δ 171.0, 155.1, 136.1, 131.4, 130.1, 121.3, 78.7, 56.9, 52.3, 28.1.

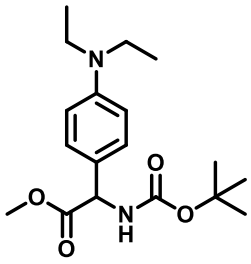

*Methyl 2-((tert-butoxycarbonyl)amino)-2-(4-(diethylamino)phenyl)acetate (**18a**)*. To a dried 20 mL microwave vessel was added **17** (250 mg, 726 µmol), $Pd_2(dba)_3$ (20.0 mg, 21.8 µmol), XPhos (34.6 mg, 72.6 µmol), Cs_2CO_3 (592 mg, 1.82 mmol), diethylamine (376 µL, 3.63 mmol), and degassed anhydrous toluene (10 mL) which was heated at reflux for overnight. After cooling, the mixture was diluted with water (6 mL) and extracted with EtOAc (3 × 20 mL). The combined organic layer was washed with brine (50 mL), dried over anhydrous Na_2SO_4 and concentrated *in vacuo*. The crude was purified by column chromatography PE/EtOAc (100:0 to 70:30) to obtain 204 mg (83%) of the desired product as a dark brown solid. ^{1}H NMR (DMSO-d_6) δ 7.51 (d, J = 7.7 Hz, 1H), 7.13 (d, J = 8.8 Hz, 2H), 6.58 (d, J = 8.8 Hz, 2H), 5.00 (d, J = 7.8 Hz, 1H), 3.58 (s, 3H), 3.34–3.12 (m, 4H), 1.38 (s, 9H), 1.06 (t, J = 7.0 Hz, 6H); ^{13}C NMR (DMSO-d_6) δ 172.1, 155.2, 147.1, 128.8, 122.3, 111.1, 78.3, 57.1, 51.9, 43.6, 28.2, 12.4.

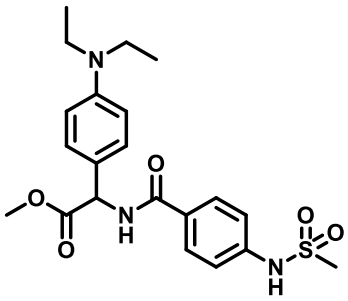

*Methyl 2-(4-(diethylamino)phenyl)-2-(4-(methylsulfonamido)benzamido)acetate (**5p**)*. Compound **18a** (292 mg, 868 µmol) was converted to the desired compound according to General Procedure E. The crude was purified by column chromatography PE/EtOAc (100:0 to 40:60) to obtain 264 mg (70%) of the desired product as an apricot solid. ^{1}H NMR (DMSO-d_6) δ 10.12 (s, 1H), 8.82 (d, J = 6.6 Hz, 1H), 7.97–7.82 (m, 2H), 7.30–7.13 (m, 4H), 6.64 (d, J = 8.9 Hz, 2H), 5.41 (d, J = 6.6 Hz, 1H), 3.62 (s, 3H), 3.33 (q, J = 7.1 Hz, 4H), 3.06 (s, 3H), 1.08 (t, J = 7.0 Hz, 6H); ^{13}C NMR (DMSO-d_6) δ 171.7, 165.8, 147.3, 141.4, 129.3, 129.2, 128.3, 121.7, 117.7, 111.2, 56.6, 51.9, 43.6, 39.6, 12.4; *m/z* MS $C_{21}H_{28}N_3O_5S$ $[MH]^+$ calcd 434.2, found 434.0.

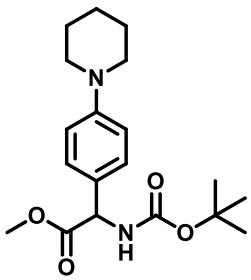

*Methyl 2-((tert-butoxycarbonyl)amino)-2-(4-(piperidin-1-yl)phenyl)acetate (**18b**)*. Compound **17** (363 mg, 1.05 mmol) was coupled to piperidine (260 µL, 2.64 mmol) according to General Procedure D. The crude was purified by column chromatography using PE/EtOAc (100:0 to 70:30) to obtain 186 mg (50%) of the desired product as a brown oil. ^{1}H NMR ($CDCl_3$) δ 7.18 (d, J = 8.7 Hz, 2H), 6.87 (d, J = 8.6 Hz, 2H), 5.46 (d, J = 6.8 Hz, 1H), 5.19 (d, J = 7.3 Hz, 1H), 3.67 (s, 3H), 3.17–3.04 (m, 4H), 1.83–1.59 (m, 4H), 1.61–1.48 (m, 2H), 1.40 (s, 9H); ^{13}C NMR ($CDCl_3$) δ 172.0, 154.9, 151.7, 128.0,

127.0, 116.5, 79.9, 57.1, 52.5, 50.4, 28.3, 25.6, 24.2; *m/z* MS $C_{19}H_{29}N_2O_4$ $[MH]^+$ calcd 349.2, found 349.1.

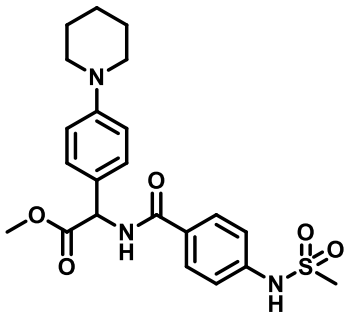

*Methyl 2-(4-(methylsulfonamido)benzamido)-2-(4-(piperidin-1-yl)phenyl)acetate (**5q**)*. Compound **18b** (186 mg, 534 µmol) was converted to the titled product according to General Procedure E. The crude was purified by column chromatography using PE/EtOAc (70:30 to 10:90) to obtain 149 mg (58%) of the desired product as a brown solid. ^{1}H NMR (DMSO-d_6) δ 10.12 (s, 1H), 8.90 (d, *J* = 6.7 Hz, 1H), 8.06–7.78 (m, 2H), 7.44–7.14 (m, 4H), 6.92 (br. d, *J* = 6.8 Hz, 2H), 5.48 (d, *J* = 6.7 Hz, 1H), 3.63 (s, 3H), 3.22–3.10 (m, 4H), 3.06 (s, 3H), 1.67–1.43 (m, 6H); ^{13}C NMR (DMSO-d_6) δ 171.5, 165.8, 151.4, 141.4, 129.2, 129.0, 128.3 (2C), 117.8, 115.8 (br.), 56.5, 52.0, 49.3, 39.6, 25.1, 23.9; *m/z* MS $C_{22}H_{28}N_3O_5S$ $[MH]^+$ calcd 446.2, found 446.0.

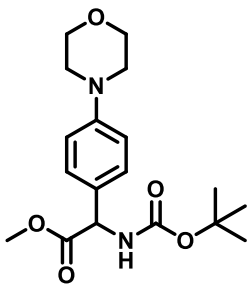

*Methyl 2-((tert-butoxycarbonyl)amino)-2-(4-morpholinophenyl)acetate (**18c**)*. Compound **17** (250 mg, 726 µmol) was coupled to morpholine (158 mg, 1.82 mmol) according to General Procedure D. The crude was purified by column chromatography using PE/EtOAc (100:0 to 50:50) to obtain 233 mg (91%) of the desired product as a yellow oil. ^{1}H NMR (DMSO-d_6) δ 7.62 (d, *J* = 7.9 Hz, 1H), 7.22 (d, *J* = 8.7 Hz, 2H), 6.89 (d, *J* = 8.8 Hz, 2H), 5.07 (d, *J* = 7.9 Hz, 1H), 3.80–3.64 (m, 4H), 3.59 (s, 3H), 3.19–2.97 (m, 4H), 1.38 (s, 9H); ^{13}C NMR (DMSO-d_6) δ 171.8, 155.2, 150.8, 128.5, 126.7, 114.8, 78.4, 66.1, 57.0, 52.0, 48.2, 28.2; *m/z* MS $C_{18}H_{27}N_2O_5$ $[MH]^+$ calcd 351.2, found 351.0.

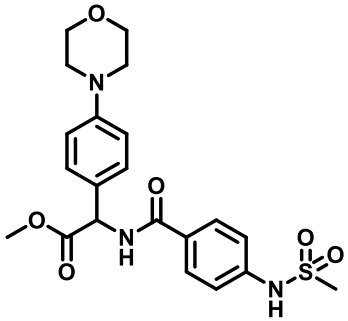

*Methyl 2-(4-(methylsulfonamido)benzamido)-2-(4-morpholinophenyl)acetate (**5r**)*. Compound **18c** (218 mg, 622 µmol) was converted to the titled compound according to General Procedure E. The crude was triturated with MeOH (10 mL) and filtered to afford 114 mg (41%) of the desired product as a white solid. ^{1}H NMR (DMSO-d_6) δ 10.12 (s, 1H), 8.91 (d, *J* = 6.8 Hz, 1H), 7.89 (d, *J* = 8.8 Hz, 2H), 7.31 (d, *J* = 8.7 Hz, 2H), 7.23 (d, *J* = 8.7 Hz, 2H), 6.95 (d, *J* = 8.8 Hz, 2H), 5.50 (d, *J* = 6.8 Hz, 1H), 3.78–3.69 (m, 4H), 3.63 (s, 3H), 3.16–3.08 (m, 4H), 3.06 (s, 3H); ^{13}C NMR (DMSO-d_6) δ 171.5, 165.8, 151.0, 141.4, 129.2., 129.0, 128.2, 126.3, 117.8, 114.9, 66.0, 56.5, 52.1, 48.3, 39.6; *m/z* MS $C_{21}H_{26}N_3O_6S$ $[MH]^+$ calcd 448.1, found 447.9.

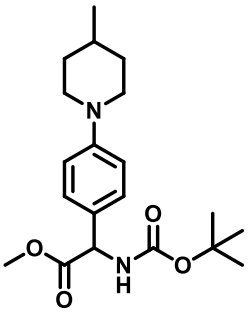

*Methyl 2-((tert-butoxycarbonyl)amino)-2-(4-(4-methylpiperidin-1-yl)phenyl)acetate (**18d**)*. Compound **17** (200 mg, 582 µmol) was coupled to 4-methylpiperidine (172 µL, 1.45 mmol) according to General Procedure D. The crude was purified by column chromatography using PE/EtOAc (100:0 to 70:30) to obtain 137 mg (65%) of the desired compound as an orange crystalline solid. ^{1}H NMR (DMSO-d_6) δ 7.59 (d, J = 7.9 Hz, 1H), 7.17 (d, J = 8.8 Hz, 2H), 6.86 (d, J = 8.8 Hz, 2H), 5.04 (d, J = 7.9 Hz, 1H), 3.74–3.62 (m, 2H), 3.59 (s, 3H), 2.63 (td, J = 12.3/2.3 Hz, 2H), 1.75–1.58 (m, 2H), 1.57–1.44 (m, 1H), 1.38 (s, 9H), 1.25–1.15 (m, 2H), 0.92 (d, J = 6.5 Hz, 3H); ^{13}C NMR (DMSO-d_6) δ 171.9, 155.2, 150.9, 128.5, 125.7, 115.3, 78.4, 57.0, 52.0, 48.5, 33.4, 30.2, 28.2, 21.8; *m/z* MS $C_{20}H_{31}N_2O_4$ $[MH]^+$ calcd 363.2, found 363.1.

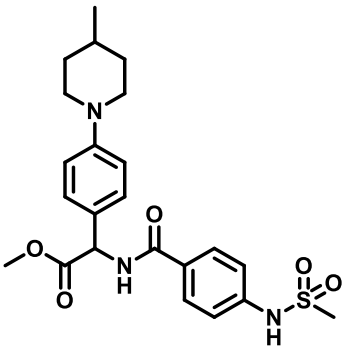

*Methyl 2-(4-(4-methylpiperidin-1-yl)phenyl)-2-(4-(methylsulfonamido)benzamido)acetate (**5s**)*. Compound **18d** (137 mg, 378 µmol) was converted to the titled compound according to General Procedure E. The crude was purified by column chromatography using PE/EtOAc (70:30 to 20:80) to obtain 99 mg (62%) as a beige solid. ^{1}H NMR ($CDCl_3$) δ 7.93 (s, 1H), 7.74 (d, J = 8.7 Hz, 2H), 7.29 (d, J = 8.7 Hz, 2H), 7.23 (d, J = 8.7 Hz, 2H), 7.12 (d, J = 6.8 Hz, 1H), 6.94 (d, J = 8.4 Hz, 2H), 5.64 (d, J = 6.8 Hz, 1H), 3.73 (s, 3H), 3.66–3.51 (m, 2H), 2.97 (s, 3H), 2.76–2.64 (m, 2H), 1.71 (app. d, J = 11.4 Hz, 2H), 1.60–1.45 (m, 1H), 1.44–1.28 (m, 2H), 0.95 (d, J = 6.4 Hz, 3H); ^{13}C NMR ($CDCl_3$) δ 172.0, 166.2, 150.7, 140.9, 129.4, 129.0, 128.5, 119.1, 117.0 (br.), 60.6, 56.6, 53.0, 50.3, 39.7, 33.6, 30.5, 21.8; *m/z* MS $C_{23}H_{30}N_3O_5S$ $[MH]^+$ calcd 460.2, found 460.0.

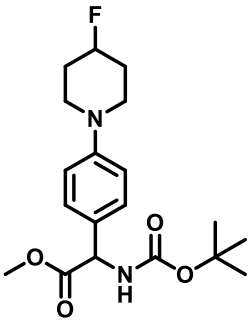

*Methyl 2-((tert-butoxycarbonyl)amino)-2-(4-(4-fluoropiperidin-1-yl)phenyl)acetate (**18e**)*. Compound **17** (250 mg, 726 µmol) was coupled to 4-fluoropiperidine hydrochloride (253 mg, 1.82 mmol) according to General Procedure D. The crude was purified by column chromatography using PE/EtOAc (100:0 to 60:40) to obtain 264 mg (99%) of the desired product as a sticky yellow solid. ^{1}H NMR (DMSO-d_6) δ 7.61 (d, J = 7.9 Hz, 1H), 7.20 (d, J = 8.7 Hz, 2H), 6.98–6.82 (m, 2H), 5.06 (d, J = 7.9 Hz, 1H), 4.95–4.65 (m, 1H), 3.59 (s, 3H), 3.45–3.31 (m, 2H), 3.21–3.05 (m, 2H), 2.07–1.87 (m, 2H), 1.82–1.68 (m, 2H), 1.38 (s, 9H); ^{19}F NMR (DMSO-d_6) δ -177.2; ^{13}C NMR (DMSO-d_6) δ 171.8, 155.2, 150.2,

128.6, 126.2, 115.5, 88.5 (d, J_{CF} = 169.4 Hz), 78.4, 57.0, 52.0, 44.8 (d, J_{CF} = 6.8 Hz), 30.5 (d, J = 19.0 Hz), 28.2; *m/z* MS $C_{19}H_{28}FN_2O_4$ $[MH]^+$ calcd 367.2, found 367.0.

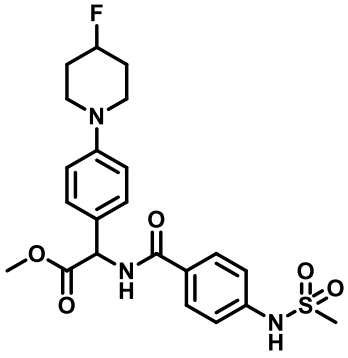

*Methyl 2-(4-(4-fluoropiperidin-1-yl)phenyl)-2-(4-(methylsulfonamido)benzamido)acetate (**5t**)*. Compound **18e** (226 mg, 617 µmol) was converted to the titled compound according to General Procedure E. The crude was taken up into 5 mL of MeOH and filtered to obtain 132 mg (46%) of the desired product as a light beige solid. ^{1}H NMR (DMSO-d_6) δ 10.06 (s, 1H), 8.91 (d, J = 6.8 Hz, 1H), 8.01–7.78 (m, 2H), 7.29 (d, J = 8.8 Hz, 2H), 7.26–7.18 (m, 2H), 6.96 (d, J = 8.8 Hz, 2H), 5.49 (d, J = 6.8 Hz, 1H), 5.01–4.65 (m, 1H), 3.63 (s, 3H), 3.44–3.33 (m, 2H), 3.21–3.09 (m, 2H), 3.06 (s, 3H), 2.04–1.86 (m, 2H), 1.86–1.69 (m, 2H); ^{19}F NMR (DMSO-d_6) δ -177.2; ^{13}C NMR (DMSO-d_6) δ 171.5, 165.8, 150.4, 141.5, 129.2, 129.0, 128.2, 125.7, 117.7, 115.6, 88.5 (d, J_{CF} = 169.4 Hz), 56.5, 52.1, 44.8 (d, J_{CF} = 6.9 Hz), 39.6, 30.5 (d, J_{CF} = 19.0 Hz); *m/z* MS $C_{22}H_{27}FN_3O_5S$ $[MH]^+$ calcd 464.2, found 464.0.

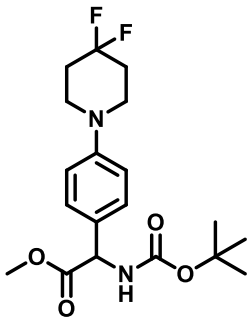

*Methyl 2-((tert-butoxycarbonyl)amino)-2-(4-(4,4-difluoropiperidin-1-yl)phenyl)acetate (**18f**)*. Compound **17** (270 mg, 784 µmol) was coupled to 4,4-difluoropiperidine hydrochloride (309 mg, 1.96 mmol) according to General Procedure D. The crude was purified by column chromatography using PE/EtOAc (100:0 to 70:30) to obtain 245 mg (81%) of the desired product as orange oil. ^{1}H NMR (DMSO-d_6) δ 7.63 (d, J = 7.9 Hz, 1H), 7.22 (d, J = 8.7 Hz, 2H), 6.96 (d, J = 8.8 Hz, 2H), 5.08 (d, J = 7.9 Hz, 1H), 3.59 (s, 3H), 3.39–3.28 (m, 4H), 2.02 (ddd, J = 19.8/14.1/6.0 Hz, 4H), 1.38 (s, 9H); ^{19}F NMR (DMSO-d_6) δ -95.2; ^{13}C NMR (DMSO-d_6) δ 171.8, 155.2, 149.3, 128.7, 126.8, 122.8 (t, J_{CF} = 240.7/240.7 Hz), 115.8, 78.4, 57.0, 52.0, 45.5 (t, J_{CF} = 5.0/5.0 Hz), 32.8 (t, J_{CF} = 22.4/22.4 Hz), 28.2; *m/z* MS $C_{19}H_{27}F_2N_2O_4$ $[MH]^+$ calcd 385.2, found 385.0.

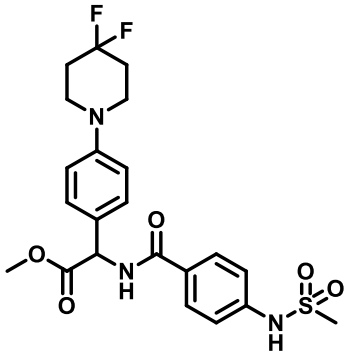

*Methyl 2-(4-(4,4-difluoropiperidin-1-yl)phenyl)-2-(4-(methylsulfonamido)benzamido)acetate (**5u**)*. Compound **18f** (225 mg, 585 µmol) was converted to the titled compound according to General Procedure E. The crude was purified by triturating with MeOH (10 mL) to obtain 123 mg (44%) of the desired product as an off-white solid. ^{1}H NMR (DMSO-d_6) δ 10.12 (s, 1H), 8.92 (d, J = 6.9 Hz, 1H), 8.06–7.77 (m, 2H), 7.31 (d, J = 8.8 Hz, 2H), 7.26–7.19 (m, 2H), 7.01 (d, J = 8.8 Hz, 2H), 5.51 (d, J = 6.8 Hz, 1H), 3.63 (s, 3H), 3.40–3.33 (m, 4H), 3.06 (s, 3H), 2.03 (ddd, J = 19.8/14.0/5.6 Hz, 4H); ^{19}F NMR (DMSO-d_6) δ -95.2; ^{13}C NMR (DMSO-d_6) δ 171.5, 165.8, 149.5, 141.5, 129.2, 129.1, 128.2, 126.3, 122.8 (t, J_{CF} = 240.7/240.7 Hz), 117.8, 115.9, 56.4, 52.1, 45.5 (t, J_{CF} = 5.2/5.2 Hz), 39.6, 32.8 (t, J_{CF} = 22.4/22.4 Hz); *m/z* MS $C_{22}H_{26}F_2N_3O_5S$ $[MH]^+$ calcd 482.1, found 482.0.

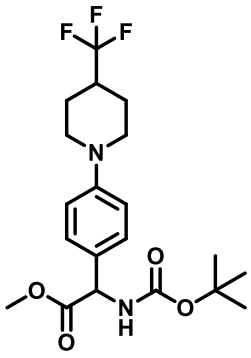

*Methyl 2-((tert-butoxycarbonyl)amino)-2-(4-(4-(trifluoromethyl)piperidin-1-yl)phenyl)acetate (**18g**)*. Compound **17** (250 mg, 726 µmol) was coupled to 4-(trifluoromethyl)piperidine hydrochloride (344 mg, 1.82 mmol) according to General Procedure D. The crude was purified by column chromatography using PE/EtOAc (100:0 to 70:30) to obtain 278 mg (92%) of the desired product as orange flakes. ^{1}H NMR (DMSO-d_6) δ 7.62 (d, J = 7.8 Hz, 1H), 7.25–7.14 (m, 2H), 6.91 (d, J = 8.8 Hz, 2H), 5.06 (d, J = 7.9 Hz, 1H), 3.91–3.72 (m, 2H), 3.59 (s, 3H), 2.79–2.62 (m, 2H), 2.49–2.42 (m, 1H), 1.98–1.77 (m, 2H), 1.66–1.42 (m, 2H), 1.38 (s, 9H); ^{19}F NMR (DMSO-d_6) δ -72.5; ^{13}C NMR (DMSO-d_6) δ 171.8, 155.2, 150.3, 129.2, 128.6, 126.4, 115.6, 78.4, 57.0, 52.0, 47.2 (d, J_{CF} = 3.4 Hz), 38.9 (d, J_{CF} = 26.5 Hz), 28.7, 23.7 *J coupling of CF_3 signal was difficult to observe; *m/z* MS $C_{20}H_{28}F_3N_2O_4$ $[MH]^+$ calcd 417.2, found 417.0.

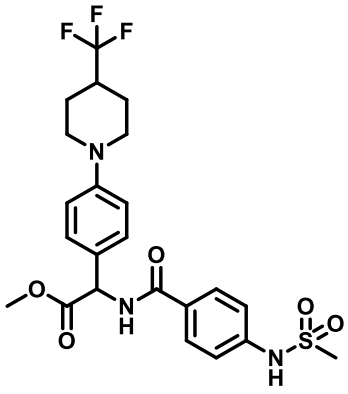

*Methyl 2-(4-(methylsulfonamido)benzamido)-2-(4-(4-(trifluoromethyl)piperidin-1-yl)phenyl)acetate (**5v**)*. Compound **18g** (258 mg, 620 µmol) was converted to the titled compound according to General Procedure E. The crude was triturated with MeOH to obtain 134 mg (56%) of the desired compound as a light beige solid. ^{1}H NMR (DMSO-d_6) δ 8.91 (d, J = 6.8 Hz, 1H), 7.95–7.79 (m, 2H), 7.29 (d, J = 8.8 Hz, 2H), 7.26–7.18 (m, 2H), 6.96 (d, J = 8.9 Hz, 2H), 5.50 (d, J = 6.8 Hz, 1H), 3.92–3.72 (m, 2H),

3.63 (s, 3H), 3.06 (s, 3H), 2.81–2.62 (m, 3H), 1.92–1.79 (m, 2H), 1.68–1.40 (m, 2H) * NH of sulfonamide was not observed; ^{19}F NMR (DMSO-d_6) δ -72.5; ^{13}C NMR (DMSO-d_6) δ 171.5, 165.8, 150.5, 141.5, 129.2, 129.1, 128.2, 125.9, 117.8, 115.7, 56.5, 52.1, 47.2, 47.1, 39.6, 38.9–38.1 (m), 23.6; *m/z* MS $C_{23}H_{27}F_3N_3O_5S$ $[MH]^+$ calcd 514.2, found 513.9.

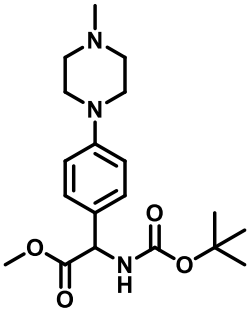

*Methyl 2-((tert-butoxycarbonyl)amino)-2-(4-(4-methylpiperazin-1-yl)phenyl)acetate (**18h**)*. Compound **17** (250 mg, 726 µmol) was coupled to 1-methylpiperazine (201 µL, 1.82 mmol) according to General Procedure D. Upon completion, the mixture was cooled to room temperature and concentrated *in vacuo*. The residue was extracted with 2 M HCl (3 × 20 mL) from Et_2O (15 mL). The aqueous layer was basified with sat. $NaHCO_3$ to pH 8 and extracted with EtOAc (3 × 100 mL). The combined organic layer was washed with brine (200 mL), dried over anhydrous Na_2SO_4 and concentrated *in vacuo* to obtain 195 mg (73%) of the desired product as yellow oil. ^{1}H NMR (DMSO-d_6) δ 7.61 (d, *J* = 7.9 Hz, 1H), 7.19 (d, *J* = 8.8 Hz, 2H), 6.88 (d, *J* = 8.8 Hz, 2H), 5.06 (d, *J* = 7.8 Hz, 1H), 3.59 (s, 3H), 3.16–3.02 (m, 4H), 2.46–2.35 (m, 4H), 2.21 (s, 3H), 1.38 (s, 9H); ^{13}C NMR (DMSO-d_6) δ 171.8, 155.2, 150.7, 128.5, 126.3, 115.0, 78.4, 57.0, 54.5, 52.0, 47.8, 45.7, 28.2; *m/z* MS $C_{19}H_{30}N_3O_4$ $[MH]^+$ calcd 364.2, found 364.1.

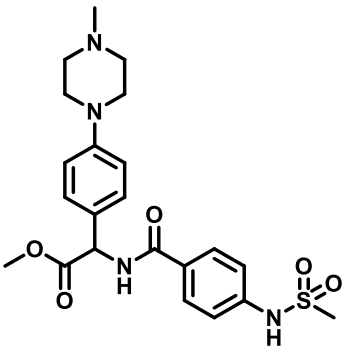

*Methyl 2-(4-(4-methylpiperazin-1-yl)phenyl)-2-(4-(methylsulfonamido)benzamido)acetate (**5w**)*. Compound **18h** (195 mg, 537 µmol) was converted to the titled compound according to General Procedure E. Brown oil obtained (131 mg, 53 %) was used for subsequent reaction without further purification. ^{1}H NMR (DMSO-d_6) δ 10.20 (s, 1H), 8.90 (d, *J* = 6.8 Hz, 1H), 7.97–7.79 (m, 2H), 7.29 (d, *J* = 8.8 Hz, 2H), 7.26–7.20 (m, 2H), 6.93 (d, *J* = 8.9 Hz, 2H), 5.49 (d, *J* = 6.8 Hz, 1H), 3.63 (s, 3H), 3.21–3.08 (m, 4H), 3.06 (s, 3H), 2.47–2.33 (m, 4H), 2.22 (s, 3H); ^{13}C NMR (DMSO-d_6) δ 171.5, 165.8, 150.9, 141.5, 129.1, 129.0, 128.2, 125.8, 117.8, 115.1, 56.5, 54.5, 52.1, 47.9, 45.7, 39.6; *m/z* MS $C_{22}H_{29}N_4O_5S$ $[MH]^+$ calcd 461.2, found 461.0.

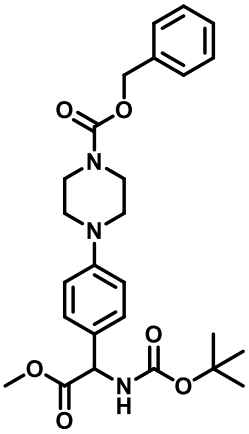

*Benzyl 4-(4-(2-methoxy-1-(4-(methylsulfonamido)benzamido)-2-oxoethyl)phenyl)piperazine-1-carboxylate (**18i**)*. Compound **17** (350 mg, 1.02 mmol) was coupled to benzyl piperazine-1-carboxylate (560 mg, 2.54 mmol) according to General Procedure D. The crude was purified by column chromatography using PE/EtOAc (100:0 to 50:50) to obtain 463 mg (94%) of the desired product as a yellow oil. ^{1}H NMR (DMSO-d_6) δ 7.63 (d, J = 8.0 Hz, 1H), 7.41–7.29 (m, 5H), 7.22 (d, J = 8.8 Hz, 2H), 7.01–6.84 (m, 2H), 5.10 (s, 2H), 5.07 (d, J = 7.8 Hz, 1H), 3.59 (s, 3H), 3.53 (br. s, 4H), 3.15–3.09 (m, 4H), 1.38 (s, 9H); ^{13}C NMR (DMSO-d_6) δ 154.4, 150.5 (2C), 145.3, 136.8, 128.6, 128.4, 127.9, 127.4, 127.0, 115.6, 78.4, 66.3, 57.0, 52.0, 48.1, 43.2, 28.2; *m/z* MS $C_{26}H_{34}N_3O_6$ $[MH]^+$ calcd 484.2, found 484.1.

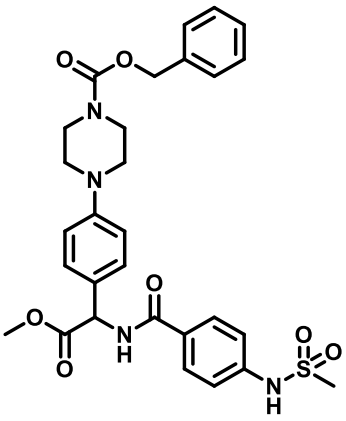

*Benzyl 4-(4-(2-methoxy-1-(4-(methylsulfonamido)benzamido)-2-oxoethyl)phenyl)piperazine-1-carboxylate (**5x**)*. Compound **18i** (493 mg, 937 µmol) was converted to the titled compound according to General Procedure E. The crude product was triturated with Et_2O to obtain 271 mg (50%) of the desired product as an off-white solid. ^{1}H NMR (DMSO-d_6) δ 10.12 (s, 1H), 8.92 (d, J = 6.8 Hz, 1H), 8.02–7.72 (m, 2H), 7.43–7.28 (m, 7H), 7.28–7.18 (m, 2H), 6.96 (d, J = 8.8 Hz, 2H), 5.51 (d, J = 6.8 Hz, 1H), 5.11 (s, 2H), 3.63 (s, 3H), 3.54 (br. s, 4H), 3.21–3.08 (m, 4H), 3.06 (s, 3H); ^{13}C NMR (DMSO-d_6) δ 171.4, 165.8, 154.4, 150.7, 141.4, 136.8, 129.2, 129.0, 128.4, 128.2, 127.9, 127.6, 126.6, 117.8, 115.8, 66.3, 56.4, 52.1, 48.1, 43.2, 39.6; *m/z* MS $C_{29}H_{33}N_4O_7S$ $[MH]^+$ calcd 581.2, found 581.0.

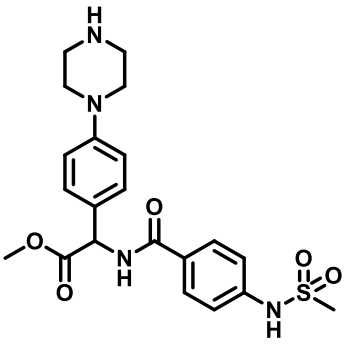

*Methyl 2-(4-(methylsulfonamido)benzamido)-2-(4-(piperazine-1-yl)phenyl)acetate (**5y**)*. A 50 mL round bottom flask was charged with **5x** (261 mg, 450 µmol), ammonium formate (283 mg, 4.49 mmol) and MeOH (10 mL). The mixture was stirred and purged with N_2 thoroughly before adding 10 % Pd/C (20 mg), which was refluxed for 4 h. Upon completion, the reaction mixture was cooled to room temperature and filtered through Celite. The filtrate was concentrated *in vacuo* and extracted with EtOAc (3 × 10 mL) from water (10 mL). The combined organic layers were dried over anhydrous Na_2SO_4 and concentrated *in vacuo* to

give 14 mg of a clear oil. LC-MS of the aqueous layer indicated the presence of the product which was recovered by lyophilisation to afford 118 mg (59%) of the desired product as a white solid. ^{1}H NMR (DMSO-d_6) δ 8.91 (d, J = 6.9 Hz, 1H), 8.32 (s, 1H), 8.03–7.74 (m, 2H), 7.30 (d, J = 8.8 Hz, 2H), 7.26–7.16 (m, 2H), 6.95 (d, J = 8.8 Hz, 2H), 5.50 (d, J = 6.8 Hz, 1H), 3.63 (s, 3H), 3.28–3.14 (m, 4H), 3.05 (s, 3H), 3.02–2.90 (m, 4H) *NH of sulfonamide was not observed; ^{13}C NMR (DMSO-d_6) δ 171.5, 165.8, 150.9, 141.7, 129.2, 129.0, 128.1, 126.4, 117.8, 115.4, 56.4, 52.1, 47.6, 44.1, 39.6; *m/z* MS $C_{21}H_{27}N_4O_5S$ $[MH]^+$ calcd 447.2, found 447.0.

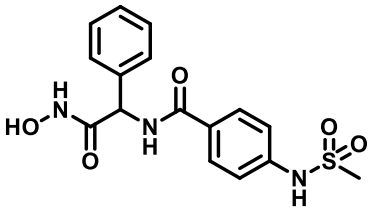

*N-(2-(Hydroxyamino)-2-oxo-1-phenylethyl)-4-(methylsulfonamido)benzamide (**6a**).* Compound **4a** (120 mg, 0.331 mmol) was converted to the corresponding hydroxamic acid according to General Procedure F. The crude was purified by column chromatography using DCM/MeOH (100:0 to 90:10) to afford 27 mg (23%) of white solid. ^{1}H NMR (DMSO-d_6) δ 11.02 (s, 1H), 10.12 (s, 1H), 9.02 (s, 1H), 8.75 (d, J = 8.2 Hz, 1H), 7.91 (d, J = 8.7 Hz, 2H), 7.55–7.46 (m, 2H), 7.41–7.32 (m, 2H), 7.32–7.27 (m, 1H), 7.27–7.20 (m, 2H), 5.60 (d, J = 8.1 Hz, 1H), 3.06 (s, 3H); ^{13}C NMR (DMSO-d_6) δ 166.7, 165.5, 141.4, 138.5, 129.2, 128.5, 128.3, 127.6, 127.4, 117.8, 54.6, 39.6; *m/z* HRMS (TOF ES$^+$) $C_{16}H_{18}N_3O_5S$ $[MH]^+$ calcd 364.0962, found 364.0950; HPLC 98%.

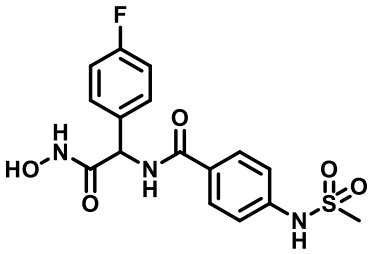

*N-(1-(4-Fluorophenyl)-2-(hydroxyamino)-2-oxoethyl)-4-(methylsulfonamido)benzamide (**6b**).* Compound **4b** (100 mg, 0.263 mmol) was converted to the corresponding hydroxamic acid according to General Procedure F. The crude was purified by column chromatography using DCM/MeOH (100:0 to 90:10) to afford 78 mg (78%) of white solid. ^{1}H NMR (DMSO-d_6) δ 11.03 (s, 1H), 10.12 (s, 1H), 9.04 (s, 1H), 8.79 (d, J = 8.1 Hz, 1H), 7.91 (d, J = 8.7 Hz, 2H), 7.58–7.50 (m, 2H), 7.25 (d, J = 8.7 Hz, 2H), 7.23–7.15 (m, 2H), 5.60 (d, J = 8.1 Hz, 1H), 3.06 (s, 3H); ^{19}F NMR (DMSO-d_6) δ -114.9; ^{13}C NMR (DMSO-d_6) δ 166.7, 165.6, 161.7 (d, J_{CF} = 243.7 Hz), 141.4, 134.8 (d, J_{CF} = 3.0 Hz), 129.5 (d, J_{CF} = 8.3 Hz), 129.3, 128.5, 117.8, 115.1 (d, J_{CF} = 21.4 Hz), 53.9, 39.5; *m/z* HRMS (TOF ES$^+$) $C_{16}H_{17}FN_3O_5S$ $[MH]^+$ calcd 382.0867, found 382.0861; HPLC 98%.

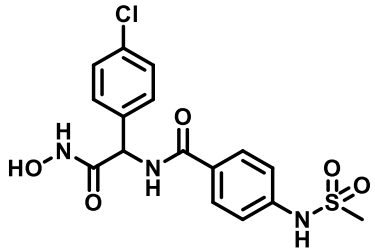

*N-(1-(4-Chlorophenyl)-2-(hydroxyamino)-2-oxoethyl)-4-(methylsulfonamido)benzamide (**6c**).* Compound **4c** (152 mg, 0.383 mmol) was converted to the corresponding hydroxamic acid according to General Procedure F. The crude was purified by column chromatography using DCM/MeOH (100:0 to 90:10) to afford 80 mg (53%) of white solid. ^{1}H NMR (DMSO-d_6) δ 11.05 (s, 1H), 10.13 (s, 1H), 9.06 (s, 1H), 8.82 (d, *J* = 8.1 Hz, 1H), 7.91 (d, *J* = 8.8 Hz, 2H), 7.52 (d, *J* = 8.5 Hz, 2H), 7.46–7.38 (m, 2H), 7.24 (d, *J* = 8.8 Hz, 2H), 5.60 (d, *J* = 8.1 Hz, 1H), 3.06 (s, 3H); ^{13}C NMR (DMSO-d_6) δ 166.4, 165.6, 141.5, 137.5, 132.3, 129.3, 129.2, 128.4, 128.3, 117.8, 54.0, 40.0; *m/z* HRMS (TOF ES$^+$) $C_{16}H_{17}ClN_3O_5S$ $[MH]^+$ calcd 398.0572, found 398.0569; HPLC 98%.

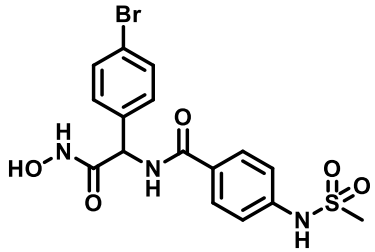

*N-(1-(4-Bromophenyl)-2-(hydroxyamino)-2-oxoethyl)-4-(methylsulfonamido)benzamide (**6d**).* Compound **4d** (600 mg, 1.36 mmol) was converted to the corresponding hydroxamic acid according to General Procedure F. The crude was purified by column chromatography using DCM/MeOH (100:0 to 90:10) to afford 109 mg (18%) of white solid. ^{1}H NMR (DMSO-d_6) δ 11.04 (app. d, *J* = 1.0 Hz, 1H), 10.12 (s, 1H), 9.05 (app. d, *J* = 1.3 Hz, 1H), 8.81 (d, *J* = 8.1 Hz, 1H), 8.01–7.85 (m, 2H), 7.62–7.54 (m, 2H), 7.50–7.42 (m, 2H), 7.26–7.19 (m, 2H), 5.57 (d, *J* = 8.1 Hz, 1H), 3.06 (s, 3H); ^{13}C NMR (DMSO-d_6) δ 166.3, 165.6, 141.4, 137.9, 131.2, 129.6, 129.2, 128.4, 120.8, 117.7, 54.0, 39.6; *m/z* HRMS (TOF ES$^+$) $C_{16}H_{17}BrN_3O_5S$ $[MH]^+$ calcd 442.0067, found 442.0073; HPLC 95%.

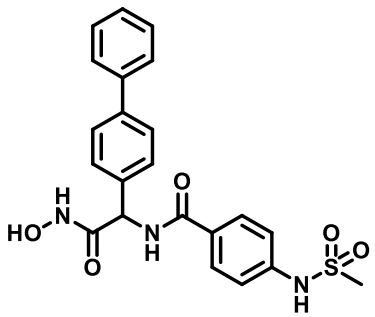

*N-(1-([1,1'-Biphenyl]-4-yl)-2-(hydroxyamino)-2-oxoethyl)-4-(methylsulfonamido)benzamide (**6e**).* Compound **5a** (126 mg, 0.287 mmol) was converted to the corresponding hydroxamic acid according to General Procedure F. The crude was purified Preparative HPLC to obtain 31 mg (14%) of the desired product as a white solid. ^{1}H NMR (DMSO-d_6) δ 11.04 (s, 1H), 10.12 (s, 1H), 9.03 (s, 1H), 8.79 (d, *J* = 8.1 Hz, 1H), 7.92 (d, *J* = 8.7 Hz, 2H), 7.71–7.63 (m, 4H), 7.58 (d, *J* = 8.3 Hz, 2H), 7.54–7.42 (m, 2H), 7.39–7.33 (m, 1H), 7.24 (d, *J* = 8.8 Hz, 2H), 5.64 (d, *J* = 8.1 Hz, 1H), 3.06 (s, 3H); ^{13}C NMR (DMSO-d_6) δ 166.6, 165.5, 141.4, 139.8, 139.6, 137.7, 129.2, 128.9, 128.5, 128.0, 127.5, 126.7, 126.6, 117.8, 54.3, 39.6; *m/z* HRMS (TOF ES$^+$) $C_{22}H_{22}N_3O_5S$ $[MH]^+$ calcd 440.1275, found 440.1276; HPLC 95%.

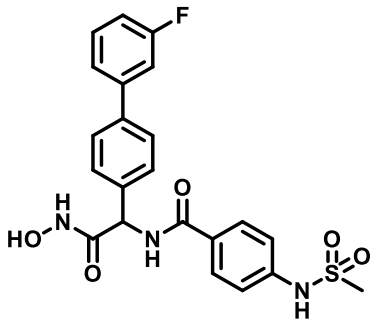

*N-(1-(3'-Fluoro-[1,1'-biphenyl]-4-yl)-2-(hydroxyamino)-2-oxoethyl)-4-(methylsulfonamido)benzamide (**6f**).* Compound **5b** (114 mg, 0.250 mmol) was converted to the corresponding hydroxamic acid according to General Procedure F. The crude was purified by column chromatography using DCM/MeOH/AcOH (99:0:1 to 84:15:1) and Preparative HPLC to obtain 4.2 mg (4%) of the desired product as a white solid. ^{1}H NMR (DMSO-d_6) δ 11.05 (s, 1H), 8.81 (d, J = 8.1 Hz, 1H), 7.92 (d, J = 8.8 Hz, 2H), 7.70 (d, J = 8.4 Hz, 2H), 7.59 (d, J = 8.3 Hz, 2H), 7.56–7.42 (m, 3H), 7.24 (d, J = 8.7 Hz, 2H), 7.23–7.10 (m, 1H), 5.64 (d, J = 8.1 Hz, 1H), 3.06 (s, 3H) *exchangeable protons NH of hydroxamic acid and sulfonamide were not observed; ^{19}F NMR (DMSO-d_6) δ -112.8; *m/z* HRMS (TOF ES$^+$) $C_{22}H_{21}FN_3O_5S$ $[MH]^+$ calcd 458.1180, found 458.1180; HPLC 95%.

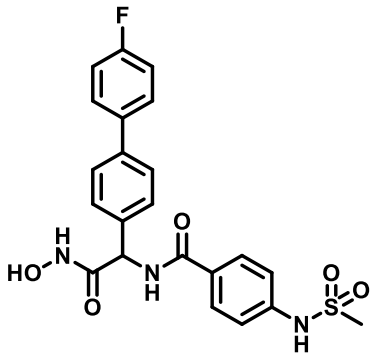

*N-(1-(4'-Fluoro-[1,1'-biphenyl]-4-yl)-2-(hydroxyamino)-2-oxoethyl)-4-(methylsulfonamido)benzamide (**6g**).* Compound **5c** was converted to the corresponding hydroxamic acid according to General Procedure F. The crude was purified by column chromatography using DCM/MeOH/AcOH (99:0:1 to 89:9:1) to obtain 60 mg (52%) of white solid. ^{1}H NMR (DMSO-d_6) δ 11.06 (s, 1H), 10.15 (s, 1H), 9.06 (s, 1H), 8.81 (d, J = 8.1 Hz, 1H), 7.93 (d, J = 8.8 Hz, 2H), 7.75–7.67 (m, 2H), 7.64 (d, J = 8.4 Hz, 2H), 7.59 (d, J = 8.4 Hz, 2H), 7.33–7.20 (m, 4H), 5.65 (d, J = 8.1 Hz, 1H), 3.07 (s, 3H); ^{19}F NMR (DMSO-d_6) δ -115.4; ^{13}C NMR (DMSO-d_6) δ 166.7, 165.6, 161.9 (d, J_{CF} = 244.3 Hz), 141.5, 138.6, 137.7, 136.3 (d, J_{CF} = 3.1 Hz), 129.2, 128.7 (d, J_{CF} = 8.2 Hz), 128.5, 128.0, 126.6, 117.8, 115.8 (d, J_{CF} = 21.3 Hz), 54.3, 39.7; *m/z* HRMS (TOF ES$^+$) $C_{22}H_{21}FN_3O_5S$ $[MH]^+$ calcd 458.1180, found 458.1185; HPLC 98%.

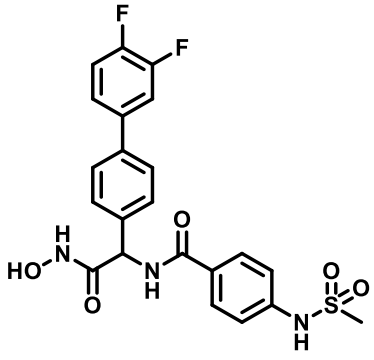

*N-(1-(3',4'-Difluoro-[1,1'-biphenyl]-4-yl)-2-(hydroxyamino)-2-oxoethyl)-4-(methylsulfonamido)benzamide (**6h**).* Compound **5d** (85.0 mg, 0.179 mmol) was converted to the corresponding hydroxamic acid according to General Procedure F. The crude was purified by column chromatography using DCM/MeOH (100:0 to 90:10) to afford 38 mg (45%) of the desired product as a white solid. ^{1}H NMR (DMSO-d_6) δ 11.06 (s, 1H), 10.12 (s,

1H), 9.05 (s, 1H), 8.82 (d, *J* = 8.1 Hz, 1H), 7.96–7.87 (m, 2H), 7.82–7.73 (m, 1H), 7.68 (d, *J* = 8.4 Hz, 2H), 7.59 (d, *J* = 8.4 Hz, 2H), 7.55–7.45 (m, 2H), 7.31–7.19 (m, 2H), 5.65 (d, *J* = 8.1 Hz, 1H), 3.07 (s, 3H); ^{19}F NMR (DMSO-d_6) δ -138.2 (d, *J* = 22.5 Hz), -140.8 (d, *J* = 22.5 Hz); ^{13}C NMR (DMSO-d_6) δ 166.6, 165.7, 149.8 (dd, J_{CF} = 245.2/12.8 Hz), 149.2 (dd, J_{CF} = 246.2/12.6 Hz), 141.5, 138.4, 137.5 (dd, J_{CF} = 6.1/3.8 Hz), 137.4, 129.3, 128.5, 128.1, 126.8, 123.5 (dd, J_{CF} = 6.4/3.3 Hz), 118.0 (d, J_{CF} = 17.0 Hz), 117.8, 115.8 (d, J_{CF} = 17.7 Hz), 54.3, 39.7; *m/z* HRMS (TOF ES$^+$) $C_{22}H_{20}F_2N_3O_5S$ [MH]$^+$ calcd 476.1086, found 476.1078; HPLC 95%.

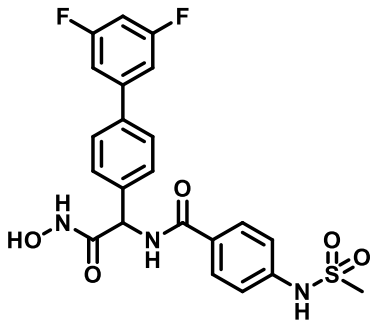

*N-(1-(3',5'-Difluoro-[1,1'-biphenyl]-4-yl)-2-(hydroxyamino)-2-oxoethyl)-4-(methylsulfonamido)benzamide (**6i**).* Compound **5e** (59.0 mg, 0.124 mmol) was converted to the corresponding hydroxamic acid according to General Procedure F. The crude was purified by column chromatography using DCM/MeOH/AcOH (100:0:1 to 89:9:1) and preparative HPLC to obtain 13.3 mg (23%) of the desired product as a white solid. ^{1}H NMR (DMSO-d_6) δ 11.06 (s, 1H), 10.13 (s, 1H), 9.05 (s, 1H), 8.83 (d, *J* = 8.1 Hz, 1H), 7.92 (d, *J* = 8.7 Hz, 2H), 7.74 (d, *J* = 8.3 Hz, 2H), 7.60 (d, *J* = 8.3 Hz, 2H), 7.45 (dd, *J* = 8.9/2.0 Hz, 2H), 7.34–7.03 (m, 3H), 5.65 (d, *J* = 8.1 Hz, 1H), 3.07 (s, 3H); ^{19}F NMR (DMSO-d_6) δ -109.4; ^{13}C NMR (DMSO-d_6) δ 166.5, 165.6, 162.9 (dd, J_{CF} = 245.5/13.7 Hz), 143.4 (d, J_{CF} = 9.8 Hz), 141.4, 139.1, 136.9, 129.2, 128.4, 128.0, 126.8, 117.8, 110.1–109.6 (m), 102.6 (d, J_{CF} = 26.2 Hz), 54.23, 39.6; *m/z* HRMS (TOF ES$^+$) $C_{22}H_{20}F_2N_3O_5S$ [MH]$^+$ calcd 476.1086, found 476.1085; HPLC 98%

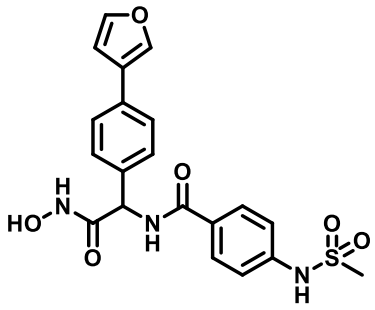

*N-(1-(4-(Furan-3-yl)phenyl)-2-(hydroxyamino)-2-oxoethyl)-4-(methylsulfonamido)benzamide (**6j**).* Compound **5f** (96.0 mg, 0.224 mmol) was converted to the corresponding hydroxamic acid according to General Procedure F. The crude was purified by column chromatography using DCM/MeOH (100:0 to 90:10) to afford 59.5 mg (62 %) of the product as a white solid. ^{1}H NMR (DMSO-d_6) δ 11.03 (s, 1H), 10.13 (s, 1H), 8.77 (d, *J* = 8.1 Hz, 1H), 8.26–8.13 (m, 1H), 7.92 (d, *J* = 8.7 Hz, 2H), 7.77–7.70 (m, 1H), 7.60 (d, *J* = 8.3 Hz, 2H), 7.51 (d, *J* = 8.3 Hz, 2H), 7.25 (d, *J* = 8.8 Hz, 2H), 6.96 (dd, *J* = 1.8/0.7 Hz, 1H), 5.60 (d, *J* = 8.1 Hz, 1H), 3.07 (s, 3H) *NH of hydroxamic acid was not observed; ^{13}C NMR (DMSO-d_6) δ 166.7, 165.6, 144.3, 141.4, 139.4, 137.1, 131.4, 129.2, 128.6, 127.9, 125.5, 125.4, 117.8, 108.8, 54.4, 39.7; *m/z* HRMS (TOF ES$^+$) $C_{20}H_{20}N_3O_6S$ [MH]$^+$ calcd 430.1067, found 430.1072; HPLC 98 %.

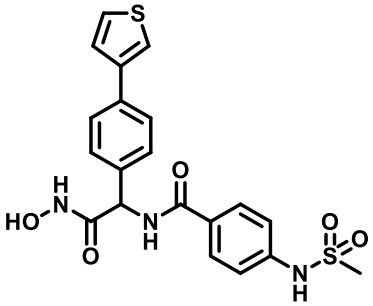

N-(2-(Hydroxyamino)-2-oxo-1-(4-(thiophen-3-yl)phenyl)ethyl)-4-(methylsulfonamido)benzamide ***(6k)***. Compound **5g** (116.0 mg, 0.260 mmol) was converted to the corresponding hydroxamic acid according to General Procedure F. The crude was purified by column chromatography using DCM/MeOH (100:0 to 90:10) to afford 64.0 mg (55%) of the product as a white solid. ^{1}H NMR (DMSO-d_6) δ 11.05 (s, 1H), 10.13 (s, 1H), 9.05 (s, 1H), 8.79 (d, *J* = 8.1 Hz, 1H), 7.93 (d, *J* = 8.7 Hz, 2H), 7.89–7.85 (m, 1H), 7.71 (d, *J* = 8.3 Hz, 2H), 7.66–7.61 (m, 1H), 7.60–7.49 (m, 3H), 7.26 (d, *J* = 8.7 Hz, 2H), 5.62 (d, *J* = 8.1 Hz, 1H), 3.07 (s, 3H); ^{13}C NMR (DMSO-d_6) δ 166.7, 165.6, 141.4, 141.1, 137.3, 134.6, 129.2, 128.5, 127.9, 127.1, 126.2, 126.0, 121.0, 117.8, 54.4, 39.7; *m/z* HRMS (TOF ES$^+$) $C_{20}H_{20}N_3O_5S_2$ $[MH]^+$ calcd 446.0839, found 446.0837; HPLC 95%

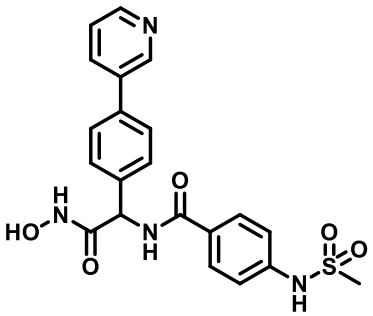

N-(2-(Hydroxyamino)-2-oxo-1-(4-(pyridin-3-yl)phenyl)ethyl)-4-(methylsulfonamido)benzamide TFA salt ***(6l)***. Compound **5h** (40.0 mg, 0.910 mmol) was converted to the corresponding hydroxamic acid according to General Procedure F. The crude was purified by preparative HPLC to afford 12.5 mg (31%) of the product as a white solid. ^{1}H NMR (DMSO-d_6) δ 11.09 (s, 1H), 10.14 (s, 1H), 9.05 (s, 1H), 8.86 (d, *J* = 8.1 Hz, 1H), 8.72 (br. s, 1H), 8.40 (app. d, *J* = 8.2 Hz, 1H), 7.92 (d, *J* = 8.7 Hz, 2H), 7.82–7.72 (m, 3H), 7.66 (d, *J* = 8.3 Hz, 2H), 7.25 (d, *J* = 8.8 Hz, 2H), 5.67 (d, *J* = 8.1 Hz, 1H), 3.07 (s, 3H); ^{19}F NMR (DMSO-d_6) δ -74.5; ^{13}C NMR (DMSO-d_6) δ 166.3, 165.5, 145.3, 144.6, 141.3, 139.2, 137.6, 135.0 (2C), 129.1, 128.3, 128.1, 126.9, 125.1, 117.7, 54.2, 39.5; *m/z* HRMS (TOF ES$^+$) $C_{21}H_{21}N_4O_5S$ $[MH]^+$ calcd 441.1227, found 441.1233; HPLC 95%

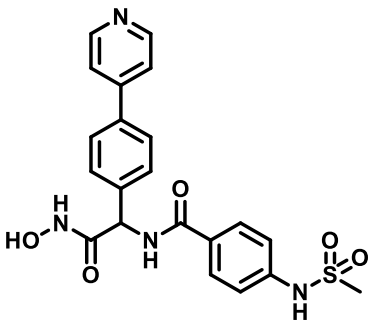

N-(2-(hydroxyamino)-2-oxo-1-(4-(pyridin-4-yl)phenyl)ethyl)-4-(methylsulfonamido)benzamide TFA salt ***(6m)***. Compound **5i** (62.0 mg, 0.141 mmol) was converted to the corresponding hydroxamic acid according to General Procedure F. The crude was purified by preparative HPLC to afford 22.4 mg (36%) of the product as a white solid. ^{1}H NMR (DMSO-d_6) δ 11.11 (s, 1H), 10.14 (s, 1H), 8.90 (d, *J* = 8.1 Hz, 1H), 8.83 (d, *J* = 6.3 Hz, 2H), 8.12 (d, *J* = 6.5 Hz, 2H), 8.04–7.86 (m, 4H), 7.70 (d, *J* = 8.4 Hz, 2H), 7.25 (d, *J* = 8.8 Hz, 2H), 5.70 (d, *J* = 8.1 Hz, 1H),

3.07 (s, 3H) *exchangeable NH proton of hydroxamic acid was not observed; ^{19}F NMR (DMSO-d_6) δ -74.3; ^{13}C NMR (DMSO-d_6) δ 166.4, 165.6, 149.8, 147.1, 141.4, 139.8, 136.4, 129.2, 128.4, 128.2, 126.8, 121.4, 117.8, 54.3, 39.6; *m/z* HRMS (TOF ES$^+$) $C_{21}H_{21}N_4O_5S$ $[MH]^+$ calcd 441.1227, found 441.1223; HPLC 95 %

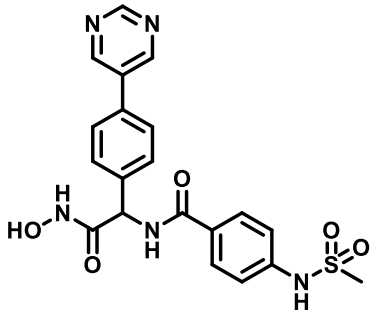

*N-(2-(Hydroxyamino)-2-oxo-1-(4-(pyrimidin-5-yl)phenyl)ethyl)-4-(methylsulfonamido)benzamide TFA salt (**6n**)*. Compound **5j** (87.0 mg, 0.198 mmol) was converted to the corresponding hydroxamic acid according to General Procedure F. The crude was purified by preparative HPLC to afford 12 mg (14%) of the product as a white solid. ^{1}H NMR (DMSO-d_6) δ 11.07 (s, 1H), 10.13 (s, 1H), 9.19 (s, 1H), 9.14 (s, 2H), 8.85 (d, *J* = 8.1 Hz, 1H), 7.92 (d, *J* = 8.7 Hz, 2H), 7.81 (d, *J* = 8.4 Hz, 2H), 7.66 (d, *J* = 8.3 Hz, 2H), 7.25 (d, *J* = 8.7 Hz, 2H), 5.66 (d, *J* = 8.1 Hz, 1H), 3.07 (s, 3H) *exchangeable NH proton of hydroxamic acid was not observed; ^{19}F NMR (DMSO-d_6) δ -74.5; ^{13}C NMR (DMSO-d_6) δ 166.4, 165.6, 154.7, 141.4, 139.4, 133.1, 132.9, 129.2 (2C), 128.4, 128.3, 126.9, 117.7, 54.3, 39.6; *m/z* HRMS (TOF ES$^+$) $C_{20}H_{20}N_5O_5S$ $[MH]^+$ calcd 442.1180, found 442.1166; HPLC 95%

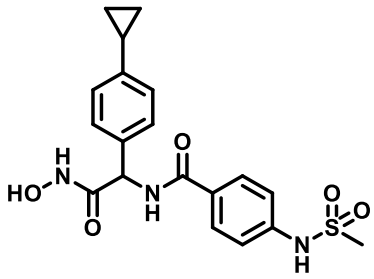

*N-(1-(4-Cyclopropylphenyl)-2-(hydroxyamino)-2-oxoethyl)-4-(methylsulfonamido)benzamide (**6o**)*. Compound **5k** (86.0 mg, 0.214 mmol) was converted to the corresponding hydroxamic acid according to General Procedure F. The crude was purified by column chromatography using DCM/MeOH (100:0 to 90:10) and preparative HPLC to afford 31.8 mg (37%) of the product as a sticky solid. ^{1}H NMR (DMSO-d_6) δ 10.94 (s, 1H), 10.10 (s, 1H), 8.97 (s, 1H), 8.66 (d, *J* = 8.1 Hz, 1H), 7.89 (d, *J* = 8.7 Hz, 2H), 7.36 (d, *J* = 8.1 Hz, 2H), 7.23 (d, *J* = 8.6 Hz, 2H), 7.05 (d, *J* = 8.2 Hz, 2H), 5.53 (d, *J* = 8.1 Hz, 1H), 3.06 (s, 3H), 2.03–1.69 (m, 1H), 1.10–0.86 (m, 2H), 0.76–0.57 (m, 2H); ^{13}C NMR (DMSO-d_6) δ 166.9, 165.4, 143.2, 141.5, 135.4, 129.2, 128.4, 127.3, 125.2, 117.8, 54.3, 39.7, 14.8, 9.4, 9.3; *m/z* HRMS (TOF ES$^+$) $C_{19}H_{22}N_3O_5S$ $[MH]^+$ calcd 404.1275, found 404.1275; HPLC 95%

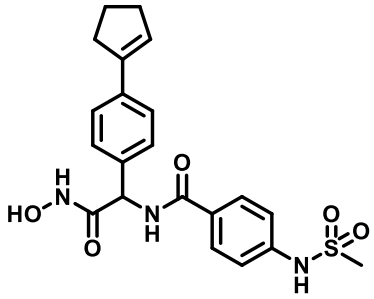

*N-(1-(4-(Cyclopent-1-en-1-yl)phenyl)-2-(hydroxyamino)-2-oxoethyl)-4-(methylsulfonamido)benzamide (**6p**)*. Compound **5l** (150 mg, 350 µmol) was converted to the corresponding hydroxamic acid according to General Procedure F. The crude was purified by a preparative HPLC to obtain 30 mg (20%) of the desired product as a light apricot coloured solid. ^{1}H NMR (DMSO-d_6) δ 11.00 (s, 1H), 10.11 (s, 1H), 9.01 (s, 1H), 8.73 (d, *J* = 8.1 Hz, 1H), 7.90 (d, *J* = 8.7 Hz, 2H), 7.44 (app. s, 4H), 7.24 (d, *J* = 8.7 Hz, 2H), 6.32–6.21 (m, 1H), 5.57 (d, *J* = 8.1 Hz, 1H), 3.06 (s, 3H), 2.71–2.59 (m, 2H), 2.50–2.43 (m, 2H), 2.03–1.87 (m, 2H); ^{13}C NMR (DMSO-d_6) δ 166.7, 165.5, 141.6, 141.4, 137.1, 135.5, 129.2, 128.5, 127.4, 126.1, 125.4, 117.8, 54.4, 39.6, 32.9, 32.7, 22.7; *m/z* HRMS (TOF ES$^+$) $C_{21}H_{24}N_3O_5S$ $[MH]^+$ calcd 430.1431, found 430.1436; HPLC 98%.

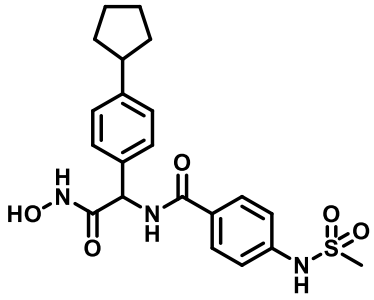

*N-(1-(4-Cyclopentylphenyl)-2-(hydroxyamino)-2-oxoethyl)-4-(methylsulfonamido)benzamide (**6q**)*. Compound **5m** (134 mg, 311 µmol) was converted to the corresponding hydroxamic acid according to General Procedure F. The crude was purified by preparative HPLC to obtain 53 mg (40%) of the desired product as a white solid. ^{1}H NMR (DMSO-d_6) δ 10.96 (s, 1H), 10.11 (s, 1H), 8.97 (s, 1H), 8.67 (d, *J* = 8.1 Hz, 1H), 7.90 (d, *J* = 8.7 Hz, 2H), 7.40 (d, *J* = 8.2 Hz, 2H), 7.38–7.07 (m, 4H), 5.53 (d, *J* = 8.0 Hz, 1H), 3.06 (s, 3H), 2.99–2.86 (m, 1H), 2.07–1.92 (m, 2H), 1.83–1.70 (m, 2H), 1.69–1.57 (m, 2H), 1.58–1.42 (m, 2H); ^{13}C NMR (DMSO-d_6) δ 166.9, 165.5, 145.4, 141.4, 135.9, 129.2, 128.6, 127.3, 126.8, 117.8, 54.4, 45.0, 39.7, 34.3, 25.0; *m/z* HRMS (TOF ES$^+$) $C_{21}H_{26}N_3O_5S$ $[MH]^+$ calcd 432.1576, found 432.1588; HPLC 98%.

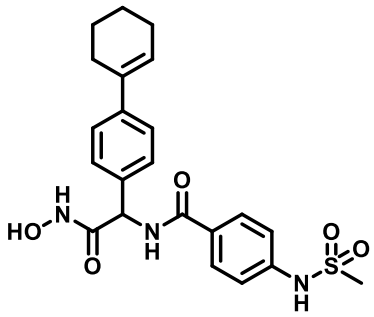

*N-(2-(Hydroxyamino)-2-oxo-1-(2',3',4',5'-tetrahydro-[1,1'-biphenyl]-4-yl)ethyl)-4-(methylsulfonamido)benzamide (**6r**)*. Compound **5n** (120 mg, 271 µmol) was converted to the corresponding hydroxamic acid according to General Procedure F. The crude was purified preparative HPLC to obtain 58 mg (48%) of the desired product as an apricot coloured solid. ^{1}H NMR (DMSO-d_6) δ 10.99 (s, 1H), 10.11 (s, 1H), 9.01 (s, 1H), 8.71 (d, *J* = 8.1 Hz, 1H), 7.91 (d, *J* = 8.7 Hz, 2H), 7.43 (d, *J* = 8.4 Hz, 2H), 7.37 (d, *J* = 8.4 Hz, 2H), 7.24 (d, *J* = 8.7 Hz, 2H), 6.13 (m, 1H), 5.57 (d, *J* = 8.1 Hz, 1H), 3.06 (s, 3H), 2.40–2.23 (m, 2H),

2.26–2.04 (m, 2H), 1.79–1.66 (m, 2H), 1.66–1.48 (m, 2H); ^{13}C NMR (DMSO-d_6) δ 166.8, 165.5, 141.4, 141.3, 136.8, 135.7, 129.2, 128.5, 127.3, 124.6, 124.4, 117.8, 54.3, 39.6, 26.7, 25.3, 22.6, 21.7; *m/z* HRMS (TOF ES$^+$) $C_{22}H_{26}N_3O_5S$ $[MH]^+$ calcd 444.1588, found 444.1600; 95%.

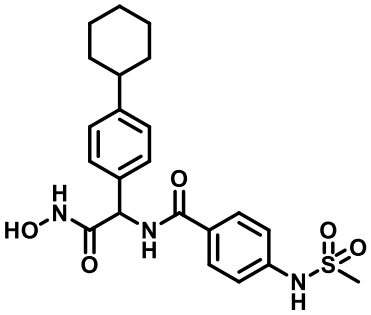

*N-(1-(4-Cyclohexylphenyl)-2-(hydroxyamino)-2-oxoethyl)-4-(methylsulfonamido)benzamide (**6s**)*. Compound **5o** (200 mg, 450 µmol) was converted to the corresponding hydroxamic acid according to General Procedure F. The crude product was purified by a preparative HPLC to obtain 73 mg (36%) of the desired product as a light pink solid. ^{1}H NMR (DMSO-d_6) δ 10.96 (s, 1H), 10.11 (s, 1H), 8.98 (s, 1H), 8.67 (d, *J* = 8.0 Hz, 1H), 7.90 (d, *J* = 8.7 Hz, 2H), 7.40 (d, *J* = 8.2 Hz, 2H), 7.28–7.14 (m, 4H), 5.54 (d, *J* = 8.0 Hz, 1H), 3.06 (s, 3H), 2.49–2.41 (m, 1H), 1.84–1.62 (m, 5H), 1.51–1.13 (m, 5H); ^{13}C NMR (DMSO-d_6) δ 166.9, 165.5, 147.0, 141.4, 135.9, 129.2, 128.5, 127.4, 126.5, 117.8, 54.4, 43.5, 39.6, 33.9, 26.4, 25.6; *m/z* HRMS (TOF ES$^+$) $C_{22}H_{28}N_3O_5S$ $[MH]^+$ calcd 446.1752, found 446.1744; HPLC 97%.

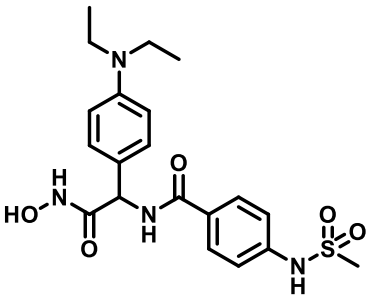

*N-(1-(4-(Diethylamino)phenyl)-2-(hydroxyamino)-2-oxoethyl)-4-(methylsulfonamido)benzamide TFA salt (**6t**)*. Compound **5p** (150 mg, 346 µmol) was converted to the corresponding hydroxamic acid according to General Procedure F. The crude was purified by column chromatography using DCM/MeOH (100:0 to 90:10) followed by preparative HPLC to obtain 88 mg (59%) of the desired product as a white solid. ^{1}H NMR (DMSO-d_6) δ 11.01 (s, 1H), 10.13 (s, 1H), 8.72 (d, *J* = 7.5 Hz, 1H), 7.90 (d, *J* = 8.7 Hz, 2H), 7.51 (br. d, *J* = 6.2 Hz, 2H), 7.31–6.71 (m, 4H), 5.56 (d, *J* = 7.9 Hz, 1H), 3.48 (br. d, *J* = 6.9 Hz, 4H), 3.06 (s, 3H), 1.02 (t, *J* = 7.1 Hz, 6H) *exchangeable NH proton of hydroxamic acid was not observed; ^{19}F NMR (DMSO-d_6) δ -74.5; ^{13}C NMR (DMSO-d_6) δ 166.7, 165.5, 141.4, 129.2, 128.9, 128.5, 117.8 (2C), 54.1, 39.6, 11.2 *Quaternary carbon atoms of the arylamine group and ethylene carbon atom were difficult to observe; *m/z* HRMS (TOF ES$^+$) $C_{20}H_{27}N_4O_5S$ $[M]^+$ calcd 435.1697, found 435.1704; HPLC 95%

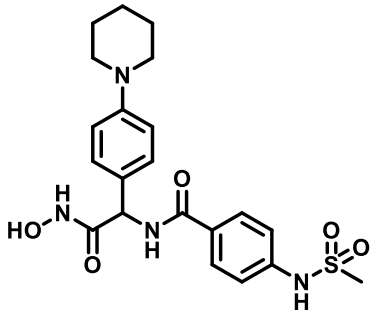

N-(2-(Hydroxyamino)-2-oxo-1-(4-(piperidin-1-yl)phenyl)ethyl)-4-(methylsulfonamido)benzamide ***(6u)***. Compound **5q** (122 mg, 274 µmol) was converted to the corresponding hydroxamic acid according to General Procedure F. The crude was purified by column chromatography using DCM/MeOH (100:0 to 90:10) to obtain 58 mg (48%) of the desired product as a light pink solid. ^{1}H NMR (DMSO-d_6) δ 10.90 (s, 1H), 10.10 (s, 1H), 8.95 (s, 1H), 8.58 (d, *J* = 8.1 Hz, 1H), 7.90 (d, *J* = 8.8 Hz, 2H), 7.31 (d, *J* = 8.8 Hz, 2H), 7.24 (d, *J* = 8.8 Hz, 2H), 6.89 (d, *J* = 8.8 Hz, 2H), 5.47 (d, *J* = 8.0 Hz, 1H), 3.16–3.08 (m, 4H), 3.06 (s, 3H), 1.68–1.46 (m, 6H); ^{13}C NMR (DMSO-d_6) δ 167.3, 165.4, 151.2, 141.3, 129.2, 128.7, 128.1, 117.8, 115.5, 54.1, 49.6, 39.6, 25.1, 24.0; *m/z* HRMS (TOF ES$^+$) $C_{21}H_{27}N_4O_5S$ $[MH]^+$ calcd 447.1697, found 447.1706; HPLC 95%

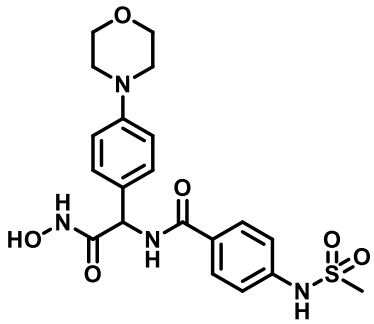

N-(2-(Hydroxyamino)-1-(4-morpholinophenyl)-2-oxoethyl)-4-(methylsulfonamido)benzamide ***(6v)***. Compound **5r** (104 mg, 232 µmol) was converted to the corresponding hydroxamic acid according to General Procedure F. The crude was purified by column chromatography using DCM/MeOH (100:0 to 90:10) to obtain 36 mg (35%) of the desired product as an off-white solid. ^{1}H NMR (DMSO-d_6) δ 10.92 (s, 1H), 10.17 (s, 1H), 8.96 (s, 1H), 8.60 (d, *J* = 8.1 Hz, 1H), 7.90 (d, *J* = 8.8 Hz, 2H), 7.35 (d, *J* = 8.8 Hz, 2H), 7.29–7.12 (m, 2H), 6.92 (d, *J* = 8.8 Hz, 2H), 5.48 (d, *J* = 8.0 Hz, 1H), 3.87–3.51 (m, 4H), 3.10–2.91 (m, 7H); ^{13}C NMR (DMSO-d_6) δ 167.2, 165.4, 150.7, 141.4, 129.2, 129.0, 128.7, 128.2, 117.8, 114.9, 66.1, 54.1, 48.6, 39.6; *m/z* HRMS (TOF ES$^+$) $C_{20}H_{25}N_4O_6S$ $[MH]^+$ calcd 449.1486, found 449.1466; HPLC 99%

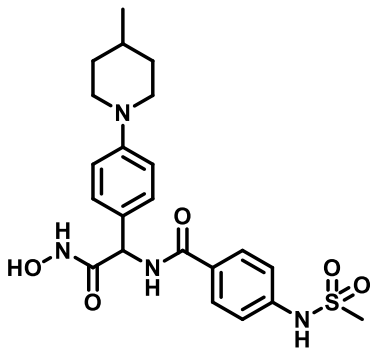

N-(2-(Hydroxyamino)-1-(4-(4-methylpiperidin-1-yl)phenyl)-2-oxoethyl)-4-(methylsulfonamido)benzamide ***(6w)***. Compound **5s** (96 mg, 209 µmol) was converted to the corresponding hydroxamic acid according to General Procedure F The crude was purified by column chromatography using DCM/MeOH (100:0 to 90:10) to obtain 60 mg (63%) of the desired product as a white solid. ^{1}H NMR (DMSO-d_6) δ 10.90 (s, 1H), 10.11 (s, 1H), 8.95 (s, 1H), 8.58 (d, *J* = 8.1 Hz, 1H), 8.01–7.80 (m, 2H), 7.31 (d, *J* = 8.8 Hz, 2H), 7.29–7.15 (m, 2H), 6.89 (d, *J* = 8.9 Hz, 2H), 5.47 (d, *J* = 8.0 Hz, 1H), 3.79–3.53 (m, 2H), 3.06 (s,

3H), 2.62 (td, *J* = 12.3/2.4 Hz, 2H), 1.84–1.58 (m, 2H), 1.48 (ddd, *J* = 11.1/9.0/5.4 Hz, 1H), 1.20 (m, 2H), 0.92 (d, *J* = 6.5 Hz, 3H); ^{13}C NMR (DMSO-d_6) δ 167.3, 165.4, 150.8, 141.3, 129.2, 128.7, 128.2, 128.0, 117.8, 115.3, 54.1, 48.9, 39.6, 33.4, 30.3, 21.8; *m/z* HRMS (TOF ES$^+$) $C_{22}H_{29}N_4O_5S$ $[MH]^+$ calcd 461.1853, found 461.1864; HPLC 95%.

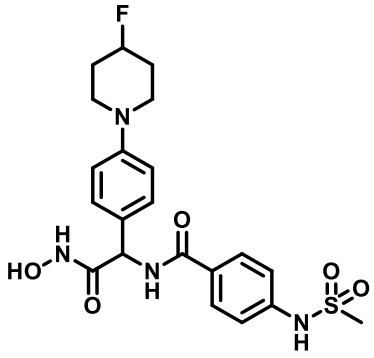

*N-(1-(4-(4-Fluoropiperidin-1-yl)phenyl)-2-(hydroxyamino)-2-oxoethyl)-4-(methylsulfonamido)benzamide (**6x**)*. Compound **5t** (122 mg, 263 µmol) was converted to the corresponding hydroxamic acid according to General Procedure F. The crude was purified by column chromatography using DCM/MeOH (100:0 to 90:10) to obtain 88 mg (72%) of the desired product as an off-white solid. ^{1}H NMR (DMSO-d_6) δ 10.92 (s, 1H), 10.12 (s, 1H), 8.96 (s, 1H), 8.60 (d, *J* = 8.1 Hz, 1H), 8.13–7.77 (m, 2H), 7.33 (d, *J* = 8.8 Hz, 2H), 7.29–7.13 (m, 2H), 6.94 (d, *J* = 8.8 Hz, 2H), 5.48 (d, *J* = 8.0 Hz, 1H), 5.10–4.60 (m, 1H), 3.49–3.26 (m, 2H), 3.17–3.08 (m, 2H), 3.01 (s, 3H), 2.13–1.81 (m, 2H), 1.86–1.60 (m, 2H); ^{19}F NMR (DMSO-d_6) δ -177.1; ^{13}C NMR (DMSO-d_6) δ 167.2, 165.4, 150.1, 141.4, 129.2, 128.7, 128.5, 128.3, 117.8, 115.5, 88.6 (d, J_{CF} = 169.3 Hz), 54.1, 45.1 (d, J_{CF} = 6.8 Hz), 39.6, 30.5 (d, J_{CF} = 18.9 Hz); *m/z* HRMS (TOF ES$^+$) $C_{21}H_{26}FN_4O_5S$ $[MH]^+$ calcd 465.1602, found 465.1592; HPLC 99%

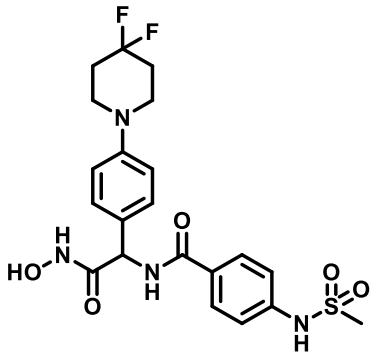

*N-(1-(4-(4,4-Difluoropiperidin-1-yl)phenyl)-2-(hydroxyamino)-2-oxoethyl)-4-(methylsulfonamido)benzamide (**6y**)*. Compound **5u** (108 mg, 224 µmol) was converted to the corresponding hydroxamic acid according to General Procedure F. The crude was purified by column chromatography using DCM/MeOH (100:0 to 90:10) to obtain 76.5 mg (71%) of the desired product as an off-white solid. ^{1}H NMR (DMSO-d_6) δ 10.93 (s, 1H), 10.08 (s, 1H), 8.98 (s, 1H), 8.63 (d, *J* = 8.1 Hz, 1H), 7.91 (d, *J* = 8.8 Hz, 2H), 7.36 (d, *J* = 8.8 Hz, 2H), 7.24 (d, *J* = 8.8 Hz, 2H), 6.98 (d, *J* = 8.8 Hz, 2H), 5.50 (d, *J* = 8.1 Hz, 1H), 3.36–3.28 (m, 4H), 3.06 (s, 3H), 2.02 (ddd, *J* = 19.8/14.0/5.5 Hz, 4H); ^{19}F NMR (DMSO-d_6) δ -95.1; ^{13}C NMR (DMSO-d_6) δ 167.2, 165.4, 149.2, 141.4, 129.2, 129.0, 128.7, 128.3, 122.8 (t, J_{CF} = 240.7/240.7 Hz), 117.8, 115.8, 54.1, 45.8 (t, J_{CF} = 5.1/5.1 Hz), 39.6, 32.8 (t, J_{CF} = 22.4/22.4 Hz); *m/z* HRMS (TOF ES$^+$) $C_{21}H_{25}F_2N_4O_5S$ $[MH]^+$ calcd 483.1508, found 483.1517; HPLC 98%

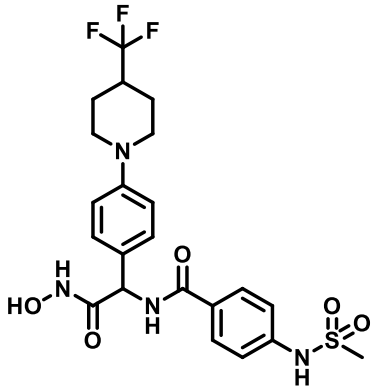

*N-(2-(Hydroxyamino)-2-oxo-1-(4-(4-(trifluoromethyl)piperidin-1-yl)phenyl)ethyl)-4-(methylsulfonamido)benzamide (**6z**)*. Compound **5v** (114 mg, 222 µmol) was converted to the corresponding hydroxamic acid according to General Procedure F. The crude was purified by column chromatography using DCM/MeOH (100:0 to 90:10) and triturated with Et_2O to obtain 55 mg (48%) of the desired product as a white solid. ^{1}H NMR (DMSO-d_6) δ 10.90 (s, 1H), 10.10 (s, 1H), 8.94 (s, 1H), 8.60 (d, *J* = 8.1 Hz, 1H), 7.89 (d, *J* = 8.8 Hz, 2H), 7.33 (d, *J* = 8.7 Hz, 2H), 7.23 (d, *J* = 8.7 Hz, 2H), 6.93 (d, *J* = 8.9 Hz, 2H), 5.47 (d, *J* = 8.1 Hz, 1H), 3.78 (app. d, *J* = 12.6 Hz, 2H), 3.05 (s, 3H), 2.70 (dd, *J* = 12.4/10.5 Hz, 2H), 1.97–1.64 (m, 2H), 1.63–1.43 (m, 2H) *CH of trifluoromethylpiperidine was is hidden under DMSO solvent peak; ^{19}F NMR (DMSO-d_6) δ -72.5; ^{13}C NMR (DMSO-d_6) δ 167.2, 165.4, 150.2, 141.3, 129.1, 128.7, 128.6, 128.2, 126.4, 117.8, 115.7, 54.0, 47.5, 39.6, 38.8–38.1 (m), 23.6; *m/z* HRMS (TOF ES$^+$) $C_{22}H_{26}F_3N_4O_5S$ $[MH]^+$ calcd 515.1571, found 515.1558; HPLC 95%.

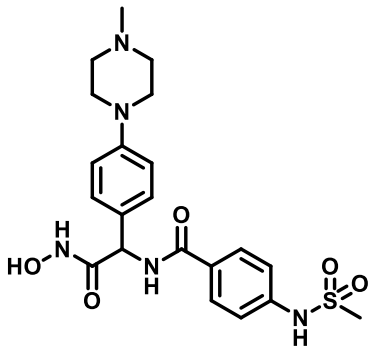

*N-(2-(Hhydroxyamino)-1-(4-(4-methylpiperazin-1-yl)phenyl)-2-oxoethyl)-4-(methylsulfonamido)benzamide TFA salt (**6aa**)*. Compound **5w** (169 mg, 367 µmol) was converted to the corresponding hydroxamic acid according to General Procedure F. Upon completion, the reaction mixture was concentrated *in vacuo*. The residue was purified by preparative HPLC to obtain (63 mg, 37%) of the desired product as a yellow fluffy solid. ^{1}H NMR (DMSO-d_6) δ 10.95 (s, 1H), 10.13 (s, 1H), 9.88 (s, 1H), 8.98 (s, 1H), 8.64 (d, *J* = 8.2 Hz, 1H), 7.88 (d, *J* = 8.7 Hz, 2H), 7.39 (d, *J* = 8.8 Hz, 2H), 7.23 (d, *J* = 8.8 Hz, 2H), 6.98 (d, *J* = 8.8 Hz, 2H), 5.50 (d, *J* = 8.1 Hz, 1H), 3.83 (br. s, 2H), 3.15 (br. s, 2H), 3.06 (s, 3H), 2.94 (br. s, 2H), 2.85 (s, 3H) * CH_2 of 1-methylpiperazine were observed as a broadened signal close to water peak; ^{19}F NMR (DMSO-d_6) δ -73.6; ^{13}C NMR (DMSO-d_6) δ 166.9, 165.3, 148.9, 141.3, 129.9, 129.0, 128.5, 128.2, 117.7, 115.6, 53.8, 52.1, 45.6, 42.0, 39.5; *m/z* HRMS (TOF ES$^+$) $C_{21}H_{28}N_5O_5S$ $[M]^+$ calcd 462.1806, found 462.1815; HPLC 95%.

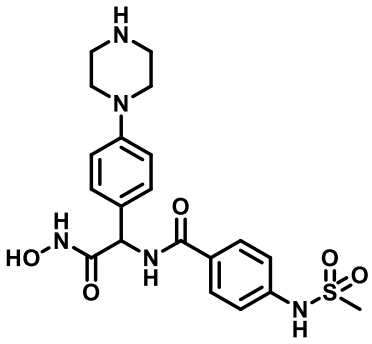

*N-(2-(Hydroxyamino)-2-oxo-1-(4-(piperazin-1-yl)phenyl)ethyl)-4-(methylsulfonamido)benzamide TFA salt (**6ab**)*. Compound **5y** (108 mg, 242 µmol) was converted to the corresponding hydroxamic acid according to General Procedure F. Upon completion the reaction mixture was concentrated *in vacuo* and purified by a preparative HPLC to obtain 67 mg (62%) of the desired product as a yellow solid. ^{1}H NMR (DMSO-d_6) δ 10.92 (s, 1H), 10.10 (s, 1H), 8.89 (s, 2H), 8.60 (d, *J* = 8.0 Hz, 1H), 7.85 (d, *J* = 8.4 Hz, 2H), 7.34 (d, *J* = 8.4 Hz, 2H), 7.20 (d, *J* = 8.5 Hz, 2H), 6.93 (d, *J* = 8.5 Hz, 2H), 5.46 (d, *J* = 8.0 Hz, 1H), 3.29 (br. s, 4H), 3.19 (br. s, 4H), 3.02 (s, 3H); ^{19}F NMR (DMSO-d_6) δ -73.9; ^{13}C NMR (DMSO-d_6) δ 167.0, 165.4, 149.6, 141.4, 123.0, 129.2, 128.6, 128.3, 117.8, 115.8, 54.0, 45.7, 42.6, 39.6; *m/z* HRMS (TOF ES$^+$) $C_{20}H_{26}N_5O_5S$ $[M]^+$ calcd 448.1649, found 448.1657; HPLC 95%.

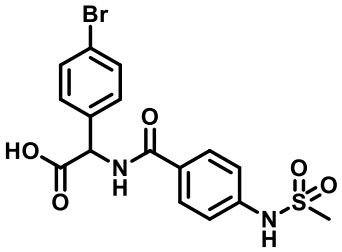

*2-(4-Bromophenyl)-2-(4-(methylsulfonamido)benzamido)acetic acid (**7**)*. To a round bottom flask was added compound **4d** (150 mg, 0.340 mmol), 2 M NaOH (0.680 µL, 1.36 mmol) and 2 mL of THF/EtOH (4:1). The mixture was heated at 50 °C overnight. Upon completion, the reaction mixture was acidified with 2 M HCl until precipitation stopped. Solid was collected by filtration and washed with minimal amount of Et_2O to afford 113 mg (78%) of the titled compound. ^{1}H NMR (DMSO-d_6) δ 13.01 (s, 1H), 10.12 (s, 1H), 8.96 (d, *J* = 7.5 Hz, 1H), 7.89 (d, *J* = 8.8 Hz, 2H), 7.58 (d, *J* = 8.5 Hz, 2H), 7.45 (d, *J* = 8.5 Hz, 2H), 7.24 (d, *J* = 8.8 Hz, 2H), 5.59 (d, *J* = 7.5 Hz, 1H), 3.06 (s, 3H); *m/z* MS $C_{16}H_{14}BrN_2O_5S$ $[M-H]^-$ calcd 425.0, found 424.8.

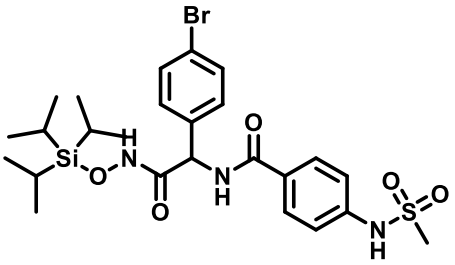

*N-(1-(4-Bromophenyl)-2-oxo-2-(((triisopropylsilyl)oxy)amino)ethyl)-4-(methylsulfonamido)benzamide (**8b**)*. To an oven dried round bottom flask, was added compound **6d** (175 mg, 396 µmol), imidazole (135 mg, 1.98 mmol), DMAP (5 mg) and anhydrous DMF (4 mL). TIPSCl (169 µL, 791 µmol) was added dropwise under inert atmosphere. The mixture was stirred at room temperature for overnight. Upon completion, the reaction mixture was diluted with water (15 mL) and extracted with EtOAc (3 × 10 mL). The combined organic layer was washed with water (2 × 20 mL), brine (10 mL), dried over

anhydrous Na_2SO_4 followed by concentrating *in* vacuo. The crude was purified by column chromatography using PE/EtOAc (100:0 to 50:50) to obtain 118 mg (50%) of the desired product as a white solid. ^{1}H NMR (DMSO-d_6) δ 10.12 (s, 1H), 8.84 (d, J = 8.1 Hz, 1H), 7.97–7.79 (m, 2H), 7.61–7.52 (m, 2H), 7.45 (d, J = 8.5 Hz, 2H), 7.29–7.17 (m, 2H), 5.65 (d, J = 8.1 Hz, 1H), 3.06 (s, 3H), 1.12–1.01 (m, 3H), 1.00–0.93 (m, 18H); ^{13}C NMR (DMSO-d_6) δ 165.6, 165.5, 141.5, 137.6, 131.1, 129.6, 129.2, 128.3, 120.8, 117.7, 56.9, 39.6, 17.4, 11.1.

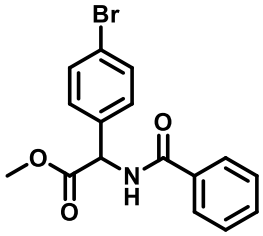

*Methyl 2-benzamido-2-(4-bromophenyl)acetate (**12**)*. Benzoic acid (300 mg, 2.46 mmol) was coupled to compound **1d** (500 mg, 2.05 mmol) according to General Procedure B. The crude was purified by column chromatography using PE/EtOAc (100:0 to 50:50) as eluent to afford 573 mg (80%) of the desired product as a yellow sticky solid. ^{1}H NMR (DMSO-d_6) δ 9.22 (d, J = 7.2 Hz, 1H), 7.90 (m, 2H), 7.64–7.53 (m, 3H), 7.51–7.42 (m, 4H), 5.70 (d, J = 7.2 Hz, 1H), 3.67 (s, 3H); ^{13}C NMR (DMSO d_6) δ 170.7, 166.4, 135.8, 133.4, 131.6, 131.5, 130.5, 128.3, 127.7, 121.6, 56.2, 52.4; *m/z* MS $C_{16}H_{15}BrNO_3$ $[MH]^+$ calcd 348.0, found 347.8

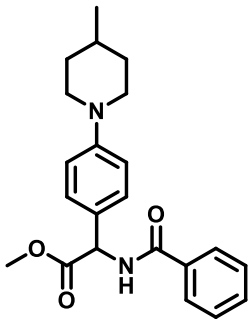

*Methyl 2-benzamido-2-(4-(4-methylpiperidin-1-yl)phenyl)acetate (**13a**)*. 4-Methylpiperidine (85.0 µL, 718 mmol) was coupled to compound **12** (100 mg, 287 mmol) according to General Procedure D to obtain 43 mg (41%) of the desired product as an orange oil. ^{1}H NMR ($CDCl_3$) δ 7.85–7.72 (m, 2H), 7.57–7.47 (m, 1H), 7.45–7.39 (m, 2H), 7.32 (d, J = 8.6 Hz, 2H), 7.10–6.95 (m, 3H), 5.67 (d, J = 6.9 Hz, 1H), 3.75 (s, 3H), 3.65 (br. d, J = 12.4 Hz, 2H), 2.75 (br. t, J = 11.6 Hz, 2H), 1.74 (br. d, J = 11.6 Hz, 2H), 1.62–1.45 (m, 2H), 1.32–1.21 (m, 1H), 0.98 (d, J = 6.3 Hz, 3H); ^{13}C NMR ($CDCl_3$) δ 171.8, 166.7, 150.0, 133.8, 132.0, 131.9, 128.7 (2C), 128.5, 127.3, 56.4, 52.9, 34.6, 33.5, 30.5, 21.8; *m/z* MS $C_{22}H_{27}N_2O3$ $[MH]^+$ calcd 367.2, found 367.2

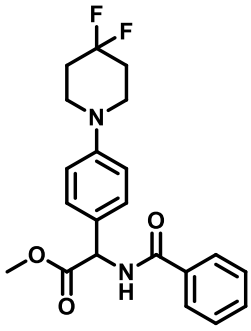

*Methyl 2-benzamido-2-(4-(4,4-difluoropiperidin-1-yl)phenyl)acetate (**13b**)*. 4,4-Difluoropiperidine hydrochloride (113 mg, 718 mmol) was coupled to compound **12** (100 mg, 287 mmol) according to General Procedure D. The crude product was purified by column chromatography using PET/EtOAc (100:0 to 60:40) to afford 80 mg (72%) of the desired compound as a brown oil. ^{1}H NMR (DMSO-d_6) δ 9.07 (d, J = 6.9 Hz, 1H), 7.91 (m, 2H), 7.59–7.50 (m, 1H), 7.49–7.42 (m, 2H), 7.34 (d, J = 8.7 Hz, 2H), 7.04 (d, J = 8.8 Hz, 2H), 5.54 (d, J = 6.9 Hz, 1H), 3.64 (s, 3H), 3.44–3.28 (m, 4H), 2.05 (ddd, J = 19.8/14.1/5.6 Hz, 4H); ^{19}F NMR (DMSO-d_6) δ -95.2; ^{13}C NMR (DMSO-d_6) δ 171.4, 166.5, 149.2, 133.6, 131.5, 129.2, 128.2, 127.7, 126.7, 122.7 (t, J_{CF} = 240.7/240.7 Hz), 116.0, 56.4, 52.1, 45.7 (t, J_{CF} = 4.9/4.9Hz), 32.8 (t, J_{CF} = 22.5/22.5 Hz); *m/z* MS $C_{21}H_{23}F_2N_2O_3$ $[MH]^+$ calcd 389.2, found 389.0

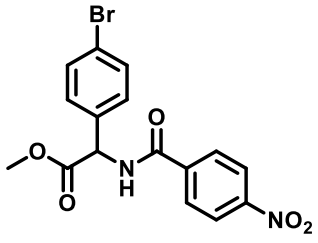

*Methyl 2-(4-bromophenyl)-2-(4-nitrobenzamido)acetate (**14**)*. 4-Nitrobenzoic acid (411 mg, 2.46 mmol) was coupled to compound **1d** according to General Procedure B. The crude was triturated from Et_2O with minimal wash with MeOH to afford 659 mg (82%) of the desired compound as a white solid. ^{1}H NMR (DMSO-d_6) δ 9.59 (d, J = 7.0 Hz, 1H), 8.39–8.25 (m, 2H), 8.15–7.96 (m, 2H), 7.69–7.55 (m, 2H), 7.53–7.24 (m, 2H), 5.72 (d, J = 7.0 Hz, 1H), 3.68 (s, 3H); ^{13}C NMR (DMSO-d_6) δ 170.4, 164.9, 149.3, 139.0, 135.3, 131.5, 130.5, 129.2, 123.5, 121.7, 56.4, 52.5; *m/z* MS $C_{16}H_{14}BrN_2O_5$ $[MH]^+$ calcd 393.0, found 392.7.

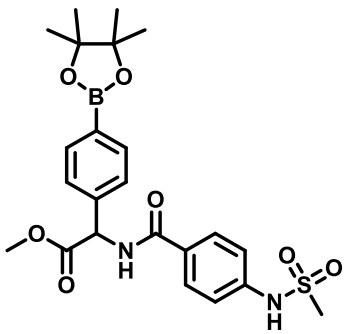

*Methyl 2-(4-(methylsulfonamido)benzamido)-2-(4-(4,4,5,5-tetramethyl-1,3,2-dioxaborolan-2-yl)phenyl)acetate (**19**)*. Compound **4d** (960 mg, 2.18 mmol), AcOK (641 mg, 6.53 mmol), Bis_2Pin_2 (663 mg, 2.61 mmol), Pd(dppf)Cl_2.DCM (107 mg, 131 µmol), and DPPF (169 mg, 305 µmol) were suspended in anhydrous 1,4-dioxane (40 mL) and purged through N_2 for 5 min before heated at reflux for 2 days. Upon completion, the mixture was filtered through Celite and washed with EtOAc followed by concentration under reduced pressure. The crude was purified by column chromatography using PE/EtOAc (50:50 to 0:100) to obtain 736 mg (69%) of a mixture of the desired product as a pale yellow solid. ^{1}H NMR (DMSO-d_6) δ 10.14 (s, 1H), 9.09 (d, J = 7.2 Hz, 1H), 8.13–7.81 (m, 2H), 7.69 (d, J = 8.1 Hz,

2H), 7.49 (d, *J* = 8.1 Hz, 2H), 7.25 (d, *J* = 8.7 Hz, 2H), 5.70 (d, *J* = 7.2 Hz, 1H), 3.65 (s, 3H), 3.06 (s, 3H), 1.29 (s, 12H); ^{13}C NMR (DMSO-d_6) δ 170.9, 165.8, 141.5, 139.6, 134.6, 129.2, 128.1, 127.7, 117.8, 83.7, 56.8, 52.3, 39.6, 24.6; *m/z* MS $C_{23}H_{30}BN_2O_7S$ $[MH]^+$ calcd 489.2 found 489.0.

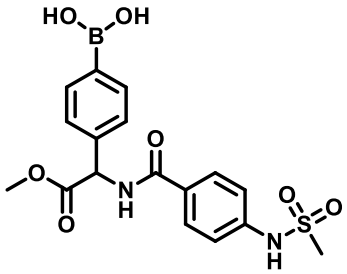

*(4-(2-Methoxy-1-(4-(methylsulfonamido)benzamido)-2-oxoethyl)phenyl)boronic acid (**20**)*. Boronic acid **19** (284 mg, 582 µmol), ammonium acetate (112 mg, 1.45 mmol) and sodium periodate (249 mg, 1.16 mmol) were stirred in acetone/water (1:1, 20 mL) for overnight. Upon completion, acetone was removed under reduced pressure and acidified to pH 3 with 1 M HCl. The mixture was extracted with EtOAc (3 × 20 mL), dried over anhydrous Na_2SO_4, and concentrated *in vacuo* to afford 116 mg (49%) of the desired product as a pale orange solid. ^{1}H NMR (DMSO-d_6) δ 10.13 (s, 1H), 9.04 (d, *J* = 7.1 Hz, 1H), 8.07 (s, 2H), 7.90 (d, *J* = 8.8 Hz, 2H), 7.79 (d, *J* = 8.1 Hz, 2H), 7.42 (d, *J* = 8.1 Hz, 2H), 7.24 (d, *J* = 8.8 Hz, 2H), 5.65 (d, *J* = 7.1 Hz, 1H), 3.65 (s, 3H), 3.06 (s, 3H); ^{13}C NMR (DMSO-d_6) δ 171.1, 165.8, 141.5, 137.8, 134.3, 129.2, 128.2, 127.2, 117.8, 56.9, 52.2, 39.6; *m/z* MS $C_{17}H_{20}BN_2O_7S$ $[MH]^+$ calcd 407.1 found 406.9.

3.7.3 Computational Chemistry

Molecular dockings of compounds **6a**, **6e**, **6f**, **6m**, **6o**, **6s**, and **6ab** were carried out using Surflex docking interfaced with SYBYL2.1.1 in SFXC mode. The final pose obtained from MD simulations of **6ad**-APN complex (in *Chapter 2*) was selected as the template structure for grid generation and ligand dockings. The coordinates of compound **6ad** bound to APN was extracted for the later use of fragment constraints. To prepare the modelled structure, water molecules were removed, and sidechain amides were protonated and fixed alongside charge addition using Gasteiger-Marsli method.[252] The charge for zinc metal was set to 2.0. The 2D ligand structures of **6a**, **6e**, **6f**, **6m**, **6o**, **6s**, and **6ab** were prepared with default settings from SYBYL2.1.1. In grid generation, the hydroxamic acid was set as fragment constraints with a constraint penalty of 10. A total of 20 poses were produced for each ligand. The coordination of hydroxamic acid to catalytic zinc ion and the positions of biaryl or alky-aryl scaffolds were manually examined. The binding poses that showed the highest total docking score were selected for more detailed analysis of predicted binding interactions between the ligand and APN.

3.8 Appendices

A. Anti-proliferative activities of **6c**, **6e**, **6f**, **6i**, **6n**, **6o**, **6q**, **6s**, **6x**, and **6b** at 10 µM. The data was generated and analysed by NCI.

Developmental Therapeutics Program
One Dose Mean Graph

NSC: D-814547 / 1	**Conc:** 1.00E-5 Molar	**Test Date:** Apr 29, 2019
Experiment ID: 1904OS99		**Report Date:** May 16, 2019

Panel/Cell Line	Growth Percent
Leukemia	
CCRF-CEM	109.59
HL-60(TB)	112.17
K-562	107.40
MOLT-4	103.21
RPMI-8226	101.08
SR	128.47
Non-Small Cell Lung Cancer	
A549/ATCC	103.36
EKVX	99.68
HOP-62	99.90
HOP-92	96.62
NCI-H23	97.29
NCI-H322M	97.71
NCI-H460	109.20
NCI-H522	100.96
Colon Cancer	
COLO 205	108.87
HCC-2998	93.24
HCT-116	99.54
HCT-15	96.56
HT29	102.74
KM12	106.94
SW-620	101.06
CNS Cancer	
SF-268	100.43
SF-295	96.25
SF-539	96.03
SNB-19	95.20
SNB-75	97.44
U251	101.22
Melanoma	
LOX IMVI	94.17
MALME-3M	95.52
M14	108.15
MDA-MB-435	105.51
SK-MEL-2	109.72
SK-MEL-28	100.73
SK-MEL-5	98.93
UACC-257	101.86
UACC-62	94.71
Ovarian Cancer	
IGROV1	101.06
OVCAR-3	107.41
OVCAR-4	96.82
OVCAR-5	87.43
OVCAR-8	108.09
NCI/ADR-RES	99.90
SK-OV-3	102.99
Renal Cancer	
786-0	91.29
A498	100.35
ACHN	97.32
CAKI-1	95.75
RXF 393	121.56
SN12C	98.67
TK-10	102.79
UO-31	91.14
Prostate Cancer	
PC-3	98.48
DU-145	105.42
Breast Cancer	
MCF7	96.64
MDA-MB-231/ATCC	102.75
HS 578T	101.48
BT-549	103.00
T-47D	88.81
MDA-MB-468	95.03
Mean	101.11
Delta	13.68
Range	41.04

Mean Growth Percent - Growth Percent

150 100 50 0 -50 -100 -150

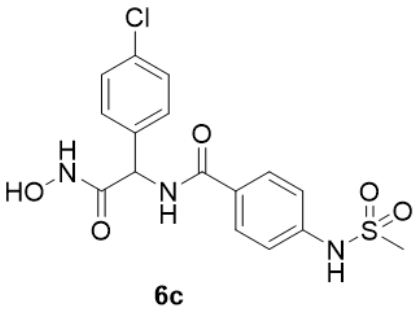

6c

Developmental Therapeutics Program	NSC: D-814548 / 1	Conc: 1.00E-5 Molar	Test Date: Apr 29, 2019
One Dose Mean Graph	Experiment ID: 1904OS99		Report Date: May 16, 2019

Panel/Cell Line	Growth Percent
Leukemia	
CCRF-CEM	97.32
HL-60(TB)	103.79
K-562	97.87
MOLT-4	97.54
RPMI-8226	108.10
SR	115.52
Non-Small Cell Lung Cancer	
A549/ATCC	107.20
EKVX	96.13
HOP-62	98.32
HOP-92	102.97
NCI-H23	97.49
NCI-H322M	99.79
NCI-H460	106.42
NCI-H522	95.74
Colon Cancer	
COLO 205	89.67
HCC-2998	104.80
HCT-116	101.60
HCT-15	104.43
HT29	107.08
KM12	106.25
SW-620	96.97
CNS Cancer	
SF-268	96.42
SF-295	99.61
SF-539	92.80
SNB-19	95.45
SNB-75	112.19
U251	98.11
Melanoma	
LOX IMVI	95.65
MALME-3M	94.29
M14	100.94
MDA-MB-435	104.46
SK-MEL-2	108.59
SK-MEL-28	99.23
SK-MEL-5	96.19
UACC-257	104.85
UACC-62	93.82
Ovarian Cancer	
IGROV1	100.97
OVCAR-3	94.90
OVCAR-4	98.45
OVCAR-5	95.84
OVCAR-8	102.95
NCI/ADR-RES	99.75
SK-OV-3	106.07
Renal Cancer	
786-0	95.84
A498	96.64
ACHN	98.92
CAKI-1	97.74
RXF 393	113.34
SN12C	103.81
TK-10	101.13
UO-31	92.12
Prostate Cancer	
PC-3	101.61
DU-145	103.96
Breast Cancer	
MCF7	92.51
MDA-MB-231/ATCC	105.84
HS 578T	105.49
BT-549	108.33
T-47D	76.68
MDA-MB-468	96.74
Mean	100.29
Delta	23.61
Range	38.84

Mean Growth Percent - Growth Percent

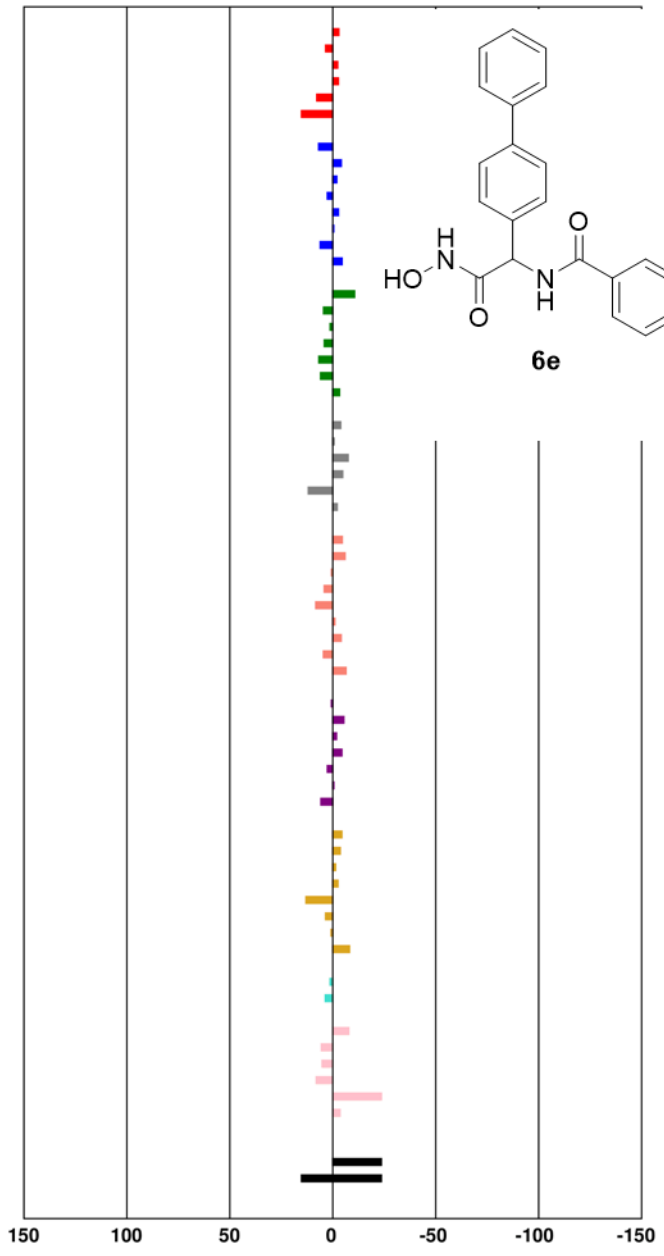

6e

Developmental Therapeutics Program

One Dose Mean Graph

NSC: D-814549 / 1	Conc: 1.00E-5 Molar	Test Date: Apr 29, 2019
Experiment ID: 1904OS99		Report Date: May 16, 2019

Panel/Cell Line	Growth Percent
Leukemia	
CCRF-CEM	95.09
HL-60(TB)	103.17
K-562	89.96
MOLT-4	103.12
RPMI-8226	82.82
SR	78.84
Non-Small Cell Lung Cancer	
A549/ATCC	103.09
EKVX	97.40
HOP-62	99.11
HOP-92	-8.77
NCI-H23	45.60
NCI-H322M	53.51
NCI-H460	89.69
NCI-H522	30.03
Colon Cancer	
COLO 205	109.27
HCC-2998	62.58
HCT-116	39.08
HCT-15	91.54
HT29	53.22
KM12	58.21
SW-620	51.25
CNS Cancer	
SF-268	47.26
SF-295	93.67
SF-539	92.61
SNB-19	45.21
SNB-75	24.78
U251	94.11
Melanoma	
LOX IMVI	44.80
MALME-3M	92.01
M14	85.28
MDA-MB-435	54.54
SK-MEL-2	73.56
SK-MEL-28	91.84
SK-MEL-5	48.01
UACC-257	100.65
UACC-62	78.97
Ovarian Cancer	
IGROV1	39.60
OVCAR-3	64.69
OVCAR-4	70.88
OVCAR-5	31.63
OVCAR-8	97.28
NCI/ADR-RES	66.62
SK-OV-3	108.09
Renal Cancer	
786-0	72.83
A498	95.65
ACHN	58.65
CAKI-1	49.87
RXF 393	106.43
SN12C	75.27
TK-10	30.32
UO-31	19.32
Prostate Cancer	
PC-3	86.89
DU-145	83.47
Breast Cancer	
MCF7	66.75
MDA-MB-231/ATCC	42.10
HS 578T	72.95
BT-549	94.12
T-47D	82.44
MDA-MB-468	95.03
Mean	71.29
Delta	80.06
Range	118.04

Mean Growth Percent - Growth Percent

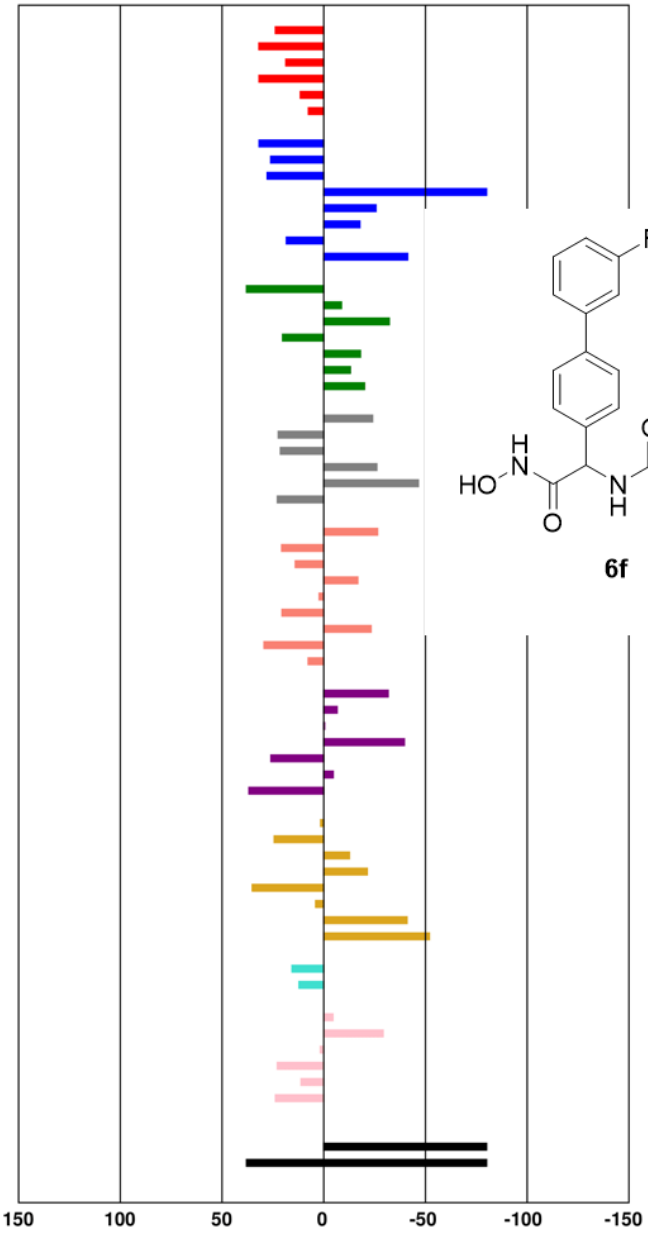

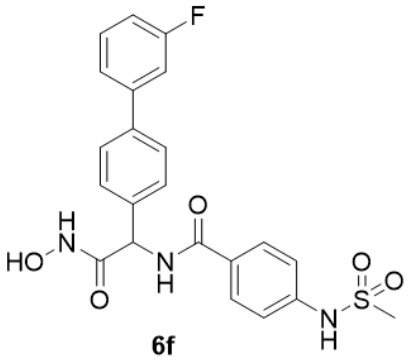

6f

Developmental Therapeutics Program

One Dose Mean Graph

NSC: D-814550 / 1	Conc: 1.00E-5 Molar	Test Date: Apr 29, 2019
Experiment ID: 1904OS99		Report Date: May 16, 2019

Panel/Cell Line	Growth Percent
Leukemia	
CCRF-CEM	85.89
HL-60(TB)	100.39
K-562	94.59
MOLT-4	98.58
RPMI-8226	96.92
SR	101.47
Non-Small Cell Lung Cancer	
A549/ATCC	102.60
EKVX	102.86
HOP-62	101.81
HOP-92	124.05
NCI-H23	102.48
NCI-H322M	96.04
NCI-H460	102.41
NCI-H522	96.08
Colon Cancer	
COLO 205	109.36
HCC-2998	108.80
HCT-116	98.29
HCT-15	102.44
HT29	108.04
KM12	103.07
SW-620	97.78
CNS Cancer	
SF-268	93.15
SF-295	102.47
SF-539	102.18
SNB-19	90.35
SNB-75	111.84
U251	95.30
Melanoma	
LOX IMVI	89.87
MALME-3M	101.01
M14	100.52
MDA-MB-435	104.89
SK-MEL-2	115.61
SK-MEL-28	100.82
SK-MEL-5	97.25
UACC-257	104.21
UACC-62	90.98
Ovarian Cancer	
IGROV1	96.10
OVCAR-3	94.51
OVCAR-4	96.38
OVCAR-5	104.52
OVCAR-8	91.47
NCI/ADR-RES	95.89
SK-OV-3	118.36
Renal Cancer	
786-0	101.50
A498	104.91
ACHN	101.76
CAKI-1	97.89
RXF 393	97.95
SN12C	95.94
TK-10	109.90
UO-31	79.67
Prostate Cancer	
PC-3	94.00
DU-145	109.69
Breast Cancer	
MCF7	87.96
MDA-MB-231/ATCC	91.23
HS 578T	101.84
BT-549	105.00
T-47D	79.15
MDA-MB-468	86.53
Mean	99.60
Delta	20.45
Range	44.90

Mean Growth Percent - Growth Percent

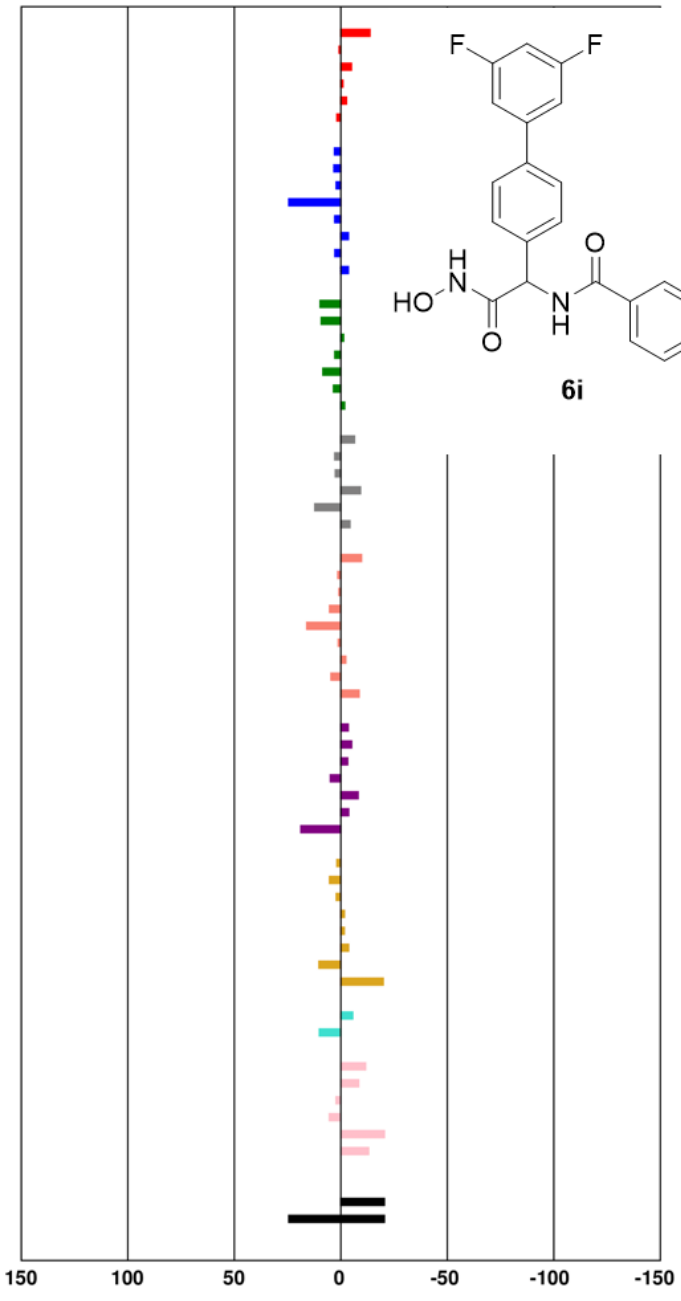

6i

Developmental Therapeutics Program

One Dose Mean Graph

NSC: D-814552 / 1	Conc: 1.00E-5 Molar	Test Date: Apr 29, 2019
Experiment ID: 1904OS99		Report Date: May 16, 2019

Panel/Cell Line	Growth Percent
Leukemia	
CCRF-CEM	107.23
HL-60(TB)	105.58
K-562	104.00
MOLT-4	100.45
RPMI-8226	105.59
SR	115.89
Non-Small Cell Lung Cancer	
A549/ATCC	102.09
EKVX	103.24
HOP-62	116.02
HOP-92	108.06
NCI-H23	108.04
NCI-H322M	95.37
NCI-H460	116.23
NCI-H522	108.68
Colon Cancer	
COLO 205	114.91
HCC-2998	100.66
HCT-116	112.56
HCT-15	103.24
HT29	104.63
KM12	102.54
SW-620	107.01
CNS Cancer	
SF-268	102.59
SF-295	99.47
SF-539	96.43
SNB-19	93.30
SNB-75	101.20
U251	108.28
Melanoma	
LOX IMVI	96.95
MALME-3M	93.16
M14	113.87
MDA-MB-435	104.94
SK-MEL-2	126.12
SK-MEL-28	105.13
SK-MEL-5	101.23
UACC-257	102.55
UACC-62	95.08
Ovarian Cancer	
IGROV1	94.57
OVCAR-3	102.60
OVCAR-4	106.14
OVCAR-5	93.95
OVCAR-8	103.58
NCI/ADR-RES	105.67
SK-OV-3	116.75
Renal Cancer	
786-0	106.19
A498	105.92
ACHN	98.49
CAKI-1	96.04
RXF 393	116.65
SN12C	97.57
TK-10	107.36
UO-31	87.00
Prostate Cancer	
PC-3	98.83
DU-145	106.42
Breast Cancer	
MCF7	97.39
MDA-MB-231/ATCC	108.95
HS 578T	106.77
BT-549	120.80
T-47D	104.33
MDA-MB-468	97.85
Mean	104.44
Delta	17.44
Range	39.12

Mean Growth Percent - Growth Percent

6n

Developmental Therapeutics Program

One Dose Mean Graph

NSC: D-814551 / 1	Conc: 1.00E-5 Molar	Test Date: Apr 29, 2019
Experiment ID: 1904OS99		Report Date: May 16, 2019

Panel/Cell Line	Growth Percent
Leukemia	
CCRF-CEM	104.19
HL-60(TB)	101.45
K-562	83.06
MOLT-4	99.33
RPMI-8226	108.78
SR	115.54
Non-Small Cell Lung Cancer	
A549/ATCC	100.96
EKVX	104.05
HOP-62	96.52
HOP-92	105.61
NCI-H23	97.28
NCI-H322M	97.92
NCI-H460	105.79
NCI-H522	99.03
Colon Cancer	
COLO 205	119.92
HCC-2998	103.67
HCT-116	105.45
HCT-15	108.72
HT29	100.41
KM12	103.93
SW-620	99.74
CNS Cancer	
SF-268	101.36
SF-295	98.05
SF-539	100.98
SNB-19	96.91
SNB-75	94.19
U251	104.85
Melanoma	
LOX IMVI	95.12
MALME-3M	96.77
M14	104.16
MDA-MB-435	107.27
SK-MEL-2	105.90
SK-MEL-28	103.76
SK-MEL-5	100.20
UACC-257	102.96
UACC-62	96.82
Ovarian Cancer	
IGROV1	97.49
OVCAR-3	105.27
OVCAR-4	104.06
OVCAR-5	98.94
OVCAR-8	98.32
NCI/ADR-RES	98.79
SK-OV-3	103.61
Renal Cancer	
786-0	104.86
A498	106.61
ACHN	98.24
CAKI-1	98.17
RXF 393	107.07
SN12C	97.06
TK-10	103.52
UO-31	94.94
Prostate Cancer	
PC-3	90.31
DU-145	113.05
Breast Cancer	
MCF7	96.01
MDA-MB-231/ATCC	113.70
HS 578T	105.75
BT-549	114.71
T-47D	92.94
MDA-MB-468	96.06
Mean	101.87
Delta	18.81
Range	36.86

Mean Growth Percent - Growth Percent

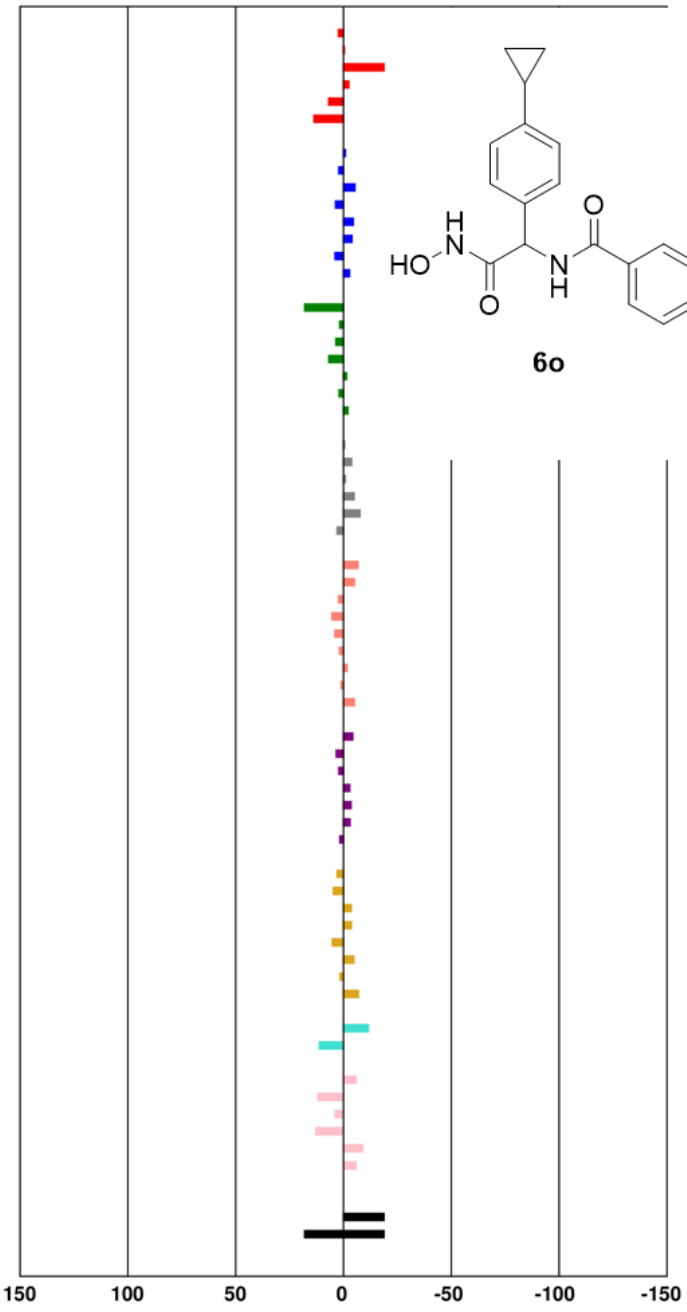

6o

Developmental Therapeutics Program

One Dose Mean Graph

NSC: D-814553 / 1	Conc: 1.00E-5 Molar	Test Date: Apr 29, 2019
Experiment ID: 1904OS99		Report Date: May 16, 2019

Panel/Cell Line	Growth Percent
Leukemia	
CCRF-CEM	83.18
HL-60(TB)	96.87
K-562	50.33
MOLT-4	97.34
RPMI-8226	91.25
SR	132.52
Non-Small Cell Lung Cancer	
A549/ATCC	107.58
EKVX	104.69
HOP-62	77.37
HOP-92	103.02
NCI-H23	92.60
NCI-H322M	98.02
NCI-H460	106.00
NCI-H522	90.17
Colon Cancer	
COLO 205	116.05
HCC-2998	99.85
HCT-116	94.63
HCT-15	104.40
HT29	99.06
KM12	110.42
SW-620	95.50
CNS Cancer	
SF-268	95.09
SF-295	99.83
SF-539	95.61
SNB-19	95.84
SNB-75	106.29
U251	98.45
Melanoma	
LOX IMVI	68.22
MALME-3M	94.08
M14	101.37
MDA-MB-435	102.46
SK-MEL-2	105.74
SK-MEL-28	92.48
SK-MEL-5	99.49
UACC-257	105.50
UACC-62	93.66
Ovarian Cancer	
IGROV1	94.47
OVCAR-3	96.74
OVCAR-4	94.83
OVCAR-5	93.37
OVCAR-8	103.93
NCI/ADR-RES	97.29
SK-OV-3	119.59
Renal Cancer	
786-0	104.53
A498	92.09
ACHN	96.62
CAKI-1	97.20
RXF 393	116.43
SN12C	96.89
TK-10	105.20
UO-31	85.80
Prostate Cancer	
PC-3	91.19
DU-145	113.68
Breast Cancer	
MCF7	92.94
MDA-MB-231/ATCC	100.84
HS 578T	97.32
BT-549	100.36
T-47D	77.53
MDA-MB-468	90.18
Mean	97.69
Delta	47.36
Range	82.19

Mean Growth Percent - Growth Percent

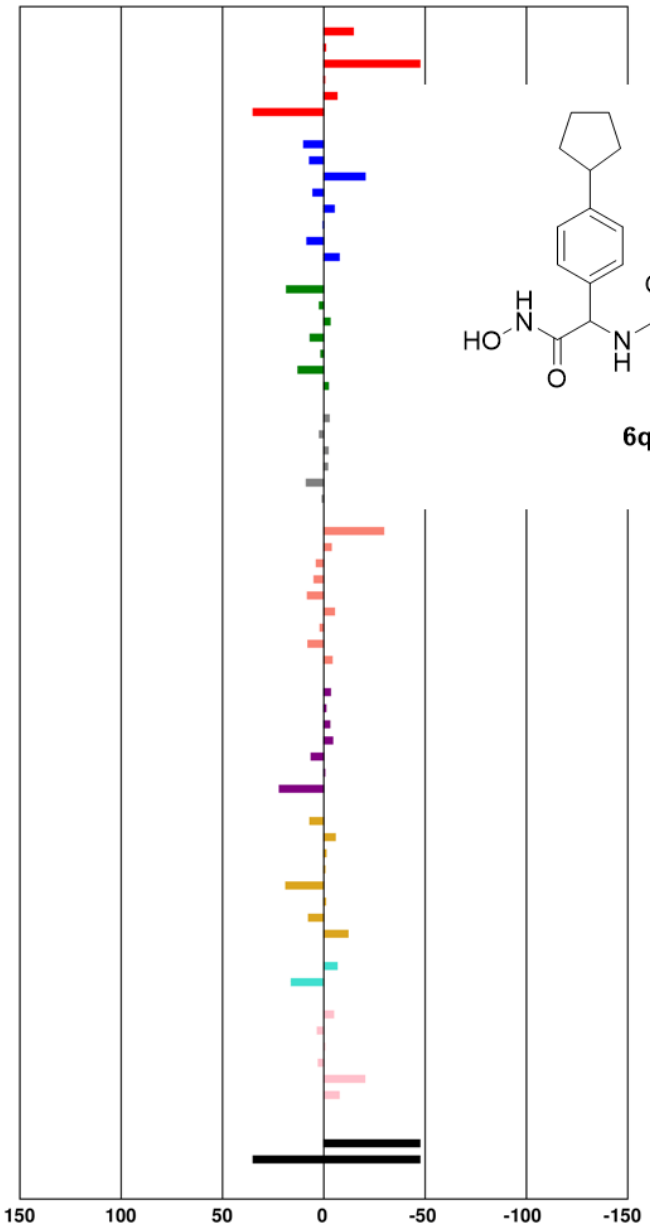

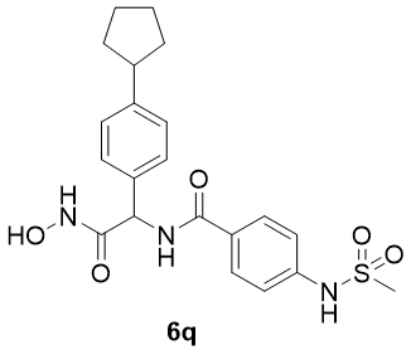

6q

Developmental Therapeutics Program

One Dose Mean Graph

NSC: D-814554 / 1	Conc: 1.00E-5 Molar	Test Date: Apr 29, 2019
Experiment ID: 1904OS99		Report Date: May 16, 2019

Panel/Cell Line	Growth Percent
Leukemia	
CCRF-CEM	66.41
HL-60(TB)	95.81
K-562	66.25
MOLT-4	87.37
RPMI-8226	83.38
SR	98.33
Non-Small Cell Lung Cancer	
A549/ATCC	100.12
EKVX	98.69
HOP-62	90.32
HOP-92	98.97
NCI-H23	100.55
NCI-H322M	94.57
NCI-H460	107.74
NCI-H522	93.26
Colon Cancer	
COLO 205	117.29
HCC-2998	90.90
HCT-116	98.34
HCT-15	102.06
HT29	104.92
KM12	102.23
SW-620	93.79
CNS Cancer	
SF-268	82.10
SF-295	101.11
SF-539	96.51
SNB-19	91.40
SNB-75	98.82
U251	84.12
Melanoma	
LOX IMVI	78.41
MALME-3M	91.84
M14	102.64
MDA-MB-435	100.49
SK-MEL-2	108.48
SK-MEL-28	95.97
SK-MEL-5	93.45
UACC-257	100.75
UACC-62	88.51
Ovarian Cancer	
IGROV1	96.96
OVCAR-3	86.30
OVCAR-4	93.32
OVCAR-5	97.70
OVCAR-8	93.52
NCI/ADR-RES	98.66
SK-OV-3	117.46
Renal Cancer	
786-0	93.43
A498	104.16
ACHN	97.12
CAKI-1	101.20
RXF 393	92.89
SN12C	96.82
TK-10	110.19
UO-31	83.92
Prostate Cancer	
PC-3	84.10
DU-145	106.89
Breast Cancer	
MCF7	88.45
MDA-MB-231/ATCC	103.80
HS 578T	100.19
BT-549	93.20
T-47D	78.84
MDA-MB-468	85.11
Mean	95.09
Delta	28.84
Range	51.21

Mean Growth Percent - Growth Percent

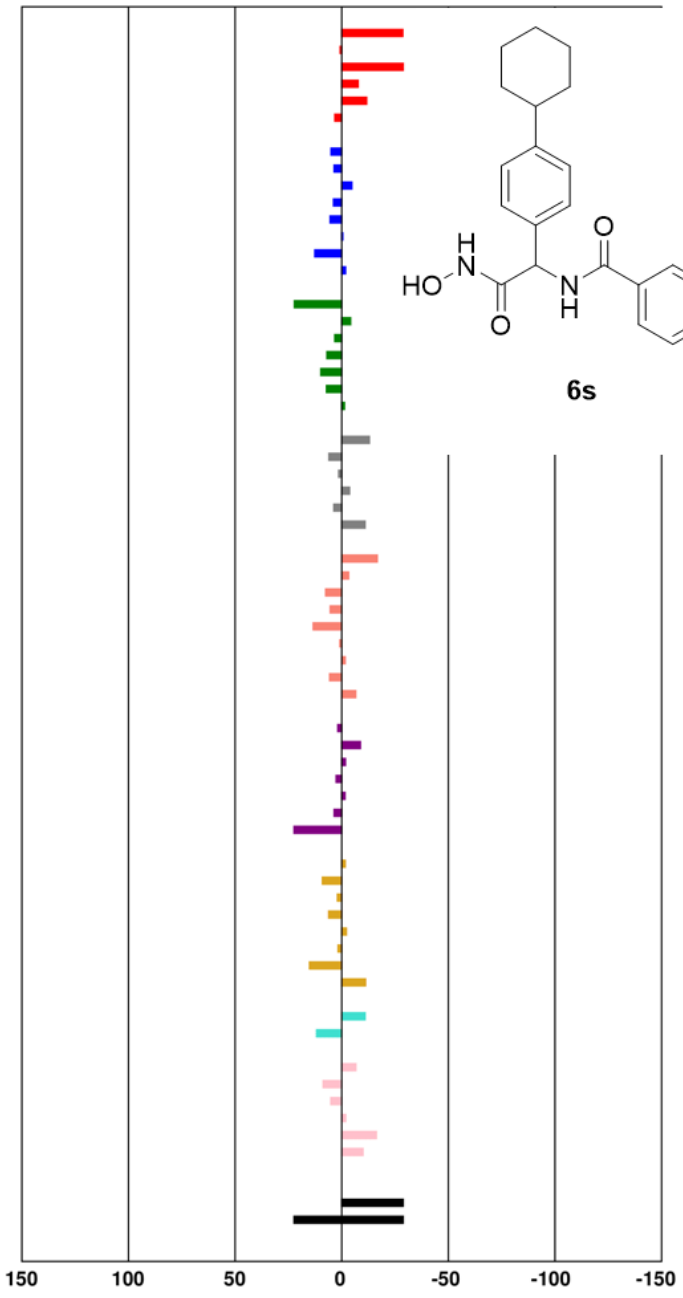

6s

Developmental Therapeutics Program

One Dose Mean Graph

NSC: D-814555 / 1	Conc: 1.00E-5 Molar	Test Date: Apr 29, 2019
Experiment ID: 1904OS99		Report Date: May 16, 2019

Panel/Cell Line	Growth Percent
Leukemia	
CCRF-CEM	114.82
HL-60(TB)	113.38
K-562	110.77
MOLT-4	103.82
RPMI-8226	111.50
SR	141.42
Non-Small Cell Lung Cancer	
A549/ATCC	103.46
EKVX	102.93
HOP-62	104.35
HOP-92	111.45
NCI-H23	96.89
NCI-H322M	96.21
NCI-H460	108.58
NCI-H522	106.18
Colon Cancer	
COLO 205	109.92
HCC-2998	93.65
HCT-116	102.23
HCT-15	98.86
HT29	105.19
KM12	110.62
SW-620	108.24
CNS Cancer	
SF-268	103.98
SF-295	98.25
SF-539	100.69
SNB-19	93.98
SNB-75	94.83
U251	105.00
Melanoma	
LOX IMVI	101.84
MALME-3M	98.02
M14	107.22
MDA-MB-435	106.50
SK-MEL-2	110.02
SK-MEL-28	96.55
SK-MEL-5	97.97
UACC-257	100.82
UACC-62	94.06
Ovarian Cancer	
IGROV1	104.55
OVCAR-3	107.32
OVCAR-4	107.97
OVCAR-5	85.05
OVCAR-8	107.20
NCI/ADR-RES	100.30
SK-OV-3	108.94
Renal Cancer	
786-0	98.84
A498	97.52
ACHN	94.89
CAKI-1	98.22
RXF 393	112.98
SN12C	97.75
TK-10	107.40
UO-31	92.60
Prostate Cancer	
PC-3	100.64
DU-145	110.51
Breast Cancer	
MCF7	100.78
MDA-MB-231/ATCC	108.52
HS 578T	106.47
BT-549	103.57
T-47D	92.72
MDA-MB-468	97.14
Mean	103.49
Delta	18.44
Range	56.37

Mean Growth Percent - Growth Percent

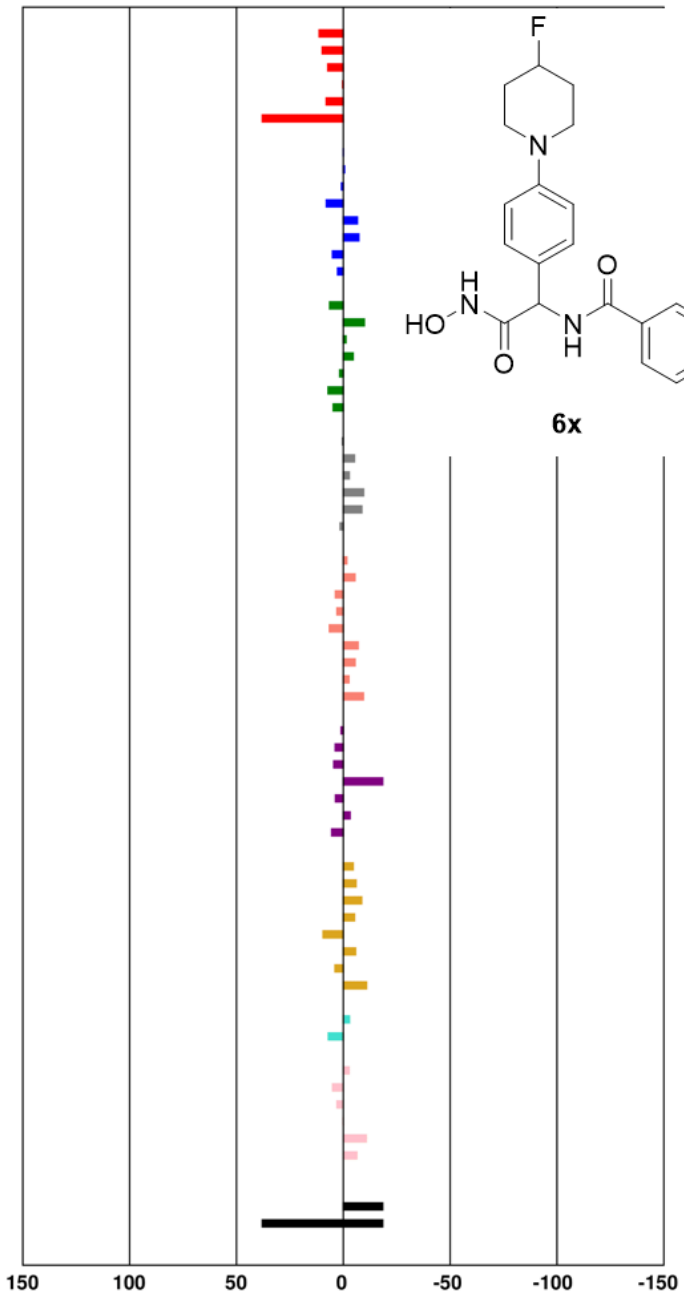

6x

Developmental Therapeutics Program

One Dose Mean Graph

NSC: D-814556 / 1	Conc: 1.00E-5 Molar	Test Date: Apr 29, 2019
Experiment ID: 1904OS99		Report Date: May 16, 2019

Panel/Cell Line	Growth Percent
Leukemia	
CCRF-CEM	115.62
HL-60(TB)	109.58
K-562	114.03
MOLT-4	105.33
RPMI-8226	120.23
SR	134.80
Non-Small Cell Lung Cancer	
A549/ATCC	109.08
EKVX	101.08
HOP-62	103.67
HOP-92	103.96
NCI-H23	99.68
NCI-H322M	100.02
NCI-H460	107.94
NCI-H522	103.16
Colon Cancer	
COLO 205	118.17
HCC-2998	105.53
HCT-116	107.97
HCT-15	106.59
HT29	105.09
KM12	100.95
SW-620	103.93
CNS Cancer	
SF-268	102.11
SF-295	99.05
SF-539	92.12
SNB-19	98.33
SNB-75	90.80
U251	103.48
Melanoma	
LOX IMVI	102.57
MALME-3M	99.66
M14	104.13
MDA-MB-435	107.44
SK-MEL-2	111.17
SK-MEL-28	97.40
SK-MEL-5	104.16
UACC-257	108.41
UACC-62	95.09
Ovarian Cancer	
IGROV1	103.98
OVCAR-3	107.80
OVCAR-4	113.21
OVCAR-5	89.96
OVCAR-8	106.66
NCI/ADR-RES	103.74
SK-OV-3	104.59
Renal Cancer	
786-0	97.76
A498	105.75
ACHN	95.84
CAKI-1	98.20
RXF 393	116.63
SN12C	99.97
TK-10	99.17
UO-31	96.74
Prostate Cancer	
PC-3	105.75
DU-145	105.02
Breast Cancer	
MCF7	97.91
MDA-MB-231/ATCC	111.35
HS 578T	104.69
BT-549	108.16
T-47D	100.00
MDA-MB-468	101.08
Mean	104.51
Delta	14.55
Range	44.84

Mean Growth Percent - Growth Percent

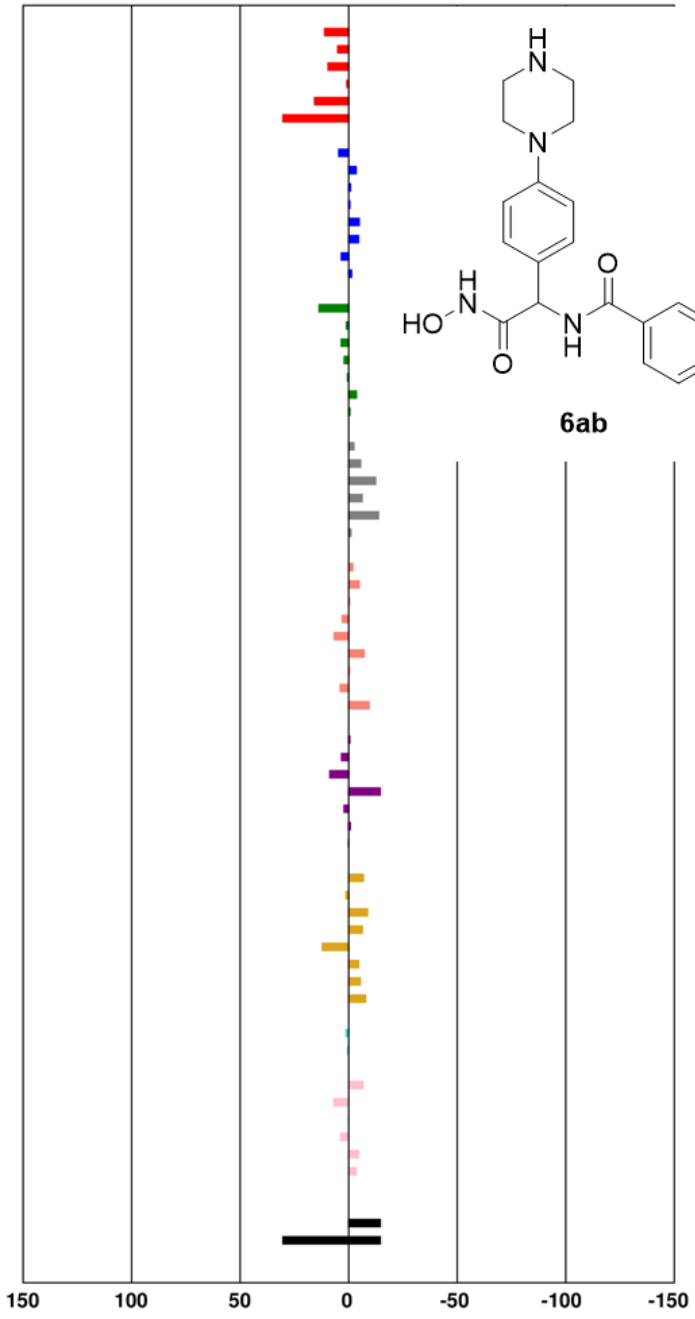

6ab

B. Binding scores of **6a**, **6e**, **6f**, **6m**, **6o**, **6s**, and **6ab.**

Total Score	Crash	Polar	FragRMSD	D score	PMF score	G score	ChemScore
Compound **6a**							
8.6429	-1.1904	6.4145	0.877	-112.243	-63.852	-216.36	-34.022
8.5111	-1.103	6.295	0.825	-112.704	-64.7495	-203.453	-33.6031
8.0252	-1.312	6.035	0.412	-114.32	-81.5735	-205.198	-39.5266
7.8118	-1.5644	6.0558	1.09	-117.19	-82.9726	-244.782	-37.0422
7.7237	-1.2875	5.8301	0.34	-120.803	-96.4463	-212.11	-38.138
7.6495	-1.0966	5.5162	1.008	-110.824	-57.2553	-179.612	-32.4251
7.5942	-1.7323	6.0093	0.418	-115.21	-71.902	-206.888	-37.1663
7.515	-1.8237	6.0811	0.414	-115.481	-72.6518	-210.365	-38.1969
7.4204	-0.7615	5.7791	0.382	-107.597	-100.8	-194.235	-37.9737
7.357	-1.4583	5.6804	0.47	-112.728	-71.7013	-208.088	-35.3211
7.3405	-1.6918	5.8973	0.701	-117.896	-71.0647	-203.936	-36.542
7.2498	-1.4265	5.7768	0.46	-112.643	-74.0138	-201.515	-36.2999
7.1291	-1.2353	4.8349	0.83	-114.678	-112.574	-203.715	-31.7405
7.1162	-0.8731	5.7119	0.736	-114.263	-105.646	-195.169	-35.6958
7.1091	-1.1537	4.3511	0.861	-111.493	-69.9055	-225.657	-27.8341
7.0966	-1.2911	4.8128	0.709	-113.683	-119.252	-212.825	-32.9145
7.0801	-1.366	4.8738	0.519	-109.58	-79.0431	-218.845	-34.4333
7.0345	-1.227	4.8289	0.778	-114.738	-112.807	-207.486	-30.8889
6.9139	-1.0428	4.8479	0.685	-112.35	-84.2305	-220.178	-29.9807
6.8392	-1.2969	4.6679	0.735	-114.782	-116.68	-204.432	-32.961
Compound **6e**							
7.429	-0.9663	4.5045	0.508	-138.387	-111.787	-241.564	-39.842
7.3377	-0.693	4.4076	0.438	-124.254	-105.841	-196.635	-37.8822
7.2375	-1.4634	3.9724	0.232	-141.882	-119.47	-240.261	-41.8665
7.0153	-1.5747	4.3332	0.231	-137.98	-117.659	-233.144	-42.0203
6.8767	-0.8368	4.4549	0.417	-124.25	-110.074	-202.975	-38.7559
6.7458	-0.6847	4.4089	0.285	-128.433	-119.088	-179.879	-43.0787
6.5785	-0.7476	4.3542	0.428	-123.692	-111	-196.016	-37.7846
6.3925	-0.7217	4.2888	0.466	-121.278	-108.589	-193.805	-36.7086
6.3756	-0.7742	4.3001	0.428	-120.141	-109.767	-193.438	-37.7904
6.3036	-0.4762	3.9746	0.386	-110.62	-117.851	-181.351	-38.4799
6.2459	-1.6727	4.8196	0.385	-106.303	-91.9616	-194.141	-35.5327

6.1588	-1.646	4.7912	0.366	-106.829	-91.4451	-193.497	-36.2726
6.1215	-0.778	4.2145	0.34	-115.279	-115.853	-186.867	-39.7264
6.1164	-0.7319	4.2278	0.346	-114.573	-120.436	-184.402	-39.7173
6.0943	-1.59	4.7249	0.351	-107.485	-90.8995	-193.685	-36.0185
6.0919	-1.6566	4.8506	0.375	-113.95	-92.5371	-203.566	-37.6131
6.0079	-0.4851	4.0034	0.372	-121.416	-132.093	-182.662	-39.4691
5.9217	-0.6834	4.1015	0.424	-127.088	-123.926	-187.291	-37.1906
5.7344	-0.9044	3.8403	0.41	-122.641	-127.296	-174.075	-40.1219
5.7265	-0.9436	3.1079	0.238	-128.197	-122.702	-199.007	-38.4512
Compound **6f**							
7.9841	-0.6706	4.3396	0.453	-127.209	-107.597	-190.377	-37.4864
7.2425	-0.7075	4.2889	0.43	-128.354	-104.97	-187.151	-37.3224
7.1943	-0.7615	3.7464	0.379	-127.838	-105.964	-185.418	-36.5526
6.9942	-0.7436	4.3284	0.435	-130.717	-108.618	-192.609	-38.1086
6.8967	-1.231	3.0296	0.279	-148.685	-133.489	-219.88	-38.9128
6.8633	-0.8203	4.0034	0.383	-127.936	-106.5	-187.878	-37.6721
6.8481	-0.73	4.3093	0.436	-132.291	-114.619	-181.503	-37.8111
6.764	-0.6627	4.0379	0.404	-132.15	-139.474	-196.145	-42.7243
6.7355	-0.663	4.2762	0.439	-131.638	-117.571	-180.925	-37.7121
6.6952	-0.6753	4.2663	0.359	-122.073	-116.685	-200.134	-39.674
6.6596	-0.6553	4.2542	0.389	-125.759	-123.285	-194.22	-38.1498
6.6055	-0.7249	4.2895	0.411	-127.596	-103.434	-193.393	-37.6738
6.5579	-0.6519	4.158	0.339	-122.303	-119.529	-197.48	-39.2034
6.5404	-0.6328	4.311	0.403	-126.623	-113.544	-186.878	-37.2745
6.5391	-0.6531	3.9511	0.356	-126.156	-125.096	-194.947	-36.4677
6.4848	-0.6633	4.1571	0.405	-123.213	-112.648	-188.172	-37.3008
6.4673	-0.5826	3.9291	0.397	-132.76	-131.266	-195.685	-42.9123
6.4655	-0.7699	4.4315	0.456	-131.368	-119.747	-199.675	-38.3925
6.2796	-0.6969	3.5312	0.351	-119.736	-120.551	-174.147	-37.7429
6.2748	-0.7763	3.691	0.353	-128.081	-101.27	-194.293	-36.5223
Compound **6m**							
7.6639	-0.7147	4.4805	0.25	-134.275	-129.776	-203.598	-41.8999
7.5126	-0.7769	4.3305	0.432	-121.371	-110.504	-193.111	-36.1502
7.426	-0.7783	4.3038	0.429	-122.072	-107.61	-192.396	-35.9283
6.3479	-0.4884	4.1235	0.402	-121.77	-143.259	-194.372	-41.4498

6.3289	-0.8513	4.3386	0.437	-119.019	-114.666	-200.401	-36.4845
6.2791	-0.6327	4.0402	0.408	-127.067	-142.758	-191.932	-41.2374
6.2476	-0.6495	4.2751	0.414	-117.123	-119.146	-186.29	-35.7476
6.1298	-0.8439	3.744	0.342	-120.121	-128.124	-183.825	-36.6454
6.0102	-0.7221	3.8023	0.374	-129.647	-142.846	-197.656	-40.9495
5.9814	-0.6678	3.7029	0.346	-128.462	-144.964	-186.585	-40.498
5.9241	-0.7584	4.134	0.4	-117.863	-122.901	-196.343	-35.833
5.8581	-0.5192	4.0129	0.42	-127.084	-140.994	-184.647	-37.5757
5.7926	-0.7988	3.879	0.388	-125.499	-111.234	-173.001	-34.6694
5.7749	-0.5627	4.1071	0.376	-112.942	-116.234	-176.931	-36.0863
5.7747	-0.5557	3.9845	0.356	-125.029	-144.516	-186.833	-41.4823
5.7587	-0.756	3.3699	0.315	-127.87	-140.891	-186.858	-38.8775
5.7313	-0.7318	3.9084	0.388	-116.457	-118.948	-193.062	-35.5206
5.7064	-0.7893	3.7755	0.373	-121.157	-117.28	-192.291	-35.3091
5.6389	-0.8676	3.9851	0.363	-117.493	-127.675	-206.775	-37.9215
5.6378	-0.6786	3.4072	0.323	-127.119	-140.219	-185.775	-39.2091
Compound **6o**							
7.2922	-1.1745	3.956	0.265	-126.197	-87.3787	-209.804	-34.9626
7.1957	-0.6128	3.7436	0.249	-114.991	-105.875	-194.073	-32.5015
7.073	-1.1847	4.06	0.245	-124.508	-90.4421	-212.379	-36.2918
7.0092	-1.3202	3.4912	0.248	-119.59	-95.9897	-207.273	-34.0889
6.9969	-1.0061	3.8023	0.225	-129.959	-105.135	-207.02	-34.341
6.9955	-1.4768	4.4873	0.22	-124.175	-93.4727	-224.098	-37.0103
6.7818	-1.0579	3.8375	0.243	-122.594	-101.072	-212.856	-34.6351
6.7542	-0.8679	3.61	0.202	-134.029	-105.759	-203.567	-33.3703
6.6765	-0.9948	3.5092	0.21	-136.432	-102.181	-207.83	-33.0777
6.6595	-1.5858	3.3753	0.24	-132.389	-98.1713	-225.138	-31.1083
6.6504	-0.8272	3.7948	0.221	-125.242	-107.475	-197.815	-33.5289
6.5782	-0.9098	4.792	0.238	-119.228	-102.603	-193.054	-37.3353
6.4616	-1.0599	3.6792	0.216	-126.295	-103.376	-208.056	-34.6131
6.4337	-1.4275	3.7398	0.27	-124.645	-99.0691	-202.371	-33.299
6.4179	-0.9798	4.7231	0.235	-118.925	-101.046	-187.419	-36.9649
6.3626	-3.4378	3.6846	0.208	-133.53	-95.0358	-226.472	-32.9437
6.2531	-1.6279	4.453	0.627	-135.834	-102.206	-237.569	-39.9425
6.2206	-1.0086	3.4647	0.528	-116.394	-105.596	-207.583	-31.5332

6.1978	-1.8765	3.4919	0.271	-138.007	-98.4803	-224.604	-33.6775
6.1854	-1.7013	3.5114	0.249	-133.5	-101.953	-218.576	-33.7577
Compound **6s**							
5.8648	-3.3753	4.7935	0.463	-116.685	-83.2182	-212.272	-34.7676
5.4732	-3.3033	4.5994	0.404	-118.564	-86.6251	-215.886	-32.7803
5.3457	-3.4838	4.6245	0.433	-115.46	-83.2	-214.31	-33.704
5.2384	-3.3108	4.2118	0.458	-143.819	-97.6079	-253.617	-37.8772
5.0622	-3.6838	4.5705	0.377	-112.258	-81.3224	-215.972	-33.9747
5.0605	-3.4543	4.3759	0.41	-116.366	-82.6337	-217.399	-32.7011
4.9221	-1.9776	3.4147	0.28	-126.106	-120.225	-213.813	-33.6986
4.8332	-2.3228	3.4254	0.288	-129.684	-125.894	-234.078	-36.4026
4.8185	-2.208	3.5429	0.291	-128.469	-124.45	-230.94	-35.5288
4.8073	-2.3721	2.5247	0.377	-137.837	-114.366	-247.219	-29.6996
4.7894	-1.8873	3.727	0.294	-124.253	-122.828	-183.839	-34.17
4.7319	-2.005	3.5081	0.277	-125.559	-122.404	-213.439	-34.2802
4.2477	-3.4854	4.2365	0.359	-119.749	-89.1278	-206.784	-32.6638
4.0799	-4.6573	4.5217	0.351	-129.557	-105.257	-217.246	-34.6633
3.9728	-4.7965	4.5154	0.342	-124.098	-108.809	-209.392	-35.9548
3.9541	-4.7929	4.4244	0.375	-118.048	-94.0504	-193.394	-33.7258
3.8482	-4.6064	4.5169	0.373	-119.99	-102.373	-196.583	-34.1744
3.7442	-4.9182	4.3957	0.324	-113.979	-98.0392	-215.238	-33.835
3.7106	-4.8731	4.2357	0.335	-119.989	-91.9887	-199.935	-33.5103
3.5759	-5.0972	4.7828	0.365	-120.335	-105.649	-234.932	-36.258
Compound **6ab**							
5.7808	-2.4741	4.6152	0.307	-158.573	-120.87	-217.188	-43.8919
5.7218	-2.9907	4.5868	0.31	-156.623	-117.392	-220.293	-43.1289
5.3024	-2.1431	3.8097	0.291	-153.594	-123.88	-225.843	-41.0438
5.1061	-2.4018	3.4861	0.32	-155.899	-121.518	-230.518	-40.5774
5.0867	-2.4613	3.3875	0.282	-156.977	-120.698	-233.674	-38.6209
4.9591	-3.2422	3.2891	0.326	-155.714	-121.28	-234.186	-38.636
4.9337	-2.2855	3.5883	0.305	-156.576	-122.138	-229.063	-41.4755
4.8386	-5.4046	4.0497	0.307	-161.953	-85.293	-267.572	-36.8002
4.789	-2.4956	3.1294	0.305	-154.857	-121.842	-226.091	-36.013
4.7339	-2.2244	3.282	0.275	-146.985	-124.37	-204.525	-34.6988
4.6988	-2.0737	3.2459	0.269	-143.12	-127.869	-197.026	-34.1361

4.6767	-2.5646	4.3072	0.368	-138.643	-115.635	-228.227	-38.0572
4.604	-3.1336	3.4039	0.263	-160.69	-138.343	-244.646	-36.3227
4.53	-2.27	3.9588	0.316	-131.452	-124.976	-217.455	-34.4083
4.4875	-2.2108	3.2755	0.29	-146.452	-136.717	-197.557	-31.3788
4.4237	-2.2736	3.6895	0.284	-134.086	-128.645	-216.775	-32.7746
4.414	-1.653	3.2506	0.285	-132.471	-123.26	-202.402	-32.4825
4.353	-2.1441	3.2292	0.297	-148.893	-126.086	-199.079	-35.3229
4.3518	-2.0288	3.0988	0.303	-131.526	-115.68	-190.328	-32.3879
4.308	-1.9343	3.1927	0.28	-129.78	-136.89	-195.592	-33.3587

Chapter 4: Introduction of New Linkers – Modification of the Central Aromatic Core

4.1 Introduction

In *Chapter 3*, the binding interactions at the S1 subsite of APN were successfully investigated, and an extremely potent APN inhibitor **6f** was discovered which had a $K_i^{(app)}$ value of 0.66 nM. After the binding interactions at the S1 and S1′ pocket of APN were optimised through modifications of the 3,4,5-trifluorophenyl and the *N*-pivaloyl group of the parent compound **1** (*Chapter 1* and *2*), the focus of this project changed to the central aromatic ring of the biphenyl core scaffold. There have been very limited studies conducted within this region for both the APN and *Pf*A-M1 inhibitors generated within our group. Therefore, it would be intriguing to explore how the changes in the structure of the centric aromatic ring affected the potency of novel inhibitors. A small series of analogues were designed as described in Figure 4.1.

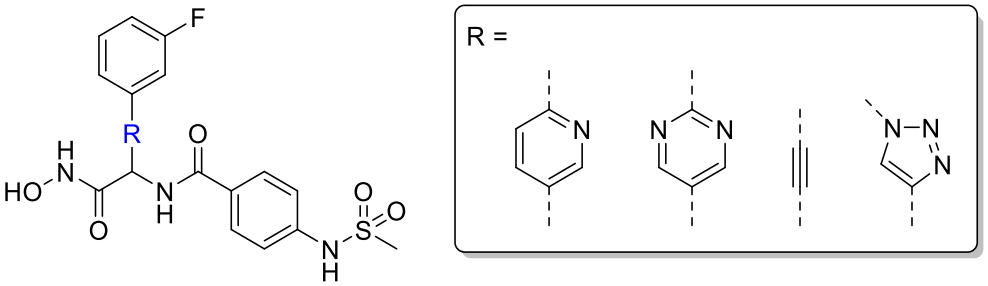

Figure 4.1. Structures of the proposed analogues.

4.2 Modifications of the central aromatic ring – designing of the proposed analogues with novel core scaffolds

The first proposed modification of the central aromatic ring was to introduce heteroaromatic groups such as pyridine and pyrimidine which are the bioisostere of benzene. As discussed in the *Chapter 3*, there are several advantages of deploying heteroaromatic groups in drug design; heteroatoms create dipole moments that can increase the potential of forming polar interactions with protein targets, and alter physicochemical properties to improve various aspects of pharmacokinetic profiles.[236-238] Replacing the central phenyl moiety with pyridine and pyrimidine not only reduces hydrophobicity of the molecule without changing the size of molecule significantly, but also allows to maintain the biaryl scaffold. This aspect is particularly imperative because although various chemical moieties were tolerated at the S1 subsite of APN, biaryl scaffold was identified as the preferred core unit to achieve potent activity. Moreover, the additional nitrogen atom(s) may boost capacity of molecules to actively engage in hydrogen bonding interactions with the backbone residues.

The second modification suggested was to install an internal alkyne group as a replacement of the centric phenyl group. This modification results into a complete loss of the biaryl scaffold, however acetylene group shares a number of similarities with a benzene ring. Alkynes are rich in π electrons and have high electron density around its C-C triple bonds. In addition, internal alkyne can act as an effective rigid spacer due to its linear structure. Furthermore, several studies demonstrated that alkynes could be non-classical isostere of phenyl moiety. Lenz *et al*. proved that the π-electronic system of enediyne could be used as a fancy bioisostere for the catechol fragment of dopamine, while Stepan *et al*. and Makarov *et al*. reported the use of bicyclo[1.1.1]pentane as a non-classical isostere of *para*-substituted phenyl and internal alkyne (Figure 4.2).[253-255] The acetylene analogue could be a precursor to generate other heterocyclic analogues such as triazole-bearing compounds through Click chemistry. Various synthetic approaches were attempted to generate the proposed analogues using previously reported procedures, which are discussed in the following section of this chapter.

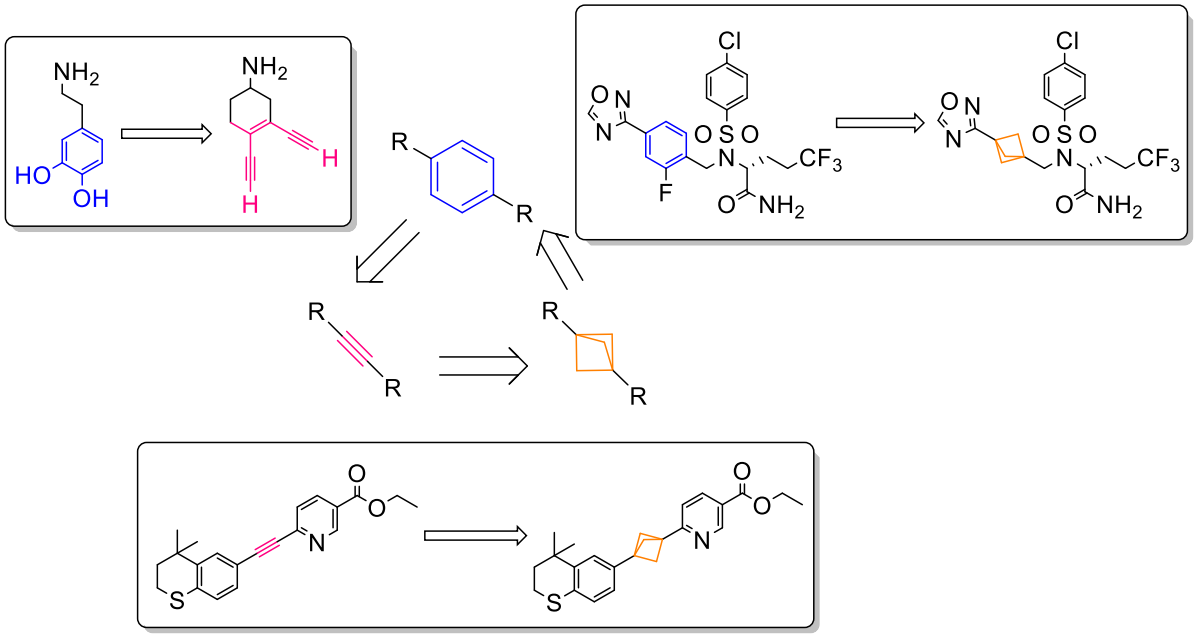

Figure 4.2. Applications of acetylene and bicyclo[1.1.1]pentane as non-classical isosteres of *para*-substituted phenyl.

4.3 Synthetic Routes Attempted to Synthesise the Desired Hydroxamic Acid Analogues

4.3.1 Synthesis of 2,5-substituted pyridine analogue

The first part of this chapter involved the synthesis of the 2,5-substituted pyridine analogue. The most efficient synthesis of the heteroaromatic analogues would start from 2-bromopyridyl glycinates, however such unusual synthetic amino acid derivatives are rarely commercially available. Therefore, the synthesis of 2-bromopyridyl glycinate was essential. In the past, several reaction procedures generating heteroaromatic amino acids were published, and some of the selected reactions are introduced in Figure 4.3. One of the approaches started from heteroaryl acetates where bromination and amination were performed to install amino groups at the α-carbon position.[256-258] Boto *et al*. reported syntheses of heteroaromatic amino acids from a primary alkoxide radical derived from serine through one-pot reaction.[259] In addition, Saaby *et al*. successfully synthesised optically active heteroaromatic amino acids from *N*-protected α-imino ester.[260]

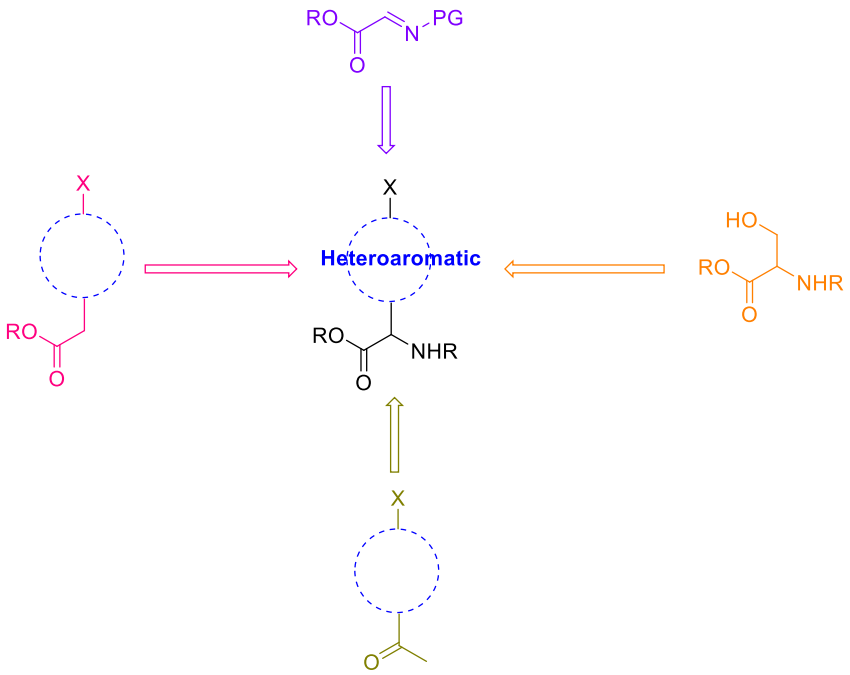

Figure 4.3. Synthetic pathways reported to generate heteroaromatic amino acids.

It was also identified that oxidation of 1-(pyridin-3-yl)ethan-1-one formed the corresponding α-keto acid in the presence of selenium dioxide.[261] This particular reaction was attractive because the conditions applied were similar to that of previously established synthetic methods (*Chapter 2*), and it also could save significant amount of time in optimising novel synthesis pathways. Therefore, the established synthetic route from *Chapter 2* was trialled to produce 2-amino-2-(6-bromopyridin-3-yl)acetic acid (Scheme 4.1).

Scheme 4.1. Proposed scheme to synthesise pyridine-containing intermediate.

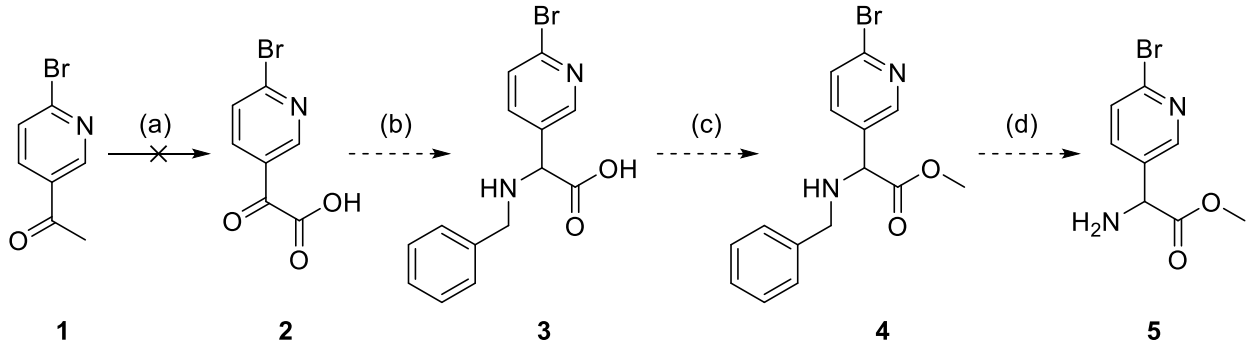

Reagents and conditions: (a) SeO_2, pyridine, 80 °C, overnight; (b) benzylamine, DCE, $NaBH(OAc)_3$, rt, overnight; (c) conc. H_2SO_4, MeOH, reflux, overnight; (d) H_2, cat. HCl, 10% Pd/C MeOH, rt, overnight.

Commercially available 1-(6-bromopyridin-3-yl)ethan-1-one **1** did undergo selenium dioxide assisted oxidation to form the keto-acid intermediate **2** using reported procedure. The conversion of the starting material was monitored qualitatively by TLC and staining with bromocresol solution produced a bright yellow spot, which indicated the presence of carboxylic acid. After filtration of SeO_2 and concentration of the filtrate, a thick residue was obtained which was not soluble in organic solvents besides DMF and DMSO. The residue was dissolved with minimal amount of DMF and added dropwise into a mixture of ice-water and the resulting precipitate was collected to give less than 10 mg of a solid. The analytical HPLC indicated that most of the product stayed in the aqueous filtrate, possibly due to the zwitterionic feature of compound **2**. Lyophilisation was performed and the collected material was analysed by running a ^1H NMR. The methyl group of the acetophenone **1** which was observed at 2.61 ppm disappeared, supporting that compound **1** was completely consumed. However, the aromatic region was extremely messy for analysis and this suggested that significant amount of impurities present. Since compound **2** is a water-soluble compound, reverse-phase chromatography and HPLC could be considered as alternative purification methods.

Instead of performing oxidation of the acetophenone, a Suzuki-Miyaura coupling reaction with 3-fluorophenyl boronic acid was carried out first to increase the lipophilicity of the intermediate, which would ease the purification step (Scheme 4.2). Moreover, the additional phenyl group provided better chromophore, which facilitated monitoring of the reaction accurately.

Scheme 4.2. Alternative synthetic pathway attempted to produce the pyridyl intermediate 9.

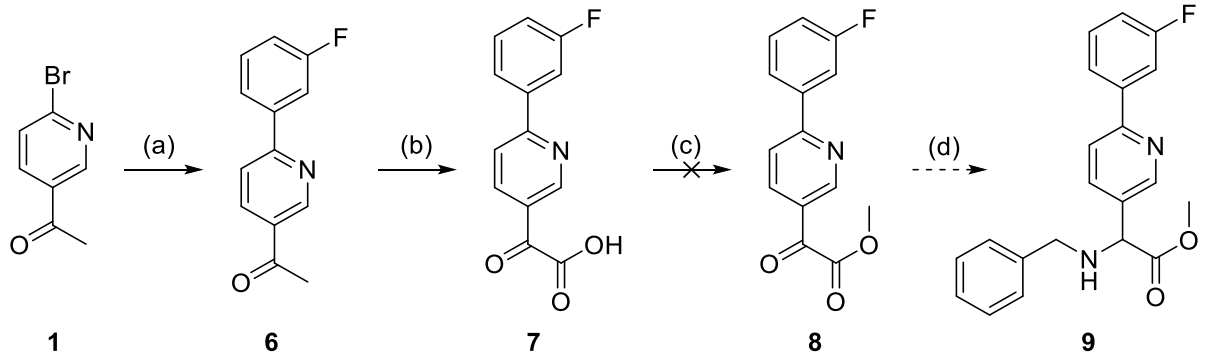

1 **6** **7** **8** **9**

Reagents and conditions: (a) 3-Fluorophenylboronic acid, 1 M Na_2CO_3, Pd $(PPh_3)_2Cl_2$, THF, reflux, overnight, 82%; (b) SeO_2, pyridine, 80 °C, overnight, quantitative; (c) MeI, Cs_2CO_3, DMF, rt, 3 d; (d) benzylamine, DCE, $NaBH(OAc)_3$, rt, overnight.

The coupling reaction afforded intermediate **6** without difficulty with a high yield of 82%. The following oxidation reaction was able to afford the desired keto-acid intermediate **7** in a quantitative yield. Successful formation of compound **7** was supported by ^{1}H NMR and LC-MS analyses where the singlet peak at 2.66 ppm for CH_3 protons of compound **6** was not observed and *m/z* of 246.0 was detected which corresponded to the positively charged molecular ion. The ^{1}H NMR of the crude also confirmed that pyridine was the only impurity present in approximately 1:1 ratio to the product. Therefore, the crude was lyophilised for two days to remove excess pyridine.

The subsequent step involved converting the carboxylic acid **7** to methyl ester **8** in the presence of methyl iodide and cesium carbonate. Previously, reductive amination with benzylamine was conducted prior to acid catalysed esterification to generate protected amino acid derivative (*Chapter 2*, pg. 33). The reason for conducting esterification in a basic condition was to convert the water-soluble intermediate **7** into more hydrophobic molecule so that successful purification could be achieved prior to the following reductive amination. Unfortunately, intermediate **7** mostly remained unreacted even with excess amount of reagents and prolonged reaction time applied. The LC-MS analysis showed a molecular ion mass of methylated compound (*m/z* = 260.0). However, it should be noted that there was also possibility of *N*-methylation to occur at the nitrogen atom of pyridyl moiety. The desired product **8** and *N*-methylpyridinium by-product have the same molecular ion mass, and LC-MS would not be able to discriminate between the two.

Instead of synthesising the methyl ester **8** from keto-acid **7** under basic conditions, acid-catalysed esterification was also attempted in the presence of concentrated sulfuric acid and methanol. It was predicted that both the carboxylic acid and ketone moieties of intermediate **7** would react simultaneously with methanol in the presence of excess acid to generate methyl ester, ketal intermediate **10**, which could be hydrolysed back to a ketone with mild acids such as trifluoroacetic acid (Scheme 4.3). Surprisingly, ^{1}H NMR of the crude revealed that only carboxylic acid group of **7** reacted to form a single methyl ester intermediate **8**. There was one singlet peak observed at 3.95 ppm which corresponded to the CH_3 of methyl ester. ^{13}C NMR further supported the formation of intermediate **8** where the CH_3 carbon atom of methyl ester was detected at 53.2 ppm. Pure methyl ester intermediate **8** was then reacted with benzylamine and $NaBH(OAc)_3$ to form the *N*-benzyl protected amino acid derivative **9**. The intermediate **8** was stirred with benzylamine for one hour prior to addition of the reducing agent $NaBH(OAc)_3$

to ensure that the ketone moiety was fully converted to the corresponding imine. However, according to the LC-MS analysis, the molecular ion of desired product **9** (*m/z* = 351.1) was not shown. Instead, the starting material achieved nearly complete conversion to a compound that had *m/z* of 262.2. Compound that could be possibly produced in the reaction was proposed to be methyl 2-(6-(3-fluorophenyl)pyridin-3-yl)-2-hydroxyacetate (**11**) where the ketone moiety of **8** was reduced to a hydroxyl group, suggesting that the imine intermediate was not produced successfully for reduction. The production of α-hydroxy ester as a side-product during reductive amination of α-keto acid has been previously reported.[232]

Scheme 4.3. Synthesis of methyl ester intermediate 8 and subsequent reductive amination reaction.

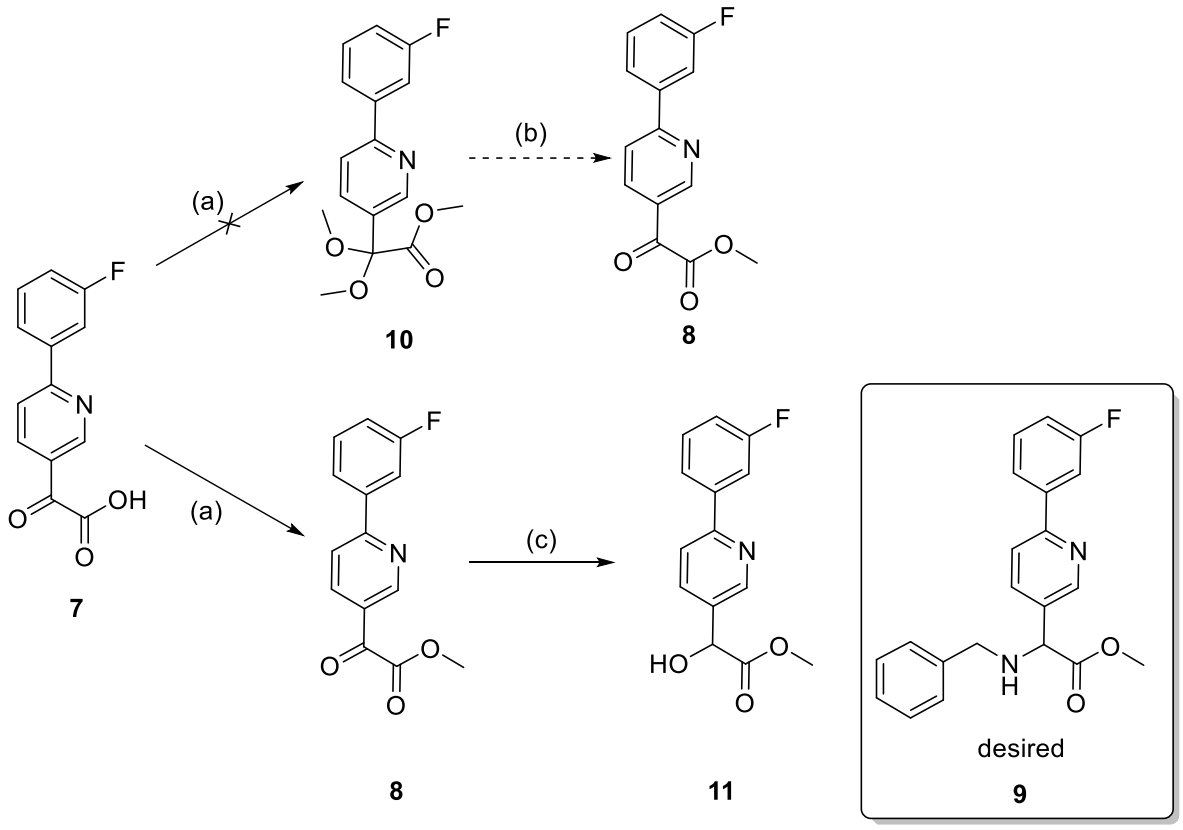

Reagents and conditions: (a) conc. H_2SO_4, MeOH, reflux, overnight, 83%; (b) TFA, H_2O, rt, overnight; (c) benzylamine, DCE, $NaBH(OAc)_3$, rt, overnight.

Several attempts were made to synthesise 2,5-substituted pyridine analogue through an established multi-synthesis pathway, however, a number of different challenges were encountered. Further investigations will be needed to identify the factors that could have

affected the reaction outcomes. In addition, alternative synthetic plans can be employed to generate the designed novel compounds successfully, which will be introduced in *Chapter 5*.

4.3.2 Introducing novel core scaffold: synthesis of acetylene-containing analogue

Alongside synthesis of 2,5-substituted pyridine analogue, the replacement of the central aromatic group with acetylene moiety was also attempted through various synthetic strategies. α-Ethynyl glycine derivatives have attracted interest of many researchers as an important building block of biologically active compounds because they can be functionalised through various modifications of the amino acid or acetylene moiety.[262] Therefore, a diverse range of syntheses of α-ethynyl glycine derivatives have been reported in the past, and this includes synthesis of optically active alkynyl glycine derivatives (Figure 4.3).[262, 263]

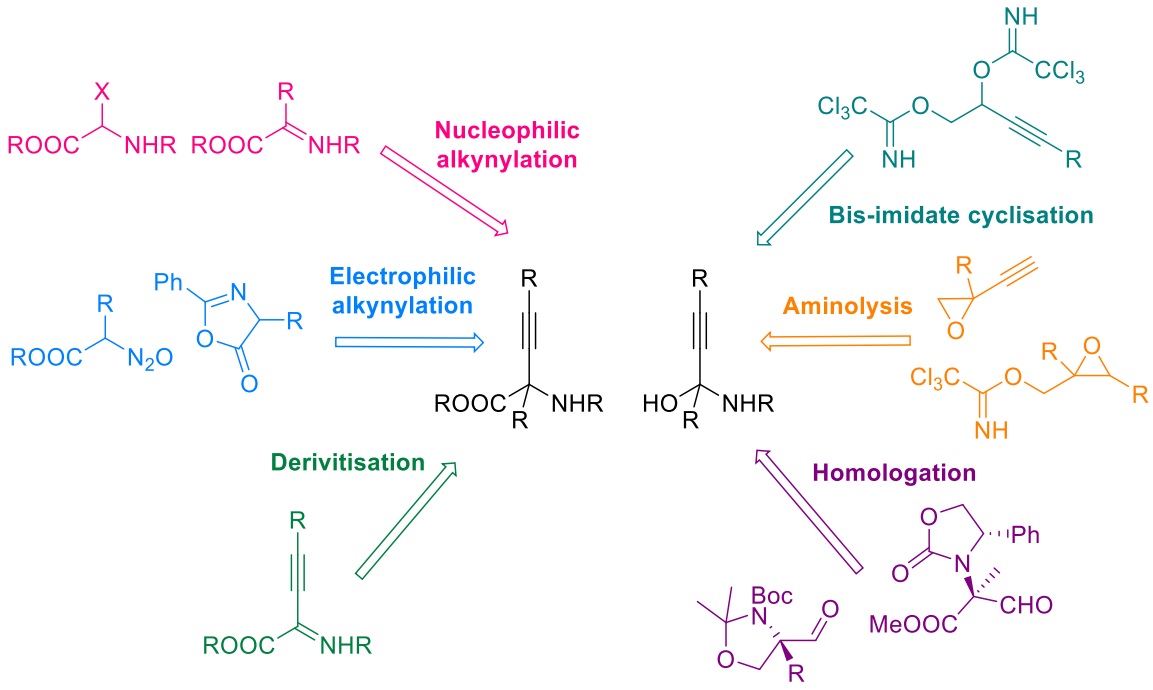

Figure 4.3. Various synthetic pathways discovered to produce alkynyl glycine derivatives. Adapted from Bolsakova *et al.*[262]

Among the reported synthetic pathways, nucleophilic alkynylation from α-halo glycinate was attempted for this project, using modified reaction conditions of Kumar *et al.* and Girijavallabhan *et al.* (Scheme 4.4).[264, 265] This proposed synthetic approach has two advantages over other pathways described in the literature because it forms TMS-protected acetylene intermediate that are structurally similar to the ultimate desired products. Moreover,

the TMS and Boc protecting groups can be easily removed to incorporate the essential 3-fluorophenyl and arylsulfonamide groups.

Scheme 4.4. Proposed synthetic pathway to generate acetylene analogue.

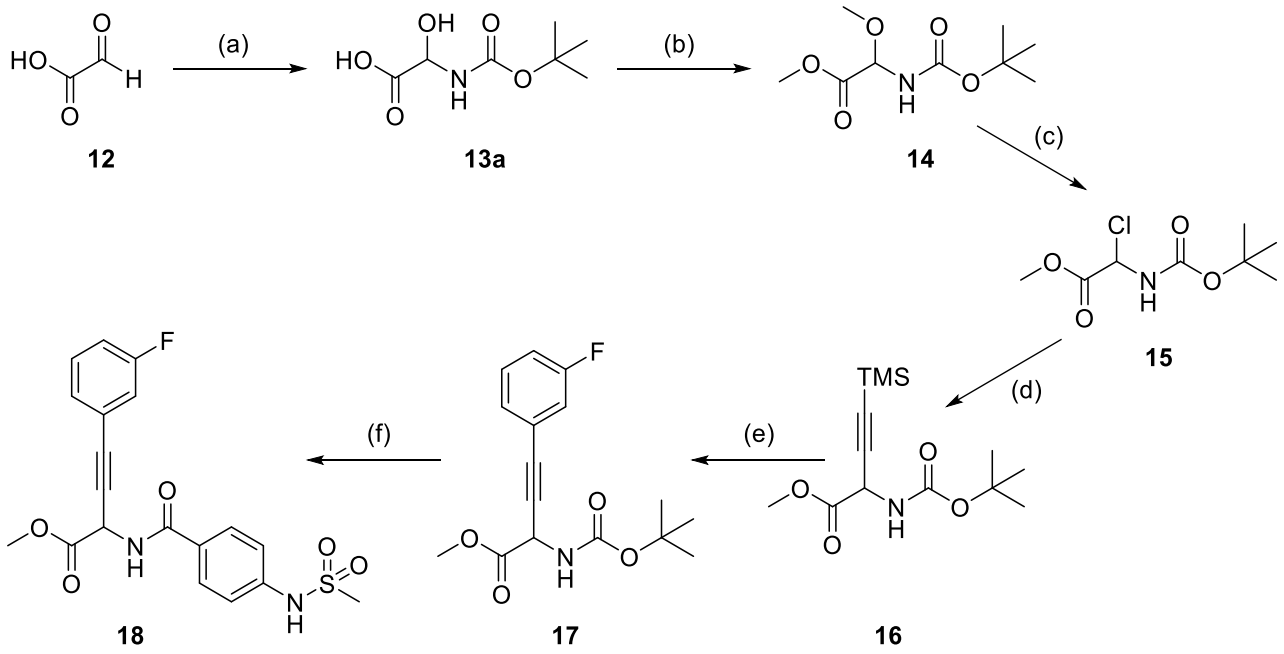

Reagents and conditions: (a) *tert*-butyl carbamate, Et_2O, rt, overnight, quantitative; (b) anhydrous MeOH, conc. H_2SO_4, 0 °C - rt, overnight; (c) PCl_5, anhydrous CCl_4, 24 h (d) bis(trimethylsilyl)acetylene, $AlCl_3$, anhydrous DCM, 0 °C - rt, overnight; (e) Sonogashira coupling (f) (i) 20% TFA/DCM, rt, 4 h (ii) DIPEA, HCTU, 4-(methylsulfonamido)benzoic acid, rt, overnight.

The first step of this synthesis involved a nucleophilic acyl addition between glyoxylic acid **12** and *tert*-butyl carbamate to generate intermediate **13a**. According to Sci-Finder database search in Jun 2019, 344 reactions between glyoxylate derivatives and carbamates were reported and it was noted that a range of solvents such as acetone, diethyl ether, cyclohexane, toluene, and benzene under both normal and anhydrous conditions were used. To investigate if the choice of different solvent affects reaction outcome, we performed a model study using anhydrous and normal diethyl ether as the solvent (Table 4.1).

Table 4.1. Summary of reactions attempted to synthesise glyoxylate derivatives.

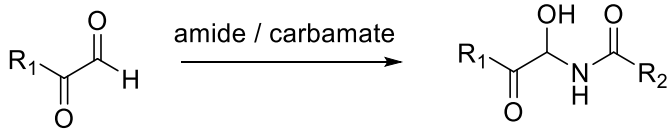

13a: (R_1) = OH (R_2) = Boc
13b: (R_1) = OH (R_2) = CH_3
13c: (R_1) = OEt (R_2) = CH_3
13d: (R_1) = OEt (R_2) = Boc

Entry	R_1	R_2	Conditions	Results	Notes
1	OH	Boc	Normal Et_2O	Successful	Boc and acetamide groups were cleaved by the acid in the subsequent reaction
2	OH	Boc	Anhydrous Et_2O	Successful	
3	OH	CH_3	Normal Et_2O	Successful	
4	OCH_2CH_3	CH_3	Toluene, 80 °C – 60 °C, 4 d	Ethyl ester group cleaved	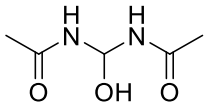 **19**
5	OCH_2CH_3	CH_3	Toluene, 60 °C, O/N		
6	OCH_2CH_3	Boc	Et_2O, RT	Product was not formed	NMR indicated a mixture of unknow compounds was formed. CH and NH protons of **13d** were missing

It turned out that the use of anhydrous solvent was not important to achieve the formation of intermediate **13a**. Both anhydrous and normal diethyl ether were able to generate intermediate **13a** in quantitative yield, and this was confirmed by the two doublet peaks at 7.55 ppm and 5.13 ppm which corresponded to the NH and methine protons, respectively (Table 4.1, Entry 1 and 2). In addition, ^{13}C NMR proved the formation of compound **13a** by showing the carbon atom of methine which was observed at 72.7 ppm. The next reaction involved introducing methyl groups to the carboxylic acid and α-hydroxy of intermediate **13a** under acidic condition. Unfortunately, ^{1}H NMR showed a mixture of unknown compounds were produced and also confirmed that the singlet peak at 1.39 ppm for CH_3 protons of the Boc group disappeared, indicating that the Boc group was cleaved through acid hydrolysis. Therefore, the Boc group was replaced with acetamide group, which is known to be more acid resistant. Synthesis of 2-acetamido-2-hydroxyacetic acid **13b** was easily achieved and both the ^{1}H NMR and ^{13}C NMR

matched with the reported values.[266] In the following reaction, there was no consumption of compound **13b** after two days of stirring. In order to facilitate the reaction, an additional equivalence of concentrated sulfuric acid was added. Similar to the reaction described above, a mixture of unidentifiable compounds was formed (Table 4.1, Entry 3). Moreover, the singlet peak at 1.84 ppm, which corresponded to the acetamide CH_3 protons of compound **13b**, was not observed in the ^{1}H NMR, which indicated cleavage of acetamide (Table 4.1, Entry 3).

Although the synthesis of intermediate **13a** and **13b** was successful, the acid hydrolysis of the Boc group or acetamide group could not be avoided in the following esterification reaction. Therefore, ethyl glyoxylate (50% w/w in toluene) was selected as the new starting molecule so that the esterification step could be avoided, which would effectively prevent the potential hydrolysis of the amide group. Reaction conditions reported by Xie *et al*. was attempted first (Table 4.1, Entry 4).[267] An extremely pure product was obtained from the reaction, however, the characteristic peaks of ethyl group were absent in the ^{1}H NMR and this suggested that the ethyl ester group was cleaved during the reaction. and formed a symmetrical compound *N*,*N*'-(hydroxymethylene)diacetamide (**19**). The formation of diacetamide compound was supported by the single peak at 1.84 ppm and double peak at 8.61 ppm, which corresponded to the six CH_3 protons and two NH protons, respectively. The mechanism of how the ester group was cleaved and formed compound **19** still needs to be elucidated. The reaction was attempted again with a reduced reaction time that could potentially prevent the cleavage of the ethyl ester (Table 4.1, Entry 5). However, formation of the compound **19** was verified by NMR analyses. The last reaction trialled was to install the Boc group on ethyl glyoxylate under the same conditions used to synthesise glyoxylic acid derivatives **13a-c** (Table 4.1, Entry 6). The ^{1}H NMR showed that the methine CH proton and NH protons which were found as double peaks between 5–8 ppm were absent, and demonstrated the desired product was not generated.

4.4 Conclusion

A small series of novel hydroxamic acid analogues were designed to investigate the effect of changes in the central aromatic ring to the inhibitory activity against APN. 3-Fluorophenyl group and methylsulfonamide groups were incorporated in the molecules to ensure the optimal potency was achieved at the S1 and S1′ of APN. Attempts were made to replace the central phenyl ring of the biaryl scaffold with heteroaromatics to synthesise 2,5-pyridyl and pyrimidyl analogues so that physicochemical properties can be enhanced while maintaining excellent

activity. It was also suggested to introduce acetylene group, which is a non-classical isostere of a *para*-substituted phenyl moiety, to introduce completely novel scaffold structure which has not been explored in previous studies.

Chemistry optimisation to synthesise the designed compounds was rather disappointing. Despite various synthetic strategies explored in different aspects, the synthesis of these designed novel APN inhibitors was unsuccessful. The previously optimised synthetic route was employed to obtain pyridyl analogue from commercially available 1-(6-bromopyridin-3-yl)ethan-1-one. Methyl 2-(6-(3-fluorophenyl)pyridin-3-yl)-2-oxoacetate intermediate **8** was successfully generated after a series of studies. However, the subsequent reductive amination led to reduction of the ketone moiety. Synthesis of acetylene analogue was also trialled which involved alkynylation of α-halo glycinate. A series of synthetic investigations were performed to generate the α-hydroxy carboxylic acid derivatives from glyoxylic acid and ethyl glyoxylate. Compound **13a** was synthesised by reacting glyoxylic acid with *tert*-butyl carbamate, but the Boc group was easily cleaved by acid hydrolysis in the following esterification reaction. Changing the amide group to acetamide, which was deemed to be more acid resistant was not able to solve the problem. Various reactions were tried with ethyl glyoxylate but none of the attempted reactions was able to synthesise the proposed compound. Nevertheless, these designed novel hydroxamic acids analogues still remain as intriguing molecules to explore, therefore, more comprehensive and thorough investigations must be carried out to optimise the synthetic pathways.

4.5 Experimental

Chemistry

General information on instrumental methods is provided in *Chapter 2*.

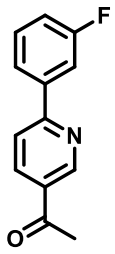

*1-(6-(3-Fluorophenyl)pyridin-3-yl)ethan-1-one (**6**).* To a nitrogen flushed 50 mL round bottom flask was added 1-(6-bromopyridin-3-yl)ethan-1-one (150 mg, 0.750 mmol), 3-fluorophenylboronic acid (136 mg, 0.974 mmol), degassed THF[*] (6 mL) and 1 M Na_2CO_3 (2 mL) the mixture was purged with N_2 before adding $Pd(PPh_3)_2Cl_2$ (15.8 mg, 22.5 µmol). The mixture was heated at reflux for overnight. The reaction mixture was concentrated under reduced pressure and extracted with EtOAc (3 × 10 mL). The organic layer was dried over anhydrous Na_2SO_4, filtered, and concentrated *in vacuo*. The crude was purified by column chromatography (PE/EtOAc 100:0 to 30:70) to obtain 132 mg (82%) of the desired product as a white solid. [*]THF was degassed by bubbling through inert N_2 gas for at least 30 min before the use. Although purging method is known to be the least effective way of generating degassed solvents, many metal-catalysed reactions described in this thesis successfully generated desired products without significant amount of side-products formed by oxidation. ^{1}H NMR (DMSO-d_6) δ 9.20 (dd, J = 2.3/0.8 Hz, 1H), 8.37 (dd, J = 8.3/2.3 Hz, 1H), 8.19 (dd, J = 8.3/0.7 Hz, 1H), 8.07–8.01 (m, 1H), 7.98 (ddd, J = 10.7/2.5/1.7 Hz, 1H), 7.58 (td, J = 8.0/6.1 Hz, 1H), 7.42–7.28 (m, 1H), 2.66 (s, 3H); ^{19}F NMR (DMSO-d_6) δ -112.6; ^{13}C NMR (DMSO-d_6) δ 196.9, 162.7 (d, J_{CF} = 243.4 Hz), 157.5 (d, J_{CF} = 2.7 Hz), 149.7 (d, J_{CF} = 2.3 Hz), 140.0 (d, J_{CF} = 7.7 Hz), 137.0, 131.0, 131.0 (d, J_{CF} = 8.3 Hz), 123.2 (d, J_{CF} = 2.6 Hz), 120.4, 116.9 (d, J_{CF} = 21.2 Hz), 113.7 (d, J_{CF} = 23.0 Hz), 27.0; *m/z* MS $C_{13}H_{11}FNO$ $[MH]^+$ calcd 216.1, found 216.0.

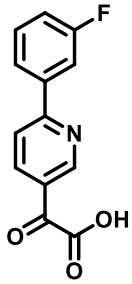

*2-(6-(3-Fluorophenyl)pyridin-3-yl)-2-oxoacetic acid (**7**).* To a solution of compound **6** (122 mg, 0.567 mmol) in pyridine (685 µL) was added SeO_2 (157 mg, 1.42 mmol) and then the mixture was stirred at 80 °C for overnight. Upon completion, the reaction mixture was cooled to room temperature and the insoluble material was removed by filtration. The filtrate was concentrated *in vacuo*. The crude product was obtained as a sticky orange solid. ^{1}H NMR of the crude indicated 1:1 ratio between compound **7** and pyridine. Excess pyridine was removed by lyophilisation to afford the desired product in quantitative yield. ^{1}H NMR (DMSO-d_6) δ 9.24–9.08 (m, 1H), 8.40 (dd, J = 8.4/2.2 Hz, 1H), 8.21 (dd, J = 20.1/8.4 Hz, 1H), 8.05 (d, J = 7.9 Hz,

1H), 8.02–7.95 (m, 1H), 7.59 (td, *J* = 8.0/6.2 Hz, 1H), 7.37 (td, *J* = 8.3/2.1 Hz, 1H) *OH exchangeable proton was not observed; ^{19}F NMR (DMSO-d_6) δ -112.5; ^{13}C NMR (DMSO-d_6) δ 187.6, 165.0, 162.7 (d, J_{CF} = 243.6 Hz), 158.7, 150.9, 139.8 (d, J_{CF} = 7.7 Hz), 138.4, 131.1 (d, J_{CF} = 8.2 Hz), 127.5, 123.4 (d, J_{CF} = 2.6 Hz), 120.6, 117.2 (d, J_{CF} = 21.2 Hz), 113.9 (d, J_{CF} = 23.0 Hz); *m/z* MS $C_{13}H_9FNO_3$ $[MH]^+$ calcd 246.1, found 246.0.

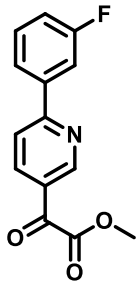

*Methyl 2-(6-(3-fluorophenyl)pyridin-3-yl)-2-oxoacetate (**8**).* To a solution of compound **7** (228 mg, 0.932 mmol) in MeOH (13 mL) was added conc. H_2SO_4 (298 µL, 5.59 mmol) dropwise. The mixture was heated at refluxed for 2 d. Upon completion, the reaction mixture was concentrated *in vacuo* and neutralised with sat. $NaHCO_3$, followed by extraction with EtOAc (3 × 30 mL). The combined organic layer was dried over anhydrous Na_2SO_4 and concentrated *in vacuo* to obtain 202 mg (83%) of the desired compound as a beige solid. ^{1}H NMR (DMSO-d_6) δ 9.32–9.14 (m, 1H), 8.47 (dd, *J* = 8.4/2.3 Hz, 1H), 8.26 (d, *J* = 8.4 Hz, 1H), 8.07 (d, *J* = 7.9 Hz, 1H), 8.07–7.96 (m, 1H), 7.61 (td, *J* = 8.0/6.1 Hz, 1H), 7.39 (td, *J* = 8.5/2.6 Hz, 1H), 3.95 (s, 3H); ^{19}F NMR (DMSO-d_6) δ -112.4; ^{13}C NMR (DMSO-d_6) δ 183.8, 162.7 (d, J_{CF} = 243.7 Hz), 162.1, 158.9, 151.3, 139.7 (d, J_{CF} = 7.5 Hz), 138.9, 131.1 (d, J_{CF} = 8.4 Hz), 127.5, 123.4, 120.5, 117.3 (d, J_{CF} = 21.2 Hz), 113.9 (d, J_{CF} = 23.0 Hz), 53.2; *m/z* MS $C_{14}H_{11}FNO_3$ $[MH]^+$ calcd 260.1, found 259.9.

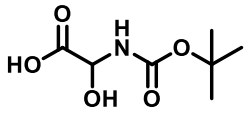

*2-((tert-Butoxycarbonyl)amino)-2-hydroxyacetic acid (**13a**).* A mixture of the *tert*-butyl carbamate (200 mg, 1.71 mmol), glyoxylic acid monohydrate (164 mg, 2.22 mmol) in Et_2O (8 mL) was stirred at room temperature for overnight. Upon completion, the reaction mixture was concentrated *in vacuo* to obtain the desired product in quantitative yield. The crude was used without further purification. ^{1}H NMR (DMSO-d_6) δ 12.74 (s, 1H), 7.55 (d, *J* = 8.6 Hz, 1H), 6.10 (br. s, 1H), 5.13 (d, *J* = 8.8 Hz, 1H), 1.39 (s, 9H); ^{13}C NMR (DMSO-d_6) δ 171.3, 154.7, 78.4, 72.7, 28.1.

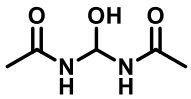

*N,N'-(Hydroxymethylene)diacetamide (**19**).* Acetamide (200 mg, 3.39 mmol) and 50% w/w ethyl glyoxylate in toluene (805 µL, 4.06 mmol) was heated at 60 °C for overnight. Upon completion, the solid cake formed was collected by filtration and dried under vacuum to obtain 41 mg (7%) as an off-white solid. ^{1}H NMR (DMSO-d_6) δ 8.61

(d, J = 7.7 Hz, 2H), 5.50 (t, J = 7.7 Hz, 1H), 1.84 (s, 6H) *exchangeable OH proton was not observed; ^{13}C NMR (DMSO-d_6) δ 169.3, 55.9, 22.2.

Chapter 5: Conclusions and Future Directions

5.1 Thesis summary

APN has been extensively studied, and there is compelling evidence that proves a relationship between APN dysregulated activity and angiogenesis or metastasis. An enormous number of inhibitors, ranging from synthetic peptidomimetic or non-peptide small molecule inhibitors to monoclonal antibodies have been developed.[98] Despite continuous efforts, only a few APN inhibitors such as bestatin and Tosedostat displayed clinical efficacy. Therefore, there is continuous interest in the discovery of novel APN inhibitors for the treatment of cancer.

This project aimed to repurpose *Pf*A-M1 inhibitors that were developed as potential anti-malarial agents.[230] APN is a human homologue of *Pf*A-M1 and investigation into the selectivity of **1** (*Chapter 1 and 2*) showed that it was a more potent inhibitor of APN than *Pf*A-M1 ($K_i^{(app)}$ = 118 nM *vs* 331 nM respectively). Based on the X-ray crystal structure of *Pf*A-M1 bound to **1**, a model of APN bound to **1** was produced. From this model, it was hypothesised that the binding interactions between the inhibitor and the S1′ subsite of APN could be improved by modifying the *N*-pivaloyl group of the inhibitor. Therefore, in a previous study, **1** was repurposed as the novel APN inhibitor to develop a series of hydroxamic acid analogues as novel anti-cancer drug candidates. A total of 11 hydroxamic acid analogues with various S1′ anchors were synthesised by replacing the *N*-pivaloyl group of **1** with a longer alkyl chain or aromatic linkers containing hydrogen bond donors and acceptors. Among the series of compounds, the 3-fluoro-4-hydroxyphenyl compound showed the most potent activity with a $K_i^{(app)}$ of 29.1 nM.

This project first aimed to further optimise the binding interactions occurring at and beyond the S1′ pocket of APN to enhance the potency of inhibitors (*Chapter 2*). The previously optimised multi-step synthesis was applied to successfully generate a total of 35 novel APN inhibitors and their inhibitory activity against APN was measured using an *in vitro*

fluorescence-based enzyme assay to establish comprehensive structure-activity relationships. Among this series of analogues, methylsulfonamide analogue **6ad** and sulfamide analogue **6ae** (Figure 5.1) were found to possess excellent potency with $K_i^{(app)}$ values of 4.5 nM and 8.2 nM, respectively. The binding interactions between the inhibitors and APN were predicted through extensive computational modelling studies. According to the MD simulations of the docked pose of **6ad** and **6ae** into APN crystal structure, the biphenyl core scaffold played a significant role in providing multiple hydrophobic interactions with the ^{891}YGGGSFSF^{898} flexible loop. It was also noted that the sulfonamide moiety of **6ad** and **6ae** engaged in dual hydrogen bonding interactions with the side chain of Asn^{900} and Arg^{442} residues. In order to assess cross-activity with other zinc-dependent enzymes, the inhibitory activity of **6ad** and **6ae** against MMP2, 7, 8, 9, and 13 was determined, and the results revealed that the inhibitors were selective against the MMPs.

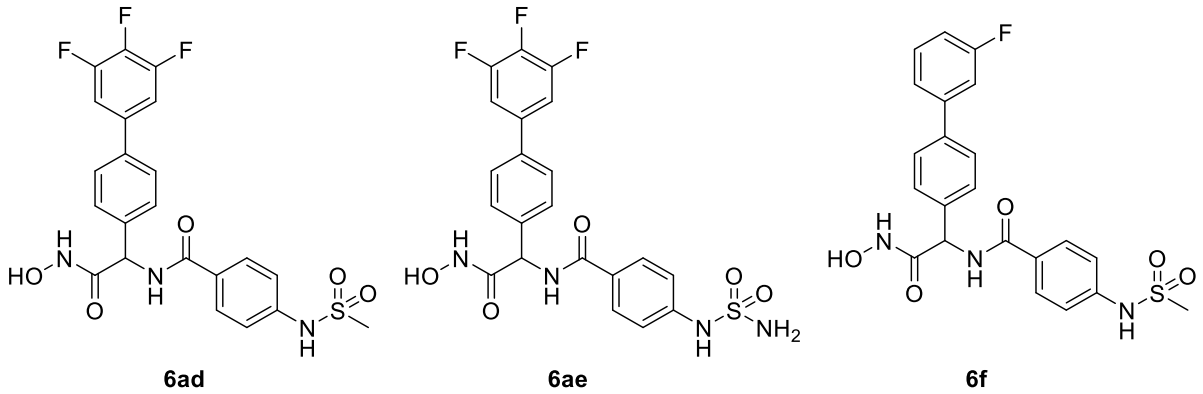

Figure 5.1. Structures of potent APN inhibitors.

Resazurin cell-based assays were also performed to measure the anti-proliferative activities of compound **6ad** and **6ae** in a cell environment. Although both compound **6ad** and **6ae** exhibited low cytotoxicity against Ad293 cells with IC_{50} values of greater than 40 µM, they only displayed very weak anti-proliferative activities against ovarian cancer cell line ES-2 and leukaemic cell line REH. The assay results also showed that both inhibitors were more active in low-APN expressing REH cell line than high-APN expressing ES-2 cell line. Growth inhibition activity of Tosedostat, **6ad** and **6ae** at a single dose of 10 µM against various cancer cell lines was also determined by NCI. Despite the weaker APN inhibition activity, Tosedostat displayed more significant growth inhibition compared to **6ad** and **6ae**. Physicochemical and pharmacokinetic studies of **6ad** and **6ae** indicated high *in vitro* metabolic and plasma stability

properties which were desirable, however, the kinetic solubilities of the inhibitors were at a sub-optimal level.

Although the novel APN inhibitor **6ad** exhibited extremely potent activity, the compound was identified to possess sub-optimal solubility, which could be further improved by medicinal chemistry approaches. Therefore, the second aspect of this project aimed to modify the hydrophobic 3,4,5-trifluorophenyl group to improve the solubility while maintaining optimal binding interactions at the S1 pocket of APN. *Chapter 3* introduced various synthetic approaches to form C-C bond between arylboronic / alkylboronic acids and the aryl bromide intermediate **4d**. Suzuki-Miyaura coupling reaction conditions were successfully optimised to synthesise 15 analogues containing biphenyl / cycloalkyl-aryl scaffolds efficiently. A diverse set of synthetic strategies were employed to produce 9 compounds with various amino groups installed through Buchwald-Hartwig aminations.

According to the enzymatic assay results, many of the hydroxamic acid analogues showed potent activity at a low nanomolar range, indicating that various chemical moieties were tolerated at the S1 subsite of APN. 3-Fluorophenyl analogue **6f** (Figure 5.1) was identified as the most potent inhibitor of this project, with an outstanding $K_i^{(app)}$ value of 0.66 nM. Binding interactions between APN and selected compounds **6a** (phenylglycine), **6e** (phenyl), **6f** (3-fluorophenyl), **6m** (4-pyridyl), **6o** (cyclopropyl), **6s** (cyclohexyl), and **6ab** (piperazinyl) were studied through molecular docking studies. While some differences in the binding interactions between each ligand were observed, the docking studies provided insufficient information to correlate with the SAR Anti-proliferative activities of 10 selected APN inhibitors **6c** (chlorophenylglycine), **6e** (phenyl), **6f** (3-fluorophenyl), **6i** (3,5-difluorophenyl), **6m** (4-pyridyl), **6o** (cyclopropyl), **6q** (cyclopentyl), **6s** (cyclohexyl), **6x** (4-fluoropiperidyl), and **6ab** (piperazinyl) were also determined. Unfortunately, compound **6f** was the only inhibitor that possessed a weak anti-proliferative activity against certain cancer cell lines.

With binding interactions at both the S1 and S1′ subsite of APN optimised, the last aspect of this project proposed to modify the centric aromatic ring to investigate the effect of such structural changes to the inhibitory activity against APN. In *Chapter 4*, a small series of novel hydroxamic acid analogues were designed where 3-fluorophenyl group and methylsulfonamide groups were incorporated to maintain the optimal potency within the S1 and S1′ of APN, respectively. The middle phenyl ring of the biaryl scaffold was suggested to replace with

heteroaromatics such as pyridine and pyrimidine. It was also proposed to install the acetylene group to introduce a completely new structure that has not been explored much in previous studies. Although considerable efforts were made to synthesise the designed compounds, chemistry optimisation was unsuccessful. The previously optimised synthetic route discussed in *Chapter 2* was employed to produce pyridyl analogue. The methyl ester intermediate **8** was successfully generated (Figure 5.2). However, the following reductive amination resulted in a reduction of the ketone moiety **11** instead of the desired product **9**. Synthesis of the acetylene analogue was attempted through multi-step synthesis developed by other research groups. Unfortunately, the earlier steps of the proposed synthetic pathway failed to afford the desired products, which require further investigations in the future.

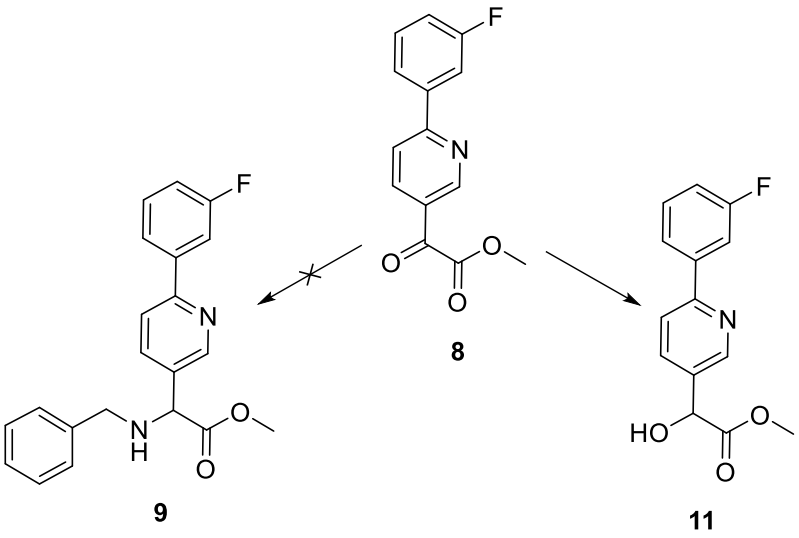

Figure 5.2. Structures of compound 8, 9, and 11.

5.2 Concluding remarks and future works

A number of tight-binding novel APN inhibitors were successfully developed through structure-based approaches and this involved applications of a wide range of synthetic chemistry and structural biology strategies. However, there were also several limitations and challenges identified which should be addressed in the future.

One of the biggest challenges of this project lies with the weak cellular activity of inhibitors observed despite their excellent inhibitory activities against APN. There have been numerous

examples of small molecules reported showing activity towards their isolated target protein in an *in vitro* screening but failed to display biological activity.[268] The major factors of such huge discrepancies were caused by poor membrane permeability and off-target effects.[268] Therefore, appropriate experiments are required to determine which properties of the inhibitors are closely associated with cellular activity. *In vitro* Caco-2 permeability assays can be performed as a measure of cell permeability of the inhibitors and their potential to interact with drug transporters.[269] The APN inhibitors bear a hydroxamic acid group which is known as strong metal chelator. Therefore, there is a possibility of non-selective binding to other metalloenzymes which can lead to off-target effects. As such, the selectivity of the inhibitors needs to be determined by measuring activities against other zinc-dependent enzymes. Moreover, the inhibitors developed in this project will be a valuable tool to establish comprehensive structure-property relationships that can assist the identification of desired features for improved cell efficacy.

Resazurin assays of **6ad** and **6ae** indicated that both inhibitors exerted stronger anti-proliferative activity against APN-negative cell line than APN-positive cell line. This result implied that APN enzymatic activity might not be associated with cell proliferation. Indeed, there are controversies about the role of APN in cell proliferation.[92 192] Another theory that explains this result would be the off-target effects of the compounds in cellular environment. In the APN positive cell line, the compounds would be more actively consumed by APN than when the compounds are present in APN-negative cell line. This would leave higher concentration of inhibitors available in the APN-negative cell line to interact with other unknown targets to exert anti-proliferative activity. Therefore, it is vital to be aware that the inhibitors may participate in cell proliferation through APN-independent mechanisms.

Additionally, it would be also interesting to explore the effects of the APN inhibitors developed on angiogenesis and metastasis. Although the inhibitors were not able to display noticeable anti-proliferative activities, they could be potential anti-cancer drug candidates as effective angiogenesis and metastasis suppressors. A classical capillary tube formation assay may provide information on the impact of the potent APN inhibitors on endothelial cell tubulogenesis which is one of the targets for angiogenesis.[15, 270] Changes in cell motility, which contributes to metastasis of cancer cells, can be evaluated by wound healing assays.[270]

The binding interactions between potent inhibitors and APN were studied through extensive molecular modelling strategies. One of the limitations of docking studies performed is that any water-mediated interactions that might be significant in affecting activity were not investigated, because water molecules were removed during the docking process. In addition, several poses that lost hydroxamic acid-zinc coordination or showed a completely flipped position of ligands were excluded for analysis. However, the results might be suggesting that those ligands are unstable within the binding site of APN, or there might be other poses available. Therefore, X-ray crystallography of the APN-inhibitor complex will be required for precise analysis of binding interactions made within the binding sites.

A wide range of synthetic chemistry strategies was explored and optimised to synthesise a total of 63 novel hydroxamic acid analogues successfully. The compounds were evaluated for pharmacological activities as a racemic mixture. Therefore, selected potent inhibitors are required to be resolved as pure enantiomeric compounds through chiral chromatography or diastereomeric salt formation to determine the active enantiomer and measure its activities in biological systems.

Synthesis of 2,5-disubstituted pyridine and alkynyl analogues through various chemistry approaches was trialled to modify the central phenyl ring. However, optimisations of proposed synthetic pathways were not achieved. As an alternative, 2,5-disubstituted pyridine or 2,5-disubstituted pyrimidine compounds can be produced by new synthetic route using modified conditions reported by Moon *et al*. and Sabbatini *et al*. as described in Scheme 5.1.[271, 272]

The first step involves decarboxylative arylation of 3-ethoxy-3-oxopropanoic acid **1** by oxidative catalysis in the presence of arylboronic acid and copper(II) triflate, followed by Suzuki-Miyaura coupling reaction optimised in *Chapter 3*.[271] The α-carbon of intermediate **3** is brominated and reacts with sodium azide which is reduced by hydrogenolysis to produce primary amine **5**. The amine is coupled with 4-(methylsulfonamide)benzoic acid, and the ethyl ester is converted to the corresponding hydroxamic acid using established methods.

Scheme 5.1. Alternative synthetic pathway proposed to produce 2,5-pyridine and pyrimidine analogues.

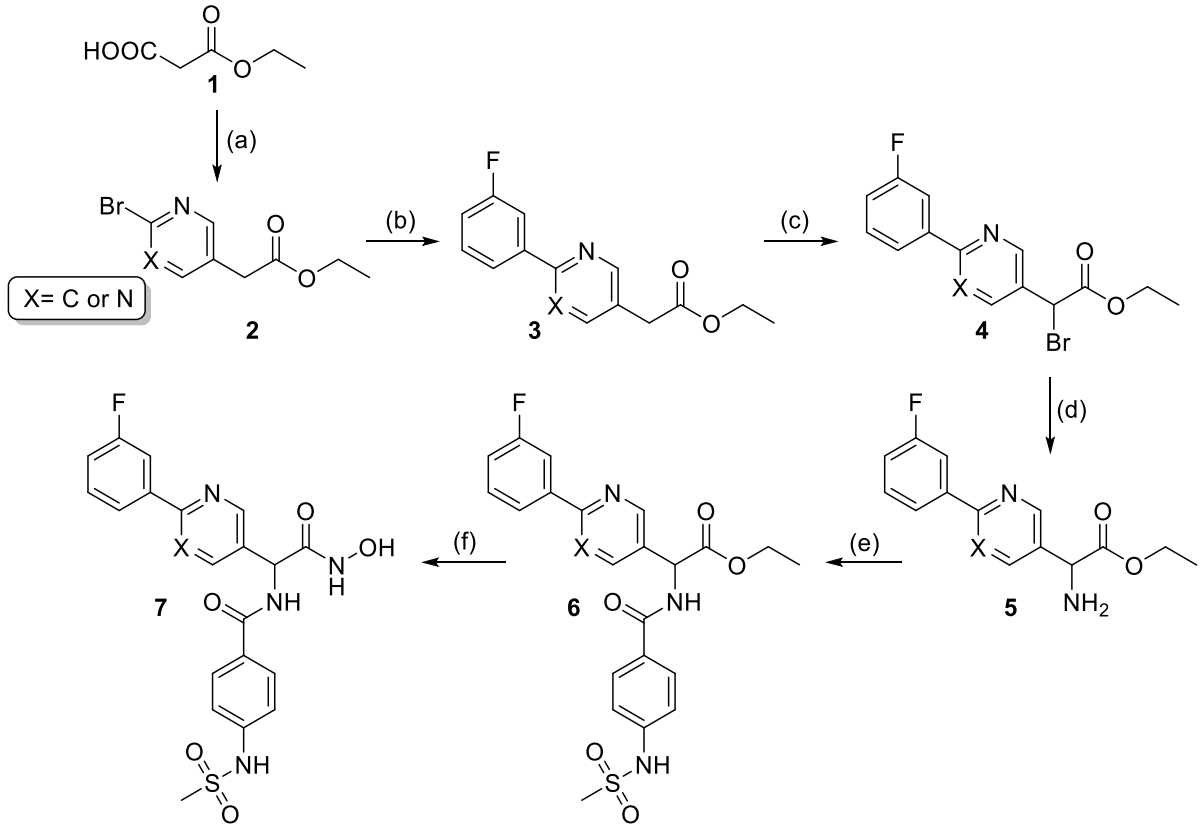

Reagents and conditions: (a) $Cu(OTf)_2$, phenylboronic ester, DMA, Et_3N, rt, overnight; (b) 3-fluorophenylboronic acid, K_3PO_4, $Pd(PPh_3)_2Cl_2$, DMF, 100 °C; (c) benzoyl chloride, NBS, CCl_4, reflux; (d) (i) $NaNH_3$, MeCN, rt, overnight; (ii) H_2, 10% Pd/C, MeOH, rt, overnight; (e) 4-(methylsulfonamido)benzoic acid, EDCI.HCl, DMAP, DCM, DMF, rt, overnight; (f) $NH_2OH{\cdot}HCl$, 5 M KOH/MeOH, anhydrous MeOH, rt, overnight.

Numerous chemistry methods to generate α-ethynyl glycines have been introduced.[262] Among them, the synthesis of β,γ-alkynyl α-amino acid derivatives optimised by Ji *et al*. can be used as an alternative approach to produce alkynyl-containing analogues (Scheme 5.2).[273]

Scheme 5.2. Synthesis of alkynyl analogue 13 from ethyl glyoxylate 8.

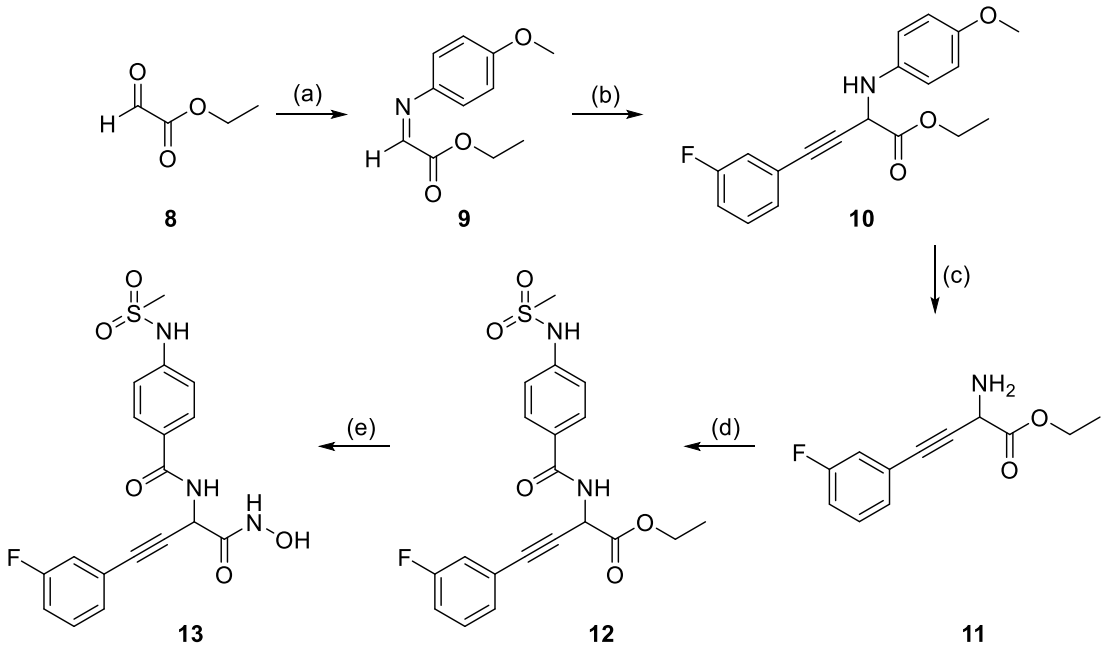

Reagents and conditions: (a) **8**, 4-methoxyaniline, DCM, rt, 30 min; (b) 3-fluorophenylacetylene, AgOTf, hexane, rt; (c) conc. H_2SO_4, H_5IO_6, MeCN/H_2O 1:1, rt or 90 °C; (d) 4-(methylsulfonamido)benzoic acid, EDCI·HCl, DMAP, DCM, DMF, rt, overnight; (e) NH_2OH·HCl, 5 M KOH/MeOH, anhydrous MeOH, rt, overnight.

Ethyl glyoxylate reacts with 4-methoxyaniline to generate imine intermediate **9**. Using the optimised conditions of silver(I)-catalysed alkynylation by Ji *et al*., 3-fluorophenylacetylene is introduced to produce alkynyl intermediate **10**, and the 4-methoxyphenyl protecting group can be reduced in the presence of periodic acid and concentrated sulfuric acid to afford free amine intermediate **11**.[273, 274] The last two steps involve installation of the methylsulfonamide moiety and formation of hydroxamic acid.

Furthermore, replacement of the hydroxamic acid moiety of APN inhibitors developed could be considered as part of the future work to solve several issues associated with hydroxamic acid. Being a strong ZBG, compounds that contain hydroxamic acid may suffer from low selectivity towards other types of zinc-dependent aminopeptidases. In addition, hydroxamic acid may cause pharmacokinetic and toxicology problems. It was also shown that hydroxamic acids might be hydrolysed to the corresponding carboxylic acid under physiological condition.[275] The downside of this effect is that compounds may lose biological efficacy

because carboxylic acid is weaker ZBG.[276] Moreover, hydroxylamine generated as a by-product can be toxic due to its mutagenicity.[277] Some of the commonly used ZBGs include carboxylate, sulfonamide, phosphonate, heteroaromatic pyrazole and tetrazole, urea, and boronic acid.[242]

The work detailed within this thesis has shown that a large series of hydroxamic acid analogues were generated and *N*-(1-(3'-fluoro-[1,1'-biphenyl]-4-yl)-2-(hydroxyamino)-2-oxoethyl)-4-(methylsulfonamido)benzamide (**6f**) achieved a remarkable improvement in potency against APN. Further modifications on this compound will be conducted to develop novel inhibitors with improved cellular activity and physicochemical properties as suitable drug candidate for the treatment of cancer.

Chapter 6: References

(1) AIHW. *Cancer in Australia 2019*; Australian Institute of Health Welfare: Canberra, 2019.

(2) Farber, S. Some observations on the effect of folic acid antagonists on acute leukemia and other forms of incurable cancer. *Blood* **1949**, *4*, 160-167.

(3) Farber, S.; Diamond, L. K. Temporary remissions in acute leukemia in children produced by folic acid antagonist, 4-aminopteroyl-glutamic acid. *N. Engl. J. Med.* **1948**, *238*, 787-793.

(4) Meienhofer, J. Syntheses of actinomycin and analogs. 3. A total synthesis of actinomycin D (Cl) via peptide cyclization between proline and sarcosine. *J. Am. Chem. Soc.* **1970**, *92*, 3771-3777.

(5) Pinkel, D. Actinomycin D in childhood cancer; a preliminary report. *Pediatrics* **1959**, *23*, 342-347.

(6) Heidelberger, C.; Chaudhuri, N. K.; Danneberg, P.; Mooren, D.; Griesbach, L.; Duschinsky, R.; Schnitzer, R. J.; Pleven, E.; Scheiner, J. Fluorinated pyrimidines, a new class of tumour-inhibitory compounds. *Nature* **1957**, *179*, 663-666.

(7) Hudis, C. A. Trastuzumab--mechanism of action and use in clinical practice. *N. Engl. J. Med.* **2007**, *357*, 39-51.

(8) Keizer, H. G.; Pinedo, H. M.; Schuurhuis, G. J.; Joenje, H. Doxorubicin (adriamycin): a critical review of free radical-dependent mechanisms of cytotoxicity. *Pharm. Ther.* **1990**, *47*, 219-231.

(9) el Saghir, N. S.; Hawkins, K. A. Hepatotoxicity following vincristine therapy. *Cancer* **1984**, *54*, 2006-2008.

(10) Patterson, W. P.; Reams, G. P. Renal toxicities of chemotherapy. *Semin. Oncol.* **1992**, *19*, 521-528.

(11) Kreisman, H.; Wolkove, N. Pulmonary toxicity of antineoplastic therapy. *Semin. Oncol.* **1992**, *19*, 508-520.

(12) Hoangland, H. C., Gastineau, D. A. *Haematological complications of cancer chemotherapy*. 2nd ed.; 1992; p 559.

(13) Gottesman, M. M. Mechanisms of cancer drug resistance. *Annu. Rev. Med.* **2002**, *53*, 615-627.

(14) Housman, G.; Byler, S.; Heerboth, S.; Lapinska, K.; Longacre, M.; Snyder, N.; Sarkar, S. Drug resistance in cancer: an overview. *Cancers* **2014**, *6*, 1769-1792.

(15) Nam, N. H.; Parang, K. Current targets for anticancer drug discovery. *Curr. Drug. Targets.* **2003**, *4*, 159-179.

(16) Burugu, S.; Dancsok, A. R.; Nielsen, T. O. Emerging targets in cancer immunotherapy. *Semin. Cancer. Biol.* **2018**, *52*, 39-52.

(17) Zhao, Y.; Adjei, A. A. Targeting Angiogenesis in Cancer Therapy: Moving Beyond Vascular Endothelial Growth Factor. *Oncologists* **2015**, *20*, 660-673.

(18) Steeg, P. S. Targeting metastasis. *Nat. Rev. Cancer.* **2016**, *16*, 201-218.

(19) Nishida, N.; Yano, H.; Nishida, T.; Kamura, T.; Kojiro, M. Angiogenesis in cancer. *Vasc. Health. Risk. Manag.* **2006**, *2*, 213-219.

(20) Bai, J.; Li, Y.; Zhang, G. Cell cycle regulation and anticancer drug discovery. *Cancer. Biol. Med.* **2017**, *14*, 348-362.

(21) Baig, S.; Seevasant, I.; Mohamad, J.; Mukheem, A.; Huri, H. Z.; Kamarul, T. Potential of apoptotic pathway-targeted cancer therapeutic research: Where do we stand? *Cell. Death. Dis.* **2016**, *7*, e2058.

(22) Bhullar, K. S.; Lagaron, N. O.; McGowan, E. M.; Parmar, I.; Jha, A.; Hubbard, B. P.; Rupasinghe, H. P. V. Kinase-targeted cancer therapies: progress, challenges and future directions. *Mol. Cancer.* **2018**, *17*, 48.

(23) Mantovani, A.; Bussolino, F.; Introna, M. Cytokine regulation of endothelial cell function: from molecular level to the bedside. *Immunol. Today.* **1997**, *18*, 231-240.

(24) Mantovani, A.; Bussolino, F.; Dejana, E. Cytokine regulation of endothelial cell function. *FASEB J.* **1992**, *6*, 2591-2599.

(25) Rajabi, M.; Mousa, S. A. The Role of Angiogenesis in Cancer Treatment. *Biomedicines* **2017**, *5*.

(26) Gupta, M. K.; Qin, R. Y. Mechanism and its regulation of tumor-induced angiogenesis. *World. J. Gastroenterol.* **2003**, *9*, 1144-1155.

(27) Folkman, J. Role of angiogenesis in tumor growth and metastasis. *Semin. Oncol.* **2002**, *29*, 15-18.

(28) Folkman, J. Tumor angiogenesis: therapeutic implications. *N. Engl. J. Med.* **1971**, *285*, 1182-1186.

(29) Dameron, K. M.; Volpert, O. V.; Tainsky, M. A.; Bouck, N. Control of angiogenesis in fibroblasts by p53 regulation of thrombospondin-1. *Science* **1994**, *265*, 1582-1584.

(30) Konda, B.; Shum, H.; Rajdev, L. Anti-angiogenic agents in metastatic colorectal cancer. *World. J. Gastrointest. Oncol.* **2015**, *7*, 71-86.

(31) Yadav, L.; Puri, N.; Rastogi, V.; Satpute, P.; Sharma, V. Tumour Angiogenesis and Angiogenic Inhibitors: A Review. *J. Clin. Diagn. Res.* **2015**, *9*, XE01-XE05.

(32) Nandikolla, A. G.; Rajdev, L. Targeting angiogenesis in gastrointestinal tumors: current challenges. *Transl. Gastroenterol. Hepatol.* **2016**, *1*, 67.

(33) Oehler, M. K.; Bicknell, R. The promise of anti-angiogenic cancer therapy. *Br. J. Cancer.* **2000**, *82*, 749-752.

(34) Griscelli, F.; Li, H.; Bennaceur-Griscelli, A.; Soria, J.; Opolon, P.; Soria, C.; Perricaudet, M.; Yeh, P.; Lu, H. Angiostatin gene transfer: inhibition of tumor growth in vivo by blockage of endothelial cell proliferation associated with a mitosis arrest. *Proc. Natl. Acad. Sci. U.S.A.* **1998**, *95*, 6367-6372.

(35) Hajitou, A.; Grignet, C.; Devy, L.; Berndt, S.; Blacher, S.; Deroanne, C. F.; Bajou, K.; Fong, T.; Chiang, Y.; Foidart, J. M.; Noel, A. The antitumoral effect of endostatin and angiostatin is associated with a down-regulation of vascular endothelial growth factor expression in tumor cells. *FASEB J.* **2002**, *16*, 1802-1804.

(36) Moser, T. L.; Stack, M. S.; Asplin, I.; Enghild, J. J.; Hojrup, P.; Everitt, L.; Hubchak, S.; Schnaper, H. W.; Pizzo, S. V. Angiostatin binds ATP synthase on the surface of human endothelial cells. *Proc. Natl. Acad. Sci. U.S.A.* **1999**, *96*, 2811-2816.

(37) Kim, Y. M.; Hwang, S.; Kim, Y. M.; Pyun, B. J.; Kim, T. Y.; Lee, S. T.; Gho, Y. S.; Kwon, Y. G. Endostatin blocks vascular endothelial growth factor-mediated signaling via direct interaction with KDR/Flk-1. *J. Biol. Chem.* **2002**, *277*, 27872-27879.

(38) Strawn, L. M.; McMahon, G.; App, H.; Schreck, R.; Kuchler, W. R.; Longhi, M. P.; Hui, T. H.; Tang, C.; Levitzki, A.; Gazit, A.; Chen, I.; Keri, G.; Orfi, L.; Risau, W.; Flamme, I.; Ullrich, A.; Hirth, K. P.; Shawver, L. K. Flk-1 as a target for tumor growth inhibition. *Cancer. Res.* **1996**, *56*, 3540-3545.

(39) Verheul, H. M.; Jorna, A. S.; Hoekman, K.; Broxterman, H. J.; Gebbink, M. F.; Pinedo, H. M. Vascular endothelial growth factor-stimulated endothelial cells promote adhesion and activation of platelets. *Blood* **2000**, *96*, 4216-4221.

(40) Ferrara, N.; Davis-Smyth, T. The biology of vascular endothelial growth factor. *Endocr. Rev.* **1997**, *18*, 4-25.

(41) Leung, D. W.; Cachianes, G.; Kuang, W. J.; Goeddel, D. V.; Ferrara, N. Vascular endothelial growth factor is a secreted angiogenic mitogen. *Science* **1989**, *246*, 1306-1309.

(42) Senger, D. R.; Galli, S. J.; Dvorak, A. M.; Perruzzi, C. A.; Harvey, V. S.; Dvorak, H. F. Tumor cells secrete a vascular permeability factor that promotes accumulation of ascites fluid. *Science* **1983**, *219*, 983-985.

(43) Gerber, H. P.; Dixit, V.; Ferrara, N. Vascular endothelial growth factor induces expression of the antiapoptotic proteins Bcl-2 and A1 in vascular endothelial cells. *J. Biol. Chem.* **1998**, *273*, 13313-13316.

(44) Hsu, J. Y.; Wakelee, H. A. Monoclonal antibodies targeting vascular endothelial growth factor: current status and future challenges in cancer therapy. *BioDrugs* **2009**, *23*, 289-304.

(45) Giantonio, B. J.; Levy, D. E.; O'Dwyer P, J.; Meropol, N. J.; Catalano, P. J.; Benson, A. B., 3rd; Eastern Cooperative Oncology, G. A phase II study of high-dose bevacizumab in combination with irinotecan, 5-fluorouracil, leucovorin, as initial therapy for advanced colorectal cancer: results from the Eastern Cooperative Oncology Group study E2200. *Ann. Oncol.* **2006**, *17*, 1399-1403.

(46) Johnson, D. H.; Fehrenbacher, L.; Novotny, W. F.; Herbst, R. S.; Nemunaitis, J. J.; Jablons, D. M.; Langer, C. J.; DeVore, R. F., 3rd; Gaudreault, J.; Damico, L. A.; Holmgren, E.; Kabbinavar, F. Randomized phase II trial comparing bevacizumab plus carboplatin and paclitaxel with carboplatin and paclitaxel alone in previously untreated locally advanced or metastatic non-small-cell lung cancer. *J. Clin. Oncol.* **2004**, *22*, 2184-2191.

(47) Kabbinavar, F.; Hurwitz, H. I.; Fehrenbacher, L.; Meropol, N. J.; Novotny, W. F.; Lieberman, G.; Griffing, S.; Bergsland, E. Phase II, randomized trial comparing bevacizumab plus fluorouracil (FU)/leucovorin (LV) with FU/LV alone in patients with metastatic colorectal cancer. *J. Clin. Oncol.* **2003**, *21*, 60-65.

(48) Zhou, M.; Yu, P.; Qu, X.; Liu, Y.; Zhang, J. Phase III trials of standard chemotherapy with or without bevacizumab for ovarian cancer: a meta-analysis. *PloS one* **2013**, *8*, e81858.

(49) Gan, H. K.; Seruga, B.; Knox, J. J. Sunitinib in solid tumors. *Expert. Opin. Investig. Drugs.* **2009**, *18*, 821-834.

(50) Wilhelm, S. M.; Adnane, L.; Newell, P.; Villanueva, A.; Llovet, J. M.; Lynch, M. Preclinical overview of sorafenib, a multikinase inhibitor that targets both Raf and VEGF and PDGF receptor tyrosine kinase signaling. *Mol. Cancer. Ther.* **2008**, *7*, 3129-3140.

(51) Rabbani, S. A. Metalloproteases and urokinase in angiogenesis and tumor progression. *In Vivo* **1998**, *12*, 135-142.

(52) Weidle, U. H.; Konig, B. Urokinase receptor antagonists: novel agents for the treatment of cancer. *Expert. Opin. Investig. Drugs.* **1998**, *7*, 391-403.

(53) Vandenbroucke, R. E.; Libert, C. Is there new hope for therapeutic matrix metalloproteinase inhibition? *Nat. Rev. Drug. Discov.* **2014**, *13*, 904-927.

(54) Coussens, L. M.; Fingleton, B.; Matrisian, L. M. Matrix metalloproteinase inhibitors and cancer: trials and tribulations. *Science* **2002**, *295*, 2387-2392.

(55) Whittaker, M.; Floyd, C. D.; Brown, P.; Gearing, A. J. Design and therapeutic application of matrix metalloproteinase inhibitors. *Chem. Rev.* **1999**, *99*, 2735-2776.

(56) Evans, J. D.; Stark, A.; Johnson, C. D.; Daniel, F.; Carmichael, J.; Buckels, J.; Imrie, C. W.; Brown, P.; Neoptolemos, J. P. A phase II trial of marimastat in advanced pancreatic cancer. *Br. J. Cancer.* **2001**, *85*, 1865-1870.

(57) Rothenberg, M. L.; Nelson, A. R.; Hande, K. R. New Drugs on the Horizon: Matrix Metalloproteinase Inhibitors. *Oncologist* **1998**, *3*, 271-274.

(58) Zervox, E. E.; Franz, M. G.; Salhab, K. F.; Shafii, A. E.; Menendez, J.; Gower, W. R.; Rosemurgy, A. S. Matrix metalloproteinase inhibition improves survival in an orthotopic model of human pancreatic cancer. *J. Gastrointest. Surg.* **2000**, *4*, 614-619.

(59) Overall, C. M.; Kleifeld, O. Towards third generation matrix metalloproteinase inhibitors for cancer therapy. *Br. J. Cancer.* **2006**, *94*, 941-946.

(60) Pirard, B. Insight into the structural determinants for selective inhibition of matrix metalloproteinases. *Drug. Discov. Today.* **2007**, *12*, 640-646.

(61) Norbury, C.; Nurse, P. Animal cell cycles and their control. *Annu. Rev. Biochem.* **1992**, *61*, 441-470.

(62) Malumbres, M.; Barbacid, M. To cycle or not to cycle: a critical decision in cancer. *Nat. Rev. Cancer.* **2001**, *1*, 222-231.

(63) Hunter, T. Signaling--2000 and beyond. *Cell* **2000**, *100*, 113-127.

(64) Diaz-Moralli, S.; Tarrado-Castellarnau, M.; Miranda, A.; Cascante, M. Targeting cell cycle regulation in cancer therapy. *Pharmacol. Ther.* **2013**, *138*, 255-271.

(65) Malumbres, M. Physiological relevance of cell cycle kinases. *Physiol. Rev.* **2011**, *91*, 973-1007.

(66) Malumbres, M.; Barbacid, M. Mammalian cyclin-dependent kinases. *Trends Biochem. Sci.* **2005**, *30*, 630-641.

(67) Mohanakumara, P.; Sreejayan, N.; Priti, V.; Ramesha, B. T.; Ravikanth, G.; Ganeshaiah, K. N.; Vasudeva, R.; Mohan, J.; Santhoshkumar, T. R.; Mishra, P. D.; Ram, V.; Shaanker, R. U. Dysoxylum binectariferum Hook.f (Meliaceae), a rich source of rohitukine. *Fitoterapia.* **2010**, *81*, 145-148.

(68) Shapiro, G. I. Preclinical and clinical development of the cyclin-dependent kinase inhibitor flavopiridol. *Clin. Cancer Res.* **2004**, *10*, 4270s-4275s.

(69) Clark, A. S.; Karasic, T. B.; DeMichele, A.; Vaughn, D. J.; O'Hara, M.; Perini, R.; Zhang, P.; Lal, P.; Feldman, M.; Gallagher, M.; O'Dwyer, P. J. Palbociclib (PD0332991)-a Selective and Potent Cyclin-Dependent Kinase Inhibitor: A Review of Pharmacodynamics and Clinical Development. *JAMA. Oncol.* **2016**, *2*, 253-260.

(70) Dhillon, S. Palbociclib: first global approval. *Drugs* **2015**, *75*, 543-551.

(71) Adams, J. M. Ways of dying: multiple pathways to apoptosis. *Genes. Dev.* **2003**, *17*, 2481-2495.

(72) Shi, Y. Mechanical aspects of apoptosome assembly. *Curr. Opin. Cell. Biol.* **2006**, *18*, 677-684.

(73) Gautschi, O.; Tschopp, S.; Olie, R. A.; Leech, S. H.; Simoes-Wust, A. P.; Ziegler, A.; Baumann, B.; Odermatt, B.; Hall, J.; Stahel, R. A.; Zangemeister-Wittke, U. Activity of a novel bcl-2/bcl-xL-bispecific antisense oligonucleotide against tumors of diverse histologic origins. *J. Natl. Cancer. Inst.* **2001**, *93*, 463-471.

(74) Kang, M. H.; Reynolds, C. P. Bcl-2 inhibitors: targeting mitochondrial apoptotic pathways in cancer therapy. *Clin. Cancer Res.* **2009**, *15*, 1126-1132.

(75) Papadopoulos, K. Targeting the Bcl-2 family in cancer therapy. *Semin. Oncol.* **2006**, *33*, 449-456.

(76) Kamal, A.; Faazil, S.; Malik, M. S. Apoptosis-inducing agents: a patent review (2010 - 2013). *Expert. Opin. Ther. Pat.* **2014**, *24*, 339-354.

(77) Bedikian, A. Y.; Millward, M.; Pehamberger, H.; Conry, R.; Gore, M.; Trefzer, U.; Pavlick, A. C.; DeConti, R.; Hersh, E. M.; Hersey, P.; Kirkwood, J. M.; Haluska, F. G.; Oblimersen Melanoma Study, G. Bcl-2 antisense (oblimersen sodium) plus dacarbazine in patients with advanced melanoma: the Oblimersen Melanoma Study Group. *J. Clin. Oncol.* **2006**, *24*, 4738-4745.

(78) Rudin, C. M.; Salgia, R.; Wang, X.; Hodgson, L. D.; Masters, G. A.; Green, M.; Vokes, E. E. Randomized phase II Study of carboplatin and etoposide with or without the bcl-2 antisense oligonucleotide oblimersen for extensive-stage small-cell lung cancer: CALGB 30103. *J. Clin. Oncol.* **2008**, *26*, 870-876.

(79) Eot-Houllier, G.; Fulcrand, G.; Magnaghi-Jaulin, L.; Jaulin, C. Histone deacetylase inhibitors and genomic instability. *Cancer. Lett.* **2009**, *274*, 169-176.

(80) Glozak, M. A.; Seto, E. Histone deacetylases and cancer. *Oncogene* **2007**, *26*, 5420-5432.

(81) Hrabeta, J.; Stiborova, M.; Adam, V.; Kizek, R.; Eckschlager, T. Histone deacetylase inhibitors in cancer therapy. A review. *Biomed Pap Med Fac Univ Palacky Olomouc Czech Repub.* **2014**, *158*, 161-169.

(82) West, A. C.; Johnstone, R. W. New and emerging HDAC inhibitors for cancer treatment. *J. Clin. Invest.* **2014**, *124*, 30-39.

(83) Mann, B. S.; Johnson, J. R.; Cohen, M. H.; Justice, R.; Pazdur, R. FDA approval summary: vorinostat for treatment of advanced primary cutaneous T-cell lymphoma. *Oncologist* **2007**, *12*, 1247-1252.

(84) Piekarz, R. L.; Frye, R.; Prince, H. M.; Kirschbaum, M. H.; Zain, J.; Allen, S. L.; Jaffe, E. S.; Ling, A.; Turner, M.; Peer, C. J.; Figg, W. D.; Steinberg, S. M.; Smith, S.; Joske, D.; Lewis, I.; Hutchins, L.; Craig, M.; Fojo, A. T.; Wright, J. J.; Bates, S. E. Phase 2 trial of romidepsin in patients with peripheral T-cell lymphoma. *Blood* **2011**, *117*, 5827-5834.

(85) Lee, H. Z.; Kwitkowski, V. E.; Del Valle, P. L.; Ricci, M. S.; Saber, H.; Habtemariam, B. A.; Bullock, J.; Bloomquist, E.; Li Shen, Y.; Chen, X. H.; Brown, J.; Mehrotra, N.; Dorff, S.; Charlab, R.; Kane, R. C.; Kaminskas, E.; Justice, R.; Farrell, A. T.; Pazdur, R. FDA Approval: Belinostat for the Treatment of Patients with Relapsed or Refractory Peripheral T-cell Lymphoma. *Clin. Cancer Res.* **2015**, *21*, 2666-2670.

(86) Hitzerd, S. M.; Verbrugge, S. E.; Ossenkoppele, G.; Jansen, G.; Peters, G. J. Positioning of aminopeptidase inhibitors in next generation cancer therapy. *Amino Acids* **2014**, *46*, 793-808.

(87) Maroux, S.; Louvard, D.; Baratti, J. The aminopeptidase from hog intestinal brush border. *Biochim. Biophys. Acta.* **1973**, *321*, 282-295.

(88) Dixon, J.; Kaklamanis, L.; Turley, H.; Hickson, I. D.; Leek, R. D.; Harris, A. L.; Gatter, K. C. Expression of aminopeptidase-n (CD 13) in normal tissues and malignant neoplasms of epithelial and lymphoid origin. *J. Clin. Pathol.* **1994**, *47*, 43-47.

(89) Look, A. T.; Ashmun, R. A.; Shapiro, L. H.; Peiper, S. C. Human myeloid plasma membrane glycoprotein CD13 (gp150) is identical to aminopeptidase N. *J. Clin. Invest.* **1989**, *83*, 1299-1307.

(90) Wickstrom, M.; Larsson, R.; Nygren, P.; Gullbo, J. Aminopeptidase N (CD13) as a target for cancer chemotherapy. *Cancer Sci.* **2011**, *102*, 501-508.

(91) Halder, A. K.; Saha, A.; Jha, T. Exploration of structural and physicochemical requirements and search of virtual hits for aminopeptidase N inhibitors. *Mol. Diversity.* **2013**, *17*, 123-137.

(92) Mina-Osorio, P. The moonlighting enzyme CD13: old and new functions to target. *Trends. Mol. Med.* **2008**, *14*, 361-371.

(93) George, A. J.; Thomas, W. G.; Hannan, R. D. The renin-angiotensin system and cancer: old dog, new tricks. *Nat. Rev. Cancer.* **2010**, *10*, 745-759.

(94) Matsas, R.; Stephenson, S. L.; Hryszko, J.; Kenny, A. J.; Turner, A. J. The metabolism of neuropeptides. Phase separation of synaptic membrane preparations with Triton X-114 reveals the presence of aminopeptidase N. *Biochem. J.* **1985**, *231*, 445-449.

(95) Proost, P.; Mortier, A.; Loos, T.; Vandercappellen, J.; Gouwy, M.; Ronsse, I.; Schutyser, E.; Put, W.; Parmentier, M.; Struyf, S.; Van Damme, J. Proteolytic processing of CXCL11 by CD13/aminopeptidase N impairs CXCR3 and CXCR7 binding and signaling and reduces lymphocyte and endothelial cell migration. *Blood* **2007**, *110*, 37-44.

(96) Ghosh, M.; McAuliffe, B.; Subramani, J.; Basu, S.; Shapiro, L. H. CD13 regulates dendritic cell cross-presentation and T cell responses by inhibiting receptor-mediated antigen uptake. *J. Immunol.* **2012**, *188*, 5489-5499.

(97) Yeager, C. L.; Ashmun, R. A.; Williams, R. K.; Cardellichio, C. B.; Shapiro, L. H.; Look, A. T.; Holmes, K. V. Human aminopeptidase N is a receptor for human coronavirus 229E. *Nature* **1992**, *357*, 420-422.

(98) Amin, S. A.; Adhikari, N.; Jha, T. Design of aminopeptidase N inhibitors as anti-cancer agents. *J. Med. Chem.* **2018**, *61*, 6468-6490.

(99) Tokuhara, T.; Hattori, N.; Ishida, H.; Hirai, T.; Higashiyama, M.; Kodama, K.; Miyake, M. Clinical significance of aminopeptidase N in non-small cell lung cancer. *Clin. Cancer Res.* **2006**, *12*, 3971-3978.

(100) Kehlen, A.; Lendeckel, U.; Dralle, H.; Langner, J.; Hoang-Vu, C. Biological significance of aminopeptidase N/CD13 in thyroid carcinomas. *Cancer. Res.* **2003**, *63*, 8500-8506.

(101) Lee, P. S.; Lin, C. N.; Liu, C.; Huang, C. T.; Hwang, W. S. Acute leukemia with myeloid, B-, and natural killer cell differentiation. *Arch. Pathol. Lab. Med.* **2003**, *127*, E93-95.

(102) Hashida, H.; Takabayashi, A.; Kanai, M.; Adachi, M.; Kondo, K.; Kohno, N.; Yamaoka, Y.; Miyake, M. Aminopeptidase N is involved in cell motility and angiogenesis: its clinical significance in human colon cancer. *Gastroenterology* **2002**, *122*, 376-386.

(103) Ishii, K.; Usui, S.; Sugimura, Y.; Yoshida, S.; Hioki, T.; Tatematsu, M.; Yamamoto, H.; Hirano, K. Aminopeptidase N regulated by zinc in human prostate participates in tumor cell invasion. *Int. J. Cancer.* **2001**, *92*, 49-54.

(104) Pasqualini, R.; Koivunen, E.; Kain, R.; Lahdenranta, J.; Sakamoto, M.; Stryhn, A.; Ashmun, R. A.; Shapiro, L. H.; Arap, W.; Ruoslahti, E. Aminopeptidase N is a receptor for tumor-homing peptides and a target for inhibiting angiogenesis. *Cancer. Res.* **2000**, *60*, 722-727.

(105) Fukasawa, K.; Fujii, H.; Saitoh, Y.; Koizumi, K.; Aozuka, Y.; Sekine, K.; Yamada, M.; Saiki, I.; Nishikawa, K. Aminopeptidase N (APN/CD13) is selectively expressed in vascular endothelial cells and plays multiple roles in angiogenesis. *Cancer. Lett.* **2006**, *243*, 135-143.

(106) Wirtz, D.; Konstantopoulos, K.; Searson, P. C. The physics of cancer: the role of physical interactions and mechanical forces in metastasis. *Nat. Rev. Cancer.* **2011**, *11*, 512-522.

(107) Mina-Osorio, P.; Shapiro, L. H.; Ortega, E. CD13 in cell adhesion: aminopeptidase N (CD13) mediates homotypic aggregation of monocytic cells. *J. Leukoc. Biol.* **2006**, *79*, 719-730.

(108) Saiki, I.; Fujii, H.; Yoneda, J.; Abe, F.; Nakajima, M.; Tsuruo, T.; Azuma, I. Role of aminopeptidase N (CD13) in tumor-cell invasion and extracellular matrix degradation. *Int. J. Cancer.* **1993**, *54*, 137-143.

(109) Hooper, N. M. Families of zinc metalloproteases. *FEBS Lett.* **1994**, *354*, 1-6.

(110) Wong, A. H.; Zhou, D.; Rini, J. M. The X-ray crystal structure of human aminopeptidase N reveals a novel dimer and the basis for peptide processing. *J. Biol. Chem.* **2012**, *287*, 36804-36813.

(111) Danziger, R. S. Aminopeptidase N in arterial hypertension. *Heart. Fail. Rev.* **2008**, *13*, 293-298.

(112) Xu, Y.; Wellner, D.; Scheinberg, D. A. Substance P and bradykinin are natural inhibitors of CD13/aminopeptidase N. *Biochem. Biophys. Res. Commun.* **1995**, *208*, 664-674.

(113) Giros, B.; Gros, C.; Solhonne, B.; Schwartz, J. C. Characterization of aminopeptidases responsible for inactivating endogenous (Met5)enkephalin in brain slices using peptidase inhibitors and anti-aminopeptidase M antibodies. *Mol. Pharmacol.* **1986**, *29*, 281-287.

(114) Bawolak, M. T.; Fortin, J. P.; Vogel, L. K.; Adam, A.; Marceau, F. The bradykinin B2 receptor antagonist icatibant (Hoe 140) blocks aminopeptidase N at micromolar concentrations: off-target alterations of signaling mediated by the bradykinin B1 and angiotensin receptors. *Eur. J. Pharmacol.* **2006**, *551*, 108-111.

(115) Garreau, I.; Chansel, D.; Vandermeersch, S.; Fruitier, I.; Piot, J. M.; Ardaillou, R. Hemorphins inhibit angiotensin IV binding and interact with aminopeptidase N. *Peptides* **1998**, *19*, 1339-1348.

(116) Hoffmann, T.; Faust, J.; Neubert, K.; Ansorge, S. Dipeptidyl peptidase IV (CD 26) and aminopeptidase N (CD 13) catalyzed hydrolysis of cytokines and peptides with N-terminal cytokine sequences. *FEBS Lett.* **1993**, *336*, 61-64.

(117) Kolb, A. F.; Hegyi, A.; Maile, J.; Heister, A.; Hagemann, M.; Siddell, S. G. Molecular analysis of the coronavirus-receptor function of aminopeptidase N. *Adv. Exp. Med. Biol.* **1998**, *440*, 61-67.

(118) Bosch, B. J.; Smits, S. L.; Haagmans, B. L. Membrane ectopeptidases targeted by human coronaviruses. *Curr. Opin. Virol.* **2014**, *6*, 55-60.

(119) Delmas, B. G., J.; L'Haridon, R.; Vogel, L. K.; Sjostrom, H.; Noren, O.; Laude, H. Aminopeptidase N is a major receptor for the entero-pathogenic coronavirus TGEV. *Nature* **1992**, *357*, 417-420.

(120) Li, W.; Hulswit, R. J. G.; Kenney, S. P.; Widjaja, I.; Jung, K.; Alhamo, M. A.; van Dieren, B.; van Kuppeveld, F. J. M.; Saif, L. J.; Bosch, B. J. Broad receptor engagement of an emerging global coronavirus may potentiate its diverse cross-species transmissibility. *Proc. Natl. Acad. Sci. U.S.A.* **2018**, *115*, E5135-E5143.

(121) Tresnan, D. B.; Levis, R.; Holmes, K. V. Feline aminopeptidase N serves as a receptor for feline, canine, porcine, and human coronaviruses in serogroup I. *J. Virol.* **1996**, *70*, 8669-8674.

(122) Tusell, S. M.; Schittone, S. A.; Holmes, K. V. Mutational analysis of aminopeptidase N, a receptor for several group 1 coronaviruses, identifies key determinants of viral host range. *J. Virol.* **2007**, *81*, 1261-1273.

(123) Reguera, J.; Santiago, C.; Mudgal, G.; Ordono, D.; Enjuanes, L.; Casasnovas, J. M. Structural bases of coronavirus attachment to host aminopeptidase N and its inhibition by neutralizing antibodies. *PLoS pathogens* **2012**, *8*, e1002859.

(124) Santiago, C.; Mudgal, G.; Reguera, J.; Recacha, R.; Albrecht, S.; Enjuanes, L.; Casasnovas, J. M. Allosteric inhibition of aminopeptidase N functions related to tumor growth and virus infection. *Sci. Rep.* **2017**, *7*, 46045.

(125) Kramer, W.; Girbig, F.; Corsiero, D.; Pfenninger, A.; Frick, W.; Jahne, G.; Rhein, M.; Wendler, W.; Lottspeich, F.; Hochleitner, E. O.; Orso, E.; Schmitz, G. Aminopeptidase N (CD13) is a molecular target of the cholesterol absorption inhibitor ezetimibe in the enterocyte brush border membrane. *J. Biol. Chem.* **2005**, *280*, 1306-1320.

(126) Kramer, W.; Glombik, H.; Petry, S.; Heuer, H.; Schafer, H.; Wendler, W.; Corsiero, D.; Girbig, F.; Weyland, C. Identification of binding proteins for cholesterol absorption inhibitors as components of the intestinal cholesterol transporter. *FEBS Lett.* **2000**, *487*, 293-297.

(127) Santos, A. N.; Langner, J.; Herrmann, M.; Riemann, D. Aminopeptidase N/CD13 is directly linked to signal transduction pathways in monocytes. *Cell Immunol.* **2000**, *201*, 22-32.

(128) Sjostrom, H.; Noren, O.; Olsen, J. Structure and function of aminopeptidase N. *Adv. Exp. Med. Biol.* **2000**, *477*, 25-34.

(129) Miki, T.; Takegami, Y.; Okawa, K.; Muraguchi, T.; Noda, M.; Takahashi, C. The reversion-inducing cysteine-rich protein with Kazal motifs (RECK) interacts with membrane type 1 matrix metalloproteinase and CD13/aminopeptidase N and modulates their endocytic pathways. *J. Biol. Chem.* **2007**, *282*, 12341-12352.

(130) Chang, Y. W.; Chen, S. C.; Cheng, E. C.; Ko, Y. P.; Lin, Y. C.; Kao, Y. R.; Tsay, Y. G.; Yang, P. C.; Wu, C. W.; Roffler, S. R. CD13 (aminopeptidase N) can associate with tumor-associated antigen L6 and enhance the motility of human lung cancer cells. *Int. J. Cancer.* **2005**, *116*, 243-252.

(131) Danielsen, E. M.; van Deurs, B. Galectin-4 and small intestinal brush border enzymes form clusters. *Mol. Biol. Cell.* **1997**, *8*, 2241-2251.

(132) Bhagwat, S. V.; Petrovic, N.; Okamoto, Y.; Shapiro, L. H. The angiogenic regulator CD13/APN is a transcriptional target of Ras signaling pathways in endothelial morphogenesis. *Blood* **2003**, *101*, 1818-1826.

(133) Mina-Osorio, P.; Ortega, E. Aminopeptidase N (CD13) functionally interacts with FcgammaRs in human monocytes. *J. Leukoc. Biol.* **2005**, *77*, 1008-1017.

(134) Reinhold, D.; Biton, A.; Pieper, S.; Lendeckel, U.; Faust, J.; Neubert, K.; Bank, U.; Tager, M.; Ansorge, S.; Brocke, S. Dipeptidyl peptidase IV (DP IV, CD26) and aminopeptidase N (APN, CD13) as regulators of T cell function and targets of immunotherapy in CNS inflammation. *Int. Immunopharmacol.* **2006**, *6*, 1935-1942.

(135) Dan, H.; Tani, K.; Hase, K.; Shimizu, T.; Tamiya, H.; Biraa, Y.; Huang, L.; Yanagawa, H.; Sone, S. CD13/aminopeptidase N in collagen vascular diseases. *Rheumatol. Int.* **2003**, *23*, 271-276.

(136) Rohnert, P.; Schmidt, W.; Emmerlich, P.; Goihl, A.; Wrenger, S.; Bank, U.; Nordhoff, K.; Tager, M.; Ansorge, S.; Reinhold, D.; Striggow, F. Dipeptidyl peptidase IV, aminopeptidase N and DPIV/APN-like proteases in cerebral ischemia. *J. Neuroinflammation.* **2012**, *9*, 44.

(137) Soderberg, C.; Giugni, T. D.; Zaia, J. A.; Larsson, S.; Wahlberg, J. M.; Moller, E. CD13 (human aminopeptidase N) mediates human cytomegalovirus infection. *J. Virol.* **1993**, *67*, 6576-6585.

(138) Luan, Y.; Xu, W. The structure and main functions of aminopeptidase N. *Curr. Med. Chem.* **2007**, *14*, 639-647.

(139) Sato, Y. Role of aminopeptidase in angiogenesis. *Biol. Pharm. Bull.* **2004**, *27*, 772-776.

(140) Enyedi, K. N.; Toth, S.; Szakacs, G.; Mezo, G. NGR-peptide-drug conjugates with dual targeting properties. *PloS one* **2017**, *12*, e0178632.

(141) Koivunen, E.; Gay, D. A.; Ruoslahti, E. Selection of peptides binding to the alpha 5 beta 1 integrin from phage display library. *J. Biol. Chem.* **1993**, *268*, 20205-20210.

(142) Healy, J. M.; Murayama, O.; Maeda, T.; Yoshino, K.; Sekiguchi, K.; Kikuchi, M. Peptide ligands for integrin alpha v beta 3 selected from random phage display libraries. *Biochemistry* **1995**, *34*, 3948-3955.

(143) Pasqualini, R.; Koivunen, E.; Ruoslahti, E. A peptide isolated from phage display libraries is a structural and functional mimic of an RGD-binding site on integrins. *J. Cell Biol.* **1995**, *130*, 1189-1196.

(144) Gregorc, V.; De Braud, F. G.; De Pas, T. M.; Scalamogna, R.; Citterio, G.; Milani, A.; Boselli, S.; Catania, C.; Donadoni, G.; Rossoni, G.; Ghio, D.; Spitaleri, G.; Ammannati, C.; Colombi, S.; Caligaris-Cappio, F.; Lambiase, A.; Bordignon, C. Phase I study of NGR-hTNF, a selective vascular targeting agent, in combination with cisplatin in refractory solid tumors. *Clin. Cancer Res.* **2011**, *17*, 1964-1972.

(145) Santoro, A.; Rimassa, L.; Sobrero, A. F.; Citterio, G.; Sclafani, F.; Carnaghi, C.; Pessino, A.; Caprioni, F.; Andretta, V.; Tronconi, M. C.; Finocchiaro, G.; Rossoni, G.; Zanoni, A.; Miggiano, C.; Rizzardi, G. P.; Traversari, C.; Caligaris-Cappio, F.; Lambiase, A.; Bordignon, C. Phase II study of NGR-hTNF, a selective vascular targeting agent, in patients with metastatic colorectal cancer after failure of standard therapy. *Eur. J. Cancer.* **2010**, *46*, 2746-2752.

(146) Bhagwat, S. V.; Lahdenranta, J.; Giordano, R.; Arap, W.; Pasqualini, R.; Shapiro, L. H. CD13/APN is activated by angiogenic signals and is essential for capillary tube formation. *Blood* **2001**, *97*, 652-659.

(147) Guzman-Rojas, L.; Rangel, R.; Salameh, A.; Edwards, J. K.; Dondossola, E.; Kim, Y. G.; Saghatelian, A.; Giordano, R. J.; Kolonin, M. G.; Staquicini, F. I.; Koivunen, E.; Sidman, R. L.; Arap, W.; Pasqualini, R. Cooperative effects of aminopeptidase N (CD13) expressed by

nonmalignant and cancer cells within the tumor microenvironment. *Proc. Natl. Acad. Sci. U.S.A.* **2012**, *109*, 1637-1642.

(148) Rangel, R.; Sun, Y.; Guzman-Rojas, L.; Ozawa, M. G.; Sun, J.; Giordano, R. J.; Van Pelt, C. S.; Tinkey, P. T.; Behringer, R. R.; Sidman, R. L.; Arap, W.; Pasqualini, R. Impaired angiogenesis in aminopeptidase N-null mice. *Proc. Natl. Acad. Sci. U.S.A.* **2007**, *104*, 4588-4593.

(149) Valastyan, S.; Weinberg, R. A. Tumor metastasis: molecular insights and evolving paradigms. *Cell* **2011**, *147*, 275-292.

(150) Su, L.; Cao, J.; Jia, Y.; Zhang, X.; Fang, H.; Xu, W. Development of synthetic aminopeptidase N/CD13 inhibitors to overcome cancer metastasis and angiogenesis. *ACS. Med. Chem. Lett.* **2012**, *3*, 959-964.

(151) Chaffer, C. L.; Weinberg, R. A. A perspective on cancer cell metastasis. *Science* **2011**, *331*, 1559-1564.

(152) Yoneda, J.; Saiki, I.; Fujii, H.; Abe, F.; Kojima, Y.; Azuma, I. Inhibition of tumor invasion and extracellular matrix degradation by ubenimex (bestatin). *Clin. Exp. Metastasis.* **1992**, *10*, 49-59.

(153) Liang, W.; Gao, B.; Xu, G.; Weng, D.; Xie, M.; Qian, Y. Possible contribution of aminopeptidase N (APN/CD13) to migration and invasion of human osteosarcoma cell lines. *Int. J. Oncol.* **2014**, *45*, 2475-2485.

(154) Drinkwater, N.; Lee, J.; Yang, W.; Malcolm, T. R.; McGowan, S. M1 aminopeptidases as drug targets: broad applications or therapeutic niche? *FEBS J.* **2017**, *284*, 1473-1488.

(155) Peer, W. A. The role of multifunctional M1 metallopeptidases in cell cycle progression. *Ann. Bot.* **2011**, *107*, 1171-1181.

(156) Chen, L.; Lin, Y. L.; Peng, G.; Li, F. Structural basis for multifunctional roles of mammalian aminopeptidase N. *Proc. Natl. Acad. Sci. U.S.A.* **2012**, *109*, 17966-17971.

(157) Vazeux, G.; Wang, J.; Corvol, P.; Llorens-Cortes, C. Identification of glutamate residues essential for catalytic activity and zinc coordination in aminopeptidase A. *J. Biol. Chem.* **1996**, *271*, 9069-9074.

(158) Wang, J.; Cooper, M. D. Histidine residue in the zinc-binding motif of aminopeptidase A is critical for enzymatic activity. *Proc. Natl. Acad. Sci. U.S.A.* **1993**, *90*, 1222-1226.

(159) Medina, J. F.; Wetterholm, A.; Radmark, O.; Shapiro, R.; Haeggstrom, J. Z.; Vallee, B. L.; Samuelsson, B. Leukotriene A4 hydrolase: determination of the three zinc-binding ligands by site-directed mutagenesis and zinc analysis. *Proc. Natl. Acad. Sci. U.S.A.* **1991**, *88*, 7620-7624.

(160) Drag, M.; Bogyo, M.; Ellman, J. A.; Salvesen, G. S. Aminopeptidase fingerprints, an integrated approach for identification of good substrates and optimal inhibitors. *J. Biol. Chem.* **2010**, *285*, 3310-3318.

(161) McGowan, S.; Porter, C. J.; Lowther, J.; Stack, C. M.; Golding, S. J.; Skinner-Adams, T. S.; Trenholme, K. R.; Teuscher, F.; Donnelly, S. M.; Grembecka, J.; Mucha, A.; Kafarski, P.; Degori, R.; Buckle, A. M.; Gardiner, D. L.; Whisstock, J. C.; Dalton, J. P. Structural basis for the inhibition of the essential Plasmodium falciparum M1 neutral aminopeptidase. *Proc. Natl. Acad. Sci. U.S.A.* **2009**, *106*, 2537-2542.

(162) Kochan, G.; Krojer, T.; Harvey, D.; Fischer, R.; Chen, L.; Vollmar, M.; von Delft, F.; Kavanagh, K. L.; Brown, M. A.; Bowness, P.; Wordsworth, P.; Kessler, B. M.; Oppermann, U. Crystal structures of the endoplasmic reticulum aminopeptidase-1 (ERAP1) reveal the molecular basis for N-terminal peptide trimming. *Proc. Natl. Acad. Sci. U.S.A.* **2011**, *108*, 7745-7750.

(163) Nguyen, T. T.; Chang, S. C.; Evnouchidou, I.; York, I. A.; Zikos, C.; Rock, K. L.; Goldberg, A. L.; Stratikos, E.; Stern, L. J. Structural basis for antigenic peptide precursor processing by the endoplasmic reticulum aminopeptidase ERAP1. *Nat. Struct. Mol. Biol.* **2011**, *18*, 604-613.

(164) Addlagatta, A.; Gay, L.; Matthews, B. W. Structure of aminopeptidase N from Escherichia coli suggests a compartmentalized, gated active site. *Proc. Natl. Acad. Sci. U.S.A.* **2006**, *103*, 13339-13344.

(165) Tholander, F.; Muroya, A.; Roques, B. P.; Fournie-Zaluski, M. C.; Thunnissen, M. M.; Haeggstrom, J. Z. Structure-based dissection of the active site chemistry of leukotriene A4 hydrolase: implications for M1 aminopeptidases and inhibitor design. *Chem. Biol.* **2008**, *15*, 920-929.

(166) Thunnissen, M. M.; Nordlund, P.; Haeggstrom, J. Z. Crystal structure of human leukotriene A(4) hydrolase, a bifunctional enzyme in inflammation. *Nat. Struct. Biol.* **2001**, *8*, 131-135.

(167) Gorvel, J. P.; Mishal, Z.; Liegey, F.; Rigal, A.; Maroux, S. Conformational change of rabbit aminopeptidase N into enterocyte plasma membrane domains analyzed by flow cytometry fluorescence energy transfer. *J. Cell Biol.* **1989**, *108*, 2193-2200.

(168) Favaloro, E. J.; Browning, T.; Facey, D. CD13 (GP150; aminopeptidase-N): predominant functional activity in blood is localized to plasma and is not cell-surface associated. *Exp. Hematol.* **1993**, *21*, 1695-1701.

(169) Lipscomb, W. N.; Strater, N. Recent Advances in Zinc Enzymology. *Chem. Rev.* **1996**, *96*, 2375-2434.

(170) Luciani, N.; Marie-Claire, C.; Ruffet, E.; Beaumont, A.; Roques, B. P.; Fournie-Zaluski, M. C. Characterization of Glu350 as a critical residue involved in the N-terminal amine binding site of aminopeptidase N (EC 3.4.11.2): insights into its mechanism of action. *Biochemistry* **1998**, *37*, 686-692.

(171) Bauvois, B.; Dauzonne, D. Aminopeptidase-N/CD13 (EC 3.4.11.2) inhibitors: chemistry, biological evaluations, and therapeutic prospects. *Med. Res. Rev.* **2006**, *26*, 88-130.

(172) Mucha, A.; Drag, M.; Dalton, J. P.; Kafarski, P. Metallo-aminopeptidase inhibitors. *Biochimie* **2010**, *92*, 1509-1529.

(173) Xu, W.; Li, Q. Progress in the development of aminopeptidase N (APN/CD13) inhibitors. *Curr. Med. Chem.* **2005**, *5*, 281-301.

(174) Suda, H.; Takita, T.; Aoyagi, T.; Umezawa, H. The structure of bestatin. *J. Antibiot.* **1976**, *29*, 100-101.

(175) Umezawa, H.; Aoyagi, T.; Suda, H.; Hamada, M.; Takeuchi, T. Bestatin, an inhibitor of aminopeptidase B, produced by actinomycetes. *J. Antibiot.* **1976**, *29*, 97-99.

(176) Leyhausen, G.; Schuster, D. K.; Vaith, P.; Zahn, R. K.; Umezawa, H.; Falke, D.; Muller, W. E. Identification and properties of the cell membrane bound leucine aminopeptidase interacting with the potential immunostimulant and chemotherapeutic agent bestatin. *Biochem. Pharmacol.* **1983**, *32*, 1051-1057.

(177) Ota, K.; Kurita, S.; Yamada, K.; Masaoka, T.; Uzuka, Y.; Ogawa, N. Immunotherapy with bestatin for acute nonlymphocytic leukemia in adults. *Cancer. Immunol. Immunother.* **1986**, *23*, 5-10.

(178) Scornik, O. A.; Botbol, V. Bestatin as an experimental tool in mammals. *Curr. Drug. Metab.* **2001**, *2*, 67-85.

(179) Ichinose, Y.; Genka, K.; Koike, T.; Kato, H.; Watanabe, Y.; Mori, T.; Iioka, S.; Sakuma, A.; Ohta, M.; Group, N. K. L. C. S. Randomized double-blind placebo-controlled trial of bestatin in patients with resected stage I squamous-cell lung carcinoma. *J. Natl. Cancer. Inst.* **2003**, *95*, 605-610.

(180) Ota, K. Review of ubenimex (Bestatin): clinical research. *Biomed. Pharmacother.* **1991**, *45*, 55-60.

(181) Urabe, A.; Mutoh, Y.; Mizoguchi, H.; Takaku, F.; Ogawa, N. Ubenimex in the treatment of acute nonlymphocytic leukemia in adults. *Ann. Hematol.* **1993**, *67*, 63-66.

(182) Yasumitsu, T.; Ohshima, S.; Nakano, N.; Kotake, Y.; Tominaga, S. Bestatin in resected lung cancer. A randomized clinical trial. *Acta. Oncol.* **1990**, *29*, 827-831.

(183) Takada, M.; Fukuoka, M.; Negoro, S.; Kusunoki, Y.; Matsui, K.; Masuda, N.; Sakai, N.; Ryu, S.; Takifuji, N.; Kudo, S. Combination therapy with bestatin in inoperable lung cancer. A randomized trial. *Acta. Oncol.* **1990**, *29*, 821-825.

(184) Niimoto, M.; Hattori, T. Prospective randomized controlled study on bestatin in resectable gastric cancer. *Biomed. Pharmacother.* **1991**, *45*, 121-124.

(185) Rich, D. H.; Moon, B. J.; Harbeson, S. Inhibition of aminopeptidases by amastatin and bestatin derivatives. Effect of inhibitor structure on slow-binding processes. *J. Med. Chem.* **1984**, *27*, 417-422.

(186) Aoyagi, T.; Tobe, H.; Kojima, F.; Hamada, M.; Takeuchi, T.; Umezawa, H. Amastatin, an inhibitor of aminopeptidase A, produced by actinomycetes. *J. Antibiot.* **1978**, *31*, 636-638.

(187) Tieku, S.; Hooper, N. M. Inhibition of aminopeptidases N, A and W. A re-evaluation of the actions of bestatin and inhibitors of angiotensin converting enzyme. *Biochem. Pharmacol.* **1992**, *44*, 1725-1730.

(188) Aoyagi, T.; Yoshida, S.; Nakamura, Y.; Shigihara, Y.; Hamada, M.; Takeuchi, T. Probestin, a new inhibitor of aminopeptidase M, produced by Streptomyces azureus MH663-2F6. I. Taxonomy, production, isolation, physico-chemical properties and biological activities. *J. Antibiot.* **1990**, *43*, 143-148.

(189) Gordon, J. J.; Kelly, B. K.; Miller, G. A. Actinonin: an antibiotic substance produced by an actinomycete. *Nature* **1962**, *195*, 701-702.

(190) Gordon, J. J.; Devlin, J. P.; East, A. J.; Ollis, W. D.; Wright, D. E.; Ninet, L. Studies concerning the antibiotic actinonin. Part I. The constitution of actinonin. A natural hydroxamic acid with antibiotic activity. *J. Chem. Soc., Perkin. 1.* **1975**, 819-825.

(191) Umezawa, H.; Aoyagi, T.; Tanaka, T.; Suda, H.; Okuyama, A.; Naganawa, H.; Hamada, M.; Takeuchi, T. Production of actinonin, an inhibitor of aminopeptidase M, by actinomycetes. *J. Antibiot.* **1985**, *38*, 1629-1630.

(192) Xu, Y.; Lai, L. T.; Gabrilove, J. L.; Scheinberg, D. A. Antitumor activity of actinonin in vitro and in vivo. *Clin. Cancer Res.* **1998**, *4*, 171-176.

(193) Shim, J. S.; Kim, J. H.; Cho, H. Y.; Yum, Y. N.; Kim, S. H.; Park, H. J.; Shim, B. S.; Choi, S. H.; Kwon, H. J. Irreversible inhibition of CD13/aminopeptidase N by the antiangiogenic agent curcumin. *Chem. Biol.* **2003**, *10*, 695-704.

(194) Chauhan, D. P. Chemotherapeutic potential of curcumin for colorectal cancer. *Curr. Pharm. Des.* **2002**, *8*, 1695-1706.

(195) Sarkar, F. H.; Li, Y. Cell signaling pathways altered by natural chemopreventive agents. *Mutat. Res.* **2004**, *555*, 53-64.

(196) Gupta, S. C.; Patchva, S.; Aggarwal, B. B. Therapeutic roles of curcumin: lessons learned from clinical trials. *AAPS J.* **2013**, *15*, 195-218.

(197) Anand, P.; Kunnumakkara, A. B.; Newman, R. A.; Aggarwal, B. B. Bioavailability of curcumin: problems and promises. *Mol. Pharm.* **2007**, *4*, 807-818.

(198) Arabshahi, L. S., F. J. Brominated tyrosine metabolites from an unidentified sponge. *J. Org. Chem.* **1987**, *52*, 3584-3586.

(199) Quinoa`, E. C., P. Phenolic constituents of *Psammaplysilla*. *Tetrahedron Lett.* **1987**, *28*, 3229-3232.

(200) Rodriguez, A. D. A. R., K.; Schuer, P. J. Two bromotyrosine-cysteine derived metabolites from a sponge. *Tetrahedron Lett.* **1987**, *28*, 4989-4992.

(201) Shim, J. S.; Lee, H. S.; Shin, J.; Kwon, H. J. Psammaplin A, a marine natural product, inhibits aminopeptidase N and suppresses angiogenesis in vitro. *Cancer. Lett.* **2004**, *203*, 163-169.

(202) Pina, I. C.; Gautschi, J. T.; Wang, G. Y.; Sanders, M. L.; Schmitz, F. J.; France, D.; Cornell-Kennon, S.; Sambucetti, L. C.; Remiszewski, S. W.; Perez, L. B.; Bair, K. W.; Crews, P. Psammaplins from the sponge Pseudoceratina purpurea: inhibition of both histone deacetylase and DNA methyltransferase. *J. Org. Chem.* **2003**, *68*, 3866-3873.

(203) Tabudravu, J. N.; Eijsink, V. G.; Gooday, G. W.; Jaspars, M.; Komander, D.; Legg, M.; Synstad, B.; van Aalten, D. M. Psammaplin A, a chitinase inhibitor isolated from the Fijian marine sponge Aplysinella rhax. *Bioorg. Med. Chem.* **2002**, *10*, 1123-1128.

(204) Melzig, M. F.; Bormann, H. Betulinic acid inhibits aminopeptidase N activity. *Planta Med.* **1998**, *64*, 655-657.

(205) Cichewicz, R. H.; Kouzi, S. A. Chemistry, biological activity, and chemotherapeutic potential of betulinic acid for the prevention and treatment of cancer and HIV infection. *Med. Res. Rev.* **2004**, *24*, 90-114.

(206) Fulda, S. Betulinic Acid for cancer treatment and prevention. *Int. J. Mol. Sci.* **2008**, *9*, 1096-1107.

(207) Zeng, A. Q.; Yu, Y.; Yao, Y. Q.; Yang, F. F.; Liao, M.; Song, L. J.; Li, Y. L.; Yu, Y.; Li, Y. J.; Deng, Y. L.; Yang, S. P.; Zeng, C. J.; Liu, P.; Xie, Y. M.; Yang, J. L.; Zhang, Y. W.; Ye, T. H.; Wei, Y. Q. Betulinic acid impairs metastasis and reduces immunosuppressive cells in breast cancer models. *Oncotarget* **2018**, *9*, 3794-3804.

(208) Krige, D.; Needham, L. A.; Bawden, L. J.; Flores, N.; Farmer, H.; Miles, L. E.; Stone, E.; Callaghan, J.; Chandler, S.; Clark, V. L.; Kirwin-Jones, P.; Legris, V.; Owen, J.; Patel, T.; Wood, S.; Box, G.; Laber, D.; Odedra, R.; Wright, A.; Wood, L. M.; Eccles, S. A.; Bone, E. A.; Ayscough, A.; Drummond, A. H. CHR-2797: an antiproliferative aminopeptidase inhibitor that leads to amino acid deprivation in human leukemic cells. *Cancer. Res.* **2008**, *68*, 6669-6679.

(209) Jenkins, C.; Hewamana, S.; Krige, D.; Pepper, C.; Burnett, A. Aminopeptidase inhibition by the novel agent CHR-2797 (tosedostat) for the therapy of acute myeloid leukemia. *Leuk. Res.* **2011**, *35*, 677-681.

(210) Moore, H. E.; Davenport, E. L.; Smith, E. M.; Muralikrishnan, S.; Dunlop, A. S.; Walker, B. A.; Krige, D.; Drummond, A. H.; Hooftman, L.; Morgan, G. J.; Davies, F. E. Aminopeptidase inhibition as a targeted treatment strategy in myeloma. *Mol. Cancer. Ther.* **2009**, *8*, 762-770.

(211) Bhatt, L.; Roinestad, K.; Van, T.; Springman, E. B. Recent advances in clinical development of leukotriene B4 pathway drugs. *Semin. Immunol.* **2017**, *33*, 65-73.

(212) Lowenberg, B.; Morgan, G.; Ossenkoppele, G. J.; Burnett, A. K.; Zachee, P.; Duhrsen, U.; Dierickx, D.; Muller-Tidow, C.; Sonneveld, P.; Krug, U.; Bone, E.; Flores, N.; Richardson, A. F.; Hooftman, L.; Jenkins, C.; Zweegman, S.; Davies, F. Phase I/II clinical study of Tosedostat, an inhibitor of aminopeptidases, in patients with acute myeloid leukemia and myelodysplasia. *J. Clin. Oncol.* **2010**, *28*, 4333-4338.

(213) Miyachi, H.; Kato, M.; Kato, F.; Hashimoto, Y. Novel potent nonpeptide aminopeptidase N inhibitors with a cyclic imide skeleton. *J. Med. Chem.* **1998**, *41*, 263-265.

(214) Li, Q.; Fang, H.; Xu, W. Novel 3-galloylamido-N'-substituted-2,6-piperidinedione-N-acetamide peptidomimetics as metalloproteinase inhibitors. *Bioorg. Med. Chem. Lett.* **2007**, *17*, 2935-2938.

(215) Cui, S. X.; Qu, X. J.; Gao, Z. H.; Zhang, Y. S.; Zhang, X. F.; Zhao, C. R.; Xu, W. F.; Li, Q. B.; Han, J. X. Targeting aminopeptidase N (APN/CD13) with cyclic-imide peptidomimetics derivative CIP-13F inhibits the growth of human ovarian carcinoma cells. *Cancer. Lett.* **2010**, *292*, 153-162.

(216) Inagaki, Y.; Tang, W.; Zhang, L.; Du, G.; Xu, W.; Kokudo, N. Novel aminopeptidase N (APN/CD13) inhibitor 24F can suppress invasion of hepatocellular carcinoma cells as well as angiogenesis. *Biosci Trends.* **2010**, *4*, 56-60.

(217) Schalk, C.; d'Orchymont, H.; Jauch, M. F.; Tarnus, C. 3-Amino-2-tetralone derivatives: novel potent and selective inhibitors of aminopeptidase-M (EC 3.4.11.2). *Arch. Biochem. Biophys.* **1994**, *311*, 42-46.

(218) Zhang, X.; Xu, W. Aminopeptidase N (APN/CD13) as a target for anti-cancer agent design. *Curr. Med. Chem.* **2008**, *15*, 2850-2865.

(219) Albrecht, S.; Al-Lakkis-Wehbe, M.; Orsini, A.; Defoin, A.; Pale, P.; Salomon, E.; Tarnus, C.; Weibel, J. M. Amino-benzosuberone: a novel warhead for selective inhibition of human aminopeptidase-N/CD13. *Bioorg. Med. Chem.* **2011**, *19*, 1434-1449.

(220) Maiereanu, C.; Schmitt, C.; Schifano-Faux, N.; Le Nouen, D.; Defoin, A.; Tarnus, C. A novel amino-benzosuberone derivative is a picomolar inhibitor of mammalian aminopeptidase N/CD13. *Bioorg. Med. Chem.* **2011**, *19*, 5716-5733.

(221) Revelant, G.; Al-Lakkis-Wehbe, M.; Schmitt, M.; Alavi, S.; Schmitt, C.; Roux, L.; Al-Masri, M.; Schifano-Faux, N.; Maiereanu, C.; Tarnus, C.; Albrecht, S. Exploring S1 plasticity and probing S1' subsite of mammalian aminopeptidase N/CD13 with highly potent and selective aminobenzosuberone inhibitors. *Bioorg. Med. Chem.* **2015**, *23*, 3192-3207.

(222) Bibby, M. C.; Double, J. A. Flavone acetic acid--from laboratory to clinic and back. *Anticancer Drugs* **1993**, *4*, 3-17.

(223) Bauvois, B.; Puiffe, M. L.; Bongui, J. B.; Paillat, S.; Monneret, C.; Dauzonne, D. Synthesis and biological evaluation of novel flavone-8-acetic acid derivatives as reversible inhibitors of aminopeptidase N/CD13. *J. Med. Chem.* **2003**, *46*, 3900-3913.

(224) Yang, K.; Wang, Q.; Su, L.; Fang, H.; Wang, X.; Gong, J.; Wang, B.; Xu, W. Design and synthesis of novel chloramphenicol amine derivatives as potent aminopeptidase N (APN/CD13) inhibitors. *Bioorg. Med. Chem.* **2009**, *17*, 3810-3817.

(225) Jia, M.; Yang, K.; Fang, H.; Xu, Y.; Sun, S.; Su, L.; Xu, W. Novel aminopeptidase N (APN/CD13) inhibitors derived from chloramphenicol amine. *Bioorg. Med. Chem.* **2011**, *19*, 5190-5198.

(226) Baker, J. O.; Wilkes, S. H.; Bayliss, M. E.; Prescott, J. M. Hydroxamates and aliphatic boronic acids: marker inhibitors for aminopeptidase. *Biochemistry.* **1983**, *22*, 2098-2103.

(227) Shenvi, A. B. alpha-Aminoboronic acid derivatives: effective inhibitors of aminopeptidases. *Biochemistry* **1986**, *25*, 1286-1291.

(228) Lejczak, B.; Kafarski, P.; Zygmunt, J. Inhibition of aminopeptidases by aminophosphonates. *Biochemistry* **1989**, *28*, 3549-3555.

(229) Chen, H.; Roques, B. P.; Fournie-Zaluski, M. C. Design of the first highly potent and selective aminopeptidase N (EC 3.4.11.2) inhibitor. *Bioorg. Med. Chem. Lett.* **1999**, *9*, 1511-1516.

(230) Drinkwater, N.; Vinh, N. B.; Mistry, S. N.; Bamert, R. S.; Ruggeri, C.; Holleran, J. P.; Loganathan, S.; Paiardini, A.; Charman, S. A.; Powell, A. K.; Avery, V. M.; McGowan, S.; Scammells, P. J. Potent dual inhibitors of Plasmodium falciparum M1 and M17 aminopeptidases through optimization of S1 pocket interactions. *Eur. J. Med. Chem.* **2016**, *110*, 43-64.

(231) Kannan Sivaraman, K.; Paiardini, A.; Sienczyk, M.; Ruggeri, C.; Oellig, C. A.; Dalton, J. P.; Scammells, P. J.; Drag, M.; McGowan, S. Synthesis and structure-activity relationships of phosphonic arginine mimetics as inhibitors of the M1 and M17 aminopeptidases from Plasmodium falciparum. *J. Med. Chem.* **2013**, *56*, 5213-5217.

(232) Mistry, S. N.; Drinkwater, N.; Ruggeri, C.; Sivaraman, K. K.; Loganathan, S.; Fletcher, S.; Drag, M.; Paiardini, A.; Avery, V. M.; Scammells, P. J.; McGowan, S. Two-pronged attack: dual inhibition of Plasmodium falciparum M1 and M17 metalloaminopeptidases by a novel series of hydroxamic acid-based inhibitors. *J. Med. Chem.* **2014**, *57*, 9168-9183.

(233) Stack, C. M.; Lowther, J.; Cunningham, E.; Donnelly, S.; Gardiner, D. L.; Trenholme, K. R.; Skinner-Adams, T. S.; Teuscher, F.; Grembecka, J.; Mucha, A.; Kafarski, P.; Lua, L.; Bell, A.; Dalton, J. P. Characterization of the Plasmodium falciparum M17 leucyl aminopeptidase. A protease involved in amino acid regulation with potential for antimalarial drug development. *J. Biol. Chem.* **2007**, *282*, 2069-2080.

(234) Ballatore, C.; Huryn, D. M.; Smith, A. B., 3rd. Carboxylic acid (bio)isosteres in drug design. *ChemMedChem* **2013**, *8*, 385-395.

(235) Riss, T. L.; Moravec, R. A.; Niles, A. L.; Benink, H. A.; Worzella, T. J.; Minor, L. Cell Viability Assays. In *Assay Guidance Manual*, Sittampalam, G. S.; Coussens, N. P.; Nelson, H.; Arkin, M.; Auld, D.; Austin, C.; Bejcek, B.; Glicksman, M.; Inglese, J.; Iversen, P. W.; Li, Z.; McGee, J.; McManus, O.; Minor, L.; Napper, A.; Peltier, J. M.; Riss, T.; Trask, O. J., Jr.; Weidner, J., Eds. Bethesda (MD), 2004.

(236) Meanwell, N. A. Synopsis of some recent tactical application of bioisosteres in drug design. *J. Med. Chem.* **2011**, *54*, 2529-2591.

(237) Meanwell, N. A. A Synopsis of the Properties and Applications of Heteroaromatic Rings in Medicinal Chemistry. In *Adv. Heterocycl. Chem.*, Scriven, E. F. V.; Ramsden, C. A., Eds. Academic Press: 2017; Vol. 123, pp 245-361.

(238) Dalvie, D.; Kang, P.; Loi, C.-M.; Goulet, L.; Nair, S. Influence of Heteroaromatic Rings on ADME Properties of Drugs. In *Metabolism, Pharmacokinetics and Toxicity of Functional Groups: Impact of Chemical Building Blocks on ADMET*, The Royal Society of Chemistry: 2010; pp 328-369.

(239) Zhang, X.; Gong, Z.; Li, J.; Lu, T. Intermolecular Sulfur...Oxygen Interactions: Theoretical and Statistical Investigations. *J. Chem. Inf. Model.* **2015**, *55*, 2138-2153.

(240) Ishikawa, M.; Hashimoto, Y. Improvement in aqueous solubility in small molecule drug discovery programs by disruption of molecular planarity and symmetry. *J. Med. Chem.* **2011**, *54*, 1539-1554.

(241) Lee, J.; Vinh, N. B.; Drinkwater, N.; Yang, W.; Kannan Sivaraman, K.; Schembri, L. S.; Gazdik, M.; Grin, P. M.; Butler, G. S.; Overall, C. M.; Charman, S. A.; McGowan, S.; Scammells, P. J. Novel Human Aminopeptidase N Inhibitors: Discovery and Optimization of Subsite Binding Interactions. *J. Med. Chem.* **2019**, *published asap online*.

(242) Kawai, K.; Nagata, N. Metal-ligand interactions: an analysis of zinc binding groups using the Protein Data Bank. *Eur. J. Med. Chem.* **2012**, *51*, 271-276.

(243) Doucet, H. Suzuki–Miyaura Cross-Coupling Reactions of Alkylboronic Acid Derivatives or Alkyltrifluoroborates with Aryl, Alkenyl or Alkyl Halides and Triflates. *Eur. J. Org. Chem.* **2008**, *2008*, 2013-2030.

(244) Jana, R.; Pathak, T. P.; Sigman, M. S. Advances in transition metal (Pd, Ni, Fe)-catalyzed cross-coupling reactions using alkyl-organometallics as reaction partners. *Chem. Rev.* **2011**, *111*, 1417-1492.

(245) Molander, G. A.; Yun, C.-S. Cross-coupling reactions of primary alkylboronic acids with aryl triflates and aryl halides. *Tetrahedron* **2002**, *58*, 1465-1470.

(246) Si, T.; Li, B.; Xiong, W.; Xu, B.; Tang, W. Efficient cross-coupling of aryl/alkenyl triflates with acyclic secondary alkylboronic acids. *Org. Biomol. Chem.* **2017**, *15*, 9903-9909.

(247) Zou, G.; Reddy, Y. K.; Falck, J. R. Ag(I)-promoted Suzuki–Miyaura cross-couplings of n-alkylboronic acids. *Tetrahedron Lett.* **2001**, *42*, 7213-7215.

(248) Lennox, A. J.; Lloyd-Jones, G. C. Selection of boron reagents for Suzuki-Miyaura coupling. *Chem. Soc. Rev.* **2014**, *43*, 412-443.

(249) Piscitelli, F.; Ligresti, A.; La Regina, G.; Coluccia, A.; Morera, L.; Allara, M.; Novellino, E.; Di Marzo, V.; Silvestri, R. Indole-2-carboxamides as allosteric modulators of the cannabinoid CB(1) receptor. *J. Med. Chem.* **2012**, *55*, 5627-5631.

(250) Vantourout, J. C.; Law, R. P.; Isidro-Llobet, A.; Atkinson, S. J.; Watson, A. J. Chan-Evans-Lam Amination of Boronic Acid Pinacol (BPin) Esters: Overcoming the Aryl Amine Problem. *J. Org. Chem.* **2016**, *81*, 3942-3950.

(251) Vantourout, J. C.; Miras, H. N.; Isidro-Llobet, A.; Sproules, S.; Watson, A. J. Spectroscopic Studies of the Chan-Lam Amination: A Mechanism-Inspired Solution to Boronic Ester Reactivity. *J. Am. Chem. Soc.* **2017**, *139*, 4769-4779.

(252) Gasteiger, J.; Marsili, M. Iterative partial equalization of orbital electronegativity—a rapid access to atomic charges. *Tetrahedron* **1980**, *36*, 3219-3228.

(253) Lenz, C.; Haubmann, C.; Hubner, H.; Boeckler, F.; Gmeiner, P. Fancy bioisosteres: synthesis and dopaminergic properties of the endiyne FAUC 88 as a novel non-aromatic D3 agonist. *Bioorg. Med. Chem.* **2005**, *13*, 185-191.

(254) Stepan, A. F.; Subramanyam, C.; Efremov, I. V.; Dutra, J. K.; O'Sullivan, T. J.; DiRico, K. J.; McDonald, W. S.; Won, A.; Dorff, P. H.; Nolan, C. E.; Becker, S. L.; Pustilnik, L. R.; Riddell, D. R.; Kauffman, G. W.; Kormos, B. L.; Zhang, L.; Lu, Y.; Capetta, S. H.; Green, M. E.; Karki, K.; Sibley, E.; Atchison, K. P.; Hallgren, A. J.; Oborski, C. E.; Robshaw, A. E.; Sneed, B.; O'Donnell, C. J. Application of the bicyclo[1.1.1]pentane motif as a nonclassical phenyl ring bioisostere in the design of a potent and orally active gamma-secretase inhibitor. *J. Med. Chem.* **2012**, *55*, 3414-3424.

(255) Makarov, I. S.; Brocklehurst, C. E.; Karaghiosoff, K.; Koch, G.; Knochel, P. Synthesis of Bicyclo[1.1.1]pentane Bioisosteres of Internal Alkynes and para-Disubstituted Benzenes from [1.1.1]Propellane. *Angew. Chem. Int. Ed. Engl.* **2017**, *56*, 12774-12777.

(256) Li, W. Z., J. Highly selective herbicide N-substituted alkyl aryloxy phenoxy propionamide compound and its preparation. CN 105669584, Jun 15, 2016.

(257) Belema, M. H., P. Preparation of biphenylacetylenes, biphenylethers, terphenyls and related derivatives end-capped with amino acid or peptide derivatives as hepatitis C virus inhibitors. WO 2012039717, Mar 29, 2012.

(258) Romine, J. L. S. L., D. R.; Belema, M.; Snyder, L. B.; Hamann, L. G.; Kadow, J. F.; Kapur, J.; Good, A. C.; Lopez, O. D.; Lavoie, R. Preparation of 1H-benzimidazole derivatives end-capped with amino acid or peptide derivatives as hepatitis C virus inhibitors. WO 2010096302, Aug 26, 2010.

(259) Boto, A.; Gallardo, J. A.; Hernandez, D.; Hernandez, R. Synthesis of unnatural amino acids from serine derivatives by beta-fragmentation of primary alkoxyl radicals. *J. Org. Chem.* **2007**, *72*, 7260-7269.

(260) Saaby, S.; Bayon, P.; Aburel, P. S.; Jorgensen, K. A. Optically active aromatic and heteroaromatic alpha-amino acids by a one-pot catalytic enantioselective addition of aromatic and heteroaromatic C-H bonds to alpha-imino esters. *J. Org. Chem.* **2002**, *67*, 4352-4361.

(261) Kusano, H. Y., K. Preparation of cephem derivatives. WO 2011136268, Nov 3,, 2011.

(262) Bolsakova, J.; Jirgensons, A. Synthesis of α-Ethynyl Glycines. *Eur. J. Org. Chem.* **2016**, *2016*, 4591-4602.

(263) Meffre, P.; Le Goffic, F. beta,gamma-Alkynylalpha-amino acids: a synthetic challenge. *Amino Acids* **1996**, *11*, 313-328.

(264) Kumar, P.; Shukhman, D.; Laughlin, S. T. A photocaged, cyclopropene-containing analog of the amino acid neurotransmitter glutamate. *Tetrahedron Lett.* **2016**, *57*, 5750-5752.

(265) Girijavallabhan, V. M.; Chen, L.; Dai, C.; Feltz, R. J.; Firmansjah, L.; Li, D.; Kim, S. H.; Kozlowski, J. A.; Lavey, B. J.; Kosinski, A.; Piwinski, J. J.; Popovici-Muller, J.; Rizvi, R.; Rosner, K. E.; Shankar, B. B.; Shih, N. Y.; Siddiqui, M. A.; Tong, L.; Wong, M. K.; Yang, D. Y.; Yang, L.; Yu, W.; Zhou, G.; Guo, Z.; Orth, P.; Madison, V.; Bian, H.; Lundell, D.; Niu, X.; Shah, H.; Sun, J.; Umland, S. Novel TNF-alpha converting enzyme (TACE) inhibitors as potential treatment for inflammatory diseases. *Bioorg. Med. Chem. Lett.* **2010**, *20*, 7283-7287.

(266) Robinson, A. J. J., W. R.; Patel, J.; Elaridi, J. Methods for the synthesis of dicarba bridges in organic compounds. WO 2007093013, Aug 23, 2007.

(267) Xie, J. G., X.; Zhao, L.; Liu, C. Process for preparation of chiral p-hydroxyphenylglycine derivatives. WO 2013120257, Aug 22, 2013.

(268) Glauner, H.; Ruttekolk, I. R.; Hansen, K.; Steemers, B.; Chung, Y. D.; Becker, F.; Hannus, S.; Brock, R. Simultaneous detection of intracellular target and off-target binding of small molecule cancer drugs at nanomolar concentrations. *Br. J. Pharmacol.* **2010**, *160*, 958-970.

(269) van Breemen, R. B.; Li, Y. Caco-2 cell permeability assays to measure drug absorption. *Expert. Opin. Drug. Metab. Toxicol.* **2005**, *1*, 175-185.

(270) Schmitt, C.; Voegelin, M.; Marin, A.; Schmitt, M.; Schegg, F.; Henon, P.; Guenot, D.; Tarnus, C. Selective aminopeptidase-N (CD13) inhibitors with relevance to cancer chemotherapy. *Bioorg. Med. Chem.* **2013**, *21*, 2135-2144.

(271) Moon, P. J.; Yin, S.; Lundgren, R. J. Ambient Decarboxylative Arylation of Malonate Half-Esters via Oxidative Catalysis. *J. Am. Chem. Soc.* **2016**, *138*, 13826-13829.

(272) Sabbatini, F. M.; Di Fabio, R.; Corsi, M.; Cavanni, P.; Bromidge, S. M.; St-Denis, Y.; D'Adamo, L.; Contini, S.; Rinaldi, M.; Guery, S.; Savoia, C.; Mundi, C.; Perini, B.; Carpenter, A. J.; Dal Forno, G.; Faggioni, F.; Tessari, M.; Pavone, F.; Di Francesco, C.; Buson, A.;

Mattioli, M.; Perdona, E.; Melotto, S. Discovery process and characterization of novel carbohydrazide derivatives as potent and selective GHSR1a antagonists. *ChemMedChem* **2010**, *5*, 1450-1455.

(273) Ji, J.-X.; Au-Yeung, T. T. L.; Wu, J.; Yip, C. W.; Chan, A. S. C. Efficient Synthesis of β,γ-Alkynyl α-Amino Acid Derivatives by Ag(I)-Catalyzed Alkynylation of α-Imino Esters. *Adv. Synth. Catal.* **2004**, *346*, 42-44.

(274) Verkade, J. M. M.; van Hemert, L. J. C.; Quaedflieg, P. J. L. M.; Alsters, P. L.; van Delft, F. L.; Rutjes, F. P. J. T. Mild and efficient deprotection of the amine protecting p-methoxyphenyl (PMP) group. *Tetrahedron Lett.* **2006**, *47*, 8109-8113.

(275) Sanderson, L.; Taylor, G. W.; Aboagye, E. O.; Alao, J. P.; Latigo, J. R.; Coombes, R. C.; Vigushin, D. M. Plasma pharmacokinetics and metabolism of the histone deacetylase inhibitor trichostatin a after intraperitoneal administration to mice. *Drug Metab. Dispos.* **2004**, *32*, 1132-1138.

(276) Flipo, M.; Charton, J.; Hocine, A.; Dassonneville, S.; Deprez, B.; Deprez-Poulain, R. Hydroxamates: relationships between structure and plasma stability. *J. Med. Chem.* **2009**, *52*, 6790-6802.

(277) Weisburger, J. H.; Weisburger, E. K. Biochemical formation and pharmacological, toxicological, and pathological properties of hydroxylamines and hydroxamic acids. *Pharmacol. Rev.* **1973**, *25*, 1-66.